BEILSTEIN JOURNAL OF ORGANIC CHEMISTRY

Functionalized polymers: synthesis and properties

Edited by Helmut Ritter

Generated on 03 November 2026, 11:28

Imprint

Beilstein Journal of Organic Chemistry
www.bjoc.org
ISSN 1860-5397
Email: journals-support@beilstein-institut.de

The *Beilstein Journal of Organic Chemistry* is published by the Beilstein-Institut zur Förderung der Chemischen Wissenschaften.

Beilstein-Institut zur Förderung der Chemischen Wissenschaften
Trakehner Straße 7–9
60487 Frankfurt am Main
Germany
www.beilstein-institut.de

The copyright to this document as a whole, which is published in the *Beilstein Journal of Organic Chemistry*, is held by the Beilstein-Institut zur Förderung der Chemischen Wissenschaften. The copyright to the individual articles in this document is held by the respective authors, subject to a Creative Commons Attribution license.

Beilstein Journal of Organic Chemistry

Functionalized polymers: synthesis and properties

Helmut Ritter

Editorial

Open Access

Address:
Institute of Organic Chemistry and Macromolecular Chemistry II,
Heinrich-Heine-University of Düsseldorf, Universitätsstraße 1,
D-40225 Düsseldorf, Germany

Email:
Helmut Ritter - h.ritter@uni-duesseldorf.de

Beilstein J. Org. Chem. **2010,** *6,* No. 55. doi:10.3762/bjoc.6.55

Received: 18 May 2010
Accepted: 19 May 2010
Published: 01 June 2010

Guest Editor: H. Ritter

© 2010 Ritter; licensee Beilstein-Institut.
License and terms: see end of document.

Materials that are used in everyday life have an immense impact on the development of the human society. During the Stone Age and Iron Age epochs, humans widely used stone or iron to make tools. In the present age, there is no question that polymers and plastics dominate our rapidly developing daily needs and show enormous potential for the development of new technologies. Constructive materials, for instance, are preferentially made of standard polymeric materials such as polyolefins, polyesters or polyamides. It is therefore obvious that the future of polymer chemistry will be influenced by the elaboration of new functional polymers. At the beginning of the application of synthetic materials, naturally occurring polymers as cellulose or polyisoprene were simply modified, for example by esterification or cross-linking to obtain the desired properties. Hermann Staudinger, for instance, chemically modified starch to prove the existence of high molecular weight substances. Nowadays, the development of various functional polymers is becoming increasingly important in specific areas of application.

In terms of technical applications, functional polymers are important, for example in the fields of optics, electronics or catalysis. They are also widely used for analytical devices, (e.g. columns for chromatography), for membranes and in the solid phase synthesis of peptides and oligonucleotides.

Focusing on the constantly developing medical field, only specifically elaborated functional polymer materials can fulfill the specific challenges required of them for use as, for example, surgical sutures, dental fillings, wound dressings, bone cements or hollow fibers for dialysis. Typical examples of such materials include hydrogels and stimulus-responsive polymers which are also the basis of ophthalmic surgery.

Thus, our aim in this Thematic Series is to bring together a broad spectrum of reports in the field of functionalized polymers to update the “state of the art” of knowledge in this field. It is therefore a great pleasure to serve as an editor for this series of articles.

Helmut Ritter

Düsseldorf, May 2010

License and Terms

This is an Open Access article under the terms of the Creative Commons Attribution License (http://creativecommons.org/licenses/by/2.0), which permits unrestricted use, distribution, and reproduction in any medium, provided the original work is properly cited.

The license is subject to the *Beilstein Journal of Organic Chemistry* terms and conditions: (http://www.beilstein-journals.org/bjoc)

The definitive version of this article is the electronic one which can be found at:
doi:10.3762/bjoc.6.55

Beilstein Journal of Organic Chemistry

Synthesis of bis(3-{[2-(allyloxy)ethoxy]methyl}-2,4,6-trimethylbenzoyl)(phenyl)phosphine oxide – a tailor-made photoinitiator for dental adhesives

Norbert Moszner*[1], Iris Lamparth[1], Jörg Angermann[1], Urs Karl Fischer[1], Frank Zeuner[1], Thorsten Bock[1], Robert Liska[2] and Volker Rheinberger[1]

Full Research Paper

Open Access

Address:
[1]Ivoclar Vivadent AG, Bendererstrasse 2, FL-9494 Schaan, Liechtenstein and [2]Institute of Applied Synthetic Chemistry, Division of Macromolecular Chemistry, Vienna University of Technology, Getreidemarkt 9/163/MA, A-1060 Vienna, Austria

Email:
Norbert Moszner* - norbert.moszner@ivoclarvivadent.com

* Corresponding author

Keywords:
adhesives; dental polymers; dimethacrylates; photoinitiator; radical polymerization

Beilstein Journal of Organic Chemistry **2010,** *6,* No. 26.
doi:10.3762/bjoc.6.26

Received: 23 November 2009
Accepted: 03 March 2010
Published: 15 March 2010

Guest Editor: H. Ritter

© 2010 Moszner et al; licensee Beilstein-Institut.
License and terms: see end of document.

Abstract

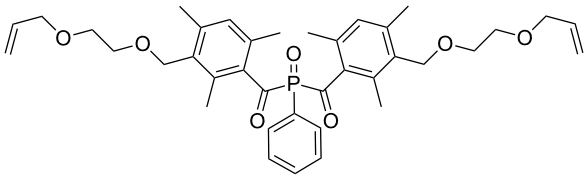
Because of the poor solubility of the commercially available bisacylphosphine oxides in dental acidic aqueous primer formulations, bis(3-{[2-(allyloxy)ethoxy]methyl}-2,4,6-trimethylbenzoyl)(phenyl)phosphine oxide (WBAPO) was synthesized starting from 3-(chloromethyl)-2,4,6-trimethylbenzoic acid by the dichlorophosphine route. The substituent was introduced by etherification with 2-(allyloxy)ethanol. In the second step, 3-{[2-(allyloxy)ethoxy]methyl}-2,4,6-trimethylbenzoic acid was chlorinated. The formed acid chloride showed an unexpected low thermal stability. Its thermal rearrangement at 180 °C resulted in a fast formation of 3-(chloromethyl)-2,4,6-trimethylbenzoic acid 2-(allyloxy)ethyl ester. In the third step, the acid chloride was reacted with phenylphosphine dilithium with the formation of bis(3-{[2-(allyloxy)ethoxy]methyl}-2,4,6-trimethylbenzoyl)(phenyl)phosphine, which was oxidized to WBAPO. The structure of WBAPO was confirmed by ^{1}H NMR, ^{13}C NMR, ^{31}P NMR, and IR spectroscopy, as well as elemental analysis. WBAPO, a yellow liquid, possesses improved solubility in polar solvents and shows UV–vis absorption, and a high photoreactivity comparable with the commercially available bisacylphosphine oxides. A sufficient storage stability was found in dental acidic aqueous primer formulations.

Introduction

Self-etching enamel-dentin adhesives (SEAs) are used in restorative dentistry to achieve a strong bond between the filling composites and dental hard tissues. The main components of currently used SEAs include strongly acidic adhesive monomers, such as polymerizable phosphonic or phosphoric acids and crosslinking dimethacrylates, such as 2,2-bis[(4-(2-hydroxy-3-methacryloyloxypropoxy)phenyl]propane (Bis-GMA) or triethylene glycol dimethacrylate (TEGDMA) [1]. In

SEAs, water is primarily used as the solvent or co-solvent. Thus, especially in the case of one-bottle adhesives, the methacrylates may undergo hydrolysis of the methacrylate ester groups in the presence of the strongly acidic adhesive monomers. Therefore, we have synthesized new crosslinkers [2], such as *N*,*N*'-diethyl-1,3-bis(acrylamido)propane (DEBAMP), or new strongly acidic monomers, such as 2,4,6-trimethylphenyl 2-[4-(dihydroxyphosphoryl)-2-oxa-butyl]acrylate [3] or 1,3-bis(methacrylamido)propane-2-yl dihydrogen phosphate (BMAMHP) [4], which show improved hydrolytic stability under acidic aqueous conditions. The visible-light (VL) photoinitiators (PIs) in current SEAs are based on mixtures of camphorquinone (CQ) and tertiary amines (A) [5]. The CQ-A PIs belong to bimolecular hydrogen abstraction PI systems: CQ shows a broad absorption spectrum between 400 and 500 nm (λ_{max} = 468 nm). The VL-excited CQ forms an excited state complex with the amine co-initiator, which generates a ketyl and an α-aminoalkyl radical by electron and subsequent proton transfer. The aminoalkyl radical may initiate the polymerization of the monomers present, while the ketyl radical is mainly deactivated by dimerization or disproportionation [6]. However, in SEAs, the acid-base reaction of acidic monomers with the basic amine co-initiators of the PI system may significantly impair the formation of initiating radicals. Moreover, especially in the aqueous medium, the polar radical ions are well solvated by the surrounding medium, thus inhibiting the proton transfer. If proton transfer occurs, both non-ionic and therefore rather hydrophobic species are kept in the solvent cage, which reduces the photoinitiating activity [7]. Therefore, in order to improve the performance of SEAs, amine-free PIs were developed. In this context, we were able to show that benzoyltrimethylgermane [8] and dibenzoyldiethylgermane (DBDEG) [9,10] can be used as VL PIs for the photopolymerization of dimethacrylate resins, dental adhesives or composites and undergo an α-cleavage with the formation of benzoyl and germyl radicals, which may initiate the free-radical polymerization of the monomers present. In addition, bisacylphosphine oxides, such as commercially available bis(2,4,6-trimethylbenzoyl)phenylphosphine oxide (BAPO), seem to be a suitable alternative because their absorption tails out into the visible range of the spectrum [7]. BAPO undergoes a monomolecular α-cleavage with the formation of two initiating radicals and shows a high photoinitiating reactivity with a good storage stability. Recently, a simple straightforward synthesis of BAPO was published [11]. However, the solubility of BAPO in polar solvents and aqueous formulations is insufficiently low, which limits the use of BAPO in water-based SEAs. In this context, we were able to synthesize a number of new substituted bisacylphosphine oxides, which show improved solubility in aqueous compositions [12].

In this paper, we report the detailed synthesis of bis(3-{[2-(allyloxy)ethoxy]methyl}-2,4,6-trimethylbenzoyl)(phenyl)phosphine oxide WBAPO (Scheme 1) and its use as a tailor-made PI in SEAs.



WBAPO

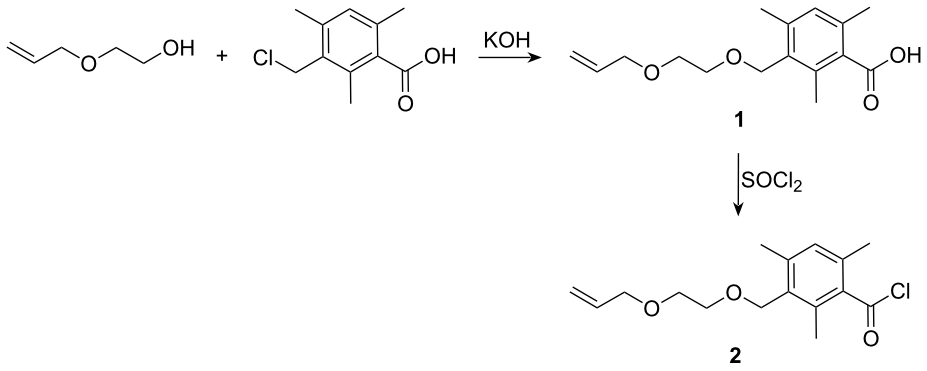
Scheme 1: Bisacylphosphine oxide with improved solubility in polar solvents.

Results and Discussion

Synthesis and characterization of WBAPO

The synthesis of bisacylphosphines and their oxides often start either from *P*,*P*-dichlorophenylphosphine ($PhPCl_2$) [13] or free phenylphosphine [14]. We chose to use the $PhPCl_2$-route since primary phosphines have an unpleasant smell, a high toxicity and are very air-sensitive. Furthermore, phenylphosphine is difficult to access commercially and is very expensive. The synthesis of WBAPO started from 3-(chloromethyl)-2,4,6-trimethylbenzoic acid, which was synthesized by chloromethylation of 2,4,6-trimethylbenzoic acid with a mixture of paraformaldehyde and hydrochloric acid, followed by treatment of the formed hydroxymethyl compound with concentrated hydrochloric acid in a one-pot reaction [15]. In the first step of the WBAPO synthesis (Scheme 2), 3-(chloromethyl)-2,4,6-trimethylbenzoic acid was coupled with 2-(allyloxy)ethanol using potassium hydroxide in excess of 2-(allyloxy)ethanol as solvent at 70 °C to afford 3-{[2-(allyloxy)ethoxy]methyl}-2,4,6-trimethylbenzoic acid **1** as an off-white powder in 62% yield. The main problem of this step was the separation of the large amount of residual 2-(allyloxy)ethanol. This was successfully accomplished by washing its toluene solution with water followed by recrystallization of the crude product from cyclohexane.

In the second step, **1** was chlorinated with thionyl chloride in toluene as solvent by a procedure analogous to that described in the literature [16]. After distillation of the dark crude product, 3-{[2-[allyloxy)ethoxy]methyl}-2,4,6-trimethylbenzoyl chloride **2** was obtained as a colorless liquid in 76% yield. However, **2** showed unexpected limited thermal stability. It was found that **2** decomposed with the formation of 3-(chloromethyl)-2,4,6-trimethylbenzoic acid 2-(allyloxy)ethyl ester **4** slowly on storage at room temperature over a few days or rapidly on heating at 180 °C for 4 h. Obviously, this reaction is a thermal

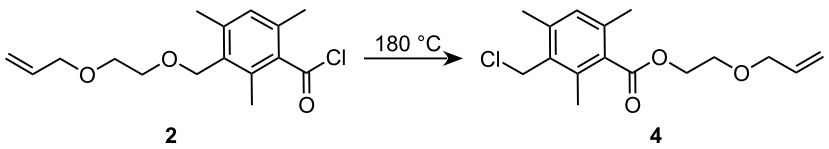


Scheme 2: Etherification of 3-(chloromethyl)-2,4,6-trimethylbenzoic acid and chlorination of **1**.

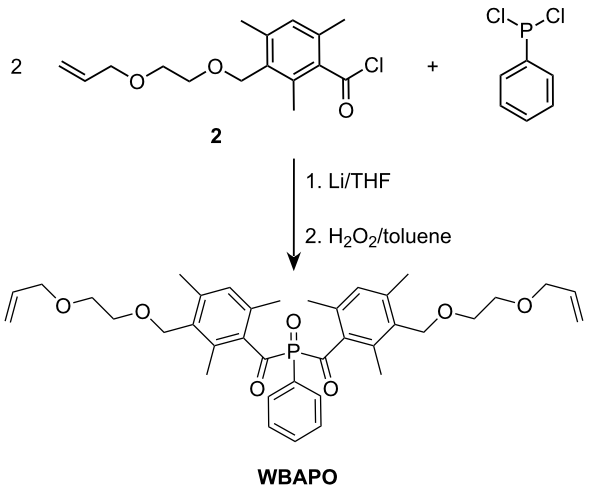
rearrangement because an exchange of chlorine with the 2-(allyloxy)ethoxy group took place as a result of heating (Scheme 3). In this context, it should be noted that we also found the exchange of chlorine in the cases of both the 2-(ethoxy)- and 2-(propoxy)ethoxy derivatives. For the successful purification of **2** by distillation both a short distillation time and a relatively low bottom temperature are crucial. Furthermore, it was found to be advantageous if the crude product was purged with nitrogen gas prior to distillation. The identity of compound **4** was established by an independent synthesis of the compound from 2-(allyloxy)ethanol and 3-(chloromethyl)-2,4,6-trimethylbenzoyl chloride **3**, prepared by chlorination of 3-(chloromethyl)-2,4,6-trimethylbenzoic acid with thionyl chloride.

In the third step, the bisacylphosphine oxide WBAPO was prepared by the reaction of **2** with *P*,*P*-dichlorophenylphosphine (Scheme 4). Thus, *P*,*P*-dichlorophenylphosphine dissolved in THF was first lithiated with metallic lithium in a dry argon atmosphere in the presence of a small amount of naphthalene. The resulting dark green phenylphosphine dilithium solution was then added to a THF solution of **2**. THF was evaporated from the intermediate bis(3-{[2-(allyloxy)ethoxy]methyl}-2,4,6-trimethylbenzoyl)(phenyl)phosphine solution, the residue dissolved in toluene and oxidized with a 30 wt % hydrogen peroxide solution at 70 °C. After column chromatography, WBAPO was obtained as a yellow oil in 67% yield with a HPLC purity of 94–95%. The characterization of WBAPO was carried out by ^{1}H NMR, ^{13}C NMR, ^{31}P NMR and IR spectroscopy, as well as by elemental analysis. The spectral data are in agreement with the expected structure. For example, the presence of the [2-(allyloxy)ethoxy]methyl substituent was supported by the presence of new signals compared to the spectrum of BAPO: a singlet for the benzyl protons at δ = 4.49 ppm and two multiplets for the vinyl protons at δ = 5.13–5.27 and 5.83–5.93 ppm were evident in the ^{1}H NMR spectrum (Figure 1). The ^{13}C NMR spectrum of WBAPO showed a doublet arising from the carbonyl carbon atom at δ = 216.2 ppm compared to 216.1 ppm in the case of BAPO, and the ^{31}P NMR spectrum featured only one signal at δ = 6.58 ppm (BAPO: 6.98 ppm).

The yield of the WBAPO synthesis was significantly lower compared to the high yield (>90%) in the case of the less substituted bisacylphosphine oxide BAPO. Therefore, a number of model reactions were carried out to elucidate possible reasons for this. We therefore investigated the formation of BAPO by the reaction of 2,4,6-trimethylbenzoylchloride with *P*,*P*-dichlorophenylphosphine under analogous conditions. The lithiation step was carried out in the presence of different model compounds for the reactive sites of the [2-(allyloxy)ethoxy]-methyl substituent, such as benzyl methyl ether, allyl ethyl ether or diethylene glycol dimethyl ether. In the case of benzyl methyl ether and allyl ethyl ether, BAPO was formed in a lower yield showing that benzyl and allyl groups had a negative effect on the yield of BAPO. Probably, these groups initiate side reac-



Scheme 3: Rearrangement of **2** under formation of **4**.



Scheme 4: Synthesis of WBAPO starting from *P*,*P*-dichlorophenylphosphine and **2**.

tions during the lithiation step. Furthermore, it was found that the temperature of the phosphine oxidation significantly influenced the yield and the purity of the formed phosphine oxide as it proved very difficult to separate the residual phosphine from the corresponding phosphine oxide. Accordingly, we used temperatures of 45, 50 or 56 °C and determined the area ratios of the WBAPO peak to the peak of the corresponding phosphine. These were found to be 3:5, 4:1 or 8:1 by HPLC. Only temperatures higher than 60 °C ensure a fast and complete oxidation of the bisacylphosphine.

Finally, different batches of WBAPO were investigated by LC-MS during the scale-up of the synthesis. The results show that a side-chain extended WBAPO with a molecular weight of 867 g/mol (Scheme 5) was formed in all cases as the main impurity in amounts of 0.5–5%. The structure of this compound was also clearly confirmed by the ^{13}C and ^{1}H NMR spectroscopic measurements of a WBAPO sample that specifically contained about 70% of this side product. The ^{13}C NMR spectrum of this sample showed three carbonyl signals: a singlet at δ = 170.4 ppm and two doublets at δ = 215.9 and 216.5 ppm. The singlet arises from the carbonyl group of the ester, whereas the two doublets can be assigned to the carbonyl groups of the differently substituted and therefore non-equivalent benzoyl moieties. Moreover, in the ^{1}H NMR spectrum the signal inten-

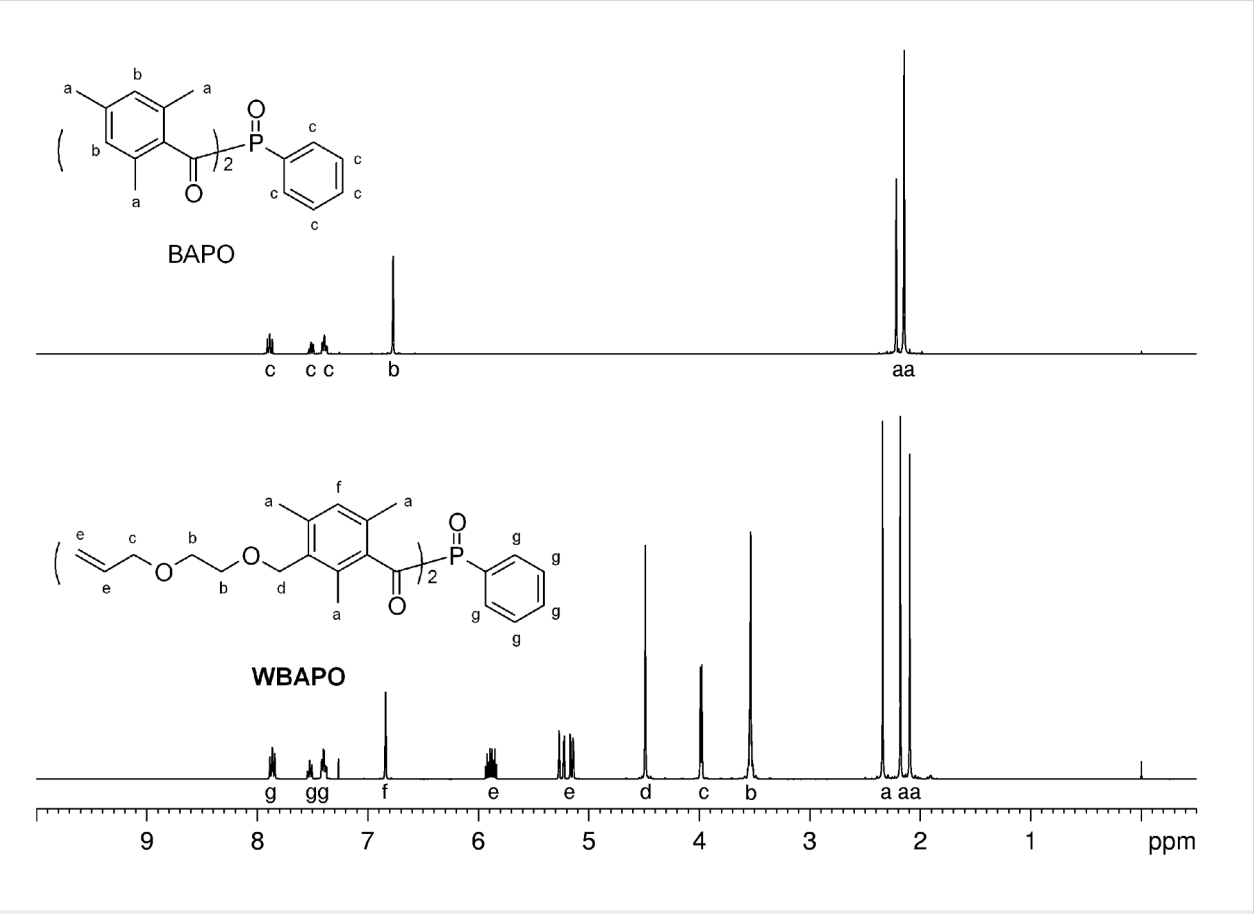
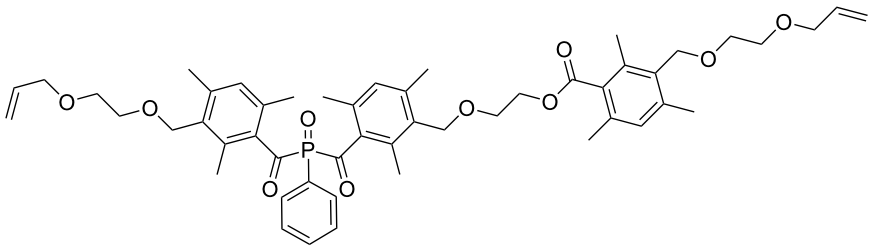


Figure 1: ^{1}H NMR spectra (400 MHz, $CDCl_3$) of BAPO and WBAPO.



Scheme 5: Structure of the main impurity in isolated WBAPO.

sities of CH_3, =CH (aromat), CH_2 (benzyl) and CH_2O protons were increased compared to pure WBAPO. In addition, a new triplet assignable to the CO-O-CH_2 protons was found at δ = 4.40 ppm. The complete separation of this side compound by repeated column chromatography would be very difficult and expensive. However, it will probably show similar photochemical properties compared to WBAPO and therefore its separation is not necessary.

Properties of WBAPO, photopolymerization and adhesives

WBAPO is a liquid that exhibits improved solubility in polar solvents compared to the solid BAPO. For example, the solubility of WBAPO in ethanol is about 50% and in acetone >50% compared to the solubility of BAPO of 3% in ethanol or 13% in acetone. As demonstrated in Figure 2, WBAPO dissolved in acetonitrile shows UV–vis absorption, which tails out into the visible range of the spectrum. WBAPO showed almost the same long wavelength absorption maximum (λ_{max}) of 368 nm and extinction coefficient (ε) of 8850 dm^2/mol compared to BAPO (λ_{max} = 369 nm, ε_{369} = 8820 dm^2/mol). The long wavelength bis(benzoyl)phosphine oxide absorption between ~360 and 400 nm can be generally assigned to symmetry forbidden n-π* transitions, which are responsible for α-cleavage and formation of free radicals [17]. After excitation with light in the near UV–vis, the excited triplet state undergoes cleavage of the carbon-phosphorus bond, thereby producing two highly efficient initiating radicals: a benzoyl and a phosphinoyl radical. CQ absorbs light in the region of 400–500 nm with a low absorption coefficient due to the n-π* transitions of the dicarbonyl group.

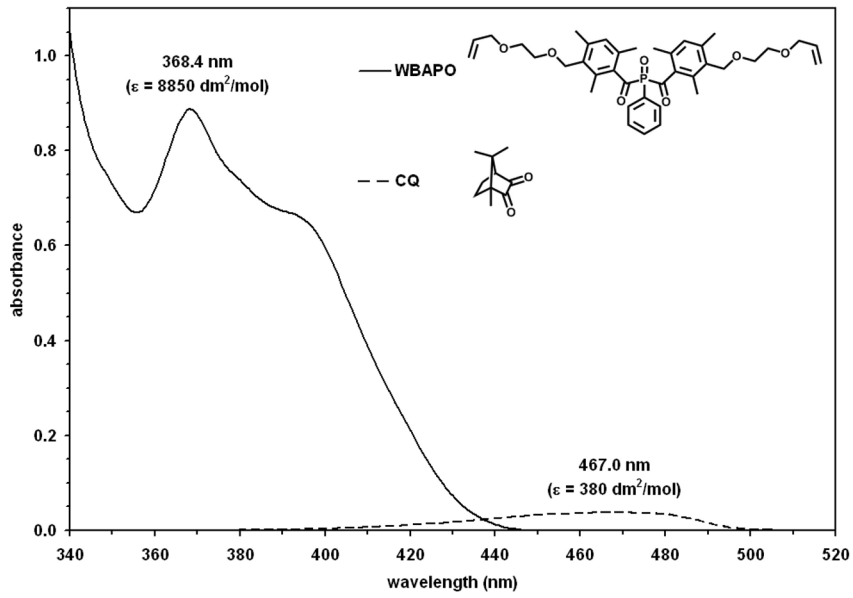


Figure 2: UV–vis absorption spectra of WBAPO and CQ dissolved in acetonitrile (10^{-3} mol/L).

Photo-DSC is a unique method for comparing the performance of different PIs. Therefore, the photopolymerization of a common dental dimethacrylate resin based on mixtures of Bis-GMA (42 wt %), UDMA (37 wt %), TEGDMA (21 wt %) and the PI WBAPO or BAPO (2.38 mmol/100 g resin) was studied by photo-DSC using a blue LED (emission spectrum: 380–515 nm, λ_{max} = 460 nm) as irradiation source. The Photo-DSC plots (Figure 3) confirmed the same photoinitiating activity of the two PIs taking into consideration the experimental accuracy of the DSC method.

Table 1: Shear bond strength (SBS, MPa) on dentin of experimental aqueous SEAs[a] measured after storage of different SEAs at 42 °C.

PI	SBS after 0 d	SBS after 14 d	SBS after 28 d
CQ/EMBO	17.0 ± 4.7	9.7 ± 3.9	n.m.[b]
WBAPO	30.3 ± 4.8	29.4 ± 3.2	30.3 ± 2.7
DBDEG	28.1 ± 3.3	32.2 ± 3.2	29.2 ± 1.6

[a]SEA based on an aqueous mixture of the cross-linker DEBAMP (43 wt %), the strongly acidic monomer BMAMHP (14 wt %) and the different PIs (0.5 wt %); [b]not measurable.

Because of the excellent performance of the synthesized WBAPO, it has been used as part of the PI system in our current SEA AdheSE® One F. This self-etching enamel-dentin adhesive is mainly based on an aqueous mixture of the hydrolytically stable cross-linker DEBAMP and the strongly acidic adhesive monomer BMAMHP. For the investigation of the adhesive properties, the shear bond strength of corresponding compositions containing different PIs was measured as a function of storage time of the adhesive at 42 °C. The results (Table 1) showed that the efficiency of the CQ-A based adhesive decreased very rapidly. In contrast, the bonding properties of the adhesives based on the bisacylphosphine oxide WBAPO or DBDEG were not influenced by the stress test.

Conclusion

WBAPO was synthesized via the dichlorophosphine route in a satisfactory yield. Benzyl and allyl groups of the introduced [2-(allyloxy)ethoxy]methyl substituent probably initiate side reactions during the lithiation step and have a negative effect on the yield of the synthesis. WBAPO, a yellow liquid, showed the expected improved solubility in polar solvents and the same photochemical properties as the commercially available bisacylphosphine oxides. Given its sufficient storage stability, WBAPO can be used as efficient PI in dental acidic aqueous primer formulations.

Experimental

2,4,6-Trimethylbenzoic acid (Jiangsu Panoxi Chemical Co., Ltd., China) and 2-(allyloxy)ethanol (Kowa Europe GmbH, Germany) were used without further purification. All other substances were purchased from Sigma-Aldrich (Switzerland). 3-(Chloromethyl)-2,4,6-trimethylbenzoic acid was prepared from 2,4,6-trimethylbenzoic acid by chloromethylation according to the literature [15]. DBDEG was synthesized as described previously [18].

DL-camphorquinone (CQ, Rahn, Switzerland), ethyl *p*-dimethylaminobenzoate (EMBO, Fluka Chemie AG, Switzerland) and Irgacure® 819 (BAPO, Ciba Specialty Chemical, Switzerland) were used without purification. Bis-GMA and

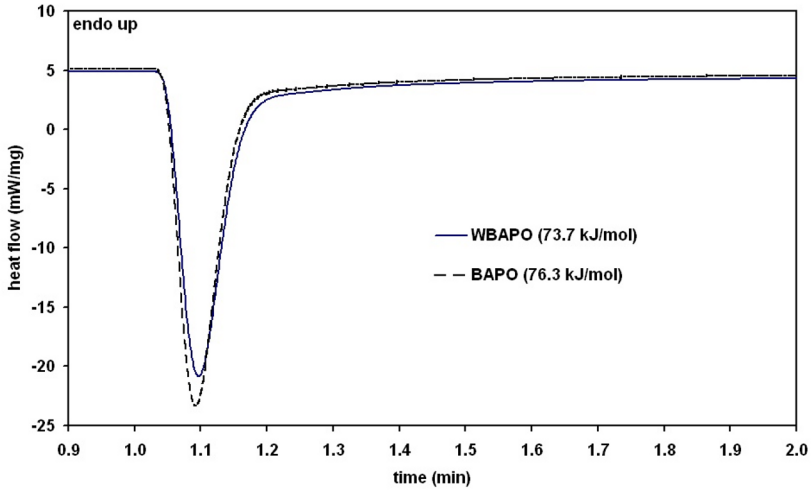


Figure 3: DSC-plot of a mixture of Bis-GMA (42 wt %), UDMA (37 wt %), TEGDMA (21 wt %) and the PI WBAPO or BAPO.

TEGDMA (Esschem, USA) and 1,6-bis(2-methacryloyloxyethoxycarbonylamino)-2,2,4-trimethylhexane (UDMA, Ivoclar Vivadent AG, Liechtenstein) were purchased from the suppliers noted above.

Synthesis of **1**

A suspension of 3-(chloromethyl)-2,4,6-trimethylbenzoic acid (84.0 g, 0.395 mol) in 2-(allyloxy)ethanol (200.0 g, 1.96 mol) was added to a solution of potassium hydroxide (88.6 g, 1.58 mol) in 2-(allyloxy)ethanol (606.7 g, 5.94 mol) and heated to 70 °C for 1 h. The mixture was poured in ice-water (600.0 g) and acidified with concentrated hydrochloric acid (pH < 1). After extraction with toluene (2 × 200 mL), the combined organic layers were washed with water (5 × 200 mL), dried with anhydrous sodium sulfate, and the solvent evaporated (50 °C, 80 mbar). Recrystallization of the crude product from cyclohexane yielded **1** as an off-white powder (68.5 g, 62%, mp: 80–81 °C) which was used without further purification.

^{1}H NMR ($CDCl_3$, 400 MHz): δ (ppm): 2.34, 2.38, and 2.43 (3 s, 3H each, CH_3), 3.61–3.68 (m, 4H, $O(CH_2)_2$), 4.02 (dt, J = 5.3 Hz, 1.4 Hz, 2H, OCH_2 allyl), 4.60 (s, 2H, OCH_2 benzyl), 5.15–5.30, and 5.86–5.96 (2 m, 2H, 1H, $HC=CH_2$), 6.90 (s, 1H, =CH aromat), 11.0 (br. s, 1H, OH). ^{13}C NMR ($CDCl_3$, 100 MHz): δ (ppm): 16.7, 19.7 and 19.8 (CH_3), 67.1, 69.4, 69.7, and 72.2 (OCH_2), 117.1 ($=CH_2$), 129.9 (=CH allyl), 132.0, 132.1, 134.5, 135.0, and 139.6 (=C aromat), 134.6 (=CH aromat), 175.4 (C=O). IR (diamond ATR): ν = 3100 (vbr, OH), 3010 (w, =CH), 2927 and 2878 (m, CH_2, CH_3), 1712 (vs, C=O), 1660 (w, C=C allyl), 1604 (w, C=C aromat), 1439 (m, CH_2, CH_3), 1352 (m, CH_3), 1040 (vs, COC), 995 and 923 cm^{-1} (s, =CH allyl). Anal. calcd. for $C_{16}H_{22}O_4$: C, 69.04; H, 7.97. Found: C, 69.17; H, 7.95.

Synthesis of **2**

1 (52.3 g, 0.188 mol) was suspended in a mixture of anhydrous toluene (300 mL) and *N*,*N*-dimethylformamide (1.4 mL). Thionyl chloride (33.5 g, 0.282 mol) was added at room temperature. After 2 h, toluene was distilled off and a stream of nitrogen was bubbled through the crude product for 4 h before it was purified by vacuum distillation (130 °C, 0.05 mbar) to give **2** as a colorless liquid (42.6 g, 76%).

^{1}H NMR ($CDCl_3$, 400 MHz): δ (ppm): 2.33, 2.39, and 2.43 (3 s, 3H each, CH_3), 3.61–3.68 [m, 4H, $O(CH_2)_2$], 4.02 (d, J = 5.3 Hz, 2H, OCH_2, allyl), 4.57 (s, 2H, OCH_2 benzyl), 5.16–5.29, and 5.86–5.96 (2 m, 2H, 1H, $HC=CH_2$), 6.91 (s, 1H, =CH aromat). ^{13}C NMR ($CDCl_3$, 100 MHz): δ (ppm): 16.5, 19.1, and 19.8 (CH_3), 66.8, 69.67, 69.69, and 72.2 (OCH_2), 117.1 ($=CH_2$), 130.1 (=CH allyl), 132.2, 132.6, 132.7, 138.1 and 140.5 (=C aromat), 134.7 (=CH aromat), 171.0 (C=O). IR (diamond ATR): ν = 3080 (w, =CH), 2980–2861 (m, CH_2, CH_3), 1786 (vs, C=O), 1647 (w, C=C allyl), 1599 (w, C=C aromat), 1449 (m, CH_2, CH_3), 1348 (m, CH_3), 1095 (vs, COC), 993, and 924 (=CH allyl), 785 cm^{-1} (vs, CCl). Anal. calcd. for $C_{16}H_{21}ClO_3$: C, 64.75; H, 7.13; Cl, 11.95. Found: C, 64.47; H, 7.15; Cl, 12.42.

Synthesis of WBAPO

1. Phenylphosphine dilithium

A solution of *P*,*P*-dichlorophenylphosphine (6.59 g, 36.8 mmol) in anhydrous tetrahydrofuran (THF, 10 mL) was added to a stirred mixture of lithium (1.53 g, 221 mmol), naphthalene (0.064 g, 0.50 mmol) and anhydrous THF (40 mL) in a flame dried flask under an argon atmosphere at room temperature. After 22 h, the dark green solution was transferred into another flame dried flask flushed with dry argon via double ended needle. This solution was directly used for the acylation step.

2. Bis(3-{[2-(allyloxy)ethoxy]methyl}-2,4,6-trimethylbenzoyl)(phenyl)phosphine

2 (21.98 g, 74.1 mmol) was dissolved in anhydrous THF (25 mL). This solution was added dropwise to the above prepared phenylphosphine dilithium solution while the temperature was kept between 30–35 °C in the dark, and subsequently stirred at ambient temperature. After 4 h, THF was removed at 40 °C under reduced pressure and the residue was used in the subsequent oxidation step.

3. Bis(3-{[2-(allyloxy)ethoxy]methyl}-2,4,6-trimethylbenzoyl)(phenyl)phosphine oxide

For this stage all manipulations were carried out in brown glass apparatus or under yellow light. The residue from the latter step was dissolved in toluene (40 mL). Hydrogen peroxide solution (30%, 4.17 g, 36.8 mmol) was added dropwise under vigorous stirring while the temperature was kept at about 70 °C. After the solution was stirred at room temperature for 30 min, it was diluted with ethyl acetate (30 mL). The two layers were separated and the organic layer washed with 0.5 N sodium hydroxide solution (5 × 20 mL) and once with brine (20 mL). After drying with anhydrous sodium sulfate, the solvent was evaporated and the crude product purified by column chromatography (silica gel 60, *n*-heptane:ethyl acetate = 2:1 → 1:2) to give WBAPO as a yellow oil (15.9 g, 67%).

^{1}H NMR (400 MHz, $CDCl_3$): δ (ppm): 2.10, 2.19, and 2.34 (3 s, 6H each, CH_3), 3.51–3.56 [m, 8H, $O(CH_2)_2$], 3.98 (dt, J = 5.6 Hz, 1.4 Hz, 4H, OCH_2 allyl), 4.49 (s, 4H, OCH_2 benzyl), 5.13–5.27, and 5.83–5.93 (2 m, 4H, 2H, $HC=CH_2$), 6.84 (s, 2H, =CH aromat), 7.37–7.42, 7.49–7.54 and 7.84–7.88 (3 m, 2H, 1H, 2H, =CH phenyl). ^{13}C NMR (100 MHz, $CDCl_3$): δ (ppm): 17.1, 19.4 and 19.9 (CH_3), 66.5, 69.2, 69.6, and 72.2 (OCH_2),

117.0 (=CH_2), 125.8 (d, J_{C-P} = 74 Hz, =CP), 128.5 (d, $^2J_{C-P}$ = 11 Hz, =CH), 130.7 (=CH allyl), 132.1 (d, $^3J_{C-P}$ = 8 Hz, =CH), 132.6, 134.8, 135.5 and 141.2 (=C aromat), 132.9 (d, $^4J_{C-P}$ = 3 Hz, =CH), 134.7 (=CH aromat), 136.7 (d, $^2J_{C-P}$ = 41 Hz, =C-C=O), 216.2 (d, J_{C-P} = 58 Hz, C=O). ^{31}P NMR (162 MHz, $CDCl_3$): δ (ppm): 6.58. IR (diamond ATR): ν = 3070 (w, =CH), 2930 and 2860 (m, CH_2, CH_3), 1735 (m, C=O), 1679 (m, C=C allyl), 1656 and 1596 (m, C=C aromat), 1437 (m, CH_2, CH_3), 1373 (m, CH_3), 1204 (s, P=O), 1096 (vs, COC), 995 and 925 cm^{-1} (s, =CH allyl). Anal. calcd. for $C_{38}H_{47}O_7P$: C, 70.57; H, 7.32; O, 17.32. Found: C, 70.23; H, 7.28; O, 18.06.

Synthesis of **3**

Compound **3** was prepared from 3-(chloromethyl)-2,4,6-trimethylbenzoic acid (21.27 g, 0.10 mol) and thionyl chloride in the same way as described for **2**. After vacuum distillation (85–86 °C, 0.1 mbar), **3** was obtained as colorless crystals (14.0 g, 61%, mp: 201–202 °C, decomp.).

^{1}H NMR (400 MHz, $CDCl_3$): δ (ppm): 2.36, 2.42 and 2.46 (3 s, 3H each, CH_3), 4.62 (s, 2H, $ClCH_2$), 6.95 (s, 1H, =CH). ^{13}C NMR (100 MHz, $CDCl_3$): δ (ppm): 16.2, 19.2 and 19.4 (CH_3), 40.1 ($ClCH_2$), 130.4 (=CH), 132.1, 132.4, 133.0, 138.2 and 140.0 (=C), 170.3 (C=O). IR (diamond ATR): ν = 3070 (w, =CH), 2980, 2910 and 2870 (w, CH_2, CH_3), 1791 (vs, C=O), 1596 and 1566 (m, C=C), 1423 (m, CH_2, CH_3), 1381 (s, CH_3), 772 cm^{-1} (vs, C-Cl). Anal. calcd. for $C_{11}H_{12}Cl_2O$: C, 57.17; H, 5.23; Cl, 30.68. Found: C, 57.56; H, 5.46; Cl, 29.82.

Synthesis of **4**

To a solution of 2-(allyloxy)ethanol (5.11 g, 50.0 mmol) and triethylamine (5.06 g, 50.0 mmol) in anhydrous methylene chloride (30 mL), **3** (11.56 g, 50.0 mmol) in anhydrous methylene chloride (20 mL) was added at 0 °C. After 2 h the white precipitate was filtered off and the filtrate was washed with water (3 × 50 mL), dried with anhydrous sodium sulfate and the solvent removed under vacuum to give **4** as a colorless liquid (11.3 g, 76%). Compound **4** was also obtained by heating **2** at 180 °C for 4 h and was the main component of its distillation residue.

^{1}H NMR (400 MHz, $CDCl_3$): δ (ppm): 2.27, 2.36 and 2.38 (3 s, 3H each, CH_3), 3.72–3.75 (m, 2H, OCH_2 ether), 4.01–4.03 (m, 2H, OCH_2 allyl), 4.48–4.50 (m, 2H, OCH_2 ester), 4.62 (s, 2H, $ClCH_2$), 5.16–5.30, and 5.84–5.94 (2 m, 2H, 1H, $HC=CH_2$), 6.90 (s, 1H, =CH aromat). ^{13}C NMR (100 MHz, $CDCl_3$): δ (ppm): 16.2, 19.3 and 19.5 (CH_3), 40.7 ($ClCH_2$), 63.9, 67.8, and 72.02 (OCH_2), 117.3 (=CH_2), 130.0 (=CH allyl), 131.9, 133.2, 134.3, 135.2, and 138.7 (=C aromat), 134.4 (=CH aromat), 170.0 (C=O). IR (diamond ATR): ν = 3090 (w, =CH), 2949, 2919 and 2862 (m, CH_2, CH_3), 1722 (vs, C=O), 1647 (w, C=C allyl), 1603 (m, C=C aromat), 1447 (s, CH_2, CH_3), 1379 (m, CH_3), 1044 (vs, COC), 992, and 924 cm^{-1} (s, =CH allyl). Anal. calcd. for $C_{16}H_{21}ClO_3$: C, 64.75; H, 7.13; Cl, 11.95. Found: C, 64.83; H, 7.12; Cl, 11.86.

Measurements

NMR spectroscopic measurements were recorded on a DPX-400 spectrometer (Bruker Biospin, ^{1}H: 400 MHz, ^{13}C: 100 MHz, ^{31}P: 162 MHz) in $CDCl_3$ or dimethyl sulfoxide-d_6 as the solvent using tetramethylsilane (TMS) as standard. A FT-IR spectrometer 1600 (Perkin-Elmer) was used to record IR spectra. Melting points were measured with a Melting Point B-540 (Büchi). Elemental analyses were performed with an elemental analyzer CHNS-O Typ EA 1108 (Fisons Instruments). UV–vis spectra were recorded with a UV–vis spectrometer Lambda 2 (Perkin Elmer) in acetonitrile.

The photopolymerization of a dimethacrylate resin (Bis-GMA: 42 wt %, UDMA: 37 wt % and TEGDMA 21 wt %) was studied by photo-DSC (Perkin Elmer DSC 7) using a blue LED Bluephase (1200 mW·cm^{-2}, Ivoclar Vivadent AG) and an irradiation time of 180 s at 37 °C.

For the measurement of the shear bond strength of the corresponding dentin adhesives, freshly extracted bovine lower incisors were embedded in unsaturated polyester resin (Castolite, Buehler, USA) in cylindrical molds. Flat dentinal surfaces were ground with water-cooled P240-grit SiC followed by P1000-grit SiC abrasive paper to expose the middle dentin of the embedded teeth. After application of the SEA, solvent evaporation, and light activation, a Teflon mould with a cylindrical hole (3.00 mm in diameter and 4 mm in height, Guillotine method [19]) was placed on the top of bonded surface and filled with two increments of the hybrid composite Tetric Ceram (Ivoclar Vivadent AG). The increments were light cured using a halogen lamp Astralis 10 (emission spectrum: 380–510 nm, 1000 mW·cm^{-2}, Ivoclar Vivadent AG) for 40 s each and the test specimens were immersed in water at 37 °C for 24 h prior to testing. Then the shear bond strength was measured using a universal testing machine (Zwick Z010, Germany) at a crosshead speed of 1.0 mm/min.

References

1. Moszner, N.; Salz, U. *Macromol. Mater. Eng.* **2007,** *292,* 245–271. doi:10.1002/mame.200600414
2. Moszner, N.; Zeuner, F.; Angermann, J.; Fischer, U. K.; Rheinberger, V. *Macromol. Mater. Eng.* **2003,** *288,* 621–628. doi:10.1002/mame.200350003
3. Pavlinec, J.; Zeuner, F.; Angermann, J.; Moszner, N. *Macromol. Chem. Phys.* **2005,** *206,* 1878–1886. doi:10.1002/macp.200500192

4. Moszner, N.; Pavlinec, J.; Lamparth, I.; Zeuner, F.; Angermann, J. *Macromol. Rapid Commun.* **2006,** *27,* 1115–1120. doi:10.1002/marc.200600209
5. Moszner, N.; Salz, U.; Zimmermann, J. *Dent. Mater.* **2005,** *21,* 895–910. doi:10.1016/j.dental.2005.05.001
6. Crivello, J. V.; Dietliker, K. In *Surface Coatings Technology: Photoinitiators for Free Radical Cationic & Anionic Photopolymerization;* Bradley, G., Ed.; Wiley & Sons: Chichester, U.K., 1998; Vol. III, pp 228–273.
7. Moszner, N.; Liska, R. Photoinitiators for direct adhesive restorative material. In *Basics and Applications of Photopolymerization Reactions;* Fouassier, J. P.; Allonas, X., Eds.; Research Signpost: Kerala, India, 2010; pp 91–112.
8. Ganster, B.; Fischer, U. K.; Moszner, N.; Liska, R. *Macromol. Rapid Commun.* **2008,** *29,* 57–62. doi:10.1002/marc.200700620
9. Ganster, B.; Fischer, U. K.; Moszner, N.; Liska, R. *Macromolecules* **2008,** *41,* 2394–2400. doi:10.1021/ma702418q
10. Moszner, N.; Fischer, U. K.; Liska, R.; Ganster, B. *Dent. Mater.* **2008,** *24,* 901–907. doi:10.1016/j.dental.2007.11.004
11. Grützmacher, H.; Geier, J.; Stein, D.; Ott, T.; Schönberg, H.; Sommerlade, R. H.; Boulmaaz, S.; Wolf, J.-P.; Murer, P.; Ulrich, T. *Chimia* **2008,** *62,* 18–22. doi:10.2533/chimia.2008.18
12. Ullrich, G.; Ganster, B.; Salz, U.; Moszner, N.; Liska, R. *J. Polym. Sci., Part A: Polym. Chem.* **2006,** *44,* 1686–1700. doi:10.1002/pola.21276
13. Leppard, D. G.; Koehler, M.; Hug, G. U. Novel Acylphosphine Oxides. PCT Int. Appl. Patent 9607662 A1, March 14, 1996.
14. Leppard, D. G.; Koehler, M. Alkoxyphenyl-substitutierte Bisacylphosphinoxide. DE Patent 19532358, Sept 2, 1994.
15. Stewart, F. H. C. *Org. Prep. Proced. Int.* **1981,** *13,* 116–118. doi:10.1080/00304948109356106
16. Leino, R.; Luttikhedde, H. J. G.; Langstedt, L.; Penninkangas, A. *Tetrahedron Lett.* **2002,** *43,* 4149–4151. doi:10.1016/S0040-4039(02)00766-9
17. Dietliker, K.; Jung, T.; Benkhoff, J.; Kura, H.; Matsumoto, A.; Oka, H.; Hristova, D.; Gescheidt, G.; Rist, G. *Macromol. Symp.* **2004,** *217,* 77–97. doi:10.1002/masy.200451307
18. Moszner, N.; Zeuner, F.; Lamparth, I.; Fischer, U. K. *Macromol. Mater. Eng.* **2009,** *294,* 877–886. doi:10.1002/mame.200900181
19. ISO, ISO/TS 11405: Dental materials – Testing of adhesion to tooth structure, 2nd ed., 2003.

License and Terms

This is an Open Access article under the terms of the Creative Commons Attribution License (http://creativecommons.org/licenses/by/2.0), which permits unrestricted use, distribution, and reproduction in any medium, provided the original work is properly cited.

The license is subject to the *Beilstein Journal of Organic Chemistry* terms and conditions: (http://www.beilstein-journals.org/bjoc)

The definitive version of this article is the electronic one which can be found at: doi:10.3762/bjoc.6.26

Beilstein Journal of Organic Chemistry

Ring opening metathesis polymerization-derived block copolymers bearing chelating ligands: synthesis, metal immobilization and use in hydroformylation under micellar conditions

Gajanan M. Pawar[1], Jochen Weckesser[2], Siegfried Blechert[*2] and Michael R. Buchmeiser[*1]

Full Research Paper

Open Access

Address:
[1]Lehrstuhl für Makromolekulare Stoffe und Faserchemie, Institut für Polymerchemie, Universität Stuttgart, Pfaffenwaldring 55, D-70550 Stuttgart, Germany; Tel.: +49 (0)711-685-64075; Fax: +49 (0)711-685-64050 and [2]Institut für Chemie, Technische Universität Berlin, Straße des 17. Juni 135, D-10623 Berlin, Germany

Email:
Siegfried Blechert[*] - blechert@chemie.tu-berlin.de;
Michael R. Buchmeiser[*] - michael.buchmeiser@ipoc.uni-stuttgart.de

* Corresponding author

Keywords:
block copolymers; catalysis; hydrophilic polymers; metathesis; micelles

Beilstein Journal of Organic Chemistry **2010,** *6,* No. 28.
doi:10.3762/bjoc.6.28

Received: 11 January 2010
Accepted: 17 March 2010
Published: 23 March 2010

Guest Editor: H. Ritter

© 2010 Pawar et al; licensee Beilstein-Institut.
License and terms: see end of document.

Abstract

Norborn-5-ene-(*N,N*-dipyrid-2-yl)carbamide (**M1**) was copolymerized with *exo,exo*-[2-(3-ethoxycarbonyl-7-oxabicyclo[2.2.1]hept-5-en-2-carbonyloxy)ethyl]trimethylammonium iodide (**M2**) using the Schrock catalyst Mo(*N*-2,6-Me_2-C_6H_3)(CHCMe$_2$Ph)(OCMe(CF$_3$)$_2$)$_2$ **[Mo]** to yield poly(**M1**-*b*-**M2**). In water, poly(**M1**-*b*-**M2**) forms micelles with a critical micelle-forming concentration (cmc) of 2.8×10^{-6} mol L^{-1}; Reaction of poly(**M1**-*b*-**M2**) with [Rh(COD)Cl]$_2$ (COD = cycloocta-1,5-diene) yields the Rh(I)-loaded block copolymer poly(**M1**-*b*-**M2**)-**Rh** containing 18 mg of Rh(I)/g of block copolymer with a cmc of 2.2×10^{-6} mol L^{-1}. The Rh-loaded polymer was used for the hydroformylation of 1-octene under micellar conditions. The data obtained were compared to those obtained with a monomeric analogue, i.e. $CH_3CON(Py)_2RhCl(COD)$ (**C1**, Py = 2-pyridyl). Using the polymer-supported catalyst under micellar conditions, a significant increase in selectivity, i.e. an increase in the *n*:*iso* ratio was accomplished, which could be further enhanced by the addition of excess ligand, e.g., triphenylphosphite. Special features of the micellar catalytic set up are discussed.

Introduction

Catalysts bound to amphiphilic block copolymers find increasing use in micellar catalysis since they combine the advantages of both homogeneous and heterogeneous catalysis in one system. Thus, with catalysts permanently linked to the block copolymer, metal leaching is substantially reduced and allows for the separation/reuse of the catalyst [1-7]. In cases where reactions are run in polar media, the catalyst is best located inside the hydrophobic micellar core, where, upon micelle formation of the functionalized block copolymer, the monomer will also accumulate. This leads to high educt concentrations at the polymer-bound catalyst, often resulting in high reaction rates in water [8]. We recently reported on the synthesis of Rh^I and Ir^I complexes of *N,N*-dipyrid-2-ylacetamide and their use in hydroformylation reactions [9]. Here, we report on the immobilization of a Rh-*N,N*-dipyrid-2-ylacetamide-based catalyst on a soluble, amphiphilic, ring-opening metathesis polymerization- (ROMP) derived block copolymer and its use in hydroformylation [10] under micellar conditions [3,5,11]. This medium activity and selectivity dipyrid-2-ylamide-based Rh(I)-catalyst was chosen in order to identify the potential advantages of a micellar setup.

Results and Discussion

Synthesis of monomers

The synthesis of norborn-5-ene-(*N,N*-dipyrid-2-yl)carbamide (**M1**) was accomplished via reaction of norborn-5-ene-2-ylcarboxylic acid chloride with dipyrid-2-ylamine in the presence of triethylamine as described elsewhere [9]. *exo,exo*-[2-(3-Ethoxycarbonyl-7-oxabicyclo[2.2.1]hept-5-ene-2-carbonyloxy)ethyl]trimethylammonium iodide (**M2**) was prepared in a four-step procedure (Scheme 1). It entailed the reaction of 7-oxanorborn-5-ene-2,3-dicarboxylic anhydride with 2-(*N,N*-dimethylamino)ethan-1-ol, conversion of the free carboxylic acid **1** into the corresponding acid chloride with $SOCl_2$ and reaction of the acid chloride with dry ethanol to form the diester **2**. Finally, compound **2** was converted into **M2** via quaternization of the tertiary amine with methyl iodide.

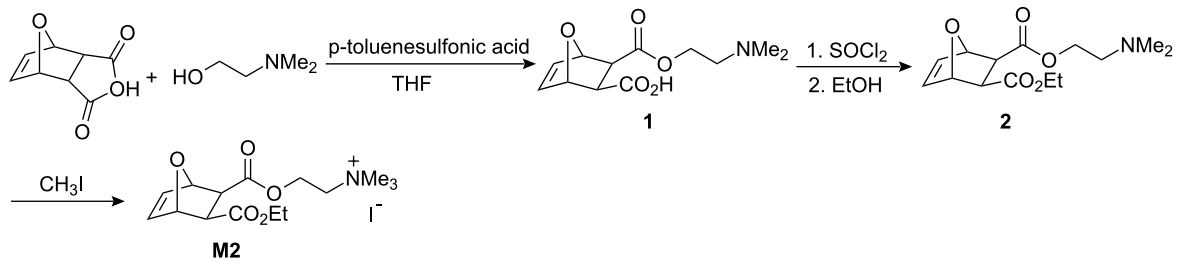
Synthesis of homo- and block copolymers via ROMP [12,13]

ROMP has already been used for the synthesis of micelle-forming block copolymers [14], however, the one used in this study, i.e. poly(**M1**-*b*-**M2**), required special attention. Though **M1** contains a chelating ligand and can be polymerized by both Schrock and Grubbs-type initiators [15-18]. **M2** is particularly problematic since it contains a quaternary ammonium moiety and has the ability to alkylate the phosphane or pyridine ligands of 1st-, 2nd-, and 3rd-generation Grubbs-type initiators. We therefore chose one of the most active Schrock-type initiator [19-21] for polymerization, i.e. $Mo(N\text{-}2,6\text{-}Me_2\text{-}C_6H_3)[CHC(CH_3)_2Ph][OCMe(CF_3)_2]_2$ (**[Mo]**) [22].

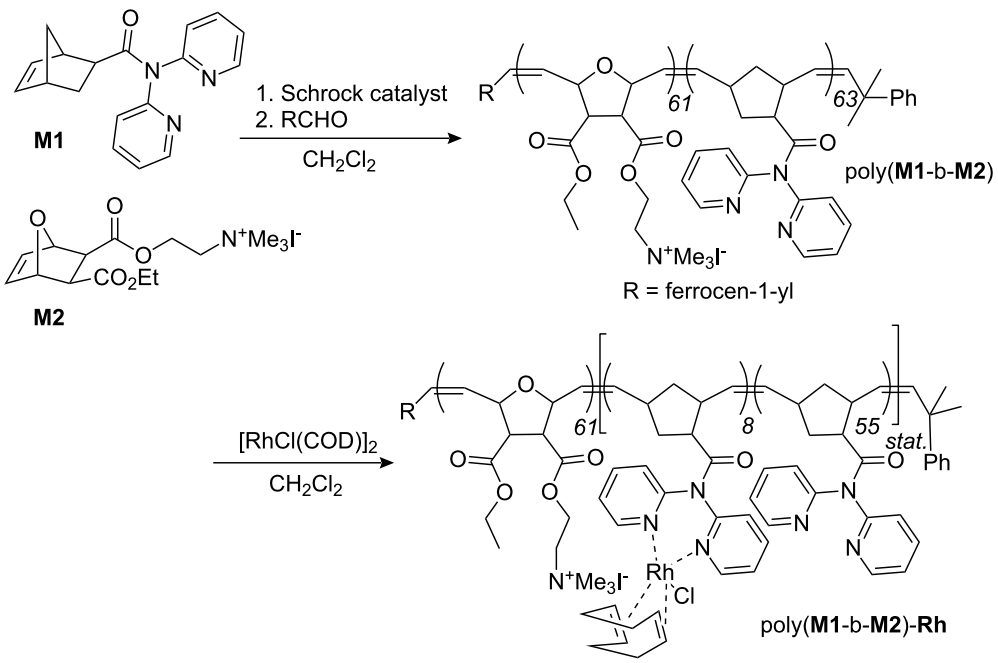
Both the homopolymerization of **M1** and **M2** by the action of **[Mo]** proceeded smoothly at room temperature. Conversion of monomer **M1** reached 100% after 10 min (Figure S1, Supporting Information File 1). The corresponding block copolymer poly(**M1**-*b*-**M2**) (M_n = 44100 g mol^{-1}, PDI = 1.38, Scheme 2) was prepared in 76% isolated yield by starting the polymerization with **M1** and adding **M2** after 20 min. The GPC-traces of the first and second block are shown in Figure S2 (Supporting Information File 1) and indicate that the diblock copolymer formed quantitatively. From GPC analysis, degrees of polymerization of 63 and 61 were found for the poly(**M1**) and the poly(**M2**) block, respectively.

Critical micelle forming concentrations, metal loading of poly(**M1**-*co*-**M2**)

The cmc of poly(**M1**-*co*-**M2**) was determined by fluorescence spectroscopy [23]. For measurements in water, 6-*p*-toluidene-2-naphthylsulfonic acid (10^{-6} mol/L) was used as the fluorescence probe. A cmc_{water} for poly(**M1**-*b*-**M2**) of 2.8 × 10^{-6} mol L^{-1} was determined (Figure S3, Supporting Information File 1). Next, poly(**M1**-*b*-**M2**) was loaded with Rh(I) via reaction of poly(**M1**-*b*-**M2**) with $[RhCl(COD)]_2$ (COD = cycloocta-1,5-diene) to yield poly(**M1**-*b*-**M2**)-**Rh** (Scheme 2).



Scheme 1: Synthesis of **M2**.



Scheme 2: Synthesis of poly(**M1**-*b*-**M2**) and of the micellar catalyst poly(**M1**-*b*-**M2**)-**Rh**.

A metal loading of 18 mg Rh/g polymer was achieved, which corresponds to 12% of the theoretical loading (assuming the formation of a mono-dipyridyl-Rh(I) complex as observed for **M1**) [9]. Consequently, almost 90% of the dipyrid-2-ylamide ligands were not involved in complex formation, which is of importance for the catalytic behavior of the supported catalyst and for metal leaching. Poly(**M1**-*b*-**M2**)-**Rh** was again subject to cmc measurements. A value of 2.2×10^{-6} mol L^{-1} was found, indicating that the loading with Rh(I) hardly changes the cmc value (Figure S4, Supporting Information File 1).

Hydroformylation under micellar conditions

Generally, micellar catalysis [3,5,24-28] and in particular micellar set-ups, where catalysts covalently bound to amphiphilic polymers are used [2,4,29-33], have been reported to present suitable catalysts for numerous catalytic reactions. The hydroformylation under micellar conditions using catalysts bound to amphiphilic block copolymers was first reported by Nuyken et al. [34]. Using a poly(2-oxazoline)-based amphiphilic copolymer and a RhBr(1,3-dialkylimidazol-2-ylidene-based catalyst, selectivities (*n*:*iso*) of ~3 at 40% conversion and an activity (TOF_0) of 1630 h^{-1} in the hydroformylation of 1-octene was observed [35]. Here, we used poly(**M1**-*b*-**M2**)-**Rh** for the hydroformylation of 1-octene in water. For purposes of comparison, the results obtained were compared to those previously obtained with the homogeneous analogue $CH_3CON(Py)_2RhCl(COD)$ (**C1**) [9].

As already described [9], the dipyridylamide-based Rh-catalyst **C1** is a very fast isomerization catalyst. Consequently, considerable amounts of *iso*-octanes and a low *n*:*iso* ratio of 0.9 was reported for this catalyst (Table 1, entry 3).

Table 1: Results for the hydroformylation of 1-octene[a].

No.	Catalyst	Solvent	TON[c]	TOF_0	*n*:*iso*
1	poly(**M1**-*b*-**M2**)-**Rh**	water	3800	1200	1.5
2	poly(**M1**-*b*-**M2**)-**Rh**[b]	water	4400	1200	2.3
3	**C1**	toluene	4500	2700	0.9
4	**C1**[b]	toluene	4700	1600	1.6

[a]catalyst:substrate ratio = 1:5000, *t* = 4 h, *T* = 70 °C.
[b]triphenylphosphite:substrate = 10:5000.
[c]based on the aldehydes formed.

When poly(**M1**-*co*-**M2**)-**Rh** was used in water, a turn-over number (TON) of 4700 and an initial turn-over frequency (TOF_0) of 1200 h^{-1} was observed. The *n*:*iso* ratio, however, was higher than the one obtained with **C1** in toluene, i.e. 1.5 vs. 0.9 for **C1** (Table 1, entry 1, Figure S5, Supporting Information File 1). At 40% conversion, an *n*:*iso* ratio of 1.6 (Figure S6, Supporting Information File 1) was found. A representative product distribution obtained with poly(**M1**-*co*-**M2**)-**Rh** is shown in Figure 1. This enhanced selectivity is attributed to the presence of a comparably large percentage (88%) of free

dipyrid-2-ylamide ligands as well as to the high concentration of educts within the micelle. Both apparently suppress β-elimination in the alkyl-metal species. Consequently, a further addition of free ligand (e.g., triphenylphosphite), which is known to favor the formation of *n*-aldehydes in homogenous catalysis [10,36], the *n*:*iso* value could be further increased to 2.3 (Table 1, entry 2, Figure 2) and to 2.5 at 40% conversion, respectively (Figure S6, Supporting Information File 1). As a matter of fact, neither ethylheptanal or propylhexanal nor the parent 3- and 4-octenes was observed in this experiment.

By contrast, the *n*:*iso* value increased only to 1.6 with **C1** in toluene upon addition of excess ligand (Figure S7, Supporting Information File 1), clearly demonstrating the effect of the micelle, where both the reactants and the additional ligand (i.e. triphenylphosphite) accumulate. Finally and importantly, the leaching of Rh from poly(**M1**-*co*-**M2**)-**Rh** into the products was very low, resulting in metal contaminations of around 9 ppm. Again, the large excess of free dipyrid-2-ylamine ligand is thought to be responsible for this finding. Moreover, the polymer-bound catalyst can be recycled by extracting the products with diethyl ether and reused with only a minor change in activity. Thus, the TONs obtained were 4300 and 3900 for the first and second run.

Conclusion

An amphiphilic block copolymer bearing a chelating *N,N*-dipyrid-2-ylamide-based ligand was prepared via ROMP using a Mo-based Schrock initiator. Loading with Rh(I) yielded a polymer-bound catalyst that was used for the hydroformylation

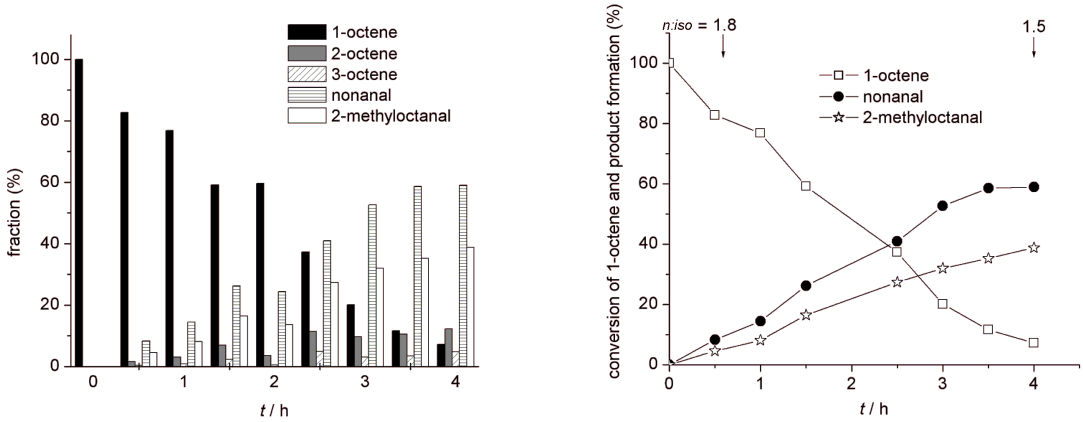


Figure 1: Conversion (%) of 1-octene, product formation, product distribution, as well as time dependant *n*:*iso* ratio in the hydroformylation of 1-octene in water in the presence of poly(**M1**-*b*-**M2**)-**Rh**.

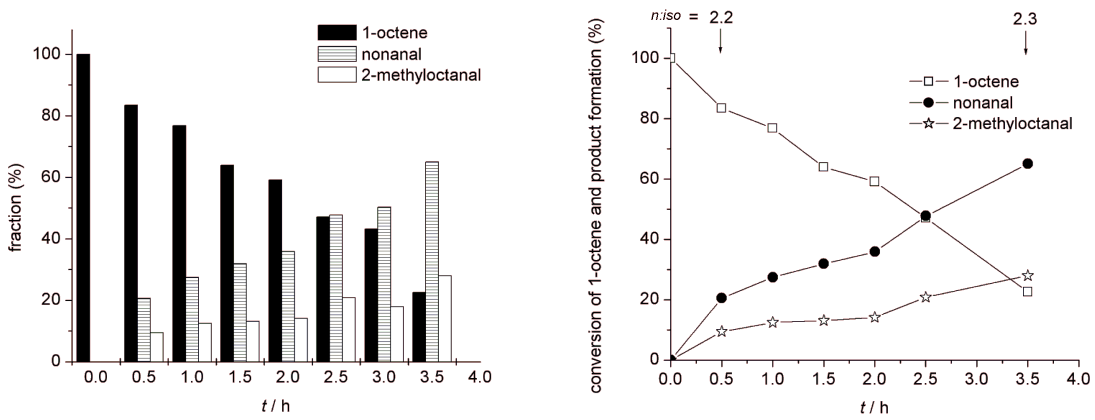


Figure 2: Conversion of 1-octene, product formation and product distribution in the hydroformylation in water in the presence of poly(**M1**-*b*-**M2**)-**Rh** and triphenylphosphite.

of 1-octene. From the hydroformylation data obtained with the polymer-bound catalyst as well as with the model catalyst, it becomes clear that the use of a micellar catalyst favors the formation of the *n*-aldehyde by suppressing the isomerization propensity of a catalyst. Apparently, the higher concentration of the starting alkene inside the micelle effectively prevents β-elimination, an effect that can be further enhanced by adding free ligand that again accumulates inside the micelle. Further advantages in favor of a micellar setup are the low metal contamination of the products as well as the possibility of reuse.

Experimental

All manipulations were performed under a N_2 atmosphere in a glove box (LabMaster 130, MBraun, Garching, Germany) or by standard Schlenk techniques unless stated otherwise. Purchased starting materials were used without any further purification. Pentane, diethyl ether, toluene, CH_2Cl_2 and tetrahydrofuran (THF) were dried using a solvent purification system (SPS, MBraun). Benzene, *n*-hexane and dimethoxyethane (DME) were dried and distilled from sodium/benzophenone ketyl under argon. NMR spectra were recorded at room temperature on a Bruker AM 400 (400 MHz for proton and 100.6 MHz for carbon) and on a Bruker Avence 600 II^+ (600.25 MHz for proton and 150.93 MHz for carbon) spectrometer, respectively, unless specified otherwise. Proton and carbon spectra were referenced to the internal solvent resonance and are reported in ppm. Molecular weights and polydispersity indices (PDIs) of the polymers were determined by GPC at 40 °C on Waters columns (Styragel HR 4 DMF, 4.6 × 300 mm) in DMF vs. poly(styrene) using a Waters 717 plus autosampler and a Waters 2414 refractive index detector. For calibration, poly(styrene) samples (PDI < 1.02) with molecular weights within the range $162 < M_n < 5{,}500{,}000$ g/mol were used. The flow rate was 1.0 mL/min. Fluorescence testing was performed using a Perkin-Elmer luminescence spectrometer LS50B. IR spectra were recorded on a Bruker Vector 22 using ATR technology. Elemental analysis was carried out on Elementar Varia El (Analytik Jena). GC-MS investigations were carried out on a Shimadzu GCMS-QP5050 with an AOC-20i Autosampler using a SPB fused silica (Rxi-5MS) column (30 m × 0.25 mm × 0.25 μm film thickness, 60.6 kPa, temperature program: 70 °C – 300 °C, 25 min). The Schrock initiator Mo(*N*-2,6-Me_2-C_6H_3)[$CHC(CH_3)_2Ph$][$OCMe(CF_3)_2$]$_2$ **[Mo]** [22], *N,N*-dipyridyl-*endo*-norborn-5-ene-2-carbamide (**M1**) [9,37] and *N*-acetyl-*N,N*-dipyrid-2-yl (cyclooctadiene) rhodium chloride (**C1**) [9] were synthesized according to the literature.

***exo,exo*-[2-(3-Ethoxycarbonyl-7-oxabicyclo[2.2.1]hept-5-en-2-carbonyloxy)ethyl]trimethylammonium iodide (M2)**

***exo,exo*-7-Oxabicyclo[2.2.1]hept-5-ene-2,3-dicarboxylic acid mono(2-dimethylaminoethyl) ester (1):** *exo*-3,6-Epoxy-1,2,3,6-tetrahydrophtalic anhydride (10.0 g, 60.0 mmol), 2-dimethylaminoethanol (6.3 mL, 62.0 mmol, 1.03 equiv) and *p*-toluenesulfonic acid (590 mg, 3.1 mmol, 5 mol%) were dissolved in 120 mL of THF and stirred at room temperature for 8 h. The white precipitate was filtered, washed with diethyl ether and dried to afford a white solid; yield: 13.8 g (90.0%). ^{1}H NMR ($CDCl_3$): δ 2.70 (s, 6H), 2.78–2.81 (m, 2H), 3.01 (ddd, 1H, ^2J = 13.7 Hz, J = 6.8 Hz, J = 2.8 Hz), 3.12 (ddd, 1H, ^2J = 13.7 Hz, J = 7.3 Hz, J = 2.8 Hz), 4.37 (ddd, 1H, ^2J = 13.3 Hz, J = 7.3 Hz, J = 2.8 Hz), 4.51 (ddd, 1H, ^2J = 13.3 Hz, J = 6.8 Hz, J = 2.8 Hz), 5.24 (s br, 2H), 6.37 (dd, 1H, J = 5.7 Hz, J = 1.6 Hz), 6.47 (dd, 1H, J = 5.7 Hz, J = 1.6 Hz).

***exo,exo*-7-Oxabicyclo[2.2.1]hept-5-ene-2,3-dicarboxylic acid 2-(2-dimethylaminoethyl) ester 3-ethyl ester (2): 1** (1.0 g, 3.9 mmol) was dissolved in 20 mL of EtOH (c = 0.2 M). $SOCl_2$ (0.4 mL, 5.9 mmol, 1.5 equiv) was added dropwise at room temperature and the reaction mixture was stirred at room temperature for 8 h. The solvent was removed in vacuo, the green residue dissolved in 25 mL of CH_2Cl_2 and washed with 10 mL of sat. $NaHCO_3$ solution. The aqueous phase was extracted with CH_2Cl_2 (3 × 10 mL) and the combined organic layers were dried over $MgSO_4$. Finally, the solvent was removed under reduced pressure to afford a yellow oil; yield: 695 mg (60%). ^{1}H NMR ($CDCl_3$): δ 1.29 (t, 3H, J = 7.2 Hz), 2.30 (s, 6H), 2.59 (t, 2H, J = 5.8 Hz), 2.81 (d, 1H, J = 9.0 Hz), 2.88 (d, 1H, J = 9.0 Hz), 4.16–4.21 (m, 3H), 4.23–4.28 (m, 1H), 5.28 (s, 1H), 5.29 (s, 1H), 6.47 (s, 2H).

***exo,exo*-[2-(3-Ethoxycarbonyl-7-oxabicyclo[2.2.1]hept-5-ene-2-carbonyloxy)ethyl]trimethylammonium iodide (M2): 2** (659 mg, 2.3 mmol) was dissolved in 2 mL of CH_3I at 0 °C. The reaction mixture was stirred for 30 min at 0 °C and for 8 h at room temperature. The resulting yellow precipitate was isolated by filtration, dried and recrystallized from boiling ethanol. The crude product was dissolved in CH_2Cl_2 and precipitated with hexane to afford a white solid; yield: 875 mg (88%). ^{1}H NMR ($CDCl_3$): δ 1.30 (t, 3H, J = 7.2 Hz), 2.86 (d, 1H, ^2J = 9.0 Hz), 2.94 (d, 1H, ^2J = 9.0 Hz), 3.54 (s, 9H), 4.16 (q, 2H, J = 7.2 Hz), 4.10–4.23 (m, 2H), 4.56 (dd, 1H, ^2J = 14.0 Hz, J = 5.1 Hz), 4.74 (dd, 1H, ^2J = 14.0 Hz, J = 6.9 Hz), 5.15 (s br, 1H), 5.43 (s br, 1H), 6.48 (dd, 1H, J = 5.8 Hz, J = 1.4 Hz), 6.50 (dd, 1H, J = 5.8 Hz, J = 1.6 Hz). ^{13}C NMR ($CDCl_3$, 100 MHz): δ 14.24 (CH_3), 46.77 (CH), 47.91 (CH), 54.88 (CH_3), 58.65 (CH_2), 61.69 (CH_2), 64.75 (CH_2), 80.10 (CH), 80.87 (CH), 136.52 (CH), 136.76 (CH), 171.19 (C_q), 172.00 (C_q). IR (ATR) ν (cm^{-1}) = 3433 (w), 3002 (w), 2977 (w), 1732 (ss), 1190 (ss), 1157 (ss) 913 (s), 887 (s). Elemental analysis**:** calcd. for $C_{15}H_{24}INO_5$: C, 42.36; H, 5.69; N, 3.29; found: C, 42.25; H, 5.71; N, 3.29.

Homopolymerization of M1: M1 (100 mg, 0.339 mmol) was dissolved in 5 mL of CH_2Cl_2 and treated with a solution of **[Mo]** (2.4 mg, 0.0034 mmol) in 1 mL of CH_2Cl_2. The yellow reaction mixture was stirred for 2 h at room temperature. A solution of ferrocene carboxaldehyde (10-fold excess based on initiator) in CH_2Cl_2 was added and the mixture was stirred for 1 h at room temperature. The polymer was precipitated by addition of pentane, filtered off, thoroughly washed with pentane and dried; yield: 85 mg (85%). Poly(**M1**): $M_{n(calc)}$ = 29400 g mol^{-1}, $M_{n(found)}$ = 37900 g mol^{-1}; PDI = 1.21. ^{1}H NMR ($CDCl_3$): δ 8.39 (broad d, 2H Py), 7.72 (broad d, 2H Py), 7.34 (broad d, 2H Py), 7.14 (broad d, 2H Py), 5.72–5.43 (broad t, 2H -CH=CH-), 3.12 (broad s, 1H NBE), 2.89–2.23 (broad d, 2H NBE), 2.20–1.20 (broad d, 4H NBE). ^{13}C NMR ($CDCl_3$): δ 175.0 (C=O), 154.8, 148.9, 137.8, 134.6 and 130.2 (all Py), 122.6 and 121.9 (-CH=CH-), 53.3, 47.6, 41.9 and 37.3 (all NBE). FT-IR (ATR mode): ν (cm^{-1}) = 2995 (w), 1672 (s), 1577 (s), 1426 (m), 1239 (w), 1048 (m), 739 (m).

Homopolymerization of M2: M2 (100 mg, 0.235 mmol) was dissolved in 5 mL of CH_2Cl_2 and treated with a solution of **[Mo]** (3.0 mg, 0.0042 mmol) in 1 mL of CH_2Cl_2. The resulting white cloudy reaction mixture was stirred for 2 h at room temperature. A solution of ferrocene carboxaldehyde (10-fold excess based on initiator) in CH_2Cl_2 was added and the mixture was then stirred for 1 h at room temperature. The polymer was filtered off, thoroughly washed with pentane and dried; yield: 90 mg (90%). Poly(**M2**): $M_{n(calc)}$ = 23600 g mol^{-1}, $M_{n(found)}$ = 24500 g mol^{-1}, PDI = 1.36. ^{1}H NMR ($CDCl_3$): δ 5.83 (broad s, 2H -CH=CH-), 5.17 (broad s, 2H CH_2), 4.70 (broad s, 2H CH_2), 4.21 (broad d, 4H CH_2), 3.51 (broad s, 13 H NBE + NCH_3), 1.26 (broad s, 3H CH_3). ^{13}C NMR ($CDCl_3$): δ 171.3 and 170.4 (C=O), 132.7(-CH=CH-), 77.2 (NBE), 64.6, 61.8, 59.4 (CH_2), 55.1, 53.8 and 52.9 (NCH_3), 14.1 (CH_3). FT-IR (ATR mode): ν (cm^{-1}) = 3428 (w), 2969 (w), 1726 (s), 1427 (m), 1181 (w), 1018 (m), 953 (m).

Synthesis of poly(M1-*b*-M2): A solution of [**Mo**] (2.4 mg, 0.0034 mmol) in 1 mL of CH_2Cl_2 was added to one of **M1** (30.0 mg, 0.102 mmol) in 1 mL of CH_2Cl_2. The reaction mixture was stirred for 20 min and a small amount was withdrawn for GPC measurements. **M2** (100 mg, 0.235 mmol) was dissolved in 2 mL of CH_2Cl_2 and this solution was added to the reaction mixture. The resulting white cloudy reaction mixture was stirred for another 90 min. The polymerization was terminated with ferrocene carboxaldehyde (10-fold excess based on initiator) and the reaction was stirred for a further hour. The polymer was filtered off, thoroughly washed with pentane and dried; yield: 100 mg (76%). M_n = 44100 g mol^{-1}, M_w = 61100 g mol^{-1}, PDI = 1.38. ^{1}H NMR ($CDCl_3$): δ 8.40, 7.92, 7.43, 7.33 (broad s, Py), 5.79 (broad s, -CH=CH-), 5.17 (broad s, CH_2), 4.70 (broad s, CH_2), 4.21 (broad d, CH_2), 3.51 (broad s, NBE + NCH_3), 1.87 (broad, NHE), 1.27 (CH_3). ^{13}C NMR ($CDCl_3$): δ 175.6 (C=O), 171.3 and 170.4 (C=O), 154.8, 148.9, 137.8, 134.6 and 130.2 (all Py), 122.8 and 122.2 (-CH=CH-), 77.0 (NBE), 64.6, 61.6, 59.3 (CH_2), 52.8 (NCH_3), 22.3, 14.1 (CH_3). FT-IR (ATR mode): ν (cm^{-1}) = 3404 (w), 2937 (w), 1727 (s), 1679 (m), 1586 (m), 1467 (m), 1432 (w), 1375 (m), 1238 (w), 1184 (s), 1097 (w), 1018 (m), 954 (m), 749 (m).

Synthesis of poly(M1-*b*-M2)-Rh: $[Rh(COD)_2Cl]_2$ (8 mg) was dissolved in CH_2Cl_2. This solution was added dropwise to a suspension of poly(**M1**-*b*-**M2**) (100 mg) in 5 mL of CH_2Cl_2. The mixture was stirred for 10 h at room temperature; then the polymer was filtered off, thoroughly washed with pentane and dried; yield: 100 mg (92%). The Rh-content was determined by ICP-OES: 18 mg Rh/g copolymer (12% of the theoretical loading).

cmc determination of poly(M1-*b*-M2) and poly(M1-*b*-M2)-Rh: The cmc in water were determined by fluorescence spectroscopy [23] using 6-*p*-toluidene-2-naphthylsufonic acid (10^{-6} M) as the fluorescence probe. Polymer solutions were prepared in a concentration range from 1×10^{-4}–1×10^{-13} mol L^{-1}. cmc of poly(**M1**-*b*-**M2**) = 2.8×10^{-6} mol L^{-1}; cmc of poly(**M1**-*b*-**M2**)-**Rh** = 2.2×10^{-6} mol L^{-1}.

Quantification of Rh: The amount of Rh bound to the block copolymers or leached into the products was determined by dissolving a 20.0 mg amount of the polymer or the product mixture in aqua regia (25 mL). Rh was quantified by ICP-OES at λ = 343.489 nm, measuring the background at λ_1 = 343.410 and λ_2 = 343.600 nm, respectively. A 1000 ppm Rh standard (1N HNO_3, Merck, Germany) was used to prepare standards of 0, 0.100, 1.00 and 10.00 ppm.

General procedure for hydroformylation: The reaction was carried out in a 300 mL Parr high-pressure reactor. The reactor was evacuated, flushed with argon and filled with the catalyst, water or toluene (30 mL), and 1-octene (1.0 g, 0.0090 mol), leading to a substrate to catalyst ratio of 5000:1. *tert*-Butylbenzene (1.00 mL) was added as internal standard. To purge the reactants, the mixture was pressurized with a 1:1 mixture of CO and H_2 up to a pressure of 30 bar and then the pressure was released. Finally, the pressure was adjusted to 50 bar with the aid of a back pressure regulator. The autoclave was heated to 70 °C and kept at this temperature. Samples were taken every 30 min. The isomeric 1-octenes and aldehydes were identified and quantified by their MS spectra as well as by their retention times using commercially available compounds as reference material.

Recyclability studies with poly(M1-*b*-M2)-Rh: Hydroformylations were carried out as described above. For recycling, the product was extracted with diethyl ether (4 × 10 mL). Fresh 1-octene (1.0 g, 0.0090 mol), and *tert*-butylbenzene (1.0 mL) were added to the aqueous, catalyst-containing phase and the reaction was run under the same conditions as before. The TONs in two consecutive cycles as determined by GC-MS were 4300 and 3900, respectively.

Supporting Information

Supporting Information contains polymerization kinetics of **M1** by the action of Mo(*N*-2,6-Me_2 C_6H_3)(CHCMe_2Ph)(OCMe$(CF_3)_2)_2$, GPC-traces (DMF) of poly(**M1**) and poly(**M1**-*b*-**M2**); cmc measurements for poly(**M1**-*b*-**M2**) and poly(**M1**-*b*-**M2**)-**Rh** in water; conversion of 1-octene, product formation, product distribution in the hydroformylation of 1-octene in toluene in the presence of **C1, C1** and triphenylphosphite; *n*:*iso* selectivities for catalysts poly(**M1**-*b*-**M2**)-**Rh**) and poly(**M1**-*b*-**M2**)-**Rh** with triphenylphosphite as a function of conversion.

Supporting Information File 1

Graphical representations of measurements.
[http://www.beilstein-journals.org/bjoc/content/supplementary/1860-5397-6-28-S1.pdf]

Acknowledgements

Our work was supported by Clariant Germany, the *Cluster of Excellence* "*Unifying Concepts in Catalysis*" *coordinated by the Technische Universität Berlin* and the *Federal Government of Germany* and the *Freistaat Sachsen*. We are grateful to Dr. Wolfgang Geyer (UFZ, Leipzig) for his kind help with the fluorescence measurements as well as to A. Prager and Dr. U. Decker (IMO, Leipzig) for ICP-OES and NMR measurements.

References

1. Kotre, T.; Zarka, M. T.; Krause, J. O.; Buchmeiser, M. R.; Weberskirch, R.; Nuyken, O. *Macromol. Symp.* **2004,** *217,* 203–214. doi:10.1002/masy.200451316
2. Nuyken, O.; Persigehl, P.; Weberskirch, R. *Macromol. Symp.* **2002,** *177,* 163–173. doi:10.1002/1521-3900(200201)177:1<163::AID-MASY163>3.0.CO;2-W
3. Nuyken, O.; Weberskirch, R.; Kotre, T.; Schoenfelder, D.; Wörndle, A. Polymers for micellar catalysis. In *Polymeric Materials in Organic Synthesis and Catalysis;* Buchmeiser, M. R., Ed.; Wiley-VCH: Weinheim, Germany, 2003; pp 277–304. doi:10.1002/3527601856.ch6
4. Nuyken, O.; Weberskirch, R.; Bortenschlager, M.; Schönfelder, D. *Macromol. Symp.* **2004,** *215,* 215–230. doi:10.1002/masy.200451118
5. Oehme, G. Micellar Systems. In *Multiphase Homogeneous Catalysis,* 1st ed.; Cornils, B.; Herrmann, W. A.; Horvath, I. T.; Leitner, W.; Mecking, S.; Olivier-Bourbigou, H.; Vogt, D., Eds.; Wiley-VCH: Weinheim, Germany, 2005; Vol. 1, pp 132–136.
6. Pawar, G.; Bantu, B.; Weckesser, J.; Blechert, S.; Wurst, K.; Buchmeiser, M. R. *Dalton Trans.* **2009,** 9043–9051. doi:10.1039/b909180g
7. Weberskirch, R.; Preuschen, J.; Spiess, H. W.; Nuyken, O. *Macromol. Chem. Phys.* **2000,** *201,* 995–1007. doi:10.1002/1521-3935(20000601)201:10<995::AID-MACP995>3.0.CO;2-T
8. Krause, J. O.; Zarka, M. T.; Anders, U.; Weberskirch, R.; Nuyken, O.; Buchmeiser, M. R. *Angew. Chem.* **2003,** *115,* 6147–6151. doi:10.1002/ange.200352637
9. Bantu, B.; Wurst, K.; Buchmeiser, M. R. *J. Organomet. Chem.* **2007,** *692,* 5272–5278. doi:10.1016/j.jorganchem.2007.08.009
10. Ungváry, F. *Coord. Chem. Rev.* **2007,** *251,* 2087–2102. doi:10.1016/j.ccr.2007.02.018
11. Holmberg, K. *Eur. J. Org. Chem.* **2007,** 731–742. doi:10.1002/ejoc.20060074
12. Buchmeiser, M. R. Ring-Opening Metathesis Polymerization. In *Handbook of Ring-Opening Polymerization,* 1st ed.; Dubois, P.; Coulembier, O., Raquez, J.-M., Eds.; Wiley-VCH: Weinheim, Germany, 2009; pp 197–225. doi:10.1002/9783527628407.ch8
13. Buchmeiser, M. R. *Chem. Rev.* **2000,** *100,* 1565–1604. doi:10.1021/cr990248a
14. Stubenrauch, K.; Moitzi, C.; Fritz, G.; Glatter, O.; Trimmel, G.; Stelzer, F. *Macromolecules* **2006,** *39,* 5865–5874. doi:10.1021/ma060451p
15. Buchmeiser, M. R.; Wurst, K. *J. Am. Chem. Soc.* **1999,** *121,* 11101–11107. doi:10.1021/ja991501r
16. Buchmeiser, M. R.; Lubbad, S.; Mayr, M.; Wurst, K. *Inorg. Chim. Acta* **2003,** *345,* 145–153. doi:10.1016/S0020-1693(02)01291-4
17. Trnka, T. M.; Grubbs, R. H. *Acc. Chem. Res.* **2001,** *34,* 18–29. doi:10.1021/ar000114
18. Grubbs, R. H. *Angew. Chem.* **2006,** *118,* 3845–3850. doi:10.1002/ange.200600680
19. Schrock, R. R. *Polyhedron* **1995,** *14,* 3177–3195. doi:10.1016/0277-5387(95)85005
20. Schrock, R. R. The Discovery and Development of High-Oxidation State Mo and W Imido Alkylidene Complexes for Alkene Metathesis. In *Handbook of Metathesis,* 1st ed.; Grubbs, R. H., Ed.; Wiley-VCH: Weinheim, Germany, 2003; Vol. 1, pp 8–32. doi:10.1002/9783527619481.ch3
21. Schrock, R. R. *Chem. Commun.* **2005,** 2773–2777. doi:10.1039/b504541j
22. Oskam, J. H.; Fox, H. H.; Yap, K. B.; McConville, D. H.; O'Dell, R.; Lichtenstein, B. J.; Schrock, R. R. *J. Organomet. Chem.* **1993,** *459,* 185–198. doi:10.1016/0022-328X(93)86071-O
23. Ananthapadmanabhan, K. P.; Goddard, E. D.; Turro, N. J.; Kuo, P. L. *Langmuir* **1985,** *1,* 352–355. doi:10.1021/la00063a015
24. Dwars, T.; Haberland, J.; Grassert, I.; Oehme, G.; Kragl, U. *J. Mol. Catal. A: Chem.* **2001,** *168,* 81–86. doi:10.1016/S1381-1169(00)00542-2
25. Morawetz, H. *Adv. Catal.* **1969,** *20,* 341–371. doi:10.1016/S0360-0564(08)60276-X
26. Lipshutz, B. H.; Aguinaldo, G. T.; Ghorai, S.; Voigtritter, K. *Org. Lett.* **2008,** *10,* 1325–1328. doi:10.1021/ol800028x

27. Mingotaud, A.-F.; Mingotaud, C.; Moussa, W. *J. Polym. Sci., Part A: Polym. Chem.* **2008,** *46,* 2833–2844. doi:10.1002/pola.22617
28. Oheme, G.; Grassert, I.; Paetzold, E.; Meisel, R.; Drexler, K.; Fuhrmann, H. *Coord. Chem. Rev.* **1999,** *185-186,* 585–600. doi:10.1016/S0010-8545(99)00012-0
29. Kotre, T.; Nuyken, O.; Weberskirch, R. *Macromol. Rapid Commun.* **2002,** *23,* 871–876. doi:10.1002/1521-3927(20021001)23:15<871::AID-MARC871>3.0.CO;2-G
30. Zarka, T. M.; Nuyken, O.; Weberskirch, R. *Chem.–Eur. J.* **2003,** *9,* 3228–3234. doi:10.1002/chem.200304729
31. Kotre, T.; Nuyken, O.; Weberskirch, R. *Macromol. Chem. Phys.* **2004,** *205,* 1187–1195. doi:10.1002/macp.200300241
32. Schönfelder, D.; Nuyken, O.; Weberskirch, R. *J. Organomet. Chem.* **2005,** *690,* 4648–4655. doi:10.1016/j.jorganchem.2005.07.053
33. Schönfelder, D.; Fischer, K.; Schmidt, M.; Nuyken, O.; Weberskirch, R. *Macromolecules* **2005,** *38,* 254–262. doi:10.1021/ma048142r
34. Zarka, M. T.; Bortenschlager, M.; Wurst, K.; Nuyken, O.; Weberskirch, R. *Organometallics* **2004,** *23,* 4817–4820. doi:10.1021/om049495h
35. Bortenschlager, M.; Wittmann, A.; Schoellhorn, N.; Weberskirch, R.; Nuyken, O. *Polym. Prepr.* **2005,** *46,* 666–667.
36. Weissermel, K.; Arpe, H. J. *Industrial Organic Chemistry;* VCH: New York, 1993.
37. Sinner, F.; Buchmeiser, M. R.; Tessadri, R.; Mupa, M.; Wurst, K.; Bonn, G. K. *J. Am. Chem. Soc.* **1998,** *120,* 2790–2797. doi:10.1021/ja973495+

License and Terms

This is an Open Access article under the terms of the Creative Commons Attribution License (http://creativecommons.org/licenses/by/2.0), which permits unrestricted use, distribution, and reproduction in any medium, provided the original work is properly cited.

The license is subject to the *Beilstein Journal of Organic Chemistry* terms and conditions: (http://www.beilstein-journals.org/bjoc)

The definitive version of this article is the electronic one which can be found at: doi:10.3762/bjoc.6.28

Beilstein Journal of Organic Chemistry

Synthesis, characterization and photoinduced curing of polysulfones with (meth)acrylate functionalities

Cemil Dizman[1,2], Sahin Ates[1,2], Lokman Torun[*1] and Yusuf Yagci[*1,2]

Full Research Paper

Open Access

Address:
[1]Chemistry Institute, TUBITAK Marmara Research Center, Gebze, Kocaeli 41470, Turkey and [2]Department of Chemistry, Istanbul Technical University, Maslak, Istanbul 34469, Turkey

Email:
Lokman Torun[*] - lokman.torun@mam.gov.tr; Yusuf Yagci[*] - yusuf@itu.edu.tr

* Corresponding author

Keywords:
acrylates; photoinitiated polymerization; polysulfone; UV-curable oligomers

Beilstein J. Org. Chem. **2010,** *6,* No. 56.
doi:10.3762/bjoc.6.56

Received: 17 March 2010
Accepted: 05 May 2010
Published: 01 June 2010

Guest Editor: H. Ritter

© 2010 Dizman et al; licensee Beilstein-Institut.
License and terms: see end of document.

Abstract

The UV-curable telechelic polysulfones with (meth)acrylate functionalities were synthesized by condensation polymerization and subsequent esterification. The final polymers and intermediates at various stages were characterized by ^{1}H NMR, FT-ATR, and GPC. The oligomeric films prepared from the appropriate solutions containing these telechelics and 2,2-dimethoxy-2-phenylacetophenone (DMPA) as the photoinitiator undergo rapid polymerization upon irradiation forming insoluble networks. The photo-curing behavior was investigated by photo-DSC and the effects of the molecular weight of the polysulfone precursor and type of functionality on the rate of polymerization and conversion were evaluated. Thermal properties of the photochemically cured films were studied by differential scanning calorimeter (DSC) and thermal gravimetric analysis (TGA).

Introduction

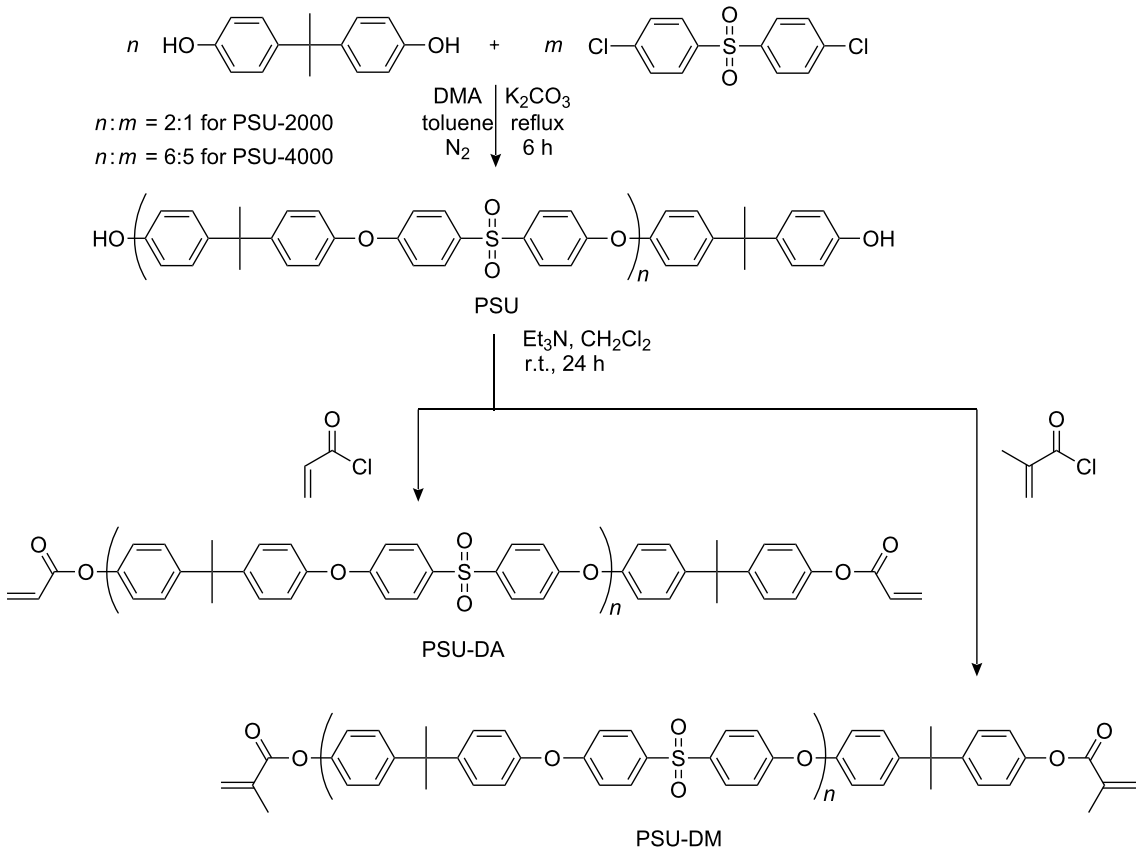
Polysulfones (PSU) show useful properties such as high strength and stiffness even at elevated temperatures, high continuous use and heat deflection temperatures, excellent resistance to hydrolysis by acids and bases, and good dimensional stability even in complex geometric shapes [1]. Despite these exceptional properties, there is need to modify the PSU structure to obtain several desired features. In general polymer modification is the one of main routes to achieve such characteristics [2,3]. There are two ways to functionalize PSUs. The first is postpolymerization modification in which the polymer is modified after polymerization. The second involves direct copolymerization of functionalized monomers [4-6]. An increasing topic of interest concerns cooperation of PSUs with epoxy resins via end group functionalization or blending. Engineering thermoplastics based on PSU have been widely used to overcome the problems associated with the brittleness of epoxy resins [7-11].

Telechelic oligomers are defined as the prepolymers carrying one or more functional end groups. They take part in further

polymerization or other reactions through their functional end groups [12]. The functionality of the end groups itself is important. When such groups are bifunctional (e.g. vinyl groups) they can participate in polymerization reactions, yielding graft copolymers or networks; such telechelic polymers are called macromolecular monomers, macromonomers. Their synthesis and modification have been studied in detail and covered by several review articles [13-15].

Photopolymerization is a frequently used process for the conversion of the multifunctional monomers into insoluble networks which are effective in various industrial fields such as, films, inks, coatings; photoresists, etc. [14]. The process is based upon the irradiation of the organic materials with light to initiate the reaction [15]. Compared to thermal polymerization, the corresponding photochemical processes have several advantages including increasing manufacturing capacity, low energy requirements, decreasing working area, production-line adjustability, low temperature processing, non-polluting and solvent-free formulations, and uncomplicated designed system. Organic materials (monomers, oligomers, polymers) with photoinitiators can be used in UV-curing systems. There are several photoinitiators acting in the UV and visible range capable of inducing rapid polymerization to form insoluble networks [16]. Because of their high reactivity leading to fast polymerization [17], multifunctional (meth)acrylates are the most commonly used monomers for many applications [18-22]. The activity of the (meth)acrylates depends on their structural properties such as the type and flexibility of incorporated molecule, number of functional groups, the presence of heteroatoms, chain length, and hydrogen bonding etc. [23-26].

In the present work, we report the preparation and characterization of UV curable (meth)acrylate telechelics with polysulfone backbones. The curing behavior of these telechelics was studied by photo-DSC with 2,2-dimethoxy-2-phenylacetophenone (DMPA) as the photoinitiator. As shown below, the rigid aromatic polysulfones with different molecular weights were deliberately used so as to demonstrate the structural and molecular weight effects on the curing behavior. Finally, the durability of the cross-linking material was investigated by TGA.



Scheme 1: Synthesis of polysulfone macromonomers.

Results and Discussion

UV-Curable PSU telechelics were synthesized by condensation polymerization and subsequent esterification. First of all, PSU-2000 and PSU-4000 were synthesized by condensation polymerization according to the procedure described in the literature [27]. Monomer concentrations were adjusted to yield oligomers possessing phenolic groups at both ends. Polysulfone macromonomers were then synthesized by esterification of the oligomers obtained with acryloyl chloride and methacryloyl chloride in the presence of Et_3N as the base. The overall procedure is presented in Scheme 1.

The characterization of the synthesized oligomers was carried out by using FTIR-ATR, ^{1}H NMR, GPC, DSC, photo-DSC and TGA. FTIR-ATR data shows the characteristic bands for the polyether sulfone backbone. The new broad but weak peak around 3435 cm^{-1} indicates the presence of phenolic end groups. Attachment of polymerizable acrylate and methylacrylate functional groups through the esterification process was evidenced by the disappearance of this peak and the formation of the new ester carbonyl peak at around 1735 cm^{-1} (Figure 1).

The structures of the macromonomers were further confirmed by ^{1}H NMR analysis. As can be seen from Figure 2, where the ^{1}H NMR spectra of the precursor polymer and telechelics are presented, the methyl group belonging to bisphenol A appears in all the spectra at 1.69 ppm. The shifts between 6.70 and 7.86 ppm correspond to the aromatic protons of the poly(ether sulfone) backbone. The phenolic protons were not observed, probably due to the relatively high molecular weight of the precursor polymers. Distinctively, the aromatic protons of the terminal benzene ring appeared at 6.77 and 7.07 ppm as relatively weak signals. Successful macromonomer formation was confirmed by the appearance of the new peaks at around 6.15 (d), 6.50 (t) and 6.75 (d) ppm for the acrylate and 6.15 (s) and 6.45 (s) ppm for methacrylate groups, respectively. Notably, in both cases, the aromatic protons were down field shifted. End chain aromatic protons overlap with the other aromatic protons. The signal at 2.02 (s) ppm was assigned to the methyl group of the methacrylate functionality.

The molecular weight characteristics of the polymers with respect to the synthesis conditions are presented in Table 1. As

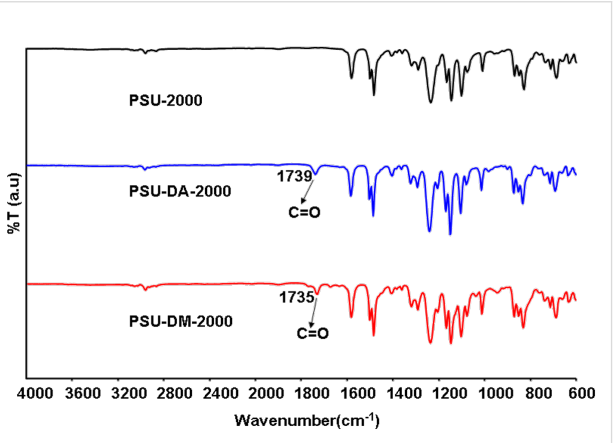


Figure 1: FT-IR spectra of PSU-2000, PSU-DA-2000 and PSU-DM-2000.

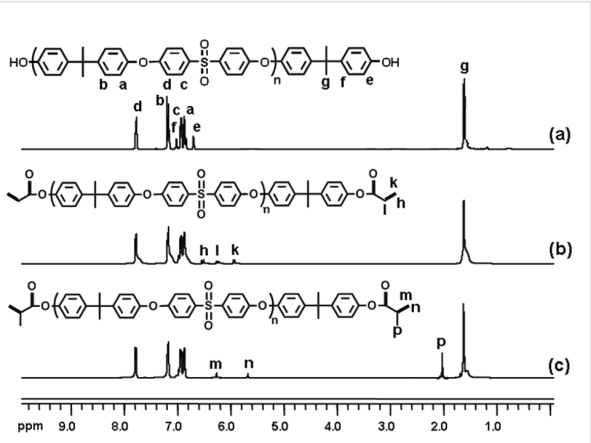


Figure 2: ^{1}H NMR spectra of PSU-2000 (a), PSU-DA-2000 (b) and PSU-DM-2000 (c) in $CDCl_3$.

Table 1: Synthesis[a] and molecular weight characteristics of polysulfones.

Polymer	Bisphenol A / Chlorosulfone (mol/mol)	Yield[b]	M_n[c] (GPC) (g/mol)	PDI	M_n[d] (NMR) (g/mol)	Acrylates		Methacrylates	
						M_n[c] (GPC) (g/mol)	M_n[d] (NMR) (g/mol)	M_n[c] (GPC) (g/mol)	M_n[d] (NMR) (g/mol)
PSU-2000	2/1	65%	1850	1.45	2150	2198	2396	2120	2323
PSU-4000	6/5	71%	4400	1.51	4000	4605	4228	–	–

[a]Reaction temperature: 170 °C, time: 6 h.
[b]Determined gravimetrically.
[c]Number average molecular weight determined from GPC measurements based on polystyrene standards.
[d]Calculated by using ^{1}H NMR spectra.

the functionalized PSUs were intended to be used in the ultimate photocuring step, the conditions of polycondensations were chosen so as to obtain relatively low molecular weight polymers with phenolic end group functionality combined with a satisfactory conversion. The efficiency of functionalization was confirmed by ^{1}H NMR spectrum by using the integration ratio of the protons corresponding to the (meth)acrylic groups to that of the methyl protons of the repeating unit. Almost quantitative functionalization was attained in both cases. Notably, the molecular weights calculated by ^{1}H NMR in general agree well with the measured values. Moreover, general agreement between the molecular weight of the final telechelic polymers and that of the precursor PSU obtained by GPC also confirms efficient esterification. The observed increase in the molecular weight is due to the additional acrylate and methacrylate moieties incorporated.

Kinetic studies concerning photopolymerization of the macromonomers were performed by photo-DSC. The results are shown in Figure 3 and Figure 4. The rate of photopolymerization vs. time plots for both PSU-DA-2000 and PSU-DM-4000 exhibit no plateau region indicating the absence of the rapid auto acceleration at the very beginning of the reaction. This behavior may be due to factors related to the cross-linking nature of the samples and solid-state measurements. Since the obtained telechelics exhibit high melting points and are solid at room temperature, free standing films can easily be prepared. The photopolymerization under these conditions leads to a suppressed center of coil diffusion resulting in rapid auto acceleration [28]. The results also indicate that conversions are lower than 50%. Although the oligomers possess long flexible chains, due to their vitreous nature dense cross-linked network formation occurs which decreases the amount of reacted double bonds significantly [29]. Figure 3 also shows that the conversion and polymerization rate of the acrylate derivative is considerably higher than that of the methacrylate macromonomer. This difference may be due to the α-methyl group present in the monomer which stabilizes the propagating radical. These results

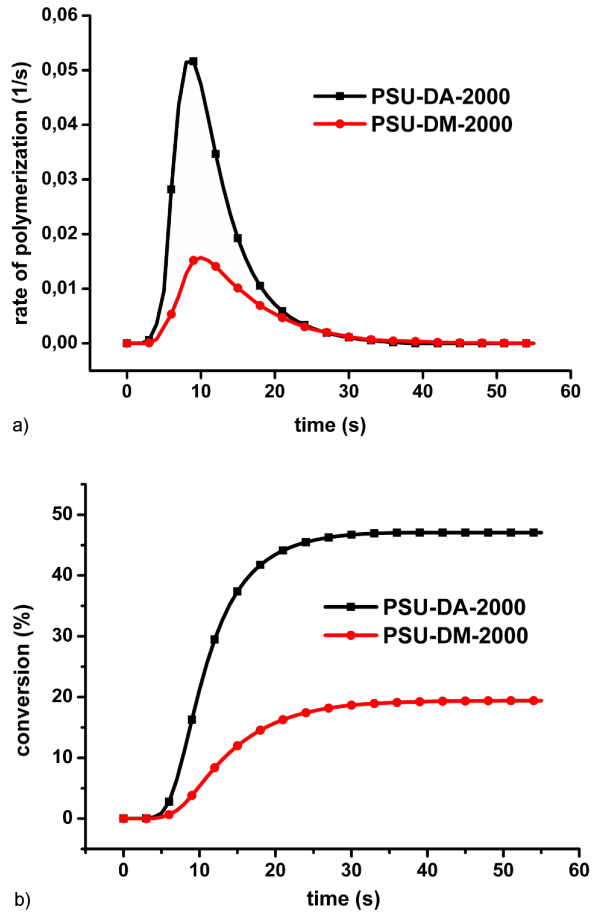


Figure 3: Rate (a) and conversion (b) of photo induced polymerization of PSU-DA-2000 and PSU-DM-2000.

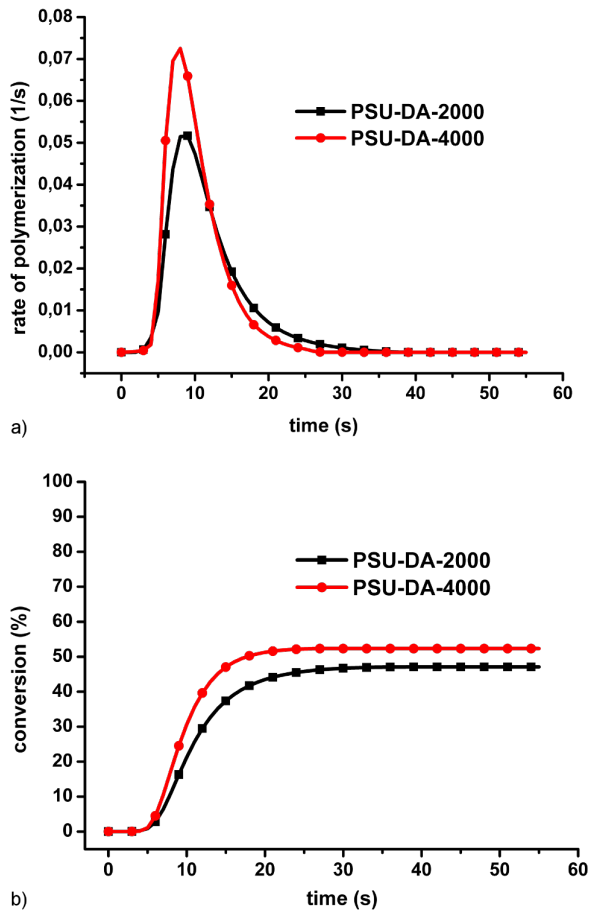


Figure 4: Rate (a) and conversion (b) of photo induced polymerization of PSU-DAs with different molecular weights.

are consistent with the literature data for the thermal initiated polymerization that gives a difference by a factor of approximately 5 in the polymerization rates at room temperature [30].

The cross-linking capability of the oligomers increased with the molecular weight of the macromonomer as a result of the increased flexibility of the longer chains. Therefore, PSU-DA-4000 displays a slightly higher conversion and a faster rate of polymerization (Figure 4) [31].

TGA thermograms of photochemically cured and precursor oligomers are shown in Figure 5. As can be seen, the initial oligomers show a small weight loss up to 200 °C. This degradation can be attributed to the elimination of water. Similar weight losses have been observed for other hydroxyl-containing polymers [32]. Major degradation of the oligomers began at around 400 °C. The overall thermal stability of the polymers is similar.

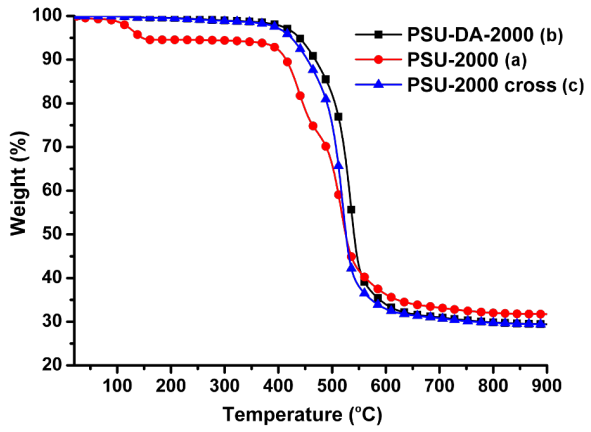


Figure 5: TGA thermograms of the precursor oligomers (PSU-2000) (a), and macromonomer, PSU-DA-2000 before (b), and after curing (PSU-DA-2000 X) (c).

As can be seen from Figure 6, the glass transition temperature (T_g) of the acrylate macromonomer is more than 20 °C higher than that of its precursor polymer because of the structural compatibility between the end groups and the inner backbone. Interestingly, the corresponding UV-cured macromonomer exhibits a much higher T_g (188 °C) which is almost the same T_g as commercially available high molecular weight PSUs such as UDEL-PSU (M_n = 30000). This behavior indicates that the properties of the high molecular weight PSUs can be attained even with oligomeric macromonomers as a result of extended chain length by UV induced cross-linking.

In conclusion, we have synthesized two types of PSU macromonomers by step-growth polymerization and subsequent esterification processes, and investigated their photocuring

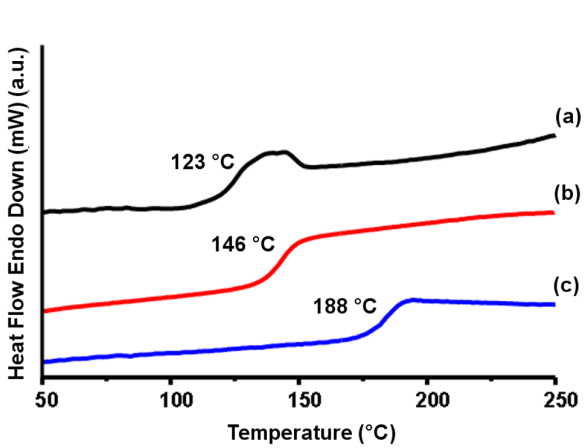


Figure 6: DSC results of the precursor oligomer (PSU-2000) (a), and macromonomer, PSU-DA-2000 before (b), and after curing (PSU-DA-2000 X) (c).

behavior. The effects of the molecular weight of the PSU precursor and type of functionality on the rate of polymerization and conversion were evaluated. The thermal stability of the photochemically cross-linked polymers indicates that these oligomers may be important components of UV curable formulations for obtaining networks that could have application in coatings and membranes.

Experimental

Materials

Bisphenol A and bis(*p*-chlorophenyl) sulfone (Hallochem Pharma Co. Ltd, China), methanol (Merck), dimethylacetamide (DMA, 99%, Merck) were used without any purification. Dichloromethane (99%, Aldrich), chloroform (+99%, Aldrich), acryloyl chloride (+97%, Merck), methacryloyl chloride (+97%, Merck) were used as received. 2,2-Dimethoxy-2-phenylacetophenone (DMPA, 99%, Across) was also used without any additional treatment.

Characterization

^{1}H NMR spectra of 5–10% (w/w) solutions of the intermediates and final polymers in $CDCl_3$ with $Si(CH_3)_4$ as an internal standard were recorded at room temperature at 250 MHz on a Bruker DPX 250 spectrometer. Fourier transform infrared-Attenuated Total Reflectance (FTIR-ATR) spectra were recorded on a Perkin-Elmer FT-IR Spectrum One B spectrometer with a Universal ATR accessory equipped with a single reflection diamond crystal. Solid oligomers were placed over the ATR crystal and maximum pressure was applied using the slip-clutch mechanism. Differential scanning calorimetry (DSC) was performed on a Perkin-Elmer Diamond DSC. Molecular weights and polydispersities of the linear oligomers were measured by gel permeation chromatography (GPC) employing an

Agilent 1100 instrument equipped with a differential refractometer with tetrahydrofuran as the eluent at a flow rate of 0.3 mL min^{-1} at 30 °C. Molecular weights were determined using polystyrene standards. Thermal gravimetric analysis (TGA) was performed on Perkin–Elmer Diamond TA/TGA with a heating rate of 10 °C min under nitrogen flow.

Preparation of the oligomers

General procedure for the synthesis of polysulfone oligomer

Bisphenol A (40 g, 175 mmol), bis(*p*-chlorophenyl) sulfone (25.16 g, 87.6 mmol) and dried potassium carbonate (25.39 g, 183.6 mmol) were added to 400 mL DMA (dimethyl acetamide) and 50 mL toluene in a 2000 mL, 2 necked round bottom flask, fitted with a condenser, nitrogen inlet, a Dean and Stark trap and an overhead mechanical stirrer. The reaction mixture was heated under reflux at 150 °C for 4 h with water removal. The reaction was stopped after about 2 h and cooled to room temperature. The solution was filtered to remove most of the salts and poured into a mixture of methanol andwater (4:1). The precipitated polymer was filtered, and washed several times with water in order to remove the remaining salts and impurities. Finally, the polymer was washed with methanol and dried in a vacuum oven at 60 °C for about 12 h to give PSU-2000 oligomer (42.2 g).

IR (ATR, cm^{-1}): 3435 (-OH), 3200–3000 (Ar), 2975 (-CH_3 sym-), 2945 (-CH_3 asym-), 1322 and 1293 (O=S=O asym-), 1240 (C-O-C), 1175 and 1151 (O=S=O sym-) and 1014 (Ar).

^{1}H NMR ($CDCl_3$, ppm): δ = 7.85 (16H), 7.26 (16H), 7.07 (4H), 7.00 (16H), 6.94 (16H), 6.75 (4H), 1.69 CMe_2 (30H).

A similar procedure using appropriate ratios of the monomers was used for the synthesis of PSU-4000.

Synthesis of polysulfone diacrylate (PSU-DA)

PSU-2000 (5 g, 2.86 mmol) was added to 20 mL CH_2Cl_2 in a 50 mL, two necked round bottomed flask fitted with a condenser and argon inlet. The flask was placed in an ice bath and the contents stirred for about 5 min. Excess triethylamine (Et_3N) 2.0 mL was added followed by excess acryloyl chloride (1.15 mL, 14.3 mmol) dissolved in 5 mL CH_2Cl_2 which was added slowly to the reaction flask over a 10 min period. The reaction mixture was stirred for 24 h then filtered to remove the salts formed and poured into methanol to precipitate the acrylate oligomer. The precipitated oligomer was filtered and washed several times with water to remove the remaining salts and impurities. Finally, the polymer was washed with methanol and dried in a vacuum oven at room temperature for about 12 h to give PSU-DA-2000 macromonomer (5 g).

IR (ATR, cm^{-1}): 3200–3000 (Ar), 2968 (-CH_3 sym-), 2875 (-CH_3 asym-), 1739 (-C=O), 1322 and 1293 (O=S=O asym-), 1238 (C-O-C), 1175 and 1151 (O=S=O sym-) and 1014 (Ar).

^{1}H NMR ($CDCl_3$, ppm): δ = 7.76 (16H), 7.16 (16H), 7.02 (4H), 6.94 (16H), 6.86 (16H), 6.84 (4H), 6.53–6.51 (2H) and 6.24–6.22 (2H) (CH2=), 5.94–5.92 (2H) (=CH-), 1.62 CMe_2 (30H).

The same procedure was applied for the synthesis of PSU-DA-4000.

Synthesis of polysulfone dimethacrylate (PSU-DM)

For the preparation of PSU-DM-2000, a similar procedure as described for the synthesis of acrylate functional macromonomers was followed with methacryloyl chloride.

IR (ATR, cm^{-1}): 3200–3000 (Ar), 2969 (-CH_3 sym-), 2875 (-CH_3 asym-), 1735 (-C=O), 1323 and 1295 (O=S=O asym-), 1243 (C-O-C), 1175 and 1151 (O=S=O sym-) and 1014 (Ar).

^{1}H NMR ($CDCl_3$, ppm): δ = 7.78 (16H), 7.17 (16H), 6.94 (16H), 6.87 (16H), 6.26 (2H) and 5.76 (2H), 1.98 (C=-Me) (6H), 1.63 CMe_2 (30H).

Preparation of Photo-curable formulations

Formulations containing macromonomers (0.003 g) and DMPA (2 mol %) in 250 μL chloroform were prepared from appropriate stock solutions. The mixture was then dropped onto an aluminum pan and the solvent allowed to evaporate completely. The film samples were placed into the sample cell of photo-DSC instrument.

Photocalorimetry (Photo-DSC)

The photo-differential scanning calorimetry (Photo-DSC) measurements were carried out by means of a modified Perkin-Elmer Diamond DSC equipped with a high pressure mercury arc lamp (320–500 nm). A uniform UV light intensity was delivered across the DSC cell to the sample and reference pans. The intensity of the light was measured as 53 mW cm^{-2} by a UV radiometer capable of broad UV range coverage. The mass of the sample was 3 mg, and the measurements were carried out in an isothermal mode at 30 °C under a nitrogen flow of 20 mL min^{-1}. The heat liberated in the polymerization was directly proportional to the number of acrylate groups reacted in the system. By integrating the area under the exothermic peak, the conversion of the acrylate groups (*C*) or the extent of the reaction was determined according to Equation 1:

$$C = \Delta H_t \big/ \Delta H_0^{theory} \quad (1)$$

where ΔH_t is the reaction heat evolved at time t and $\Delta H_0^{\text{theory}}$ is the theoretical heat for complete conversion. $\Delta H_0^{\text{theory}}$ = 86 kJ mol^{-1} for an acrylic double bond [33]. The rate of polymerization (R_p) is directly related to the heat flow (dH/dt) by Equation 2:

$$R_p = dC/dt = \left(dH/dt\right)/\Delta H_0^{theory} \qquad (2)$$

Acknowledgements

The authors thank the State Planning Organization of Turkey (DPT) for the financial support (Project no: 2005K120920). We also want to thank Nursen Turdu for NMR studies and Zekayi Korlu for TGA studies. Special thanks go to Turgay Balci for the technical support.

References

1. Olabisi, O. *Handbook of thermoplastics;* Marcel Dekker: New York, 1997.
2. Jouanneau, J.; Mercier, R.; Gonon, L.; Gebel, G. *Macromolecules* **2007,** *40,* 983–990. doi:10.1021/ma0614139
3. Bishop, M. T.; Karasz, F. E.; Russo, P. S. *Macromolecules* **1985,** *18,* 86–93. doi:10.1021/ma00143a014
4. Stephen, R.; Gibon, C. M.; Weber, M.; Gaymans, R. J. *J. Polym. Sci., Part A: Polym. Chem.* **2009,** *47,* 3904–3913. doi:10.1002/pola.23457
5. Matsumoto, K.; Higashihara, T.; Ueda, M. *J. Polym. Sci., Part A: Polym. Chem.* **2009,** *47,* 3444–3453. doi:10.1002/pola.23403
6. Yu, X.; Roy, A.; Dunn, S.; Badami, A. S.; Yang, J.; Good, A. S.; McGrath, J. E. *J. Polym. Sci., Part A: Polym. Chem.* **2009,** *47,* 1038–1051. doi:10.1002/pola.23194
7. Lin, H. T.; Lin, C. H.; Hu, Y. M.; Su, W. C. *Polymer* **2009,** *50,* 5685–5692. doi:10.1016/j.polymer.2009.09.075
8. Scamporrino, E.; Mineo, P.; Scamporrino, A.; Dattilo, S.; Vitalini, D.; Alicata, R. *J. Polym. Sci., Part A: Polym. Chem.* **2009,** *47,* 5682–5689. doi:10.1002/pola.23611
9. Mimura, K.; Ito, H.; Fujioka, H. *Polymer* **2000,** *41,* 4451. doi:10.1016/S0032-3861(99)00700-4
10. Pethrick, R. A.; Hollins, E. A.; McEwan, I.; MacKinnon, A. J.; Hayward, D.; Cannon, L. A. *Macromolecules* **1996,** *29,* 5208. doi:10.1021/ma9518464
11. Bonnet, A.; Pascault, J. P.; Sautereau, H.; Rogozinski, J.; Kranbuehl, D. *Macromolecules* **2000,** *10,* 3833. doi:10.1021/ma991363q
12. Odian, G. *Principles of Polymerization;* Wiley and Sons, 1991. Chapter 2.
13. Ebdon, J. R.; Eastmond, G. C., Eds. *New Methods of Polymer Synthesis;* Blackie Academic and Professional, 1995.
14. Ates, S.; Aydogan, B.; Torun, L.; Yagci, Y. *Polymer* **2010,** *51,* 825–831. doi:10.1016/j.polymer.2010.01.005
15. Yagci, Y.; Nuyken, O.; Graubner, V.-M. Telechelic Polymers. In *Encyclopedia of Polymer Science and Technology,* 3rd ed.; Kroschwitz, J. I., Ed.; Wiley and Sons: New York, 2005; Vol. 12, pp 57–130.
16. Chaisuriyathepkul, A.; Klinpituksa, P.; Phinyocheep, P.; Nakason, C.; Kittipoom, S. *E-Polymers* **2008,** 141.
17. Lee, T. Y.; Roper, T. M.; Jönsson, E. S.; Guymon, C. A.; Hoyle, C. E. *Macromolecules* **2004,** *37,* 3659–3665. doi:10.1021/ma0305277
18. Anseth, K. S.; Kline, L. M.; Walker, T. A.; Anderson, K. J.; Bowman, C. N. *Macromolecules* **1995,** *28,* 2491–2499. doi:10.1021/ma00111a050
19. Moussa, K.; Decker, C. *J. Polym. Sci., Part A: Polym. Chem.* **1993,** *31,* 2197–2203. doi:10.1002/pola.1993.080310903
20. Kannurpatti, R. A.; Anseth, J. W.; Bowman, C. N. *Polymer* **1998,** *39,* 2507–2513. doi:10.1016/S0032-3861(97)00585-5
21. Anseth, K. S.; Bowman, C. N.; Peppas, N. A. *Polym. Bull.* **1993,** *31,* 229–233. doi:10.1007/BF00329970
22. Andrzejewska, E. *Polymer* **1996,** *37,* 1039–1045. doi:10.1016/0032-3861(96)87288-0
23. Dietz, J. E.; Peppas, N. A. *Polymer* **1997,** *38,* 3767–3781. doi:10.1016/S0032-3861(96)00902-0
24. Cook, W. D. *J. Polym. Sci., Part A: Polym. Chem.* **1993,** *31,* 1053–1067. doi:10.1002/pola.1993.080310428
25. Hoyle, C. E.; Mathias, L. J.; Jariwala, C.; Sheng, D. *Macromolecules* **1996,** *29,* 3182–3187. doi:10.1021/ma9464377
26. Boutevin, B.; Pietrasanta, Y.; Parisi, J. P. *Makromol. Chem.* **1987,** *188,* 1621–1629. doi:10.1002/macp.1987.021880708
27. Viswanathan, R.; Johnson, B. C.; McGrath, J. E. *Polymer* **1984,** *25,* 1827. doi:10.1016/0032-3861(84)90258-1
28. Young, J. S.; Bowman, C. N. *Macromolecules* **1999,** *32,* 6073–6081. doi:10.1021/ma9902955
29. Davidson, S. *Exploring the science, technology and applications of UV and EB curing;* SITA Technology Limited: London, 1999.
30. Brandrup, J.; Immergut, E. H. *Polymer Handbook,* 2nd ed.; John Wiley and Sons: New York, 1975.
31. Anseth, K. S.; Kline, L. M.; Walker, T. A.; Anderson, K. J.; Bowman, C. N. *Macromolecules* **1995,** *28,* 2491–2499. doi:10.1021/ma00111a050
32. Holland, B. J.; Hay, J. N. *Polymer* **2001,** *42,* 6775–6783. doi:10.1016/S0032-3861(01)00166-5
33. Andrzejewska, E.; Andrzejewski, M. *J. Polym. Sci., Part A: Polym. Chem.* **1998,** *36,* 665–673. doi:10.1002/(SICI)1099-0518(199803)36:4<665::AID-POLA15>3.0.CO;2-K

License and Terms

This is an Open Access article under the terms of the Creative Commons Attribution License (http://creativecommons.org/licenses/by/2.0), which permits unrestricted use, distribution, and reproduction in any medium, provided the original work is properly cited.

The license is subject to the *Beilstein Journal of Organic Chemistry* terms and conditions: (http://www.beilstein-journals.org/bjoc)

The definitive version of this article is the electronic one which can be found at: doi:10.3762/bjoc.6.56

Beilstein Journal of Organic Chemistry

Polar tagging in the synthesis of monodisperse oligo(*p*-phenyleneethynylene)s and an update on the synthesis of oligoPPEs

Dhananjaya Sahoo, Susanne Thiele, Miriam Schulte, Navid Ramezanian and Adelheid Godt*

Full Research Paper

Open Access

Address:
Bielefeld University, Faculty of Chemistry, Universitätsstr. 25, D-33615 Bielefeld, Germany

Email:
Adelheid Godt* - godt@uni-bielefeld.de

* Corresponding author

Keywords:
alkyne protecting group; carbometalation; C–C coupling; phenyleneethynylene; polar tagging

Beilstein J. Org. Chem. **2010,** *6,* No. 57.
doi:10.3762/bjoc.6.57

Received: 02 February 2010
Accepted: 22 April 2010
Published: 01 June 2010

Guest Editor: H. Ritter

© 2010 Sahoo et al; licensee Beilstein-Institut.
License and terms: see end of document.

Abstract

One important access to monodisperse (functionalized) oligoPPEs is based on the orthogonality of the alkyne protecting groups triisopropylsilyl and hydroxymethyl (HOM) and on the polar tagging with the hydroxymethyl moiety for an easy chromatographic separation of the products. This paper provides an update of this synthetic route. For the deprotection of HOM protected alkynes, γ-MnO_2 proved to be better than (highly) activated MnO_2. The use of HOM as an alkyne protecting group is accompanied by carbometalation as a side reaction in the alkynyl–aryl coupling. The extent of carbometalation can be distinctly reduced through substitution of HOM for 1-hydroxyethyl. The strategy of polar tagging is extended by embedding ether linkages within the solubilising side chains. With building blocks such as 1,4-diiodo-2,5-bis(6-methoxyhexyl) less steps are needed to assemble oligoPPEs with functional end groups and the isolation of pure compounds becomes simple. For the preparation of 1,4-dialkyl-2,5-diiodobenzene a better procedure is presented together with the finding that 1,4-dialkyl-2,3-diiodobenzene, a constitutional isomer of 1,4-dialkyl-2,5-diiodobenzene, is one of the byproducts.

Introduction

Oligo(*p*-phenyleneethynylene)s (oligoPPEs) have been frequently used as structural units for nanoscopic molecules because of their geometry and their electronic and photophysical properties [1-19]. For their preparation three widely used synthetic routes have emerged:

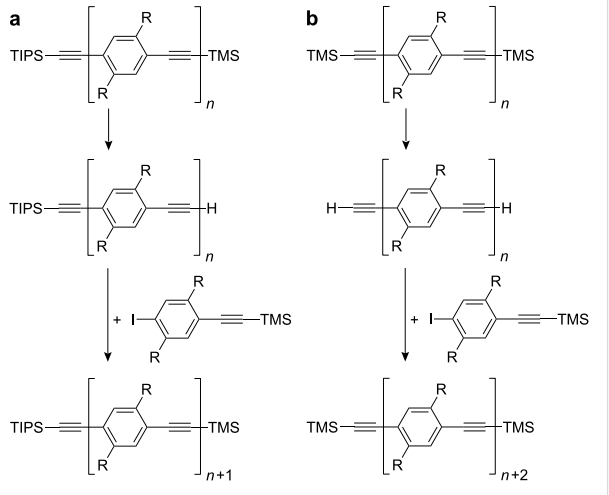
1. The repeating unit by repeating unit approach (Scheme 1a) with desilylation and coupling of the (functionalized) arylethyne with 1-iodo-4-(2-trimethylsilylethynyl)benzene as the two repeating steps [6,9,20-24]. The oligomer grows slowly repeating unit by repeating

unit. In the related bidirectional approach two repeating units are added in each coupling step (Scheme 1b) [25].

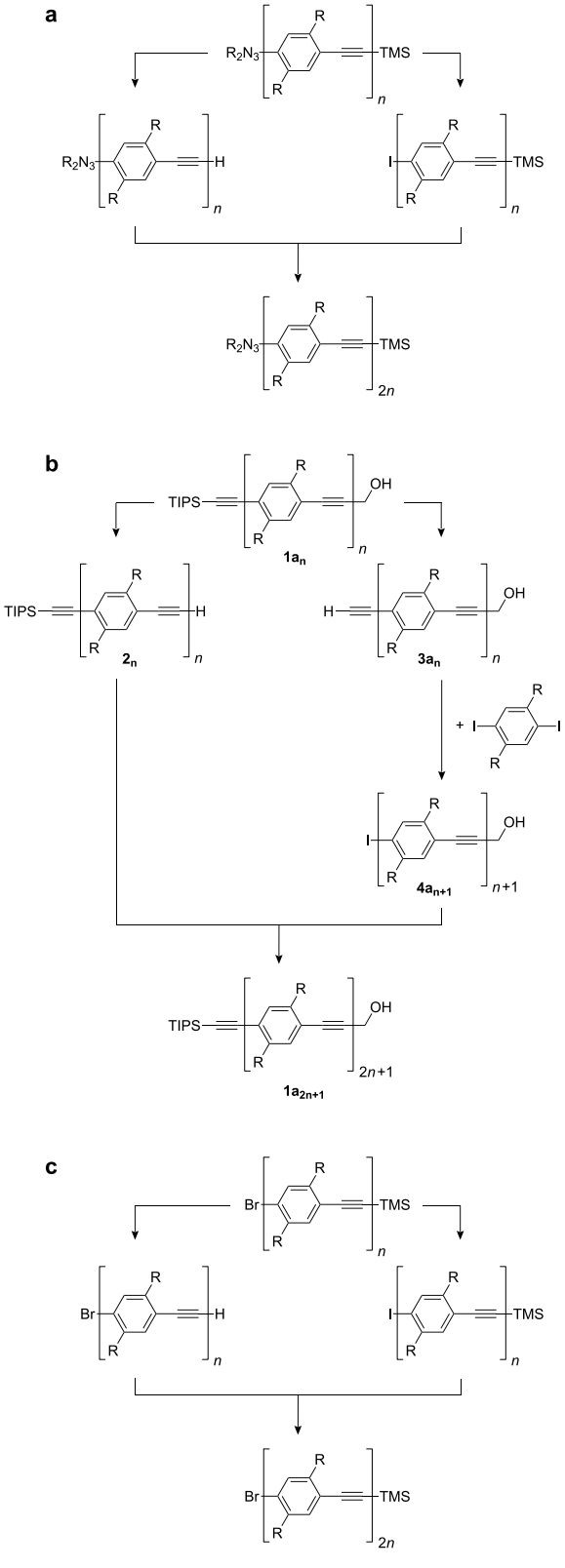
2. The divergent-convergent Moore–Tour-route (Scheme 2a) [26-29] which employs the diethyltriazenyl group to mask an iodo substituent [30,31]. 1-(Diethyltriazenyl)-4-(2-trimethylsilylethynyl)benzene is the parent compound. Desilylation and exchange of the triazenyl substituent for an iodo substituent are the two divergent steps followed by the alkynyl–aryl coupling, the convergent step. The dialkyltriazenyl group decomposes during chromatography on silica gel [28].
3. The divergent-convergent route which makes use of the orthogonality of the two alkyne protecting groups triisopropylsilyl (TIPS) and hydroxymethyl (HOM) (Scheme 2b) [32]. The reaction sequence starts with the HOM and TIPS protected 1,4-diethynylbenzene **1a$_1$** from which the monoprotected 1,4-diethynylbenzenes **2$_1$** and **3a$_1$** are derived by the removal of either the HOM or the TIPS group. The HOM protected 1,4-diethynylbenzene **3a$_1$** is coupled with 1,4-diiodobenzene to obtain aryl iodide **4a$_2$**. This is coupled with the TIPS protected 1,4-diethynylbenzene **2$_1$** in the convergent step. It has been shown that HOM can be exchanged for 1-hydroxy-1-methylethyl (2-hydroxyprop-2-yl, HOP) [33-38].

A rather rarely utilized third divergent-convergent approach (Scheme 2c) [39-41] relies on the bromo iodo selectivity of the alkynyl–aryl coupling and bromo iodo exchange via halogen metal exchange.

The principles underlying these methods have been applied to building blocks with additional substituents including func-



Scheme 1: Synthesis of oligoPPEs by a unidirectional (a) or bidirectional (b) repeating unit by repeating unit approach. R denotes solubilising substituents.



Scheme 2: Three divergent-convergent routes to oligoPPEs. R denotes solubilising substituents such as hexyl.

tional groups as well as to other aromatic building blocks, such as biphenyl [33], bipyridine [36,42], thiophene [36,43,44], fluorene [45], and triptycene [46], and other shapes, e.g. starlike compounds [2,7,12,34,37].

The divergent-convergent route that employs the two orthogonal alkyne protecting groups TIPS and HOM (Scheme 2b) does not only allow the fast growth of oligomers – only four steps for doubling the number of repeating units with two of the four steps being experimentally extremely simple – but is especially satisfying because of a trouble-free separation of the desired alkynyl–aryl coupling product and the accompanying oxidative alkyne dimerization product (Glaser coupling product). In our experience, under the standard coupling conditions – i.e. $Pd(PPh_3)_2Cl_2$, CuI, piperidine, THF, room temperature – Glaser coupling is much faster than the alkynyl–aryl coupling. Therefore, even traces of oxygen in the reaction vessel will lead to alkyne dimerization. Furthermore, most experimentalists prefer to work up the reaction mixtures under standard conditions which means exposing the reaction mixture to air. Opening the flask will immediately cause any unreacted terminal alkyne to undergo Glaser coupling. This is of no concern provided the alkyne dimer and the alkynyl–aryl coupling product can be easily separated, and this is what the HOM and related HOP group guarantee since they act as polar tags for the chromatographic separation. Polar tagging with HOM [47-49] or HOP [34,42,45,50-57] has been the key to the successful syntheses of a variety of aryleneethynylene building blocks and oligomers [42,45,47-52] and of oligoeneynes [53] including the natural marine compound callyberyne [54].

Since we disclosed this strategy several years have elapsed during which time we have gained more experience with it, became aware of some problems concerning it and improved it. Because the strategy has been adopted in whole or in part by other groups [33,34,47,49,58,59] and oligoPPEs are still a topic of great interest [1-19], we would like to share our results and present an update and an extension of our route in this paper. There are four issues that we want to address: (1) The type of MnO_2 used for the removal of the HOM group, (2) carbometalation, a side reaction when using hydroxymethyl as an alkyne protecting group, (3) purity of 1,4-dihexyl-2,5-diiodobenzene, and (4) polar tags in the side chains of building blocks to reduce the number of steps in oligomer synthesis.

Results and Discussion

Type of MnO_2 used for alkyne deprotection

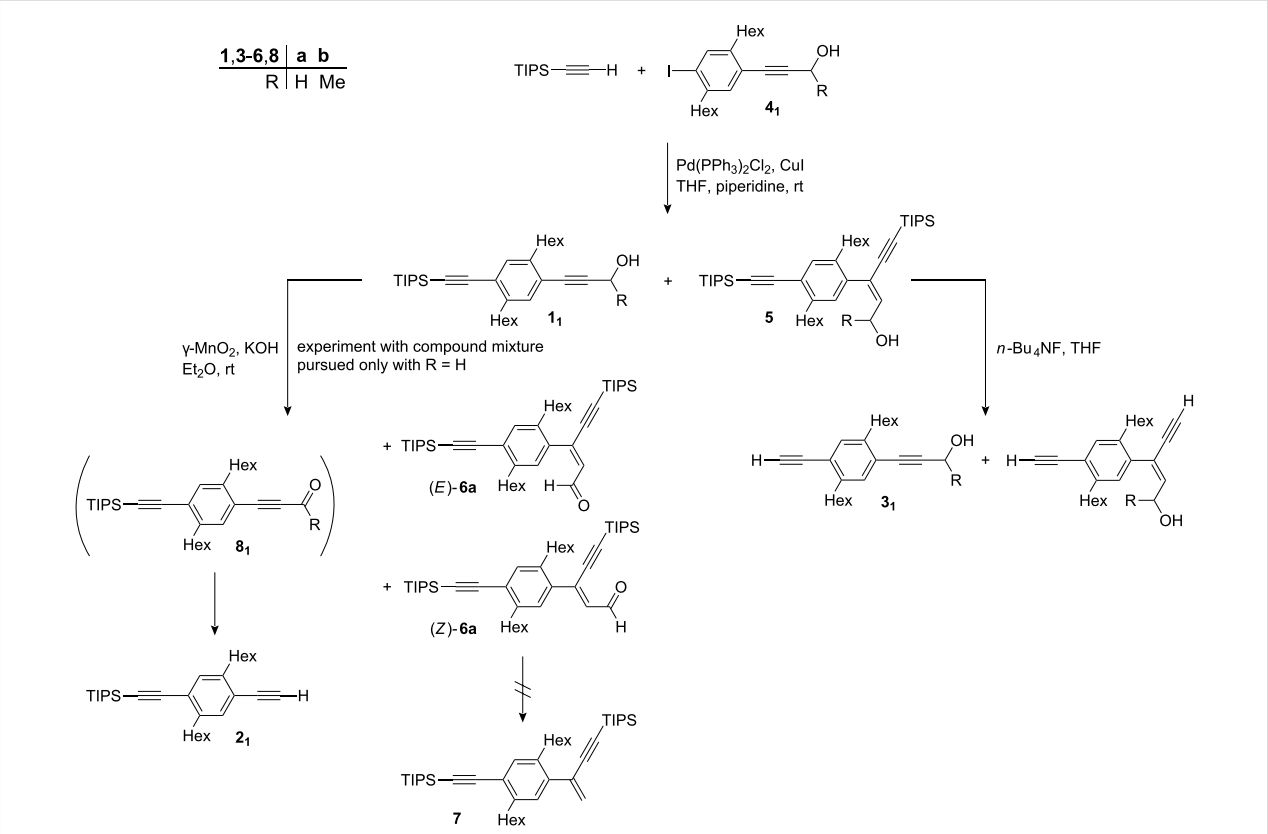
The original paper on the oxidation-decarbonylation of HOM-protected alkynes [60,61] through treatment with MnO_2 and powdered KOH does not contain any details about the type of MnO_2. We applied this method to the synthesis of oligoPPEs, only exchanging benzene for diethyl ether, and obtained satisfactory results with commercially available active MnO_2 (Aldrich) [32]. However, the deprotection of the HOM-protected arylalkynes $\mathbf{1a_n}$ took several hours, especially when the reaction was run on larger scale, i.e. with 500 mg or more of starting material [62]. Even more annoying was that the required reaction time varied drastically from one experiment to another. The best procedure was to add portions of a mixture of MnO_2 and KOH in intervals of 15 to 60 minutes until the reaction was complete. The reaction can be easily monitored by thin layer chromatography.

To improve the procedure, we tested the activated MnO_2 (purchased; Aldrich), highly activated MnO_2 (self-made) [63-65], $BaMnO_4$ (purchased) [66-68], and γ-MnO_2 (self-made) [63,64] on 3-(4-bromophenyl)prop-2-ynol in the presence of powdered KOH in diethyl ether at room temperature. The reaction with γ-MnO_2 was the fastest. Even more important, γ-MnO_2 when applied to the oligomers $\mathbf{1a_n}$ proved to be highly reliable in its oxidizing power making it the reagent of choice for the removal of HOM groups. Some experimental results hint at a reduced activity of γ-MnO_2 after it was stored for more than half a year in a closed jar under ambient conditions.

Carbometalation

When we published the synthesis of oligoPPEs via the divergent-convergent route which is based on the orthogonality of the alkyne protecting groups TIPS and HOM, we reported the carbometalation product **5a** (Scheme 3) which formed as a side product in the coupling of iodo monomer $\mathbf{4a_1}$ with TIPSethyne [32]. In the original procedure a reaction temperature of 50 °C was employed. Much later we found that the reaction goes to completion even at room temperature. Lowering the temperature reduced the amount of the carbometalation product **5a** from 2–16% to 1–5%. Nevertheless, large scale preparative chromatographic separation on silica gel is tedious. Carbometalation product **5a** and monomer $\mathbf{1a_1}$ have very similar R_f-values and, unfortunately, the byproduct is eluted first.

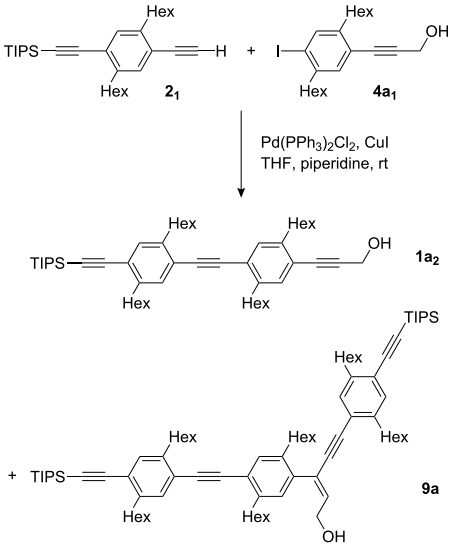
Luckily, contamination of monomer $\mathbf{1a_1}$ with carbometalation product **5a** is of no concern if this material is used to prepare the TIPS protected 1,4-diethynylbenzene $\mathbf{2_1}$ (Scheme 3). Under standard reaction conditions – γ-MnO_2, powdered KOH, Et_2O, room temperature – the alcohol groups of both compounds $\mathbf{1a_1}$ and **5a** are oxidized. Whereas the oxidation product of $\mathbf{1a_1}$, aldehyde $\mathbf{8a_1}$, reacts with KOH to give the ethynyl anion and formic acid which immediately exchange a proton providing deprotected alkyne $\mathbf{2_1}$, the oxidation product of **5a**, aldehyde **6a**, is inert under the reaction conditions [69,70]. This finding is attributed to the higher energy content and therefore lower nucleofugicity of a vinyl anion as compared to an ethynyl



Scheme 3: Synthesis of the building blocks $\mathbf{1}_1$, $\mathbf{2}_1$, and $\mathbf{3}_1$. The depicted alkene configuration of **5** was chosen assuming a carbometalation process for the formation of **5** and thus a *syn* addition of the alkyne onto the hydroxypropyne moiety.

anion. The products, alkyne $\mathbf{2}_1$ and the oxidized carbometalation product **6a**, are easily separable by chromatography, which resembles a simple filtration through silica gel because **6a** stays anchored on the solid phase through its polar carbonyl group. In this way pure alkyne $\mathbf{2}_1$ can be obtained even if carbometalation product **5a** is present in the starting material.

The case is quite different when monomer $\mathbf{1a}_1$ is used as the precursor for the HOM protected 1,4-diethynylbenzene $\mathbf{3a}_1$. Treatment of a mixture of $\mathbf{1a}_1$ and **5a** with *n*-Bu_4NF will not only remove the TIPS group of $\mathbf{1a}_1$ but also the two TIPS groups of **5a** (Scheme 3). The two products are as difficult to separate as the starting compounds. Furthermore, the ethynyl groups of both products are expected to have the same reactivity which can make the isolation of pure compounds of subsequent coupling reactions even more challenging. Finally, we found that carbometalation not only occurs during the preparation of monomer $\mathbf{1a}_1$ and its trimethylsilyl (TMS)-analogue but also, even though extremely rarely, at later stages of the oligoPPE synthesis. For example, on one occasion we isolated compound **9a** (2%, isolated yield) from the reaction between alkyne $\mathbf{2}_1$ and iodo monomer $\mathbf{4a}_1$ which gave dimer $\mathbf{1a}_2$ as the major product (79%, isolated yield) (Scheme 4).



Scheme 4: Carbometalation, an occasionally detected side reaction. The depicted alkene configuration was chosen assuming a carbometalation process and thus a *syn* addition of the alkyne onto the hydroxypropyne moiety.

In other reactions of this type, the carbometalation product may have remained undetected due to the limited sensitivity of ^{1}H NMR spectroscopy, which we use as a routine method to assess the composition of the crude product and the chromatographic fractions, although the characteristic triplet at 6.38 ppm (J = 7 Hz) [71] arising from the vinyl proton of the carbometalation products is easily observed. If the ^{1}H NMR spectrum displays the carbon satellites of an aromatic proton signal from the major product, the threshold for detection the carbometalation product is as low as 0.5%.

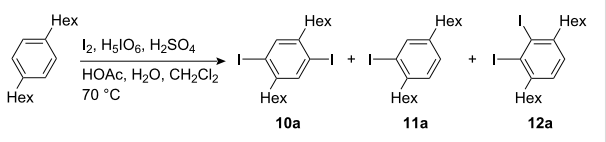
While compiling records on carbometalation of hydroxymethyl protected arylalkynes we never found any evidence for carbometalation of TMS or TIPS protected arylalkynes, even when conducting the aryl–alkyne coupling at 50 °C [72-75]. Possibly, the OH-group of the HOM group coordinates to the alkyne loaded Pd(II)-complex and thus acts as a directing and rate increasing group. It may as well be that the bulky trialkylsilyl substituents simply act as steric shields for the arylalkyne. If the latter is true, then the use of 1-hydroxyethyl (HOE) or HOP instead of HOM as polar protecting groups for alkynes could prevent carbometalation. Although HOP is a sterically more demanding group, we decided in favor of HOE because the removal of HOP requires refluxing in toluene for several hours in the presence of sodium hydride or potassium hydroxide [34,36-38,42,50-52,76] whereas we expected that HOE could be detached through treatment with γ-MnO_2 and powdered KOH in diethyl ether at room temperature, i.e. under the same, comparatively mild reaction conditions that had been used for HOM protected alkynes.

For a comparison of the influence of HOM and HOE on the carbometalation, the iodo monomers **4a$_1$** and **4b$_1$** were coupled with TIPSethyne in THF and piperidine using $Pd(PPh_3)_2Cl_2$ and CuI as the catalysts. A reaction temperature of 40 °C was chosen in order to boost carbometalation. These two experiments were carried out at the same time, thus providing the best basis for a comparison. After an aqueous workup, the reaction products were analyzed by ^{1}H NMR spectroscopy. In both cases the conversion of **4$_1$** was complete and the main component of the crude product was the coupling product **1$_1$**. The spectra gave no indication of the presence of carbometalation product **5b** whereas carbometalation product **5a** (ca. 3%) had formed. However, when another member of our group performed the coupling of TIPSethyne with HOE protected iodo monomer **4b$_1$**, he found a trace of carbometalation product **5b** (1%; as determined by ^{1}H NMR spectroscopy; the characteristic signal is the doublet at 6.15 ppm with J = 9 Hz in $CDCl_3$ which is assigned to the vinyl proton) in his crude product, although the reaction had been performed at room temperature. The same co-worker generally obtains a comparatively large amount of carbometalation product. Thus, the extent to which carbometalation occurs varies with the operator. So far we have no clue what the relevant factor is. The conclusion is that the alkyne protecting group HOE reduces the amount of accompanying carbometalation product when compared with HOM, however it does not inhibit it completely.

As expected, the HOE group is as smoothly removed as the HOM group through treatment of the protected alkynes **1b$_n$** with γ-MnO_2 and powdered KOH in diethyl ether at room temperature. This is illustrated for the conversion of hexamer **1b$_6$** and heptamer **1b$_7$** into the alkynes **2$_6$** (98% isolated yield) and **2$_7$** (90% isolated yield), respectively.

Iodination of 1,4-dihexylbenzene

The preparation of 1,4-dihexyl-2,5-diiodobenzene (**10a**) by the iodination of 1,4-dihexylbenzene with a mixture of iodine and potassium iodate in HOAc, H_2SO_4, and water at 70 °C [32,77,78] gave variable yields and on occasions failed. We obtained **10a** much more reliably via iodination with iodine and periodic acid in HOAc, H_2SO_4, water, and dichloromethane at 70 °C [79,80]. Dichloromethane probably acts as a phase compatibiliser. Nevertheless, the reaction never went to completion: In all cases monoiodination product **11a** was found (Scheme 5). Additionally, irrespective of which procedure was followed, the crude product always contained 1,4-dihexyl-2,3-diiodobenzene (**12a**) (ca. 3%), a constitutional isomer of **10a**. The structure elucidation of these byproducts based on ^{1}H NMR spectra is outlined in Supporting Information File 1.

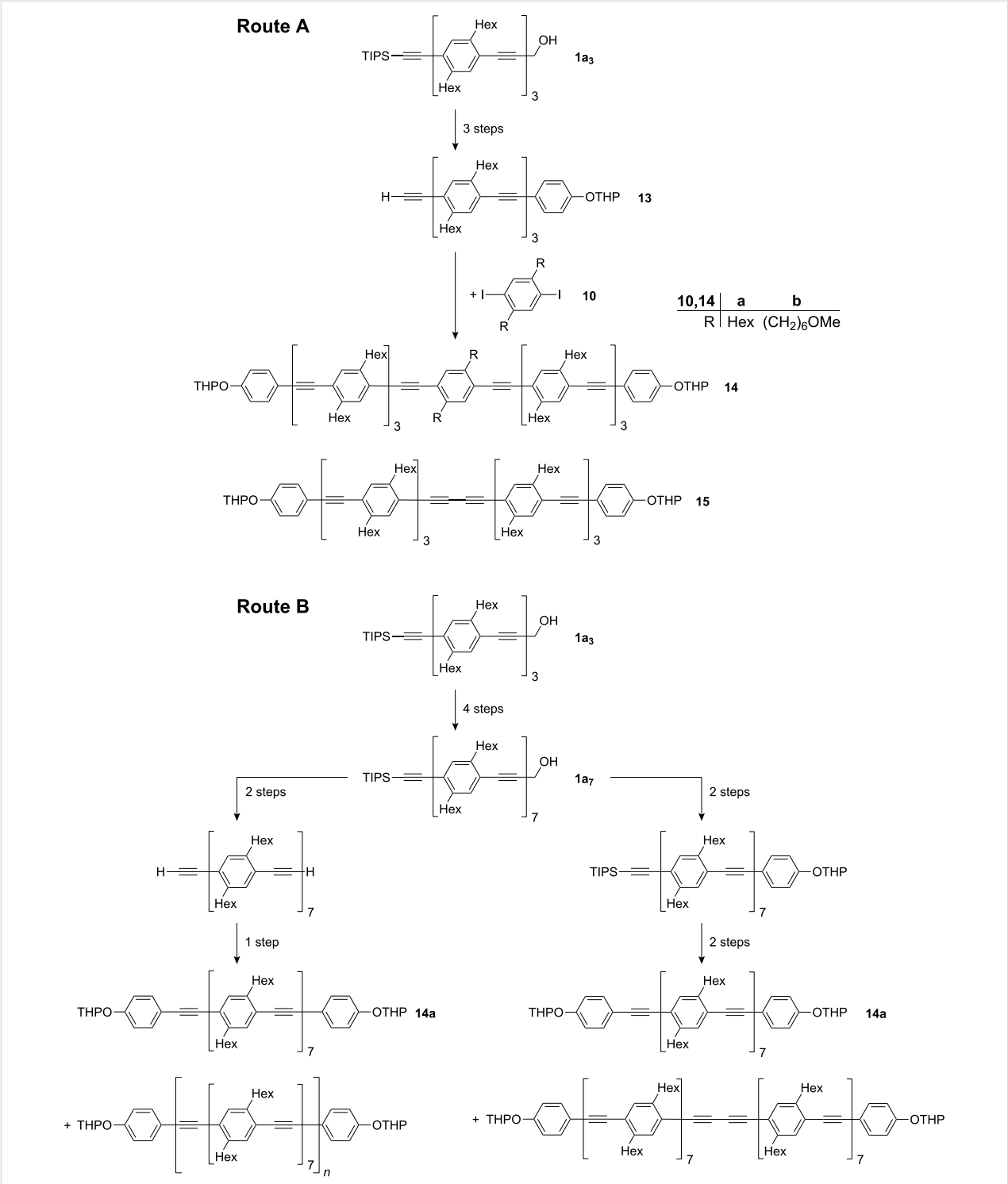


Scheme 5: Iodination of 1,4-dihexylbenzene.

At least twofold recrystallization is needed to obtain material which contains less than 0.5% of these byproducts (as determined by ^{1}H NMR spectroscopy. The ^{13}C-satellites of the signal of the aromatic protons of **10a** were used as the reference). Whereas monoiodination product **11a** is of minor concern because it is monofunctional, the constitutional isomer **12a** is a severe threat to the structural purity of oligoPPEs and especially polyPPEs. To illustrate this point let us assume that **10a** and thereof derived 1,4-diethynyl-2,5-dihexylbenzene, both contaminated with only 0.1% of the respective constitutional isomers, are polymerized to give a polymer batch with an average polymerisation degree of 1000. The consequence is that on average each of the polymer chains in this sample will have a kink, i.e. a severe structural defect.

Polar tags in the side chain

In spite of its efficiency, the divergent-convergent synthesis of oligoPPEs involves considerable effort, especially as a result of the chromatography which is required after each alkynyl–aryl coupling. In the case of the synthesis of oligoPPEs with terminal functional groups, it is tempting to reduce the number of steps through the coupling of a diiodo compound with oligoPPEs which carry one functional group and have about half of the number of repeating units of the target compound. To give one concrete example (Scheme 6): Starting from **1a$_3$**



Scheme 6: Different routes to compound **14**, a representative of the large group of functionalized oligoPPEs.

the synthesis of **14a** through the coupling of **13** with diiodobenzene **10a** (Scheme 6, route A) requires only two alkynyl–aryl couplings (four steps overall), whereas the alternative (Scheme 6, route B) via heptamer $\mathbf{1a_7}$ would take three or four cross coupling reactions (seven or eight steps overall) [81,82].

However, all of these routes will be plagued by the difficulty in separating **14a** from the accompanying alkyne dimer (Glaser coupling product). These two products differ only in the number of repeating units. In our experience with functionalized oligoPPEs their chromatographic properties on silica gel are very weakly influenced by the number of the non polar repeating unit, 2,5-dihexyl-1,4-phenyleneethynylene, but dominated by the polar functional groups. Therefore, if the two products differ in the number of polar groups, chromatographic separation can become easy. This idea was put to the test for the shortest route, route A, by employing methoxyhexyl substituted diiodobenzene **10b** instead of hexyl substituted diiodobenzene **10a**. The two methoxy groups influence the chromatographic behaviour distinctly (R_f(**14b**) = 0.29, R_f(**15**) = 0.71; silica gel, CH_2Cl_2/*n*-pentane 6:4). The oxygen atoms are intentionally inserted remote from the polyconjugated backbone in order not to change the optical properties of the oligomers.

Polar tagging with e.g. the rather inert ether moiety within the side chains at a site distant from the backbone appears to us a generally useful concept for the synthesis of mesoscopic molecules which very often have unbranched or slightly branched alkyl substituents present for solubility reasons.

Supporting Information

Supporting information features the syntheses of compounds used for the discussed experiments, the detailed experimental procedures, and the structure elucidation of the products from the iodination of 1,4-dihexylbenzene.

Supporting Information File 1

[http://www.beilstein-journals.org/bjoc/content/supplementary/1860-5397-6-57-S1.pdf]

Acknowledgements

Financial support by DFG (GO 555/4-3) is gratefully acknowledged.

References

1. Daniell, H. W.; Klotz, E. J. F.; Odell, B.; Claridge, T. D. W.; Anderson, H. L. *Angew. Chem.* **2007,** *119,* 6969–6972. doi:10.1002/ange.200702349
2. Tour, J. M. *J. Org. Chem.* **2007,** *72,* 7477–7496. doi:10.1021/jo070543s
3. Hu, W.; Zhu, N.; Tang, W.; Zhao, D. *Org. Lett.* **2008,** *10,* 2669–2672. doi:10.1021/ol800753z
4. Blakskjær, P.; Gothelf, K. V. *Org. Biomol. Chem.* **2006,** *4,* 3442–3447. doi:10.1039/b605844b
5. Andersen, C. S.; Gothelf, K. V. *Org. Biomol. Chem.* **2009,** *7,* 58–60. doi:10.1039/b815099k
6. Ljungdahl, T.; Pettersson, K.; Albinsson, B.; Mårtensson, J. *Eur. J. Org. Chem.* **2006,** 3087–3096. doi:10.1002/ejoc.200600240
7. Zhao, Y.; Shirai, Y.; Slepkov, A. D.; Cheng, L.; Alemany, L. B.; Sasaki, T.; Hegmann, F. A.; Tour, J. M. *Chem.–Eur. J.* **2005,** *11,* 3643–3658. doi:10.1002/chem.200401198
8. Huber, R.; Gonzáles, M. T.; Wu, S.; Langer, M.; Grunder, S.; Horhoiu, V.; Mayor, M.; Bryce, M. R.; Wang, C.; Jitchati, R.; Schönenberger, C.; Calame, M. *J. Am. Chem. Soc.* **2008,** *130,* 1080–1084. doi:10.1021/ja0767940
9. Mayr, A.; Srisailas, M.; Zhao, Q.; Gao, Y.; Hsieh, H.; Hoshmand-Kochi, M.; St. Fleur, N. *Tetrahedron* **2007,** *63,* 8206–8217. doi:10.1016/j.tet.2007.05.116
10. Guo, X.; Whalley, A.; Klare, J. E.; Huang, L.; O'Brien, S.; Steigerwald, M.; Nuckolls, C. *Nano Lett.* **2007,** *7,* 1119–1122. doi:10.1021/nl070245a
11. Lu, Q.; Liu, K.; Zhang, H.; Du, Z.; Wang, X.; Wang, F. *ACS Nano* **2009,** *3,* 3861–3868. doi:10.1021/nn9012687
12. Jeschke, G.; Sajid, M.; Schulte, M.; Godt, A. *Phys. Chem. Chem. Phys.* **2009,** *11,* 6580–6591. doi:10.1039/b905724b
13. Polyhach, Y.; Godt, A.; Bauer, C.; Jeschke, G. *J. Magn. Reson.* **2007,** *185,* 118–129. doi:10.1016/j.jmr.2006.11.012
14. Godt, A.; Schulte, M.; Zimmermann, H.; Jeschke, G. *Angew. Chem.* **2006,** *118,* 7722–7726. doi:10.1002/ange.200602807
15. Babgi, B.; Rigamonti, L.; Cifuentes, M. P.; Corkery, T. C.; Randles, M. D.; Schwich, T.; Petrie, S.; Stranger, R.; Teshome, A.; Asselberghs, I.; Clays, K.; Samoc, M.; Humphrey, M. G. *J. Am. Chem. Soc.* **2009,** *131,* 10293–10307. doi:10.1021/ja902793z
16. Ochi, T.; Yamaguchi, Y.; Wakamiya, T.; Matsubara, Y.; Yoshida, Z. *Org. Biomol. Chem.* **2008,** *6,* 1222–1231. doi:10.1039/b717832h
17. Albinsson, B.; Mårtensson, J. *J. Photochem. Photobiol., C: Photochem. Rev.* **2008,** *9,* 138–155. doi:10.1016/j.jphotochemrev.2008.01.002
18. Myahkostupov, M.; Piotrowiak, P.; Wang, D.; Galoppini, E. *J. Phys. Chem. C* **2007,** *111,* 2827–2829. doi:10.1021/jp0679257
19. Yatabe, T.; Suzuki, Y.; Kawanishi, Y. *J. Mater. Chem.* **2008,** *18,* 4468–4477. doi:10.1039/b808036d
20. Lavastre, O.; Ollivier, L.; Dixneuf, P. H.; Sibandhit, S. *Tetrahedron* **1996,** *52,* 5495–5504. doi:10.1016/0040-4020(96)00240-2
21. Aujard, I.; Baltaze, J.-P.; Baudin, J.-B.; Cogné, E.; Ferrage, F.; Jullien, L.; Perez, E.; Prévost, V.; Qian, L. M.; Ruel, O. *J. Am. Chem. Soc.* **2001,** *123,* 8177–8188. doi:10.1021/ja010019h
22. Hwang, J.-J.; Tour, J. M. *Tetrahedron* **2002,** *58,* 10387–10405. doi:10.1016/S0040-4020(02)01409-6
23. Zhi, Y.-G.; Lai, S.-W.; Chan, Q. K.-W.; Law, Y.-C.; Tong, G. S.-M.; Che, C.-M. *Eur. J. Org. Chem.* **2006,** 3125–3139. doi:10.1002/ejoc.200600103
24. Nierengarten, J.-F.; Gu, T.; Hadziioannou, G.; Tsamouras, D.; Krasnikov, V. *Helv. Chim. Acta* **2004,** *87,* 2948–2966. doi:10.1002/hlca.200490266
    Another stepwise approach consisting of coupling with 4-iodobenzaldehyde and conversion of the aldehyde group into an ethyne moiety via the Corey-Fuchs reaction.

25. Huang, S.; Tour, J. M. *Tetrahedron Lett.* **1999,** *40,* 3347–3350. doi:10.1016/S0040-4039(99)00463-3
26. Zhang, J.; Pesak, D. J.; Ludwick, J. L.; Moore, J. S. *J. Am. Chem. Soc.* **1994,** *116,* 4227–4239. doi:10.1021/ja00089a012
27. Jones, L., II; Schumm, J. S.; Tour, J. M. *J. Org. Chem.* **1997,** *62,* 1388–1410. doi:10.1021/jo962336q
28. Li, G.; Wang, X.; Wang, F. *Tetrahedron Lett.* **2005,** *46,* 8971–8973. doi:10.1016/j.tetlet.2005.10.113
29. Hortholary, C.; Coudret, C. *J. Org. Chem.* **2003,** *68,* 2167–2174. doi:10.1021/jo026735z
30. The use of the triflate group for the alkynyl–aryl coupling and its masking as the precursory OH group offers an alternative that was applied to the synthesis of phenyleneethynylene dendrimers [31], however, not (yet) to the synthesis of oligoPPEs.
31. Pan, Y.; Peng, Z.; Melinger, J. S. *Tetrahedron* **2003,** *59,* 5495–5506. doi:10.1016/S0040-4020(03)00827-5
32. Kukula, H.; Veit, S.; Godt, A. *Eur. J. Org. Chem.* **1999,** 277–286. doi:10.1002/(SICI)1099-0690(199901)1999:1<277::AID-EJOC277>3.0.CO;2-R
33. Wang, C.; Batsanov, A. S.; Bryce, M. R. *J. Org. Chem.* **2006,** *71,* 108–116. doi:10.1021/jo051711o
34. Chandra, K. L.; Zhang, S.; Gorman, C. B. *Tetrahedron* **2007,** *63,* 7120–7132. doi:10.1016/j.tet.2007.05.006
35. We like to call attention to the recent reports that trimethylsilyl and HOP are orthogonal alkyne protecting groups which make HOP a very interesting protecting group [36,37]. The same is true for *tert*-butyldimethylsilyl and HOP [38].
36. Goeb, S.; De Nicola, A.; Ziessel, R. *J. Org. Chem.* **2005,** *70,* 1518–1529. doi:10.1021/jo048435i
37. Rodríguez, J. G.; Esquivias, J.; Lafuente, A.; Díaz, C. *J. Org. Chem.* **2003,** *68,* 8120–8128. doi:10.1021/jo034972b
38. Shimizu, H.; Fujimoto, K.; Furusyo, M.; Maeda, H.; Nanai, Y.; Mizuno, K.; Inouye, M. *J. Org. Chem.* **2007,** *72,* 1530–1533. doi:10.1021/jo061959t
39. Ziener, U.; Godt, A. *J. Org. Chem.* **1997,** *62,* 6137–6143. doi:10.1021/jo970548x
40. Acharya, J. R.; Zhang, H.; Li, X.; Nesterov, E. E. *J. Am. Chem. Soc.* **2009,** *131,* 880–881. doi:10.1021/ja807621z
41. Hsung, R. P.; Chidsey, C. E. D.; Sita, L. R. *Organometallics* **1995,** *14,* 4808–4815. doi:10.1021/om00010a049
42. Ley, K. D.; Li, Y.; Johnson, J. V.; Powell, D. H.; Schanze, K. S. *Chem. Commun.* **1999,** 1749–1750. doi:10.1039/a903476e
43. Li, G.; Wang, X.; Li, J.; Zhao, X.; Wang, F. *Tetrahedron* **2006,** *62,* 2576–2582. doi:10.1016/j.tet.2005.12.043
44. Pearson, D. L.; Tour, J. M. *J. Org. Chem.* **1997,** *62,* 1376–1387. doi:10.1021/jo962335y
45. Zeng, X.; Wang, C.; Bryce, M. R.; Batsanov, A. S.; Sirichantaropass, S.; García-Suárez, V. M.; Lambert, C. J.; Sage, I. *Eur. J. Org. Chem.* **2007,** 5244–5249. doi:10.1002/ejoc.200700507
46. Maag, D.; Kottke, T.; Schulte, M.; Godt, A. *J. Org. Chem.* **2009,** *74,* 7733–7742. doi:10.1021/jo9009744
47. Yang, J.; Ng, M.-K. *Synthesis* **2006,** 3075–3079. doi:10.1055/s-2006-942529
48. Robinson, J. M. A.; Kariuki, B. M.; Harris, K. D. M.; Philp, D. *J. Chem. Soc., Perkin Trans. 2* **1998,** 2459–2469. doi:10.1039/a804676j
49. Harriman, A.; Mallon, L.; Ziessel, R. *Chem.–Eur. J.* **2008,** *14,* 11461–11473. doi:10.1002/chem.200801384
50. Zhao, Z.; Yu, S.; Xu, L.; Wang, H.; Lu, P. *Tetrahedron* **2007,** *63,* 7809–7815. doi:10.1016/j.tet.2007.05.095
51. Rodríguez, J. G.; Tejedor, J. L. *J. Org. Chem.* **2002,** *67,* 7631–7640. doi:10.1021/jo0203589
52. Kaneko, T.; Horie, T.; Matsumoto, S.; Teraguchi, M.; Aoki, T. *Macromol. Chem. Phys.* **2009,** *210,* 22–36. doi:10.1002/macp.200800429
53. Takayama, Y.; Delas, C.; Muraoka, K.; Uemura, M.; Sato, F. *J. Am. Chem. Soc.* **2003,** *125,* 14163–14167. doi:10.1021/ja037975e
54. López, S.; Fernández-Trillo, F.; Midón, P.; Castedo, L.; Saá, C. *J. Org. Chem.* **2006,** *71,* 2802–2810. doi:10.1021/jo052609u
55. Silicon based alkyne protecting groups with a cyano group as the polar tag [54,56,57].
56. Höger, S.; Bonrad, K. *J. Org. Chem.* **2000,** *65,* 2243–2245. doi:10.1021/jo991746m
57. Gaefke, G.; Höger, S. *Synthesis* **2008,** 2155–2157. doi:10.1055/s-2008-1067141
58. Keller, J. M.; Schanze, K. S. *Organometallics* **2009,** *28,* 4210–4216. doi:10.1021/om900195p
59. Weibel, N.; Mishchenko, A.; Wandlowski, T.; Neuburger, M.; Leroux, Y.; Mayor, M. *Eur. J. Org. Chem.* **2009,** 6140–6150. doi:10.1002/ejoc.200900751
60. Bumagin, N. A.; Ponomaryov, A. B.; Beletskaya, I. P. *Synthesis* **1984,** 728–729. doi:10.1055/s-1984-30947
61. Atkinson, R. E.; Curtis, R. F.; Jones, D. M.; Taylor, J. A. *J. Chem. Soc. C* **1969,** 2173–2176. doi:10.1039/J39690002173
    The suggestion to use the HOM group as a protecting group that can be removed via oxidation–decarbonylation was made much earlier here.
62. The largely different reaction times given in the experimental part of [48] probably indicate that the experimenters of that reference experienced the same difficulties.
63. Burke, S. D.; Danheiser, R. L., Eds. *Handbook of Reagents for Organic Synthesis, Oxidizing and Reducing Agents;* Wiley: Chichester, U.K., 2004; p 232.
64. Fatiadi, A. J. *Synthesis* **1976,** 65–104. doi:10.1055/s-1976-23961
65. For the preparation of highly activated MnO_2 we followed the procedure given in [63]. In this procedure less $MnCl_2 \cdot 4\ H_2O$ (200 g vs. 220 g) but the same amount of $KMnO_4$ (160 g) and of solvent was used in comparison to the procedure given in [64].
66. As purchased; 80% technical grade.
67. Fatiadi, A. J. *Synthesis* **1987,** 85–127. doi:10.1055/s-1987-27859
68. Firouzabadi, H.; Ghaderi, E. *Tetrahedron Lett.* **1978,** *19,* 839–840. doi:10.1016/S0040-4039(01)85412-5
69. Experimental proof: Carbometalation product **5a** was treated with γ-MnO_2 and powdered KOH in diethylether at room temperature. The ^{1}H NMR spectrum of the crude product shows unambigously the signals of the expected aldehyde **6a**. There are no signals that fit to the characteristic signals of the unsymmetrically 1,1-disubstituted alkene **7**, the product in case **6a** had lost the formyl group.
    The two sets of ^{1}H NMR signals in an intensity ratio of 22:1 for the aryl protons, the aldehyde proton, and the vinyl proton indicate a mixture of *E*- and *Z*-alkene. Alkene isomerization upon oxidation with MnO_2 has been reported [70]. The alkene isomerization can also be explained by a reversible addition of hydroxide to the electron acceptor substituted alkene of aldehyde **6a**. Characteristic signals of the major isomer: δ = 9.38 (d, *J* = 8.2 Hz, 1 H, CHO), 7.32 and 7.00 (2 s, 1 H each, ArH), 6.47 (d, *J* = 8.2 Hz, 1 H, C=CH); Characteristic signals of the minor isomer: δ = 10.28 (d, *J* = 8.2 Hz, 1 H, CHO), 7.30 and 7.09 (2 s, 1 H each, ArH), 6.31 (d, *J* = 8.2 Hz, 1 H, C=CH).

70. Burrell, J. W. K.; Garwood, R. F.; Jackman, L. M.; Oskay, E.; Weedon, B. C. L. *J. Chem. Soc. C* **1966,** 2144–2154. doi:10.1039/J39660002144
71. Characteristic ^{1}H NMR signals of the carbometalation product **9a** in $CDCl_3$: δ = 7.37, 7.31, 7.29, 7.22, 7.17, 6.98 (6 s, 1 H each, ArH), 6.38 (t, *J* = 7 Hz, 1 H, C=C<u>H</u>CH_2OH), 4.06 (t-shaped signal, slightly broadened, *J* = 6 Hz, 2 H, C<u>H</u>$_2$OH).
72. We know of only two publications that report on carbometalation of 1-aryl-2-trialkylsilylethynes [73,74]. The carbometalation reported in [73] is possibly induced by the hydroxy group of the hydroxymethyl substituent in ortho-position to the 2-(trimethylsilyl)ethynyl group. Note also the related Pd-catalyzed addition of TMSethyne onto 3-(trimethylsilyl)prop-2-ynol giving *Z*-2-(2-trimethylsilylethynyl)-3-trimethylsilylprop-2-enol in [75].
73. Stará, I. G.; Starý, I.; Kollárovič, A.; Teplý, F.; Šaman, D.; Fiedler, P. *Tetrahedron* **1998,** *54,* 11209–11234. doi:10.1016/S0040-4020(98)00655-3
74. Batenburg-Nguyen, B.; Ung, A. T.; Pyne, S. G. *Tetrahedron* **2009,** *65,* 318–327. doi:10.1016/j.tet.2008.10.052
75. Trost, B. M.; McIntosh, M. C. *Tetrahedron Lett.* **1997,** *38,* 3207–3210. doi:10.1016/S0040-4039(97)00614-X
76. Mal'kina, A. G.; Brandsma, L.; Vasilevsky, S. F.; Trofimov, B. A. *Synthesis* **1996,** 589–590. doi:10.1055/s-1996-4265
77. McQuade, D. T.; Kim, J.; Swager, T. M. *J. Am. Chem. Soc.* **2000,** *122,* 5885–5886. doi:10.1021/ja000553+
78. Werz, D. B.; Fischer, F. R.; Kornmayer, S. C.; Rominger, F.; Gleiter, R. *J. Org. Chem.* **2008,** *73,* 8021–8029. doi:10.1021/jo801378p
79. The use of CCl_4 instead of CH_2Cl_2 as described in [80] for iodination of 1,4-dialkoxybenzene resulted in an even higher conversion. However, the aromatic substitution reaction was no longer the only occuring reaction as especially the signals around 6 ppm in the ^{1}H NMR spectrum of the crude product reveal.
80. Bao, Z.; Chen, Y.; Cai, R.; Yu, L. *Macromolecules* **1993,** *26,* 5281–5286. doi:10.1021/ma00072a002
81. The eight step synthesis is outlined in analogy to the synthesis of the corresponding oligoPPE diesters in [82]. The eight step route is to be preferred over the seven step route because of the instability of oligoPPEs with two unprotected terminal ethyne moieties.
82. Hensel, V.; Godt, A.; Popovitz-Biro, R.; Cohen, H.; Jensen, T. R.; Kjaer, K.; Weissbuch, I.; Lifshitz, E.; Lahav, M. *Chem.–Eur. J.* **2002,** *8,* 1413–1423. doi:10.1002/1521-3765(20020315)8:6<1413::AID-CHEM1413>3.0.CO;2-6

License and Terms

This is an Open Access article under the terms of the Creative Commons Attribution License (http://creativecommons.org/licenses/by/2.0), which permits unrestricted use, distribution, and reproduction in any medium, provided the original work is properly cited.

The license is subject to the *Beilstein Journal of Organic Chemistry* terms and conditions: (http://www.beilstein-journals.org/bjoc)

The definitive version of this article is the electronic one which can be found at: doi:10.3762/bjoc.6.57

Beilstein Journal of Organic Chemistry

New amphiphilic glycopolymers by click functionalization of random copolymers – application to the colloidal stabilisation of polymer nanoparticles and their interaction with concanavalin A lectin

Otman Otman[1,2], Paul Boullanger[2], Eric Drockenmuller[1] and Thierry Hamaide[*1]

Full Research Paper

Open Access

Address:
[1]Université de Lyon; Université Lyon 1; Ingénierie des Matériaux Polymères, (IMP UMR CNRS 5223). 15, boulevard Latarjet, Villeurbanne, F-69622, France and [2]Université de Lyon; Université Lyon 1; Institut de Chimie et Biochimie Moléculaires et Supramoléculaires (ICBMS), Chimie Organique 2 – Glycochimie, UMR CNRS 5246, CPE-Lyon. 43, boulevard du 11 Novembre 1918, Villeurbanne, F-69622, France

Email:
Thierry Hamaide[*] - thierry.hamaide@univ-lyon1.fr

* Corresponding author

Keywords:
click chemistry; con A lectin; dynamic light scattering; glycopolymer; polymer nanoparticles

Beilstein J. Org. Chem. **2010,** *6,* No. 58. doi:10.3762/bjoc.6.58

Received: 30 March 2010
Accepted: 18 May 2010
Published: 01 June 2010

Guest Editor: H. Ritter

© 2010 Otman et al; licensee Beilstein-Institut.
License and terms: see end of document.

Abstract

Glycopolymers with mannose units were readily prepared by click chemistry of an azido mannopyranoside derivative and a poly(propargyl acrylate-co-*N*-vinyl pyrrolidone). These glycopolymers were used as polymer surfactants, in order to obtain glycosylated polycaprolactone nanoparticles. Optimum stabilization for long time storage was achieved by using a mixture of glycopolymers and the non-ionic triblock copolymer Pluronic® F-68. The mannose moieties are accessible at the surface of nanoparticles and available for molecular recognition by concanavalin A lectin. Interaction of mannose units with the lectin were evaluated by measuring the changes in nanoparticles size by dynamic light scattering in dilute media.

Introduction

Over the last decades, research efforts in pharmaceutical, food and cosmetics technologies have been directed not only towards the syntheses of new bioactive entities or medicines, but also towards new formulations that can enhance the activity of drugs, as well as the elaboration of new drug delivery systems. The main objectives are the transport of active hydrophilic or lipophilic substances, while minimizing drug degradation, increasing drug availability and localization in the required organ. At the same time, the development of "all in one" formulations encourages manufacturers to introduce more and more

active components in the finished products, so that new systems are nowadays widely investigated in order to get synergies in one product, to propose innovative properties and to combine immediate and delayed effects, through the selection of an efficient drug and the design of a suitable dosage form. Encapsulation of hydrophobic substances in aqueous dispersed media can be performed by a number of methods. Notably, synthetic polymer-based nanoparticles have received considerable attention because of their potential since they represent attractive alternatives to conventional pharmaceutical applications. In addition, the size, morphology and composition of the polymer particles can be tuned to optimize the drug release kinetics in order to reduce, e.g., toxicity and improve efficacy. These parameters are closely connected. For instance, the chemical composition of the polymer matrix may affect the particle morphology because of thermodynamic interactions between the hydrophobic drug and the polymer.

Whatever the drug delivery system, surfactants, and in particular polymer non-ionic surfactants, are required to assure the colloidal stabilization of the polymer nanoparticles in aqueous medium. The properties of micelles (cmc, size and dynamics) depend on the chemical structures of amphiphilic copolymers. Macromolecular non-ionic surfactants appear to be the best suited from both the stability and the biological points of view. In such block copolymers, the hydrophobic part is enhanced in comparison to molecular surfactants, which allows a better adsorption (by reducing the exchange dynamics) and increases the long term stability. This stronger adsorption also reduces the residual concentration of free surfactant in the aqueous phase. The hydrophilic part is most often constructed from PEG chains. In addition to the steric stabilization, this PEG coating reduces the detection of particles or liposomes by the immune system and consequently, the reticular endothelial uptake of nanoparticles, thus increasing their circulation in the body. The polyether triblock copolymer PEO-b-PPO-b-PEO Pluronic® F-68 (PF-68) is approved by the US Food and Drug Administration and is thus widely used in pharmaceutical formulations.

Glycopolymers can advantageously replace these block copolymers. In addition to the hydrophilicity conferred by the carbohydrate moiety, specific targeting may be result from coating nanoparticles with oligo- or polysaccharide chains since the carbohydrate moieties play an essential role in molecular recognition processes. Although the carbohydrate ligands occur naturally as glycoconjugates or as high molecular weight polymers, the actual "recognized" fractions are most often small oligosaccharides (3 to 10 carbohydrate units). Efficient binding has also been reported for monosaccharide ligands; for instance, galactose residues are targetable moieties for hepatocytes [1] whilst mannose units can be used for nerve cells targeting [2]. Besides naturally occurring polysaccharides, macromolecular engineering allows quite interesting possibilities for modelling of synthetic glycopolymers [3].

The hydrophobic component can be introduced by any convenient polymer moiety. Some of these are obtained using methodologies based on living polymerizations in order to achieve controlled molecular weights and narrow polydispersity indexes. Depending on the chemistry, carbohydrate moieties can be grafted either at the polymer chain end or as pendant groups on the polymer backbone. Thus, polycaprolactones (PCL) functionalized with galactopyranose end-groups have been synthesized by ring opening polymerization and used for the stabilization of PCL nanoparticles [4]. Glucose or cellobiose moieties have been grafted at both ends of short PDMS chains and used as polymer surfactants for mini-emulsion polymerization [5,6]. Amphiphilic block copolymers with pendant glucosamine units have been obtained by living cationic polymerization and their interaction with wheat germ agglutinin lectin investigated [7]. More recently, the synthesis of neoglycopolymers by living radical polymerization and click chemistry has been reported [8,9].

Besides homopolymers or block copolymers, statistical copolymers obtained from conventional radical polymerization deserve special attention because of their ease of synthesis. Well controlled MW as well as narrow PI are not always prerequisites to achieve interesting colloidal stabilization properties. Carbohydrate residues such as galactosyl moieties have also been incorporated as side groups through the ring opening of maleic anhydride based copolymers [10,11]. We recently reported the synthesis and characterization of amphiphilic copolymers bearing carbohydrate and oligocaprolactone side chains, obtained via copolymerization of a PCL macromonomer and maleic anhydride, and further functionalization by ring opening of the anhydride moiety with amino mannopyranoside. These copolymers were then used as polymer surfactants for the stabilization of PCL nanoparticles coated with carbohydrate on their surface [12].

This paper reports the first results on another class of glycopolymers obtained from the functionalization of poly(propargyl acrylate-co-*N*-vinyl pyrrolidone) by click chemistry with ω-mannopyranoside. These copolymers were used as polymer surfactants for the colloidal stabilization of polycaprolactone (PCL) nanoparticles. Preliminary studies towards the recognition of these glyco-nanoparticles by specific concanavalin A (con A) lectin have been carried out, which provided clear evidence for the presence of carbohydrate units on the surface of the nanoparticles

Results and Discussion

Synthesis and characterization of the polymer surfactants

Besides well-known functionalization of anhydride-based copolymers, the grafting of carbohydrate moieties on a polymer backbone by Huisgen [2 + 3] cycloaddition (CuI-catalyzed 1,3-dipolar cycloaddition of azide and alkynes, CuAAC) constitutes another interesting approach. The versatile nature of this reaction has led to a tremendous amount of work, mainly due to the quantitative yields and the possibility of carrying out the synthesis in either organic solvents or water. Moreover, since various other functional groups can be tolerated, one-pot tandem approaches can be considered [13]. Similarly, in the carbohydrate field, this unique feature makes it possible to conduct syntheses by simplified pathways without protection–deprotection steps. We chose to use poly(propargyl acrylate-co-*N*-vinyl pyrrolidone) as the starting copolymer. Poly(NVP) is known to be biocompatible and to promote adhesion. NVP-based maleic copolymers have been reported for BSA immobilization [14] as well as for the preparation of polymer nanoparticles [10,15].

The choice of the carbohydrate moieties to be grafted onto the copolymer and their related syntheses were based on the following criteria: 1 - the monosaccharide must be anchored onto the polymer backbone by the use of a hydrophilic spacer in order to allow more freedom inside the aqueous phase after adsorption onto the polymer particles; 2 - syntheses must be simple enough to allow scale-up.

Thus, we elected to use the simplest carbohydrates, i.e., those which are easy to prepare and easy to handle, e.g., the peracetylated monosaccharide **1** [16]. Although other derivatives, such as the 2,3,4,6-tetra-*O*-acetyl-1-*O*-trichloroacetimidoyl mannose might give rise to better glycosylation yields, the scale-up of these reactions was shown to be difficult. As a spacer, we chose triethylene glycol. The reaction of **1** with 8-azido-3,6-dioxaoctyloctan-1-ol (prepared in several steps from triethylene glycol) [17] was found to be unsatisfactory since the by-products formed in the reaction were difficult to separate from the desired compounds. The addition of triethylene glycol derivatives was also attempted by coupling triethylene glycol, or an activated triethylene glycol derivative bearing a tosylate or a chlorine atom at the ω-position. This latter approach proved to be better. The best result was obtained with commercially available triethylene glycol monochloride. Thus, peracetylated mannose **1** was reacted with triethyleneglycol monochloride, in the presence of boron trifluoride etherate to afford glycoside **2** [12] in 50–55% yield. After purification, the latter was converted to the azido derivative **3** in almost quantitative yield, by nucleophilic displacement of the chlorine atom by azide ion. Deprotection of the latter under Zemplén conditions [17] afforded the expected derivative **4** in quantitative yield (Figure 1).

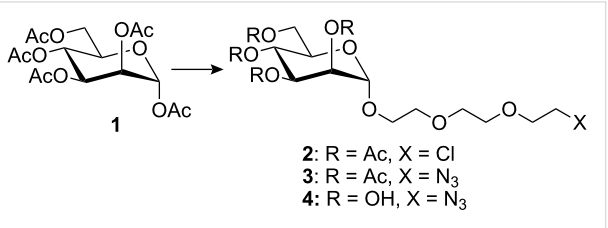


Figure 1: Preparation of the 8-azido-3,6-dioxaoctyl α-D-mannopyranoside.

The copolymer backbones, namely the poly(propargyl acrylate-co-*N*-vinyl pyrrolidone), were prepared by conventional radical copolymerization using propargyl acrylate and *N*-vinyl pyrrolidone as comonomers. The reactions were carried out in dry THF at 65 °C under an argon atmosphere with lauroyl peroxide as the initiator. The copolymers were obtained as a white powders by precipitation in diethyl ether which were dried under vacuum and characterized by IR, ^{1}H and ^{13}C NMR and SEC. Kinetics were also monitored by ^{1}H NMR from the disappearance of the monomer signals. Yields were in the range of 60 to 90%. Although some radical transfer reactions leading to addition to the acetylene groups has been reported on reaching high yields [18], no gel formation was observed in our case during polymerization, so that protection of the propargyl monomer was not required. Molecular weights were around 10000 g/mol with $M_w/M_n \approx 1.6–2.0$. The molar fraction of PA units in the copolymer was in the range of 0.25 to 0.75.

As previously outlined, coupling reactions with sugar moieties generally require protection and deprotection steps of the hydroxyl functions. Click chemistry can of course be performed with peracetylated mannose followed by deprotection, but this involves all the drawbacks inherent to polymer structures. Due to the high versatility of click chemistry in the presence of functional groups, it was then of interest to attempt the reaction with unprotected sugars. Moreover, this chemistry can be carried out not only in various organic solvents, but also in aqueous alcoholic media and water. In our case, the click reaction was performed with $CuSO_4$ and sodium ascorbate in a THF/water mixture (Figure 2). This approach was preferred to the use of other catalysts because of the applications listed in the specific area of colloidal stabilization and the ease of removal of copper salts with ethyl xanthogenate or cation exchange resin. Moreover, sodium ascorbate is far easier to remove in contrast to DIPEA or bipyridine and additionally, it would not be of any great consequence if some residual sodium ascorbate remained in the medium. The resulting grafted copolymers were fully

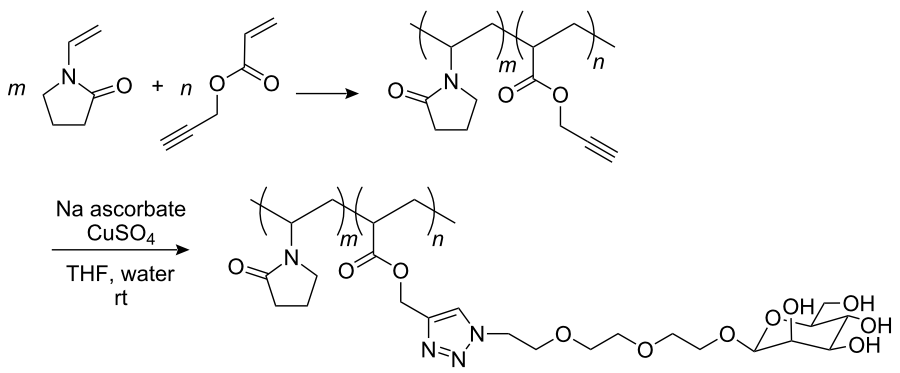


Figure 2: Preparation of poly(propargyl-co-*N*-vinyl pyrrolidone) and subsequent addition of the mannose derivative by click chemistry.

characterized by IR (disappearance of $\nu(N_3)$ at 2121 cm^{-1} and $\nu(C{\equiv}C)$ at 2129 cm^{-1}) and NMR: ^1H (δ H_{12} at 8.06 ppm) and ^{13}C (δ C_{11} and C_{12} respectively, at 143.32 and 125.82 ppm). DEPT experiments were used to ascertain the chemical shifts and to ensure the complete conversion of the azide functions. These copolymers are water soluble.

Recognition of PCL nanoparticles by concanavalin A

Lectins are proteins of non-immunological origin, able to bind carbohydrate ligands, without any enzymatic or immunological function. They are multivalent and can bind several ligands simultaneously and participate in biological phenomena such as cell adhesion or cell–cell recognition. The specific binding of a lectin receptor with a carbohydrate ligand (usually called recognition) is obtained, provided that the ligands are orientated in a specific manner that can fit several lectin receptors and is usually referred to as the cluster effect [19,20]. The lectin–carbohydrate specificity strongly depends on the lectin. Several of these are very sensitive to the nature of the carbohydrate (e.g. Man vs Gal), whereas others are more sensitive to the orientation of the anomeric substituent (i.e. α vs β). Concanavalin A, used in the present work, belongs to the latter group and displays strong specificity towards α-D-mannopyranose. This lectin is dimeric and divalent at pH < 5.6 and tetrameric and tetravalent at pH > 5.6. Its specificity is directed to α-D-mannopyranosides and to a lesser extent to α-D-glucopyranosides and α-D-galactopyranosides, and shows no affinity at all towards β-D-monosaccharides [21].

Consequently, the addition of a tetravalent lectin to a suspension of nanoparticles covered with large amounts of its specific ligands should lead to agglutination of the particles, thus giving rise to flocculation or precipitation, whereas the suspension should remain unchanged on the addition of "naked" nanoparticles (without any carbohydrate on their surface) or nanoparticles covered with non specific carbohydrates. This increase in size can be observed either by the naked eye, turbidity or fluorescence measurements as previously reported in the literature [7,22]. Measurements by light scattering have only occasionally been reported in the literature [23].

Polycaprolactone nanoparticles were prepared according to the emulsification–diffusion procedure as proposed by Quintanar and Fessi [24,25] by using a mixture of PEO-b-PPO-b-PEO triblock copolymer (Pluronic® F-68) and our functionalized copolymers as polymer surfactants. This technique is based on the rapid diffusion of the organic solvent from the internal into the external phase, which causes the precipitation of the polymer as colloidal nanoparticles. We previously used this procedure to obtain polycaprolactone nanoparticles with end-capped oligocaprolactones with galactopyranose moieties as polymer surfactants [4].

In this case, some previous studies have clearly shown that the glycopolymers employed alone are unable to assure colloidal stabilization of polymers in dispersed media. This behavior was observed when using other types of glycopolymers [6,12] where a second polymer surfactant was required to assure a stable colloidal stabilization upon long time storage. This was tentatively interpreted in terms of layer thickness of the polymer surfactant adsorbed onto the particles.

We used here Pluronics instead of poly(vinyl alcohol) (PVA), as proposed by Quintanar and Fessi, to get a higher solid content for the nanoparticles suspensions (the evaporation step rapidly leads to highly viscous suspensions because of the high molecular weight of PVA). Some other advantages of Pluronics for biomedical applications have already been detailed in the introduction. Nanoparticles stabilized by Pluronic® F-68 and 20% (w/w) of the glycopolymers previously prepared were used in our investigations.

In a first set of experiments, increasing amounts (10 to 1000 µL) of a con A solution (8.7 mg/10 mL of PBS, pH 6.8) were added to nanoparticles stabilized by only Pluronic® F-68. No changes in size were observed over a 2 h period irrespective of the con A concentration. Similarly, no significant change in size was recorded over 2 h on the addition of increasing amounts of con A to PCL particles stabilized by a mixture of Pluronic® F-68 and the precursor poly(PA-co-NVP) (20% w/w).

The same results were observed when either crude suspensions of nanoparticles or their supernatants after centrifugation (2000 g; 1 h) were used. The same tendencies were also observed with the re-suspended pellets, but the results were not so relevant since more important variations in size were observed from one sample to another. Thus, the recognition experiments then conducted only with the supernatant fractions of the particle suspensions. All the observations that will be described were also true for crude suspensions as well as re-suspended pellets however, the supernatants are more homogenous and the more abundant fractions, and contain about 65 % (of the dry weight) of nanoparticles.

This time increasing amounts of con A were added to the supernatant fraction of colloidal suspensions of nanoparticles stabilized by the mixture of PF-68 and NVP-PA-Man. A very important increase in size was observed, even with low amounts of lectin (50 µL). The kinetics of size increase was proportional to the amount of lectin added (Figure 3). Furthermore, flocculation occurred with the highest concentrations and the suspensions changed from clear colorless to milky. As can be seen from Figure 3, changes in size were drastic, giving rise to aggregates of almost 2 µm in diameter, i.e. ten times the size of isolated nanoparticles.

Particles covered with β-D-galactose were used as control experiments since concanavalin A has no affinity for this monosaccharide. Some of the experiments were repeated under the same conditions with nanoparticles covered with D-galactose, i.e. stabilized by a mixture of PF-68 and NVP-PA-Gal. No change in size was observed over 2 h (<30 nm) irrespective of the amount of added lectin. This result corroborates the previous assumption regarding the observations made with the first group of nanoparticles, i.e. the apparent non specific binding of the lectin can be attributed the formation of a covalent bond between the protein and the residual anhydride functions of the glycopolymer.

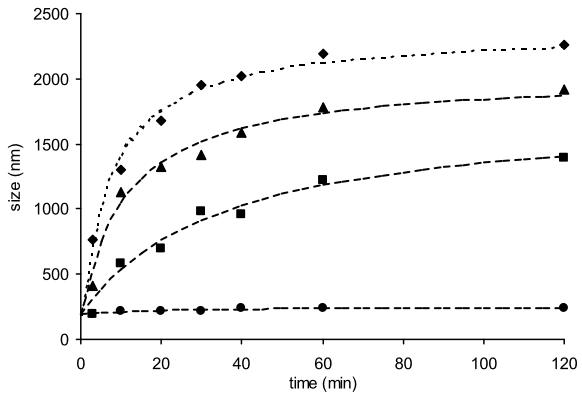


Figure 3: Size of the nanoparticles stabilized with Pluronic® F-68/NVP-PA-Man (0.8/0.2), after addition of increasing amounts of con A. ● 10 µL; ■ 50 µL; ▲ 100 µL; ♦ 1000 µL. Measurements realized on supernatant of centrifuged nanoparticles.

Conclusion

Water soluble glycopolymers can easily be prepared by the CuI-catalyzed cycloaddition of an azido mannopyrannoside derivative and a poly(propargyl acrylate-co-*N*-vinyl pyrrolidone). These glycopolymers can be used as polymer surfactants, in conjunction with another non-ionic triblock copolymer in order to obtain glycosylated polycaprolactone nanoparticles stable over a long period of storage.

The carbohydrates covalently bound to the copolymers are accessible at the surface of the nanoparticles and are available for molecular recognition. The recognition of α-D-mannose at the surface of the nanoparticles by con A is specific, provided that no further reactive groups which could covalently bind the lectin are present on the polymer. In addition, light scattering appears to be the method of choice to detect carbohydrate recognition by a lectin at the surface of nanoparticles in dilute media. This approach can be easily extended to multifunctional polymer nanoparticles containing encapsulated drugs inside their core.

Experimental

The syntheses of 8-chloro-3,6-dioxaoctyl 2,3,4,6-tetra-*O*-acetyl-α-D-mannopyranoside (**2**) and 8-azido-3,6-dioxaoctyl 2,3,4,6-tetra-*O*-acetyl-α-D-mannopyranoside (**3**) were reported in a previous paper [12].

Materials

Polycaprolactone (MW 80000 g/mol), Pluronic® F-68 and propargyl acrylate were purchased from Aldrich. *N*-Vinyl pyrrolidone and lauroyl peroxide were purchased from Fluka. Thin layer chromatography was performed on aluminium sheets coated with Silica gel 60 F_{254} (Merck). Compounds were visualized by spraying the TLC plates with dilute 15% aq. H_2SO_4, followed by charring at 150 °C for a few minutes. Column chromatography was performed on Silica-gel Geduran Si 60

(Merck). ^{1}H and ^{13}C NMR spectra were recorded with a Bruker DRX-300 spectrometer at 300 MHz and 75 MHz respectively, or with a Bruker DRX-500 spectrometer at 500 MHz and 125 MHz respectively, with TMS as internal standard. High resolution mass spectra were recorded with a ThermoFinnigan MAT95XL double focusing mass spectrometer equipped with an ESI III source.

8-Azido-3,6-dioxaoctyl α-D-mannopyranoside (**4**)

The protected derivative **3** (500 mg, 0.99 mmol) was dissolved in dry methanol (10 mL) and stirred for 1h at room temperature in the presence of a catalytic amount of sodium. The mixture was then neutralized with Amberlist IR 120 H^+ resin, filtered and evaporated to afford compound **4** in quantitative yield as a clear oily material. $[\alpha]_D$ +38.7 (c 1.0, 25 °C, MeOH). R_f 0.49 (5:1, ethyl acetate/methanol). ^{1}H NMR (D_2O): δ (ppm) 4.79 (d, 1H, $J_{1,2}$ 1.5 Hz, H-1), 3.86 (dd, 1H, $J_{2,3}$ 3.6 Hz, $J_{3,4}$ 9.2 Hz, H-3), 3.81 (t, 1H, H-4), 3.77 (dd, 1H, H-2), 3.63 (m, 12H, H-6, H-6′, (OCH_2CH_2)$_2CH_2$), 3.56 (m, 1H, H-5), 3.42 (t, 2H, CH_2N_3). ^{13}C NMR (CD_3OD): δ (ppm) 100.30 (C-1), 73.09 (C-5), 70.00, 69.92, 69.87 (OCH_2CH_2)$_2OCH_2$), 70.87 (C-2), 70.32 (C-3), 67.09 (C-4), 61.28 (C-6), 50.51 (CH_2N_3). HRMS (ESI) *m/z* Calcd for $[C_{12}H_{25}O_8N+Na]^+$ 360.13830; Found 360.13837.

Poly(propargyl acrylate-co-*N*-vinyl pyrrolidone)

Copolymerizations were carried out in dry THF at 65 °C under an argon atmosphere with 3–5% of lauroyl peroxide as the initiator. For example, propargyl acrylate (0.309 g, 2.93 mmole) and *N*-vinyl pyrrolidone (0.095 g, 0.85 mmol) were dissolved in dry THF (20 mL) at 65 °C. The solution was degassed for 15 min with argon, before the addition of lauroyl peroxide (0.060 g, 0.15 mmol). After 8 h, the copolymer was recovered as a white powder by precipitation in diethyl ether (three times), dried under vacuum (85% yield) and characterized by IR (ν(C≡C) at 2129 cm^{-1}), ^{1}H and ^{13}C NMR (Figure 4).

^{1}H NMR ($CDCl_3$, 300 MHz): δ (ppm) 5.75 (H-1); 4.5–4.95 (H-10); 3.6–4.2 (H-2); 3.25 (H-7); 2.55 (H-12); 2.35 (H-4); 1.3–2.1 (H-3, H-6, H-8). ^{13}C NMR ($CDCl_3$, 125 MHz): δ (ppm) 174.19–175.79 (C-5, C-9), 75.77 (C-11), 79.36 (C-12), 52.68 (C-10), 47.91 (C-1), 39.03 (C-78), 35.42 (C-2), 31.67 (C-4), 26.00–26.07 (C-6, C-8), 18.57 (C-3).

Coupling of azido functionalized carbohydrates by CuAAC

The dry copolymer (100 mg, containing approximately 75 mg, 0.68 mmol of propargyl acrylate) and compound **4** (229 mg, 1.0 equiv vs propargyl acrylate) were dissolved in a 1:1 mixture of THF and water (4 mL) at room temperature. After the addition of $CuSO_4$ (6 mg, 0.02 mmol) and sodium ascorbate (18 mg, 0.09 mmol), the mixture was stirred at room temperature for 12 h, the solution evaporated to dryness and dried under vacuum. The light green product thus obtained was dissolved in de-ionized water (5 mL) containing 50 mg of potassium ethyl xanthogenate to remove the copper salts. After filtration through celite and evaporation to dryness, the desired mannose-functionalized copolymer was obtained as a pale yellow solid in 73% yield.

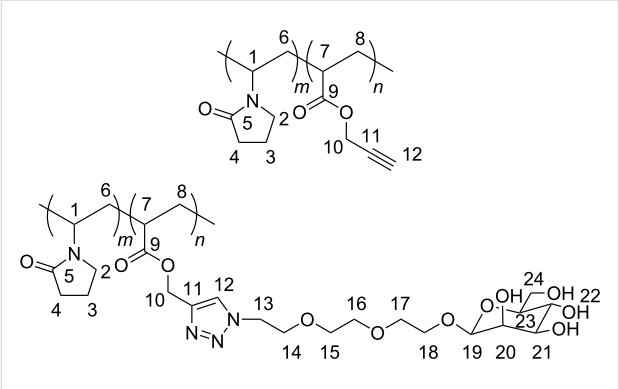


Figure 4: Hydrogen and carbon numbering for NMR assignment.

^{1}H NMR (CD_3OD, 500 MHz): δ (ppm) 8.06 (H-12), 5.8 (H-1), 5.10 (H-10), 4.6–4.85 (4 OH, H-19), 4.56 (H-2), 3.50–4.10 (H-13/H-18, H-20/H-24), 3.10 (H-8), 2.35 (H-4), 1.20–2.10 (H-3, H-6, H-7). ^{13}C NMR (CD_3OD, 125 MHz): δ (ppm) 174.20–178.50 (C-5, C-9), 143.32 (C-11), 125.82 (C-12), 100.75 (C-19), 73.37 (C-20), 71.74 (C-21), 71.10 (C-23), 69.50 (C-15, C-16, C-17, C-18), 67.82 (C-22), 66.93 (C-14), 62.05 (C-24), 58.07 (C-10), 50.65 (C-13), 48.40 (C-1), 40.04 (C-7), 35.00 (C-2), 31.48 (C-4), 26.00–26.50 (C-6, C-8), 18.27 (C-3).

Nanoparticle formation

Ethyl acetate and water were contacted for 2 h in order to obtain mutually saturated solutions. Polycaprolactone (80000 g/mol) (1.0 g) was dissolved in ethyl acetate (25 mL) under gentle stirring and heating for 2 h (ethyl acetate was added in order to adjust the volume to 25 mL). Pluronic® F-68 and the glycopolymer, dissolved in water (50 mL), were then added to the preceding solution, the mixture stirred for 10 min and then emulsified by sonication (ultrasonic processor Vibra Cell VCX-750) for 2 min at 525 W. De-ionized water (175 mL) was then added while stirring the solution at 700–800 rpm. The nanoparticle suspension was then concentrated at atmospheric pressure to 30–35 mL by stirring and heating to 70–80 °C.

The sizes of nanoparticles were measured by dynamic light scattering (each measurement was repeated five times) at 25 °C

with a Malvern Zetasizer 1000HSa series (wavelength 633.0 nm, RI (dispersant) 1.330, angle 90°); data treatments were made in intensity, with water viscosity 0.89 cP.

Interaction of the nanoparticles containing D-mannose with con A

In a 20 mL flask, 8.7 mg of concanavalin A was dissolved without stirring in 10 mL of phosphate-buffered saline (PBS, pH = 6.8, 0.1 M) over 16 hours. The flask was then stored at 4 °C. The nanoparticle stock solution (200 mg of dry matter in 3.5 mL H_2O) was diluted in PBS and various volumes of con A solution in the same buffer solution (10, 20, 50, 100, 200, 500, 1000 μL) were added; the final volume was adjusted to 5 mL by addition of PBS.

References

1. Muraji, Y.; Nakagawa, Y.; Yamane, S.; Kawanami, S.; Aoki, T.; Saito, S.; Ikai, A. *Jpn. J. Appl. Phys.* **2006,** *45,* 2298–2300. doi:10.1143/JJAP.45.2298
2. Galea, I.; Palin, K.; Newman, T. A.; Van Rooijen, N.; Perry, H. V.; Boche, D. *Glia* **2005,** *49,* 375–384. doi:10.1002/glia.20124
3. Okada, M. *Prog. Polym. Sci.* **2001,** *26,* 67–104. doi:10.1016/S0079-6700(00)00038-1
4. Hamaide, T.; Pantiru, M.; Fessi, H.; Boullanger, P. *Macromol. Rapid Commun.* **2001,** *22,* 659–663. doi:10.1002/1521-3927(20010601)22:9<659::AID-MARC659>3.0.CO;2-4
5. Racles, C.; Hamaide, T. *Macromol. Chem. Phys.* **2005,** *206,* 1757–1768. doi:10.1002/macp.200500139
6. Berson, S.; Halila, S.; Driguez, H.; Viet, D.; Fleury, E.; Hamaide, T. *Macromol. Chem. Phys.* **2008,** *209,* 1814–1825. doi:10.1002/macp.200800194
7. Yamada, K.; Minoda, M.; Miyamoto, T. *Macromolecules* **1999,** *32,* 3553–3558. doi:10.1021/ma9816315
8. Ladmiral, V.; Mantovani, G.; Clarkson, G. J.; Cauet, S.; Irwin, J. L.; Haddleton, D. M. *J. Am. Chem. Soc.* **2006,** *128,* 4823–4830. doi:10.1021/ja058364k
9. Geng, J.; Mantovani, G.; Tao, L.; Nicolas, J.; Chen, G.; Wallis, R.; Mitchell, D. A.; Johnson, B. R. G.; Evans, S. D.; Haddleton, D. M. *J. Am. Chem. Soc.* **2007,** *129,* 15156–15163. doi:10.1021/ja072999x
10. Cade, D.; Ramus, E.; Rinaudo, M.; Auzely-Velty, R.; Delair, T.; Hamaide, T. *Biomacromolecules* **2004,** *5,* 922–927. doi:10.1021/bm034504b
11. Satoh, A.; Kojima, K.; Koyama, K.; Ogawa, H.; Matsumoto, I. *Anal. Biochem.* **1998,** *260,* 96–102. doi:10.1006/abio.1998.2668
12. Otman, O.; Boullanger, P.; Lafont, D.; Hamaide, T. *Macromol. Chem. Phys.* **2008,** *209,* 2410–2422. doi:10.1002/macp.200800300
13. Damiron, D.; Desorme, M.; Ostaci, R. V.; El Akhrass, S.; Hamaide, T.; Drockenmuller, E. *J. Polym. Sci., Part A: Polym. Chem.* **2009,** *47,* 3803–3813. doi:10.1002/pola.23438
14. Veron, L.; Revol, M.; Mandrand, B.; Delair, T. *J. Appl. Polym. Sci.* **2001,** *81,* 3327–3337. doi:10.1002/app.1789
15. Iojoiu, C.; Cade, D.; Fessi, H.; Hamaide, T. *Polym. Int.* **2005,** *55,* 222–228. doi:10.1002/pi.1964
16. Wilhelm, F.; Chatterjee, S. K.; Rattay, B.; Nuhn, P.; Benecke, R.; Ortwein, J. *Liebigs Ann.* **1995,** *9,* 1673–1679. doi:10.1002/jlac.1995199509232
17. Thompson, A.; Wolfrom, M. L. In *Methods in Carbohydrate Chemistry;* Whistler, R. L.; Wolfrom, M. L., Eds.; Academic Press, Inc.: New York, 1963; Vol. 2, pp 215–220.
18. Summerlin, B. S.; Tsarevsky, N. V.; Louche, G.; Lee, R. Y.; Matyjaszewski, K. *Macromolecules* **2005,** *38,* 7540–7545. doi:10.1021/ma0511245
19. Mammen, M.; Choi, S. K.; Whitesides, G. M. *Angew. Chem., Int. Ed.* **1998,** *37,* 2754–2794. doi:10.1002/(SICI)1521-3773(19981102)37:20<2754::AID-ANIE2754>3.0.CO;2-3
20. Lundquist, J. J.; Toone, E. J. *Chem. Rev.* **2002,** *102,* 555–578. doi:10.1021/cr000418f
21. Goldstein, I. J.; Hayes, C. E. *Adv. Carbohydr. Chem. Biochem.* **1978,** *35,* 127–340. doi:10.1016/S0065-2318(08)60220-6
22. Kitano, H.; Kawabata, J.; Muramoto, T. *Macromol. Chem. Phys.* **1996,** *197,* 3657–3666. doi:10.1002/macp.1996.021971113
23. Kanellopoulos, P. N.; Pavlou, K.; Perrakis, A.; Agianian, B.; Vorgias, C. E.; Mavrommatis, C.; Soufi, M.; Tucker, P. A.; Hamodrakas, S. J. *J. Struct. Biol.* **1996,** *116,* 345–355. doi:10.1006/jsbi.1996.0052
24. Quintanar-Guerrero, D.; Allemann, E.; Doelker, E.; Fessi, H. *Colloid Polym. Sci.* **1997,** *275,* 640–647. doi:10.1007/s003960050130
25. Quintanar-Guerrero, D.; Allemann, E.; Doelker, E.; Fessi, H. *Pharm. Res.* **1998,** *15,* 1056–1062. doi:10.1023/A:1011934328471

License and Terms

This is an Open Access article under the terms of the Creative Commons Attribution License (http://creativecommons.org/licenses/by/2.0), which permits unrestricted use, distribution, and reproduction in any medium, provided the original work is properly cited.

The license is subject to the *Beilstein Journal of Organic Chemistry* terms and conditions: (http://www.beilstein-journals.org/bjoc)

The definitive version of this article is the electronic one which can be found at: doi:10.3762/bjoc.6.58

Beilstein Journal of Organic Chemistry

Synthesis and crossover reaction of TEMPO containing block copolymer via ROMP

Olubummo Adekunle, Susanne Tanner and Wolfgang H. Binder*

Full Research Paper

Open Access

Address:
Institute of Chemistry, Faculty of Natural Sciences II (Chemistry and Physics), Martin-Luther University, Halle-Wittenberg, von Danckelmannplatz 4, D-06120 Halle, Germany

Email:
Olubummo Adekunle - olubummo.adekunle-ayodele@student.uni-halle.de;
Susanne Tanner - susanne.tanner@chemie.uni-halle.de;
Wolfgang H. Binder* - wolfgang.binder@chemie.uni-halle.de

* Corresponding author

Keywords:
block copolymer (BCP); crossover reaction; MALDI; NEOLYST™; ROMP

Beilstein J. Org. Chem. **2010,** *6,* No. 59. doi:10.3762/bjoc.6.59

Received: 25 February 2010
Accepted: 14 May 2010
Published: 01 June 2010

Guest Editor: H. Ritter

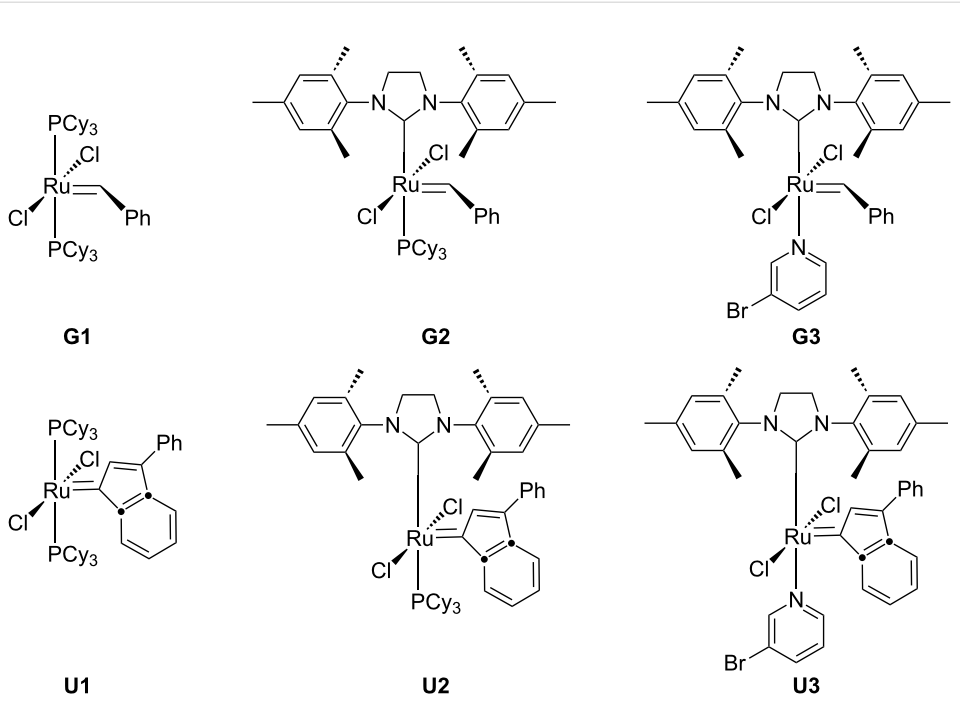
© 2010 Adekunle et al; licensee Beilstein-Institut.
License and terms: see end of document.

Abstract

We report on the block copolymerization of two structurally different norbornene monomers (±)-*endo*,*exo*-bicyclo[2.2.1]-hept-5-ene-2,3-dicarboxylic acid dimethylester (**7**), and (±)-*endo*,*exo*-bicyclo[2.2.1]-hept-5-ene-2,3-dicarboxylic acid bis(1-oxyl-2,2,6,6-tetramethyl-piperidin-4-yl) ester (**9**) using ruthenium based Grubbs' type initiators [$(PCy_3)_2Cl_2Ru$(benzylidene)] **G1** (PCy_3 = tricyclohexylphosphine), [$(H_2IMes)(PCy_3)Cl_2Ru$(benzylidene)] **G2** (H_2IMes = 1,3-bis(mesityl)-2-imidazolidinylidene), [$(H_2IMes)(py)_2Cl_2Ru$(benzylidene)] **G3** (py = pyridine or 3-bromopyridine) and Umicore type initiators [$(PCy_3)_2Cl_2Ru$(3-phenylinden-1-ylidene)] **U1** (PCy_3 = tricyclohexylphosphine), [$(H_2IMes)(PCy_3)Cl_2Ru$(3-phenylinden-1-ylidene)] **U2** (H_2IMes = 1,3-bis(mesityl)-2-imidazolidinylidene), [$(H_2IMes)(py)Cl_2Ru$(3-phenylinden-1-ylidene)] **U3** (py = pyridine or 3-bromopyridine) via ring opening polymerization (ROMP). The crossover reaction and the polymerization kinetics were investigated using matrix assisted laser desorption ionization mass spectroscopy (MALDI-TOF) and nuclear magnetic resonance (NMR), respectively. MALDI showed that there was a complete crossover reaction after the addition of 25 equivalents of the second monomer. NMR investigation showed that **U3** gave a faster rate of polymerization in comparison to **U1**. The synthesis of block copolymers with molecular weights up to M_n = 31 000 g/mol with low polydispersities (M_w/M_n = 1.2) is reported.

Introduction

Block copolymers are macromolecules composed of linear or non-linear arrangements of chemically different polymeric chains. If the different blocks are incompatible, a rich variety of well defined self-assembled structures both in bulk and selective solvents arises [1]. The synthetic approach to block copolymers has been widely discussed [1] and achieved extensively via living polymerization methods. Thus, besides acyclic diene metathesis polymerization (ADMET) [2], ring opening

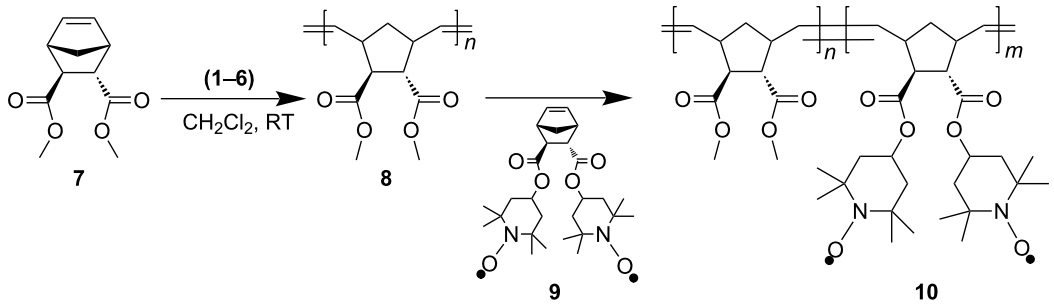


Scheme 1: Grubbs **G1**–**G3** and Umicore **U1**–**U3** catalyst.

metathesis polymerization (ROMP) [3-5] is another type of olefin metathesis polymerization that can be used for the synthesis of block copolymers.

Early examples of catalysts for ROMP were based on molybdenum alkylidene catalysts, however, the true breakthrough of the method was hampered by the restricted functional group tolerance of Schrock initiators due to their sensitivity towards protic solvents and air [6]. With the advent of the Grubbs' catalyst **G1** (see Scheme 1) and related complexes as initiators, polymerization reactions can now not only be performed in protic media but also without rigorous exclusion of molecular oxygen. However, these advantages are hampered by the considerable lower activity of catalysts such as **G1** when compared with Schrock's molybdenum catalysts [7-9]. Often, the polydispersity indices of the resulting polymers obtained with initiator **G1** are large with values ranging between 1.3 and 1.5 arising from an unfavorable rate of initiation (k_i) relative to propagation (k_p) as well as considerable secondary metathesis (backbiting). Grubbs' second generation catalyst **G2** displays an activity comparable to the Schrock type initiators. It exhibits a higher functional group tolerance than **G1**, but initiation by catalyst **G2** is often slow as a result of the slow dissociation of the phosphine group, sometimes limiting its application in polymer synthesis. Alternatively, Grubbs' third generation catalyst **G3** introduced by Grubbs et al. [10] has an ultrafast initiating ruthenium benzylidene. The rate of reaction of **G3** with ethyl vinyl ether thus is six orders of magnitude higher than for **G2** [10], leading to a faster initiation and often lower polydispersities of the resulting polymers.

Recently, structural variations of **G1**–**G3** catalysts generated a new series of catalysts **U1**–**U3** bearing indenyl-carbenes instead of benzylidene-carbenes. These new catalysts are now commercially available and are well known as the Umicore catalysts (NEOLYST™). However, their synthetic profile with respect to the synthesis of block copolymers is largely unexplored. As we recently have reported extensively on the use of ROMP methods in blockcopolymer synthesis [11-13], either via direct copolymerization or coupled to postmodification methods via azide/alkyne-"click"-chemistry [14-17], the crossover reaction of more complex monomers remains the crucial factor in achieving defined BCP's with low polydispersities. In a recent example, the crossover reaction of various monomers with the Grubbs' type catalysts **G1**–**G3** was studied in detail via MALDI mass spectrometry [11], revealing a more detailed picture of the crossover reaction (Scheme 2). Thus mass spectrometry could often demonstrate insufficient crossover reactions between monomers of different reactivity such as monomer A **7** and monomer T **9**, despite a low polydispersity when the crossover reaction was monitored by conventional GPC methods [11]. A semi-quantification method of the respective spectra allowed a good correlation between the rate-constants of initiation and propagation of the different monomers.



Scheme 2: Synthetic pathway to BCP-A_nT_m using Grubbs' (**1**–**3**) and Umicore (**4**–**6**) type catalysts.

The current publication describes the synthesis of block copolymers A_nT_m composed of monomers **7** and **9**, initiated via the catalysts **U1**–**U3**, as well as mass spectrometric investigations of the crossover reactions via MALDI methods. The incorporation of the free radical **9** into block copolymer is an important contribution in the generation of polymers for reversible charge storage materials, as monomer **9** can accept or donate electrons reversibly.

Results and Discussion

The polymerization of monomer **7** was investigated using catalysts **U1**–**U3** (see Table 1). Basically, the catalyst **U3** showed good polymerization behavior, furnishing the homopolymers (entries 2, 3) with excellent control of chain length and low polydispersities (M_w/M_n = 1.2). The catalysts **U1** and **U2** gave poor results (see entries 4 and 5) presumably due to slow initiation and fast polymerization, which is in accord with the struc-

Table 1: Overview of polymerization result of monomer A **7** and monomer T **9** with the catalysts **U1**–**U3** and **G1**–**G3**.

entry	polymer	1st monomer	2nd monomer	catalyst	molecular weight (g/mol)		PDI
					GPC	calculated	
1	Homo-A_{15}[a]	Mon-A	—	**G3**	3700	3100	1.1
2	Homo-A_{15}[a]	Mon-A	—	**U3**	2700	3150	1.2
3	Homo-A_{25}[a]	Mon-A	—	**U3**	4410	5250	1.2
4	Homo-A_{50}[b]	Mon-A	—	**U1**	8500	10500	1.2
5	Homo-A_{50}[b]	Mon-A	—	**U2**	418000	10500	1.4
6	Homo-T_{20}	Mon-T	—	**G2**	12900	9800	1.7
7	Homo-T_{100}[b]	Mon-T	—	**G3**	48800	49000	1.3
8	Homo-T_{50}[b]	Mon-T	—	**U3**	24100	24500	1.3
9	BCP-$A_{15}T_1$[a]	Mon-A	Mon-T	**U3**	3200	3640	1.1
10	BCP-$A_{15}T_2$[a]	Mon-A	Mon-T	**U3**	4020	4130	1.2
11	BCP-$A_{15}T_4$[a]	Mon-A	Mon-T	**U3**	4400	5110	1.1
12	BCP-$A_{25}T_1$[a]	Mon-A	Mon-T	**U3**	5100	5740	1.1
13	BCP-$A_{25}T_2$[a]	Mon-A	Mon-T	**U3**	5500	6230	1.1
14	BCP-$A_{25}T_4$[a]	Mon-A	Mon-T	**U3**	6100	7770	1.1
15	BCP-$A_{15}T_1$[a]	Mon-A	Mon-T	**G3**	4600	3640	1.1
16	BCP-$A_{15}T_2$[a]	Mon-A	Mon-T	**G3**	4900	4140	1.1
17	BCP-$A_{15}T_5$[a]	Mon-A	Mon-T	**U3**	5680	7700	1.1
18	BCP-$A_{25}T_{25}$	Mon-A	Mon-T	**U3**	17000	17500	1.1
19	BCP-$A_{50}T_{50}$	Mon-A	Mon-T	**U3**	31300	35000	1.2
20	BCP-$A_{10}T_{10}$	Mon-A	Mon-T	**U3**	7300	7000	1.1
21	BCP-$A_{20}T_{20}$	Mon-A	Mon-T	**U3**	13400	14000	1.1

[a]The polymer was synthesized for MALDI analysis.
[b]The experiment was performed for kinetic measurements by taking samples every 5 minutes.

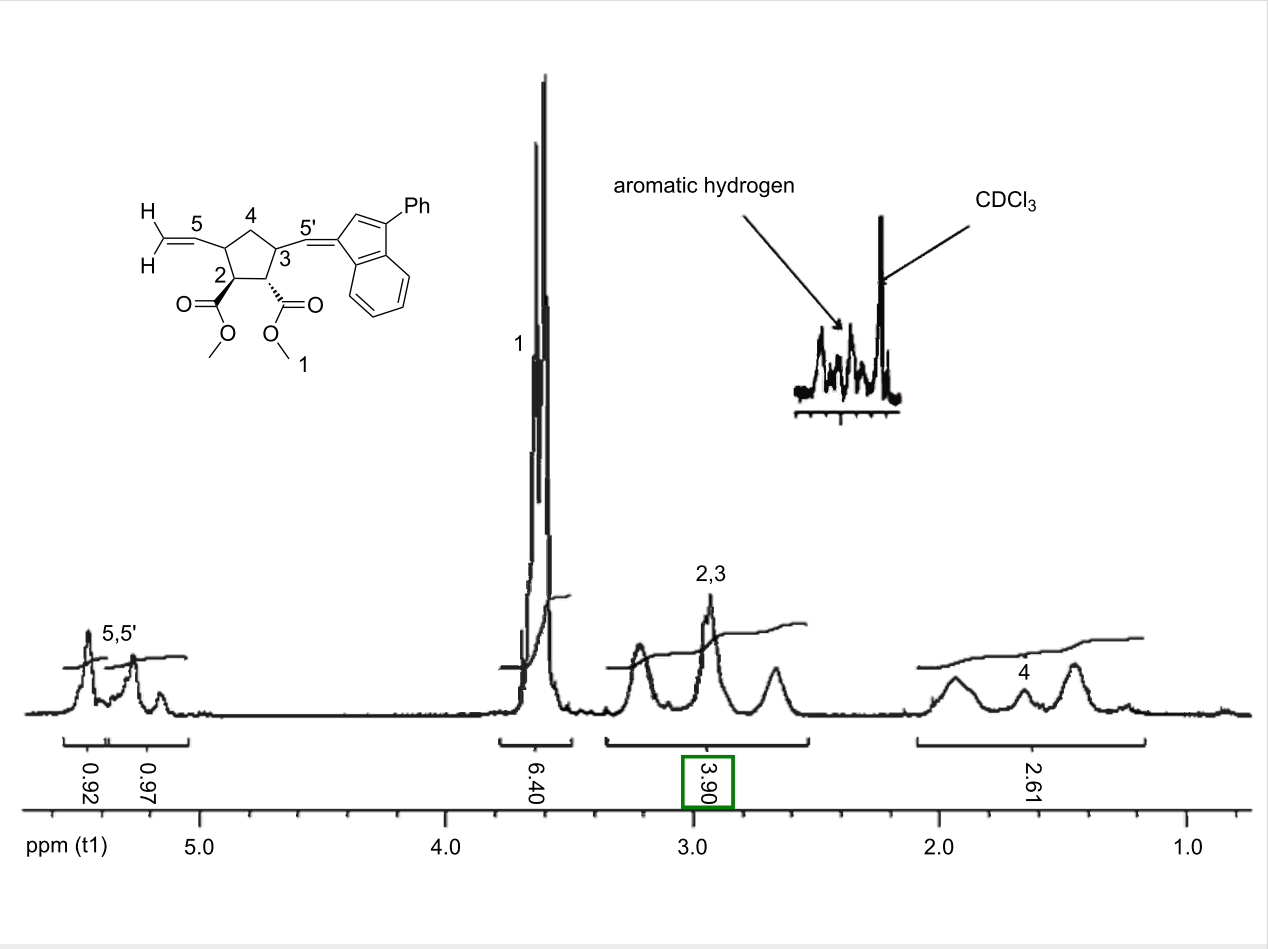


Figure 1: ^{1}H NMR spectrum of the homopolymer A_{50} synthesized with the catalyst **U3**.

turally similar catalysts **G1** and **G2** (see Scheme 1). Similarly, the polymerization of monomer T **9** was investigated, which gave good results with the catalysts **G2**, **G3**, and **U3** (entries 6, 7, and 8). The other catalysts **G1**, **U1**, and **U2** did not yield good polymerization results (data not shown) and were therefore not considered further for the synthesis of the respective block copolymers.

The ^{1}H NMR spectrum (Figure 1) of the respective homopolymer (A_{50}) clearly shows the expected resonances together with the resonances of the indenyl-moieties of the initiator-structure. The spectrum further revealed that the unsaturated polymer exhibited no stereoregularity (*cis*/*trans* ~ 50/50 see the peaks at 5.2 and 5.4 ppm in Figure 1) which is in accordance with results reported in the literature [18]. Figure 2 shows the relevant region of the ^{13}C NMR spectrum, with the approximately equal peak intensities indicating an equal *m*:*r* ratio. Thus the polymerization yields the respective polymer, although in poor yields which is underlined when monitoring the kinetics of the polymerization of monomer A **7** using catalysts **U1** and **U3** (see Figure 3, Figure 4 and Figure 5). As expected in accordance with the known polymerization reactions of the respective Grubbs' type catalysts, catalyst **U3** polymerizes significantly faster (the polymerization reaction is complete after ~20 seconds) whereas the polymerization initiated with catalyst **U1** takes significantly longer and never yields significant amounts of the homopolymer (yield < 10 %).

As the polymerization kinetics of **7** using catalyst **U3** could not be monitored effectively with GPC because it was too fast (50 units were polymerized in less than 1 minute), the kinetics were monitored by NMR. NMR measurements were conducted every 8 seconds and the result showed that the polymerization was complete within ~20 seconds as shown in Figure 4 and Figure 5. The rate of polymerization (k_p) was calculated by integrating the peaks (6.25 and 6.07 ppm) corresponding to the alkene protons of monomer A **7** as they disappeared. Plotting $\ln([M]_0/[M]_t)$ vs. time (t) gave a straight line as shown in Figure 5 and indicated linear chain growth. The slope of the straight line was divided by the initial initiator concentration $[I]_0$ assuming a first order kinetics which gave k_p as 18.5 $l \cdot mol^{-1} \cdot s^{-1}$.

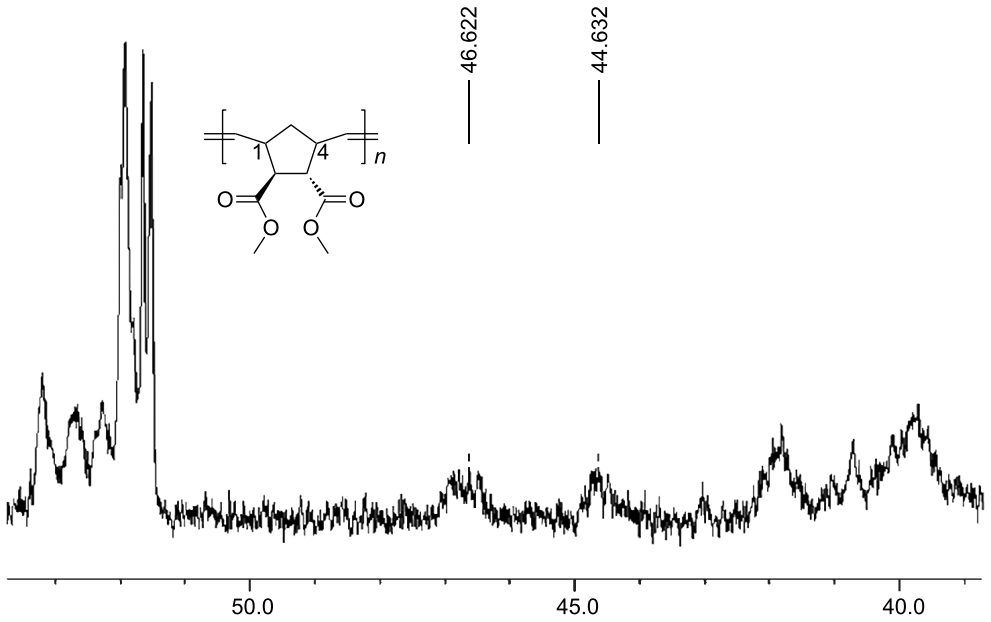


Figure 2: ^{13}C NMR spectrum of the homopolymer A_{50} synthesized with catalyst **U3**.

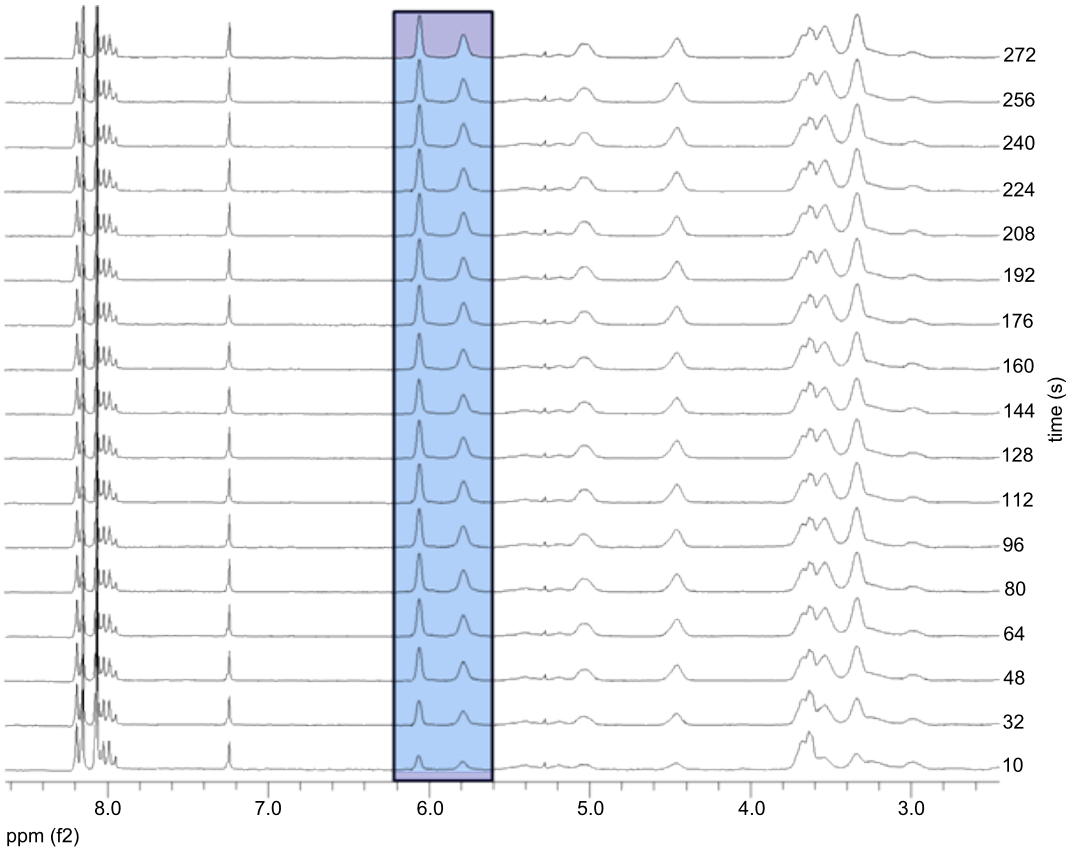


Figure 3: Kinetic progress monitored via ^1H NMR spectroscopy of the polymerization of monomer A **7** with catalyst **U1**; [**7**]/[**U1**] = 20/1.

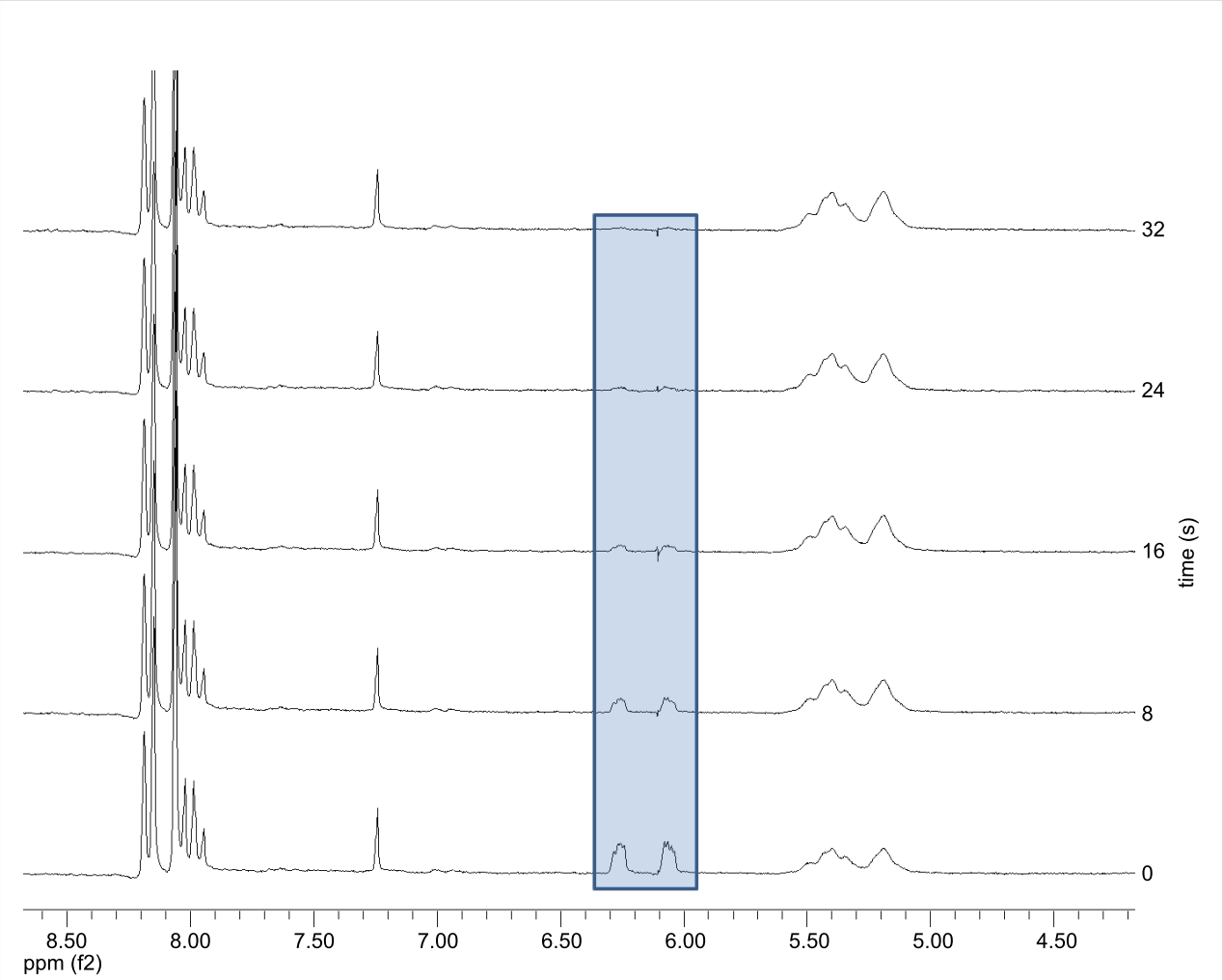


Figure 4: Kinetic progress monitored via ^{1}H NMR spectroscopy of the polymerization of **7** with catalyst **U3**; [**7**]/[**U3**] = 20/1.

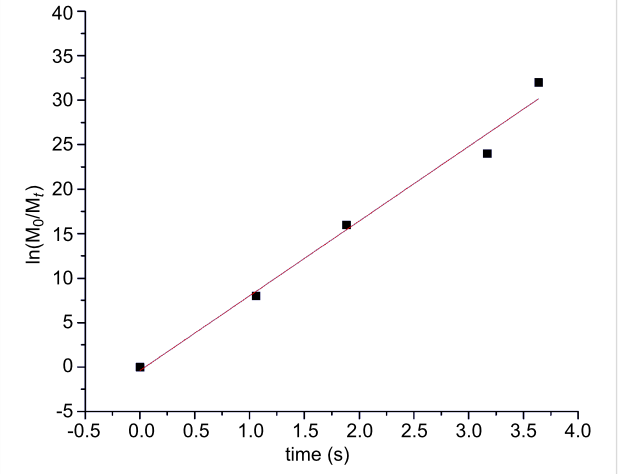


Figure 5: ln([M]$_0$/[M]$_t$) vs. time (t) plot obtained from ^{1}H NMR spectra for homopolymer-A_{50} using catalyst **U3**; [**7**]/[**U3**] = 20/1.

As monomer T **9** is a free stable radical, the progress of its polymerization with catalyst **U3** could not be monitored by ^{1}H NMR spectroscopy. Therefore, the conventional method of following the M_n vs. time (t) profile was carried out as shown in Figure 6. Chain growth with a maximum polydispersity of M_w/M_n ~1.3 was observed, clearly proving the high precision of this type of polymerization reaction.

As the polymerization of both, monomer A **7** and monomer T **9** proceeded well with catalyst **U3**, the synthesis of the BCP was achieved by use of this initiating system to yield the respective BCP-$A_{10}T_{10}$, $A_{20}T_{20}$, $A_{25}T_{25}$ and $A_{50}T_{50}$ with the expected molecular weight and with low polydispersity (see Table 1, entries 18–21). The GPC traces of A_{25} block and the $A_{25}T_{25}$ block copolymer are shown in Figure 7, indicating the expected shift in the retention time after addition of monomer T **9** after all of the monomer A **7** had been consumed.

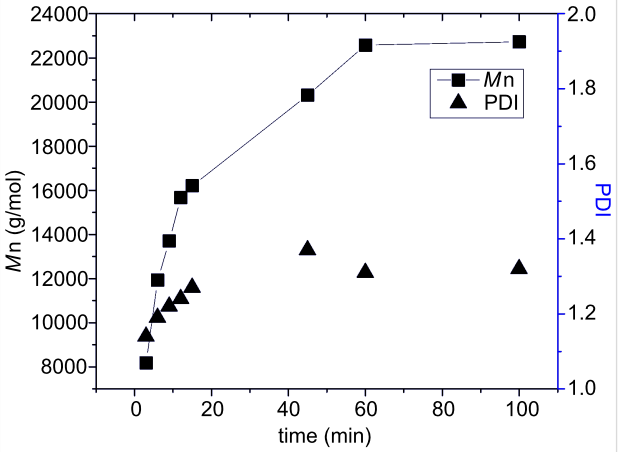


Figure 6: M_n vs. time (t) kinetic plot and M_w/M_n (PDI) of the polymerization of monomer T **9** with catalyst **U3**; [**9**]/[**U3**] = 50/1.

In order to achieve a deeper insight into the exact nature of the crossover reaction when changing from monomer A **7** to monomer T **9** with catalyst **U3**, the respective reaction was monitored according to our previous methods using MALDI mass spectrometry [11]. Thus homopolymer A_{25} was initiated with catalyst **U3** and subsequently reacted with 1, 2, 5 and 25 equivalents of monomer T after all of the monomer A **7** had been consumed. The respective samples were then quenched with ethyl vinyl ether, and subsequently analyzed by MALDI-TOF mass spectrometry and GPC. The GPC results are shown in Table 1, entries 9–14 and 18–21, indicating that with increasing amount of added monomer T an equal increase of M_n can be observed. However, in order to check for the detailed composition of the reaction mixture, MALDI spectra were measured. As shown in Figure 8, homopolymer A_{25} can be desorbed well in MALDI, featuring the respective A_nNa^+-ions as a pure series. Thus the homopolymer A_n can serve as molecular probe for the subsequent desorption of the individual $A_nT_{1,\ 2,\ 5}$-species.

The MALDI spectrum of the crossover reaction of A_{25} with exactly one equivalent of monomer T **9** using **U3** as initiator is shown in Figure 9. Thus, together with the still present A_n-series (visible as A_nNa^+-series), the respective crossover species A_nT_1, and A_nT_2 can be seen as the respective Na^+-ions. These results demonstrate that a large amount of A_n-species did not participate in the crossover reaction, since due to the fast polymerization of monomer T **9**, it was rapidly consumed, leading to A_nT_2-species and its respective higher homologues.

The respective MALDI spectrum of the crossover reaction of the homopolymer A_{25} with exactly two equivalents of monomer T **9** is shown in Figure 10. Again, a significant amount of

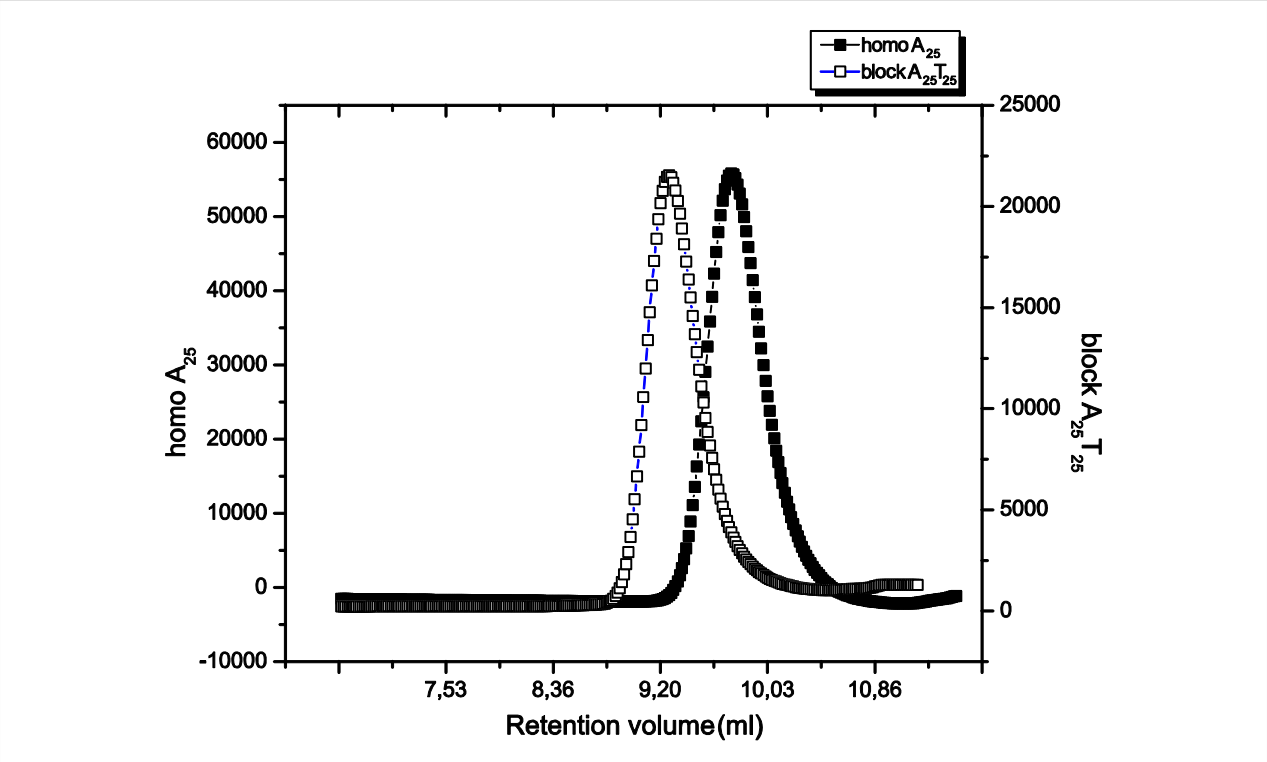


Figure 7: GPC trace of the block copolymer $A_{25}T_{25}$ synthesized with catalyst **U3**.

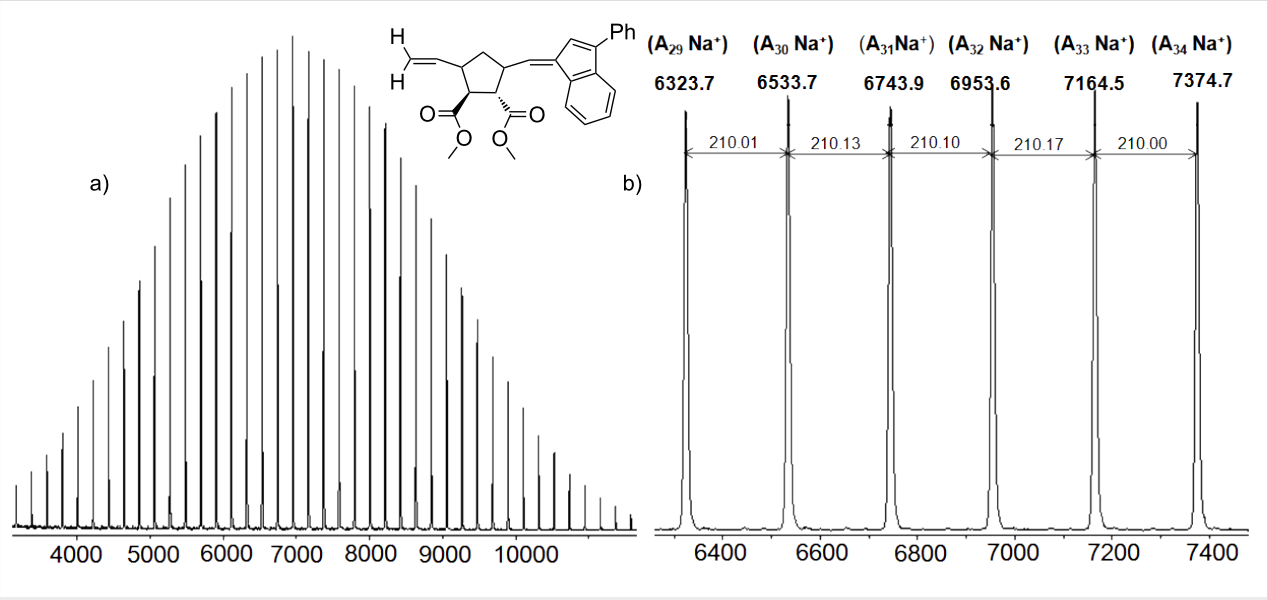


Figure 8: MALDI-TOF mass spectra of homopolymer A_{25} **4** synthesized with catalyst **U3**: (a) full spectrum, (b) expansion.

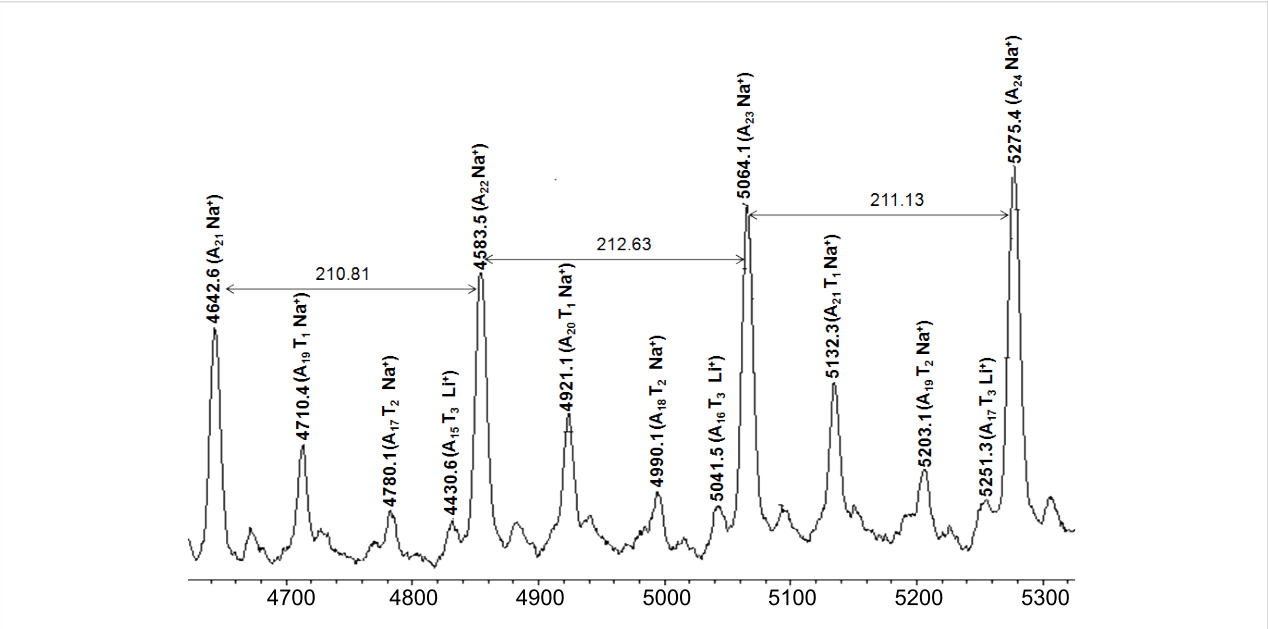


Figure 9: MALDI-TOF mass spectrum of BCP-$A_{25}T_1$ synthesized with catalyst **U3**.

homopolymer A_n (visible as A_nNa^+-series) is present in the reaction mixture, the respective crossover-species A_nT_1, and A_nT_2 can be seen as the respective Na^+-ions. Additionally, the respective series A_nT_3 is visible, indicative of the further chain growth process after the crossover reaction. Again, despite the excess of T_n-species a large amount of A_n-species did not participate in the crossover reaction due to the fast polymerization of monomer T **9**. MALDI spectra of a further series of block copolymers $A_{25}T_5$ and $A_{25}T_{25}$ was carried out in order to check for the presence of residual homopolymer A_{25} in the polymer mixture (see Figure 11). We could not detect any residual homopolymer in either of these final samples. As it is known from our previous investigations, that the homopolymer A_n in MALDI is desorbed preferentially by a factor of 13 with respect to the $A_{25}T_n$-species, this now indicates a complete cross-over reaction and thus the successful preparation of block copolymers A_nT_m via this methodology. Basically, this synthetic approach now allows the synthesis of AT type BCP's with high precision and chain length control up to molecular weights of ~31000 g/mol.

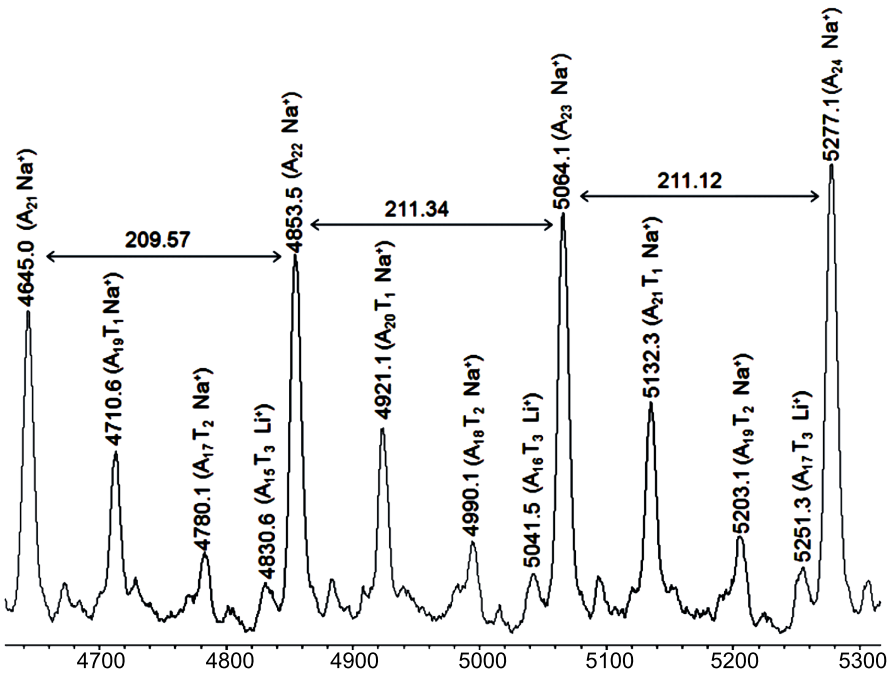


Figure 10: MALDI-TOF mass spectrum of BCP-$A_{25}T_2$ **13** synthesized with catalyst **U3**.

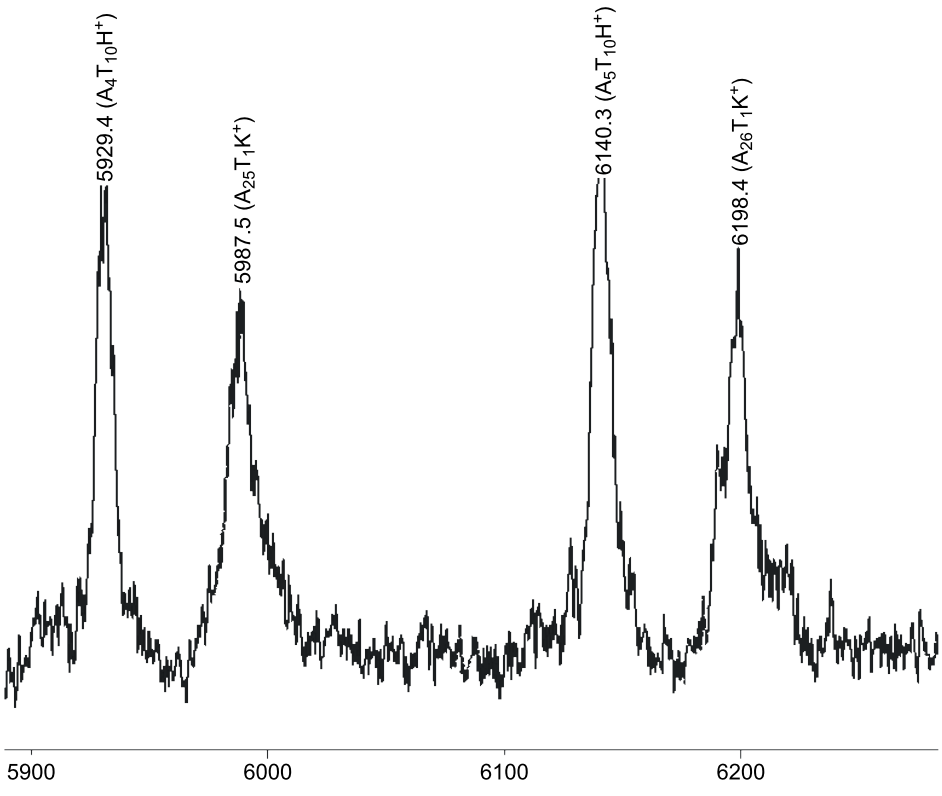


Figure 11: MALDI-TOF mass spectrum of BCP-$A_{25}T_{25}$ synthesized with catalyst **U3**.

Conclusion

The synthesis of new block copolymers containing free radical centers within one block via ROMP has been described. MALDI analyses especially provide a detailed picture of the crossover reaction. Basically, the NEOLYST™ catalysts are comparable to the well known Grubbs' catalysts, indicating a similar profile of initiation and propagation. However, the catalyst **U3** is especially a highly potent catalyst for ROMP and displays a broad profile of tolerance against functional groups within the monomer, enabling the successful synthesis of block copolymers containing free-radical species in high densities.

Experimental

General Remarks

Solvents/Reagents/Materials: Catalysts **G1**, **G2** and **G3** were obtained from Sigma-Aldrich. Catalysts **U1**, **U2** and **U3** were obtained as gifts from the Umicore chemical company. All reagents used for the synthesis of norbornene monomers **7** and **9** were obtained from Sigma-Aldrich Chemical Co. (Germany) and used as received without further purification unless otherwise indicated. Bicyclopentadiene (100%), fumaric acid (99+%), thionyl chloride (99+%, Fluka), pyridine (99.8%), methanol and 4-hydroxy-2,2,6,6-tetramethyl-piperidin-1-oxyl (TEMPOL) were obtained from Sigma-Aldrich and used without further purification. Dichloromethane (CH_2Cl_2) was freshly distilled over CaH_2 and degassed with argon prior to use. Other solvents such as hexane and ethyl acetate were used after distillation.

Instrumentation: ^{1}H NMR spectra were recorded on a Varian Gemini 400 MHz FT-NMR spectrometer, and MestRec (4.9.9.9) was used for data interpretation. The polymerization kinetics of the polymerization reactions with both catalysts **U1** and **U3** were measured at 25 °C on a 200 MHz FT-NMR spectrometer using $CDCl_3$ as a solvent. GPC analysis was performed on a Viscotek VE2001 system with THF as the eluant at a flow rate of 1 ml/min and an injection volume of 100 µL. Polystyrene standards were used for conventional external calibration using a Viscotek VE3580 refractive index detector. Positive ion MALDI-TOF (matrix-assisted laser desorption ionization time-of-flight) measurements were performed on a Bruker Autoflex-III instrument equipped with a smart ion beam laser. Measurements were carried out in linear and reflector mode. Samples were prepared from THF solution by mixing matrix (20 mg/ml), polymer (20 mg/ml), and salt (20 mg/ml solution) in a ratio of 100:10:1. Dithranol (1,8-dihydroxy-9(10*H*)-anthracetone, Aldrich 97%) was used as the matrix. Sodium trifluoroacetate (Aldrich, 98%), silver trifluoroacetate (Aldrich, 99.99%) or lithium trifluoroacetate (Aldrich, 99.8%) were added for ion formation, with sodium trifluoroacetate as the optimal salt for obtaining the highest S/N ratio.

Monomer synthesis

5-Norbornene-*endo*,*exo*-2,3-dicarboxylic acid dimethylester, monomer A **7** was synthesised according to reference [11], 5-norbornene-*endo, exo*-2,3-dicarboxylic acid bis(1-oxyl-2,2,6,6-tetramethyl-piperidin-4-yl) ester, monomer T **9**, was prepared according to references [19,20].

Synthesis of homopolymers A_{15} and T_{20}

Monomer A **7** (50.0 mg, 0.23 mmol) dissolved in 1 ml of CH_2Cl_2 was introduced into a heated and argon flushed glass tube equipped with a magnetic stirring bar. A solution of catalyst **U3** (11.8 mg, 0.015 mmol) dissolved in 1 ml of CH_2Cl_2 was then added. After 5 min of stirring at room temperature, the total consumption of monomer A **7** was confirmed by thin layer chromatography (TLC). The reaction was then quenched with 5 drops of cold ethyl vinyl ether, and the resulting polymer purified by column chromatography (SiO_2). The homo-polymerization of monomer T **9** was carried out in the same manner with catalyst **G2**. Homopolymers (A_n) with different chain lengths (n = 15, 50, 25) with the catalysts **G3**, **U1**, **U2** and **U3** as initiators were also synthesized using the same procedure by adopting the required polymerization times.

Block copolymer syntheses

The synthesis of block copolymers (A_n-*b*-T_n) was carried out analogously to methods developed previously in our laboratory [14,16]. For example the synthesis of BCP-$A_{50}T_{50}$ was performed by sequential addition of monomers. Monomer A **7** (15 mg, 0.071 mmol) dissolved in 1 ml of CH_2Cl_2 was introduced into a heated and argon flushed glass tube equipped with a magnetic stirring bar. To this solution, catalyst **G3** (1.26 mg, 0.0014 mmol) dissolved in 1 ml of CH_2Cl_2 was then added. The mixture was allowed to stir at room temperature for 1 h until all of the monomer A **7** was consumed as confirmed by GPC and TLC. Subsequently, monomer T **9** (35 mg, 0.071 mmol) dissolved in 1 ml of CH_2Cl_2 was then added to the above reaction mixture and stirred for 2 h at room temperature until all of monomer T **9** was consumed, as confirmed by GPC and TLC. The polymerization was quenched by the addition of cold ethyl vinyl ether. The polymer was isolated by column chromatography (SiO_2) (eluent: DCM).

Kinetic experiments

A pyrene stock solution was prepared from 70 mg of pyrene dissolved in 2 ml of $CDCl_3$. Monomer A **7** (20.83 mg, 0.099 mmol) dissolved in $CDCl_3$ (0.2 ml) was first introduced into the NMR tube and then the pyrene stock solution (0.2 ml) was added. Before adding the initiator solution, the ratio of the monomer to the internal standard was determined by NMR. On the basis of this value, the monomer concentration at t = 0 was determined. A solution of the catalyst **U3** (1.48 mg,

0.0019 mmol), dissolved in $CDCl_3$ (0.2 ml) (in case of catalyst **U1** (1.83 mg, 0.0019 mmol)) dissolved in $CDCl_3$ (0.2 ml) was added via a syringe to yield the desired monomer to initiator ratio. After shaking, the tube was inserted into the NMR spectrometer, and the decrease in the monomer with respect to time was monitored by integrating the resonance peaks at 6.27 and 6.07 ppm. For determination of the monomer concentration at $t = 0$ and the monomer consumption, the corresponding signals at 6.27 and 6.07 ppm from monomer A **7** compared with the one at 8.20 ppm from the internal standard pyrene were integrated. The time between the addition of the initiator solution and the first measurement was added to the first measuring point.

Acknowledgements

Grants from the DFG INST 271/249-1; INST 271/247-1 and INST 271/248-1 are gratefully acknowledged.

References

1. Hadjichristidis, N.; Pispas, S.; Floudas, G. A. *Block Copolymers-synthetic strategies, physical properties and application;* John Wiley and Sons: New York, 2002.
2. Baughman, T. W.; Wagener, K. B. *Adv. Polym. Sci.* **2005,** *176,* 1–42.
3. Buchmeiser, M. R. *Chem. Rev.* **2000,** *100,* 1565–1604. doi:10.1021/cr990248a
4. Frenzel, U.; Nuyken, O. *J. Polym. Sci., Part A: Polym. Chem.* **2002,** *40,* 2895–2916. doi:10.1002/pola.10324
5. Schrock, R. R. *Acc. Chem. Res.* **1990,** *23,* 158–165. doi:10.1021/ar00173a007
6. Slugovc, C. *Macromol. Rapid Commun.* **2004,** *25,* 1283–1297. doi:10.1002/marc.200400150
7. Novak, B. M.; Grubbs, R. H. *J. Am. Chem. Soc.* **1988,** *110,* 960–961. doi:10.1021/ja00211a043
8. Bazan, G. C.; Schrock, R. R.; Choj, H. N.; Gibson, V. C. *Macromolecules* **1991,** *24,* 4495–4502. doi:10.1021/ma00016a003
9. Malcolmson, S. J.; Meek, S. J.; Sattely, E. S.; Schrock, R. R.; Hoveyda, A. H. *Nature* **2008,** *456,* 933–937. doi:10.1038/nature07594 Letter.
10. Love, J. A.; Morgan, J. P.; Trnka, T. M.; Grubbs, R. H. *Angew. Chem., Int. Ed.* **2002,** *41,* 4035–4037. doi:10.1002/1521-3773(20021104)41:21<4035::AID-ANIE4035>3.0.CO;2-I
11. Binder, W. H.; Pulamagatta, B.; Kir, O.; Kurzhals, S.; Barqawi, H.; Tanner, S. *Macromolecules* **2009,** *42,* 9457–9466. doi:10.1021/ma902115j
12. Binder, W. H.; Kurzhals, S.; Pulamagatta, B.; Decker, U.; Manohar Pawar, G.; Wang, D.; Kühnel, C.; Buchmeiser, M. R. *Macromolecules* **2008,** *41,* 8405–8412. doi:10.1021/ma801465r
13. Kluger, C.; Binder, W. H. *J. Polym. Sci., Part A: Polym. Chem.* **2007,** *45,* 485–499. doi:10.1002/pola.21867
14. Binder, W. H.; Kluger, C.; Josipovic, M.; Straif, C. J.; Friedbacher, G. *Macromolecules* **2006,** *39,* 8092–8101. doi:10.1021/ma061256d
15. Binder, W. H.; Kluger, C.; Straif, C. J.; Friedbacher, G. *Macromolecules* **2005,** *38,* 9405–9410. doi:10.1021/ma0518252
16. Binder, W. H.; Kluger, C. *Macromolecules* **2004,** *37,* 9321–9330. doi:10.1021/ma0480087
17. Binder, W. H.; Lomoschitz, M.; Sachsenhofer, R.; Friedbacher, G. *J. Nanomater.* **2009**. doi:10.1155/2009/613813. Article ID 613813.
18. Lee, W. L.; Register, A. R. *Macromolecules* **2005,** *38,* 1216–1222. doi:10.1021/ma048013a
19. Katsumata, T.; Qu, J.; Shiotsuki, M.; Satoh, M.; Wada, J.; Igarashi, J.; Mizoguchi, K.; Masuda, T. *Macromolecules* **2008,** *41,* 1175–1183. doi:10.1021/ma7020425
20. Katsumata, T.; Satoh, M.; Wada, J.; Shiotsuki, M.; Sanda, F.; Masuda, T. *Macromol. Rapid Commun.* **2006,** *27,* 1206–1211. doi:10.1002/marc.200600286

License and Terms

This is an Open Access article under the terms of the Creative Commons Attribution License (http://creativecommons.org/licenses/by/2.0), which permits unrestricted use, distribution, and reproduction in any medium, provided the original work is properly cited.

The license is subject to the *Beilstein Journal of Organic Chemistry* terms and conditions: (http://www.beilstein-journals.org/bjoc)

The definitive version of this article is the electronic one which can be found at: doi:10.3762/bjoc.6.59

Beilstein Journal of Organic Chemistry

Free radical homopolymerization of a vinylferrocene/cyclodextrin complex in water

Helmut Ritter*[1], Beate E. Mondrzik[1], Matthias Rehahn[2] and Markus Gallei[2]

Full Research Paper

Open Access

Address:
[1]Institute of Organic Chemistry and Macromolecular Chemistry II, Heinrich-Heine-University of Duesseldorf, Universitaetsstrasse 1, D-40225 Duesseldorf, Germany and [2]Ernst-Berl-Institute for Technical and Macromolecular Chemistry, Technical University of Darmstadt, Petersenstrasse 22, D-64287 Darmstadt, Germany

Email:
Helmut Ritter* - H.Ritter@uni-duesseldorf.de

* Corresponding author

Keywords:
cyclodextrin; free radical polymerization; polyvinylferrocene; vinylferrocene

Beilstein J. Org. Chem. **2010,** *6,* No. 60. doi:10.3762/bjoc.6.60

Received: 13 January 2010
Accepted: 31 March 2010
Published: 01 June 2010

Guest Editor: H. Ritter

© 2010 Ritter et al; licensee Beilstein-Institut.
License and terms: see end of document.

Abstract

We report the radical initiated homopolymerization of a soluble vinylferrocene cyclodextrin-complex in water. Uncomplexed vinylferrocene **1** and the corresponding homopolymer are hydrophobic and completely insoluble in water. Complexation of **1** with methyl-β-cyclodextrin **2** results in clearly water-soluble structures due to incorporation of the ferrocene moiety into the cyclodextrin cavity. After free radical polymerization of the water-soluble complexed monomer, corresponding to polyvinylferrocene (PVFc), the water-soluble polymer is obtained due to the host guest interactions. Those polymeric complexes are stable in water up to about 90 °C. Above this temperature the polymer precipitates due to decomplexation. The complex was investigated by ^{1}H NMR spectrometry, dynamic light scattering (DLS), differential scanning calorimetry (DSC), and lower critical solution temperature (LCST) measurements.

Introduction

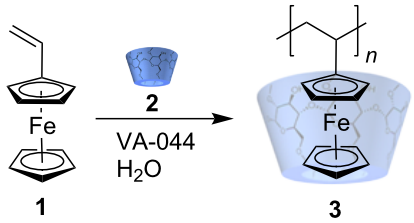
Since its discovery in 1951, ferrocene [1] and its derivatives and their applications have been the subject of numerous papers [2-7]. One derivative, vinylferrocene **1**, is of particular interest because of its anionic and radical polymerization behavior [8-12]. Due to its electrical semiconductivity properties the polymer of **1** has several practical applications. It is mainly used in biochemical sensors [13,14], batteries [15] and in the fuel industry [16]. However, the polymerization of the hydrophobic vinylferrocene in water has not been investigated.

Recently, we studied the radical polymerization of various vinyl monomers in water using cyclodextrin as the hydrophilic host component [17-25]. The hydrophobic part of the monomer molecule is included in the more hydrophobic cyclodextrin

cavity yielding completely water-soluble complexes capable of polymerization. In this publication we wish to present our results of the aqueous free radical homopolymerization of vinylferrocene **1** as a guest in the host methyl-β-cyclodextrin (methyl-β-CD) **2**. The stability of the resulting complexed polymers in water is also reported.

Results and Discussion

Vinylferrocene **1** was added to an aqueous solution of methyl-β-CD **2** and the complex obtained was subjected to radical polymerization in water at 50 °C. During the reaction an increase in viscosity was observed, due to the formation of complexed polyvinylferrocene **3**, which did not precipitate during the chain growth as a consequence of a strong host-guest interaction (Scheme 1). The complex remains in solution.



Scheme 1: Homopolymerization of vinylferrocene **1**.

The ratio of insertion of vinylferrocene **1** and methyl-β-CD **2** in the complexed polymer **3** was analyzed by ^{1}H NMR spectrometry by comparing the integrated signals of vinylferrocene **1** (singlets at 1.83 and 4.11 ppm, triplets at 4.25 and 4.44 ppm, doublet of doublets at 6.47 ppm) with the integrated signals of methyl-β-CD **2** (3.10–3.31, 3.45–3.65 and 4.75–5.30 ppm). From this data 1:1 complexation was indicated.

The DLS results showed the hydrodynamic radii in water for molecular dispersed cyclodextrin **2** to be 1.3 nm. By comparison, the radius of the complex of monomer **1** with methyl-β-CD **2** is slightly increased at 1.5 nm. However, the complexed polymer **3** shows a significantly larger hydrodynamic radius of 164 nm (Figure 1).

The complexed polyvinylferrocene **3** was thermally stable up to about 90 °C in water, as demonstrated by turbidity measurements. The complex between methyl-β-CD **2** and polyvinylferrocene **4** remains stable almost up to boiling point of water. Heating above 90 °C, results in destabilization of the complex and causes the polymer to precipitate.

Furthermore, the reversibile redox behavior of complexed polyvinylferrocene **3** was evaluated by cyclic voltammetry. Oxidation of complexed polyvinylferrocene **3** to the polyvinylferricinium cation **6** takes place at 0.5 V and its reduction at −0.45 V (Figure 2).

By contrast, irreversible oxidation occurred on heating the solution of complexed polyvinylferrocene **3** in aqueous hydrogen peroxide, which was accompanied with a change in color from yellow (Figure 3a) to green (Figure 3b). In a second step, the reduction of $PVFc^+$ **6** to PVFc **4** was exothermic, hence the complexed polyvinylferrocene **3** was destabilized and the

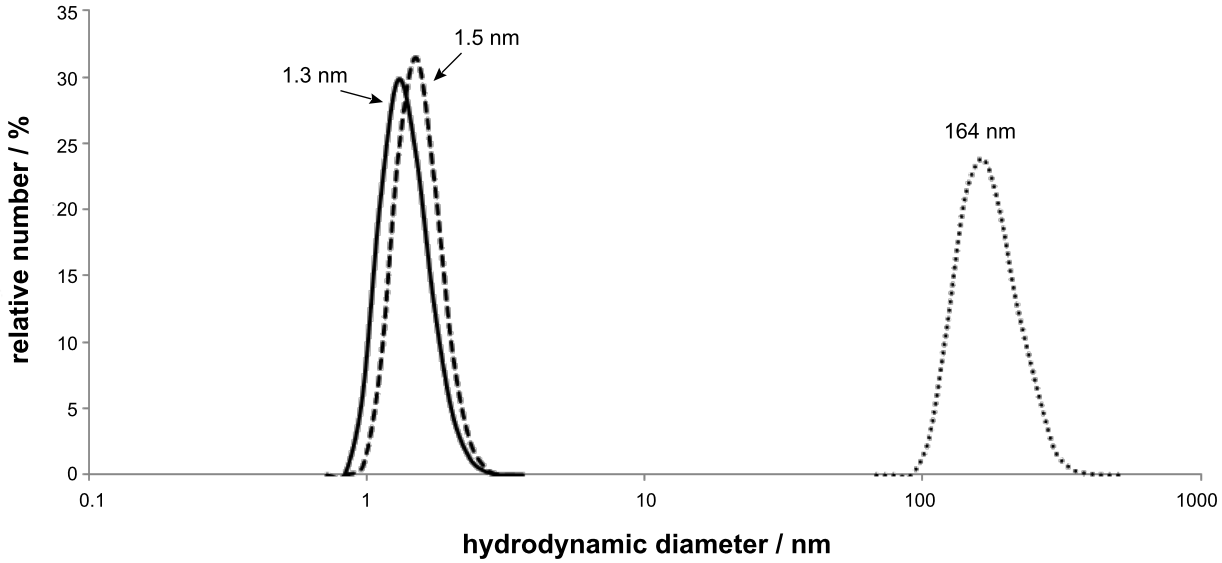


Figure 1: Dynamic light scattering of methyl-β-CD **2** (solid line), vinylferrocene **1** complexed with methyl-β-CD (dashed line) and complexed polyvinylferrocene **3** (dotted line).

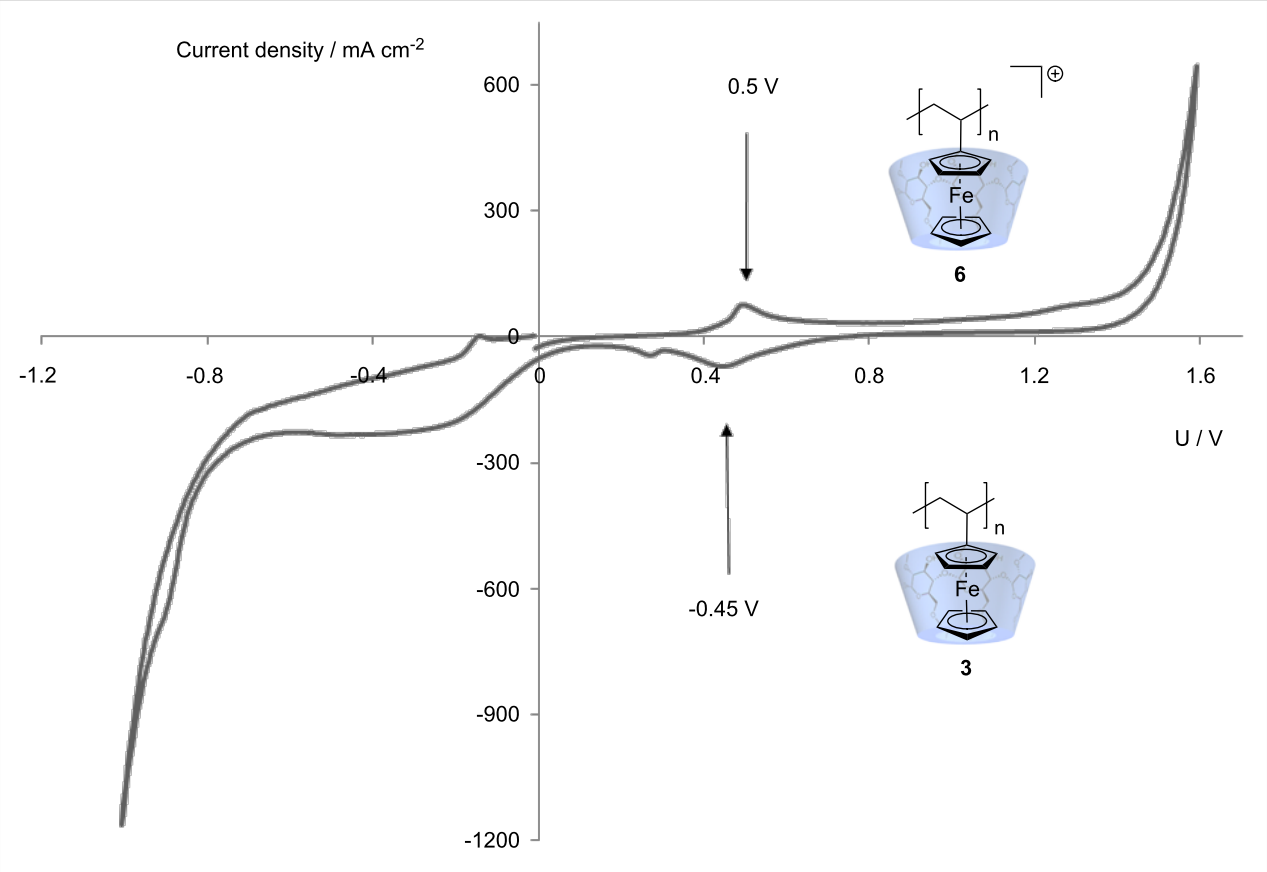


Figure 2: The cyclic voltammetry for the complexed PVFc/PVFc$^+$-system **3**/**6**: 1.0 × 10^{-3} M substance in Na_2SO_4 | Ag/AgCl.

orange colored reduced form of polyvinylferrocene **4** precipitated, indicating that the individual ferrocene units along the chain no longer fit into the cavity of the cyclodextrin (Figure 3c).

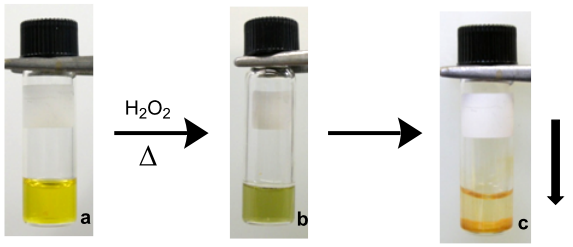
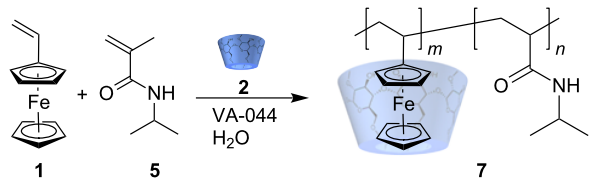


Figure 3: Redox behaviour of PVFc **3**: (a) the complexed PVFc **3** mixed with aqueous hydrogen peroxide solution was heated to 50 °C. The orange **3** oxidized to green PVFc$^+$ **6** cation (b), which is reduced to the PVFc **4** and precipitated (c).

In addition, when potassium 1-adamantane carboxylate was added as a guest molecule, which competes with the complexed homopolymer solution, the polymer precipitated due to the hydrophobic character of the uncomplexed ferrocene. This uncomplexed polyvinylferrocene was investigated by MALDI-TOF which indicated a mass of 6172.7 $[M+Na]^+$.

Very recently a paper was published, reporting the expected LCST properties of the copolymer consisting of *N*-allylferrocenecarboxamide and *N*-isopropylacrylamide (poly(N*i*PAAM/FCN)) [26]. However, in this instance the copolymer was prepared by a classical synthesis in an organic solvent. Thus, we were encouraged to prepare a similar copolymer by free radical polymerization in water starting from cyclodextrin complexed vinylferrocene **1** and the water-soluble co-monomer *N*-isopropylacrylamide **5**, the latter in a 20 fold molar excess. The copolymer obtained (PVFc-co-P(N*i*PAAM)) **7** was water-soluble, since the cyclodextrin is not covalently attached to the ferrocene moiety (Scheme 2).

The strong complexation was shown by correlations between methyl-β-CD **2** and polyvinylferrocene-co-poly(*N*-isopropylacrylamide) **7** at 4.16 ppm (cp) + 3.54 ppm (**2**) and at 4.17 (cp) + 3.52 ppm (**2**) in $^1H^1H$ ROESY-NMR spectrum. The LCST of the copolymer in water was slightly increased from 17 °C to 19 °C (Figure 4) after the addition of cyclodextrin.



Scheme 2: Copolymerization of vinylferrocene **1** with N*i*PAAM **5** (1:20).

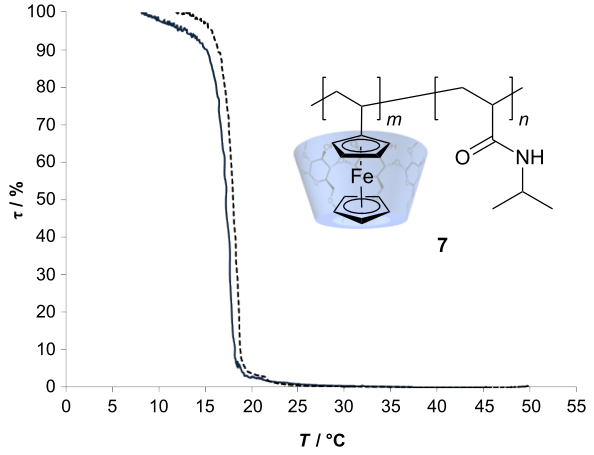


Figure 4: Lower critical solution temperature of PVFc-co-P(N*i*PAAM) **7** (1:20) (solid line): 17 °C and complexed N*i*PAAM with additional methyl-β-CD (dashed line): 19 °C.

Conclusion

It can be concluded from the experiments described above that vinylferrocene can be easily polymerized in water after complexation with cyclodextrin. The strong polymer-CD complex obtained remained unchanged up to about 90 °C. The removal of cyclodextrin by the addition of a competing guest, potassium 1-adamantane carboxylate, was demonstrated. Additionally, the polymer shows redox behavior even in the presence of the cyclodextrin ring.

Experimental Part

Materials and Instrumentation

Methyl-β-cyclodextrin was obtained from Wacker-Chemie GmbH, Burghausen, Germany, and used after drying overnight with a vacuum oil pump over P_4O_{10}. Dimethyl-d_6 sulfoxide (99.9 atom % D) was obtained from Euriso-Top SA, France. 2,2-Azobis[2-(2-imidazolin-2-yl)-propane] dihydrochloride (VA-044) was obtained from Cayman Europe, Estonia. *N*-Isopropylacrylamide (N*i*PAAM) was obtained from Aldrich, Germany. Vinylferrocene (VFc) was obtained from Sigma-Aldrich, Germany.

IR spectra were recorded with a Nicolet 5 SXB FTIR (Fourier transform infrared) spectrometer equipped with an ATR unit. The measurements were performed in the range of 4000–300 cm^{-1} at room temperature. ^1H NMR spectra were recorded with a Bruker AC 500 at 20 °C. Chemical shifts were referenced to the solvent value δ 2.51 for dimethyl-d_6 sulfoxide. Matrix-assisted laser desorption/ionization-time-of-flight mass spectrometry (MALDITOF-MS) was performed on a Bruker Ultraflex TOF mass spectrometer. Cyclic voltammetry measurements were performed on a simplot instrument with a resolution of <100 pA. Dynamic light scattering (DLS) experiments were carried out with a Malvern HPPS-ET at 25 °C. The particle size distribution was derived from a deconvolution of the measured intensity autocorrelation function of the sample by the general purpose mode algorithm included in the DTS software. DLS measurements were performed in water; the concentrations of the substances were 10 mg × mL^{-1}. Each experiment was performed at least five times to obtain statistical information. Differential scanning calorimetry (DSC) measurements were performed on a Mettler DSC-30 instrument in a temperature range of −25 to 200 °C at a heating rate of 15 °C × min^{-1} as the average of five measurements using the midpoint method.

Homopolymerization of vinylferrocene **1**

An aqueous solution of methyl-β-CD **2** in water (617.72 mg, 0.47 mmol) was prepared and purged with argon for 5 min. Vinylferrocene **1** (100 mg, 0.47 mmol) was added under an argon atmosphere and the mixture heated to 50 °C. VA-044 (1.53 mg, 4.7×10^{-3} mmol) was added to the mixture followed by the addition of a similar amount of the initiator after 8 h. After a reaction time of 48 h, the reaction mixture was freeze-dried. No residual monomer was evident by thin layer chromatography. According to differential scanning calorimetry (DSC), the obtained polyvinylferrocene **3** had a glass transition temperature (T_g) of 145 °C.

FT-IR (film) **3**: 2902 cm^{-1} (–C–H), 1643 cm^{-1} (–C=C), 1452 cm^{-1} (CH_2), 1153, 1033 cm^{-1} (–C–O), 1082 cm^{-1} (C–O–C), 964, 758, 702 cm^{-1} (=C–H); ^1H NMR: (500 MHz, DMSO-d_6, 298 K) **3**: δ (ppm) = 1.83 (CH_2), 3.10–3.31 (14H, 5-H) 3.45–3.65 (28H, 6-H) 4.11 (s, 5H, 1-H), 4.25 (t, 2H, 2-H, ^3J = 1.73 Hz), 4.44 (t, 2H, 3-H, ^3J = 1.73 Hz), 4.75–5.30 (7H, 7-H) 6.47 (dd,1H, 4-H, ^3J = 10.72 Hz (*cis*), ^3J = 17.34 Hz (*trans*)).

Copolymerization of vinylferrocene **1** and *N*-isopropylacrylamide **5**

An aqueous solution of methyl-β-CD **2** (617.72 mg, 0.47 mmol) was prepared and purged with argon for 5 min. Vinylferrocene **1** (100 mg, 0.47 mmol) was added under an argon atmosphere. After vinylferrocene **1** had completely dissolved, *N*-isopropylacrylamide (N*i*PAAM) **5** (1067.10 mg, 9.43 mmol) was added.

The mixture was heated to 50 °C and VA-044 (32.02 mg, 0.10 mmol) added. After 3 h an orange solid precipitated.

FT-IR (film) **7**: 2970 cm^{-1} (–C–H), 1637 cm^{-1} (–C=C), 1533 cm^{-1} (–N–H), 1458 cm^{-1} (-CH_2), 1385 cm^{-1} (–CH_3), 1365 cm^{-1} (–C–N); ^{1}H NMR: (500 MHz, DMSO-d_6, 298 K) **7**: δ (ppm) = 1.05 (120H, 1-H), 1.46 (40H, 2-H), 1.98 (20 H, 3-H), 3.10–3.30 (42H, 11-H), 3.45–3.65 (84H, 12-H), 3.86 (20 H, 4-H), 4.25–3.96 (9 H, 7-H), 4.71–5.20 (21H, 10-H), 6.18 (1H, 6-H), 7.20 (20H, 5-H); MALDI-TOF **7**: m/z 1.6 × 10^4.

References

1. Kealy, T. J.; Pausen, P. L. *Nature* **1951,** *168,* 1039–1040. doi:10.1038/1681039b0
2. Wilkinson, G.; Rosenblum, M.; Whiting, M. C.; Woodward, R. B. *J. Am. Chem. Soc.* **1952,** *74,* 2125–2126. doi:10.1021/ja01128a527
3. Fischer, E. O.; Pfab, W. *Z. Naturforsch., B* **1952,** *7,* 377–379.
4. Miller, S. A.; Tebboth, J. A.; Tremaine, J. F. *J. Chem. Soc.* **1952,** 632–635.
5. Harada, A.; Takahashi, S. *J. Inclusion Phenom.* **1984,** *2,* 791–798. doi:10.1007/BF00662247
6. Ueno, A.; Osa, T.; Chen, Q.; Suzuki, I. *Anal. Chem.* **1992,** *64,* 1650–1655. doi:10.1021/ac00039a005
7. Casas-Solvas, J. M.; Ortiz-Salmerón, E.; Giménez-Martínez, J. J.; García-Fuentes, L.; Capitán-Vallvey, L. F.; Santoyo-González, F.; Vargas-Berenguel, A. *Chem.–Eur. J.* **2009,** *15,* 710–725. doi:10.1002/chem.200800927
8. George, M. H. *J. Polym. Sci., Polym. Chem. Ed.* **1975,** *13,* 1049–1070.
9. Hayes, G. F.; George, M. H. *Coat. Plast. Prepr. Pap. Meet. (Am. Chem. Soc., Div. Org. Coat. Plast. Chem.)* **1977,** *37,* 430–434.
10. Saito, T.; Watanabe, M. *React. Funct. Polym.* **1998,** *37,* 263–269. doi:10.1016/S1381-5148(97)00146-6
11. Brooks, J. S.; Care, C. M.; Plimley, S.; Corfield, G. C. *Hyperfine Interact.* **1984,** *20,* 151–167. doi:10.1007/BF02073559
12. Higashihara, T.; Faust, R. *Macromolecules* **2007,** *40,* 7453–7463. doi:10.1021/ma070903d
13. Himuro, Y.; Takai, M.; Ishihara, K. *Sens. Actuators, B* **2009,** *136,* 122–127. doi:10.1016/j.snb.2008.09.049
14. Gasser, G.; Hüsken, N.; Köster, S.; Metzler-Nolte, N. *Chem. Commun.* **2008,** 3675–3677. doi:10.1039/b805369c
15. Tamura, K.; Akutagawa, N.; Sawoh, M.; Wada, J.; Masuda, T. *Macromol. Rapid Commun.* **2008,** *29,* 1944–1949. doi:10.1002/marc.200800526
16. Lohmann, G.; Kalischewski, W.; Marschewski, A. Additive für flüssige Kraftstoffe. DE Patent 10208326 B4, June 19, 2008.
17. Amajjahe, S.; Munteanu, M.; Ritter, H. *Macromol. Rapid Commun.* **2009,** *30,* 904–908. doi:10.1002/marc.200900007
18. Amajjahe, S.; Choi, S. W.; Munteanu, M.; Ritter, H. *Angew. Chem., Int. Ed.* **2008,** *47,* 3435–3437. doi:10.1002/anie.200704995 *; Angew. Chem.* **2008**, *120*, 3484–3486. doi: 10.1002/ange.200704995.
19. Koopmans, C.; Ritter, H. *Macromolecules* **2008,** *41,* 7418–7422. doi:10.1021/ma801202f
20. Kretschmann, O.; Steffens, C.; Ritter, H. *Angew. Chem., Int. Ed.* **2007,** *46,* 2708–2711. doi:10.1002/anie.200603753
21. Koopmans, C.; Ritter, H. *J. Am. Chem. Soc.* **2007,** *129,* 3502–3504. doi:10.1021/ja068959v
22. Kretschmann, O.; Choi, S. W.; Miyauchi, M.; Tomatsu, I.; Harada, A.; Ritter, H. *Angew. Chem., Int. Ed.* **2006,** *45,* 4361–4365. doi:10.1002/anie.200504539
23. Köllisch, H.; Barner-Kowollik, C.; Ritter, H. *Macromol. Rapid Commun.* **2006,** *27,* 848–853. doi:10.1002/marc.200600067
24. Schmitz, S.; Ritter, H. *Angew. Chem., Int. Ed.* **2005,** *44,* 5658–5661. doi:10.1002/anie.200501374
25. Ohga, K.; Takashima, Y.; Takahashi, H.; Kawaguchi, Y.; Yamaguchi, H.; Harada, A. *Macromolecules* **2005,** *38,* 5897–5904. doi:10.1021/ma0508606
26. Zuo, F.; Luo, C.; Ding, X.; Zheng, Z.; Cheng, X.; Peng, Y. *Supramol. Chem.* **2008,** *20,* 559–564. doi:10.1080/10610270701491227

License and Terms

This is an Open Access article under the terms of the Creative Commons Attribution License (http://creativecommons.org/licenses/by/2.0), which permits unrestricted use, distribution, and reproduction in any medium, provided the original work is properly cited.

The license is subject to the *Beilstein Journal of Organic Chemistry* terms and conditions: (http://www.beilstein-journals.org/bjoc)

The definitive version of this article is the electronic one which can be found at: doi:10.3762/bjoc.6.60

Beilstein Journal of Organic Chemistry

Poly(glycolide) multi-arm star polymers: Improved solubility via limited arm length

Florian K. Wolf, Anna M. Fischer and Holger Frey*

Full Research Paper

Open Access

Address:
Institut für Organische Chemie, Johannes Gutenberg-Universität Mainz, Duesbergweg 10–14, D-55099 Mainz, Germany

Email:
Holger Frey* - hfrey@uni-mainz.de

* Corresponding author

Keywords:
block copolymer; hyperbranched; PGA; polyester; polyglycerol; poly(glycolide); star polymer

Beilstein J. Org. Chem. **2010,** *6,* No. 67.
doi:10.3762/bjoc.6.67

Received: 14 February 2010
Accepted: 02 June 2010
Published: 21 June 2010

Guest Editor: H. Ritter

© 2010 Wolf et al; licensee Beilstein-Institut.
License and terms: see end of document.

Abstract

Due to the low solubility of poly(glycolic acid) (PGA), its use is generally limited to the synthesis of random copolyesters with other hydroxy acids, such as lactic acid, or to applications that permit direct processing from the polymer melt. Insolubility is generally observed for PGA when the degree of polymerization exceeds 20. Here we present a strategy that allows the preparation of PGA-based multi-arm structures which significantly exceed the molecular weight of processable oligomeric linear PGA (<1000 g/mol). This was achieved by the use of a multifunctional hyperbranched polyglycerol (PG) macroinitiator and the tin(II)-2-ethylhexanoate catalyzed ring-opening polymerization of glycolide in the melt. With this strategy it is possible to combine high molecular weight with good molecular weight control (up to 16,000 g/mol, PDI = 1.4–1.7), resulting in PGA multi-arm star block copolymers containing more than 90 wt % GA. The successful linkage of PGA arms and PG core via this core first/grafting from strategy was confirmed by detailed NMR and SEC characterization. Various PG/glycolide ratios were employed to vary the length of the PGA arms. Besides fluorinated solvents, the materials were soluble in DMF and DMSO up to an average arm length of 12 glycolic acid units. Reduction in the T_g and the melting temperature compared to the homopolymer PGA should lead to simplified processing conditions. The findings contribute to broadening the range of biomedical applications of PGA.

Introduction

Linear aliphatic polyesters such as polylactic acid (PLA) and poly(ε-caprolactone) [1] are of great interest due to their biodegradability, biocompatibility and permeability for many drugs. In contrast, poly(glycolic acid) (PGA) is scarcely used because of its high degree of crystallinity and its insolubility in all common solvents. However, glycolic acid is widely employed in copolymers of varying composition with the above-mentioned lactone comonomers [2]. For the PGA homopolymers, special processing techniques for the polymer melt are required and characterization is limited to solid-state techniques [3].

In recent works, PLA and poly(ε-caprolactone) [4] have been successfully used for the synthesis of numerous star [5] and

multi-arm star [6] as well as (hyper)branched polymers [7]. Although PGA-rich polymers exhibit a superior degradation rate in comparison to poly(lactide), star copolymers primarily composed of this building unit have hardly been described in literature [8]. However, star copolymers, in a general sense, have attracted increasing interest for the fabrication of unimolecular micelles [9]; in particular when they consist of a hydrophilic, hyperbranched (or dendritic) core and a hydrophobic corona [10]. Their potential arises from their ability to encapsulate and release hydrophilic molecules slowly. Particularly, PEG/PLA-based copolymers have been intensely studied in this context [11-13]. Apart from this special application in solution, analogs of well-known linear polymers with star architectures exhibit significantly altered physical properties [14,15]. This is often considered the primary motivation for the choice of this interesting polymer architecture [16].

A suitable multifunctional core molecule is required to prepare multi-arm star polymers with core–shell characteristics. Apart from dendrimers [17,18], well-defined hyperbranched polymers [19] fulfill this requirement and benefit from their accessibility via a facile one-step synthesis, which makes a tedious, generation-wise build-up ubiquitous. Besides poly(ethylene imine) (PEI) [20], hyperbranched polyglycerol [21-26] has proven to be a versatile and highly potent multifunctional core molecule [27-29]. Derivatization and functionalization of the peripheral hydroxy groups of this polyether-polyol have afforded a number of carrier systems [30-34], matching the concept outlined above. In contrast to dendrimers, where functional groups are exclusively located at the surface, poly(glycerol) scaffolds also contain hydroxy groups throughout the structure. At first glance this might be considered a disadvantage, however, this is in fact beneficial for the significantly hydrophilized core environment when core–shell topologies for encapsulation are desired.

Here we present a solvent-free synthetic strategy for multi-arm star block copolymers with a hyperbranched polyether core and PGA arms, systematically varying arm length. The combination of glycolide with a multifunctional initiator studied in this paper is of a rather fundamental nature. Our primary objective is to improve the solubility of PGA in standard organic solvents and thus facilitate characterization as well as processing, while keeping the overall glycolide weight fraction high. Multi-arm star copolymers [35] should permit the combination of short average chain length with high molecular weight. Since the high number of functionalities of the core molecules is ideally translated into a matching number of arms with a respective chain end, end-group effects are expected to exert a significant influence on solubility and crystallization tendencies of the polymer.

Results and Discussion

The hyperbranched poly(glycerol)s (PGs) with multiple poly(glycolide) arms were prepared by a straightforward two-step approach as shown in Figure 1. In the first step, we polymerized glycidol anionically by the method described previously [19], using trimethylolpropane as a trifunctional initiator. The hydroxy groups of PG were deprotonated to an extent of

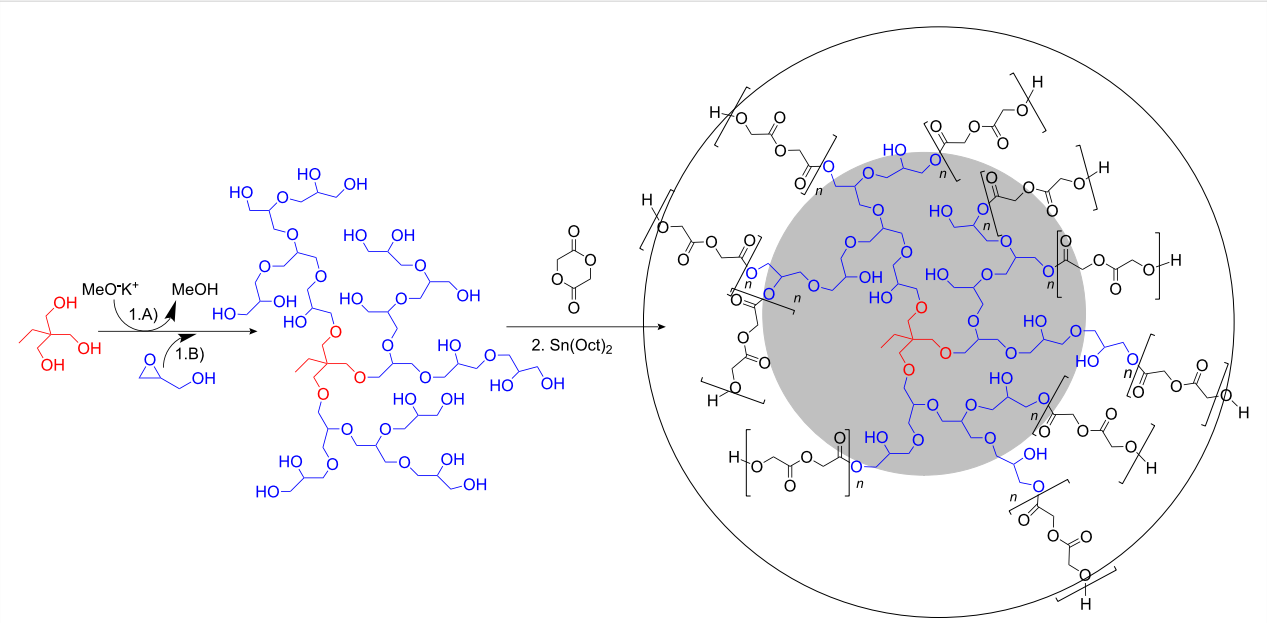


Figure 1: Synthetic route to *hb*-PG-*b*-(P)GA multi-arm star copolymers in a two-step sequence. The well-established anionic ring-opening multibranching polymerization of glycidol is followed by the $Sn(Oct)_2$-mediated copolymerization of glycolide.

10% before the slow addition of glycidol monomer was started. The subsequent polymerization proceeds via a ring-opening branching reaction where branching occurs due to a fast proton exchange equilibrium which is a well-known phenomenon in oxyanionic polymerizations.

In the second step, the polyether-polyols were used as macroinitiators for the ring-opening polymerization of glycolide via $Sn(Oct)_2$ catalysis. All polymerization experiments were carried out in bulk (with a minimum of toluene present for transfer of the catalyst) at 120 °C for 24 h with systematic variation of the glycolide monomer/*hb*-PG-OH ratios. Since each glycidol unit leads to the formation of an additional end-group after ring opening and attachment to the growing PG, the corresponding total number of primary and secondary hydroxy groups of the polymer n(OH) is equal to the sum of the initiator functionality f and the degree of polymerization DP_n.

$$n(\mathrm{OH}) = \mathrm{DP}_n + f \quad (1)$$

By varying of the initiator/monomer ratio, two hyperbranched poly(glycerol) samples with different degrees of polymerization DP_n were obtained. Their theoretical number of initiating hydroxy groups was calculated from the degree of polymerization which is available from ^{1}H NMR according to Equation 1. PG_{14} and PG_{38} thus offer an average of 17 and 41 potential initiating moieties for the grafting-from reaction with glycolide. It should be emphasized that according to Equation 1, the number of hydroxy groups is independent of the degree of branching (DB). Typically, the poly(glycerol) macroinitiators possess primary as well as secondary –OH groups, which likely show different reactivities in the initial reaction with glycolide. Since the accessibility of functional groups of PG is believed to play an important role in the properties of the resulting star block copolymer, the branched topology and the distribution of OH groups therein are key factors that will also be addressed in the following text.

Careful drying of the PG cores under vacuum is a crucial step for the controlled synthesis of the multi-arm star polymers in order to avoid initiation by trace amounts of water, which leads to concurrent glycolide homopolymerization and thus an undesired mixture of linear and star-like PGAs. In order to prevent possible precipitation from solution, the polymerization was conducted in bulk without added solvent under $Sn(Oct)_2$ catalysis with an average catalyst loading of 0.1 mol % of the glycolide feed. The mixed compounds yielded a homogeneous melt at 120 °C, fulfilling a prerequisite for an efficient grafting-from approach. Under the reaction conditions employed and taking the high number of initiating groups into account, the conversion proceeds to high values within short reaction times. The polymers obtained show improved solubility properties compared to linear PGA and thus permit the use of common characterization methods such as NMR in DMSO-d_6 and SEC in DMF. This is largely attributed to the high end-group concentration in combination with a short average PGA chain length in the multi-arm structure.

With increasing glycolide content, a second high-molecular-weight distribution mode appears together with a gradual shift of the main distribution mode to lower elution volume (Figure 2) which is in line with expectations. These apparent impurities could be caused by compounds capable of co-initiation such as water or other hydroxy functionalities. Table 1 illustrates the correlation between theoretical molecular weight and values obtained from SEC measurements via calibration with polyethylene glycol (PEG) standards. The obvious underestimation of the molecular weight by SEC is attributed to the peculiar spherical geometry of the multi-arm star copolymer and has also been observed with other star polymers. The polydispersities of the materials are in the range of 1.3–1.7 for the series of star polymers prepared, which is moderate. These values can be explained by the non-monodisperse multifunctional initiator (PDI: 1.9–2.0), although transesterification/cyclization reactions during the synthesis cannot be completely excluded.

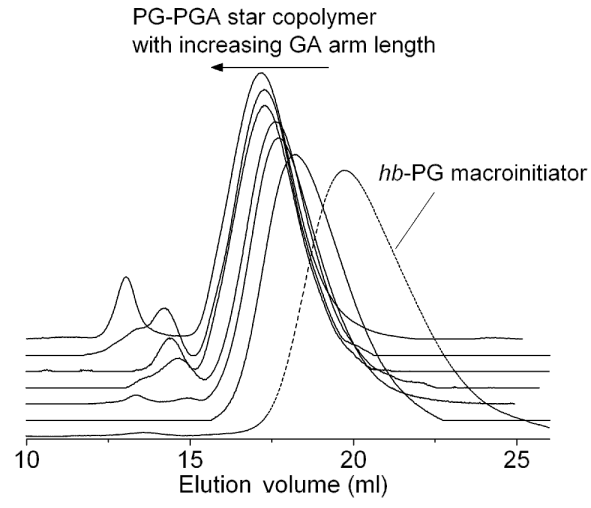


Figure 2: SEC-elugrams of the obtained multi-arm star block copolymers derived from PG_{38}. The grafting of polyglycolide on the poly(glycerol) macroinitiator is accompanied by a significant decrease in elution volume.

A detailed account of the NMR studies aimed at determining the PGA arm length of the polymers is given in the following text. In this context, it should be emphasized that solubility in DMF and DMSO was generally limited to star polymers with

targeted arm length of up to 12 glycolic acid units. Obviously, samples exceeding these values have not been characterized by SEC or NMR and are thus not listed in Table 1.

The ^{1}H NMR spectra of multi-arm polymer samples with varying composition (based on PG_{38}) are shown in Figure 3. As expected, an increase in the glycolide feed results in an increase in the glycolide backbone signal at 4.91 ppm (**B**) and a relative decrease in signal intensity of the PG core. The resonances of the core are mainly distributed between 3.1 and 3.8 ppm (**e**). Special attention was paid to the terminal glycolic acid unit, since it enables the determination of the average chain length of

Table 1: Characterization data of the multi-arm star block copolymers originating from two different *hb*-PG macroinitiators from NMR and SEC.

sample	glycolide content (weight ratio)	yield (%)	M_n (theor./NMR*)	M_n (GPC)	PDI (GPC)	average arm length (NMR)
PG_{14}	0	–	1,140*	1,130	2.0	–
$P(G_{14}GA_4)$	0.77	48	5,000	5,400	1.6	7
$P(G_{14}GA_8)$	0.87	90	8,800	6,500	1.5	10.6
$P(G_{14}GA_{12})$	0.91	94	–	–	–	12.1
PG38	0	–	2,900*	2,450	1.9	–
$P(G_{38}GA_2)$	0.62	45	7,600	6,300	1.7	3.9
$P(G_{38}GA_4)$	0.76	72	12,300	9,300	1.5	5.6
$P(G_{38}GA_6)$	0.83	88	17,000	11,000	1.4	7.2
$P(G_{38}GA_8)$	0.87	83	21,700	14,300	1.5	8.6
$P(G_{38}GA_{10})$	0.89	92	26,400	15,600	1.4	9.5
$P(G_{38}GA_{12})$	0.91	93	31,100	17,000	1.3	9.8

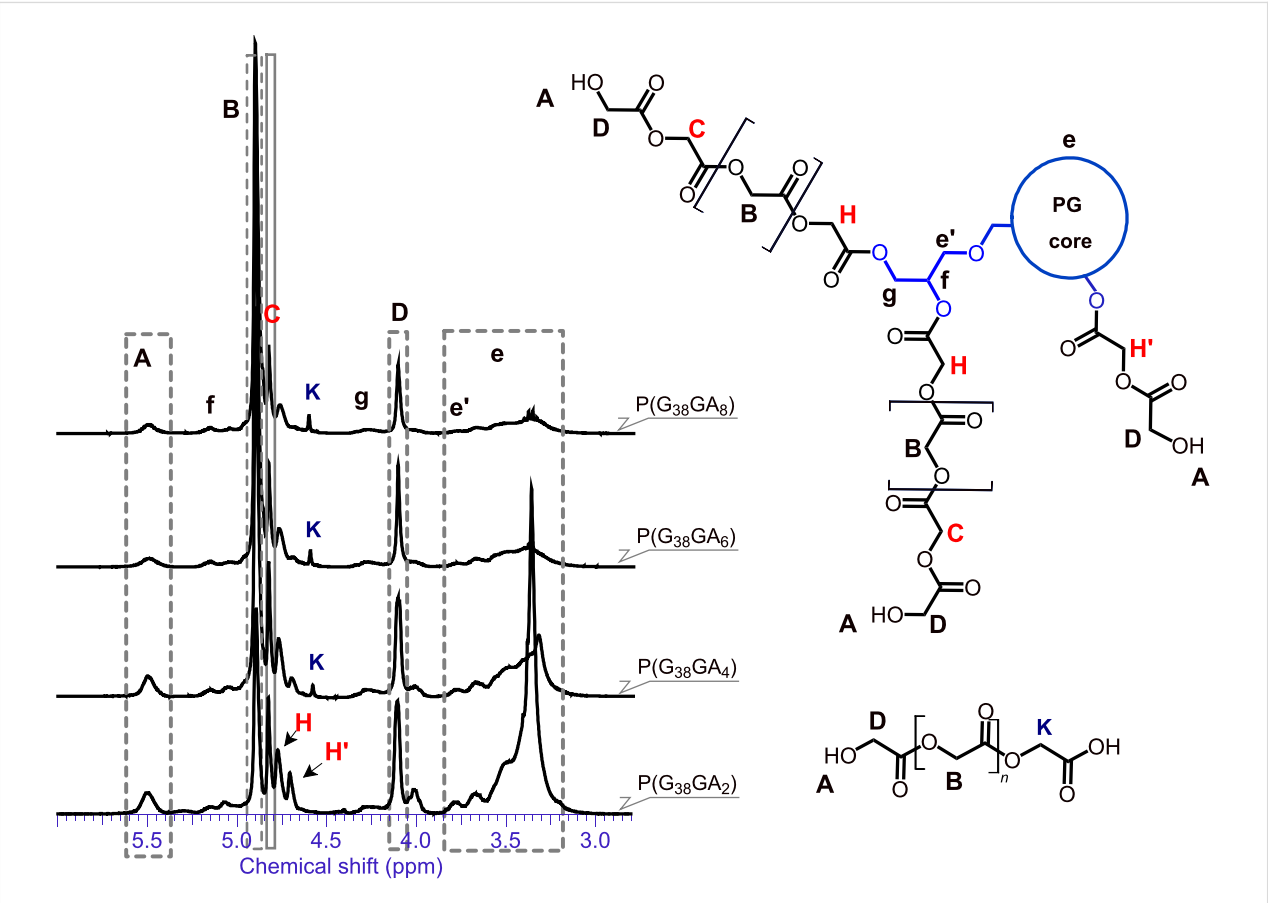


Figure 3: ^{1}H NMR analysis of the star block copolymers with increasing glycolide to poly(glycerol) ratio, using PG_{38} as core molecule.

the oligoglycolide arms. The respective signal can be found at 4.12 ppm and is thus well separated from the other glycolide arm-related signals **B**, **C**, **H** and **H′**. Furthermore, the signal denoted **A** at 5.5 ppm can be assigned to the terminal hydroxy group of the arms. This important signal assignment was confirmed by an ^{1}H COSY NMR experiment (Figure 4), relying on the cross correlation of the methylene group **D** with the hydroxy proton **A**. Verification of the assignment of methylene and methine protons of the esterified primary and secondary OH groups of the PG core is crucial, since they evidence the successful linkage of arms and core. Unequivocal proof of attachment is obtained from the cross correlation of the methine/methylene proton of the major initiating species, the terminal glycerol units of *hb*-PG. Clear cross correlations between esterified secondary PG-OH (methine proton) groups (**f**) and esterified primary PG-OH (methylene proton) units (**g**) as well as esterified secondary PG-OH methine (**f**)/primary ether (**e′**) methylene protons can be observed. In the 2D NMR spectra of the star polymers, these protons have undergone a significant downfield shift (5.0–5.4 ppm), compared to the non-functionalized *hb*-PG-related signals, which are mainly found between 3.82 and 3.1 ppm. Although direct experimental proof could not be provided via 2D NMR, the signal denoted **C** at 4.84 ppm is assigned to the penultimate glycolic acid repeat unit. The first glycolic acid repeat unit, directly attached to the PG core, is represented by two different signals: **H** (4.78 ppm) or **H′** (4.72 ppm). While **H** corresponds to the first glycolic acid unit of a PGA chain, directly attached to the poly(glycerol) core, **H′** represents the special case of an α-unit of a glycolic acid dimer directly attached to the PG core (i.e. first and penultimate unit at the same time). Hence **H′** is predominantly observed for low glycolide fractions. This signal assignment is consistent with literature data for PGA-*co*-poly(ε-caprolactone) copolymers [36,37], as well as PLLA–PG star block copolymers which have recently been developed by our group [22].

The ^{1}H COSY NMR spectrum further suggests that the linear and terminal glycolic acid units do not suffer from signal superposition and can thus be evaluated for the determination of the average arm length, which was achieved by the comparison of end-group- and backbone-related signals (**B** and **D**). Although a precise signal-to-structure correlation is difficult to establish, differentiation between PG and poly(glycolide) signals was achieved, confirming successful grafting of poly(glycolide) onto the PG core. Even more important, it was confirmed that the majority of the hydroxy groups of PG, particularly in the periphery of the core, was esterified.

An interesting correlation between the high-molecular-weight modes observed in SEC and the NMR spectra was found in the

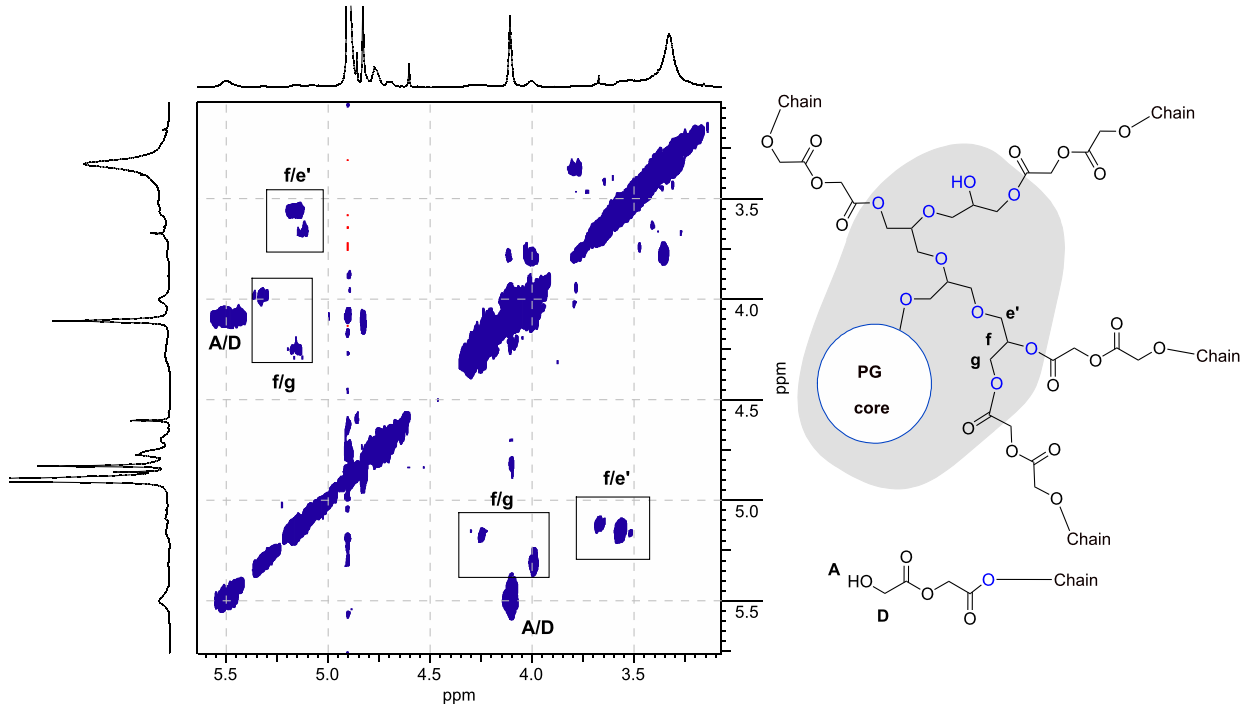


Figure 4: ^{1}H, ^{1}H-correlation COSY NMR: this experiment visualizes correlations of terminal groups with their adjacent hydroxy groups as well as correlations within esterified glycerol units (**f**/**g** and **f**/**e′**). The most pronounced cross correlation peak can be assigned to the terminal hydroxy-methyl group of polyglycolide at 5.5/4.12 ppm (**A**/**D**).

singlet, present at 4.61 ppm (**K**). According to literature data, this can be related to a carboxylic acid chain end of PGA homopolymer [38]. It can be observed for samples that exhibit an additional mode in SEC. This therefore supports the assumed formation of PGA homopolymer by co-initiation with water. Despite careful drying of the hygroscopic PG macroinitiator in vacuo, contamination with water could obviously not be fully eliminated. Since glycolide has been used as received and not stored in vacuo or under an inert gas atmosphere, this is the most likely cause for the introduction of traces of moisture into the system.

The graph shown in Figure 5 relates the number of glycolic acid repeat units per arm, calculated from ^{1}H NMR for the series of PG_{38}-derived star polymers. These values are compared with the theoretical number expected from the ratio of glycolide monomer to the sum of possible initiating sites in *hb*-PG.

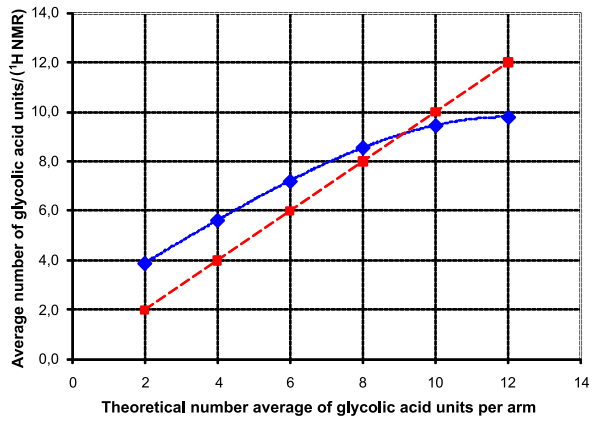


Figure 5: Comparison of average number of repeat units vs the theoretical number based on the ratio of PG and glycolic acid. The dotted line represents the ideal case of matching numbers and is added as a visual guide.

Indeed, an interesting trend can be observed. This trend is most likely influenced by two factors:

1. For very low and moderate numbers of GA repeat units, the observed chain length of the glycolide stars exceeds theoretical expectations. This difference can be attributed to the difference in accessibility and nature (primary/secondary) of the hydroxy groups of the hyperbranched PG core. A certain fraction of potential initiating sites suffers from a reduced reactivity towards the employed glycolide lactone monomer. Especially, the hydroxy groups close to the core of the hyperbranched structure and/or those of a secondary nature are less active toward glycolide addition. The first ring-opening step of the glycolide lactone always generates/retains a primary hydroxy group which is more reactive for the attachment of further glycolide monomers than the average PG-hydroxy groups. Nevertheless, the observed yield of the precipitated star polymers (Table 1) was high enough to assume conversions exceeding 90% before the polymer melt congealed. In addition, ^{1}H NMR spectra of the samples showed no residual glycolide monomer with its distinct singlet signal at 5.06 ppm (in DMSO-d_6).
2. With increasing arm length, the observed number of units drops below the theoretical value. As stated above, we assume that water was introduced via the glycolide monomer (indicated by signal **K**). Hence, co-initiation by trace amounts of water increases with increase in the glycolide/macroinitiator ratio.

Since the effect discussed in the second postulate counteracts that in the first, we observe the described trend as an overestimation of the chain length rather than an underestimation.

During the polymerization in the melt, continuous polymer melts with high viscosity are only observed for samples with a targeted average of up to 5–6 GA units. For longer arm lengths, the high mobility of the oligo-GA chains contributes to the consolidation of the melt via crystallization when reaching high conversion with a lack of molten glycolide monomer that can act as a plasticizer. This is supported by the results of the DSC measurements (Figure 6) of the star copolymers *hb*-PG_{38}-*b*-GA_4, *hb*-PG_{38}-*b*-GA_8 and *hb*-PG_{38}-*b*-GA_{12} which confirm the variety of glycolide arm lengths achieved.

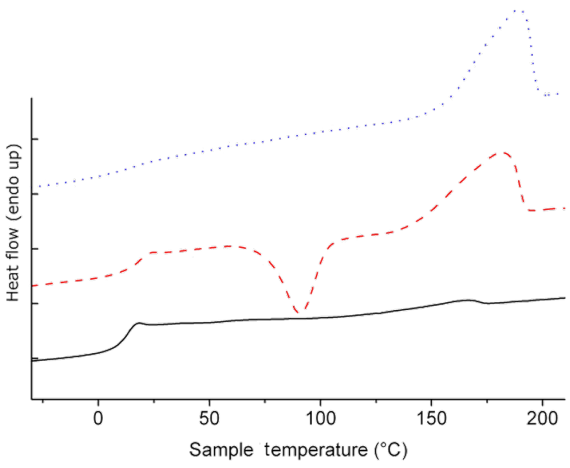


Figure 6: DSC heating traces (second heating run at 20 °C/min) for *hb*-PG_{38}-*b*-GA_4 (bottom), *hb*-PG_{38}-*b*-GA_8 (middle) and *hb*-PG_{38}-*b*-GA_{12} (top), reflecting the increasing influence of polyglycolide chain length.

Generally, the observed glass transition (T_g) of the glycolide arms for *hb*-PG_{38}-*b*-GA_2 and *hb*-PG_{38}-*b*-GA_4 is significantly depressed (10–18 °C) in comparison to literature data for PGA homopolymers [39] (approximately 40–50 °C). This reflects the influence of the flexible PG core. The T_g increased slightly with molecular weight, as it is also observed for most linear polymers. Both findings can be attributed to the low average number of repeating units per arm and are often observed for oligomers. This generally ensures increased chain mobility. As expected, this increased mobility enables efficient crystalline packing for a very short average chain length of 8.6 GA repeating units (for *hb*-PG_{38}-*b*-GA_8). Even for *hb*-PG_{38}-*b*-GA_4 with very low average PGA arm length a slight endothermic melting peak is visible in the DSC heating trace. The high crystallization tendency of the star block copolymers, despite the generally impeded crystallization due to the strongly branched PG core, is obvious from the data. An average chain length of less than 8–9 glycolic acid units is sufficient for a crystallization-induced vitrification of the polymer melt at 120 °C. The observed melting temperatures for star-shaped PGA range between 170 and 190 °C (Table 2) and are significantly depressed compared to PGA homopolymers of comparable molecular weight. This should allow polymer processing at lower temperatures which is, in particular, advantageous for such a thermolabile material.

Conclusion

This work presents the first synthesis of star block copolymers based on glycerol and glycolide. *hb*-PG-*b*-PGA multi-arm star copolymers have been prepared via a core first approach, using hyperbranched poly(glycerol) with different hydroxy functionalities as core molecules. The melt copolymerization with *hb*-PG as macroinitiator via $Sn(Oct)_2$ catalysis afforded well-defined complex polymer structures with predictable molecular weights. In contrast to their linear analogs of comparable molecular weight, the polymers exhibited superior solubility in organic solvents such as DMF and DMSO. This permitted detailed characterization via 1D and 2D NMR, SEC and DSC. It should be emphasized that the multi-arm star polymers presented possess molecular weights up to 31,000 g/mol and high glycolide weight content up to approximately 91 wt %. The short chain lengths of the oligoglycolic acid chains along with the increased number of end-groups are expected to enhance hydrolytic degradability significantly, rendering the novel materials promising candidates for drug release applications.

Experimental

Instrumentation

^{1}H NMR spectra were recorded at 300 MHz on a Bruker AC 300. The spectra were measured in DMSO-d_6 and the chemical shifts were referenced to residual solvent signals (^{1}H proton NMR signal: 2.50 ppm). 2D NMR experiments were performed on a Bruker Avance-II-400 (400 MHz) equipped with an inverse multinuclear 5 mm probe head and a *z*-gradient coil. Standard pulse sequences for gs-COSY and gs-NOESY experiments were used. The refocusing delays for the inverse hetero-correlations were set to 3.45 and 62.5 ms, corresponding to $^1J_{C,H}$ = 145 Hz and $^nJ_{C,H}$ = 8 Hz, respectively.

For SEC measurements in DMF (containing 1 g/l of lithium bromide as an additive), an Agilent 1100 series was used as an integrated instrument, including a PSS Gral column (10^4/10^4/10^2 Å porosity) and RI detector. Calibration was achieved with poly(ethylene glycol) standards provided by Polymer Standards Service (PSS)/Germany. Differential scanning calorimetry (DSC) measurements were carried out on a Perkin-Elmer 7 Series Thermal Analysis System with auto sampler in the temperature range from −40 to 230 °C at a heating rate of 20 K/min. The melting points of indium (T_m = 156.6 °C) and Millipore water (T_m = 0 °C) were used for calibration.

Reagents

Diglyme (99%) and glycidol (Sigma Aldrich) were purified by vacuum distillation over CaH_2 directly prior to use. Tetrahydrofuran (THF) was refluxed with sodium/benzophenone before distillation. Glycolide was purchased from Purac®/Gorinchem (Netherlands) and used as received. Tin(II)-2-ethylhexanoate ($Sn(Oct)_2$), 97% was obtained from Acros and used as received.

The synthesis of *hb*-PG was conducted as described in previous publications, using the slow monomer addition technique [21,25,26].

Table 2: Thermal properties of selected multi-arm star copolymers.

samples	GA units/arm (theor.)	GA units/arm (found)	T_g (°C)	ΔH_m (J/g)	T_m (°C)
$P(G_{38}GA_4)$	4	5.6	10.13	3.1	161.4
$P(G_{38}GA_8)$	8	8.6	15.44	57.6	180.7
$P(G_{38}GA_{12})$	12	9.8	17.5	59.9	189.5

"Grafting from" polymerization of glycolide with hyperbranched polyglycerol-polyol as a macroinitiator. In a typical experiment, exemplified for the synthesis of star block copolymers *hb*-PG_{38}-*b*-GA_6, 0.530 g *hb*-PG_{38} (0.181 mmol/ 7.33 mmol of primary and secondary hydroxy groups, according to Equation 1) was placed in a flask immersed in an oil bath at 120 °C and evacuated for at least 20 min. Glycolide 2.55 g (22.0 mmol) was charged into the flask, which was then re-immersed in the oil bath. To the homogeneous melt, 75 μL of a 10% solution of $Sn(Oct)_2$ (0.022 mmol) was injected. The mixture was stirred vigorously under N_2 atmosphere for 24 h. After cooling, the mixture was dissolved in hexafluoroisopropanol and precipitated in excess diethyl ether. The precipitation/ purification process was carried out twice to yield pure polymer. The product was isolated by filtration and dried in vacuum at room temperature for 24 h to yield a white powder in all cases, except for the copolymer with an average targeted GA amount of two units per arm ($P(G_{38}GA_2)$), which was a viscous, non-transparent white oil.

Acknowledgements

Florian Wolf acknowledges the IMPRS (International Max Planck-Research School) of the Max Planck Society for continuous support. The authors thank Heinz Kolshorn for his valuable help with the detailed NMR characterization of the materials. Holger Frey acknowledges valuable support from the Fonds der Chemischen Industrie as well as from the SFB 625.

References

1. Sanda, F.; Sanada, H.; Shibasaki, Y.; Endo, T. *Macromolecules* **2002,** *35,* 680–683. doi:10.1021/ma011341f
2. Li, Y.; Kissel, Th. *Polymer* **1998,** *39,* 4421–4427. doi:10.1016/S0032-3861(97)10362-7
3. Sekine, S.; Yamauchi, K.; Aoki, A.; Asakura, T. *Polymer* **2009,** *50,* 6083–6090. doi:10.1016/j.polymer.2009.10.040
4. Lu, C.; Liu, L.; Guo, S.-R.; Zhang, Y.; Li, Z.; Gu, J. *Eur. Polym. J.* **2007,** *43,* 1857–1865. doi:10.1016/j.eurpolymj.2007.02.039
5. Buwalda, S. J.; Dijkstra, P. J.; Calucci, L.; Forte, C.; Feijen, J. *Biomacromolecules* **2010,** *11,* 224–232. doi:10.1021/bm901080d
6. Burgath, A.; Sunder, A.; Neuner, I.; Mülhaupt, R.; Frey, H. *Macromol. Chem. Phys.* **2000,** *201,* 792–797. doi:10.1002/(SICI)1521-3935(20000401)201:7<792::AID-MACP792>3.0.CO;2-K
7. Wolf, F. K.; Frey, H. *Macromolecules* **2009,** *42,* 9443–9456. doi:10.1021/ma9016746
8. Joziasse, C. A. P.; Grablowitz, H.; Pennings, A. J. *Macromol. Chem. Phys.* **2000,** *201,* 107–112. doi:10.1002/(SICI)1521-3935(20000101)201:1<107::AID-MACP107>3.0.CO;2-W
9. Satoh, T. *Soft Matter* **2009,** *5,* 1972–1982. doi:10.1039/b819748b
10. Jones, M.-C.; Gao, H.; Leroux, J.-C. *J. Controlled Release* **2008,** *132,* 208–215. doi:10.1016/j.jconrel.2008.05.006
11. Lemmouchi, Y.; Perry, M. C.; Amass, A. J.; Chakraborty, K.; Schacht, E. *J. Polym. Sci., Part A: Polym. Chem.* **2007,** *45,* 3966–3974. doi:10.1002/pola.22150
12. Jie, P.; Venkatraman, S. S.; Min, F.; Freddy, B. Y. C.; Huat, G. L. *J. Controlled Release* **2005,** *110,* 20–33. doi:10.1016/j.jconrel.2005.09.011
13. Lapienis, G. *Prog. Polym. Sci.* **2009,** *34,* 852–892. doi:10.1016/j.progpolymsci.2009.04.006
14. Finne, A.; Albertsson, A.-C. *Biomacromolecules* **2002,** *3,* 684–690. doi:10.1021/bm020009o
15. Tsuji, H.; Miyase, T.; Tezuka, Y.; Saha, S. K. *Biomacromolecules* **2005,** *6,* 244–254. doi:10.1021/bm049552q
16. Nagahama, K.; Shimizu, K.; Ouchi, T.; Ohya, Y. *React. Funct. Polym.* **2009,** *69,* 891–897. doi:10.1016/j.reactfunctpolym.2009.09.004
17. Zhao, Y.; Shuai, X.; Chen, C.; Xi, F. *Chem. Mater.* **2003,** *15,* 2836–2843. doi:10.1021/cm0210694
18. Zhao, Y.; Shuai, X.; Chen, C.; Xi, F. *Macromolecules* **2004,** *37,* 8854–8862. doi:10.1021/ma048303r
19. Wolf, F. K.; Frey, H. *Macromolecules* **2009,** *42,* 9443–9456. doi:10.1021/ma9016746
20. Cao, P.-F.; Xiang, R.; Liu, X.-Y.; Zhang, C.-X.; Cheng, F.; Chen, Y. *J. Polym. Sci., Part A: Polym. Chem.* **2009,** *47,* 5184–5193. doi:10.1002/pola.23568
21. Sunder, A.; Hanselmann, R.; Frey, H.; Mülhaupt, R. *Macromolecules* **1999,** *32,* 4240–4246. doi:10.1021/ma990090w
22. Sunder, A.; Frey, H.; Mülhaupt, R. *Macromol. Symp.* **2000,** *153,* 187–196. doi:10.1002/1521-3900(200003)153:1<187::AID-MASY187>3.0.CO;2-I
23. Sunder, A.; Mülhaupt, R.; Haag, R.; Frey, H. *Adv. Mater.* **2000,** *12,* 235–239. doi:10.1002/(SICI)1521-4095(200002)12:3<235::AID-ADMA235>3.0.CO;2-Y
24. Wilms, D.; Wurm, F.; Nieberle, J.; Böhm, P.; Kemmer-Jonas, U.; Frey, H. *Macromolecules* **2009,** *42,* 3230–3236. doi:10.1021/ma802701g
25. Wilms, D.; Stiriba, S.-E.; Frey, H. *Acc. Chem. Res.* **2010,** *43,* 129–141. doi:10.1021/ar900158p
26. Calderón, M.; Quadir, M. A.; Sharma, S. K.; Haag, R. *Adv. Mater.* **2010,** *22,* 190–218. doi:10.1002/adma.200902144
27. Knischka, R.; Lutz, P. J.; Sunder, A.; Mülhaupt, R.; Frey, H. *Macromolecules* **2000,** *33,* 315–320. doi:10.1021/ma991192p
28. Frey, H.; Haag, R. *Rev. Mol. Biotechnol.* **2002,** *90,* 257–267. doi:10.1016/S1389-0352(01)00063-0
29. Shen, Y.; Kuang, M.; Shen, Z.; Nieberle, J.; Duan, H.; Frey, H. *Angew. Chem., Int. Ed.* **2008,** *47,* 2227–2230. doi:10.1002/anie.200704572
30. Sunder, A.; Krämer, M.; Hanselmann, R.; Mülhaupt, R.; Frey, H. *Angew. Chem., Int. Ed.* **1999,** *38,* 3552–3555. doi:10.1002/(SICI)1521-3773(19991203)38:23<3552::AID-ANIE3552>3.0.CO;2-G
31. Slagt, M. Q.; Stiriba, S.-E.; Klein Gebbink, R. J. M.; Kautz, H.; Frey, H.; van Koten, G. *Macromolecules* **2002,** *35,* 5734–5737. doi:10.1021/ma020094s
32. Stiriba, S.-E.; Kautz, H.; Frey, H. *J. Am. Chem. Soc.* **2002,** *124,* 9698–9699. doi:10.1021/ja026835m
33. Burakowska, E.; Quinn, J. R.; Zimmerman, S. C.; Haag, R. *J. Am. Chem. Soc.* **2009,** *131,* 10574–10580. doi:10.1021/ja902597h
34. Gottschalk, C.; Wolf, F.; Frey, H. *Macromol. Chem. Phys.* **2007,** *208,* 1657–1665. doi:10.1002/macp.200700168

35. Chen, Y.; Shen, Z.; Barriau, E.; Kautz, H.; Frey, H. *Biomacromolecules* **2006,** *7,* 919–926. doi:10.1021/bm050784e
36. Kasperczyk, J. *Macromol. Chem. Phys.* **1999,** *200,* 903–910. doi:10.1002/(SICI)1521-3935(19990401)200:4<903::AID-MACP903>3.0.CO;2-6
37. Dali, S.; Lefebvre, H.; El Gharbi, R.; Fradet, A. *e-Polym.* **2007,** No. 65.
38. Dali, S.; Lefebvre, H.; El Gharbi, R.; Fradet, A. *J. Polym. Sci., Part A: Polym. Chem.* **2006,** *44,* 3025–3035. doi:10.1002/pola.21405
39. Baker, G. L.; Vogel, E. B.; Smith, M. R., III. *Polym. Rev.* **2008,** *48,* 64–84. doi:10.1080/15583720701834208

License and Terms

This is an Open Access article under the terms of the Creative Commons Attribution License (http://creativecommons.org/licenses/by/2.0), which permits unrestricted use, distribution, and reproduction in any medium, provided the original work is properly cited.

The license is subject to the *Beilstein Journal of Organic Chemistry* terms and conditions: (http://www.beilstein-journals.org/bjoc)

The definitive version of this article is the electronic one which can be found at: doi:10.3762/bjoc.6.67

Beilstein Journal of Organic Chemistry

Synthesis, electronic properties and self-assembly on Au{111} of thiolated (oligo)phenothiazines

Adam W. Franz[1], Svetlana Stoycheva[2], Michael Himmelhaus[2] and Thomas J. J. Müller[*1]

Full Research Paper

Open Access

Address:
[1]Institut für Organische Chemie und Makromolekulare Chemie, Heinrich-Heine-Universität Düsseldorf, Universitätsstr. 1, D-40225 Düsseldorf, Germany and [2]Physikalisch-Chemisches Institut, Ruprecht-Karls-Universität Heidelberg, Im Neuenheimer Feld 253, D-69120 Heidelberg, Germany

Email:
Thomas J. J. Müller[*] - ThomasJJ.Mueller@uni-duesseldorf.de

* Corresponding author

Keywords:
cyclic voltammetry; ellipsometry; phenothiazines; SAM; thiols

Beilstein J. Org. Chem. **2010,** *6,* No. 72. doi:10.3762/bjoc.6.72

Received: 15 April 2010
Accepted: 02 June 2010
Published: 02 July 2010

Guest Editor: H. Ritter

© 2010 Franz et al; licensee Beilstein-Institut.
License and terms: see end of document.

Abstract

(Oligo)phenothiazinyl thioacetates, synthesized by a one-pot sequence, are electrochemically oxidizable and highly fluorescent. SAMs can be readily formed from thiols prepared by in situ deprotection of the thioacetates in the presence of a gold-coated silicon wafer. Monolayer formation is confirmed by ellipsometry and the results compared to those obtained by force field and DFT calculations.

Introduction

Functional organic π-systems [1] are of great relevance in the miniaturization of electronic devices particularly since they could serve as molecular switches, wires, and transistors [2-5]. As a consequence, the molecule-based bottom-up approach to nanodimensional structured self-assembled monolayers (SAMs) on well-defined metal surfaces has become a groundbreaking strategy in the development of molecular electronics [6]. In recent years, many investigations into SAMs of organic molecules on gold surfaces have been carried out [7]. Thiols, thiol esters, and disulfides can be easily chemisorbed on gold to form SAMs by exposure of well-defined gold substrates to solutions of sulfur functionalized molecules [7-14]. These "alligator-clips" [15-17] are able to bind functional molecules covalently to gold{111}-surfaces. Phenyl derivatives [18,19], conjugated bi- [18,20] and oligophenyls [18,20,21], oligothiophenes [18], porphyrin derivatives [20], phenanthrenes [22,23], fullerenes [24], and optically active naphthalenes [25] adsorbed on gold were studied in break-junction experiments and their properties on conductance, 1-bit random access memory and, especially, with regard to their ability to function as conductive molecular wires investigated. Among many heteroaromatic systems, phenothiazines, their derivatives and oligomers are interesting building blocks for rigid-rod and wire-like molecular modules for single-molecule electronics as a

consequence of their electronic properties. In particular, their reversible formation of stable radical cations [26-31], their tunable redox and fluorescence properties [32-34], and their tendency to self-assemble on surfaces by π–π interactions [35] make them eligible for use as redox-switchable molecular entities. In addition, the inherent folded conformation of phenothiazines [36], with a folding angle of 158.5°, represents an intriguing new aspect for the formation of self-assembled monolayers (SAMs) of this class of compounds. Furthermore, the transformation of phenothiazines into stable planar radical cations with excellent delocalization [37] qualifies them as excellent models for switchable conductive or semiconductive molecular wires. Encouraged by successful electrode modifications with conjugated thiolated anilines [38] and SAM formation of thiolated phenylethynyl phenothiazines [39], and in continuation of our investigations directed towards the synthesis and study of (oligo)phenothiazine-based functional π-systems [40-46], we have now focused our attention on thiolated phenothiazines and (oligo)phenothiazines as "alligator-clips". Here, we report the synthesis of phenothiazines and their oligomers bearing "alligator-clips" and their electronic properties as studied by cyclic voltammetry (CV), spectroscopic and spectrometric methods. Furthermore, their chemisorption and SAM formation on Au{111} were studied by ellipsometry.

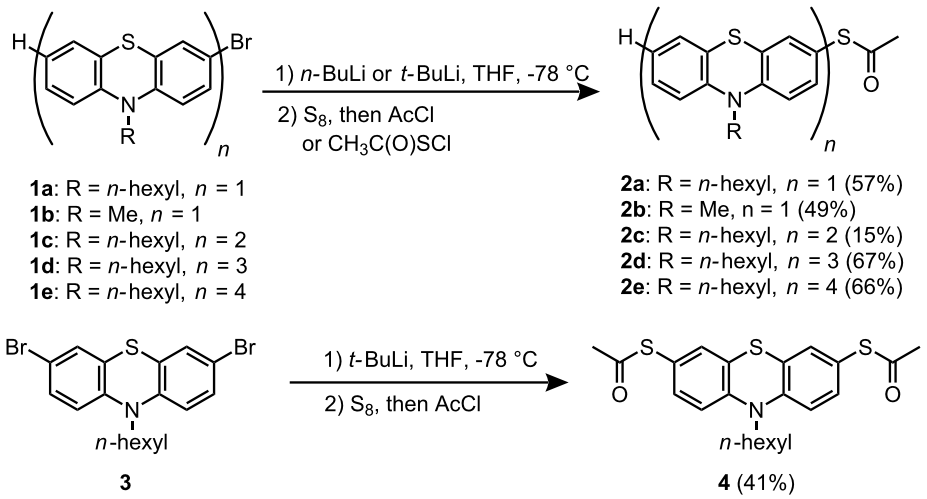
Results and Discussion

Synthesis

The facile bromine–lithium exchange of bromo phenothiazines [47-49] and the subsequent electrophilic trapping reactions of the resulting lithio phenothiazines [50,51] with different electrophiles set the stage for a straightforward synthesis of thiolated (oligo)phenothiazines. Therefore, the synthesis of thiofunctionalized phenothiazines can be accomplished according to a standard protocol [18]. Thus, solutions of bromo phenothiazines **1** [32,52] were cooled to −78 °C and reacted with *n*-BuLi (**1a** and **1b**) or *t*-BuLi (**1c–e** and **3**), respectively, to give the corresponding lithio phenothiazines via bromine–lithium exchange. Subsequent addition of elemental sulfur, followed by stirring for 5 min at −78 °C, and the addition of freshly distilled acetyl chloride furnished the desired (oligo)phenothiazinyl thioacetates **2** and **4** in moderate to good yields (Scheme 1). However, in the case of dyad **1c** thiolation was only accomplished by addition of acetylsulfur chloride [53] to the lithio species at low temperature, albeit the thiofunctionalized derivative **2c** was obtained in only 15% yield. The structures of the (oligo)phenothiazinyl thioacetates **2** and **4** were unambiguously supported by ^{1}H and ^{13}C NMR spectroscopy, mass spectrometry and elemental analysis.

Electronic properties

The electronic properties of the (oligo)phenothiazinyl thioacetates **2** and **4** were investigated by absorption and emission spectra, and cyclic voltammetry (Table 1). Optical spectroscopy (UV–vis and fluorescence spectra) revealed that only the triad **2d** and the tetrad **2e** displayed considerable fluorescence with emission of greenish-blue light and large Stokes shifts (Figure 1, $\Delta\tilde{\nu}$ 6400–6600 cm^{-1}). While the absence of fluorescence of monophenothiazines **2a**, **2b**, and **4** with heavy atom substitution and consequently, increased spin–orbit coupling is not too surprising, the presence of a diphenothiazine unit (**2c**) is not sufficient. Hence, at least two covalently bound phenothiazines without an additional sulfur substituent appears to be the prerequisite for intense fluorescence of oligophenothiazinyl thioacetates.



Scheme 1: Synthesis of (oligo)phenothiazinyl thioacetates **2** and **4**.

Table 1: Selected electronic properties of (oligo)phenothiazinyl thioacetates **2** and **4** (absorption[a] and emission spectra[a] and cyclic voltammetry[b]).

	Absorption $\lambda_{max,abs}$ (nm)	Emission $\lambda_{max,em}$ (nm)	Stokes shift $\Delta\tilde{\nu}$ (cm^{-1})	$E_0^{0/+1}$ (mV)	$E_0^{+1/+2}$ (mV)	$E_0^{+2/+3}$ (mV)
2a	266, 310	–	–	800	–	–
2b	264, 316	–	–	838	–	–
2c	276, 324, 366	–	–	668	853	–
2d	280, 326, 364	474	6400	608	765	876
2e	282, 326, 362	476	6600	597	690	842[c]
4	272, 326	–	–	875	–	–

[a]Recorded in CH_2Cl_2.
[b]Recorded in CH_2Cl_2, 20 °C, v = 100 mV/s, electrolyte: n-$Bu_4N^+PF_6^-$, Pt working electrode, Pt counter-electrode, Ag/AgCl reference electrode.
[c]The third and fourth oxidation waves coincide.

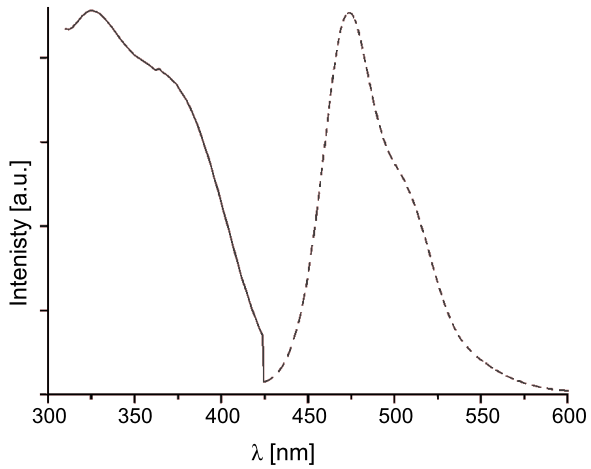


Figure 1: Normalized absorption (solid line) and emission (dashed line) spectra of thioacetate **2d** (recorded in dichloromethane, T = 298 K).

Electrochemical data for (oligo)phenothiazinyl thioacetates **2** and **4** were obtained by cyclic voltammetry in the anodic region (scan area up to 1.5 V). The reversible first oxidations to the radical cations of monophenothiazines **2a**, **2b**, and **4** were shifted anodically in comparison to unsubstituted monophenothiazines [54] as a consequence of the electron-withdrawing nature of the thioacetate. Due to unsymmetrical substitution, the dyad **2c** showed two distinctly separated, reversible oxidations at $E_0^{0/+1}$ = 668 mV and $E_0^{+1/+2}$ = 853 mV. The cyclic voltammogram of the triad **2d** displayed three distinctly separated, reversible oxidations at $E_0^{0/+1}$ = 608 mV, $E_0^{+1/+2}$ = 765 mV, and $E_0^{+2/+3}$ = 876 mV (Figure 2). However, the electrochemistry of the tetrad **2e** is more complicated. Only three distinctly separated, reversible oxidations were evident. The first oxidations at $E_0^{0/+1}$ = 597 mV and $E_0^{+1/+2}$ = 690 mV are in accordance with Nernstian behavior, while the third oxidation at E_0 = 842 mV reveals a large difference of ΔE = 132 mV for the current peaks of the oxidation and the reduction wave. Presumably, the expected third and fourth oxidations coincide and give rise to a combined quasi-reversible peak.

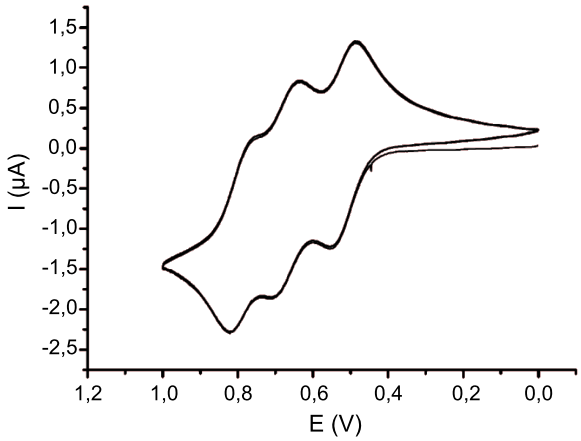
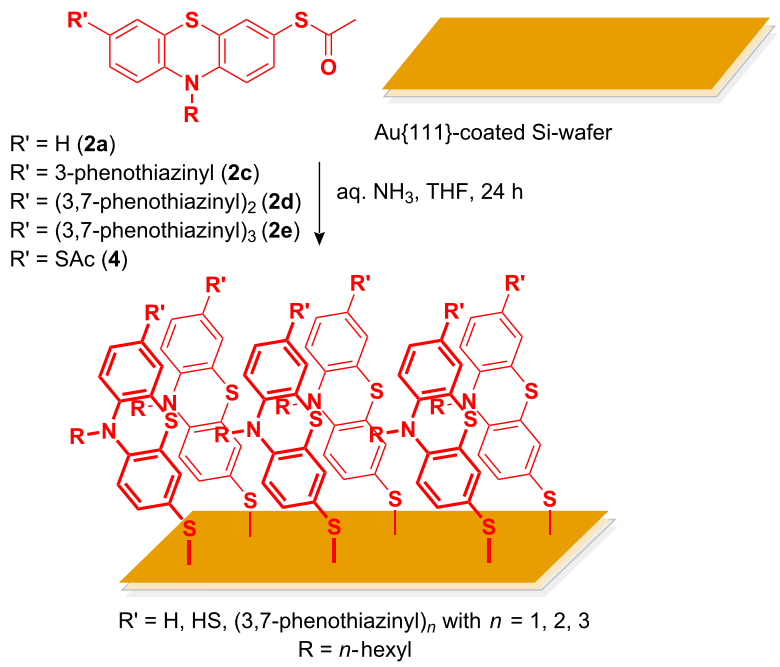


Figure 2: Cyclic voltammogram of thioacetate **2d** (recorded in CH_2Cl_2, T = 293 K; 0.1 M electrolyte $[Bu_4N][PF_6]$; v = 100 mV/s; Pt-working electrode, Ag/AgCl-reference and Pt-counter electrode.

Self-assembly and ellipsometry

SAMs on a Au{111}-coated silicon wafer substrate were prepared from (oligo)phenothiazinyl thioacetates **2** or **4** by in situ saponification with degassed aqueous ammonia in THF at room temperature for 24 h (Scheme 2).

Based upon thorough surface analysis of the previously studied thiolated phenylethynyl phenothiazines chemisorbed on Au{111} by ellipsometry, contact angle measurements, X-ray photoelectron spectroscopy, and infrared reflection absorption spectroscopy (IRRAS) [39], we applied ellipsometry in combination with molecular modeling at the force field and DFT levels of theory for the characterization of SAMs of in situ liberated (oligo)phenothiazinyl thiols on Au{111}. The ability of the molecules to form SAMs was investigated by solution adsorption of different systems onto gold films of 100 nm thickness



Scheme 2: Preparation of SAMs from (oligo)phenothiazinyl thioacetates **2** or **4** on a Au{111}-coated silicon wafer substrate.

thermally evaporated onto Si wafers using 10 nm of Ti as adhesion promoter. This procedure is known to yield polycrystalline gold films with preferential {111} orientation [55].

The thickness of the layer was determined by ellipsometry as described above. As an estimate for the molecular dimensions of the monolayers, the structures of the (oligo)phenothiazines **2** and **4** were computed at the MM2 and DFT levels of theory (Table 2) [56].

To minimize computational time in the latter calculations, the hexyl substituents were truncated to methyl groups. From these calculations, the theoretical layer thickness was calculated according to $d_{th} = l_{mol} \cos \varphi + l_{Au-S}$, where l_{mol} is the calculated length of the respective molecule, φ is the molecules' tilt angle with the surface normal, and $l_{Au-S} = 2.1$ Å is the Au–S bond length [57]. For φ, we refer to a recent electron spectroscopic analysis on similar aromatic systems, which determined φ = 23° for anthracene-2-thiol [58]. Using this value, we made the reasonable assumption that the Au–S–C bond is mainly influenced by the adjacent phenyl system. Table 2 shows d_{th} for the different molecules along with the experimental thickness d_{exp} as determined by ellipsometry. The theoretical thicknesses are given for MM2 as well as DFT calculations. As a simple

Table 2: Measured (ellipsometry) and calculated (MM2, DFT) layer thickness of (oligo)phenothiazinyl thioacetates **2a**, **2c–e**, and **4** on Au{111}-coated silicon wafers.

Compound[a]	Measured layer thickness d_{exp}[b] (Å)	Calculated molecule length l_{mol}		Calculated layer thickness d_{th}[d]		Coverage θ[e]		Monolayer
		MM2 (Å)	DFT[c] (Å)	MM2 (Å)	DFT[c] (Å)	MM2 (%)	DFT[c] (%)	
2a	9.0 ± 1.00	9.04	9.10	10.4	10.5	86.6 ± 9.56	86.1 ± 9.50	Yes
2c	11.4 ± 0.99	17.5	15.3	18.2	16.2	62.6 ± 5.41	70.4 ± 6.09	Poor
2d	18.0 ± 1.44	19.1	21.6	19.7	22.0	91.5 ± 7.32	81.9 ± 6.56	Yes
2e	10.9 ± 1.61	25.5	22.4	25.6	22.7	42.6 ± 6.28	48.0 ± 7.07	Poor
4	12.9 ± 1.06	11.7	10.4	12.9	11.7	100.2 ± 8.22	110.5 ± 9.07	Yes

[a]Thioacetate precursor.
[b]Measured by ellipsometry. Errors given are the figures of merit of the least squares fitting routine as determined by the ellipsometer built-in software. [c]DFT calculations (B3LYP/3-21G), the hexyl group was replaced by a methyl group [28]. [d]$d_{th} = l_{mol} \cos \varphi + l_{Au-S}$; $l_{Au-S} = 2.1$ Å; $\varphi_{anthracene-2-thiol} = 23°$. [e]$\theta = d_{exp}/d_{th}$.

measure of monolayer formation of the different systems, the relative coverage θ obtained experimentally is calculated from $\theta = d_{exp}/d_{th}$ as given in Table 2. From these values it is clear that of **2**, only **2a** and **2d** show good SAM formation, suggesting an odd–even effect on film growth, which might be related to steric hindrance during adsorption when an even number of phenothiazine units are present, e.g., because of a back bending of the thiol-bound molecule to the gold surface in these cases, supported by additional gold-π-interactions with the terminal phenothiazine, which thus would hamper the formation of a SAM with an almost parallel intermolecular orientation. In corroboration of such disorder effects, coverage seems to decrease with increasing molecule length for even-numbered molecules (cf. Table 2). The highest coverage was obtained with **4**, which is not surprising, because the thiol bifunctionality allows chemisorption of the molecule at either side, which reduces the impact of steric effects on the adsorption kinetics and thus may lead to a more densely packed film. As a consequence, thiolated mono- and terphenothiazines **2** (n = 1, 3) and the dithiolated derivative **4** can be easily self-assembled to give stable monolayers on gold surfaces. This feature makes this class of redox-active molecular entities highly interesting for the fabrication of functionalized electroactive surfaces and nanostructured devices.

Conclusion

In summary we have shown a concise, general synthetic access to (oligo)phenothiazinyl thioacetates that are suitable precursors for the formation of thiol-bound (oligo)phenothiazines on gold surfaces. Whereas the first oligomers are non-fluorescent, the triad and the tetrad display intense greenish-blue fluorescence in addition to distinct multiple reversible oxidation. The in situ deprotection of the thioacetates to thiols in the presence of a gold-coated silicon wafer was used to prepare self-assembled monolayers, which were unambiguously characterized by ellipsometry and accompanying force field and DFT calculations. The chemical trigger of gradual thiol liberation enables better control of film formation and adsorption kinetics, which can be very useful, for example, for co-adsorption of the moieties with a second, nonconductive molecule, which serves as an insulating matrix. Further studies directed toward such more-complex (oligo)phenothiazine SAMs on gold and functionalized redox manipulable surfaces, the nanoscopic characterization of the monolayers as well as their manipulation with external stimuli are currently underway.

Experimental

General considerations

Reagents, catalysts, ligands, and solvents were purchased reagent grade materials and used without further purification. THF and acetyl chloride were dried and distilled according to standard procedures [59]. The bromo phenothiazines **1a** [50,51], **1b** [50,51], **1c** and **1d** [32,52] and **3** [50,51], and acetylsulfur chloride [53] were prepared according to literature procedures. Column chromatography: silica gel 60, mesh 70–230. TLC: silica gel coated plates. ^{1}H and ^{13}C NMR spectra: CD_2Cl_2, $CDCl_3$, and [D_6]-acetone (locked to Me_4Si) [60]. The assignments of quaternary C, CH, CH_2, and CH_3 were made by using DEPT spectra. Elemental analyses were carried out in the Microanalytical Laboratories of the Organisch-Chemisches Institut, Ruprecht-Karls-Universität Heidelberg, Germany.

Electrochemistry

Cyclic voltammetry experiments (EG & G potentiostatic instrumentation) were performed under an argon atmosphere in dry and degassed CH_2Cl_2 at room temperature and at scan rates of 100, 250, 500, and 1000 mV/s. The electrolyte was Bu_4NPF_6 (0.025 M). The working electrode was a 1 mm platinum disk, the counter-electrode was a platinum wire, and the reference electrode was an Ag/AgCl electrode. The potentials were corrected to the internal standard of Fc/Fc^+ in CH_2Cl_2 ($E_0^{0/+1}$ = 450 mV) [61].

7-Bromo-10,10′,10″,10‴-tetrahexyl-10*H*,10′*H*,10″*H*,10‴*H*-3,3′:7′,3″:7″,3‴-quaterphenothiazine (**1e**)

1.90 g (2.95 mmol) 7-Bromo-10,10′-dihexyl-10*H*,10′*H*-3,3′-biphenothiazine (**1c**) [32,52], 2.37 g (4.43 mmol) 10-hexyl-3,7-bis-(4,4,5,5-tetramethyl-[1,3,2]-dioxaborolan-2-yl)-10*H*-phenothiazine [50,51], and 2.45 g (17.7 mmol) potassium bicarbonate were dissolved in 100 mL of DME and 20 mL of water. The mixture was degassed by purging with argon gas for 20 min. After the addition of 136 mg of tetrakis(triphenylphosphan)palladium (118 μmol, 4 mol %), the reaction mixture was stirred for 12 h at 85 °C. After cooling to room temperature, 50 mg of Na_2SO_3 was added and the reaction mixture stirred for 14 h at room temperature. Then, 3.17 g (6.49 mmol) of 3-bromo-10-hexyl-7-iodo-10*H*-phenothiazine [51] was added and the mixture stirred for 4 d at 85 °C. After the addition of 100 mL of water, the crude product was extracted several times with dichloromethane. The combined organic phases were dried with magnesium sulfate and the solvents removed in vacuo. The residue was chromatographed on silica gel (hexane/acetone 50:1) to give 1.53 g (36%) of **1e** as a yellow resin. ^{1}H NMR (300 MHz, CD_2Cl_2): δ = 0.76–0.81 (m, 12H), 1.18–1.26 (m, 16H), 1.30–1.40 (m, 8H), 1.63–1.75 (m, 8H), 3.69–3.77 (m, 8H), 6.61–6.64 (m, 2H), 6.78–6.84 (m, 7H), 7.02–7.10 (m, 3H), 7.14–7.31 (m, 13H). ^{13}C NMR (75 MHz, CD_2Cl_2): δ = 14.2 (CH_3), 23.0 (CH_2), 26.9 (CH_2), 27.0 (CH_2), 31.8 (CH_2), 31.8 (CH_2), 47.9 (CH_2), 114.5 (C_{quat}), 115.9 (CH), 116.0 (CH), 116.9 (CH), 122.7 (CH), 124.6 (CH), 125.2 (CH), 125.4 (CH), 125.5 (CH), 125.7 (CH), 126.9 (C_{quat}), 127.6 (CH), 129.7 (CH),

130.2 (C_{quat}), 134.6 (C_{quat}), 144.7 (C_{quat}). MS (MALDI-TOF) *m*/*z* (%): 1206.3 (M^+, 100), 1126.4 ($M^+ - Br$), 1121.2 ($M^+ - C_6H_{13}$, 6), 1041.2 ($M^+ - Br - C_6H_{13}$, 6). MS (FAB^+) *m*/*z* (%): 1206.2 (M^+, 100), 1121.1 ($M^+ - C_6H_{13}$, 45), 1037.0 ($M^+ - 2C_6H_{13}$, 10), 951.0 ($M^+ - 3C_6H_{13}$, 9), 865.9 ($M^+ - 4C_6H_{13}$, 23). IR (KBr): ν = 2953, 2927, 2868, 2854, 1604, 1457, 1415, 1378, 1332, 1295, 1252, 1240, 1193, 1147, 806, 746 cm^{-1}. UV–vis (CH_2Cl_2): λ_{max} (ε) = 238 (6700), 282 (10500), 326 (3500), 376 nm (4300). Anal. Calcd for $C_{72}H_{77}BrN_4S_4$ (1206.6): C, 71.67; H, 6.43; N, 4.64; Br, 6.62; S, 10.63. Found: C, 71.54; H, 6.53; N, 4.64; Br, 6.91; S, 10.58.

Thioacetic acid *S*-(10-hexyl-10*H*-phenothiazin-3-yl) ester (**2a**)

To a cooled solution of 500 mg (1.38 mmol) of 3-bromo-10*H*-hexylphenothiazine (**1a**) in 25 mL of dry THF, 0.55 mL (1.52 mmol, 1.1 equiv) of 2.5 M *n*-butyllithium in hexanes was added dropwise over 5 min at −78 °C (dry ice/acetone). After stirring for 5 min at −78 °C, 49 mg (1.52 mmol, 1.1 equiv) of sulfur was added to the reaction mixture. After stirring for a further 5 min at −78 °C, 0.11 mL (1.52 mmol, 1.1 equiv) of acetyl chloride was added dropwise over 5 min. The solution was allowed to come to room temperature and stirred overnight. Then, 50 mL of water was added and the aqueous phase was extracted several times with small portions of dichloromethane. The combined organic phases were dried with magnesium sulfate and the solvents removed in vacuo. The residue was chromatographed on silica gel (hexane/acetone 10:1) to give 279 mg (57%) of **2a** as a yellow oil. R_f (hexane/acetone 5:1) = 0.45. ^{1}H NMR (D_6-acetone, 300 MHz): δ = 0.88 (t, ^3J = 6.9 Hz, 3H), 1.28 (m, 4H), 1.46 (m, 2H), 1.77 (m, 2H), 2.35 (s, 3H), 3.97 (t, ^3J = 7.2 Hz, 2H), 6.94 (m, 1H), 7.08 (m, 2H), 7.13 (m, 2H), 7.24 (m, 2H). ^{13}C NMR (D_6-acetone, 75 MHz): δ = 14.2 (CH_3), 23.2 (CH_2), 27.1 (CH_2), 27.4 (CH_2), 29.9 (CH_3), 32.1 (CH_2), 47.9 (CH_2), 116.9 (CH), 116.9 (CH), 121.9 (C_{quat}), 123.8 (CH), 126.2 (C_{quat}), 126.7 (C_{quat}), 128.1 (CH), 128.5 (CH), 133.7 (CH), 134.7 (CH), 145.6 (C_{quat}), 147.5 (C_{quat}), 194.2 (C_{quat}). MS (FAB^+) *m*/*z* (%): 357.3 (M^+, 100), 314.3 ($M^+ - COCH_3$, 18). IR (film): ν = 3061, 2954, 2928, 2855, 1708, 1593, 1486, 1462, 1393, 1377, 1126, 878, 812, 749, 615 cm^{-1}. UV–vis (CH_2Cl_2): λ_{max} (ε) = 240 (11600), 266 (24800), 310 nm (6200). Anal. Calcd for $C_{20}H_{23}NOS_2$ (357.1): C, 67.19; H, 6.48; N, 3.92. Found: C, 67.16; H, 6.52; N, 3.86.

Thioacetic acid *S*-(10-methyl-10*H*-phenothiazin-3-yl) ester (**2b**)

To a cooled solution of 292 mg (1.00 mmol) of 3-bromo-10*H*-methylphenothiazine (**1b**) in 10 mL of dry THF, 0.7 mL (1.1 mmol, 1.1 equiv) of 1.58 M *n*-butyllithium in hexanes was added dropwise over 5 min at −78 °C (dry ice/acetone). After stirring for 5 min at −78 °C, 35 mg (1.1 mmol, 1.1 equiv) of sulfur was added to the reaction mixture. After stirring for a further 5 min at −78 °C, 0.07 mL (1.1 mmol, 1.1 equiv) of acetyl chloride was added dropwise over 5 min. The solution was allowed to come to room temperature and stirred overnight. Then, 50 mL of water was added and the aqueous phase extracted several times with small portions of dichloromethane. The combined organic phases were dried with magnesium sulfate and the solvents removed in vacuo. The residue was chromatographed on silica gel (hexane/acetone 50:1) to give 141 mg (49%) of **2b** as a yellow oil. R_f (hexane/acetone 5:1) = 0.29. ^{1}H NMR (CD_2Cl_2, 300 MHz): δ = 2.38 (s, 3H), 3.36 (s, 3H), 6.84 (m, 2H), 6.96 (dt, ^dJ = 1.2 Hz, ^tJ = 4.5 Hz, 1H), 7.13 (m, 2H), 7.20 (m, 2H). ^{13}C NMR (CD_2Cl_2, 75 MHz): δ = 30.2 (CH_3), 35.7 (CH_3), 114.7 (CH), 114.8 (CH), 121.2 (C_{quat}), 122.9 (C_{quat}), 123.1 (CH), 124.5 (C_{quat}), 127.4 (CH), 127.9 (CH), 133.1 (CH), 134.4 (CH), 145.6 (C_{quat}), 147.4 (C_{quat}), 194.8 (C_{quat}). MS (EI^+) *m*/*z* (%): 287.0 (M^+, 100), 245.0 ($M^+ - COCH_3$, 62), 230.3 ($M^+ - COCH_3 - CH_3$, 68), 212.0 ($M^+ - SCOCH_3$, 16). HR-MS (EI^+) *m*/*z* Calcd for $C_{15}H_{13}NOS_2$: 287.0438. Found: 287.0458. IR (KBr): ν = 3057, 2965, 2883, 2819, 1598 cm^{-1}. UV–vis (CH_2Cl_2): λ_{max} (ε) = 264 (71200), 316 nm (12800). Anal. Calcd for $C_{15}H_{13}NOS_2$ (287.0): C, 62.69; H, 4.56; N, 4.87. Found: C, 62.68; H, 4.78; N, 4.81.

S-(10,10′-Dihexyl-10*H*,10′*H*-3,3′-biphenothiazin-7-yl) ethanethioate (**2c**)

To a cooled solution of 500 mg (0.78 mmol) of 7-bromo-10,10′-dihexyl-10*H*,10′*H*-3,3′-biphenothiazine (**1c**) in 25 mL of dry THF, 0.91 mL (1.55 mmol, 2.0 equiv) of 1.7 M *t*-butyllithium in pentane was added dropwise over 5 min at −78 °C (dry ice/acetone). After stirring for 10 min at −78 °C, 95 mg (0.78 mmol, 1.0 equiv) of acetylsulfur chloride [25] was added to the reaction mixture. The solution was allowed to come to room temperature and stirred overnight. Then 30 mL of water was added and the aqueous phase was extracted several times with small portions of dichloromethane. The combined organic phases were dried with magnesium sulfate and the solvents were removed in vacuo. The residue was chromatographed on silica gel (hexane/acetone 50:1) to give 76 mg (15%) of **2c** as a yellow resin. R_f (hexane/acetone 5:1) = 0.42. ^{1}H NMR (CD_2Cl_2, 300 MHz): δ = 0.87 (t, ^3J = 6.6 Hz, 6H), 1.31 (m, 8H), 1.43 (m, 4H), 1.79 (m, 4H), 2.36 (s, 3H), 3.85 (t, ^3J = 6.9 Hz, 4H), 6.86 (m, 1H), 6.90 (m, 4H), 7.14 (m, 3H), 7.29 (m, 4H), 7.31 (m, 1H). ^{13}C NMR (CD_2Cl_2, 75 MHz): δ = 14.2 (CH_3), 23.0 (CH_2), 27.1 (CH_2), 27.1 (CH_2), 30.1 (CH_3), 31.9 (CH_2), 48.1 (CH_2), 115.8 (CH), 116.0 (CH), 116.2 (CH), 121.2 (C_{quat}), 122.7 (CH), 124.7 (C_{quat}), 124.9 (C_{quat}), 125.3 (C_{quat}), 125.3 (CH), 125.4 (C_{quat}), 125.6 (CH), 127.7 (CH), 133.4 (CH), 134.2 (CH), 134.4 (C_{quat}), 135.1 (C_{quat}), 143.9 (C_{quat}), 144.7 (C_{quat}), 146.9 (C_{quat}), 194.9 (C_{quat}). MS (FAB^+) *m*/*z* (%): 638.6 (M^+, 100), 595.5 ($M^+ - COCH_3$, 12), 553.4 ($M^+ - C_6H_{13}$, 14). HR-MS

(FAB$^+$) m/z Calcd for $C_{38}H_{42}N_2OS_3$: 638.2459. Found: 683.2445. IR (film): ν = 2960, 2927, 2854, 1706, 1601, 1575, 1459, 1416, 1393, 1377, 1334, 1040, 876, 809, 745, 616 cm^{-1}. UV–vis (CH_2Cl_2): λ_{max} (ε) = 276 nm (44900), 324 (18900), 366 nm (15400).

S-[10,10′-Dihexyl-7′-(10-hexyl-10*H*-phenothiazin-3-yl)-10*H*,10′*H*-3,3′-biphenothiazin-7-yl] ethanethioate (**2d**)

To a cooled solution of 800 mg (0.87 mmol) of 7-bromo-10,10′-dihexyl-7′-(10-hexyl-10*H*-phenothiazin-3-yl)-10*H*,10′*H*-3,3′-biphenothiazine (**1d**) in 25 mL of dry THF, 1.07 mL (1.82 mmol, 2.1 equiv) of 1.7 M *t*-butyllithium in pentane was added dropwise over 5 min at °C (dry ice/acetone). After stirring for 10 min at −78 °C, 29 mg (0.91 mmol, 1.1 equiv) of sulfur was added to the reaction mixture. After stirring for a further 10 min at −78 °C, 0.07 mL (0.95 mmol, 1.1 equiv) of acetyl chloride was added dropwise over 5 min. The solution was allowed to come to room temperature and stirred overnight. Then, 50 mL of water was added and the aqueous phase extracted several times with small portions of dichloromethane. The combined organic phases were dried with magnesium sulfate and the solvents removed in vacuo. The residue was chromatographed on silica gel (hexane to hexane/acetone 10:1) to give 536 mg (67%) of **2d** as a yellow resin. R_f (hexane/acetone 5:1) = 0.35. ^{1}H NMR (CD_2Cl_2, 300 MHz): δ = 0.88 (t, ^3J = 3 Hz, 9H), 1.31 (m, 12H), 1.44 (m, 6H), 1.80 (m, 6H), 2.36 (s, 3H), 3.85 (t, ^3J = 6 Hz, 6H), 6.90 (m, 7H), 7.14 (m, 5H), 7.29 (m, 7H). ^{13}C NMR (CD_2Cl_2, 75 MHz): δ = 14.2 (CH_3), 23.0 (CH_2), 27.0 (CH_2), 27.1 (CH_2), 30.2 (CH_3), 31.9 (CH_2), 36.3 (CH_2), 48.0 (CH_2), 115.8 (C_{quat}), 116.0 (CH), 116.2 (CH), 121.1 (C_{quat}), 122.7 (CH), 124.8 (C_{quat}), 125.2 (CH), 125.6 (CH), 127.7 (CH), 133.4 (CH), 134.2 (CH), 143.9 (C_{quat}), 144.7 (C_{quat}), 146.8 (C_{quat}), 194.9 (C_{quat}). MS (MALDI-TOF) m/z (%): 919.4 (M$^+$, 100), 877.4 (M$^+$ − $COCH_3$, 4). IR (KBr): ν = 2954, 2928, 2855, 1700, 1635, 1458, 1416, 1379, 1241, 1193, 873, 807, 747 cm^{-1}. UV–vis (CH_2Cl_2): λ_{max} (ε) = 280 (101000), 326 (38100), 364 nm (31400). Anal. calcd. for $C_{56}H_{61}N_3OS_4$: C, 73.08; H, 6.68; N, 4.57; S, 13.94. Found: C, 73.08; H, 6.60; N, 4.69; S, 13.99.

S-[10,10′,10″-Trihexyl-7′-(10-hexyl-10*H*-phenothiazin-3-yl)-10*H*,10′*H*,10″*H*-3,3′:7′,3″-terphenothiazin-7-yl] ethanethioate (**2e**)

To a cooled solution of 200 mg (0.17 mmol) of 7-(7′-bromo-10,10′-dihexyl-10*H*,10′*H*-3,3′-biphenothiazin-7-yl)-10,10′-dihexyl-10*H*,10′*H*-3,3′-biphenothiazine (**1e**) in 10 mL of dry THF, 0.20 mL (0.35 mmol, 2.1 equiv) of 1.7 M *t*-butyllithium in pentane was added dropwise over 5 min at −78 °C (dry ice/acetone). After stirring for 10 min at −78 °C, 6.0 mg (0.17 mmol, 1.0 equiv) of sulfur was added to the reaction mixture. After stirring for a further 10 min at −78 °C, 0.013 mL (0.18 mmol, 1.1 equiv) of acetyl chloride was added dropwise over 5 min. The solution was allowed to come to room temperature and stirred overnight. Then, 20 mL of water was added and the aqueous phase extracted several times with small portions of dichloromethane. The combined organic phases were dried with magnesium sulfate and the solvents removed in vacuo. The residue was chromatographed on silica gel (hexane to hexane/acetone 50:1) to give 132 mg (66%) of **2e** as a yellow resin. R_f (hexane/acetone 5:1) = 0.24. ^{1}H NMR (CD_2Cl_2, 300 MHz): δ = 0.87 (m, 12H), 1.31 (m, 16H), 1.43 (m, 8H), 1.79 (m, 8H), 2.36 (s, 3H), 3.86 (m, 8H), 6.89 (m, 8H), 7.12 (m, 7H), 7.31 (m, 10H). ^{13}C NMR (CD_2Cl_2, 75 MHz): δ = 14.2 (CH_3), 23.0 (CH_2), 27.0 (CH_2), 30.2 (CH_3), 31.9 (CH_2), 48.3 (CH_2), 115.9 (CH), 121.8 (C_{quat}), 125.5 (C_{quat}), 127.8 (C_{quat}), 131.1 (CH), 132.8 (CH), 133.5 (CH), 134.3 (CH), 140.1 (C_{quat}), 140.8 (C_{quat}), 146.3 (C_{quat}), 148.1 (C_{quat}), 194.9 (C_{quat}). MS (MALDI-TOF) m/z: 1200.5 (M$^+$), 1158.5 (M$^+$ − $COCH_3$), 1126.5 (M$^+$ − $SCOCH_3$), 1116.4 (M$^+$ − C_6H_{13}). IR (KBr): ν = 2955, 2928, 2854, 1706, 1634, 1604, 1575, 1459, 1415, 1379, 1333, 1241, 1192, 1106, 1062, 874, 807, 746, 616 cm^{-1}. UV/vis (CH_2Cl_2): λ_{max} (ε) = 282 (92900), 326 (33800), 362 nm (31000).

S,*S*′-(10-Hexyl-10*H*-phenothiazine-3,7-diyl) bis(ethanethioate) (**4**)

To a cooled solution of 800 mg (1.82 mmol) of 3,7-dibromo-10*H*-hexylphenothiazine (**3**) in 25 mL of dry THF, 4.38 mL (7.44 mmol, 4.1 equiv) of 1.7 M *t*-butyllithium in pentane was added dropwise over 5 min at −78 °C (dry ice/acetone). After stirring for 5 min at −78 °C, 122 mg (3.81 mmol, 2.1 equiv) sulfur was added to the reaction mixture. After stirring for a further 10 min at −78 °C, 0.27 mL (3.72 mmol, 2.1 equiv) of acetyl chloride was added dropwise over 5 min. The solution was allowed to come to room temperature and stirred overnight. Then, 50 mL of water was added and the aqueous phase extracted several times with small portions of dichloromethane. The combined organic phases were dried with magnesium sulfate and the solvents removed in vacuo. The residue was chromatographed on silica gel (hexane to hexane/acetone 50:1) to give 317 mg (41%) of **4** as a yellow oil. R_f (hexane/acetone 5:1) = 0.18. ^{1}H NMR (CD_2Cl_2, 300 MHz): δ = 0.91 (t, ^3J = 6.9 Hz, 3H), 1.33 (m, 4H), 1.42 (m, 2H), 1.80 (m, 2H), 2.38 (s, 6H), 3.85 (t, ^3J = 7.2 Hz, 2H), 6.88 (m, 1H), 6.90 (m, 1H), 7.12 (m, 2H), 7.17 (m, 1H), 7.20 (m, 1H). ^{13}C NMR (CD_2Cl_2, 75 MHz): δ = 14.2 (CH_3), 23.0 (CH_2), 26.9 (CH_2), 27.0 (CH_2), 30.2 (CH_3), 31.8 (CH_2), 48.2 (CH_2), 116.3 (CH), 121.8 (C_{quat}), 125.2 (C_{quat}), 133.5 (CH), 134.3 (CH), 146.3 (C_{quat}), 194.7 (C_{quat}). MS (MALDI-TOF) m/z: 431.0 (M$^+$), 388 (M$^+$ − $COCH_3$), 356 (M$^+$ − $SCOCH_3$). IR (film): ν = 2955, 2927, 2858, 1707, 1590, 1564, 1463, 1393, 1352, 1332, 1265, 1250,

1124, 949, 813, 615 cm^{-1}. UV–vis (CH_2Cl_2): λ_{max} (ε) = 272 (36000), 326 nm (7100). Anal. Calcd for $C_{20}H_{25}NO_2S_3$ (431.1): C, 61.22; H, 5.84; N, 3.24; S, 22.29. Found: C, 61.27; H, 5.95; N, 3.25; S, 20.70.

SAM preparation and ellipsometry

The (oligo)phenothiazinyl thioacetates **2a**, **2c–e**, and **4** were dissolved under an argon atmosphere in dry THF to give a 10^{-4} M solutions. Au-coated silicon wafers (surface area: 1 cm^2) were placed in these solutions. Upon the addition of a few drops of a concentrated solution of aqueous ammonia the thioacetates were saponified to liberate the thiol functionality necessary for chemisorption and SAM formation on gold. After 24 h the wafers were removed from the solution and rinsed several times with dry THF.

The thickness of the formed organic layers was determined by means of spectral ellipsometry (M-44, J.A. Woollam, USA) applying a 3-layer model consisting of gold substrate, organic layer, and ambient [62]. The organic layer was described by means of a Cauchy model, with the first two Cauchy parameters chosen such to yield a refractive index of 1.490 at 500 nm, which resulted from a study on biphenylthiolates on gold in excellent agreement with theory [63].

Supporting Information

Supporting Information File 1

Molecular modeling coordinates of **2a**, **2c**, **2d**, **2e**, and **4**, cyclic voltammograms of **2a**, **2b**, **2c**, **2d**, **2e**, and **4**, and absorption and emission spectra of **2d** and **2e**.
[http://www.beilstein-journals.org/bjoc/content/supplementary/1860-5397-6-72-S1.pdf]

Acknowledgements

The financial support of this work by the Deutsche Forschungsgemeinschaft (Graduate College 850, stipend for A. W. F.) and by the Fonds der Chemischen Industrie is gratefully acknowledged. The authors also thank the BASF SE for the generous donation of chemicals.

References

1. *Functional Organic Materials – Synthesis, Strategies, and Applications;* Müller, T. J. J.; Bunz, U. H. F., Eds.; Wiley-VCH: Weinheim, 2007. (see e.g., for a monography).
2. Timp, G. L. *Nanotechnology;* AIP Press/Springer: New York, 1999.
3. Waser, R. *Nanoelectronics and Information Technology: Advanced Electronic Materials and Novel Devices Information Technology;* Wiley-VCH: Weinheim, Germany, 2003.
4. Joachim, C.; Gimzewski, J. K.; Aviram, A. *Nature* **2000,** *408,* 541–548. doi:10.1038/35046000
5. Forrest, S. R. *Nature* **2004,** *428,* 911–918. doi:10.1038/nature02498
6. Tour, J. M. *Molecular Electronics: Commercial Insights, Chemistry, Devices, Architecture and Programming;* World Scientific: River Edge, NJ, 2003.
7. Love, J. C.; Estroff, L. A.; Kriebel, J. K.; Nuzzo, R. G.; Whitesides, G. M. *Chem. Rev.* **2005,** *105,* 1103–1170. doi:10.1021/cr0300789 (and references therein).
8. Tao, F.; Bernasek, S. L. *Chem. Rev.* **2007,** *107,* 1408–1453. doi:10.1021/cr050258d
9. Kriegisch, V.; Lambert, C. *Top. Curr. Chem.* **2005,** *258,* 257–313. doi:10.1007/b135682
10. Otsubo, T.; Aso, Y.; Takimiya, K. *J. Mater. Chem.* **2002,** *12,* 2565–2575. doi:10.1039/b203780g
11. Ulman, A. *Acc. Chem. Res.* **2001,** *34,* 855–863. doi:10.1021/ar0001564
12. Ulman, A. *Chem. Rev.* **1996,** *96,* 1533–1554. doi:10.1021/cr9502357
13. Kumar, A.; Abbott, N. L.; Kim, E.; Biebuyck, H. A.; Whitesides, G. M. *Acc. Chem. Res.* **1995,** *28,* 219–226. doi:10.1021/ar00053a003
14. Berry, J. F.; Cotton, F. A.; Murillo, C. A. *Organometallics* **2004,** *23,* 2503–2506. doi:10.1021/om049979d
15. Maya, F.; Flatt, A. K.; Stewart, M. P.; Shen, D. E.; Tour, J. M. *Chem. Mater.* **2004,** *16,* 2987–2997. doi:10.1021/cm049504c
16. Seminario, J. M.; Zacarias, A. G.; Tour, J. M. *J. Am. Chem. Soc.* **1999,** *121,* 411–416. doi:10.1021/ja982234c
17. Pearson, D. L.; Tour, J. M. *J. Org. Chem.* **1997,** *62,* 1376–1387. doi:10.1021/jo962335y
18. Tour, J. M.; Jones, L., II; Pearson, D. L.; Lamba, J. J. S.; Burgin, T. P.; Whitesides, G. M.; Allara, D. L.; Parikh, A. N.; Atre, S. *J. Am. Chem. Soc.* **1995,** *117,* 9529–9534. doi:10.1021/ja00142a021
19. Reed, M. A.; Zhou, C.; Muller, C. J.; Burgin, T. P.; Tour, J. M. *Science* **1997,** *278,* 252–254. doi:10.1126/science.278.5336.252
20. Tour, J. M.; Rawlett, A. M.; Kozaki, M.; Yao, Y.; Jagessar, R. C.; Dirk, S. M.; Price, D. W.; Reed, M. A.; Zhou, C.-W.; Chen, J.; Wang, W.; Campbell, I. *Chem.–Eur. J.* **2001,** *7,* 5118–5134. doi:10.1002/1521-3765(20011203)7:23<5118::AID-CHEM5118>3.0.CO;2-1
21. Bumm, L. A.; Arnold, J. J.; Cygan, M. T.; Dunbar, T. D.; Burgin, T. P.; Jones, L., II; Allara, D. L.; Tour, J. M.; Weiss, P. S. *Science* **1996,** *271,* 1705–1707. doi:10.1126/science.271.5256.1705
22. Dameron, A. A.; Ciszek, J. W.; Tour, J. M.; Weiss, P. S. *J. Phys. Chem. B* **2004,** *108,* 16761–16767. doi:10.1021/jp049442d
23. Ciszek, J. W.; Tour, J. M. *Tetrahedron Lett.* **2004,** *45,* 2801–2803. doi:10.1016/j.tetlet.2004.02.028
24. Shirai, Y.; Cheng, L.; Chen, B.; Tour, J. M. *J. Am. Chem. Soc.* **2006,** *128,* 13479–13489. doi:10.1021/ja063451d
25. Zhu, Y.; Gergel, N.; Majumdar, N.; Harriott, L. R.; Bean, J. C.; Pu, L. *Org. Lett.* **2006,** *8,* 355–358. doi:10.1021/ol0517168
26. Oka, H. *J. Mater. Chem.* **2008,** *18,* 1927–1934. doi:10.1039/b716919a
27. Okamoto, T.; Kuratsu, M.; Kozaki, M.; Hirotsu, K.; Ichimura, A.; Matsushita, T.; Okada, K. *Org. Lett.* **2004,** *6,* 3493–3496. doi:10.1021/ol048698z
28. Sun, D.; Rosokha, S. V.; Kochi, J. K. *J. Am. Chem. Soc.* **2004,** *126,* 1388–1401. doi:10.1021/ja038746v
29. Kochi, J. K.; Rathore, R.; Le Maguères, P. *J. Org. Chem.* **2000,** *65,* 6826–6836. doi:10.1021/jo000570h
30. Nishinaga, T.; Inoue, R.; Matsuura, A.; Komatsu, K. *Org. Lett.* **2002,** *4,* 1435–1438. doi:10.1021/ol0255662
31. Pan, D.; Phillips, D. L. *J. Phys. Chem. A* **1999,** *103,* 4737–4743. doi:10.1021/jp990399h

32. Sailer, M.; Franz, A. W.; Müller, T. J. J. *Chem.–Eur. J.* **2008,** *14,* 2602–2614. doi:10.1002/chem.200701341
33. Franz, A. W.; Popa, L. N.; Müller, T. J. J. *Tetrahedron Lett.* **2008,** *49,* 3300–3303. doi:10.1016/j.tetlet.2008.03.071
34. Franz, A. W.; Popa, L. N.; Rominger, F.; Müller, T. J. J. *Org. Biomol. Chem.* **2009,** *7,* 469–475. doi:10.1039/b814850c
35. Barkschat, C. S.; Guckenberger, R.; Müller, T. J. J. *Z. Naturforsch.* **2009,** *64b,* 707–718.
36. McDowell, J. J. H. *Acta Crystallogr., Sect. B: Struct. Crystallogr. Cryst. Chem.* **1976,** *B32,* 5–10. doi:10.1107/S0567740876002215
37. Uchida, T.; Ito, M.; Kozawa, K. *Bull. Chem. Soc. Jpn.* **1983,** *56,* 577–582. doi:10.1246/bcsj.56.577
38. Lambert, C.; Kriegisch, V. *Langmuir* **2006,** *22,* 8807–8812. doi:10.1021/la061404t
39. Barkschat, C. S.; Stoycheva, S.; Himmelhaus, M.; Müller, T. J. J. *Chem. Mater.* **2010,** *22,* 52–63. doi:10.1021/cm901514t
40. Müller, T. J. J. *Tetrahedron Lett.* **1999,** *40,* 6563–6566. doi:10.1016/S0040-4039(99)01402-1
41. Krämer, C. S.; Zeitler, K.; Müller, T. J. J. *Org. Lett.* **2000,** *2,* 3723–3726. doi:10.1021/ol0066328
42. Krämer, C. S.; Müller, T. J. J. *Eur. J. Org. Chem.* **2003,** 3534–3548. doi:10.1002/ejoc.200300250
43. Sailer, M.; Nonnenmacher, M.; Oeser, T.; Müller, T. J. J. *Eur. J. Org. Chem.* **2006,** 423–435. doi:10.1002/ejoc.200500539
44. Bucci, N.; Müller, T. J. J. *Tetrahedron Lett.* **2006,** *47,* 8323–8327. doi:10.1016/j.tetlet.2006.09.076
45. Bucci, N.; Müller, T. J. J. *Tetrahedron Lett.* **2006,** *47,* 8329–8332. doi:10.1016/j.tetlet.2006.09.075
46. Hauck, M.; Schönhaber, J.; Zucchero, A. J.; Hardcastle, K. I.; Müller, T. J. J.; Bunz, U. H. F. *J. Org. Chem.* **2007,** *72,* 6714–6725. doi:10.1021/jo070922l
47. Ebdrup, S. *Synthesis* **1998,** 1107–1109. doi:10.1055/s-1998-2121
48. Ebdrup, S. *J. Chem. Soc., Perkin Trans. 1* **1998,** 1147–1150. doi:10.1039/a705813f
49. Ebdrup, S.; Schou Jensen, M.; Vedsø, P. *J. Chem. Soc., Perkin Trans. 1* **1998,** 351–354. doi:10.1039/a704120i
50. Krämer, C. S.; Zimmermann, T. J.; Sailer, M.; Müller, T. J. J. *Synthesis* **2002,** 1163–1170. doi:10.1055/s-2002-32527
51. Sailer, M.; Gropeanu, R.-A.; Müller, T. J. J. *J. Org. Chem.* **2003,** *68,* 7509–7512. doi:10.1021/jo034555z
52. Franz, A. W.; Müller, T. J. J. *Synthesis* **2008,** 1121–1125. doi:10.1055/s-2008-1032118
53. Grassi, G.; Tyblewski, M.; Bauder, A. *Helv. Chim. Acta* **1985,** *68,* 1876–1879. doi:10.1002/hlca.19850680710
54. Krämer, C. S.; Zeitler, K.; Müller, T. J. J. *Tetrahedron Lett.* **2001,** *42,* 8619–8624. doi:10.1016/S0040-4039(01)01848-2
55. Stoycheva, S.; Himmelhaus, M.; Fick, J.; Korniakov, A.; Grunze, M.; Ulman, A. *Langmuir* **2006,** *22,* 4170–4178. doi:10.1021/la0531188
56. *Gaussian 03,* Revision C.02; Gaussian, Inc.: Wallingford, CT, 2004.
57. Leung, T. Y. B.; Schwartz, P.; Scoles, G.; Schreiber, F.; Ulman, A. *Surf. Sci.* **2000,** *458,* 34–52. doi:10.1016/S0039-6028(00)00385-X
58. Frey, S.; Stadler, V.; Heister, K.; Eck, W.; Zharnikov, M.; Grunze, M.; Zeysing, B.; Terfort, A. *Langmuir* **2001,** *17,* 2408–2415. doi:10.1021/la001540c
59. Becker, H. G. O.; Berger, W.; Domschke, G.; Fanghänel, E.; Faust, J.; Fischer, M.; Gentz, F.; Gewald, K.; Gluch, R.; Mayer, R.; Müller, K.; Pavel, D.; Schmidt, H.; Schollberg, K.; Schwetlick, K.; Seiler, E.; Zeppenfeld, G. *Organikum,* 20th ed.; Johann Ambrosius Barth Verlag: Heidelberg, Leipzig, 1996.
60. Hesse, M.; Meier, H.; Zeeh, B. *Spektroskopische Methoden in der organischen Chemie;* Georg Thieme Verlag: Stuttgart, New York, 1991; p 69.
61. Zanello, P. In *Ferrocenes;* Togni, A.; Hayashi, T., Eds.; VCH: Weinheim, New York, Basel, Cambridge, Tokyo, 1995; pp 317–430.
62. Tompkins, H. G.; McGahan, W. A. *Spectroscopic Ellipsometry and Reflectivity, A User's Guide;* John Wiley & Sons, Inc., 1999.
63. Gilchrist, V. A.; Lu, J. R.; Keddie, J. L.; Staples, E.; Garrett, P. *Langmuir* **2000,** *16,* 740–748. doi:10.1021/la9906572

License and Terms

This is an Open Access article under the terms of the Creative Commons Attribution License (http://creativecommons.org/licenses/by/2.0), which permits unrestricted use, distribution, and reproduction in any medium, provided the original work is properly cited.

The license is subject to the *Beilstein Journal of Organic Chemistry* terms and conditions: (http://www.beilstein-journals.org/bjoc)

The definitive version of this article is the electronic one which can be found at: doi:10.3762/bjoc.6.72

Beilstein Journal of Organic Chemistry

Chromo- and fluorophoric water-soluble polymers and silica particles by nucleophilic substitution reaction of poly(vinyl amine)

Katja Hofmann[1], Ingolf Kahle[1], Frank Simon[2] and Stefan Spange[*1]

Full Research Paper

Open Access

Address:
[1]Department of Polymer Chemistry, Chemnitz University of Technology, Straße der Nationen 62, Chemnitz 09111, Germany and [2]Leibniz Institute of Polymer Research Dresden, Hohe Straße 6, Dresden 01069, Germany

Email:
Katja Hofmann - katja.hofmann@chemie.tu-chemnitz.de; Ingolf Kahle - ingolf.kahle@chemie.tu-chemnitz.de; Frank Simon - frsimon@ipfdd.de; Stefan Spange* - stefan.spange@chemie.tu-chemnitz.de

* Corresponding author

Keywords:
carbonitrile; cyclodextrin; fluorescence; hybridmaterials; poly(vinyl amine)

Beilstein J. Org. Chem. **2010,** *6,* No. 79. doi:10.3762/bjoc.6.79

Received: 21 May 2010
Accepted: 07 July 2010
Published: 22 July 2010

Guest Editor: H. Ritter

© 2010 Hofmann et al; licensee Beilstein-Institut.
License and terms: see end of document.

Abstract

Novel chromophoric and fluorescent carbonitrile-functionalized poly(vinyl amine) (PVAm) and PVAm/silica particles were synthesized by means of nucleophilic aromatic substitution of 8-oxo-8*H*-acenaphtho[1,2-*b*]pyrrol-9-carbonitrile (**1**) with PVAm in water. The water solubility of **1** has been mediated by 2,6-*O*-β-dimethylcyclodextrin or by pre-adsorption onto silica particles. Furthermore, **1** was converted with isopropylamine into the model compound **1-M**. All new compounds were characterized by NMR, FTIR, UV–vis and fluorescence spectroscopy. The solvent-dependent UV–vis absorption and fluorescence emission band positions of the model compound and the carbonitrile-functionalized PVAm were studied and interpreted using the empirical Kamlet–Taft solvent parameters π^* (dipolarity/polarizability), α (hydrogen-bond donating capacity) and β (hydrogen-accepting ability) in terms of the linear solvation energy relationship (LSER). The solvent-independent regression coefficients a, b and s were determined using multiple linear correlation analysis. It is shown, that the chains of the polymer have a significant influence on the solvatochromic behavior of **1-P**. The structure of the carbonitrile **1-Si** bound to polymer-modified silica particles was studied by means of X-ray photoelectron spectroscopy (XPS) and Brunauer–Emmett–Teller (BET) measurements. Fluorescent silica particles were obtained as shown by fluorescence spectroscopy with a diffuse reflectance technique.

Introduction

Fluorescent polymers are an important tool for the study of molecular dynamics and also find use as sensor probes for biologically active compounds [1]. In recent years, there has been great interest in the synthesis, characterization and applications of fluorescent polymers [2-4]. In general, there are two approaches for the synthesis of fluorescent polymers: First, the

polymerization of a monomer that contains a fluorescent chromophore is possible. However, in some cases the new fluorophore-carrying polymer [1,5] is accompanied by a non-adequate effort concerning its synthesis and purification. An alternative pathway is the chemical modification of commercially available polymers containing reactive groups which can react with fluorescent dyes [6]. Poly(vinyl amine)s (PVAm) are copolymers made by the hydrolysis of poly(vinyl formamide) (PVFA). Fully hydrolyzed PVFA contains ca. 5% of formamido groups and 95% of primary amino groups. The water-soluble PVAm copolymer has been widely applied for a number of purposes, e.g., in catalysis [7], chelation [8], treatment of waste water [9], paper making [10], recovery of oil [11] and as superabsorber [12]. Modified PVAm is expected to be useful in the preparation of polymeric water-soluble dyes [13], in mimicking natural enzymes [14] and as a polymeric surfactant [15]. Depending on the pH of the aqueous solution, the primary amino groups of PVAm can be partly protonated ($-NH_3^+$) or they can be present as charge-neutral amines ($-NH_2$). In this context, PVAm can be considered as a weak cationic polyelectrolyte.

The pH-variation is an excellent tool to control and adjust the net-charge density along the polymer chain or in a layer made from PVAm [16,17]. Full conversion of the amino groups into their cationic form leads to a polymer with the highest known charge density along the polymer backbone. Such highly protonated polymers appear to be very interesting compounds for the prevention of bacteria adhesion on surfaces [18]. Non-protonated primary amino groups in the PVAm polymer have a high synthetic potential which can be used for versatile subsequent derivatization reactions [17,19-21].

In previous articles we reported the nucleophilic aromatic substitution of activated fluoroaromatic compounds with PVAm [22-24]. Reactions of PVAm with derivatization agents seem at first glance to be simple to carry out, but in fact they require a considerable synthetic effort because the reactants must share a solvent or a homogeneous mixture of solvents. For many reactions it is profitable to remove or to buffer low-molecular mass products formed during the reaction between PVAm and the derivatization agent.

High molecular mass products of PVAm copolymers (M_r > 1500 g mol^{-1}) are soluble in water only, while fluoroaromatic compounds are sparingly soluble or even insoluble in water. The lack of solvents capable of dissolving all the reactants complicates subsequent derivatization reactions or requires a high synthetic effort. Micelle techniques commonly used to carry out reactions between water-soluble and insoluble compounds cannot be cleanly applied to modify polyelectrolytes [25]. Alternatively, water-soluble polymers can be modified by the introduction of alkyl or aryl groups, thus mediating solubility in organic solvents [26].

The use of cyclodextrins (CD) provides a further opportunity to solve these problems. Due to the formation of host–guest complexes with CD both reactants become completely soluble in water. According to Ritter et al., the 2,6-*O*-β-dimethylcyclodextrin (β-DMCD) derivative has been found to be suitable because of its higher solubility in water compared to β-cyclodextrin (800.5 g L^{-1} vs. 18.5 g L^{-1}) [27-29].

Chemical reactions between two incompatible reactants can also be achieved under heterogeneous reaction conditions (the reaction is localized at the interphase of the two contacting phases). This approach was developed to carry out functionalization reactions between the water-soluble PVAm and suitable chromophores [30] or fluorophores. In these reactions, silica can be considered as 'solubilizer' because PVAm, as well as the reactants, are consecutively adsorbed on the silica particles. The functionalization reactions take place on the silica surface simultaneously. The large specific surface area of the silica particles employed (ca. 400 m^2 g^{-1}) guarantees the presence of a high amount of the adsorbed polymer and modifiers [31].

The electron-deficient heterocycle 8-oxo-8*H*-acenaphtho[1,2-*b*]pyrrol-9-carbonitrile (**1**) is a type of novel fluorescent chromophore with long-wavelength absorption and fluorescence, the excitation and emission wavelengths of which can reach 530 nm and 590 nm, respectively [36]. It is well known, that carbonitrile **1** is able to react with nitrogen-, oxygen-, or sulfur-containing nucleophiles by nucleophilic aromatic substitution reactions (S_NAr^H) [32-36]. The reaction of **1** with 3-thiopropionic acid has used to produce a fluorescent sensor for cys/Hcy with a 75-fold fluorescence enhancement [34]. The S_NAr^H reaction of **1** with the thiolated RGD peptide cyclo(Arg-Gly_Asp-Phe-Lys(mpa))(c(RGDFK)-SH) leads to a fluorescent sensor for imaging tumor cells [37].

In this paper we report our current studies on the functionalization of PVAm with carbonitrile **1** to introduce a chromophore as well as a fluorophore into the polymer chain. The synthesis was achieved by two different approaches. The first method included the use of β-DMCD to render **1** compatible to PVAm dissolved in water. The S_NAr^H reaction between the two reactants was carried out in homogeneous phase. The second approach was to synthesize a hybrid material by the consecutive adsorption of PVAm and **1** onto silica particles. The adsorbed substances were reacted directly on the silica particle surface. The reaction products (yield on the surface of silica particles) were analyzed using high-resolution X-ray photoelectron spectroscopy (XPS). The XPS method is very surface-sen-

sitive and gives spectroscopic information for sample depths of less than 8 nm.

Results and Discussion

Synthesis

Synthesis and characterization of the fluorescent polymer

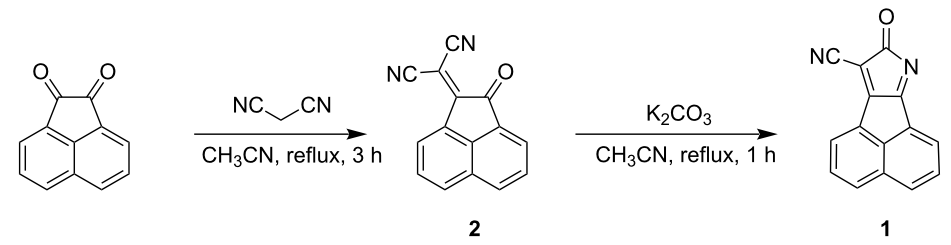
Carbonitrile **1** was synthesized by a very efficientl two-step literature procedure [32,34]. As shown in Scheme 1, the starting material acenaphthylene-1,2-dione undergoes a Knoevenagel condensation with malononitrile to give mono-adduct **2**.

Compound **2** was originally synthesized by Junek et al. [38]. However, no detailed NMR data were reported. In a second step, cyclization with anhydrous K_2CO_3 converted **2** to **1** in a good yield. In contrast to the procedure described in [34], a ten-fold excess of K_2CO_3 did not give rise to the target compound **1**. Only the use of a 10 % mol. equivalent of the base led to **1**.

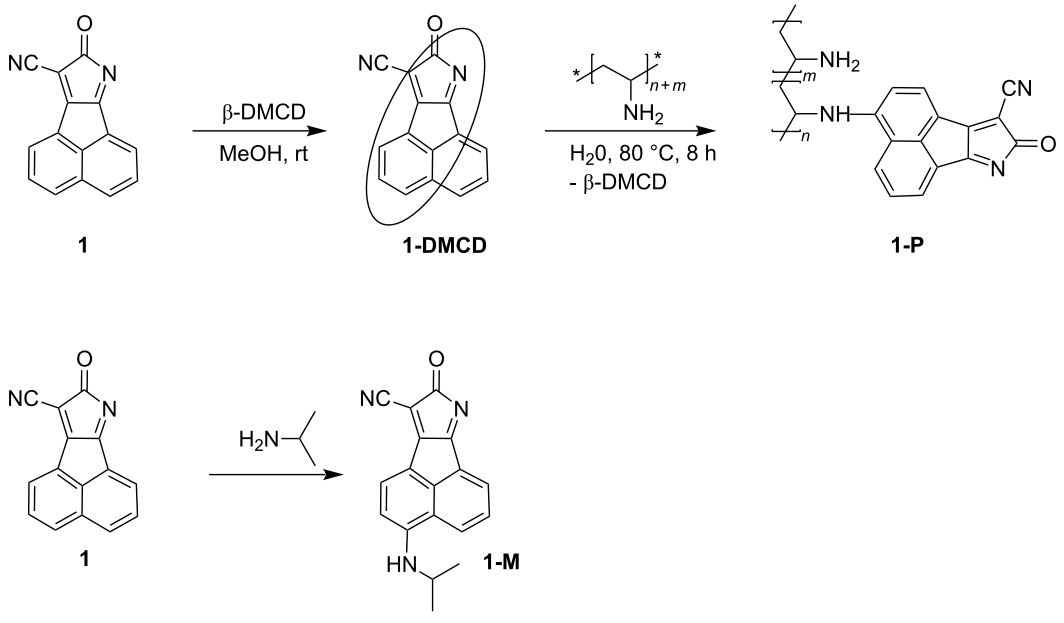
The success of the S_NAr^H reaction of **1** with PVAm (Scheme 2) mediated by β-DMCD in water could be established using ^{13}C-{^1H}-CP-MAS NMR spectroscopy.

Figure 1 compares the solid state ^{13}C NMR spectra of pure PVAm, fluorophore-functionalized PVAm **1-P** and the model compound **1-M**. It can be seen that the signals observed for **1-M** and pure PVAm are also visible in the ^{13}C-{^1H}-CP-MAS NMR spectrum of **1-P**. This is an excellent evidence for the functionalization of the PVAm fluorophore **1**. The signal at δ = 169 ppm in the solid state ^{13}C NMR spectra [(a) and (b), Figure 1] are due to the residual formamido groups while the signal at δ = 67 ppm is caused by the methine carbon of poly(vinyl alcohol) [39,40].

Further confirmation of the success of the S_NAR^H reaction was obtained from the FTIR spectra. Pure PVAm copolymers show characteristic IR absorption of N–H groups in the range of



Scheme 1: Synthesis of carbonitrile **1**.



Scheme 2: Coupling of the β-DMCD-caged carbonitrile derivative **1-DMCD** with PVAm to yield the fluorophore-functionalized PVAm **1-P** and synthesis of the model compound **1-M**.

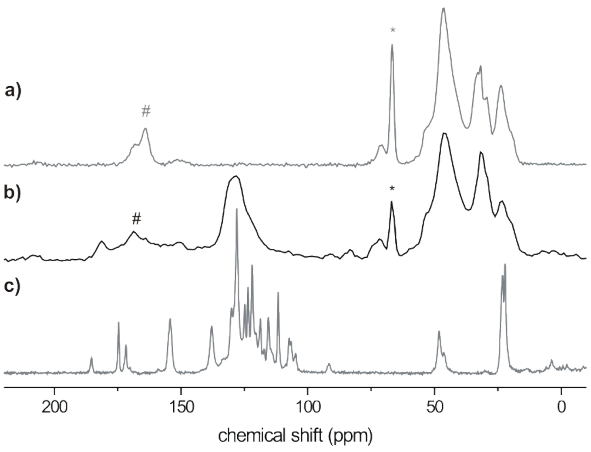


Figure 1: Solid state ^{13}C-{^1H}-CP-MAS NMR spectra of pure PVAm (a), functionalized PVAm **1-P** (b) and the model compound **1-M** (c) ["*" indicates the signals of the methine carbon of poly(vinyl alcohol) (PVA) and "#" corresponds to non-hydrolized formamido groups still present in the PVAm chains].

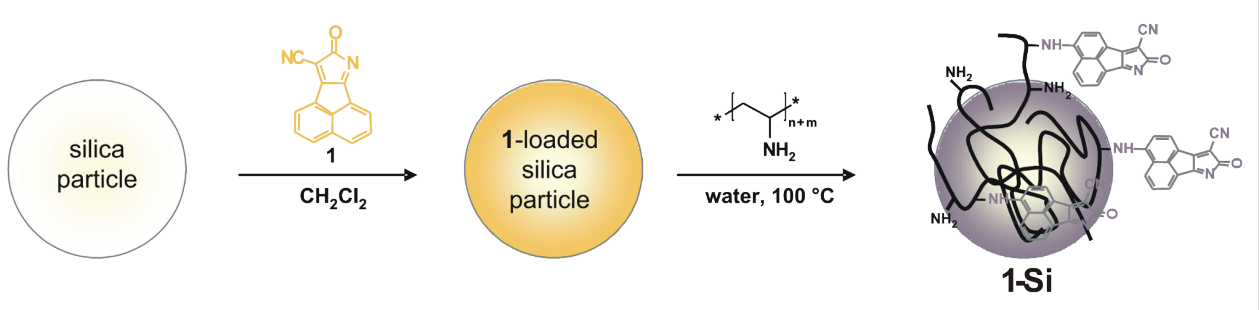
$\tilde{\nu}$ = 3450–3150 cm^{-1} due to the stretching vibration and at $\tilde{\nu}$ = 1600 cm^{-1} due to the deformation vibration. Asymmetric as well as symmetric stretching modes of C–H groups ($\tilde{\nu}$ = 2880–2950 cm^{-1}) and deformation vibrations of the CH_2 and CH group at $\tilde{\nu}$ = 1430 cm^{-1} as well as 1381 cm^{-1} were observed. Additionally, the IR band at $\tilde{\nu}$ = 1665 cm^{-1} corresponds to residual formamido groups. The IR spectrum of the model compound shows a sharp N–H stretch band at ca. $\tilde{\nu}$ = 3334 cm^{-1}, stretching modes of aromatic and aliphatic C–H groups between 2879–3080 cm^{-1}, C≡N stretching at 2213 cm^{-1} and aromatic C=C stretching vibrations at 1627 cm^{-1}. The IR spectrum of the carbonitrile-functionalized PVAm **1-P** shows the characteristic absorption bands of both the PVAm and carbonitrile moiety which confirms the functionalization. A broad N–H stretching band of the NH_2 groups of the polymer and the NH group of the fluorophore at $\tilde{\nu}$ = 3550–3150 cm^{-1} was observed. Bands between $\tilde{\nu}$ = 2890–2990 cm^{-1} correspond to the stretching modes of the aliphatic CH groups of the polymer backbone. The IR absorption of the aromatic C=C units occurs at ca. $\tilde{\nu}$ = 1665 cm^{-1} which appear to be overlapped by N–H deformation vibration bands. The presence of the C≡N stretching band at $\tilde{\nu}$ = 2221 cm^{-1} confirms the existence of the organo-substituted fluorophore.

The glass transition temperature T_g is an important parameter for polymers, which indicates the transition of the amorphous phase of the polymer from its rubbery to its glassy state (and vice versa). Pure PVAm shows a T_g of 103 °C. The glass transition temperature is a function of chain flexibility. Because of the presence of hydrogen-bond donor and -acceptor centers along the polymer backbone, PVAm is able to form hydrogen bonds between the amino groups (and residual formamido groups). The carbonitrile-functionalized PVAm **1-P** shows a lower T_g of 87 °C. Obviously, the introduction of the rigid fluorophore leads to a separation of the individual polymer chains, resulting in a decreased glass transition temperature.

Synthesis and characterization of the hybrid material

As can be seen from Scheme 3, carbonitrile **1** was adsorbed from its dichloromethane solution onto carefully dried silica particles (Kieselgel 60, Merck). The **1**-loaded silica particles were transferred into an aqueous solution of PVAm. In order to initiate the S_NAR^H reaction between **1** and PVAm the solution was heated and kept for 16 h at its boiling point. The silica particles were extracted twice, first with water to remove non-adsorbed functionalized PVAm and then with acetone to remove unreacted **1**. **1-Si** was obtained as intensively colored purple solid.

The ^{13}C-{^1H}-CP-MAS NMR spectrum of **1-Si** shows the characteristic signals of the fluorophore as well as those of the aliphatic carbons of the polymer backbone. The FTIR spectrum of **1-Si** confirms the adsorption of the functionalized PVAm onto the silica particle surface. As expected, a strong IR absorption band was present in the range of $\tilde{\nu}$ = 1200–1000 cm^{-1} corresponding to Si–O–Si stretching vibrations. Furthermore, a broad N–H stretching vibration at $\tilde{\nu}$ = 3150–3500 cm^{-1} was



Scheme 3: Synthesis of **1-Si** by nucleophilic aromatic substitution of **1** adsorbed onto silica particles.

observed. Additionally, the IR spectrum shows stretching vibrations at 2207 cm^{-1}, 1651 cm^{-1} and 1372 cm^{-1} ($\nu_{C\equiv N}$, $\nu_{C=C}$ and δ_{CH}) which are evidence for the adsorption of carbonitrile-functionalized PVAm.

XPS spectra were taken from the unmodified silica, PVAm adsorbed onto silica and the fluorophore PVAm-modified silica particles **1-Si** (Figure 2).

Figure 2a shows a typical XPS wide-scan spectrum of the bare silica support which was unloaded. The spectrum contains the expected peaks from silicon (Si 2s and Si 2p) and oxygen (O 1s, O 2s and the O KLL Auger series). The small C 1s peak shows the presence of typical hydrocarbon surface contaminations. PVAm, adsorbed onto the silica particle surface, strongly increases the amount of carbon on the silica surface. Nitrogen atoms of the amino (and residual formamido) groups lead to the N 1s peak (Figure 2b). The corresponding C 1s high-resolution spectrum of the PVAm-loaded silica shows saturated hydrocarbons from the methylene units of the polymer backbone and surface contaminations (component peak *A*). Component peak *B* shows C–N bonds of primary amino groups of the polymer and the amine-side carbon atoms (O=CH–NH–C) of residual amido groups. Formamido groups (O=CH–NH–C) contribute to the component peak *C*. The area of component peak *C* is ca. 4.9% of the C 1s area. As noted above, the amino groups of the PVAm polymer can be protonated by hydronium ions. In Figure 2b the N 1s high-resolution spectrum of the PVAm/silica hybrid material shows such protonated amino groups (component peak *G*), clearly separated from the non-protonated amino groups (component peak *F*). Nitrogen involved in amide groups contributes to component peak *F*. The ratio of the two

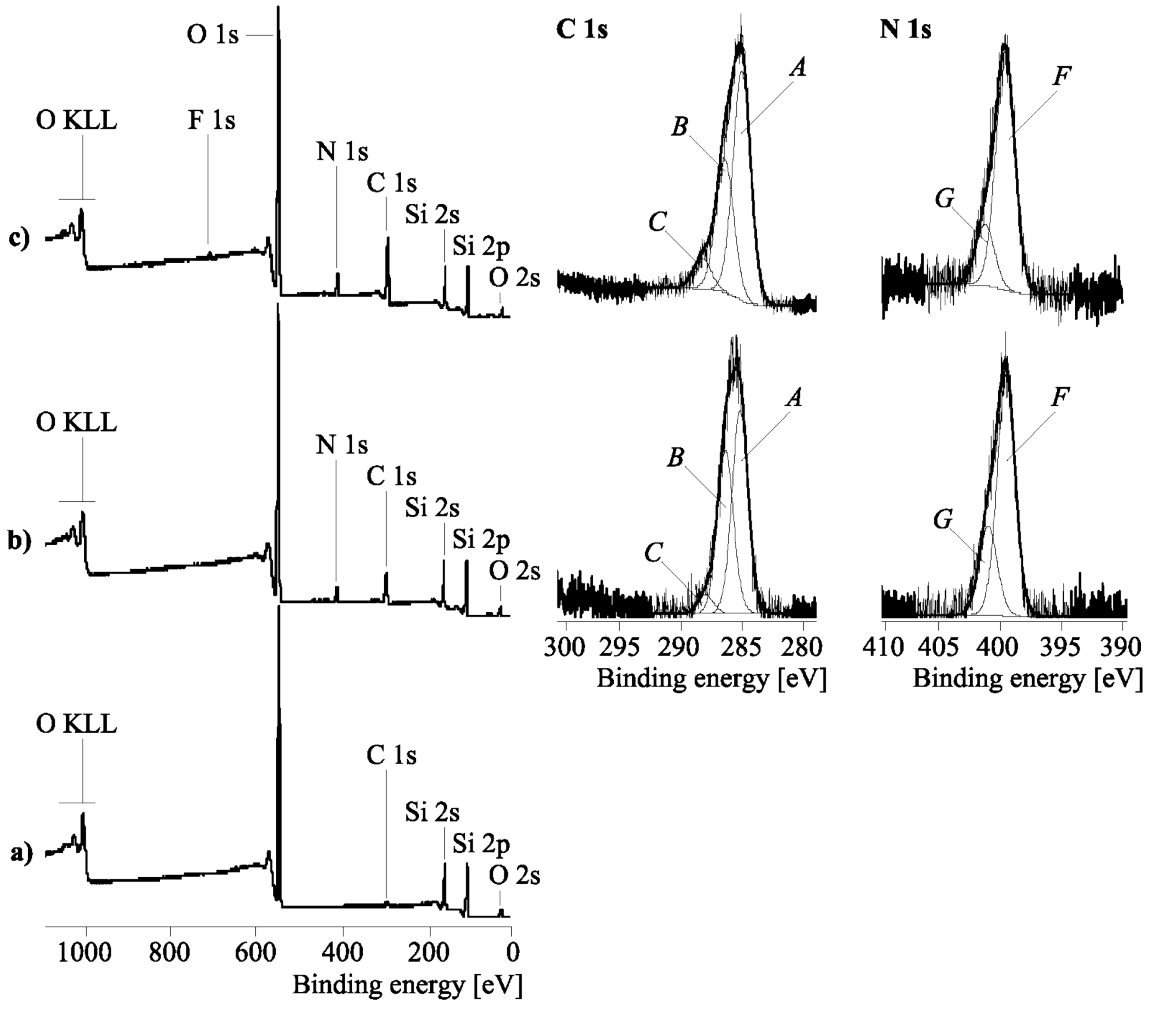


Figure 2: Wide-scan X-ray photoelectron spectra (left), C 1s and N 1s high-resolution spectra (right) of bare silica particles (a), PVAm adsorbed onto silica particles (b) and PVAm reacted with **1** on the surface of silica particles (c).

component peak areas [*G*]:[*F*] can be considered as the protonation–deprotonation equilibrium of the amine-functionalized hybrid surface.

The reaction of adsorbed PVAm with adsorbed **1** changes the corresponding XPS spectra slightly (Figure 2c). In the wide-scan spectrum the amounts of carbon and nitrogen increase: The elemental ratio [N]:[O] of the PVAm loaded silica sample was found to be [N]:[O] = 0.094, while the ratio after reaction of PVAm with **1** was [N]:[O] = 0.152 (nitrogen can be considered as label for the organic adsorption layer and oxygen the label for the silicon support). The coupling of PVAm with the fluorophore group **1** introduces an additional amount of carbonyl groups (carbon atoms of the cyclic amide in structure **1-P**) into the organic adsorption layer. Hence, in the corresponding C 1s spectrum (Figure 2c) the area of component peak *C* is increased to 8.11%. Carbon atoms of the C≡N group, C–N bonds in structure **1** and C–NH–C links between **1** and the PVAm polymer contribute to component *B*. The attachment of the fluorophore to the PVAm also changes the ability of the nitrogen atoms to be protonated. Nitrogen atoms in structure **1** cannot be involved in the protonation–deprotonation equilibrium of the amino groups of the PVAm polymer. The N 1s spectrum in Figure 2c shows a significantly decreased area of component peak *G* which is due to the C–N^+ species (its binding energy is BE ≈ 401.4 eV while the binding energy of the non-protonated species is BE ≈ 399.5 eV).

Table 1 summarizes the results of the BET analysis. In addition, Figure 3 shows the pore-size distribution histograms of bare silica, a typical PVAm/silica hybrid material and **1-Si**.

The bare silica support used for the functionalization reaction showed a BET surface of 411 $m^2\ g^{-1}$. The main average pore radius ranges between 2 and 4 nm. The adsorption of PVAm as well as **1-Si** significantly reduces the specific surface area. Small molecules such as the fluorophore **1** preferably fill the narrow pores. Hence, the fraction of the narrow pore radii 2–4 nm is considerably decreased. PVAm also reduces this. But the macromolecules are also able to cover the porous silica surface and prevent the access of the BET probe molecules (nitrogen) to the inner silica surface. The corresponding BET measurements show a smaller value of specific surface area (Table 1). After the adsorption of **1** or PVAm the fraction of the pore sizes between 4 and 10 nm is apparently higher. However, the values given in Figure 3 are expressed in percent terms. The increased values profit from the decreased value of the accessible narrow-size pores.

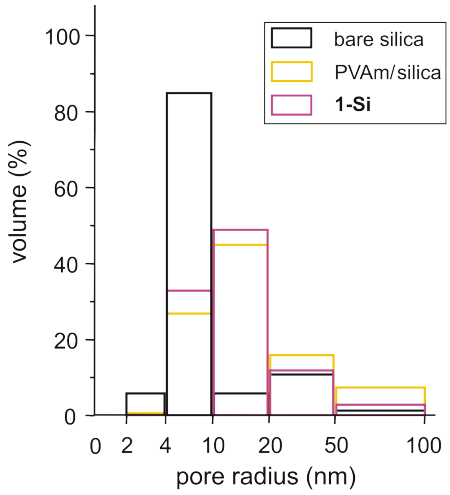


Figure 3: Pore-size distribution of bare silica, PVAm/silica and **1-Si**.

Solvatochromic and fluorescence properties

Interactions of solvatochromic dyes with pure solvents or solvent mixtures are a combination of many effects [41-44]. We wanted to investigate the influence of the PVAm on the chromophoric and fluorophoric π-electron system of **1** resulting from intermolecular interactions with the surroundings of the molecules, and which of these are dipole–dipole and/or hydrogen-bond interactions. To separate the effects of non-specific van der Waals interactions including electrostatic effects (dipolarity/polarizability) from specific interactions (hydrogen bonding), we used the simplified Kamlet–Taft equation (Equation 1) [45,46].

$$\tilde{\nu}_{max} = \tilde{\nu}_{max,0} + a\alpha + b\beta + s\pi^* \quad (1)$$

Table 1: Specific surface areas (according to BET, A_{BET}) and fractions of the average pore-size radii range of the bare silica support, a PVAM/silica hybrid material and **1-Si**, compared with the relative carbon-content (C_{found}/C_{calc}·100%) determined from data of the elemental analysis.

sample		Fraction of the average pore radii (%)		C_{found}/C_{calc}
	A_{BET} ($m^2\ g^{-1}$)	2–4 nm	4–10 nm	100%
bare silica	411	85	6	–
PVAm/silica	207	27	45	75.50
1-Si	197	0.3	33	89.05

According to Equation 1, the influence of the hydrogen-bond donor capacity (HBD) [47], the hydrogen-bond acceptor capacity (HBA) [48] and the dipolarity/polarizability [45,49] of a solvent can be expressed by α, β and π^*, respectively. $\tilde{\nu}_{max,0}$ corresponds to a standard process, referenced to a nonpolar medium. a, b and s represent solvent-independent regression coefficients which reflect the relative influence of each of the three parameters.

UV–vis spectroscopy

The solvatochromism of **1-M** and **1-P** was investigated in a set of only ten solvents due to the low solubility of **1-P** in organic solvents. Table 2 shows the UV–vis absorption maxima of **1-M** and **1-P** measured in solvents of different polarity and hydrogen-bonding ability, and the Kamlet–Taft parameters used for the multiple linear correlation analysis.

For both compounds, the shortest UV–vis absorption maxima were observed at λ_{max}(**1-M**) = 568 nm and λ_{max}(**1-P**) = 513 nm in HFIP. **1-M** shows the longest wavelength UV–vis absorption band at λ_{max} = 580 nm in DMSO, whereas **1-P** has the strongest bathochromic shift in ethanol at λ_{max} = 538 nm. These band shifts correspond to a small solvatochromic range of $\Delta\tilde{\nu}$ (**1-M**) = 333 cm^{-1} and $\Delta\tilde{\nu}$ (**1-P**) = 905 cm^{-1}, respectively. In general, the carbonitrile-functionalized PVAm **1-P** absorbs at shorter wavelengths as compared to the model compound **1-M**, which at firstl indicates an influence of the polymer chains on the solvatochromic behavior of the chromophoric unit.

In order to determine the relative contributions of the solvent properties on $\tilde{\nu}_{max}$, the simplified form of the Kamlet–Taft linear solvation energy relationship was used (Equation 1). The qualitatively best regressions of **1-M** and **1-P** are shown in Table 3.

The correlation coefficients r are greater than 0.92 for LSERs, which indicates a high quality of the two multi-parameter equations and allows significant conclusions to be drawn. When increasing the HBA strength of the solvent, a bathochromic shift of the UV–vis absorption maxima of **1-M** is observed, which is readily explained by interaction of the solvents with the NH function of the chromophore. The negative sign of the correlation coefficient s of **1-M** indicates that the electronically excited state of these molecules becomes more strongly solvated and is consequently stabilized with increasing the solvent's dipolarity/polarizability. This correlates with a higher

Table 2: UV–vis absorption maxima, $\tilde{\nu}_{max}$, of **1-M** and **1-P** investigated in ten solvents of different polarity and hydrogen-bond ability and the empirical Kamlet–Taft parameter α, β and π^* [41,43].

Solvent	Kamlet–Taft parameters			**1-M**		**1-P**	
	α	β	π^*	λ_{max} (nm)	$\tilde{\nu}_{max,abs}$ (10^3 cm^{-1})	λ_{max} (nm)	$\tilde{\nu}_{max,abs}$ (10^3 cm^{-1})
DMF[a]	0	0.69	0.88	578	17.30	534	18.73
DMAA[b]	0	0.76	0.88	579	17.27	535	18.69
DMSO[c]	0	0.76	1.00	580	17.24	532	18.79
DCM[d]	0.13	0.10	0.82	571	17.51	— [g]	— [g]
acetonitrile	0.19	0.41	0.75	573	17.45	531	18.83
1-propanol	0.84	0.90	0.52	575	17.39	536	18.66
ethanol	0.86	0.75	0.54	574	17.42	538	18.59
methanol	0.98	0.66	0.60	575	17.39	535	18.69
TFE[e]	1.51	0	0.73	569	17.57	521	19.19
HFIP[f]	1.96	0	0.65	568	17.61	513	19.49

[a]*N*,*N*-dimethylformamide, [b]*N*,*N*-dimethylacetamide, [c]dimethyl sulfoxide, [d]dichloromethane, [e]2,2,2-trifluoroethanol, [f]1,1,1,3,3,3-hexafluoro-2-propanol, [g]probe is insoluble in this solvent.

Table 3: Solvent-independent correlation coefficients a, b and s of the Kamlet–Taft parameters α, β and π^*; solute property of the reference system $\tilde{\nu}_{max,0}$, correlation coefficient (r), standard deviation (sd), number of solvents (n) and significance (f) for the solvatochromism of **1-M** and **1-P**.

comp.	$\tilde{\nu}_{max,0}$ (10^3 cm^{-1})	a	b	s	r	sd	n	f
1-M	17.857	0	−0.311	−0.386	0.995	0.014	10	< 0.001
1-P	18.260	0	−0.813	0	0.922	0.122	9	4×10^{-4}

dipole moment of the electronically excited state. In contrast to **1-M**, **1-P** shows no significant influence of the π^* term of the solvent on $\tilde{\nu}_{max}$, whereas the influence of the β term is greater compared to that of **1-M**. This effect reflects the impact of the NH_2 groups of the PVAm on the UV–vis absorption maxima of the chromophore. Probably, the chains of the polymer are able to insulate the chromophores from the solvent molecules. Hence, the chromophores interact more strongly with the polymer chains than they do with the solvents. The HBD ability of the solvents shows no influence on the solvatochromic behavior of **1-M** and **1-P**.

In addition, all compounds were measured as powders by means of the diffuse reflectance technique. The UV–vis absorption bands of the solids are non-symmetric and show several UV–vis absorption maxima. The longest-wavelength UV–vis absorption maxima were observed at λ_{max} (**1-P**, **1-Si**) = 545 nm and λ_{max} (**1-M**) = 546 nm. Figure 4 shows the UV–vis absorption and the emission diffuse reflectance spectra of **1-Si**.

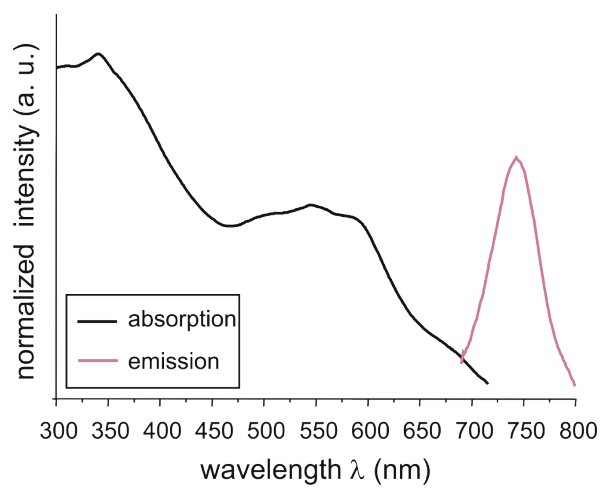


Figure 4: UV–vis absorption and emission diffuse reflectance spectra of sample **1-Si**.

Fluorescence

Both the carbonitrile-functionalized PVAm **1-P** and the model compound **1-M** show strong fluorescence. This can be explained by two factors: Firstly, the fluorophore is a very rigid and planar molecule and secondly, the fluorophore contains both strongly electron-withdrawing and electron-donating groups along the axis of the π-conjugated system. Therefore, an efficient intramolecular charge transfer (ICT) system is possible [32]. The fluorescence emission maxima of **1-M** and **1-P** are shown in Table 4.

Figure 5 shows an UV–vis absorption spectrum and a fluorescence emission spectrum of **1-M** and **1-P** measured in methanol as well as a photograph of solutions of these compounds.

Similar to the UV–vis measurements, **1-M** shows the longest-wavelength emission maximum in DMSO at λ_{max} = 595 nm and **1-P** in ethanol at λ_{max} = 586 nm. The longest hypsochromic shifts of the fluorescence emission maximum were observed at λ_{max}(**1-M**) = 577 nm in HFIP and λ_{max}(**1-P**) = 561 nm in DMMA. These band shifts correspond to a small solvatochromic range of $\Delta\tilde{\nu}$(**1-M**) = 524 cm^{-1} and $\Delta\tilde{\nu}$(**1-P**) = 760 cm^{-1}, respectively. Furthermore, for **1-M** only a small Stokes

Table 4: Fluorescence emission maxima $\tilde{\nu}_{max}$ of **1-M** and **1-P**, measured in ten solvents of different polarity and hydrogen-bond ability and the corresponding Stokes shifts.

Solvent	**1-M**			**1-P**		
	$\lambda_{max,em}$ (nm)	$\tilde{\nu}_{max,em}$ (10^3 cm^{-1})	Stokes shift (nm)	$\lambda_{max,em}$ (nm)	$\tilde{\nu}_{max,em}$ (10^3 cm^{-1})	Stokes shift (nm)
DMF[a]	593	16.86	15	562	17.79	28
DMAA[b]	592	16.89	13	561	17.83	26
DMSO[c]	595	16.81	15	564	17.73	32
DCM[d]	584	17.06	13	— [g]	— [g]	—
acetonitrile	586	17.06	13	563	17.76	32
1-propanol	586	17.06	11	585	17.09	49
ethanol	587	17.04	13	586	17.06	48
methanol	588	17.01	13	582	17.18	61
TFE[e]	582	17.18	13	580	17.24	59
HFIP[f]	577	17.33	9	576	17.36	63

[a]*N*,*N*-dimethylformamide, [b]*N*,*N*-dimethylacetamide, [c]dimethyl sulfoxide, [d]dichloromethane, [e]2,2,2-trifluoroethanol, [f]1,1,1,3,3,3-hexafluoro-2-propanol, [g]probe is insoluble in this solvent.

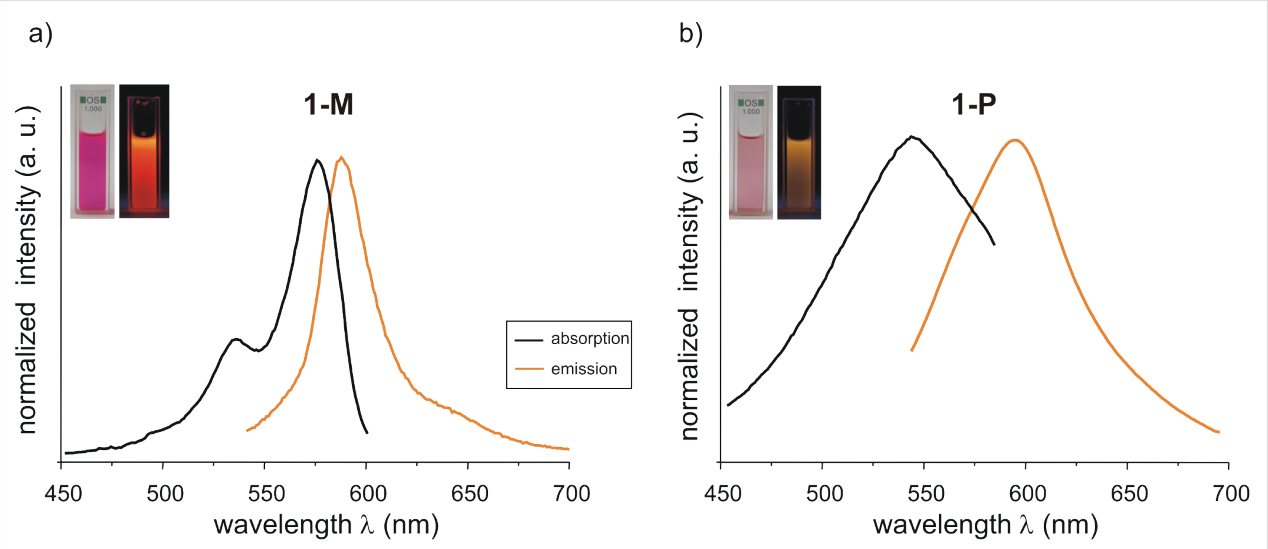


Figure 5: Normalized absorption and emission spectra of **1-M** (a) and **1-P** (b).

shift (9–15 nm) is observed, whereas **1-P** shows a larger one (26–63 nm), which reaches a maximum in strong HBD solvents (HFIP).

Again, the solvent-dependent fluorescence emission maxima can be interpreted with regard to the dipolarity/polarizabilty and the hydrogen-bond capacity of the solvents using the simplified Kamlet–Taft equation (Equation 1). The qualitatively best regressions are shown in Table 5.

In both, absorption and fluorescence of **1-M**, the polarity as well as the hydrogen-bond accepting ability of the solvents leads to a bathochromic band shift and both contribute to the stabilization of the excited state as well as to the interaction with the NH group. However, this effect is slightly more pronounced on the fluorescence side, as shown by the slightly higher b and s coefficients. In contrast to the results of the regression analysis obtained from the UV–vis absorption spectra, the HBD ability of the solvents shows a significant influence on the emission maxima of **1-P**. With increasing HBD strength of the solvent a bathochromic shift of the emission maximum was observed. Additionally, solvents which can act as hydrogen-bond acceptors also interact with the NH function of **1-P**, which leads to an enhancement of the push character of this group resulting in a band shift to longer wavelengths ($b < 0$). To confirm these conclusions drawn from the regression analysis with regard to the α term of the solvents, the emission spectra of **1-P** were measured in aqueous solutions at four different pH values (Figure 6).

In comparison to the UV–vis absorption measurements of the solids of **1-M**, **1-P** and the hybrid material **1-Si**, the fluorescence spectra recorded by diffuse reflection seem to be smaller (Figure 4). The model compound **1-M** exhibits an emission maximum at $\lambda_{em} = 753$ nm. For the compounds **1-Si** and **1-P** a hypsochromic band shift to λ_{em}(**1-Si**) = 745 nm and λ_{em}(**1-P**) = 741 nm was observed. This behavior also shows the strong influence of the chains of the PVAm on the solvatochromic behavior of the polymer.

As depicted in Figure 6, in aqueous solution at pH = 11, **1-P** shows two emission bands at $\lambda_{em,1} = 515$ nm and $\lambda_{em,2} = 579$ nm. With decreasing pH value, the intensity of the first emission band decreases, whereas for the emission band at the longer wavelength a slightly bathochromic shift is observed. This result confirms the conclusions drawn by the LSER of **1-P** with regard to the HBD strength of the solvents. A possible explanation is that at higher pH values the polymer chains are

Table 5: Solvent-independent correlation coefficients a, b and s of the Kamlet–Taft parameters α, β and π^*; solute property of the reference system $\tilde{\nu}_{max,0}$, correlation coefficient (r), standard deviation (sd), number of solvents (n) and significance (f) for the fluoro-solvatochromism of **1-M** and **1-P**.

comp.	$\tilde{\nu}_{max,0}$ (10^3 cm^{-1})	a	b	s	r	sd	n	f
1-M	17.638	0	−0.357	−0.573	0.970	0.043	10	< 0.001
1-P	17.465	−0.576	−0.772	0	0.922	0.144	9	0.003

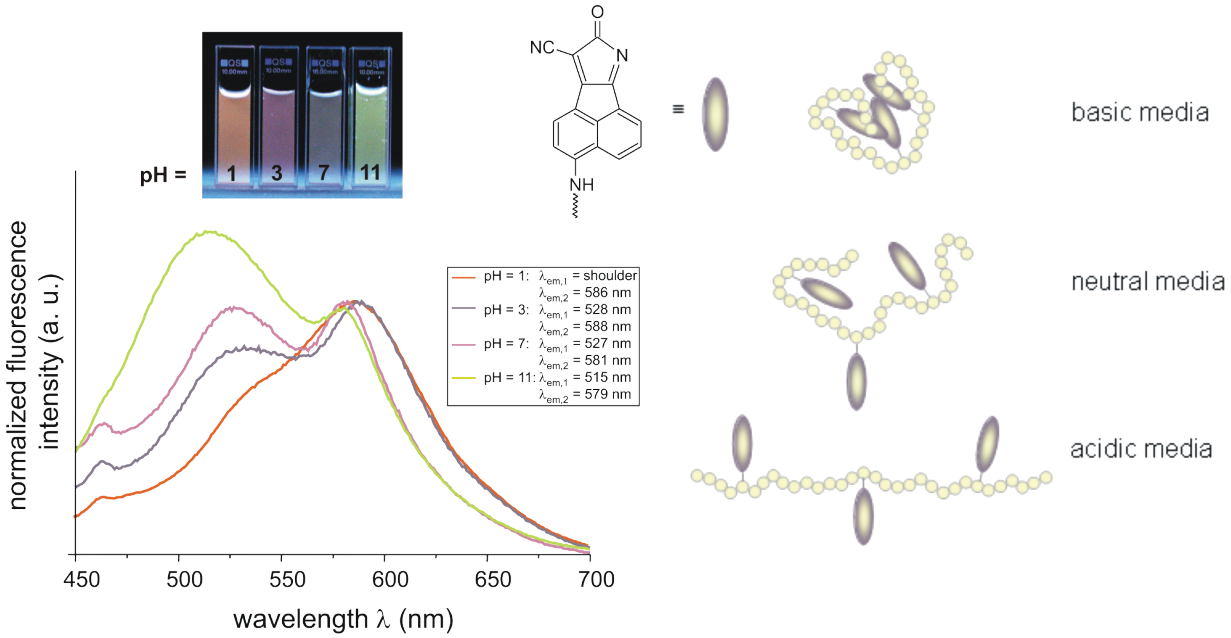


Figure 6: Normalized emission spectra of **1-P** in water at four different pH values and a sketch of the assumed chain conformations of PVAm.

coiled and the fluorophore is not accessible for interactions with the surrounding molecules. At lower pH values the polymer has a more straight conformation and interactions of the solvent with the fluorophore are possible. The explanation is in good agreement with the known behavior of weak cationic polyelectrolyte molecules. With lowering the pH of the surrounding aqueous solution the degree of protonation increases. The increased net charge along the polymer stretches and strengthens the chain.

Conclusion

In this paper we present the functionalization of PVAm with the known fluorophore **1** in water, mediated by 2,6-*O*-β-dimethylcyclodextrin. The characterization of the new fluorescent PVAm **1-P** has been carried out by means of ^{13}C-{^{1}H}-CP-MAS NMR, FTIR spectroscopy and DSC.

The influence of the solvents on the solvatochromic behavior of **1-M** and **1-P** can be quantitatively described by means of a LSE relationship using the well-established empirical Kamlet–Taft equation. The most dominant effect on the UV–vis absorption and fluorescence is caused by the HBA strength as well as by the dipolarity/polarizabilty of the solvents. In particular it has been shown that the polymer chains have a significant influence on the solvatochromic behavior of **1-P**. With decreasing pH value in aqueous solutions a bathochromic band shift was observed.

Pre-adsorption of carbonitrile **1** on silica and subsequent nucleophilic substitution of PVAm in water at 100 °C results in fluorophore-functionalized PVAm/silica particles. The PVAm–carbonitrile layer remains irreversibly bound to the silica, as shown by extraction experiments. Hence, the synthesis of a fluorescent hybrid material was possible.

Experimental

General details: The aqueous solution of poly(vinyl amine) copolymer (M_n = 15,000 g mol^{-1}, pH = 11) was kindly provided by BASF SE (Ludwigshafen, Germany). 2,6-*O*-β-dimethylcyclodextrin (β-DMCD) was supplied by Wacker Chemie (Burghausen, Germany).

2-(2-Oxo-2*H*-acenaphthylene-1-ylidene)-malononitrile (**2**)

Compound 2 was synthesized as described earlier [34]. Acenaphthene-1,2-dione (2.00 g, 11 mmol) and malononitrile (0.73 g, 11 mmol) were dissolved in 40 mL of CH_3CN and refluxed for 3 h. After cooling, the orange precipitate was filtered off and washed several times with CH_3CN to yield **2** as an orange crystalline solid (2.00 g, 8.3 mmol). Yield 80%, mp 241–244 °C (lit. 243–245 °C); ^{1}H NMR (250 MHz, CD_2Cl_2): δ (ppm) 8.61 (dd, J = 7.5 Hz, J = 0.6 Hz, 1H), 8.33–8.29 (m, 2H), 8.21 (dd, J = 7.2 Hz, J = 0.8 Hz, 1H), 7.96–7.88 (m, 2H); ^{13}C NMR (69 MHz, CD_2Cl_2): δ (ppm); 142.9, 132.6 (Ar*H*), 132.3 (Ar*H*), 130.5, 128.3, 112.7, 129.2 (Ar*H*), 129.0 (Ar*H*),

124.5 (Ar*H*), 123.6 (Ar*H*); FTIR (KBr): $\tilde{\nu}$ (cm^{-1}) 3093, 2225, 1717, 1597, 1574; $C_{15}H_6N_2O$ (230.23) Anal. calcd. C, 78.26; H, 2.63; N, 12.17; found C, 78.03; H, 2.66; N, 12.18.

8-Oxo-8*H*-acenaphtho[1,2-*b*]pyrrol-9-carbonitrile (**1**)

2-(2-Oxo-2*H*-acenaphthylene-1-ylidene)-malononitrile (**2**) (0.80 g, 3.5 mmol) and K_2CO_3 (48 mg, 0.35 mmol) in 5 mL of CH_3CN were refluxed for 1 h. After cooling, the yellow-orange precipitate was filtered off and washed several times with CH_3CN to yield **1** as a yellow–orange solid (0.70 g, 3.1 mmol). Yield 88%, mp 278–280 °C (lit. 275–277 °C [32]); ^{1}H NMR (250 MHz, CD_2Cl_2): δ (ppm) 8.80 (dd, J = 7.4 Hz, J = 1.3 Hz, 1H), 8.51–8.41 (m, 3H), 7.99 (dd, J = 7.6 Hz, J = 0.5 Hz, 1H), 7.89 (dd, J = 8.3 Hz, J = 1.0 Hz, 1H); FTIR (KBr): $\tilde{\nu}$ (cm^{-1}) 3084, 2231, 1713, 1645, 1576, 1549; $C_{15}H_6N_2O$ (230.23) Anal. calcd. C, 78.26; H, 2.63; N, 12.17; found C, 77.96; H, 2.61; N, 11.79.

Fluorophoric, carbonitrile-functionalized PVAm (**1-P**)

For the β-cyclodextrin complex formation, stoichiometric amounts of **1** (0.29 g, 1.28 mmol) and β-DMCD (1.68 g, 1.28 mmol) were dissolved in methanol and stirred overnight at room temperature [29]. The light orange solid complex of **1-DMCD** was isolated by removing the methanol in vacuum and was used without further purification.

For functionalization of PVAm in aqueous media, the solid β-DMCD complexes (10 mol %) was dissolved in 50 mL of distilled water and 6.10 g of the aqueous solution of PVAm containing 0.50 g of the polymer added. The mixture was refluxed for 8 h. Then the fluorophore-functionalized PVAm was precipitated by addition to ice-cold acetone (refrigerator), washed with acetone and dried in vacuum to yield an intensive purple-colored solid.

^{13}C-{^{1}H}-CP-MAS NMR (100 MHz, 12.5 kHz): δ (ppm) 181.3, 168.6, 128.4, 71.5, 46.0, 31.6, 23.5; FTIR (KBr): $\tilde{\nu}$ (cm^{-1}) 3239, 2895, 2838, 2221, 1665, 1590, 1497, 1386; Anal. calcd (for 100% substitution). C, 55.73; H, 10.11; N, 31.20; found C, 57.27; H, 7.45; N, 15.71.

3-Isopropylamino-8-oxo-8*H*-acenaphtho[1,2-*b*]pyrrol-9-carbonitrile (**1-M**)

8-Oxo-8*H*-acenaphtho[1,2-*b*]pyrrol-9-carbonitrile (**1**) (88 mg, 0.38 mmol) and isopropylamine (45 mg, 0.76 mmol) in 15 mL of CH_3CN were stirred for 3 h at room temperature. The dark purple-colored precipitate was filtered off and washed several times with CH_2Cl_2 to yield **1-M** (51 mg, 18 mmol). Yield 47%, mp > 300 °C (lit. >300 °C [33]); ^{1}H NMR (250 MHz, CD_2Cl_2): δ (ppm) 8.41 (d, 1H, J = 7.7 Hz), 8.15 (t, J = 7.6 Hz, J = 9.4 Hz, 2H), 7.69 (t, J = 7.6 Hz, J = 7.7 Hz, 1H), 7.36 (d, J = 9.4 Hz, 1H), 4.22–4.31 (m, 1H) NHC*H*) 1.49–1.51 (m, 6H, CH(CH_3)$_2$; ^{13}C-{^{1}H}-CP-MAS NMR (100 MHz, 12.5 kHz): δ (ppm) 185.3, 174.7, 171.8, 154.3, 137.9, 130.0, 1278.0, 124.8, 123.5, 121.9, 118.7, 117.3, 115.5, 111.6, 107.3, 104.8, 48.2, 23.2, 22.2; FTIR (KBr): $\tilde{\nu}$ (cm^{-1}) 3334, 3049, 2982, 2213, 1627, 1576, 1539; $C_{18}H_{13}N_3O$ (287.32) Anal. calcd. C, 75.25; H, 4.56; N, 14.63; found C, 74.85; H, 4.37; N, 14.49.

Fluorophoric, carbonitrile-functionalized PVAm/silica particles (**1-Si**)

For functionalization of silica with fluorophores and PVAm in aqueous media, **1** (0.1 g, 0.4 mmol) was dissolved in 50 mL of CH_2Cl_2, then suspended with silica (2.5 g, 41 mmol) and kept overnight. The solvent was removed in a rotary evaporator at 40 °C. Distilled water (60 mL) and 2.2 g of the aqueous solution of PVAm (0.18 g of polymer, 4.1 mmol) were added to the freshly prepared **1**-loaded silica particles. The mixture was refluxed for 16 h. After cooling to room temperature, the PVAm-functionalized silica was filtered off and washed carefully with water. In order to remove non-adsorbed functionalized PVAm and unreacted **1** from the silica particles surface, two Soxhlet extraction cycles were carried out, the first one with water and the second with acetone. **1-Si** was obtained as purple solid.

^{13}C-{^{1}H}-CP-MAS NMR (100 MHz, 12.5 kHz): δ (ppm) 181.2, 164.7, 151.4, 128.3, 44.6, 37.4; FTIR (KBr): $\tilde{\nu}$ (cm^{-1}) 3277, 2207, 1651, 1572, 1569; 1087, 1025; Anal. calcd. C, 6.30; H, 0.82; N, 2.52; found C, 5.61; H, 1.24; N, 2.08.

Acknowledgements

Financial support from the Deutsche Forschungsgemeinschaft, Bonn and the delivery of chemicals from the BASF SE, Ludwigshafen, is gratefully acknowledged. The 2,6-*O*-β-dimethylcyclodextrin was kindly supplied by Wacker Chemie. The authors thank Dr. A. Seifert and R. Jaeschke for ^{13}C-{^{1}H}-CP-MAS NMR measurements and the determination of the glass-transition temperatures by means of differential scanning calorimetry (DSC).

References

1. Smitha, P.; Asha, S. K. *J. Phys. Chem. B* **2007,** *111,* 6364–6373. doi:10.1021/jp071303j
2. Cai, H.; He, X.-H.; Zheng, D.-Y.; Qiu, J.; Li, Z.-C.; Li, F.-M. *J. Polym. Sci., Part A: Polym. Chem.* **1996,** *34,* 1245–1250. doi:10.1002/(SICI)1099-0518(199605)34:7<1245::AID-POLA11>3.0.CO;2-9
3. Smith, R. C.; Chen, X.; Protasiewicz, J. D. *Inorg. Chem.* **2003,** *42,* 5468–5470. doi:10.1021/ic0345471

4. Li, H.; Jäkle, F. *Angew. Chem.* **2009,** *121,* 2349–2352. doi:10.1002/ange.200805863
5. Grabchev, I.; Petkov, C.; Bojinov, V. *Macromol. Mater. Eng.* **2002,** *287,* 904–908. doi:10.1002/mame.200290025
6. Wang, K.; Huang, W.; Xia, P.; Gao, C.; Yan, D. *React. Funct. Polym.* **2002,** *52,* 143–148. doi:10.1016/S1381-5148(02)00088-3
7. Prabhakaran, P. V.; Venkatachalam, S.; Ninan, K. N. *Eur. Polym. J.* **1999,** *35,* 1743–1746. doi:10.1016/S0014-3057(98)00246-8
8. Kobayashi, S.; Suh, K. D.; Shirokura, Y. *Macromolecules* **1989,** *22,* 2363–2366. doi:10.1021/ma00195a062
9. Brunnmüller, F.; Schneider, R.; Kröner, M.; Müller, H.; Linhart, F.; Burkert, H.; Beyer, K.-H. EP 071 050, 1981.
10. Linhart, F.; Auhorn, W. *Das Papier* **1992,** *10A,* V38–V45.
11. Pinschmidt, R. K.; Vijayendran, B. R.; Lai, Ta-W. US 5 085787, 1992.
12. Beihoffer, T.; Mitchell, M.; Truzpek, L. T.; Darlington, J. W.; Anderson, M. US 6 194 631, 2001.
13. Dawson, D. J.; Gless, R. D.; Wingard, R. E., Jr.. *J. Am. Chem. Soc.* **1976,** *98,* 5996–6000. doi:10.1021/ja00435a036
14. Martel, B.; Pollet, A.; Morcellet, M. *Macromolecules* **1994,** *27,* 5258–5262. doi:10.1021/ma00097a003
15. Qui, Y.; Zang, T.; Ruegsegger, M.; Marchant, R. E. *Macromolecules* **1998,** *31,* 165–171. doi:10.1021/ma9707401
16. Dautzenberg, H.; Jaeger, W.; Kötz, J.; Phillip, B.; Seidel, C.; Stscherbina, D. *Polyelectrolytes: Formation, Characterization and Application;* Carl Hanser Verlag: Munich, 1994.
17. Caroll, W. E.; Chen, N.; Drescher, J.; Nordquist, A. F.; Pinschmidt, R. K., Jr..; Renz, W. L. *J. Macromol. Sci., Part A: Pure Appl. Chem.* **1997,** *A34,* 1885–1905.
18. Bratskaya, S.; Marinin, D.; Simon, F.; Synytska, A.; Zschoche, S.; Busscher, H. J.; Jager, D.; van der Mei, H. C. *Biomacromolecules* **2007,** *8,* 2960–2968. doi:10.1021/bm700620j
19. Badesso, R. J.; Nordquist, A. F.; Pinschmidt, R. K., Jr..; Sagl, D. J. *Adv. Chem. Ser.* **1996,** *248,* 489–504. doi:10.1021/ba-1996-0248.ch025
20. Yamamoto, K.; Imamura, Y.; Nagatomo, E.; Serizawa, T.; Muraoka, Y.; Akashi, M. *J. Appl. Polym. Sci.* **2003,** *89,* 1277–1283. doi:10.1002/app.12230
21. Chen, W.; Lu, C.; Pelton, R. *Biomacromolecules* **2006,** *7,* 701–702. doi:10.1021/bm050925c
22. Roth, I.; Spange, S. *Macromol. Rapid Commun.* **2001,** *22,* 1288–1291. doi:10.1002/1521-3927(20011001)22:15<1288::AID-MARC1288>3.0.CO;2-Z
23. Roth, I.; Spange, S. *Macromolecules* **2005,** *38,* 10034–10041. doi:10.1021/ma0518609
24. Roth, I.; Jbarah, A. A.; Holze, R.; Friedrich, M.; Spange, S. *Macromol. Rapid Commun.* **2006,** *27,* 193–199. doi:10.1002/marc.200500722
25. Correa, N. M.; Durantini, E. N.; Silber, J. J. *J. Org. Chem.* **2000,** *65,* 6427–6433. doi:10.1021/jo000714s
26. Jang, T.; Rasmussen, P. G. *J. Polym. Sci., Part A: Polym. Chem.* **1989,** *36,* 2616–2629.
27. Glöckner, P.; Metz, N.; Ritter, H. *Macromolecules* **2000,** *33,* 4288–4290. doi:10.1021/ma992012e
28. Casper, P.; Glöckner, P.; Ritter, H. *Macromolecules* **2000,** *33,* 4361–4364. doi:10.1021/ma0001382
29. Glöckner, P.; Ritter, H. *Macromol. Rapid Commun.* **1999,** *20,* 602–605. doi:10.1002/(SICI)1521-3927(19991101)20:11<602::AID-MARC602>3.0.CO;2-K
30. Roth, I.; Simon, F.; Bellmann, C.; Seifert, A.; Spange, S. *Chem. Mater.* **2006,** *18,* 4730–4739. doi:10.1021/cm0601483
31. Voigt, I.; Simon, F.; Estel, K.; Spange, S. *Langmuir* **2001,** *17,* 3080–3086. doi:10.1021/la001366s
32. Xiao, Y.; Liu, F.; Qian, X.; Cui, J. *Chem. Commun.* **2005,** 239–241. doi:10.1039/b413537g
33. Liu, F.; Xiao, Y.; Qian, X.; Zhang, Z.; Cui, J.; Cui, D.; Zhang, R. *Tetrahedron* **2005,** *61,* 11264–11269. doi:10.1016/j.tet.2005.08.106
34. Zhang, M.; Yu, M.; Li, F.; Zhu, M.; Li, M.; Gao, Y.; Li, L.; Liu, Z.; Zhang, J.; Zhang, D.; Yi, T.; Huang, C. *J. Am. Chem. Soc.* **2007,** *129,* 10322–10323. doi:10.1021/ja073140i
35. Coskun, A.; Yilmaz, M. D.; Akkaya, E. U. *Tetrahedron Lett.* **2006,** *47,* 3689–3691. doi:10.1016/j.tetlet.2006.03.128
36. Liu, Y.; Xu, Y.; Qian, X.; Xiao, Y.; Liu, J.; Shen, L.; Li, J.; Zhang, Y. *Bioorg. Med. Chem. Lett.* **2006,** *16,* 1562–1566. doi:10.1016/j.bmcl.2005.12.031
37. Xiong, L.; Yu, M.; Cheng, M.; Zhang, M.; Zhang, X.; Xu, C.; Li, F. *Mol. BioSyst.* **2009,** *5,* 241–243. doi:10.1039/b820576k
38. Junek, H.; Hamböck, H.; Hornischer, B. *Monatsh. Chem.* **1967,** *98,* 315–323. doi:10.1007/BF00899947
39. Pinschmidt, R. K., Jr..; Wasowski, L. A.; Orphanides, G. G.; Yacoub, K. *Prog. Org. Coat.* **1996,** *27,* 209–218. doi:10.1016/0300-9440(95)00537-4
40. Witek, E.; Pazdro, M.; Bartel, E. J. *J. Macromol. Sci., Part A: Pure Appl. Chem.* **2007,** *44,* 503–507.
41. Reichardt, C. *Solvents and Solvent Effects in Organic Chemistry,* 2nd ed.; VCH: Weinheim, 1988. And references therein.
42. Reichardt, C. *Chem. Rev.* **1994,** *94,* 2319–2358. doi:10.1021/cr00032a005
43. Marcus, Y. *Chem. Soc. Rev.* **1993,** *22,* 409–416. doi:10.1039/cs9932200409
44. Gutmann, V. *The Donor-Acceptor Approach to Molecular Interactions;* Plenum Press: New York, 1978.
45. Kamlet, M. J.; Abboud, J. L.; Taft, R. W. *J. Am. Chem. Soc.* **1977,** *99,* 6027–6038. doi:10.1021/ja00460a031
46. Kamlet, M. J.; Abboud, J. L. M.; Abraham, M. H.; Taft, R. W. *J. Org. Chem.* **1983,** *48,* 2877–2887. doi:10.1021/jo00165a018
47. Taft, R. W.; Kamlet, M. J. *J. Am. Chem. Soc.* **1976,** *98,* 2886–2894. doi:10.1021/ja00426a036
48. Kamlet, M. J.; Taft, R. W. *J. Am. Chem. Soc.* **1976,** *98,* 377–383. doi:10.1021/ja00418a009
49. Kamlet, M. J.; Hall, T. N.; Boykin, J.; Taft, R. W. *J. Org. Chem.* **1979,** *44,* 2599–2604. doi:10.1021/jo01329a001

License and Terms

This is an Open Access article under the terms of the Creative Commons Attribution License (http://creativecommons.org/licenses/by/2.0), which permits unrestricted use, distribution, and reproduction in any medium, provided the original work is properly cited.

The license is subject to the *Beilstein Journal of Organic Chemistry* terms and conditions: (http://www.beilstein-journals.org/bjoc)

The definitive version of this article is the electronic one which can be found at: doi:10.3762/bjoc.6.79

Beilstein Journal of Organic Chemistry

Novel multi-responsive P2VP-*block*-PNIPAAm block copolymers via nitroxide-mediated radical polymerization

Cathrin Corten[1], Katja Kretschmer[1] and Dirk Kuckling[*1,2]

Full Research Paper

Open Access

Address:
[1]Fachrichtung Chemie und Lebensmittelchemie, Technische Universität Dresden, D-01062 Dresden, Germany and [2]Department Chemie, Universität Paderborn, Warburger Str. 100, D-33098 Paderborn, Germany

Email:
Dirk Kuckling[*] - dirk.kuckling@uni-paderborn.de

* Corresponding author

Keywords:
block copolymers; *N*-isopropylacrylamide; nitroxide-mediated radical polymerization; stimuli-responsive polymers; 2-vinylpyridine

Beilstein J. Org. Chem. **2010,** *6,* 756–765.
doi:10.3762/bjoc.6.89

Received: 05 May 2010
Accepted: 09 August 2010
Published: 20 August 2010

Guest Editor: H. Ritter

© 2010 Corten et al; licensee Beilstein-Institut.
License and terms: see end of document.

Abstract

Linear soluble multi-responsive block copolymers are able to form so called schizophrenic micelles in aqueous solution. Here, such polymers are prepared via nitroxide-mediated radical polymerization (NMRP). In a first step nitroxide-terminated poly(2-vinylpyridine) (P2VP) was prepared with different molecular weights and narrow molecular weight distributions. The best reaction conditions, optimized by kinetic studies, were bulk polymerization at 110 °C. Using P2VP as a macroinitiator, the synthesis of new soluble linear block copolymers of P2VP and poly(*N*-isopropylacrylamide) (PNIPAAm) (P2VP-*block*-PNIPAAm) was possible. The nitroxide terminated polymers were characterized by nuclear magnetic resonance (NMR) spectroscopy, size exclusion chromatography (SEC) and matrix-assisted laser desorption ionization time-of-flight mass spectrometry (MALDI-TOF MS). Thermal properties were investigated by the differential scanning calorimetry (DSC). Block copolymers showed pH- and temperature-responsive solubility in aqueous media. By increasing the P2VP content, the phase transition temperature shifted to lower temperatures (e.g. 26 °C for $P2VP_{114}$-*block*-$PNIPAAm_{180}$). Depending on the resulting block length, temperature and pH value of aqueous solution, the block copolymers form so called schizophrenic micelles. The hydrodynamic radius R_h of these micelles associated with pH values and temperature was analyzed by dynamic light scattering (DLS). Such kind of block copolymers has potential for many applications, such as controlled drug delivery systems.

Introduction

Functional polymers have attracted much attention because of their technological and scientific importance. Polymers, which respond with large property changes to small external chemical or physical stimuli, are so called “smart”, “responsive” or “intelligent” polymers [1,2], constitute a very interesting group of functional polymers. Such polymers have found applications

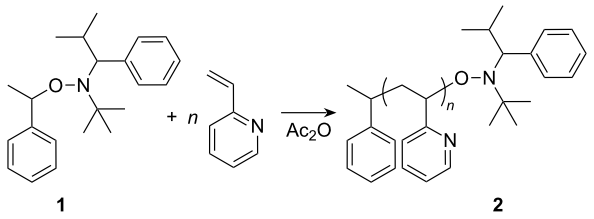
as reactive surfaces [3], in drug delivery and separation systems [4], as well as chemo-mechanical actuators [5], e.g., in valves where their characteristics have been studied extensively by a large range of methods [6,7].

One of the most intensively studied polymers in this field is poly(*N*-isopropylacrylamide) (PNIPAAm), which exhibits a sharp phase transition in water at 32 °C [8]. PNIPAAm undergoes a temperature-induced collapse from an extended coil to a globular structure, a transition revealed on the macroscopic scale by sudden decrease in the solubility of PNIPAAm. This behavior is derived from changes in the balance of interactions between hydrophilic and hydrophobic groups in the polymer chains at the critical temperature.

In order to prepare multi-responsive polymers, it is necessary to combine different kinds of monomers. For this purpose the preparation of defined block copolymers with different architectures is demanded. Amphiphilic or smart block and graft copolymers are already known in the literature [9]. Block copolymers in a wide range of variety are synthesized by using living anionic polymerization [10], living cationic polymerization [11] or controlled radical polymerizations techniques [12]. The development of the controlled radical polymerization (CRP), based on the idea of reversible chain termination, decreases the disadvantage of the free radical polymerization and permits the synthesis of defined block copolymer structures [13]. The growing demand for well-defined and functional soft materials in nanoscale applications has led to a dramatic increase in the development of procedures that combine architectural control with flexibility in the incorporation of functional groups. Thus, there has been a considerable increase in the understanding of a variety of controlled polymerization strategies [14-17] over the last few years. This includes nitroxide-mediated radical polymerization (NMRP) [18], atom transfer radical polymerization (ATRP) [19,20] and radical addition fragmentation chain transfer procedures (RAFT) [21,22]. The controlled polymerization of styrene, and analogous monomers such as 2-vinylpyridine (2VP), is one point of interest because at pH values lower than 5 it is possible to protonate the 2VP units and hence P2VP can be used as a pH-responsive component. Several techniques such as NMRP, ATRP and RAFT led to well-defined homo and block copolymers of different architectures whose behavior was investigated in solution and on surfaces [23,24].

The synthesis of NIPAAm homopolymers through different controlled polymerization techniques is described in the literature. Using RAFT it was possible to obtain amphiphilic block copolymers of PNIPAAm (hydrophilic) and poly(styrene) (PS) or poly(*tert*-butylmethacrylate) (PtBMA) as the hydrophobic compounds [25]. The design of bi-responsive narrowly distributed block copolymers consisting of NIPAAm and acrylic acid (AAc) was also feasible [26]. By the use of the ATRP catalyst system of tris(2-dimethylaminoethyl)amine (Me_6TREN) and Cu(I) chloride, well-defined PNIPAAm could be synthesized at room temperature [27]. Several graft copolymers are described in previous reports such as Chitosan-*graft*-PNIPAAm [28] and PNIPAAm-*graft*-P2VP polymers [29]. Both polymers show a temperature- and pH-responsive phase behavior in aqueous solutions.

While there are advantages and disadvantages to each procedure, our recent work concentrated on nitroxide mediated processes because of the ease of the reaction and the absence of transition metal impurities (binding easily to 2VP moieties) in the product. A major recent advance in nitroxide mediated polymerization has been the development of a hydrido nitroxide, in which the presence of a hydrogen atom on the α-carbon leads to a significant increase in the range of vinyl monomers that undergo controlled polymerization [30]. From that point of view, alkoxyamine **1** as an initiator for the polymerization of the 2VP has been selected and the resulting polymer was used as a macroinitiator **2** (Scheme 1).



Scheme 1: Synthesis of the nitroxide-terminated P2VP-macroinitiator.

Amphiphilic diblock copolymers undergo a self-assembly micellar process in solvents that are selective for one of the blocks [31]. By choosing selective conditions for each block, conventional micelles and so-called inverse micelles can be formed. In recent papers some examples of so called schizophrenic micelles are described [31,32]. In this case hydrophilic AB diblock copolymers can form micelles in aqueous solution, in which the A block forms the inner core and inverted micelles (with the B block forming the inner core) [33]. Armes et al. described the synthesis of a diblock copolymer with two weak polybases (poly(2-(*N*-morpholino)ethyl methacrylate-*block*-2-(diethylamino)ethyl methacrylate) PMEMA-*block*-PDEA) via group transfer polymerization. By adjusting the pH value of the solution, it was possible to from stable micelles with PDEA cores. The formation of inverted micelles (PMEMA core) was achieved by a "salting out" effect by adding electrolytes to the aqueous solution.

The synthesis of polyampholytes from P2VP as a basic block was reported in several papers, e.g., poly(2-vinylpyridine-*block*-sodium-4-styrenesulfonate) [34], poly(2-vinylpyridine-*block*-acrylic acid) [35], and poly(2-vinylpyridine-*block*-ethylene oxide) [31]. In this case according to the corresponding pH value of the solution, it was possible to obtain precipitation, aggregation or micellation.

An example of double-responsive diblock copolymers is reported by Müller et al. [26]. Diblock copolymers of poly(*N*-isopropylacrylamide-*block*-acrylic acid) were synthesized via RAFT. The resulting behavior in aqueous solution is influenced by hydrogen bonding interactions between the *N*-isopropylacrylamide and acrylic acid units.

Herein, we describe the synthesis of new multi-responsible diblock copolymers poly(2-vinylpyridine-*block*-*N*-isopropylacrylamide), which form schizophrenic micelles. Such micellation behavior is interesting for drug delivery systems in the gastro-intestinal tract [36,37].

Results and Discussion

Polymerization of 2-vinylpyridine

By using the unimolecular initiator 2,2,5-trimethyl-3-(1-phenylethoxy)-4-phenyl-3-azahexane (St-TIPNO) (**1**), it was possible to synthesize macroinitiators based on 2VP. In order to analyze the controlled character of the 2VP homo polymerization (Scheme 1), a kinetic study of this reaction with varying synthesis parameters (temperature, time and different molar ratios of [initiator]/[monomer]) was performed. A constant value of 2 equiv Ac_2O according to the amount of the alkoxyamine to each reaction mixture was added. The necessary addition of acetic anhydride or other organic acids is described in the literature [38].

After starting the reaction of 2VP in bulk at different temperatures (90 °C, 110 °C, 130 °C), a sample of 0.2 mL of the reaction mixture was taken after certain periods of time. 0.1 mL of this portion was analyzed by ^{1}H NMR spectroscopy in perdeuterated chloroform. The conversion was calculated by using the typical signal for C<u>H</u>=CH_2 of the monomer at 5.45 ppm and the peak at 8.44 ppm for the CH_{arom}–N of the 2VP polymer. The molecular weight and molecular weight distribution were determined by SEC measurements using THF as the mobile phase.

Figure 1 shows the plots of $\ln(M_0/M_t)$ and molecular weight distribution versus time at different temperatures. Here, characteristics known for controlled polymerizations are found, i.e., conversion increases within prolonged reaction time, molecular weight increases linearly with conversion, and products possess narrow molecular weight distribution. Increased temperature caused an enhancement of the reaction speed, which was also influenced by the molar ratio of [initiator]/[monomer]. This corresponds to various reports on the existence of the persistent radical effect (PRE) as a kinetic phenomenon [39].

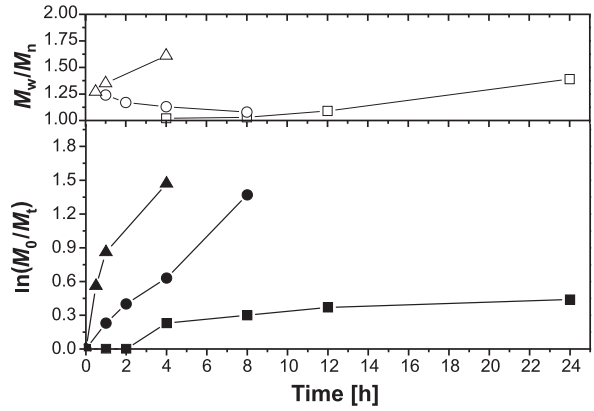


Figure 1: Plots of $\ln(M_0/M_t)$ and molecular weight distribution vs time of the homopolymerization of 2VP at ■ 90 °C, ● 110 °C, ▲ 130 °C (molar ratio [initiator]/[monomer] 1:140).

At 90 °C a very long induction period was found. After 4 h a conversion of 21% and after 8 h of 36% was determined. Despite this low polymer conversion, the molecular weight distribution was very narrow. However, for a practical process this reaction temperature is not useful because at extended reaction times, side reactions, e.g., elimination of the end capping nitroxide group by β-elimination, can occur terminating chain growth. Hence, an increased molecular weight distribution was observed. At 130 °C the reaction was very fast leading to a strong increase in conversion. After 30 min 40% of polymer was obtained. Apart from a high conversion, a broad molecular weight distribution of the products was obtained. The best reaction temperature was found to be 110 °C. At this temperature a linear relationship between conversion and reaction time was observed. For example, after 6 h a conversion of 50% corresponding to a molecular weight of 7550 g/mol (Figure 2).

During the progress of the reaction, a decrease of the molecular weight distribution could be found corresponding to the living character of this reaction [14]. In Figure 3 the molecular weight of P2VP prepared with different molar ratios of [initiator]/[monomer] at a constant temperature of 110 °C, compared with the theoretical molecular weights as function of conversion, are presented. The ratios [initiator]/[monomer] of 1:70 and 1:140 showed a linear increase of the molecular weight with increasing conversion, and are in good agreement with the calculated data. For a [initiator]/[monomer] ratio of 1:210, the obtained molecular weights are higher than the calculated ones.

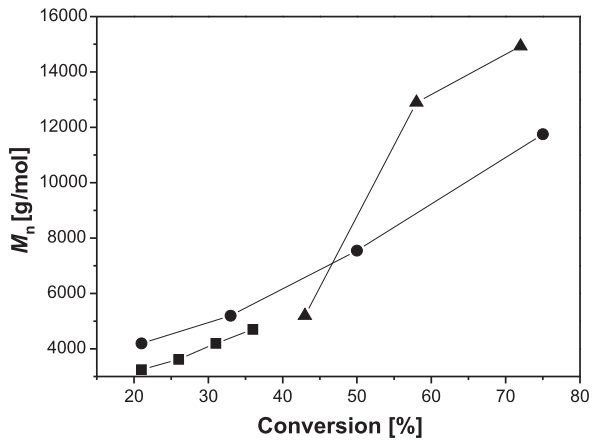


Figure 2: Plots of number average molecular weight vs conversion for the homopolymerization of 2VP for ■ 90 °C, ● 110 °C, ▲ 130 °C, (molar ratio [initiator]/[monomer] 1:140).

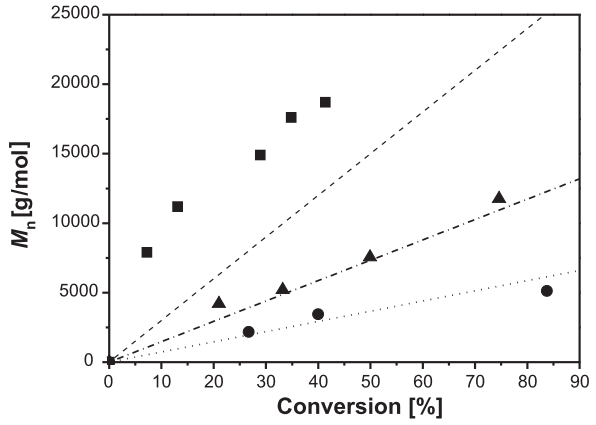


Figure 3: Plot of number average molecular weight vs conversion for the homopolymerization of 2VP at 110 °C with different molar ratios of [initiator]/[monomer] ■ 1:210, ▲ 1:140, ● 1:70. The dashed lines describe the theoretical behavior.

This is an indication that the amount of initiator was too small to control the polymerization. An increasing number of non-living processes occurred, yielding polymer chains having higher molecular weights.

By performing NMRP on 2VP, the resulting polymer should possess defined end groups (Scheme 1). In order to analyze the polymer structure MALDI-TOF MS was employed. The spectra of samples obtained from the polymerization at 110 °C with a [initiator/monomer] ratio of 1:140 stopped after 2, 4, 6 and 8 h are depicted in Figure 4. All distributions of the polymers exhibited differences between the *m/z*-peaks in the MALDI-TOF spectra that can be attributed to the weight of the 2VP

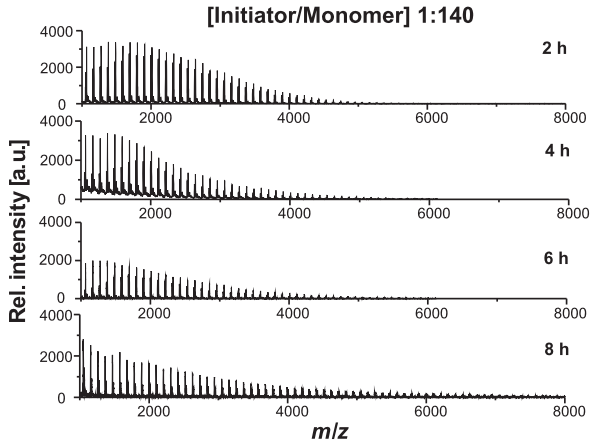
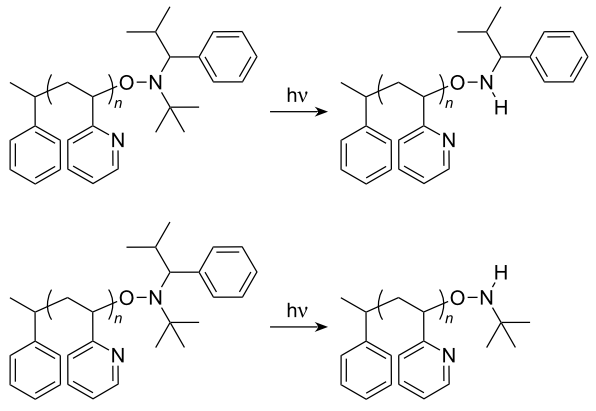


Figure 4: MALDI-TOF MS of P2VP obtained for polymerizations stopped after 2, 4, 6, and 8 h. The samples were prepared by the dried droplet method dissolving the polymer, DT, and KOTf in THF. To gain representative information, the spot was probed at several locations and 100 spectra were accumulated.

monomer unit. In contrast to the molecular weight data obtained by SEC analysis, the molecular weight determined by MALDI-TOF MS only increased from M_n = 1530 g/mol to M_n = 2800 g/mol. One reason might be the laser energy used to desorb the polymer led to P2VP chain degradation or fragmentation. Since SEC calibration has been done with P2VP standards, one can assume that the different results can be ascribed to significant ionization biases during MALDI-TOF analysis leading to incorrect molecular weights.

In addition, Dempwolf et al. [40] tested different alkoxyamines in different MALDI experiments. Supported by a comparison with other methods, they postulate a fragmentation mechanism inside the nitroxide-group, which takes place during the MALDI measurement. Disregarding the mechanism, Scheme 2 describes the possible reactions.



Scheme 2: Degradation of nitroxide-terminated P2VP-macroinitiator by laser light irradiation.

Since this process is accompanied by other degradation processes such as ß-abstraction [41] and by the instability of the C–O bond, it was not possible to detect the complete end groups. Figure 5 shows a section of typical spectra. Three different distributions could be observed, each of them has a repeating unit of m/z = 105.13, which corresponds to the monomer unit of 2VP. In Table 1 possible polymer structures according to suitable sum formula are summarized. For peak B different compositions could be assigned. At this point it is not possible to decide, if the measured distribution belongs to a thermal or nitroxide started polymer chain.

In summary, the analysis of such nitroxide capped polymers by MALDI-TOF MS is complex. However, by using St-TIPNO as an alkoxyamine initiator, it was possible to obtain 2VP-macromonomers of different molecular weights with narrow molecular weight distributions.

Synthesis of linear multi-responsive soluble polymers

Based on the results of homo polymerization for NIPAAm known from literature [9], it was possible to create suitable block copolymers with nitroxide-terminated P2VP macroinitiators and NIPAAm (Scheme 3). Chain extension of nitroxide capped polymers is only possible in intact polymers. Figure 6 illustrates typical SEC traces for the NIPAAm containing block copolymers. The shift of the peak to a smaller elution volume relative to the macroinitiator indicated successful block

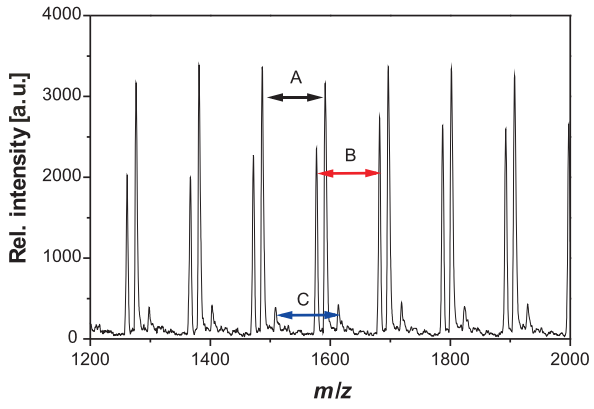


Figure 5: MALDI-TOF MS of P2VP obtained for polymerizations stopped after 2 h. The samples were prepared by the dried droplet method dissolving the polymer, DT, and KOTf in THF.

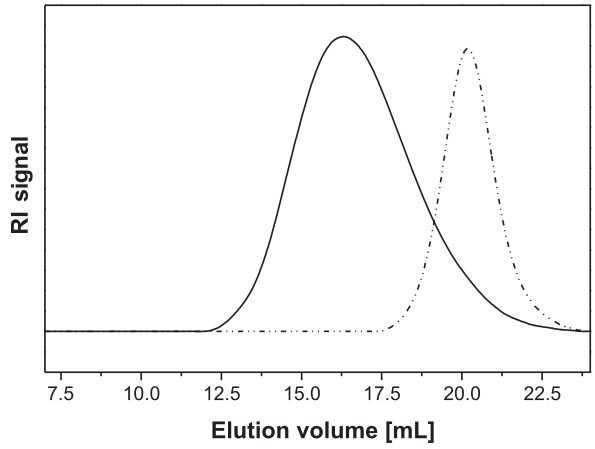
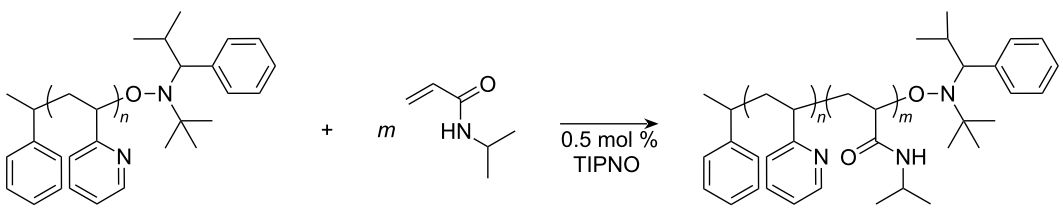


Figure 6: SEC traces for P2VP-*block*-PNIPAAm (solid line) and P2VP macroinitiator (dashed line).

Table 1: End group determination of the macroinitiators via MALDI-TOF MS.

Peak	m/z [exp.]	m/z [th.]	Chain	n	Cation	Δ m/z
A	1591.12	1597.97	$[CH_3(C_7H_6)–[2VP]_n–C_4H_{10}NO]$	13	K^+	6.82
B	1577.12	1578.08	$[CH_3(C_7H_6)–[2VP]_n–H]$	14	H^+	0.96
		1579.07	$[CH_3(C_5H_6N)–[2VP]_n–H]$	14	H^+	1.95
C	1513.13	1510.90	$[CH_3(C_7H_6)–[2VP]_n–H]$	13	K^+	2.23



Scheme 3: Synthesis of the bi-responsive block copolymers.

copolymer formation. No shoulder or second peak at elution volumes for macroinitiator was found, indicating that most of the polymers possessed intact structure. Additionally, the SEC traces show an overlap between the two traces, which might be taken as hint for the existence of unreacted macroinitiator.

After 48 h at 135 °C block copolymers with an average yield of 65% could be obtained. As described in previous papers, the process of the NIPAAm polymerization with nitroxide-mediated compounds is neither a well-controlled process nor does it result in a real living character [41]. However, PNIPAAm homo polymer of M_n = 7500 g/mol could be obtained with a molecular weight distribution of 1.21. After block copolymerization, the molecular weight distribution increased. Nevertheless, for most of the block copolymers the molecular weight distribution remained moderate. The results of copolymer characterization are summarized in Table 2. DSC measurements revealed two separated T_gs, indicating a microphase separation of the block copolymers in the dry state.

Aqueous solutions of these block copolymers showed an LCST behavior. Due to the hydrophobic character of P2VP, the resulting polymers possessed lower phase transition temperatures compared to pure PNIPAAm [42]. With increase of the 2VP/NIPAAm ratio within the block copolymers, the critical temperature dropped to 26.3 °C. Although all polymers showed a temperature-dependent solution behavior, only block copolymers with a high P2VP content showed pH sensitivity. Solubilization of such polymers was possible below pH 5 only due to the protonation of pyridine moieties. In Figure 7 the solution behavior of such polymers is demonstrated.

Figure 7a shows that the P2VP macroinitiator and $P2VP_{114}$-*block*-$PNIPAAm_{244}$ were not soluble in aqueous solution of pH 7 at lower temperatures, while PNIPAAm and $P2VP_{85}$-*block*-$PNIPAAm_{351}$ were completely dissolved under these conditions. By increasing the temperature above 35 °C, none of polymers were soluble. A decrease of the pH value to pH 4, resulted in protonation of the P2VP fraction, which also led to completely soluble polymers at lower temperatures. The phase separation behavior was also observable at higher temperatures. Above the critical temperatures, all polymer solutions with a PNIPAAm fraction became opaque.

A typical titration curve for the multi-responsive *block* copolymers is presented in Figure 8. By adding 0.1 N NaOH to a stirred solution of $P2VP_{105}$-*block*-$PNIPAAm_{332}$ in 0.02 N HCl, scattering polymer particles were produced at a pH range of 4–5 around the added NaOH droplets (high local concentration). When the solution is homogenized by stirring, the scattering disappeared. This indicates that the micelle formation is a dynamic and reversible process. When the pH value reaches 4.8 (point 1), aggregates were visible over the entire volume, and above 5.3 (point 2) the micelles formation was complete.

The pK_a for 2-ethylpyridine is 5.9. As described in the literature [31], due to the concentrated pyridine groups along the polymer backbone, the effective pK_a is lower than for this model substance as a result of charge repulsion along the chain, decreasing the pK_a value to 4.4. It has been shown [43] that the effective pK_a varies with the fraction of protonation of P2VP. Hence, by titration it is not possible to measure the real pK_a.

In order to investigate the size of the micelles, dynamic light scattering experiments were performed on diluted block copolymer solutions under various conditions. The resulting hydrodynamic radii of the diblock copolymers are summarized in Table 3. Polymers with short P2VP blocks, $P2VP_{85}$-*block*-$PNIPAAm_{351}$ and $P2VP_{22}$-*block*-$PNIPAAm_{181}$, behave similar to homo PNIPAAm at 20 °C. No association, due to the incorporation of the 2VP block, could be observed. The two aqueous solutions were completely clear and showed no scattering indicating that the polymers were molecularly dissolved. Above the critical temperature, micelles, with R_h of 55 nm and 79 nm, respectively, were formed stabilized by partly ionized P2VP blocks. Interestingly, the decrease of the pH value to pH 2 led to formation of large aggregates instead of micellation at higher temperatures. This instability of the polymeric material

Table 2: Characterization of soluble linear P2VP-*block*-PNIPAAm copolymers created by NMRP.

Polymer	M_n [g/mol]	M_w / M_n	T_c [°C]	T_g [°C]
PNIPAAm	7500	1.21	32.3	—
$P(2VP)_{22}$-*block*-$P(NIPAAm)_{181}$	16600	1.35	30.5	131.7
$P(2VP)_{85}$-*block*-$P(NIPAAm)_{351}$	22600	1.74	29.3	107.4 / 132.7
$P(2VP)_{105}$-*block*-$P(NIPAAm)_{332}$	28900	1.62	28.0	97.8 / 130.4
$P(2VP)_{114}$-*block*-$P(NIPAAm)_{180}$	21700	1.43	26.3	103.9 / 131.2
$P(2VP)_{114}$-*block*-$P(NIPAAm)_{244}$	24700	1.57	27.6	97.4 / 131.6
$P(2VP)_{114}$-*block*-$P(NIPAAm)_{648}$	45500	2.19	28.6	104.9 / 128.9

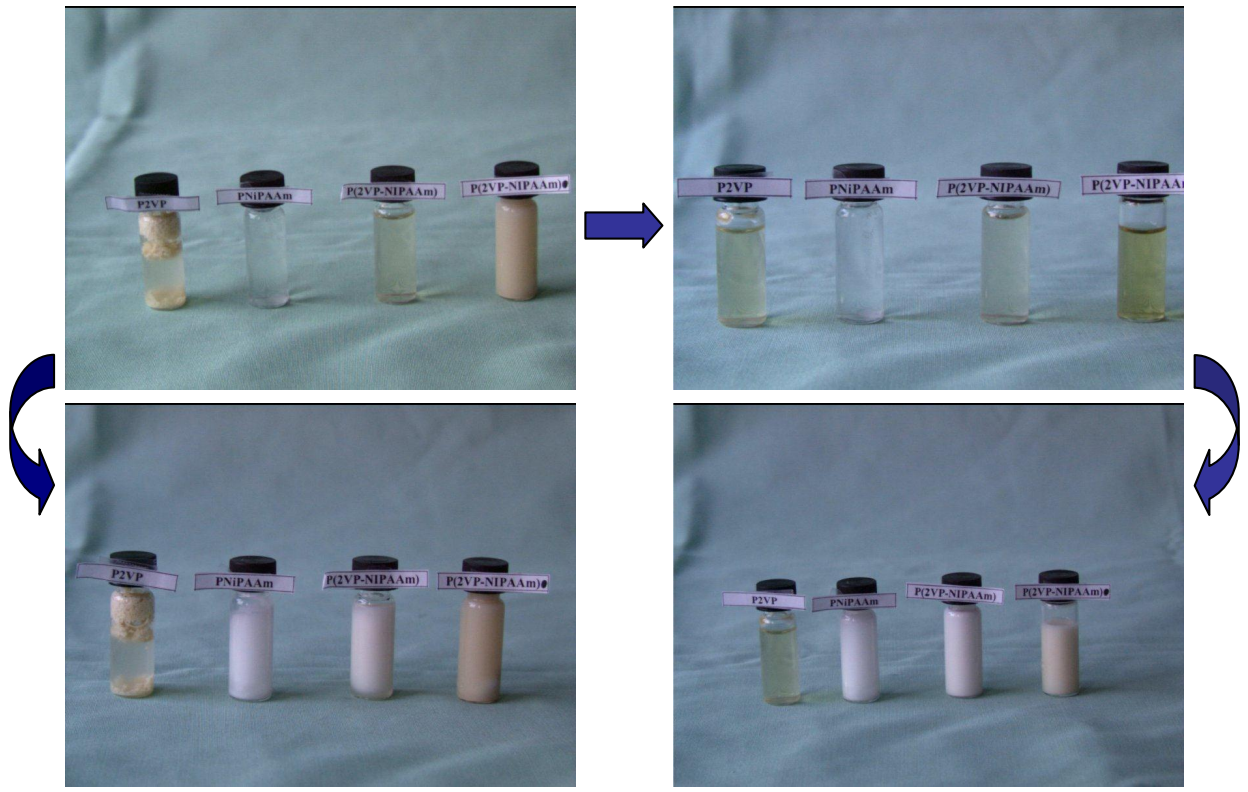


Figure 7: Demonstration of the solution behavior. Polymers from left to right: P2VP, PNIPAAm, $P(2VP)_{85}$-*block*-$P(NIPAAm)_{351}$, $P(2VP)_{114}$-*block*-$P(NIPAAm)_{244}$; a) pH7 and RT, b) pH 4 and RT, c) pH 7 and $T > 35$ °C, d) pH 4 and $T > 35$ °C.

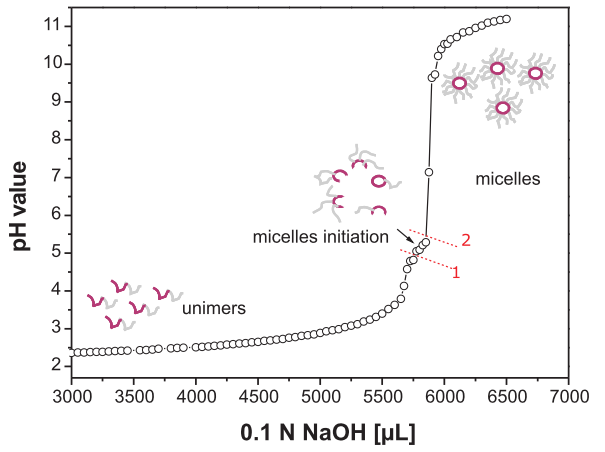


Figure 8: Titration of $P2VP_{105}$-*block*-$PNIPAAm_{332}$ (1g/L) in 0.02 N HCl with 0.1 N NaOH at room temperature.

in the presence of an HCl solution above the critical temperature can be explained by increased ionic strength at pH 2. Chloride ions can bind to polar amide groups of the PNIPAAm units, and might interact with the water molecules associated with polar or hydrophobic polymer segments [44]. Hence, driving forces for inter- and intramolecular hydrophobic interactions are increased leading to a decrease in the stability of the NIPAAm polymers, which then tend to form larger aggregates. The protonated P2VP units are too small to inhibit this process. The results of the P2VP-*block*-PNIPAAm copolymers with longer P2VP segments showed the expected results. In neutral aqueous solutions, micelles with a hydrophobic P2VP core and an outer shell of PNIPAAm were formed. By increasing the temperature to 45 °C, the PNIPAAm units became more hydrophobic, and were not able to stabilize the micelles anymore. Finally, the micelles were forming large aggregates and precipitated. By dissolving the polymers in 0.02 N HCl at 20 °C, the P2VP segments were completely protonated forming soluble unimers. Polymers with larger P2VP/PNIPAAm ratios were forming inverted micelles above the critical temperature. The protonation of the 2VP units led to electrostatic repulsion and the longer P2VP blocks were able to stabilize the micelles preventing PNIPAAm forming larger aggregates even in diluted HCl. Due to the longer PNIPAAm block with respect to the P2VP block, micelles formed by a PNIPAAm core and by a P2VP outer shell showed larger hydrodynamic radius. The schizophrenic behavior of $P2VP_{105}$-*block*-$PNIPAAm_{332}$ is summarized in Figure 9.

Table 3: Dynamic light scattering characterization of bi-responsive P2VP-*block*-PNIPAAm copolymers in aqueous solution.

Polymer	Ratio P2VP/PNIPAAm	R_h pH 7 20 °C [nm]	R_h pH 7 45 °C [nm]	R_h pH 2 20 °C [nm]	R_h pH 2 45 °C [nm]
$P(2VP)_{22}$-*block*-$P(NIPAAm)_{181}$	1:8	4.5	55.3	5	Agg[a]
$P(2VP)_{85}$-*block*-$P(NIPAAm)_{351}$	1:4	8	79.4	7.5	Agg
$P(2VP)_{105}$-*block*-$P(NIPAAm)_{332}$	1:3	85.6	Agg	5	116.2
$P(2VP)_{114}$-*block*-$P(NIPAAm)_{244}$	1:2	71.2	Agg	6	112.3

[a]Agg: aggregates larger than R_h = 1100 nm.

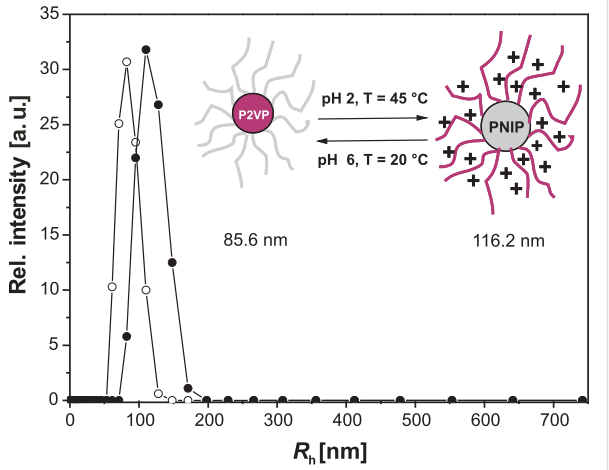


Figure 9: Hydrodynamic radius distribution of $P(2VP)_{105}$-b-$P(NIPAAm)_{332}$ at ○ pH 7, T = 20 °C and ● pH 2, T= 45 °C.

Conclusion

Well-defined P2VP macroinitiators were prepared using NMRP. The kinetic study showed the controlled behavior of the polymerization for this vinyl monomer. Best polymerizations were carried out in bulk at 110 °C with a molar ratio of [initiator]/[monomer] of 1:140. Under these conditions, nitroxide-terminated P2VP with different molecular weights and a narrow molecular weight distribution could be synthesized. It is well known that the MALDI process causes severe degradation of nitroxide end capped polymers. This fragmentation could be observed as well for P2VP. Despite this fact, chain extension of such polymers is only possible by intact polymers. No shoulder or second peak at elution volumes for macroinitiator was found indicating that most of the polymers possessed intact structure. Using P2VP as a macroinitiator, new soluble linear block copolymers of P2VP and PNIPAAm were synthesized, which showed a pH- and temperature-responsive solubility. With increased P2VP content, the phase transition temperature shifted to lower temperatures (e.g., 26 °C for $P2VP_{114}$-*block*-$PNIPAAm_{180}$). DLS measurements of the block copolymers underlined the multi-responsive and schizophrenic behavior in aqueous solutions. DSC measurement of the glass transition temperature revealed a microphase separation behavior for these block copolymers in the dry state.

Experimental Section

Materials

N-isopropylacrylamide (NIPAAm, Acros) was purified by recrystallization from hexane and dried in vacuum. 2-Vinylpyridine (2VP, 98 %, Merck) was stirred over calcium hydride for 24 h and freshly distilled before use. Dimethylformamide (DMF) was distilled over calcium hydride. All other chemicals were used as received.

Characterization

NMR spectra were recorded on a Bruker NMR spectrometer DRX500. Elemental analysis was done with a Hekatech EA 3000 Euro Vector CHNSO Elementaranalysator. DSC measurements were carried out with a Mettler-Toledo DSC 30 to determine the glass transition temperature (T_g) of the block copolymers (heating rate 10 °C/min) and with a TA Instruments DSC 2290 to measure the phase transition temperature (T_c) (heating rate of 5 °C/min) as an average of 4 cycles. The polymer concentration was 50 mg/mL in a pH 4 buffer solution (CertiPUR® Merck). Molecular weight and the molecular weight distribution of P2VP were determined by size exclusion chromatography with a JASCO instrument set up with UV and RI detector using a P2VP-calibration. The samples were measured at 30 °C in THF as the mobile phase with a flow rate 1 mL/min. BHT was used as an internal standard on Polymer Laboratories linear columns (PLgel MIXED-BLS 10 mm). The parameters of the copolymers were determined by size exclusion chromatography (SEC) with a PL120 instrument equipped with RI detector using PSS 'GRAM' columns using a P2VP-calibration. The samples were measured at 50 °C in dimethylacetamide (DMAc) containing 0.42 g/L lithium bromide as mobile phase with a flow rate of 1 mL/min. Matrix assisted laser desorption ionization time of flight mass spectrometry (MALDI-TOF MS) was performed on a BiFlex IV (Bruker Daltonics). 1,8,9-Anthracenetriol (DT) (Bruker Daltonics) was used as the matrix and potassium triflouromethanesulfonate (98% ACROS) was added to improve the ionization process.

The samples were prepared by mixing THF solutions of the polymer, matrix and salt (10 mg/mL) in a typical ratio of 1:10:1 (v/v/v, polymer/matrix/salt), and a droplet (1 µL) of the mixture was dried on the target. As calibration standard poly(ethylene oxide) [M_w = 2000 g/mol, Sigma-Aldrich] was used.

Dynamic light scattering (DLS) was measured on a Zetasizer Nanoseries Nano-ZS (Malvern instruments) with a laser at 633 nm, a constant angle of 173° and a temperature of 25 °C. The hydrodynamic radius (R_h) was calculated using the Stokes–Einstein relation. The polymeric solutions were prepared from double-destilled water or 0.02 M HCl (aq) solution with polymer concentration of 0.5 g/L. All solutions were prepared 60 min before measurements. The solutions were treated with ultrasound for 5 min and filtered through PES filters (pore size 0.45 µm).

Synthesis

2,2,5-Trimethyl-3-(1-phenylethoxy)-4-phenyl-3-azahexane (St-TIPNO) (**1**) and the corresponding nitroxide 2,2,5-trimethyl-4-phenyl-3-azahexane 3-nitroxide (TIPNO) were prepared according to the literature [45,46].

General procedure of 2VP polymerization

A mixture of 2VP, 0.1 mL acetic anhydride and the alkoxyamine **1** was degassed by three freeze/thaw cycles, sealed under argon, and heated at 110 °C for different periods of time. Afterwards the polymerization was stopped by cooling with liquid nitrogen. The reaction mixture was then diluted with THF and precipitated in *n*-pentane (ratio 1:5). The obtained powder was dried in vacuum to give the desired alkoxyamine-terminated P2VP.

Preparation of multi-responsive block copolymers

A mixture of the alkoxyamine-terminated P2VP macroinitiator, NIPAAm, and TIPNO dissolved in DMF was degassed by three freeze/thaw cycles, sealed under argon and heated to 135 °C for 48 h. Afterwards the reaction was stopped by cooling with liquid nitrogen. The solvent was almost removed by evaporation under reduced pressure. The residue was redissolved in chloroform and precipitated in cold diethyl ether. The resulting brownish powder was dried in vacuum. Block copolymer was obtained with up to a yield of 65%.

Acknowledgements

The DFG (Deutsche Forschungsgemeinschaft) is gratefully acknowledged for their financial support of this work within the Sonderforschungsbereich 287 “Reaktive Polymere”. The authors are thankful to A. Rudolph for recording NMR spectra, I. Poitz and M. Dziewiencki for DSC measurements.

References

1. Hoffman, A. S. *Macromol. Symp.* **1995,** *96,* 645–664.
2. Hoffman, A. S.; Stayton, P. S. *Macromol. Symp.* **2004,** *207,* 139–152. doi:10.1002/masy.200450314
3. Yakushiji, T.; Sakai, K.; Kikuchi, A.; Aoyagi, T.; Sakurai, Y.; Okano, T. *Langmuir* **1998,** *14,* 4657–4662. doi:10.1021/la980090+
4. Freitas, R. F. S.; Cussler, E. L. *Chem. Eng. Sci.* **1987,** *42,* 97–103. doi:10.1016/0009-2509(87)80213-0
5. Kuckling, D.; Richter, A.; Arndt, K.-F. *Macromol. Mater. Eng.* **2003,** *288,* 144–151. doi:10.1002/mame.200390007
6. Kuckling, D.; Harmon, M. E.; Frank, C. *Langmuir* **2003,** *19,* 10660–10665. doi:10.1021/la030232m
7. Kuckling, D. *Colloid Polym. Sci.* **2009,** *287,* 881–891. doi:10.1007/s00396-009-2060-x
8. Schild, H. G. *Prog. Polym. Sci.* **1992,** *17,* 163–249. doi:10.1016/0079-6700(92)90023-R
9. Bosman, A. W.; Vestberg, R.; Heumann, A.; Frechet, J. M. J.; Hawker, C. J. *J. Am. Chem. Soc.* **2003,** *125,* 715–728. doi:10.1021/ja028392s
10. Rempp, P.; Lutz, P. *Makromol. Chem., Macromol. Symp.* **1993,** *67,* 1–14.
11. Kennedy, J. P.; Iván, B. *Designed polymers by carbocationic macromolecular engineering: theory and practice;* Carl Hanser Verlag: München, Germany, 1991.
12. Matyjaszewski, K. *Curr. Opin. Solid State Mater. Sci.* **1996,** *1,* 769–776. doi:10.1016/S1359-0286(96)80101-X
13. Riess, G.; Hurtrez, G.; Bahadur, P. Block Copolymers. In *Encyclopedia of Polymer Science and Engineering,* 2nd ed.; Mark, H. F., Ed.; Wiley: New York, 1985.
14. Matyjaszewski, K., Ed. *Controlled radical polymerization;* ACS Symposium Series, Vol. 685; American Chemical Society: Washington, DC, 1998.
15. Fischer, H. *J. Polym. Sci., Part A: Polym. Chem.* **1999,** *37,* 1885–1901. doi:10.1002/(SICI)1099-0518(19990701)37:13<1885::AID-POLA1>3.3.CO;2-T
16. Boyer, C.; Bulmus, V.; Davis, T. P.; Ladmiral, V.; Liu, J.; Perrier, S. *Chem. Rev.* **2009,** *109,* 5402–5436. doi:10.1021/cr9001403
17. Rosen, B. M.; Percec, V. *Chem. Rev.* **2009,** *109,* 5069–5119. doi:10.1021/cr900024j
18. Rodlert, M.; Harth, E.; Rees, I.; Hawker, C. J. *J. Polym. Sci., Part A: Polym. Chem.* **2000,** *38,* 4749–4763. doi:10.1002/1099-0518(200012)38:1+<4749::AID-POLA140>3.0.CO;2-D
19. Matyjaszewski, K. *J. Phys. Org. Chem.* **1995,** *8,* 197–207. doi:10.1002/poc.610080403
20. Kato, M.; Kamigaito, M.; Sawamoto, M.; Higashimura, T. *Macromolecules* **1995,** *28,* 1721–1723. doi:10.1021/ma00109a056
21. Otsu, T.; Matsumoto, A.; Tazaki, T. *Polym. Bull.* **1987,** *17,* 323–330. doi:10.1007/BF00955715
22. Convertine, A. J.; Ayres, N.; Scales, C. W.; Lowe, A. B.; McCormick, C. L. *Biomacromolecules* **2004,** *5,* 1177–1180. doi:10.1021/bm049825h
23. Yu, K.; Wang, H.; Xue, L.; Han, Y. *Langmuir* **2007,** *23,* 1443–1452. doi:10.1021/la062159g
24. Zetterlund, P. B.; Kagawa, Y.; Okubo, M. *Chem. Rev.* **2008,** *108,* 3747–3794. doi:10.1021/cr800242x
25. Nuopponen, M.; Ojala, J.; Tenhu, H. *Polymer* **2004,** *45,* 3643–3650. doi:10.1016/j.polymer.2004.03.083

26. Schilli, C. M.; Zhang, M.; Rizzardo, E.; Thang, S. H.; Chong, Y. K.; Edwards, K.; Karlsson, G.; Müller, A. E. *Macromolecules* **2004,** *37,* 7861–7866. doi:10.1021/ma035838w
27. Masci, G.; Giacomelli, L.; Crescenzi, V. *Macromol. Rapid Commun.* **2004,** *25,* 559–564. doi:10.1002/marc.200300140
28. Lee, S. B.; Ha, D. I.; Cho, S. K.; Kim, S. J.; Lee, Y. M. *J. Appl. Polym. Sci.* **2004,** *92,* 2612–2620. doi:10.1002/app.20265
29. Wohlrab, S.; Kuckling, D. *J. Polym. Sci., Part A: Polym. Chem.* **2001,** *39,* 3797–3804. doi:10.1002/pola.10026
30. Benoit, D.; Hawker, C. J.; Huang, E. E.; Lin, Z.; Russell, T. P. *Macromolecules* **2000,** *33,* 1505–1507. doi:10.1021/ma991721p
31. Prochazka, K.; Martin, J. T.; Webber, S. E.; Munk, P. *Macromolecules* **1996,** *29,* 6526–6530. doi:10.1021/ma9606317
32. Liu, S.; Billingham, N. C.; Armes, S. P. *Angew. Chem., Int. Ed.* **2001,** *40,* 2328–2331. doi:10.1002/1521-3773(20010618)40:12<2328::AID-ANIE2328>3.0.CO;2-M
33. Bütun, V.; Billingham, N. C.; Armes, S. P. *J. Am. Chem. Soc.* **1998,** *120,* 11818–11819. doi:10.1021/ja982295a
34. Varoqui, R.; Tran, Q.; Pfefferkorn, E. *Macromolecules* **1979,** *12,* 831–835. doi:10.1021/ma60071a008
35. Kamachi, K.; Kurihara, M.; Stille, J. K. *Macromolecules* **1972,** *5,* 161–167. doi:10.1021/ma60026a013
36. Satturwar, P.; Eddine, M. N.; Ravenelle, F.; Leroux, J.-C. *Eur. J. Pharm. Biopharm.* **2007,** *65,* 379–387. doi:10.1016/j.ejpb.2006.09.012
37. Jones, M.-C.; Leroux, J.-C. *Eur. J. Pharm. Biopharm.* **1999,** *48,* 101–111. doi:10.1016/S0939-6411(99)00039-9
38. Baumann, M.; Schmidt-Naake, G. *Macromol. Chem. Phys.* **2001,** *202,* 2727–2731. doi:10.1002/1521-3935(20010901)202:13<2727::AID-MACP2727>3.0.CO;2-L
39. Fukuda, T.; Goto, A.; Ohno, K. *Macromol. Rapid Commun.* **2000,** *21,* 151–165. doi:10.1002/(SICI)1521-3927(200003)21:4<151::AID-MARC151>3.0.CO;2-3
40. Dempwolf, W.; Flakus, S.; Schmidt-Naake, G. *Macromol. Symp.* **2007,** *259,* 416–420. doi:10.1002/masy.200751347
41. Schulte, T.; Siegenthaler, K. O.; Luftmann, H.; Letzel, M.; Studer, A. *Macromolecules* **2005,** *38,* 6833–6840. doi:10.1021/ma050343n
42. Hirokawa, Y.; Tanaka, T. *J. Chem. Phys.* **1984,** *81,* 6379–6380. doi:10.1063/1.447548
43. Kirsh, Y. E.; Komarova, O. P.; Lukovikin, G. M. *Eur. Polym. J.* **1973,** *9,* 1405–1415. doi:10.1016/0014-3057(73)90110-9
44. Eliassaf, J. *J. Appl. Polym. Sci.* **1978,** *22,* 873–874. doi:10.1002/app.1978.070220328
45. Krause, T.; Habicher, W. D.; Messerschmidt, M.; Voit, B. *Des. Monomers Polym.* **2004,** *7,* 391–397. doi:10.1163/1568555041475275
46. Benoit, D.; Chaplinski, V.; Braslau, R.; Hawker, C. *J. Am. Chem. Soc.* **1999,** *121,* 3904–3920. doi:10.1021/ja984013c

License and Terms

This is an Open Access article under the terms of the Creative Commons Attribution License (http://creativecommons.org/licenses/by/2.0), which permits unrestricted use, distribution, and reproduction in any medium, provided the original work is properly cited.

The license is subject to the *Beilstein Journal of Organic Chemistry* terms and conditions: (http://www.beilstein-journals.org/bjoc)

The definitive version of this article is the electronic one which can be found at: doi:10.3762/bjoc.6.89

Beilstein Journal of Organic Chemistry

Novel 2-(ω-phosphonooxy-2-oxaalkyl)acrylate monomers for self-etching self-priming one part adhesive

Joachim E. Klee* and Uwe Lehmann

Full Research Paper

Open Access

Address:
Dentsply De Trey, De-Trey-Str. 1, 78467 Konstanz, Germany

Email:
Joachim E. Klee* - joachim.klee@dentsply.com

* Corresponding author

Keywords:
adhesion to enamel and dentin; hydrolysis stable 2-(ω-phosphonooxy-2-oxaalkyl)acrylates; phosphorylation using $POCl_3$; polymerization enthalpy; shear bond strength

Beilstein J. Org. Chem. **2010,** *6,* 766–772.
doi:10.3762/bjoc.6.95

Received: 04 May 2010
Accepted: 09 August 2010
Published: 07 September 2010

Guest Editor: H. Ritter

© 2010 Klee and Lehmann; licensee Beilstein-Institut.
License and terms: see end of document.

Abstract

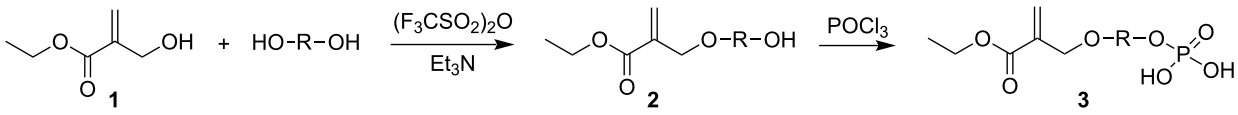
Novel hydrolysis stable 2-(ω-phosphonooxy-2-oxaalkyl)acrylate monomers **3** with phosphoric acid moieties were synthesized by a three step synthesis via Baylis–Hillman reaction of ethyl acrylate and formaldehyde, and subsequent etherification of the obtained product with diols and phosphorylation using $POCl_3$. The polymerization enthalpy of 2-(ω-phosphonooxy-2-oxaalkyl)acrylates **3** as measured by DSC ranges from −29 to −53 kJ·mol^{-1}. The shear bond strength of adhesive compositions **4,** comprising of polymerizable acids **3,** ranges from 5.8 to 19.3 MPa on enamel and from 8.7 to 16.9 MPa on dentin.

Introduction

Dental adhesives have been employed for fixation of direct and indirect restorations since the 80s of the last century. The first of these adhesives were composed of three-part systems, consisting of an etch gel, a primer and a bonding. Each of these adhesive parts was applied step-by-step in a relatively time consuming procedure that is prone to failure during the procedure. Therefore, a reduction of the complexity of the adhesives during application was desirable. Furthermore, the adhesion procedure should be more safe, easy and robust. In order to fulfill these demands some generations of adhesives were developed which combined the etch and prime function or the prime and bond function together in one part.

The first self-etching, self-priming dental adhesives were composed of two-part systems for stability reasons, i.e., low hydrolysis stability of conventional polymerizable acidic ester monomers and adhesive monomers in water or water/solvent mixtures. Newer one-part systems are based on conventional polymerizable acidic ester monomers and adhesive monomers, and these must be stored in a refrigerator to guarantee stability.

Today the demand is to have a one-part self-etching adhesive, which can be stored under ambient conditions and which combines all three steps of the adhesive procedure in one. Besides polymerizable monomers and acidic monomers, water



Scheme 1: Synthesis of novel ethyl 2-(ω-phosphonooxy-2-oxaalkyl)acrylates **3**.

is required in such a system for the acidic etch function. Therefore, such adhesives require novel hydrolysis stable monomers and novel hydrolysis stable acidic monomers.

Recently, some interesting approaches to acidic monomers were developed based on derivatives of α-hydroxymethylacrylate esters [1], with one [2-4] or two phosphonic acid moieties [5], or with phosphoric [4,6] or sulfonic acid groups [7] as well as with carboxylic acid groups [7]. These acidic monomers are constructed in such a way that no hydrolysis sensitive moiety is present between the polymerizable moiety and the acidic group. The latter etches enamel and dentin surface, and is an anchor group, especially on dentin, due to the formation of calcium phosphate linkages.

The aim of the present investigation is the synthesis of novel polymerizable phosphoric acid ester monomers and their comparison concerning their adhesive performance in dental formulations. Furthermore, the aim is to clarify whether, under strong acidic conditions, hydrolysis of phosphoric acid ester moieties takes place in a similar manner to carboxylic acid esters, and to establish whether acidic molecules with 2-(ω-phosphonooxy-2-oxaalkyl)acrylate moieties exhibit the same adhesive performance as their ester analogues.

Results and Discussion

A series of novel 2-(ω-phosphonooxy-2-oxaalkyl)acrylates **3,** comprising of phosphoric acid ester moieties, were synthesized via a three step synthesis via Baylis–Hillman reaction of ethyl acrylate and formaldehyde, and subsequent etherification of the obtained product with diols and phosphorylation using $POCl_3$ (Scheme 1, Table 1).

The double bonds in **3** are evident in the IR spectrum at 1637 (**3a**) and 1639 cm^{-1} (**3e, 3h, 3i**) and in the ^1H NMR spectrum at 5.87/6.27 ppm (**3a**). In the ^{13}C NMR spectra signals of the sp^2 hybridized C-atoms of the double bonds appear at 127.11/136.281 ppm (**3a**). Signals of the P–OH moiety were found in the ^1H NMR spectrum at 10.71 ppm (**3a**) and in the ^{31}P NMR spectra at 0.16 ppm (**3h**) and −0.11/0.07 ppm (**3i**).

DSC Investigation of 3

The polymerization behavior of 2-(ω-phosphonooxy-2-oxaalkyl)acrylates **3** was investigated by photo-polymerization using a DSC 7/DPA 7 unit. The polymerization enthalpy of 2-(ω-phosphonooxy-2-oxaalkyl)acrylates **3** (Table 2) ranged from −29 to −53 $kJ \cdot mol^{-1}$ per double bond, which is rather comparable to the polymerization enthalpy of methacrylic esters (−52.8 to −59.9 $kJ \cdot mol^{-1}$) [8-10] and lower compared to the

Table 1: Yields, viscosities and refraction indexes of molecules **2a–2i** and **3a–3i**.



	R		M_n g/mol	Yield **2** g (%)	Yield **3** g (%)	η Pa*s	n_D^{20}
a	$(CH_2)_2$	$C_8H_{15}O_7P$	254.18	10.12 (50.0)	14.2 (55.0)	40.13 ± 0.62	1.4760 ± 0.002
b	$(CH_2)_3$	$C_9H_{17}O_7P$	268.20	37.28 (21.4)	31.0 (58.8)	4.01 ± 0.10	1.4662 ± 0.001
c	$(CH_2)_6$	$C_{12}H_{23}O_7P$	310.28	16.01 (36.2)	8.8 (44.5)	2.04 ± 0.05	1.4652 ± 0.0003
d	$(CH_2)_{10}$	$C_{16}H_{31}O_7P$	366.39	40.49 (40.9)	11.5 (20.9)	-	-
e	$(CH_2)_{10}$[a]	$C_{14}H_{27}O_7P$	338.34	-	8.6 (60.0)	-	-
f	$(CH_2)_{12}$	$C_{18}H_{35}O_7P$	394.45	7.07 (8.8)	7.8 (91.0)	-	-
g	$CH_2CH_2OCH_2CH_2$	$C_{10}H_{19}O_8P$	298.23	19.45 (46.0)	17.0 (65.0)	6.26 ± 0.16	1.4691 ± 0.002
h	$(CH_2CH_2O)_2CH_2CH_2$	$C_{12}H_{23}O_9P$	342.28	28.34 (46.9)	31.1 (88.6)	4.16 ± 0.05	1.4692 ± 0.0002
i	$(CH_2CH_2O)_3CH_2CH_2$	$C_{14}H_{27}O_{10}P$	386.34	51.91 (73.5)	32.9 (50.2)	2.35 ± 0.01	1.4702 ± 0.0003

[a]**3e** with free carboxylic acid moiety.

polymerization enthalpy of acrylic esters (−77.5 to −80.5 kJ·mol^{-1}) [9,10]. This may be due to the substitution of the double bond in **3,** which is comparable with a methacrylic moiety rather than with an acrylic group.

Table 2: Polymerization enthalpy $\Delta_R H$ of **3a–3i**.

3	R	$\Delta_R H$ kJ/mol
a	$(CH_2)_2$	−30.7
b	$(CH_2)_3$	−45.7
c	$(CH_2)_6$	−44.8
d	$(CH_2)_{10}$	−45.1
e	$(CH_2)_{10}$[a]	−53.2
f	$(CH_2)_{12}$	−52.0
g	$CH_2CH_2OCH_2CH_2$	−29.3
h	$(CH_2CH_2O)_2CH_2CH_2$	−41.8
i	$(CH_2CH_2O)_3CH_2CH_2$	−50.8

[a]**3e** with free carboxylic acid moiety.

Obviously, molecules **3** with relatively short alkyl or oxyalkyl spacers exhibit the lowest polymerization enthalpy of −30.7 (**3a**) and −29.3 kJ·mol^{-1} (**3g**). The longer the spacers are, the higher is the polymerization enthalpy, up to −50.8 (**3i**) and −52.0 kJ·mol^{-1} (**3f**), which is only slightly lower than those of methacrylates. Probably, the steric proximity of the phosphoric acid moiety has an influence on the polymerization behavior due to the competitive reactions of protonation and radical formation of the amine co-initiator.

Assuming that there was complete polymerization at 80 °C, the polymerization enthalpy of **3b** was measured under these conditions. It was found that the polymerization enthalpy increases from −45.7 at 37 °C to −52.3 kJ/mol at 80 °C, which corresponds to a degree of double bond conversion of 87.3% at 37 °C.

Adhesion of phosphoric acids 3

The shear bond strength of adhesive compositions **4** [11], comprising of polymerizable acids **3,** ranges from 5.8 to 19.3 MPa on enamel and from 8.7 to 16.9 MPa on dentin (Table 3, Figure 1). With increasing length of the aliphatic spacers of **3a**–**3f** between the phosphoric acid ester and the ether linkage, adhesion both on enamel and dentin reach a maximum at **3e** (*n* = 10 CH_2 moieties). Obviously, a balance of the hydrophobic and hydrophilic nature is achieved with **3e,** which is essential for adhesion on the very different substrates such as enamel and dentin.

Whilst the inclusion of larger oxymethylene moieties in **3** has no influence on the adhesion on dentin (**3a**, **3g**–**3h**), it has a pronounced effect on the adhesion on enamel which drops significantly with larger numbers of oxymethylene moieties.

Table 3: Adhesion of an adhesive composition **4,** comprising of polymerizable acids **3,** on enamel and dentin.

4	Adhesion on enamel/MPa	Adhesion on dentin/MPa
a	10.9 ± 3.0	13.4 ± 2.0
c	10.8 ± 1.4	16.9 ± 1.4
d	19.3 ± 1.8	15.1 ± 2.2
e	10.5 ± 2.4	23.7 ± 3.4
f	17.5 ± 1.5	8.7 ± 1.0
g	12.6 ± 2.2	14.3 ± 1.4
h	5.4 ± 0.9	13.3 ± 3.4
i	6.8 ± 2.4	13.4 ± 1.3

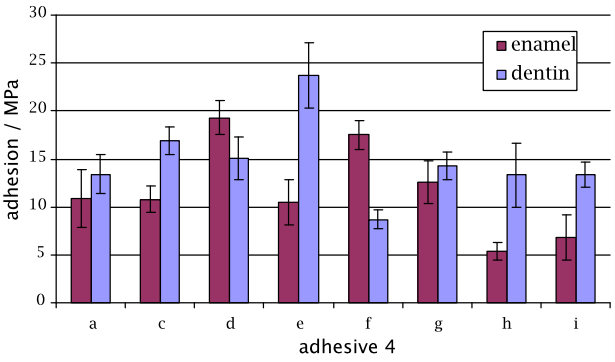


Figure 1: Adhesion of an adhesive composition **4,** comprising of polymerizable acids **3,** on enamel and dentin.

Conclusion

Novel hydrolysis stable 2-(ω-phosphonooxy-2-oxaalkyl)acrylate monomers **3** with phosphoric acid moieties and alkyl as well as oxyalkyl spacers were synthesized in three steps via Baylis–Hillman reaction of ethyl acrylate and formaldehyde, and subsequent etherification of the obtained product with diols and phosphorylation using $POCl_3$. The polymerization enthalpy of 2-(ω-phosphonooxy-2-oxaalkyl)acrylates **3** measured by DSC ranges from −29 to −53 kJ·mol^{-1}. The shear bond strength of adhesive compositions **4,** comprising of polymerizable acids **3,** ranges from 5.8 to 19.3 MPa on enamel and from 8.7 to 16.9 MPa on dentin.

Experimental

The following commercial products were purchased from Sigma-Aldrich: formalin, ethyl acrylate, diazabicyclo[2.2.2]-octane, dioxane, trifluoromethane sulphonic anhydride, dichloromethane, conc. HCl, triethylamine, 1,2-ethanediol, 1,6-

hexanediol, 1,8-octanediol 1,10-decanediol, 1,12-dodecanediol, diethylene glycol, triethylene glycol, tetraethylene glycol, phosphorous oxychloride, diethyl ether and 2,6-di-*tert*-butyl-4-methylphenol Bis(2,4,6-trimethylbenzoyl)phenyl phosphine oxide was purchased from BASF Interorgana. *N*,*N*′-bisacrylamido-*N*,*N*′-diethyl-1,3-propane, and 3(4)8(9)-bis(acrylamidomethyl)tricyclo[5.2.1.$0^{2,6}$]decane were obtained from DENTSPLY. Spectrum TPH (DENTSPLY) is a dental composite comprising of methacrylate based resins and a glass filler.

Ethyl 2-hydroxymethylacrylate (1)

1 was prepared according to [1].

Ethyl 2-(4-hydroxy-2-oxabutyl)acrylate (2a)

To a solution of 32.52 g trifluoromethane sulphonic anhydride in 100 mL dichloromethane, a solution of 15 g (0.115 mol) **1** and 11.66 g (0.115 mol) triethylamine in 200 mL dichloromethane was added slowly at such a rate that the temperature of the reaction mixture remained below 5 °C. The solution was then added dropwise at room temperature to 210 g (3.387 mol) 1,2-ethanediol. After stirring for 12 h at room temperature, the solution was washed successively with 1 × 200 mL water, 2 × 250 mL of an aqueous sodium carbonate solution (25 wt %) and 1 × 200 mL water. The organic layer was dried over magnesium sulfate and filtered. After the evaporation of the solvent, the oily crude product was stabilized with 15 mg 2,6-di-*tert*-butyl-4-methylphenol and purified by vacuum distillation (63 °C/0.032 mbar) to give 10.12 g (yield: 50%) of **2a** as a clear, colorless oil.

IR (film, cm^{-1}) 3436 (OH), 2979, 2931, 2871 (CH_3/CH_2), 1710 (CO), 1638 (C=C), 1453, 1373, 1304 (CH_3/CH_2), 1270, 1173, 1109, 1052, 953. ^{1}H NMR (250 MHz, $CDCl_3$, ppm) 1.27 (t, 3H, CH_3), 2.52 (broad s, 1H, OH), 3.54–3.63 (m, 2H, O$CH_2$$CH_2$O), 3.67–3.78 (m, 2H, O$CH_2$$CH_2$O), 4.15–4.24 (m, 4H, CH_2 (1) and O$CH_2$$CH_3$), 5.84 (s, 1H, CH=*C*), 6.28 (s, 1H, CH=C). ^{13}C NMR (63 MHz, $CDCl_3$, ppm) 14.06 (CH_3), 60.74 (O*C*$H_2$$CH_3$), 61.56 (*C*$H_2$OH), 69.31 (*C*$H_2$$CH_2$OH), 71.80 (=C*C*$H_2$O), 126.21 (*C*$H_2$=C), 137.03 (*C*=$CH_2$), 165.82 (CO).

Ethyl 2-(4-phosphonooxy-2-oxabutyl)acrylate (3a)

To a stirred solution of 15.46 g (0.1008 mol) phosphorus oxychloride in 280 mL diethyl ether, a solution of 17.56 g (0.1008 mol) **2a** and 10.2 g (0.1008 mol) triethylamine in 250 mL diethyl ether was added dropwise at such a rate that the temperature of the reaction mixture remained below 5 °C. After stirring for 14 h at room temperature, the mixture was filtered and then added slowly at 0 °C to 200 mL of water. The emulsion was stirred for 40 min. The layers were separated and the aqueous layer was washed with 2 × 100 mL diethyl ether. The aqueous layer was reduced in volume to 100 mL and extracted with 4 × 100 mL dichloromethane. The combined organic extracts were dried over magnesium sulfate, filtered and evaporated to yield 19 g of a yellow oil. The oil was dissolved in 400 mL of water and washed with 3 × 200 mL of diethyl ether. Concentration of the aqueous phase at reduced pressure and drying under vacuum (10^{-3}mbar) afforded 14.18 g (yield: 55%) of a clear colorless oil, which was stabilized with 6.11 mg 2,6-di-*tert*-butyl-4-methylphenol.

IR (film, cm^{-1}) 3500–2500 broad absorption (OH), 2912 (CH_3/CH_2), 1709 (CO), 1637 (C=C), 1456, 1374 (CH_3/CH_2), 1261, 1178, 1105, 1014, 949. ^{1}H NMR (250 MHz, $CDCl_3$, ppm) 1.25 (t, 3H, CH_3), 3.70 (broad s, 2H, CH_2), 4.30–4.13 (m, 6H, CH_2), 5.87 (s, 1H, CH=C), 6.27 (s, 1H, CH=C), 10.71 (broad s, 2 H, PO_3H_2). ^{13}C NMR (63 MHz, $CDCl_3$, ppm) 13.94 (CH_3), 60.94 (O*C*$H_2$$CH_3$), 66.01 (O$CH_2$*C*$H_2$), 69.25 (O*C*$H_2$$CH_2$), 69.40 (=C*C*$H_2$O), 127.11 (*C*$H_2$=C), 136.28 (*C*=$CH_2$), 166.00 (CO). ^{31}P NMR (CD_3OD; ppm): −0.21/0.01 (d, PO_3H_2).

2b–**2i** and **3b**–**3i** were synthesized as described for **2a** and **3a**.

Ethyl 2-(5-hydroxy-2-oxapentyl)acrylate (2b)

bp 100–120 °C/0.093 mbar. IR (film, cm^{-1}): 3500–2500 broad absorption (OH), 2877 (CH_3/CH_2), 1705 (CO), 1637 (C=C), 1469, 1381, 1177, 1101, 1002, 953, 819, 746. ^{1}H NMR (250 MHz, d_6-DMSO, ppm): δ = 1.18 (t, 3H, CH_3), 1,72–1,87 (m, 2H, CH_2), 3.43–3,51 (m, 2H, CH_2), 3.81–3,94 (m, 2H, CH_2), 4.00–4.19 (m, 4H, CH_2), 5.79 (s, 1H, CH=C), 6.12 (s, 1H, CH=C). ^{13}C NMR (63 MHz, d_6-DMSO, ppm): δ = 14.35 (CH_3), 30.58, 30.65 (CH_2*C*$H_2$$CH_2$), 60.79 (O*C*$H_2$$CH_3$), 63.15, 63.18 (O*C*$H_2$$CH_2$), 66.88 (O*C*$H_2$$CH_2$), 68.76 (=C*C*$H_2$O), 125.77 (*C*$H_2$=C), 137.84 (*C*=$CH_2$), 165.61 (CO).

Ethyl 2-(8-hydroxy-2-oxaoctyl)acrylate (2c)

The substance was dried in vacuum without distillation. IR (film, cm^{-1}): 3383 (OH), 2935/2866 (CH_3/CH_2), 1710 (CO), 1638 (C=C), 1452, 1383, 1303, 1269, 1158, 1100, 1055, 949, 816.

Ethyl 2-(12-hydroxy-2-oxadodecyl)acrylate (2d)

bp 129–140 °C/0.039 mbar. IR (film, cm^{-1}): 3425 (OH), 2926/2855 (CH_3/CH_2), 1714 (CO), 1638 (C=C), 1459/1375/1303 (CH_3/CH_2), 1270/1172/1102/1031/949. ^{1}H NMR (250 MHz, $CDCl_3$, ppm): δ = 1.08–1.24 (m, 15H, C*H*$_2$,C*H*$_3$), 1.24–1.49 (m, 4H, CH_2), 3.17 (broad s, 1H, OH), 3.27 (t, 2H, OCH_2) 3.37 (t, 2H, OCH_2), 3.96 (s, 2H, CH_2(1)), 4.01 (q, 2H, O$CH_2$$CH_3$) 5.65 (s, 1H, CH=C), 6.07 (s, 1H, CH=C). ^{13}C NMR (63 MHz, $CDCl_3$, ppm): δ = 13.64 (CH_3), 25.36, 25.68, 28.98, 29.07, 29.11, 29.17 and 32.24 (CH_2 (8-15)), 60.10 (CH_2OH), 68.31 (O*C*$H_2$$CH_2$), 70.52 (=C*C*$H_2$O), 124.69 (*C*$H_2$=C), 137.12 (*C*=$CH_2$), 165.37 (CO).

Ethyl 2-(14-hydroxy-2-oxatetradecyl)acrylate (2f)

Purification was performed by recrystallization from CH_2Cl_2 followed by column chromatography on silica gel (115 g) with CH_2Cl_2 as eluent. IR (film, cm^{-1}): 3412 (OH), 2924/2855 (CH_3/CH_2), 1715 (CO), 1638 (C=C), 1460/1375/1303 (CH_3/CH_2), 1270/1173/1103/1054/1029/951.

Ethyl 2-(7-hydroxy-2,5-dioxaheptyl)acrylate (2g)

bp 94–102 °C/0.026 mbar. IR (film, cm^{-1}): 3426 (OH), 2871 (CH_3/CH_2), 1712 (CO), 1639 (C=C), 1456, 1374, 1303, 1270, 1174, 1099, 1028, 953, 887, 816.

Ethyl 2-(10-hydroxy-2,5,8-trioxadecyl)acrylate (2h)

bp 138–141 °C/0.041 mbar. IR (film, cm^{-1}): 3433 (OH), 2964/2929/2874 (CH_3/CH_2), 1711 (CO), 1638 (C=C), 1453/1385/1302 (CH_3/CH_2), 1269/1151/1099/1056/984/882. ^{13}C NMR (63 MHz, $CDCl_3$, ppm): δ = 13.0 (CH_3), 60.3 (CH_2O), 68.0–71.5 (CH_2), 124.3 (CH_2=C), 136.1 (C=CH_2), 164.5 (CO).

Ethyl 2-(13-hydroxy-2,5,8,11-tetraoxatridecyl)acrylate (2i)

bp 147–153 °C/0.037 mbar. IR (film, cm^{-1}): 3370 (OH), 2870 (CH_3/CH_2), 1713 (CO), 1639 (C=C), 1458/1375 (CH_3/CH_2), 1266 (CH_2O), 1198/1028/947/816.

Ethyl 2-(5-phosphonooxy-2-oxapentyl)acrylate (3b)

The compound was obtained as a clear, colorless oil. IR (film, cm^{-1}): 2926/2855 (CH_3/CH_2), 1715 (CO), 1639 (C=C), 1461/1375 (CH_3/CH_2), 1265/ 1169/1101/1023/951.

Ethyl 2-(8-phosphonooxy-2-oxaoctyl)acrylate (3c)

The compound was obtained as a clear, slightly yellow oil. IR (film, cm^{-1}): 2934/2872 (CH_3/CH_2), 1714 (CO), 1640 (C=C), 1456/1376 (CH_3/CH_2), 1269/1170/1098/1027/950. ^1H NMR (250 MHz, CD_3OD, ppm): δ = 1.20–1.36 (t, 3H, CH_3), 1.43–1.44 (m, 4H, CH_2), 3.30 (s, 2H, CH_2), 3.51 (t, 2H, CH_2), 3.97–3.98 (m, 2H, CH_2), 4.99 (m, 6H, $CH_2OPO_3H_2$, OCH_2CH_3), 5.86 (s, 1H, CH=C), 6.32 (s, 1H, CH=C). ^{13}C NMR (63 MHz, CD_3OD, ppm): δ = 13.6 (CH_3), 26.5/26.9/30.6 (CH_2), 31.4 (CH_2CH_2OP), 31.5 (OCH_2CH_2), 60.8 (CH_2O), 68.0 (CH_2OP), 70.1 (OCH_2CH_2), 71.8 (=CCH_2O), 126.4 (CH_2=C), 139.8 (C=CH_2), 169.5 (CO). ^{31}P NMR (CD_3OD; ppm): −0.36/0.14 (d, PO_3H_2).

Ethyl 2-(12-phosphonooxy-2-oxadodecyl)acrylate (3d)

The compound was obtained as a yellowish solid. IR (film, cm^{-1}): 2926/2855 (CH_3/CH_2), 1715 (CO), 1639 (C=C), 1461/1375 (CH_3/CH_2), 1265/1169/1101/1023/951. ^1H NMR (250 MHz, $CDCl_3$, ppm): δ = 1.15–1.36 (m, 15H, CH_3), 1.45–1.77 (m, 4H, CH_2), 3.41 (t, 2H, CH_2(3)), 4.03–4.24 (m, 4H, $CH_2OPO_3H_2$, OCH_2CH_3), 4.11 (s, 2H, CH_2), 5.79 (s, 1H, CH=C), 6.22 (s, 1H, CH=C). ^{13}C NMR (63 MHz, $CDCl_3$, ppm): δ = 13.98 (CH_3), 25.08, 25.93, 28.92, 29.19, 29.25, 29.30 and 29.45 (CH_2 (8-15)), 60.42 (CH_2CH_3, CH_2OP), 68.63 (OCH_2CH_2), 70.86 (=CCH_2O), 125.08 (CH_2=C), 137.38 (C=CH_2), 165.69 (CO).

2-(12-phosphonooxy-2-oxadodecyl)acrylic acid (3e)

To an ice cold solution (0–5 °C) of 3.470 g (10.14 mmol) of **3d** dissolved in 20 mL water, an aqueous solution of 1.217 g (30.41 mmol) sodium hydroxide dissolved in 12.165 mL of water was added slowly. The solution was then stirred for 24 h at ambient temperature. The basic solution was acidified with 25 mL of a 1N HCl, saturated with NaCl and extracted three times with 50 mL THF. The extracts were dried over Na_2SO_4 and the solvent was removed. Yield: 2.01 g (62.8%), of a yellowish solid, mp 63.2 °C

IR (film, cm^{-1}): 3500–3100 (COOH, broad), 2924/2854 (CH_3/CH_2), 1697 (CO), 1633 (C=C), 1458/1373 (CH_3/CH_2), 1173/1010/827. ^1H NMR (250 MHz, $CDCl_3$, ppm): δ = 1.95–2.18 (m, 16H, CH_2), 3.90 (t, 2H, $CH_2OPO_3H_2$), 4.37–4.43 (m, 2H, OCH_2CH_2), 4.6 (s, 2H, =CCH_2O), 5,75 (s, 1H, CH=C), 6.30 (s, 1H, CH=C). ^{13}C NMR (63 MHz, $CDCl_3$, ppm: δ = 25.08–31.6 (CH_2), 67.3 (CH_2OP), 69.5 (OCH_2CH2), 71.2 (=CCH_2O), 125.8 (CH_2=C), 137.6 (CH_2=C), 168.7 (CO).

Ethyl 2-(14-phosphonooxy-2-oxatetradecan)acrylate (3f)

The compound was obtained as a white wax-like solid. IR (film, cm^{-1}): 2918/2854 (CH_3/CH_2), 1712 (CO), 1637 (C=C), 1470/1379 (CH_3/CH_2), 1304/1238/1165/1116/1026/853. ^1H NMR (250 MHz, CD_3OD, ppm): δ = 1.28–1.41 (m, 17H, CH_3), 1.58–1.69 (m, 4H, CH_2), 3.48-3.51 (t, 2H, CH_2), 3.94–3.98 (q, 2H, OCH_2CH_3), 4.15 (s, 2H, CH_2), 5.20 (s, 2H, CH_2), 5.85 (s, 1H, CH=C), 6.26 (s, 1H, CH=C). ^{13}C NMR (63 MHz, CD_3OD, ppm): δ = 15.50 (CH_3), 26.69, 27.31, 30.37, 30.61, 30.75, 31.49 and 31.56, (CH_2), 62.52 (CH_2CH_3), 67.81, 67.69 (CH_2OP), 70.21 (OCH_2CH_2), 71.99 (=CCH_2O), 126.28 (CH_2=C), 139.51 (C=CH_2), 169.51 (CO). ^{31}P NMR (CD_3OD; ppm): −0.57/0.13 (d, PO_3H_2).

Ethyl 2-(7-phosphonooxy-2,5-dioxaheptyl)acrylate (3g)

The compound was obtained as a clear, colorless oil. IR (film, cm^{-1}): 2926/2878 (CH_3/CH_2), 1712 (CO), 1640 (C=C), 1453/1379 (CH_3/CH_2), 1240/1169/1105/818. ^1H NMR (250 MHz, CD_3OD, ppm): δ = 1.30–1.38 (m, 3H, CH_2CH_3), 1.70–1.85 (m, 2H, CH_2), 3.31–3.46 (t, 2H, CH_2), 3.61–3.73 (m, 4H, OCH_2CH_3), 4.07–4.25 (m, 2H, CH_2), 4.88 (s, 2H, CH_2), 5.92 (s, 1H, CH=C), 6.27 (s, 1H, CH=C). ^{13}C NMR (63 MHz,

CD_3OD, ppm): δ = 14.47 (CH_3), 61.88 (CH_2CH_3), 66.89/66.73 (CH_2OP), 70.4 (CH_2CH_2O), 70.48 (OCH_2CH_2), 71.42 (=CCH_2O), 71.49 (OCH_2CH_2), 126.65 (CH_2=C), 139.01 (C=CH_2), 164.72 (CO). ^{31}P NMR (CD_3OD; ppm): −0.01/0.79 (d, PO_3H_2).

Ethyl 2-(10-phosphonooxy-2,5,8-trioxadecyl)acrylate (3h)

The compound was obtained as a clear, colorless oil. IR (film, cm^{-1}): 2874 (CH_3/CH_2), 1711 (CO), 1639 (C=C), 1459/1372 (CH_3/CH_2), 1246/982/820. ^{1}H NMR (250 MHz, CD_3OD, ppm): δ = 1.28–1.32 (m, 3, CH_3), 3.67/3.72 (m, 10H, CH_2), 4.09–4.10 (q, 2H, OCH_2CH_3), 4.21–4.23 (t, 2H, CH_2), 5.34 (s, 2H, CH_2), 5.91 (s, 1H, CH=C), 6.30 (s, 1H, CH=C). ^{13}C NMR (63 MHz, CD_3OD, ppm): δ = 13.57 (CH_3), 61.95 (CH_2CH_3), 66.86/66.91 (CH_2OP), 70.4 (CH_2CH_2O), 70.5 (OCH_2CH_2), 71.19 (=CCH_2O), 71.60 (OCH_2CH_2), 126.74 (CH_2=C), 139.21 (C=CH_2), 165.6 (CO). ^{31}P NMR (CD_3OD; ppm): 0.81/0.01/−0.81 (m, PO_3H_2).

Ethyl 2-(13-phosphonooxy-2,5,8,11-tetraoxatridecyl)acrylate (3i)

The compound was obtained as a clear, colorless oil. IR (film, cm^{-1}): 2879 (CH_3/CH_2), 1714 (CO), 1639 (C=C), 1465/1398 (CH_3/CH_2), 1258/1150/1026/796. ^{1}H NMR (250 MHz, CD_3OD, ppm): δ = 1.21–1.28 (m, 3, CH_3), 3.59/3.63 (m, 14H, CH_2), 4.06–4.14 (q, 2H, OCH_2CH_3), 4.21–4.23 (t, 2H, CH_2), 5.34 (s, 2H, CH_2), 5.92/5.94 (s, 1H, CH=C), 6.24/6.28 (s, 1H, CH=C), 8.71 (s, 2H, PO_3H_2). ^{13}C NMR (63 MHz, $CDCl_3$, ppm): δ = 13.7 (CH_3), 60.5 (CH_2CH_3), 65.5 (CH_2OP), 68.8 (CH_2CH_2O), 69.3 (OCH_2CH_2), 69.7 (=CCH_2O), 127.9 (CH_2=C), 136.4 (C=CH_2), 168.5 (CO). ^{31}P NMR (CD_3OD; ppm): −0.11/0.07 (d, PO_3H_2).

Adhesive composition **4a**: 1.5261 g *N*,*N*′-bisacrylamido-1,3-propane, 2.2150 g 3,(4),8,(9)-bis(acrylamidomethyl)-tricyclo[5.2.1.$0^{2,6}$]decane, 0.5551 g of **3a**, 0.2776 g 2-acrylamido-2-methylpropanesulfonic acid, 0.0337 g camphorquinone, 0.0849 g bis(2,4,6-trimethylbenzoyl)phenyl phosphine oxide and 0.0392 g 4-(*N*,*N*-dimethylamino)benzoic acid ethyl ester were dissolved in a solvent mixture of 3.5201 g ethanol and 1.7484 g water.

Adhesive compositions **4c–i** were prepared from **3c–i** in the same manner as described above.

The following procedure was applied prior to adhesion measurements:

- First the teeth were abraded with 200 and 500 grit abrasive paper.
- Then the teeth were stored at 37 °C in water.
- The teeth were treated with adhesive formulation for 20 s and the solvents evaporated by an air stream for 10 s.
- Light curing of adhesive layer for 20 s.
- A polymerized Spectrum TPH body applied on the adhesive was cured on the teeth 3 times for 20 s.
- Finally, the prepared teeth were stored in water at 37 °C for 2 h before the measurement.

IR spectra were measured with a FT-IR spectrometer (Nicolet 6700 FT-IR spectrometer, Thermo Scientific). The ^{1}H NMR, ^{13}C NMR and ^{31}P NMR spectra were obtained with a Bruker AC 250 MHz spectrometer. Viscosities were measured with a Bohlin-Rheometer CS-50 at 23 °C.

The melting points were taken with a DSC 7 (Perkin-Elmer). Polymerization enthalpies were measured in the isothermal mode at 37 °C with a photo-calorimeter DSC 7/DPA 7 (Perkin-Elmer). The light intensity in the visible portion of the spectrum was 108 $mW \cdot cm^{-2}$. Each DSC experiment included a short dark period (typically 6 s) and a subsequent illumination period. After the first run, an additional run was made using the polymerized material under the same experimental conditions. The subtraction of these runs from one another removed the effect of different baselines for the dark and the illumination periods. In the monomers were dissolved 0.3 mol % camphorquinone and 0.35 mol % 4-(*N*,*N*-dimethylamino)benzoic acid ethyl ester.

References

1. Mathias, L. J.; Warren, R. M. *Polym. Prepr.* **1989,** *30,* 235.
2. Moszner, N.; Zeuner, F.; Fischer, U. K.; Rheinberger, V. *Macromol. Chem. Phys.* **1999,** *200,* 1062.
3. Moszner, N.; Zeuner, F.; Rheinberger, V. Hydrolysestabile und polymerisierbare Acrylphsophonsäuren. DE 197 46 708, Oct 16, 1997.
4. Avci, D.; Mathias, L. J. *J. Polym. Sci., Part A: Polym. Chem.* **2002,** *40,* 3221. doi:10.1002/pola.10413
5. Erdmann, C.; Ziegler, S.; Nefgen, S.; Bolln, C.; Mühlbauer, W.; Lück, R. Dental material containing phosphonic acids. WO 02/02057 A1, July 3, 2001.
6. Klee, J. E.; Lehmann, U.; Walz, U.; Liu, H. A polymerizable phosphoric acid ester derivative and a dental composition employing it. EP 1 454 911, March 7, 2003.
7. Hoffmann, M.; Erdrich, A. Hydrolysestabile Monomere mit Säuregruppen. EP 1 681 283 A1, Dec 24, 2005.
8. Dainton, F. S.; Ivin, K. J.; Walmsley, D. A. G. *Trans. Faraday Soc.* **1960,** *56,* 1784. doi:10.1039/tf9605601784
9. Joshi, R. M. *J. Polym. Sci.* **1962,** *56,* 313. doi:10.1002/pol.1962.1205616404
10. Flammersheim, H.-J.; Klemm, E. *Acta Polym.* **1985,** *36,* 443. doi:10.1002/actp.1985.010360810
11. Klee, J. E.; Lehmann, U.; Walz, U. One-part self-etching, self-priming dental adhesive composition. EP 1 548 021 B1, Dec 23, 2003.

License and Terms

This is an Open Access article under the terms of the Creative Commons Attribution License (http://creativecommons.org/licenses/by/2.0), which permits unrestricted use, distribution, and reproduction in any medium, provided the original work is properly cited.

The license is subject to the *Beilstein Journal of Organic Chemistry* terms and conditions: (http://www.beilstein-journals.org/bjoc)

The definitive version of this article is the electronic one which can be found at: doi:10.3762/bjoc.6.95

Beilstein Journal of Organic Chemistry

Synthesis and crystal structures of multifunctional tosylates as basis for star-shaped poly(2-ethyl-2-oxazoline)s

Richard Hoogenboom[*1,2], Martin W. M. Fijten[1], Guido Kickelbick[3] and Ulrich S. Schubert[*1,4]

Full Research Paper

Open Access

Address:
[1]Laboratory of Macromolecular Chemistry and Nanoscience, Eindhoven University of Technology, Den Dolech 2, 5612AZ Eindhoven, The Netherlands, [2]Supramolecular Chemistry group, Department of Organic Chemistry, Ghent University, Krijgslaan 281 S4, 9000 Ghent, Belgium, [3]Inorganic Solid State Chemistry, Saarland University, Am Markt Zeile 3, 66125 Saarbrücken, Germany and [4]Laboratory of Organic and Macromolecular Chemistry, Friedrich-Schiller-University Jena, Humboldtstrasse 10, 07743 Jena, Germany

Email:
Richard Hoogenboom[*] - r.hoogenboom@tue.nl; Ulrich S. Schubert[*] - ulrich.schubert@uni-jena.de

* Corresponding author

Keywords:
cationic polymerization; crystal structure; living polymerization; star-polymer; tosylate

Beilstein J. Org. Chem. **2010,** *6,* 773–783.
doi:10.3762/bjoc.6.96

Received: 09 June 2010
Accepted: 19 August 2010
Published: 09 September 2010

Guest Editor: H. Ritter

© 2010 Hoogenboom et al; licensee Beilstein-Institut.
License and terms: see end of document.

Abstract

The synthesis of well-defined polymer architectures is of major importance for the development of complex functional materials. In this contribution, we discuss the synthesis of a range of multifunctional star-shaped tosylates as potential initiators for the living cationic ring-opening polymerization (CROP) of 2-oxazolines resulting in star-shaped polymers. The synthesis of the tosylates was performed by esterification of the corresponding alcohols with tosyl chloride. Recrystallization of these tosylate compounds afforded single crystals, and the X-ray crystal structures of di-, tetra- and hexa-tosylates are reported. The use of tetra- and hexa-tosylates, based on (di)pentaerythritol as initiators for the CROP of 2-ethyl-2-oxazoline, resulted in very slow initiation and ill-defined polymers, which is most likely caused by steric hindrance in these initiators. As a consequence, a porphyrin-cored tetra-tosylate initiator was prepared, which yielded a well-defined star-shaped poly(2-ethyl-2-oxazoline) by CROP as demonstrated by SEC with RI, UV and diode-array detectors, as well as by ^{1}H NMR spectroscopy.

Introduction

Nowadays, well-defined polymer structures are of major importance for the development of ever more sophisticated and complex materials, e.g., applications in drug delivery or as adaptive materials. Star-shaped polymers are especially interesting since their properties are distinctly different from their linear analogues with regard to, e.g., number of functional end-groups, hydrodynamic volume and thermal properties [1,2].

Poly(2-oxazoline)s represent a class of versatile polymer structures that can be prepared by the (CROP) of 2-substituted-2-oxazoline monomers (see the bottom right corner of Figure 1 for the structure of poly(2-ethyl-2-oxazoline), as an example of the polymer structure) [3,4]. The versatility of this class of polymers comes from the living nature of the polymerization, allowing control over the length of the polymer with a narrow molar mass distribution and allowing the introduction of specific end-groups by initiation and termination [4]. Moreover, variation of the 2-substituent of the 2-oxazoline results in a variety of the amidic side chains of the poly(2-oxazoline)s [5,6], which strongly influences the properties of the resulting polymers: ranging from hydrophilic to hydrophobic; and from hard materials, with a high glass transition temperature via crystalline and chiral polymers [7], to soft materials, with a very low glass transition temperature [8,9].

The synthesis of star-shaped poly(2-oxazoline)s has been reported using a range of multifunctional electrophilic halide initiators, such as tetrakis(bromomethyl)ethylene, yielding 4-armed star-shaped polymers [10], as well as other multi-halide initiators based on, e.g., cyclotriphosphazine [11], silesquioxane [12], porphyrin [13,14] and bipyridine metal complex [15,16] cores. More recently, Jordan and coworkers reported the use of multi-triflate initiators for the preparation of well-defined star-shaped poly(2-methyl-2-oxazoline)s [17]. However, these multi-halide as well as multi-triflate initiators are not easily prepared and are not stable upon storage, in particular in the presence of air. Therefore, we recently reported a post-modification route for the synthesis of star-shaped poly(2-ethyl-2-oxazoline) by coupling of an acetylene-functionalized poly(2-ethyl-2-oxazoline) to a *heptakis*-azido functionalized *β*-cyclodextrin [18]. However, this method required chromatographic separation of the star-shaped polymer from the acetylene-precursor polymer.

To overcome the limitations of multi-halide, multi-triflate initiators and post-modification methods, we investigated the use of multi-tosylate initiators for the CROP of 2-oxazolines as depicted in Figure 1. The advantages of multi-tosylate initiators are their straightforward syntheses starting from commercially

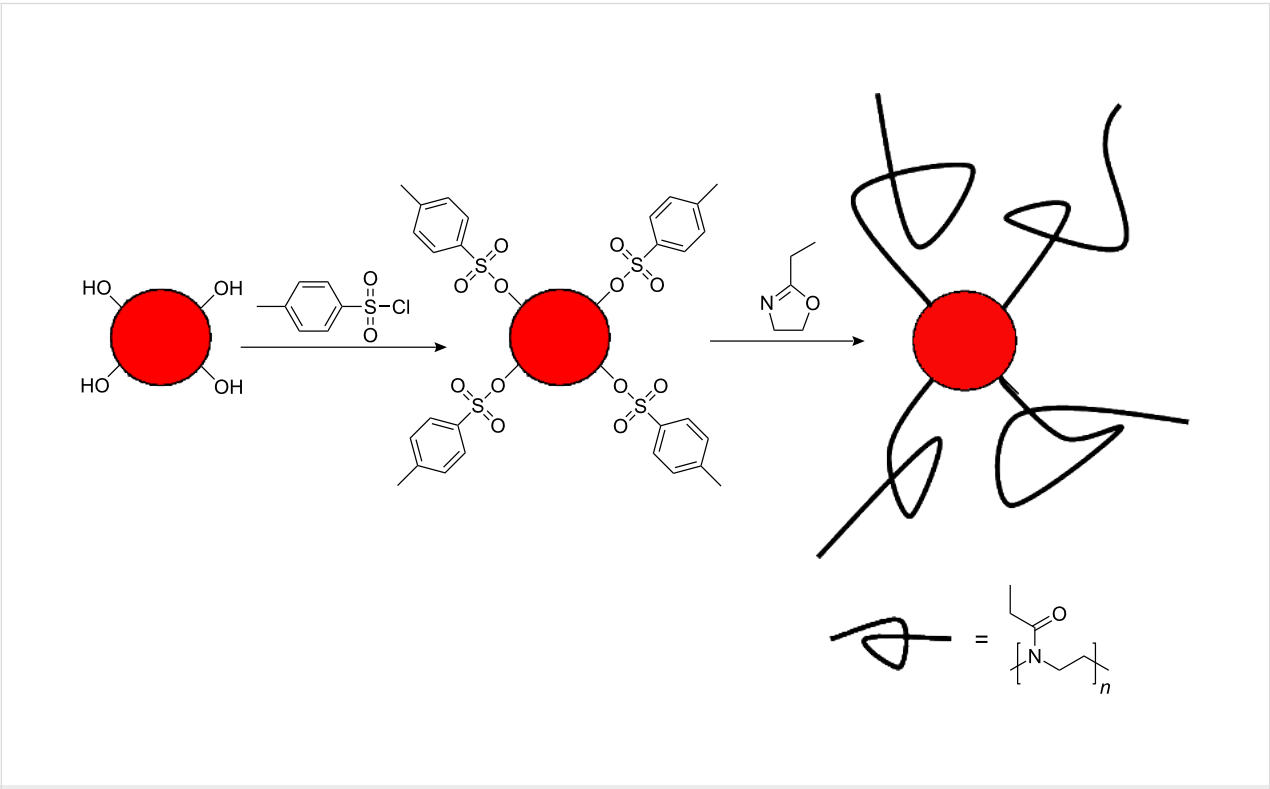


Figure 1: Schematic representation of the investigated strategy for the synthesis of star-shaped poly(2-ethyl-2-oxazoline)s based on multi-tosylate initiators.

available alcohols, their easy purification based on their high tendency to crystallize [19,20] and their stability under ambient conditions. In this contribution, we report the synthesis and crystal structures of various multi-tosylate initiators as well as their use for the initiation of the CROP of 2-ethyl-2-oxazoline for the formation of star-shaped poly(2-oxazoline)s.

Results and Discussion

Multi-tosylate preparation

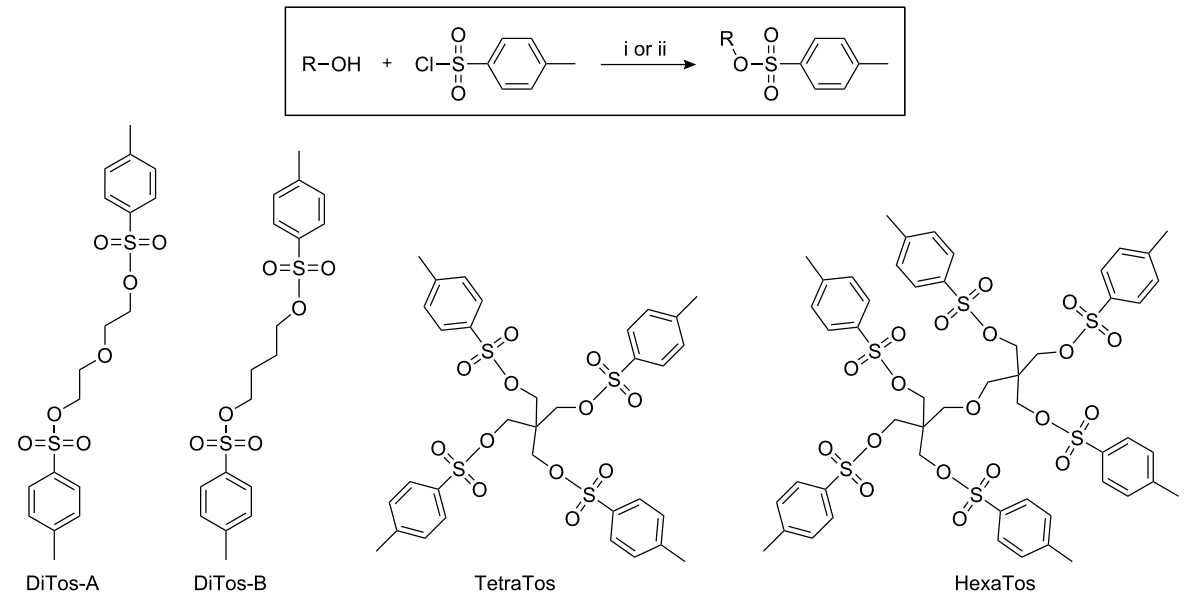
The preparation of tosylates from alcohols is a straightforward synthetic procedure using *p*-toluenesulfonic acid chloride (tosyl chloride) in the presence of a base. Commonly applied procedures are performed in dichloromethane using triethylamine as base or using pyridine both as solvent and base (Scheme 1, top). The synthesis of diethyleneglycol ditosylate (DiTos-A; Scheme 1) was not required since this compound is commercially available. Recrystallization of this compound from ethanol resulted in single crystals suitable for X-ray analysis. Butane ditosylate (DiTos-B; Scheme 1) was synthesized from 1,4-butanediol and an excess of tosyl chloride using dichloromethane as solvent and triethylamine as base. After 24 h stirring at ambient temperature, ethanolamine was added to this reaction mixture to react with the excess of tosyl chloride resulting in the water-soluble 1-hydroxy-2-ethyl tosylamide, which could be removed by washing with 3 N hydrochloric acid and brine. Final purification was performed by recrystallization from ethanol.

The synthesis of the tetra-tosylate (TetraTos; Scheme 1) and hexa-tosylate (HexaTos; Scheme 1) compounds was based on tosylation of pentaerythritol and dipentaerythritol, respectively, which are both insoluble in dichloromethane. Therefore, the solvent was changed to pyridine, which also acts as a base. After the reaction, the mixture was poured into acidified water resulting in the precipitation of the product that could be purified by recrystallization from a mixture of ethanol and acetone.

Besides the common characterization techniques to prove the purity of the compounds, i.e. ^{1}H and ^{13}C NMR spectroscopy and elemental analysis, the chemical structures of the TetraTos and HexaTos were verified by MALDI-TOF MS, revealing only the desired mass peak corresponding to full tosylation (Figure 2). The absence of residual hydroxyl groups is of major importance for the use of these multi-tosylates as initiators for the CROP of 2-oxazolines since they lead to side reactions with the cationic oxazolinium propagating species.

Multi-tosylate crystal structures

Recrystallization of the prepared multi-tosylates from ethanol or ethanol–acetone mixtures directly gave single crystals suitable for X-ray analysis as we previously also observed for a tosylate adduct of *2,2':6',2''*-terpyridine [20]. The obtained molecular structures and the packing diagrams for DiTos-A, DiTos-B, TetraTos and HexaTos are displayed in Figures 3–6, respectively. The crystallographic data, selected bond lengths



Scheme 1: General reaction scheme for the preparation of multi-tosylates from multifunctional alcohols (top) and schematic representation of the structures of the investigated multi-tosylates (bottom). i: triethylamine in dichloromethane; ii: pyridine.

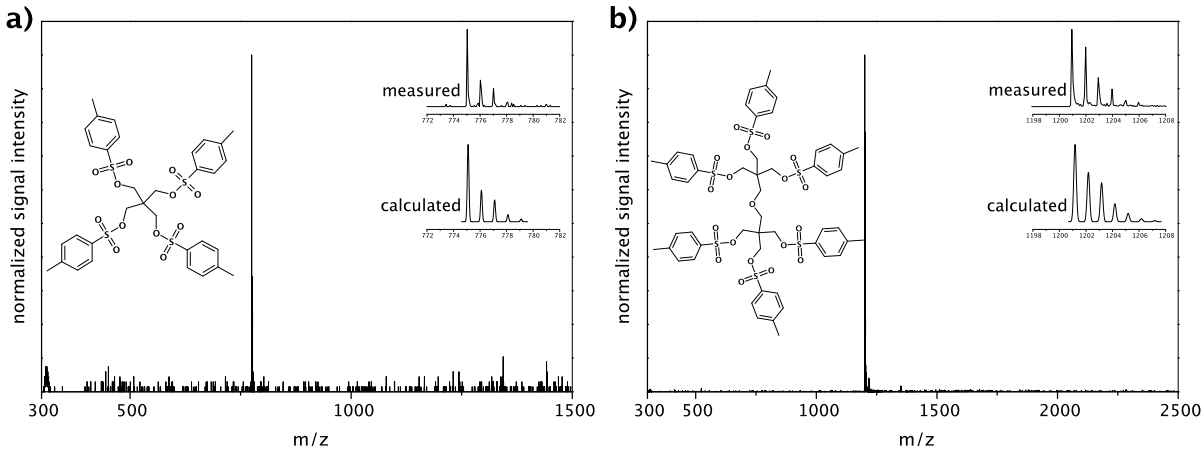


Figure 2: MALDI-TOF MS spectra of TetraTos a) and HexaTos b) Matrix: dithranol.

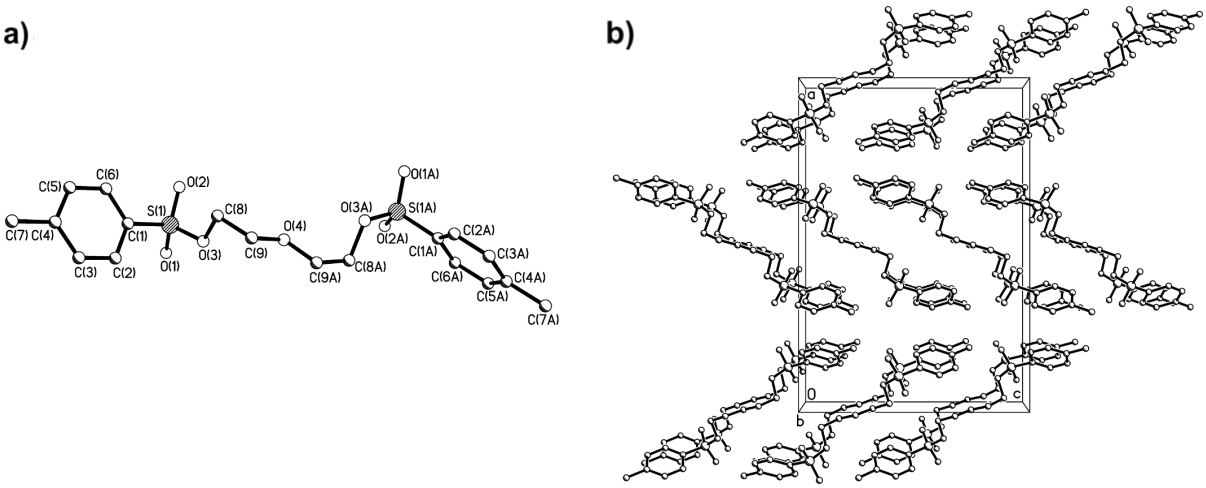


Figure 3: Molecular structure a) and packing diagram b) of the structure of diethyleneglyclol ditosylate (DiTos-A).

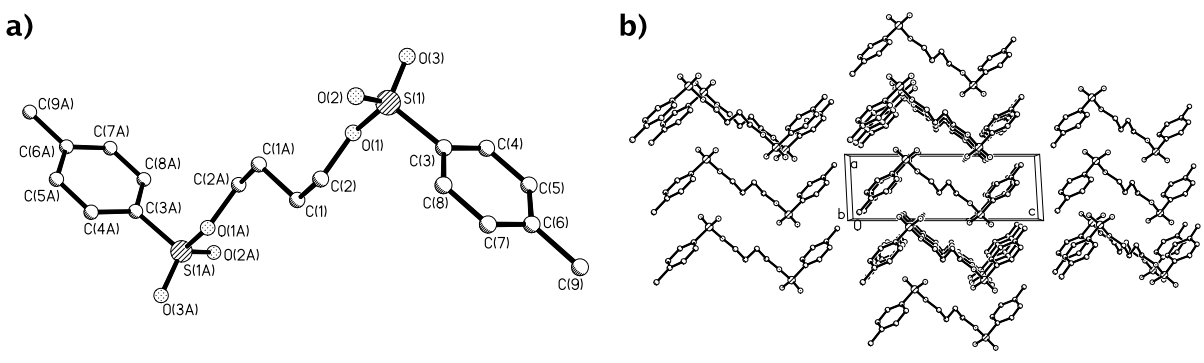


Figure 4: Molecular structure a) and packing diagram b) of the structure of 1,4-butanediol ditosylate (DiTos-B).

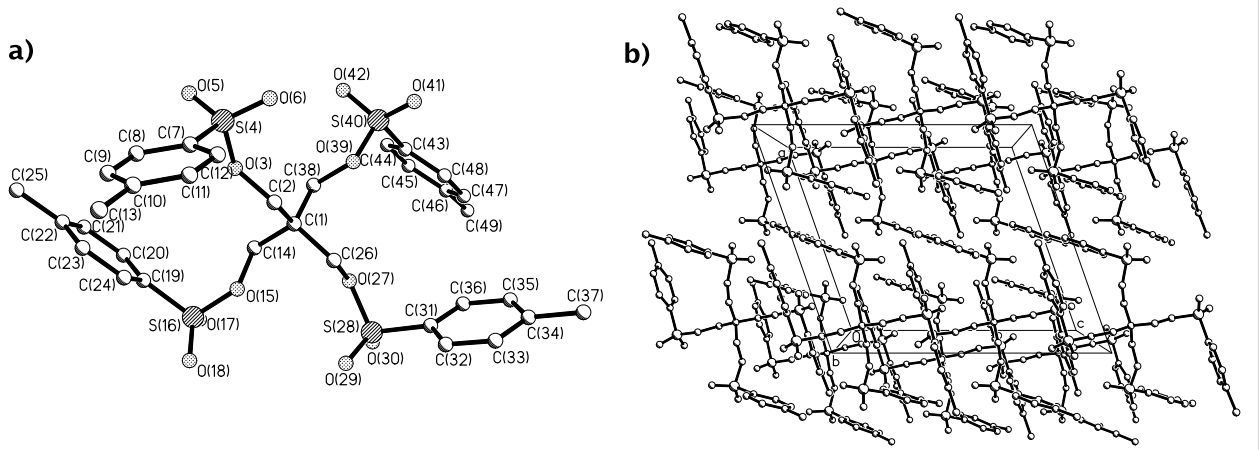


Figure 5: Molecular structure a) and packing diagram b) of the structure of penthaerythritol tetra-tosylate (TetraTos).

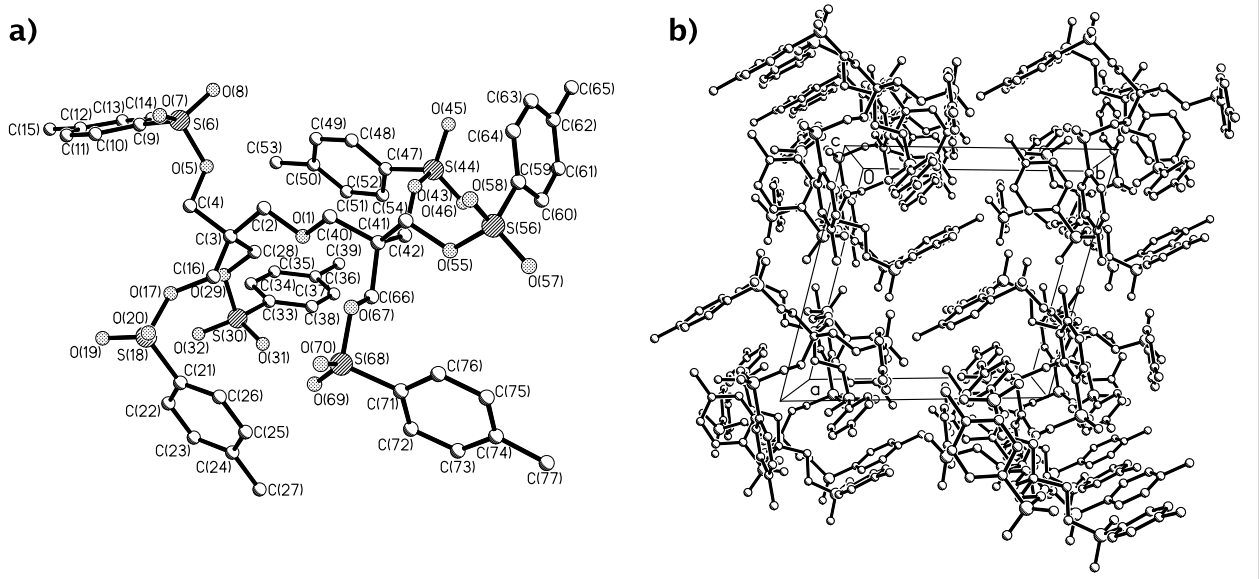


Figure 6: Molecular structure a) and packing diagram b) of the structure of dipenthaerythritol tetra-tosylate (HexaTos).

and angles for the crystal structures can be found in the supporting information. All structures show the expected bond length and angles. The packing diagrams reveal space filling packing without any π-stacking between the molecules.

Polymerizations

Since the goal of this research was the development of multi-tosylate initiators for the preparation of well-defined star-shaped poly(2-oxazoline)s, TetraTos and HexaTos were utilized for the CROP of 2-ethyl-2-oxazoline under microwave irradiation. Using the optimal polymerization conditions that were previously determined for 2-ethyl-2-oxazoline with methyl tosylate as initiator, i.e. 4 M monomer concentration in acetonitrile, at 140 °C and 10 min for a monomer to initiator ratio of 60 [21,22]; no polymerization was observed at all when using TetraTos or HexaTos as initiators. By contrast, when the polymerization with TetraTos was performed at a further elevated temperature of 200 °C, the formation of polymer was observed by SEC (Figure 7a). However, the resulting polymer had a broad molar mass distribution with tailing at the low molar mass side. In addition, residual tosylate initiator was still observed after heating to 200 °C for 10 min. These results clearly demonstrate that initiation with TetraTos is very slow, which has also been observed for the polymerization with, e.g. 1-butyne tosylate, due to the decreased electrophilicity of the initiator when compared to methyl tosylate [18]. However, the

rate of initiation is further decreased for TetraTos compared to 1-butyne tosylate, which is most likely due to steric hindrance in TetraTos resulting in a decreased accessibility of the initiating groups. Similar disappointing polymerization results were obtained with HexaTos as initiator as depicted in Figure 7b. In fact, even less of the HexaTos was consumed after 10 min heating to 200 °C at 4 M monomer concentration as a result of the further increased steric hindrance. Variation of temperature or concentration did not improve the polymerization results. Therefore, it can be concluded that these pentaerythritol based multi-tosylate initiators are not suitable for the CROP of 2-oxazolines, which is in sharp contrast with the rather similar pluritriflate initiators reported by Jordan [17]. This difference is most likely related to both the smaller size and the higher reactivity of the triflate groups compared to the tosylates.

To circumvent the poor initiation efficiency with the multi-tosylate pentaerythritol derivatives, a tetra-tosylated porphyrin (TetraTos-B) was designed in which the rigid porphyrin keeps the tosylate groups far apart. Scheme 2 depicts the schematic path that was followed to synthesize TetraTos-B, and subsequently, the four-armed star pEtOx. *Tetrakis*(hydroxyphenyl)porphyrin (porphyrin) was used to synthesize the rigid star-shaped TetraTos-B initiator by reaction with a 20-fold excess of 1,4-butane ditosylate (DiTos-B), followed by chromatographic purification. This is not a straightforward synthesis compared to the previously discussed multi-tosylates, partly counteracting the advantages of multi-tosylate initiators compared to multi-halides and multi-triflates. Figure 8 depicts the MALDI-TOF MS spectrum of the porphyrin initiator TetraTos-B. The formation of TetraTos-B (mass 1582) and a minor fraction, with only three tosylate groups and one methoxybutoxy group (mass 1446), next to the utilized matrix dithranol (mass 226), are clearly evident in the spectrum (Figure 8). This latter methoxylated side chain might have been present in the DiTOs-B. Importantly, no hydroxyl groups remained that might cause side reactions during the polymerizations.

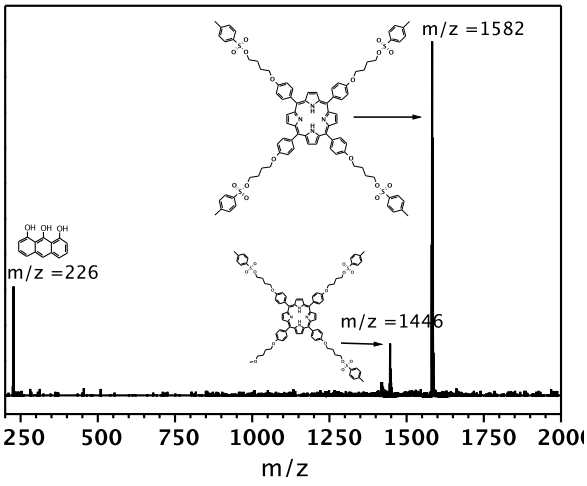


Figure 8: MALDI-TOF MS spectrum of the tetra-tosylate-porphyrin (TetraTos-B). Matrix: dithranol.

Subsequently, this tetrafunctional initiator was applied for the microwave-assisted cationic ring-opening polymerization of EtOx. The polymerization of EtOx with TetraTos-B as initiator was performed with 2 M monomer concentration in CH_3CN at 140 °C under microwave irradiation with a [M]/[I] ratio of 200, corresponding to 50 monomer units per tosylate group. After

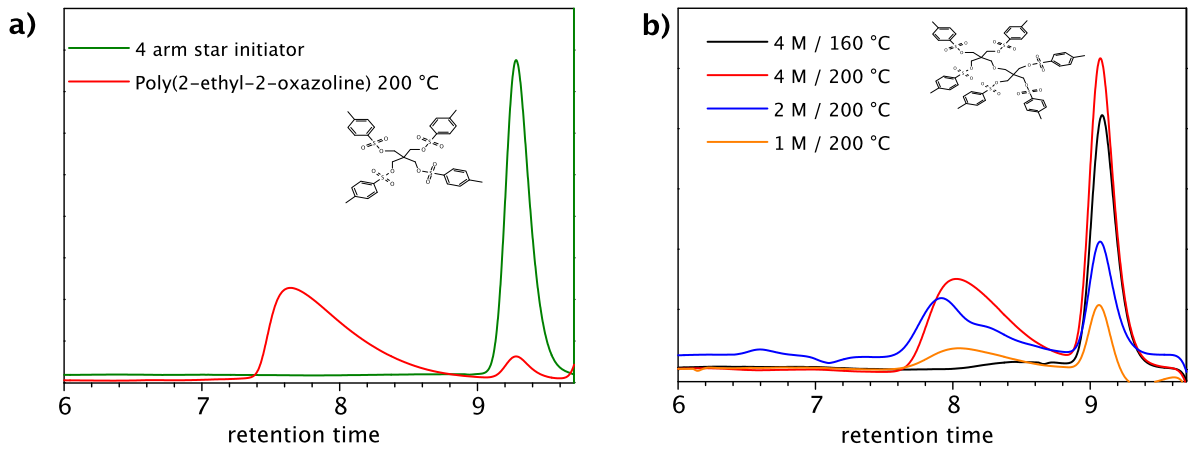
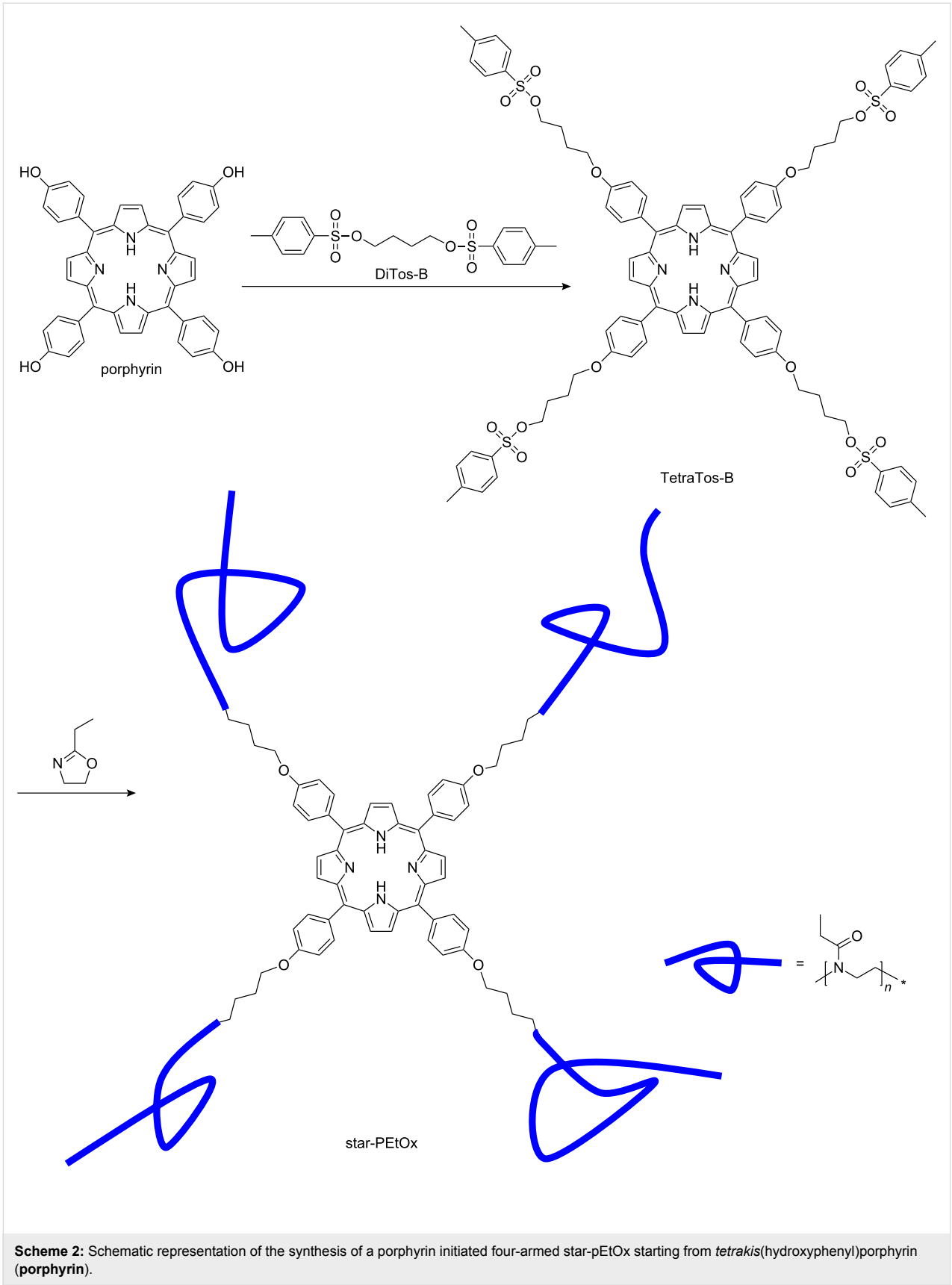


Figure 7: SEC traces obtained for the polymerization of 2-ethyl-2-oxazoline initiated with TetraTos a) and HexaTos b). The large signals at 9 to 9.5 min retention time correspond to the multi-tosylate initiators.



Scheme 2: Schematic representation of the synthesis of a porphyrin initiated four-armed star-pEtOx starting from *tetrakis*(hydroxyphenyl)porphyrin (**porphyrin**).

20 min polymerization time, the formation of the polymer was observed and the initiator was completely consumed, which is in clear contrast with TetraTos-A, indicating that indeed decreasing the steric hindrance significantly improves the initiation efficiency of the polymerization. The resulting porphyrin centered star-shaped poly(2-ethyl-2-oxazoline) star-PEtOx was purified by preparative SEC to remove unreacted monomer since precipitation was unsuccessful due to the small scale of the polymerization. Figure 9a depicts the ^{1}H NMR spectra of the tosylate-porphyrin TetraTos-B (bottom) and the star-PEtOx (top). The porphyrin signals are still present in the star-PEtOx spectrum, indicating that indeed a four-armed pEtOx with a porphyrin core was synthesized. Integration of both the polymer backbone signals (l and m) and the porphyrin signals (a and b) revealed that 188 EtOx units were incorporated into the polymer, corresponding to 47 monomers per arm, which is close to the theoretical number of 50.

SEC characterization of the TetraTos-B resulted in a negative signal in the RI-detector, indicating that the porphyrin has a lower RI than the eluent, and a positive signal in the UV-detector at 500 nm, where the porphyrin has a strong UV-absorption (Figure 9b). The M_n was calculated to be 1,580 g/mol with a polydispersity index (PDI) of 1.06 (against polystyrene standards). This PDI value results from diffusion of the organic compound in the column since it is almost monodisperse (see MALDI in Figure 8). The star-PEtOx could not be characterized with the RI-detector due to the combination of a positive signal of the polymer and a negative signal of the porphyrin. However, detection with the UV-detector at 500 nm revealed a relatively narrow molar mass distribution (Figure 9b), proving that the porphyrin is incorporated into the polymer. The SEC analysis with the UV-detector yielded a M_n of 10,700 g/mol and a PDI of 1.18 based on linear poly(ethylene glycol) standards. The M_n is lower than the theoretical molar mass (~21,000 g/mol) due to calibration with linear standards with a different molecular structure. The hydrodynamic volume, that determines the retention time, will be very different for a star-shaped polymer when compared to a linear polymer. Nonetheless, the narrow molar mass distribution indicates that the star-PEtOx was synthesized in a controlled manner. Critical examination of the SEC trace does show a slight shoulder at shorter retention times, indicating the occurrence of minor side reaction leading to star-star coupling. In addition, the specific porphyrin absorption spectrum could be detected in the entire molar mass distribution using SEC with a photodiode-array detector, indicating that the porphyrin is indeed incorporated in all polymer chains (Figure 10).

Conclusion

The synthesis of various multi-tosylates was successfully performed by esterification of the corresponding alcohols with tosyl chloride. The tosylation of (di)pentaerythritols was only successful using pyridine as solvent due to the limited solubility of the respective educts in dichloromethane. Recrystallization of these tosylate compounds yielded single crystals, and the X-ray crystal structures of di-, tetra- and hexa-tosylates were centrosymmetric with ideal space filling packing. The use of tetra- and hexa-tosylates, based on (di)pentaerythritol as initiators for the living cationic ring-opening polymerization (CROP) of 2-ethyl-2-oxazoline, resulted in very slow initiation and ill-defined polymers, which is most likely due to the steric

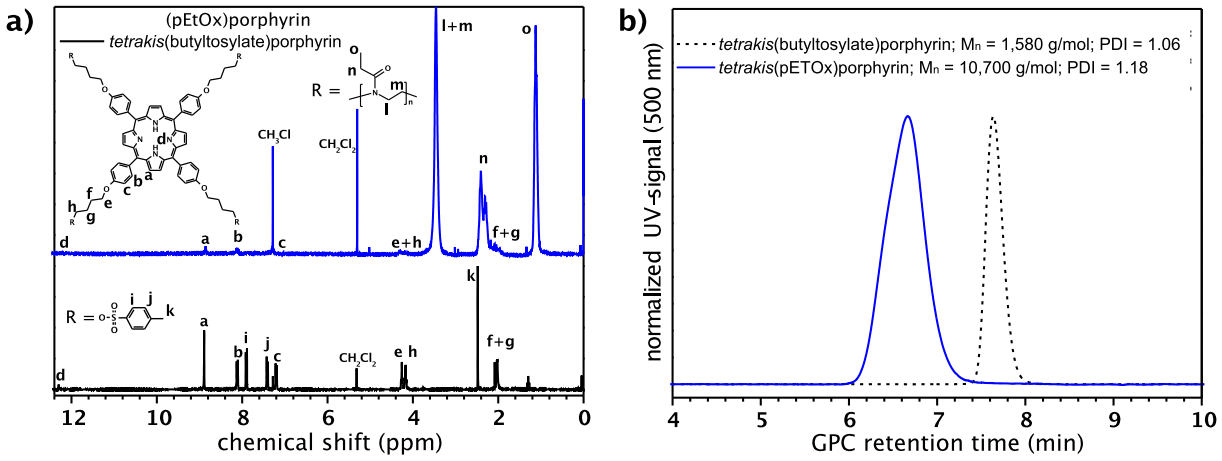


Figure 9: a) ^{1}H NMR spectra (in $CDCl_3$) of the porphyrin initiator TetraTos-B (bottom) and star-pEtOx (top). b) SEC traces of TetraTos-B and star-PEtOx (in $CHCl_3$:NEt_3:2-PrOH; UV-detector at 500 nm).

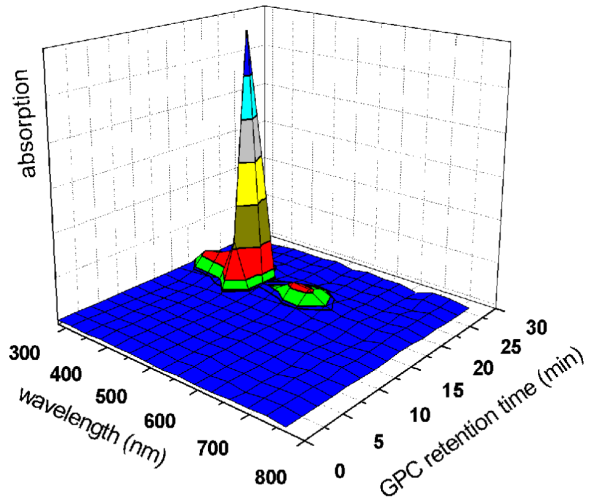


Figure 10: SEC spectrum obtained for star-pEtOx utilizing a photodiode-array detector (eluent: DMF containing 5 mM NH_4PF_6).

hindrance of the multiple tosylate groups in these initiators. Therefore, a porphyrin-cored tetra-tosylate initiator with significantly reduced steric hindrance was successfully prepared by reaction of 1,4-butane-ditosylate with 5,10,15,20-*tetrakis*(4-hydroxyphenyl)porphyrin. Utilization of this star-shaped initiator yielded a well-defined star-shaped poly(2-ethyl-2-oxazoline) by CROP.

Experimental

Materials

Solvents were purchased from Biosolve Ltd. Acetonitrile (size 3 Å) was dried over molecular sieves. CH_2Cl_2 was distilled over potassium. All other solvents were used without further purification. EtOx (Aldrich) was distilled over barium oxide (BaO) and stored under argon. Methyl tosylate (Aldrich) was distilled over P_2O_5 and stored under argon. Diethyleneglycol ditosylate (DiTos-A; Aldrich) was recrystallized from ethanol and 5,10,15,20-*tetrakis*(4-hydroxyphenyl)porphyrin (porphyrin; Aldrich) was used without further purification.

Instrumentation

Polymerizations were carried out in an Emrys Liberator (Biotage, formerly PersonalChemistry) with capped reaction vials. All microwave polymerizations were performed with temperature control (IR sensor).

NMR spectra were recorded on a Varian AM-400 spectrometer or on a Varian Gemini 300 spectrometer. Chemical shifts are given in ppm relative to TMS or residual solvent signals.

Size exclusion chromatography (SEC) was measured on a Shimadzu system with a SCL-10A system controller, a LC-10AD pump, a RID-6A refractive index detector, a SPD-10A UV detector and a PLgel 5 µm Mixed-D column with chloroform: triethylamine:2-propanol (94:4:2) as eluent and the column oven set to 50 °C (polystyrene calibration). SEC with photodiode-array detector was measured on a Waters system with a 1515 pump, a 2414 refractive index detector and a Waters Styragel HT4 column utilizing DMF containing 5 mM NH_4PF_6 at a flow rate of 0.5 mL/min as eluent and the column oven set to 50 °C (PEG calibration).

MALDI-TOF-MS was performed on a Voyager-DE™ PRO Biospectrometry™ Workstation (Applied Biosystems) time-of-flight mass spectrometer using the linear mode for operation (positive ion mode; ionization with a 337 nm pulsed nitrogen laser). Elemental analyses were performed on a EuroEA3000 Series EuroVector Elemental Analyzer for CHNS-O.

X-ray crystal structures were measured by mounting selected crystals on a Bruker-AXS APEX diffractometer with a CCD area detector. Graphite-monochromated Mo-K_α radiation (71.073 pm) was used for the measurements. The nominal crystal-to-detector distance was 5.00 cm. A hemisphere of data was collected by a combination of three sets of exposures at 292 K. Each set had a different Φ angle for the crystal, and each exposure took 20 s and in steps of 0.3° in ω. The data were corrected for polarization and Lorentz effects, and an empirical absorption correction (SADABS) was applied [23]. The cell dimensions were refined with all unique reflections. The structures were solved by direct methods (SHELXS97). Refinement was carried out with the full-matrix least-squares method based on F^2 (SHELXL97) [24] with anisotropic thermal parameters for all non-hydrogen atoms. Hydrogen atoms were inserted in calculated positions and refined riding with the corresponding atom.

Synthesis of 1,4-butanediol ditosylate (DiTos-B)

To a solution of 1,4-butanediol (4.5 g, 50 mmol) and triethylamine (6.07 g, 60 mmol) in dry CH_2Cl_2 (100 mL), a solution of tosyl chloride (23.8 g, 125 mmol) in CH_2Cl_2 (100 mL) was added dropwise over 75 min. The resulting solution was stirred for 24 h under argon and subsequently, ethanolamine (6 mL) was added to react with excess tosyl chloride. The resulting mixture was poured into water (200 mL). The aqueous layer was extracted with CH_2Cl_2, and the combined organic layers were washed successively with 3 N HCl (2 × 100 mL) and brine (150 mL). After drying with $MgSO_4$ and filtration, the solvent was evaporated under reduced pressure. Recrystallization of the product from ethanol yielded the desired 1,4-butanediol ditosylate as white platelets in 58% yield (11,5 g, 28,9 mmol).

^{1}H NMR ($CDCl_3$): δ 7.74 (d, 8.3 Hz, 4H, *o*-CH), 7.33 (d, 8.3 Hz, 4H, *m*-CH), 3.97 (t, 5.5 Hz, 4H, OCH_2), 2.43 (s, 6H, CH_3), 1.68 (t, 5.5 Hz, 4H, $OCH_2C\underline{H}_2$). ^{13}C NMR ($CDCl_3$): δ 144.8 ($\underline{C}CH_3$), 132.7 (CS), 129.8 (*m*-C), 127.7 (*o*-C), 69.2 (OCH_2), 24.9 ($OCH_2\underline{C}H_2$), 21.5 ($C\underline{C}H_3$).

Synthesis of pentaerythritol tetra-tosylate (TetraTos)

Pentaerythritol (1.36 g; 10 mmol) and pyridine (20 mL) were weighed into a round-bottom flask and cooled to 0 °C. Subsequently, solid tosyl chloride (9.5 g; 50 mmol) was added portionwise ensuring that the temperature remained below 5 °C. The resulting solution was stirred overnight, during which time it was allowed to warm slowly to ambient temperature. The formed white-pinkish slurry was poured into 125 mL of a 6M HCl solution yielding a white precipitate that was collected by filtration. This solid was washed with water (2 × 100 mL). Further purification was performed by recrystallization from a mixture of ethanol (100 mL) and acetone (100 mL) yielding 4.7 g (62%) of the desired product as white crystals. Partial evaporation of the acetone (~75 mL) from the filtrate yielded another 1.6 g (22%) of crystals, resulting in a total isolated yield of 84%.

^{1}H NMR ($CDCl_3$): δ 7.68 (d, 8.2 Hz, 8H, *o*-CH_{tos}), 7.36 (d, 8.2 Hz, 8H, *m*-CH_{tos}), 3.82 (s, 8H, $SOCH_2$), 2.47 (s, 12H, CH_3). ^{13}C NMR ($CDCl_3$): δ 145.3, 131.0, 129.8, 127.6, 65.2, 42.9, 21.4. $C_{33}H_{36}O_{12}S_4$: calcd. C 52.65, H 4.82, S 17.03; found C 52.87, H 4.89, S 17.21.

Synthesis of dipentaerythritol hexa-tosylate (HexaTos)

This compound was prepared in a similar manner as TetraTos using the following amounts: dipentaerythritol (2.5 g; 10 mmol), pyridine (20 mL) and tosyl chloride (14.3 g; 75 mmol). Recrystallization of the crude product from ethanol yielded the desired product as white crystals (~8 g; 68%).

^{1}H NMR ($CDCl_3$): δ 7.66 (d, 8.2 Hz, 12H, *o*-CH_{tos}), 7.35 (d, 8.2 Hz, 12H, *m*-CH_{tos}), 3.77 (s, 12H, $SOCH_2$), 3.14 (s, 4H, OCH_2) 2.44 (s, 18H, CH_3). ^{13}C NMR ($CDCl_3$): δ 145.4, 131.7, 130.0, 127.8, 67.8, 66.5, 43.6, 21.5. $C_{52}H_{58}O_{19}S_6$: calcd. C 52.96, H 4.96, S 16.31; found C 53.30, H 5.10, S 15.97.

Synthesis of 5,10,15,20-tetrakis(4-hydroxybutyloxy tosylate)-21H,23H-porphyrin (TetraTos-B)

A mixture of 5,10,15,20-*tetrakis* (4-hydroxyphenyl)porphyrin 1 (170 mg, 0.25 mmol), 1,4-butanediol ditosylate 2 (2 g, 5 mmol) and potassium carbonate (190 mg, 1,37 mmol) in dry CH_3CN was refluxed for 75 h. After this period, the solvent was evaporated under reduced pressure and the residue was redissolved in $CHCl_3$. This solution was washed successively with water (100 mL), saturated sodium hydrogen carbonate solution (100 mL) and brine (100 mL). After drying with $MgSO_4$ and filtration, the solvent was removed under reduced pressure. The resulting solid was purified by column chromatography (SiO_2 with CH_2Cl_2) and preparative size exclusion chromatography (biobeads SX-1 in CH_2Cl_2) resulting in the title compound 3 (38 mg, 0.024 mmol, 10% yield).

^{1}H NMR ($CDCl_3$): δ 12.3 (s, 2H, NH), 8.89 (s, 8H, CH_{por}), 8.20 (d, 8.5 Hz, 8H, OCCHC$\underline{H}$), 7.90 (d, 8.2 Hz, 8H, *o*-CH_{tos}), 7.42 (d, 8.2 Hz, 8H, *m*-CH_{tos}), 7.21 (d, 8.5 Hz, 8H, OCC$\underline{H}$), 4.26 (t, 5.6 Hz, 8H, $COCH_2$), 4.15 (t, 7.2 Hz, 8H, $SOCH_2$), 2.48 (s, 12H, CH_3), 2.03 (m, 16H, $OCH_2C\underline{H}_2C\underline{H}_2$). ^{13}C NMR ($CDCl_3$): δ 158.3, 144.5, 135.3, 134.4, 132.9, 129.6, 127.7, 119.4, 112.3, 70.0, 66.8, 25.6, 25.2, 21.3. $C_{88}H_{86}N_4O_{16}S_4$: calcd. C 66.73, H 5.47, N 3.54, S 8.10; found C 66.22, H 5.38, N 3.67, S 7.74. GPC ($CHCl_3$:NEt_3:2-PrOH = 94:4:2; UV detector at 500 nm): M_n = 1,580 g/mol; PDI = 1.06. MALDI-TOF-MS: *m/z* [M^+] 1582, [M^+-tosyl] 1446.

General polymerization procedure

The polymerizations of 2-ethyl-2-oxazoline with TetraTos and HexaTos as initiators were performed under microwave irradiation. Before use, the microwave vials were heated to 105 °C, allowed to cool to ambient temperature and filled with argon prior to use. Subsequently, the initiator, monomer and acetonitrile were weighed in so that a 1.0 mL polymerization mixture was obtained in which the ratio of monomer per tosylate group is 25 and the desired monomer concentration is 1, 2 or 4 M. This polymerization mixture was heated by microwaves to the desired temperature for a fixed time (5 min at 140 °C; 2 min at 160 °C; 30 seconds or 10 min at 200 °C). After heating, the polymerization mixtures were investigated by size exclusion chromatography.

Microwave synthesis of 5,10,15,20-tetrakis(pEtOx)-21H,23H-porphyrin (star-PEtOx)

A mixture of porphyrin tosylate 3 (7.92 mg, 0.005 mmol) and EtOx (100 mg, 1 mmol) in CH_3CN (0.4 mL) was heated to 140 °C for 20 min under microwave irradiation. After heating, the solvent and residual monomer were evaporated under vacuum and the resulting residue was purified by preparative size exclusion chromatography (biobeads SX-1 with CH_2Cl_2), resulting in 60 mg of polymer 4 (56% yield).

^{1}H NMR ($CDCl_3$): δ 12.23 (s, 2H, NH), 8.85 (br, 8H, CH_{por}), 8.10 (br, 8H, 8H, OCCHC$\underline{H}$), 7.23 (br, 8H, OCC$\underline{H}$), 4.35–4.17 (br, 16H, $COCH_2$ + $SOCH_2$), 3.75–3.20 (br, 752H, NCH_2), 2.57–2.05 (br, 395H, $COCH_2$ + $OCH_2C\underline{H}_2C\underline{H}_2$), 1.11–1.09 (br, 574H, CH_3). GPC ($CHCl_3$:NEt_3:2-PrOH = 94:4:2; UV detector at 500 nm): M_n = 10,700 g/mol; PDI = 1.18.

Supporting Information

Supporting Information File 1

Details of the reported crystal structures.
[http://www.beilstein-journals.org/bjoc/content/supplementary/1860-5397-6-96-S1.pdf]

Acknowledgements

RH (Veni-grant) and USS (Vici award) are grateful to the Netherlands Scientific Organisation (NWO) for financial support.

References

1. Mishra, M.; Kobayashi, S. *Star and Hyperbranched Polymers;* Marcel Dekker Inc.: New York, 1999.
2. Inoue, K. *Prog. Polym. Sci.* **2000,** *25,* 453–571. doi:10.1016/S0079-6700(00)00011-3
3. Kobayashi, S. *Prog. Polym. Sci.* **1990,** *15,* 751–823. doi:10.1016/0079-6700(90)90011-O
4. Aoi, K.; Okada, M. *Prog. Polym. Sci.* **1996,** *21,* 151–208. doi:10.1016/0079-6700(95)00020-8
5. Hoogenboom, R. *Macromol. Chem. Phys.* **2007,** *208,* 18–25. doi:10.1002/macp.200600558
6. Hoogenboom, R. *Angew. Chem., Int. Ed.* **2009,** *48,* 7978–7994. doi:10.1002/anie.200901607
7. Bloksma, M. M.; Hendrix, M. M. R. M.; Schubert, U. S.; Hoogenboom, R. *Macromolecules* **2010,** *43,* 4654–4659. doi:10.1021/ma100128q
8. Kranenburg, J. M.; Tweedie, C. A.; Hoogenboom, R.; Wiesbrock, F.; Thijs, H. M. L.; Hendriks, C. E.; Van Vliet, K. J.; Schubert, U. S. *J. Mater. Chem.* **2007,** *17,* 2713–2721. doi:10.1039/b701945a
9. Kempe, K.; Jacobs, S.; Lambermont-Thijs, H. M. L.; Fijten, M. W. M.; Hoogenboom, R.; Schubert, U. S. *Macromolecules* **2010,** *43,* 4098–4104. doi:10.1021/ma9028536
10. Kobayashi, S.; Uyama, H.; Narita, Y. *Macromolecules* **1992,** *25,* 3232–3236. doi:10.1021/ma00038a031
11. Chang, J. Y.; Ji, H. J.; Han, M. J.; Rhee, S. B.; Cheong, S.; Yoon, M. *Macromolecules* **1994,** *27,* 1376–1380. doi:10.1021/ma00084a015
12. Kim, K. M.; Ouchi, Y.; Chujo, Y. *Polym. Bull.* **2003,** *49,* 341–348. doi:10.1007/s00289-002-0113-0
13. Jin, R.-H. *J. Mater. Chem.* **2004,** *14,* 320–327. doi:10.1039/b307439k
14. Jin, R.-H. *Adv. Mater.* **2002,** *14,* 889–892. doi:10.1002/1521-4095(20020618)14:12<889::AID-ADMA889>3.0.CO;2-6
15. Schubert, U. S.; Nuyken, O.; Hochwimmer, G. *J. Macromol. Sci., Part A: Pure Appl. Chem.* **2000,** *A37,* 645–658.
16. McAlvin, J. E.; Scott, S. B.; Fraser, C. L. *Macromolecules* **2000,** *33,* 6953–6964. doi:10.1021/ma000024q
17. Luxenhofer, R.; Bezen, M.; Jordan, R. *Macromol. Rapid Commun.* **2008,** *29,* 1509–1513. doi:10.1002/marc.200800293
18. Fijten, M. W. M.; Haensch, C.; Van Lankvelt, B. M.; Hoogenboom, R.; Schubert, U. S. *Macromol. Chem. Phys.* **2008,** *209,* 1887–1895. doi:10.1002/macp.200800226
19. Hoogenboom, R.; Fijten, M. W. M.; Paulus, R. M.; Thijs, H. M. L.; Hoeppener, S.; Kickelbick, G.; Schubert, U. S. *Polymer* **2006,** *47,* 75–84. doi:10.1016/j.polymer.2005.11.025
20. Hoogenboom, R.; Nakahashi, A.; Kickelbick, G.; Chujo, Y.; Schubert, U. S. *Acta Crystallogr., Sect. E* **2007,** *63,* o2311–o2313. doi:10.1107/S1600536807017229
21. Wiesbrock, F.; Hoogenboom, R.; Abeln, C. H.; Schubert, U. S. *Macromol. Rapid Commun.* **2004,** *25,* 1895–1899. doi:10.1002/marc.200400369
22. Wiesbrock, F.; Hoogenboom, R.; Leenen, M. A. M.; Meier, M. A. R.; Schubert, U. S. *Macromolecules* **2005,** *38,* 5025–5034. doi:10.1021/ma0474170
23. Blessing, R. H. *Acta Crystallogr., Sect. A* **1995,** *51,* 33–38. doi:10.1107/S0108767394005726
24. *SHELX97 Programs for Crystal Structure Analysis,* Release 97-2; Universität Göttingen: Göttingen, Germany, 1998.

License and Terms

This is an Open Access article under the terms of the Creative Commons Attribution License (http://creativecommons.org/licenses/by/2.0), which permits unrestricted use, distribution, and reproduction in any medium, provided the original work is properly cited.

The license is subject to the *Beilstein Journal of Organic Chemistry* terms and conditions: (http://www.beilstein-journals.org/bjoc)

The definitive version of this article is the electronic one which can be found at:
doi:10.3762/bjoc.6.96

Beilstein Journal of Organic Chemistry

Calix[4]arene-click-cyclodextrin and supramolecular structures with watersoluble NIPAAM-copolymers bearing adamantyl units: *"Rings on ring on chain"*

Bernd Garska, Monir Tabatabai and Helmut Ritter*

Full Research Paper

Open Access

Address:
Institut für Organische Chemie und Makromolekulare Chemie, Heinrich-Heine-Universität Düsseldorf, Universitätsstraße 1, 40225 Düsseldorf, Germany

Email:
Bernd Garska - bernd.garska@uni-duesseldorf.de; Monir Tabatabai - tabatabai@uni-duesseldorf.de; Helmut Ritter* - h.ritter@uni-duesseldorf.de

* Corresponding author

Keywords:
β-cyclodextrin; calix[4]arene; click chemistry; poly(NIPAAM)

Beilstein J. Org. Chem. **2010,** *6,* 784–788.
doi:10.3762/bjoc.6.83

Received: 16 June 2010
Accepted: 08 July 2010
Published: 05 August 2010

Guest Editor: H. Ritter

© 2010 Garska et al; licensee Beilstein-Institut.
License and terms: see end of document.

Abstract

We describe the calixarene-cyclodextrin-coupling via click reaction starting from 5,11,17,23-tetra-*tert*-butyl-25,27-dipropargyl-ether-26,28-hydroxy-calix[4]arene (calix[4]arene-dipropargylether) (**2**) onto 6I-azido-6I-deoxycyclomaltoheptaose (**3**) under microwave assisted conditions. The coupling was proven by MALDI-TOF mass spectrometry, ^{1}H NMR and IR-spectroscopy. The pH dependent supramolecular complex formation with poly(NIPAAM) bearing attached adamantyl units was investigated by dynamic light scattering (DLS) and turbidity measurements.

Introduction

Supramolecular interactions of macrocycles with different types of guest molecules are of increasing practical and theoretical interest [1-3]. In this context, we recently coupled cyclodextrin (CD) with cucubituril via a click reaction and investigated the special interactions with some suitable copolymers [4]. Because of their capability to form host–guest superstructures, CDs and calixarenes turned out to be very attractive not only as molecular receptors but also as building blocks for the construction of supramolecular architectures [5]. For that reason, we were encouraged to couple these two different types of macrocycles via click type reactions. Recent progress in the field of supramolecular chemistry is based on click chemistry, a versatile and powerful tool that permits the modular assembly of new molecular entities [6,7]. Both CDs as well as calixarenes have already been modified by click chemistry [8-14]. However, the coupling of calixarenes and β-CD via click reaction and their application in the field of supramolecular chemistry has not yet been reported. Herein, we describe the synthesis and complexa-

tion behavior of a dual type calix[4]arene-click-cyclodextrin (**4**) receptor by the cycloaddition of a dipropargylether of calix[4]arene (**2**) onto 6I-azido-β-CD (**3**) under microwave assisted conditions.

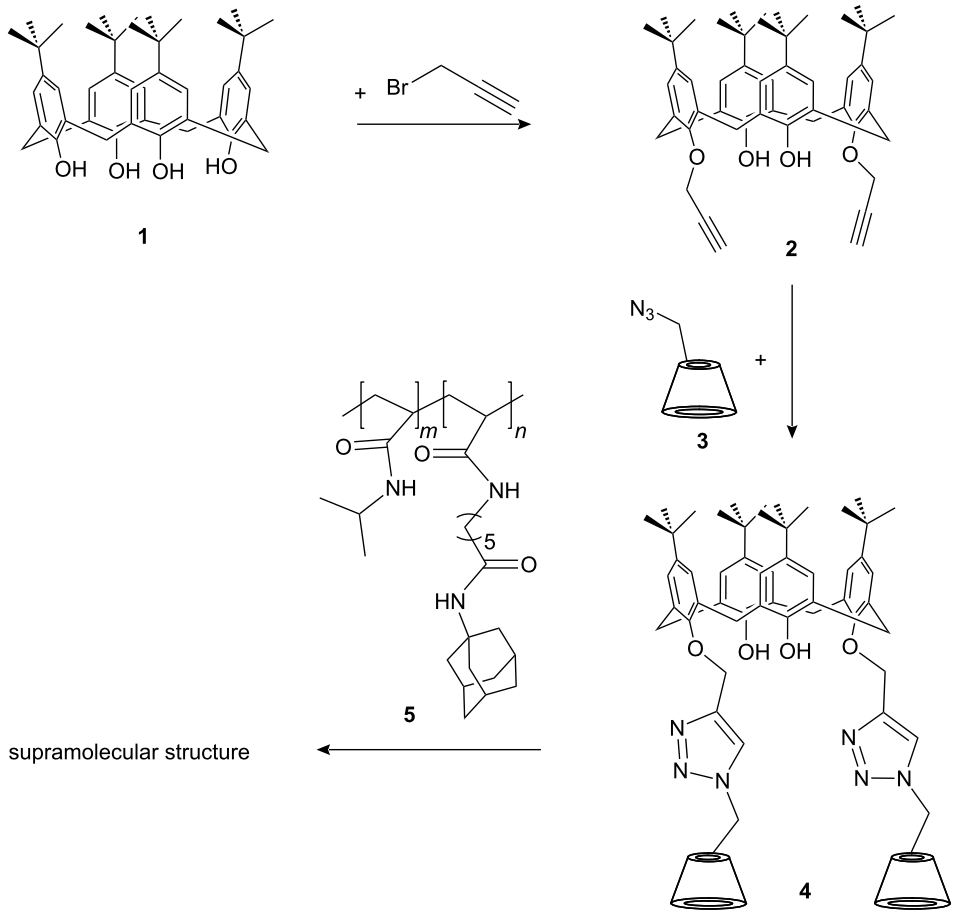
Results and Discussion

Synthesis and characterization of compound 4

The calixarene-click-CD compound (**4**) was synthesized as shown in Scheme 1.

The successful microwave assisted cycloaddition of 5,11,17,23-tetra-*tert*-butyl-25,27-dipropargylether-26,28-hydroxy-calix[4]arene (calix[4]arene-1,3-dipropargylether) (**2**) onto 6I-azido-6I-deoxycyclomaltoheptaose (**3**) was proven by IR spectroscopy by the disappearance of the bands for the azide group at 2105 cm^{-1} and for the propargyl group at 2115 cm^{-1}, whilst the formation of the triazole ring was confirmed by the appearance of a new band at 1654 cm^{-1}. The structure of compound **4** was additionally confirmed by ^1H NMR spectroscopy with the appearance of an olefinic proton signal at 8.07 ppm (–C=CH–N) and the disappearance of the characteristic propargyl proton signal at 2.50 ppm. Furthermore, the aromatic signals at about 7.0 ppm and the *tert*-butyl groups at 1.0 to 1.2 ppm indicates the presence of the calix[4]arene component. The CD was confirmed by the presence of the H2–H6 protons at about 3.3 to 3.6 ppm, the primary hydroxy group at 4.5 ppm and the secondary hydroxy groups at 5.7 ppm. The ^1H NMR spectrum of the successful cycloaddition of **2** and **3** indicates that the di-substituted calix[4]arene **4** was the major product along with a little amount of the mono-substituted compound. In addition, the MALDI-TOF-MS clearly confirmed the existence of the covalently combined rings (**4**) with a molecular mass of $[M + Na^+]$ = 3066 *m/z* (1 calix[4]arene-click- 2 CD).

DLS measurements were performed to evaluate the hydrodynamic diameter of the prepared compounds. Surprisingly, the number averaged hydrodynamic diameter of **4**, which is about 150 nm in aqueous solution, which suggests the formation of aggregates. In comparison, the hydrodynamic diameter of β-CD in water is about 1.5 nm, and that of calix[4]arene-1,3-dipropargylether (**2**) in $CHCl_3$ is only 0.64 nm. To reduce the agglomeration, compound **4** was deprotonated by dissolution in



Scheme 1: Synthesis of calixarene-click-cyclodextrin **4** via click chemistry and structure of copolymer **5**.

aqueous NaOH at pH 12. The negative charge was expected to cause intermolecular electrostatic repulsion. Accordingly, the hydrodynamic diameter of **4** decreased in NaOH solution from 150 nm to 9.0 nm, which can actually be attributed to the existence of trimers.

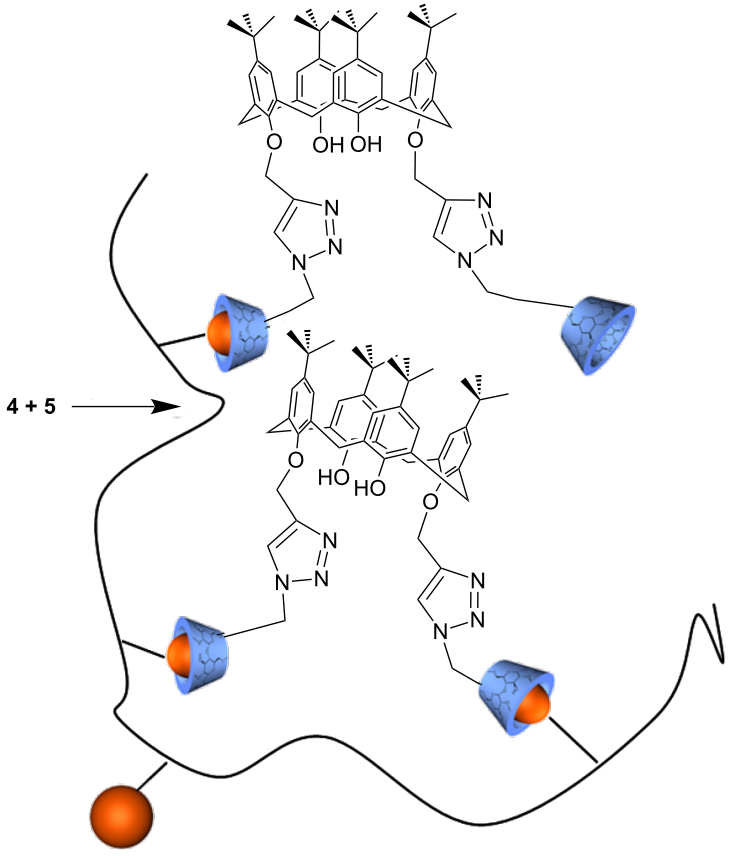
Host–guest complexion of 4 and 5

An adamantane containing copolymer **5** was prepared via free radical polymerization of 6-acrylamido-*N*-adamantyl-hexane amide and NIPAAM. Copolymer **5** was mixed with **4** subsequently (Scheme 2) to form supermolecular structures.

The hydrodynamic diameter of copolymer **5** increased from 8.5 nm to 53 nm after addition of **4**. This clearly indicates the inclusion of a polymer attached adamantane moiety into the cavity of CD. The adamantane moiety is known to be one of the best guest molecules for β-CD [15]. A relatively high complex stability constant for a polymer attached adamantane groups with CD is about 5000 M^{-1} [16]. Therefore, as shown in Scheme 2, compound **4** obviously is expected to act as an intermolecular linker between the copolymer chains. To prove the assumed agglomeration of the CD-moieties in water [17], adamantyl carboxylate was added to the solution as a competitive guest molecule. As expected, a decrease of the hydrodynamic diameter from 53 nm to 13 nm was observed. Adamantyl carboxylate is known to be a more effective guest [15] than the polymer attached adamantane moiety itself. Thus, the inclusion of the low molecular weight adamantyl carboxylate into the cavity of the CD component of **4** leads to a replacement of copolymer **5**.

pH-Depending and LCST measurements of the host–guest complex

To prevent the agglomeration effects of the CD in compound **4** as discussed above, copolymer **5** and compound **4** were dissolved in an aqueous NaOH solution at pH 12 to deprotonate the free phenolic groups of the calix[4]arene-derivative **4**. After that, the hydrodynamic diameter of copolymer **5** increased due to complexation with negatively charged **4** from 8.5 nm to 17.5 nm. This increase of the hydrodynamic diameter again indicates the inclusion of the polymer attached adamantane moiety into the cavity of the CD-component. Comparing the diameters of complex (**4** + **5**) at pH 7 (53 nm) and at pH 12 (17.5 nm), it can be supposed, that due to deprotonation inter-



Scheme 2: Superstructure of calixarene-click-cyclodextrin **4** and copolymer **5**.

molecular electrostatic repulsion takes place which decreases the agglomeration in the system.

The turbidity point of copolymer **5** in water, 29 °C, is significant lower than that of the unmodified poly(NIPAAM) at 34 °C, which can be ascribed to the existence of the hydrophobic adamantyl units in the copolymer. The host–guest effect of the coupled rings **4** on the cloud point of copolymer **5** was evaluated by turbidity measurements. Only a slight positive shift of the cloud point temperature from 29 °C to 30 °C was found (Table 1). The temperature shift relative to the cloud point of poly(NIPAAM) itself, can be explained by the inclusion of the hydrophobic adamantyl units of **5** by the CD moiety of **4**, which, in principal, should increase the cloud point temperature. In contrast to this, the unavoidable presence of the hydrophobic calixarene units of **4** leads to a reduction of the cloud point temperature. Repeating the turbidity experiment at pH of 12, the cloud point temperature of the copolymer **5** decreased from the original 29 °C to 23 °C due to salt and pH effects [18]. However, after adding the calixarene-click-cyclodextrin (**4**) to copolymer **5** under similar conditions at pH 12, the cloud point increased to 30.5 °C. This increase of the cloud point can be explained by the deprotonation of the calixarene moiety of **4** to the corresponding phenolate structure, which causes an increase in hydrophilicity.

Table 1: Experimental cloud point temperature (LCST) and hydrodynamic diameter[a] depending on the balance of hydrophobic/hydrophilic interactions of calixarene-click-cyclodextrin **4** with copolymer **5** depending on pH.

Compound number (pH)	Turbidity point (°C)	Number averaged hydrodynamic diameter (nm)
4 (7)		150
4 (12)		9.0
5 (7)	29.0	8.5
5 (12)	23.0	8.5
5 + **4** (7)	30.0	53.0
5 + **4** (12)	30.5	17.5

[a]DLS measurements were performed at 10 °C, below the turbidity point of the copolymer.

Conclusion

A calixarene-click-cyclodextrin combi-receptor (**4**) was synthesized via copper-catalyzed Huisgen 1,3-dipolar cycloaddition. Investigations of the interactions with an adamantyl moiety containing copolymer have been carried out, showing the existence of a supramolecular structure. Due to deprotonation of the calixarene moieties at higher pH values, a significant change in solubility and hydrodynamic diameter was observed and correlated to the formation of superstructures.

Experimental

Materials. β-Cyclodextrin (β-CD) was purchased from Wacker Chemie GmbH (Burghausen, Germany) and used after drying overnight over P_4O_{10} under an oil pump vacuum. *N*-Isopropylacrylamide (NIPAAM) 97%, sodium azide (99.5%) and azobisisobutyronitrile (98%) were purchased from Aldrich Chemicals (Germany) and used as received. Copper-(II)-sulfate pentahydrate (99%) was obtained from Carl Roth GmbH & CO., and sodium L(+)-ascorbate (99%) obtained from AppliChem (Germany). *N*,*N*-Dimethylformamide (DMF) and sodium hydroxide (NaOH) were purchased from VWR (USA). Dimethylsulfoxide-d_6 99.9% atom% D was obtained from Deutero GmbH (Germany). Commercially available reagents and solvents were used without further purification. calix[4]arene **1** [19], calix[4]arene-1,3-dipropargylether **2** [8], 6I-azido-6I-deoxycyclomaltoheptaose **3** [20] and poly(6-acrylamido-*N*-adamantyl-hexane amide-co-NIPAAM) **5** [4] (M_w: 94900 g/mol, PDI: 3.5) were prepared according to methods described in literature.

Measurements. IR spectra were recorded with a Nicolet 6700 FTIR (Fourier transform infrared) spectrometer equipped with an ATR unit. The measurements were performed in the rage of 4000–300 cm^{-1} at room temperature. ^1H NMR spectra were recorded on a Bruker Avance DRX 200 at 20 °C. Chemical shifts were referenced to the solvent value δ 2.51 for DMSO-d_6. Matrix assisted laser desorption ionization time of flight mass spectrometry (MALDI-TOF-MS) was performed on a Bruker Ultraflex TOF mass spectrometer. Ions formed with a pulsed nitrogen laser (25 Hz, 337 nm) were accelerated to 25 kV, the molecular masses being recorded in linear mode. 2-(4-Hydroxyphenylazo)benzoic eacid (HABA) in DMF (25 mg/mL) was used as matrix. The samples (1 mg/mL in DMF) were mixed with the matrix solution at volumetric ratios of 1:10. Gel permeation chromatography (GPC) analyses were performed on a GPC system from PPS with PPS-WIN-GPC software 4.01, 6.1 with *N*,*N*-dimethylformamide as eluent. The flow rate was 1 ml min^{-1} and the column temperature was maintained at 60 °C. A 0.1% (w/w) polymer solution (100 µL) was applied to a hydroxyethyl methacrylate (HEMA) column combination that consisted of a precolumn of 40 Å and main columns of 40, 100 and 3000 Å porosities. The weight-average molecular weight (M_w) and the polydispersity (PD) were calculated by a calibration curve generated by polystyrene standards with a molecular weight range from 370 to 1000000 Da. DLS experiments were carried out on a Malvern HPPS-ET apparatus at a temperature value of 10 °C. The particle size distribution was derived from a deconvolution of the measurement number averaged autocorrelation function of the sample by the general purpose mode algorithm included in the DTS software. Each experiment was preformed five times to obtain statistical information. Cloud

points were determined by transmission changes (at 500 nm) of the solution heated at 1 K/min in a magnetically stirred cell; cloud points were defined as the temperature at which the transmission decreases by 50%. Microwave assisted synthesis was performed using a CEM Discover synthesis unit (monomode system). The temperature was measured by infrared detection with control and maintained at constant value by power modulation. Reactions were performed in closed vessels under controlled pressure.

Synthesis of calix[4]arene-click-cyclodextrin 4. The microwave assisted click reaction of calix[4]arene-1,3-dipropargylether (**2**) (100 mg, 0.14 mmol) with 6I-azido-6I-deoxycyclomaltoheptaose (**3**) (324.8 mg, 0.28 mmol) was carried out in DMF in the presence of Cu(I) generated by the reduction of copper sulfate (0.014 mmol) with sodium ascorbate (0.07 mmol). The tube was sealed, placed in the CEM monomode microwave and irradiated at 150 °C and 100 W for 30 min. The solvent was removed under reduced pressure. The crude product **4** was washed with water and dried in vacuum to afford a brown solid (yield: 70%).

MALDI-TOF: *m/z* 3066 [M + Na^+]. ^{1}H NMR (DMSO-d_6, δ(ppm)): 1.05 (s, 9H, -C-$(CH_3)_3$), 1.13 (s, 9H, -C-$(CH_3)_3$), 1.17 (s, 9H, -C-$(CH_3)_3$), 1.19 (s, 9H, -C-$(CH_3)_3$), 3.37 (br, 28H, H-2,4), 3.66 (br, 56H, H-3,5,6), 4.48 (br, 7H, O-CH-O), 4.75 (br, 7H, O-CH-O), 4.85 (br, 12H, OH-6), 5.78 (br, 2H, Ar-OH), 6.97 (s, 2H, Ar-H), 7.01 (s, 2H, Ar-H), 7.06 (s, 2H, Ar-H), 7.10 (s, 2H, Ar- H), 7.78 (s, 1H, N-CH=C), 8.07 (s, 1H, N-CH=C). IR: 3328 (-OH), 2929 (aryl, alkyl), 1654 (triazole), 1482 (-C=N-), 1386 (-C(CH_3)); further intensive signals, 1151, 1078, 1022 cm^{-1}.

Host–guest complexion of polymer 5 and calix[4]arene-click-cyclodextrin 4. For further investigations, polymer **5** (50 mg, 5.3×10^{-3} mmol) was dissolved in 5 ml water or aqueous NaOH at pH 12. Product **4** (10 mg, 3.2×10^{-3} mmol) was added and the solution was mechanical stirred for 24 h. This solution was centrifuged to remove undissolved particles.

References

1. Abraham, W. *J. Inclusion Phenom. Macrocyclic Chem.* **2002,** *43,* 159–174. doi:10.1023/A:1021288303104
2. Ikeda, A.; Shinkai, S. *J. Am. Chem. Soc.* **1994,** *116,* 3102–3110. doi:10.1021/ja00086a045
3. Gutsche, C. D.; Alam, I. *Tetrahedron* **1988,** *15,* 4689–4694. doi:10.1016/S0040-4020(01)86171-8
4. Munteanu, M.; Choi, S. W.; Ritter, H. *Macromolecules* **2009,** *42,* 3887–3891. doi:10.1021/ma900397m
5. De Zorzi, R.; Guidolin, N.; Randaccio, L.; Purrello, R.; Geremia, S. *J. Am. Chem. Soc.* **2009,** *131,* 2487–2489. doi:10.1021/ja808850d
6. Kolb, H. C.; Finn, M. G.; Sharpless, K. B. *Angew. Chem., Int. Ed.* **2001,** *40,* 2004–2021. doi:10.1002/1521-3773(20010601)40:11<2004::AID-ANIE2004>3.0.CO;2-5
7. Rostovtsev, V. V.; Green, L. G.; Fokin, V. V.; Sharpless, K. B. *Angew. Chem.* **2002,** *114,* 2708–2711. doi:10.1002/1521-3757(20020715)114:14<2708::AID-ANGE2708>3.0.CO;2-0
8. Zhan, J.; Tian, D.; Li, H.; New, J. *New J. Chem.* **2009,** *33,* 725–728. doi:10.1039/b816467c
9. Bew, S. P.; Brimage, R. A.; L'Hermite, N.; Sharma, S. V. *Org. Lett.* **2007,** *9,* 3713–3716. doi:10.1021/ol071047t
10. Pérez-Balderas, F.; Ortega-Muñoz, M.; Morales-Sanfrutos, J.; Hernández-Mateo, F.; Calvo-Flores, F. G.; Calvo-Asín, J. A.; Isac-García, J.; Santoyo-González, F. *Org. Lett.* **2003,** *5,* 1951–1954. doi:10.1021/ol034534r
11. Ortega-Muñoz, M.; Morales-Sanfrutos, J.; Pérez-Balderas, F.; Hernández-Mateo, F.; Girón-González, M. D.; Sevillano-Tripero, N.; Salto-González, R.; Santoyo-González, F. *Org. Biomol. Chem.* **2007,** *5,* 2291–2301. doi:10.1039/b706331h
12. Chan, T. R.; Hilgraf, R.; Sharpless, K. B.; Fokin, V. V. *Org. Lett.* **2004,** *6,* 2853–2855. doi:10.1021/ol0493094
13. Hoogenboom, R.; Moore, B. C.; Schubert, U. S. *Chem. Commun.* **2006,** *38,* 4010–4012. doi:10.1039/b608313g
14. Munteanu, M.; Choi, S. W.; Ritter, H. *Macromolecules* **2008,** *41,* 9619–9623. doi:10.1021/ma8018975
15. Rekharsky, M. V.; Inoue, Y. *Chem. Rev.* **1998,** *98,* 1875–1918. doi:10.1021/cr970015o
16. Amajjahe, S.; Ritter, H. *Macromolecules* **2008,** *41,* 716–718. doi:10.1021/ma702271p
17. Bonini, M.; Rossi, S.; Karlsson, G.; Almgren, M.; Lo Nostro, P.; Baglioni, P. *Langmuir* **2006,** *22,* 1478–1484. doi:10.1021/la052878f
18. Saeed, A.; Georget, D. M. R.; Mayes, A. G. *React. Funct. Polym.* **2010,** *70,* 230–237. doi:10.1016/j.reactfunctpolym.2009.12.004
19. Gutsche, C. D.; Iqbal, M. *Org. Synth.* **1990,** *68,* 234–237.
20. Ohga, K.; Takashima, Y.; Takahashi, H.; Kawaguchi, Y.; Yamaguchi, H.; Harada, A. *Macromolecules* **2005,** *38,* 5897–5904. doi:10.1021/ma0508606

License and Terms

This is an Open Access article under the terms of the Creative Commons Attribution License (http://creativecommons.org/licenses/by/2.0), which permits unrestricted use, distribution, and reproduction in any medium, provided the original work is properly cited.

The license is subject to the *Beilstein Journal of Organic Chemistry* terms and conditions: (http://www.beilstein-journals.org/bjoc)

The definitive version of this article is the electronic one which can be found at: doi:10.3762/bjoc.6.83

Beilstein Journal of Organic Chemistry

Functionalized copolyimide membranes for the separation of gaseous and liquid mixtures

Nadine Schmeling, Roman Konietzny, Daniel Sieffert, Patrick Rölling and Claudia Staudt*

Full Research Paper

Open Access

Address:
Institute for Organic and Macromolecular Chemistry, Heinrich-Heine University of Duesseldorf, Universitaetsstr. 1, 40225 Duesseldorf, Germany

Email:
Claudia Staudt* - staudt@uni-duesseldorf.de

* Corresponding author

Keywords:
aromatics/aliphatics; copolyimides; cross-linking; gas separation; membranes; natural gas treatment; olefins/paraffins; pervaporation

Beilstein J. Org. Chem. **2010,** *6,* 789–800.
doi:10.3762/bjoc.6.86

Received: 17 May 2010
Accepted: 02 August 2010
Published: 12 August 2010

Guest Editor: H. Ritter

© 2010 Schmeling et al; licensee Beilstein-Institut.
License and terms: see end of document.

Abstract

Functionalized copolyimides continue to attract much attention as membrane materials because they can fulfill the demands for industrial applications. Thus not only good separation characteristics but also high temperature stability and chemical resistance are required. Furthermore, it is very important that membrane materials are resistant to plasticization since it has been shown that this phenomenon leads to a significant increase in permeability with a dramatic loss in selectivity. Plasticization effects occur with most polymer membranes at high CO_2 concentrations and pressures, respectively. Plasticization effects are also observed with higher hydrocarbons such as propylene, propane, aromatics or sulfur containing aromatics. Unfortunately, these components are present in mixtures of high commercial relevance and can be separated economically by single membrane units or hybrid processes where conventional separation units are combined with membrane-based processes. In this paper the advantages of carboxy group containing 6FDA (4,4′-hexafluoroisopropylidene diphthalic anhydride) -copolyimides are discussed based on the experimental results for non cross-linked, ionically and covalently cross-linked membrane materials with respect to the separation of olefins/paraffins, e.g. propylene/propane, aromatic/aliphatic separation e.g. benzene/cyclohexane as well as high pressure gas separations, e.g. CO_2/CH_4 mixtures. In addition, opportunities for implementing the membrane units in conventional separation processes are discussed.

Introduction

Over 50% of energy costs in the chemical industry are used for the separation of gaseous or liquid mixtures [1]. Separations in petrochemical processes, e.g. low temperature distillation of olefin/paraffin mixtures or extractive distillation for the production of benzene as well as the separation of isomeric xylenes by low temperature fractional crystallization are highly energy intensive. If these separation processes could be improved, the costs of basic chemicals as ethylene, propylene and benzene could be drastically reduced.

Membrane devices offer new opportunities for the separation of gaseous or liquid mixtures. Compared to conventional distilla-

tion units, membrane devices are much smaller and processes can be conducted at lower temperatures. In certain cases, the combination of distillation and membrane units, so called hybrid processes, have been established. For the separation of olefin/paraffin mixtures it has been estimated that membrane based hybrid processes could save approximately 40–50% of the production costs [2]. The worldwide membrane market currently has a steady growth of approximately 10–15% each year [3]. Membrane based separations of gaseous mixtures have been well established for natural gas treatments (removal of carbon dioxide), for hydrogen removal (e.g. in cracking processes) for oxygen enrichment from air (medical devices) and for nitrogen enrichment from air (used as an inert atmosphere for oxygen sensitive compounds). Other areas with fast growing market relevance are vapor recovery systems [4], monomer recovery units, e.g. ethylene/nitrogen or propylene/nitrogen [5,6], the dehydration of organic solvents and the removal of polar low molecular weight components in equilibrium reactions [7].

Background and theory

In general, membranes are very thin layers, which can have different structures. They are divided into porous membranes and solution-diffusion membranes. Porous membranes are well established in typical filtration processes e.g. micro-, ultra-, and nanofiltration. The particles to be separated have diameters between 10 and 1000 nanometers and will be held back from the membrane due to the fact that the pores of the membrane are smaller than the particle size.

If the size of the components to be separated is less than 1 nanometer – which is the case for many gaseous, vaporous and also liquid components that have to be removed from process streams – then mainly so called solution-diffusion membranes are used. This type of membrane does not have pores but free volume sites which exist due to restricted motion and packing density of the polymer chains.

Figure 1 shows the principle of a membrane-based separation process. The feed mixture is transported along one side of the membrane and the different feed components permeate through the membrane at different rates. The stream leaving the membrane unit on the same side as the feed is depleted in the components which permeate preferentially. Consequently the stream, which is collected on the back side of the membrane, is enriched in the preferentially permeating component. The driving force for the mass transport through a polymeric membrane is the difference in the chemical potential between the feed and permeate side and depends on temperature, pressure and concentration. In pervaporation, a membrane based process for separating liquid mixtures and also employed in gas separation processes, the difference in chemical potential is mainly achieved by keeping the permeate pressure much lower than the feed pressure.

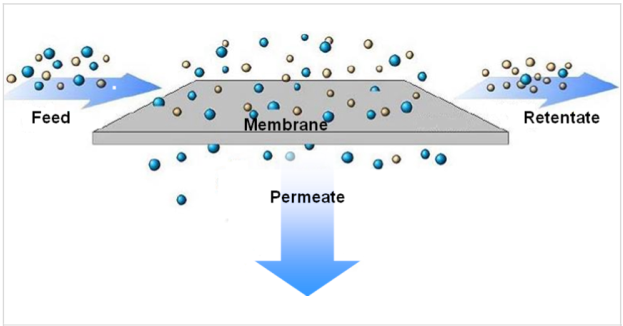


Figure 1: Membrane based separation process.

The mass transport through solution-diffusion membranes can be described with the solution-diffusion model [8]. Based on this model the components permeate through a polymeric membrane in a three step process, i.e., the sorption of the component on the membrane surface (feed side), the diffusion of the component through the free volume of the polymer and the desorption of the component on the permeate side of the membrane.

In order to optimize material properties for the solution-diffusion process through the polymer matrix, approaches can be made taking the molecular structure into account [9].

Thus, it is supposed that a certain free volume exists in polymers. This is the volume, which cannot be occupied by polymer chains due to conformational constraints. Within this free volume, transient gaps are formed which can accommodate, e.g., gas molecules. According to the driving force, the components have to be transported by successive movement between transient gaps close to the feed side to those close to the permeate side. The movement necessary for the transport of the components between the microvoids is possible due to thermal motion of segments of the polymer chains.

Polymeric membrane materials are generally characterized by the transport properties permeability and selectivity. Permeability is a measure of the productivity of the membrane and selectivity is a measure of the separation efficiency. For polymer films without any support, which are used as membrane materials in this review, the flux (n_A), normalized by the transmembrane partial pressure (Δp_A) and thickness (ℓ), the permeability (P_A) is defined, as shown in Equation 1.

$$P_A = n_A \frac{\ell}{\Delta p_A} \quad (1)$$

In gas separation devices the permeability values are typically reported in Barrer,

$$\left(1\ \text{Barrer}\ = 10^{-10}\ \frac{\text{cc(STP)} \cdot \text{cm}}{\text{cm}^2\ \cdot \text{cm Hg} \cdot \text{s}}\right) \tag{2}$$

whereas in pervaporation processes the mass flux is reported in $kg \cdot \mu m \cdot m^{-2} \cdot h^{-1}$. The ideal selectivity α^*_{AB} (i.e. pure feed components) between A and B is defined as the ratio of their permeabilities (Equation 3).

$$\alpha^*_{AB} = P_A / P_B \tag{3}$$

The permeability can be written as the product of the diffusion coefficient D, and the solubility coefficient S (Equation 4).

$$P_A = D_A S_A \tag{4}$$

From this relationship, the ideal selectivity α^*_{AB} can be expressed by Equation 5.

$$\alpha^*_{AB} = \frac{D_A S_A}{D_B S_B} \tag{5}$$

Thereby the solubility coefficient S is determined by the polymer-penetrant interactions and by the amount of free volume in the polymer. The average diffusion coefficient D is a measure of the mobility of the penetrants between the feed and permeate side of the membrane. The diffusion coefficient D depends on packing and motion of the polymer segments and on the size and shape of the penetrating molecules.

For binary feed mixtures in gas separation and also in pervaporation processes, the selectivity can be calculated from Equation 6.

$$\alpha_{AB} = \frac{\left(y_A / y_B\right)}{\left(x_A / x_B\right)} \tag{6}$$

In which x_i is the mole fraction of the preferred permeating component i on the feed side and y_i is the mole fraction of the preferred permeating component i on the permeate side, as measured by gas chromatography.

Results and Discussion

Material selection

For the separation of liquid and gaseous mixtures, in general, porous as well as solution-diffusion membranes can be used. Although porous inorganic membranes, e.g., different zeolite types are characterized by their high thermal and chemical resistance, the application in large scale industrial processes seems to be rather difficult since preparing defect free membranes in huge areas is still difficult and expensive. The manufacturing of polymeric materials as composites or hollow fibers has been well established over the past 10–15 years, which is the reason why most of the commercial membrane units used for gas separation contain, e.g., polymer membranes [10]. Furthermore, strategies for new large-scale applications with polymeric membranes are under investigation [11-13].

Polymeric membrane materials can be divided into rubbery and glassy polymers. Extensive research in the area of gas separation has found correlations between the polymer structure and the separation characteristics. Thus glassy polymers show very attractive separation characteristics – high selectivity combined with medium permeability, whilst rubbery polymers show comparably low selectivity with high permeability for common gas pairs such as O_2/N_2, H_2/CH_4, CO_2/CH_4, etc. [14-16]. This correlation is demonstrated for the CO_2/CH_4 separation as shown in Table 1.

Table 1: Comparison of glassy and rubbery polymer membranes in CO_2/CH_4 separation [12].

Polymer	α* = $P(CO_2)/P(CH_4)$	P (CO_2) [Barrer]
Cellulose derivatives	3	4550
Polycarbonates	11–33	75–15
Polyimides	15–25	110–6.5
Polydimethylsiloxane	55–65	23–0.6

High selectivity is achieved with glassy polymers as a result of several factors, e.g., the lower free volume, a narrower distribution of the free volume as well as the lower flexibility of the polymer chains, compared to those of rubbery polymers. Within the class of glassy polymers, polyimides have been found to be very attractive as membrane materials because they have better separation characteristics compared to other glassy polymers, e.g., polycarbonates as also shown in Table 1. Additionally, polyimides offer good thermal and chemical resistance and are easy to process. Polyimide membranes are manufactured by several companies, e.g., Evonic, UBE, GKSS, MTR, etc., and are used mainly in gas separation processes but also find application in pervaporation and vapor recovery systems [17]. In order to improve the separation characteristics of this polymer

class, systematic studies have been carried out over the last 10 years in order to find correlations between polyimide structure and separation performance. Thus it was found that with monomers having $-CF_3$ groups, e.g. the 6FDA dianhydride, as shown in Figure 2, the bulky $-CF_3$ groups restrict chain mobility and simultaneously chain packing, and consequently lead to significantly improved selectivity as well as permeability [18-22].

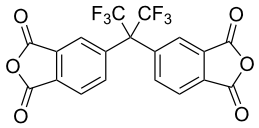


Figure 2: Chemical structure of the 6FDA (= 4,4′-hexafluoroisopropylidene diphthalic anhydride).

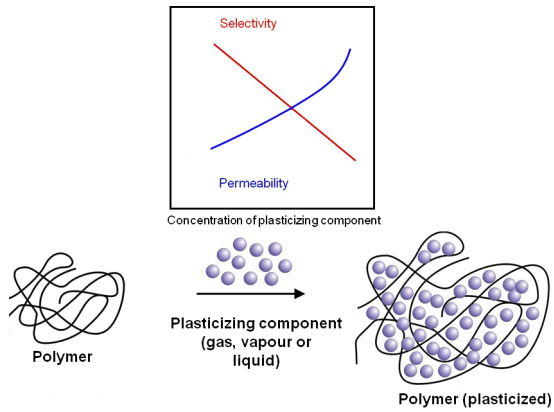


Figure 3: Plasticization phenomenon and resulting effects on separation characteristics.

Cross-linked polymers

6FDA-polyimides show excellent separation characteristics for different gaseous and liquid mixtures. However, in the presence of certain feed components plasticization occurs. Plasticization leads to an increase in the intermolecular distance and to a decrease in inter- and/or intra-molecular forces. As a consequence, the molecular motion of the polymer chains increases and as a result of this the permeabilities for all feed components also increase with an associated decrease in selectivity (Figure 3). It has been found in several studies that plasticization occurs if polyimides are exposed to high partial pressure of CO_2 [23,24], hydrocarbons, e.g., propylene and propane [25,26] or ethylene oxide [27]. Strong plasticization can even lead to a partial dissolution of the membrane as it has been found in aromatic/aliphatic separation [28]. These results indicate that if new markets for membrane systems are found, then it will be definitely necessary to develop new plasticization resistant, robust membrane materials.

Cross-linking of polymer structures has been found to be a suitable method to improve plasticization resistance as well as the separation characteristics for pervaporation [29-33] and gas separation [34-39]. Carboxy group containing 6FDA-based polyimides and copolyimides have been developed resulting in functional polymers which can be cross-linked or further modified. Consequently, plasticization effects can be reduced very efficiently [25,27,40,41]. As shown in Figure 4, such carboxy

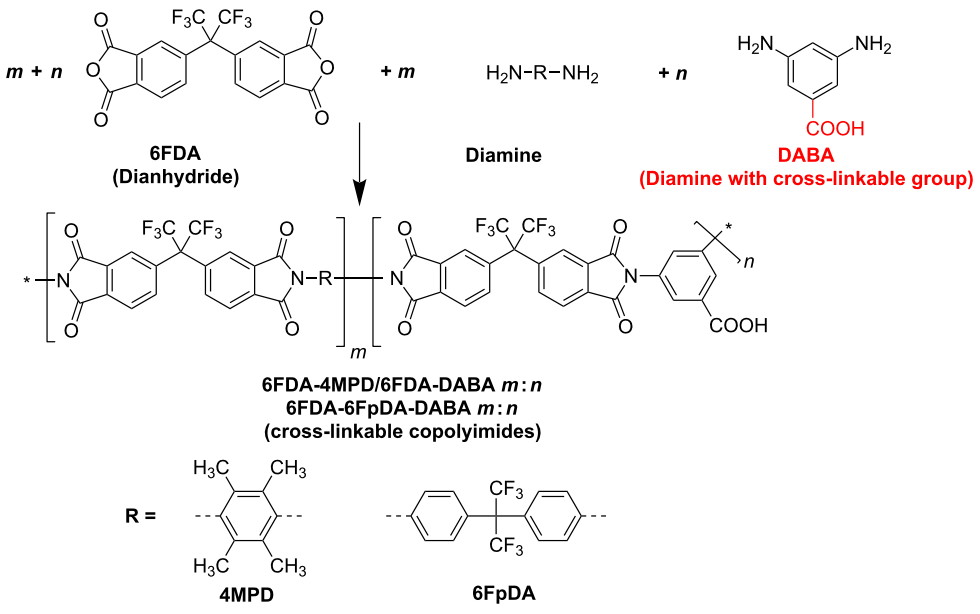


Figure 4: Synthesis of cross-linkable copolyimide structures.

group containing copolyimides can be synthesized by using 3,5-diaminobenzoic acid as one of the monomers. Due to the lower reactivity of the carboxy groups on the diaminobenzoic acid (DABA) monomer compared to the dianhydride on the 6FDA, the carboxy groups are still present after the polymerization reaction and can be used in further reactions, e.g., cross-linking. Polymerization takes place in a two step reaction. Firstly, the purified diamino monomers were dissolved in dry *N*,*N*-dimethylacetamide and the 6FDA dianhydride is added under a nitrogen atmosphere in order to form the polyamic acid. After stirring for 24 h at room temperature, the viscous polyamic acid solution was chemically converted to the polyimide by treatment with a mixture of acetic anhydride and triethylamine. A detailed description of the synthesis is given in [28].

In Figure 5 the three different types of copolyimides investigated are shown schematically. It is assumed that the polymer chains of copolyimides containing free carboxy groups are associated via hydrogen bonds. This is indicated by comparing the CO_2 permeabilities for pure polyimides and copolyimides containing DABA. It was found that the presence of carboxy groups reduces the CO_2 plasticization slightly due to the hydrogen bonds between the carboxylic acid groups [23]. Copolyimides with carboxy groups can be further modified via covalent cross-linking with, e.g., diols or diamines or cross-linked ionically with aluminium acetylacetonate or zirconium acetylacetonate as shown in Figure 5.

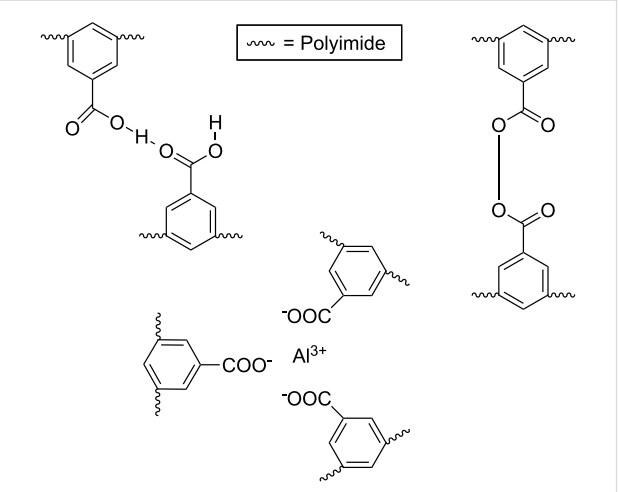


Figure 5: Investigated cross-linking variations (non cross-linked, covalently and ionically cross-linked).

Covalent cross-linked membranes were prepared by dissolving the carboxy group containing copolyimide in dry *N*,*N*-dimethylacetamide and adding 6 times the stoichiometric amount of diol (based on the number of cross-linkable carboxy groups) together with *p*-toluenesulfonic acid as a catalyst to the casting solution. After the solvent has been evaporated at 70 °C, the membranes obtained are stored for another 24 h at 150 °C at 80 mbar in order to carry out the cross-linking reaction.

Ionically cross-linked membranes have been prepared by dissolving the carboxy group containing copolyimide in tetrahydrofuran (THF) and adding a stoichiometric amount of aluminium acetylacetonate or zircon(IV) acetylacetonate to the casting solution. After evaporation of the solvent, the membranes are dried in a vacuum oven at 150 °C and 80 mbar in order to perform the cross-linking reaction.

In the following sections it will be shown which cross-linking method, ionic or covalent, will be the most effective to reduce undesired plasticization effects occurring in different separations. Furthermore, different ionic cross-linkers are compared, since it was expected that higher cation loadings would lead to more effective cross-linking.

Experimental set-up

According to Equation 4 and Equation 5, the separation characteristics, permeability and selectivity are dependent on the solubility and diffusivity of the single components in the membrane material. In order to estimate if the synthesized membrane polymer is suitable for a given separation problem, the solubility properties for the different feed components can be determined by means of gas or vapor sorption experiments. Diffusion coefficients can be determined by time dependent sorption measurements. For gas sorption experiments and for vapor sorption experiments, a microbalance and a quartz spring balance can be used, respectively [42,43]. It has been shown that polymeric membranes having significant differences in solubility for different feed components are particularly suitable for separating a mixture containing these components. However, sorption experiments do not give sufficient information about permeability and selectivity behavior if plasticization occurs. Therefore thorough gas permeation or pervaporation experiments are necessary with varying feed pressures and/or feed compositions. Only then reliable statements on potential applications of membrane systems are possible.

Investigated separation problems

Several membrane-based separations are already well established commercially. However, the number of new potential applications is steadily increasing [5,6]. Therefore, it is absolutely necessary to develop new, economic and reliable membrane materials. In the following section, three examples of new applications, namely, the separation of gaseous olefin/paraffin mixtures, aromatic/aliphatic separation and the removal of carbon dioxide from natural gas a with high CO_2 content, are discussed in detail.

Olefin/paraffin separation

The separation of olefin/paraffin mixtures is rather difficult because of the small differences in physical properties, e.g., boiling points. Currently, such separations are carried out by energy intensive low temperature distillation. Huge splitter columns are necessary to separate the mixtures of saturated and unsaturated hydrocarbons to obtain, e.g., propylene of sufficient purity for polymerization reactions. As shown in Figure 6, a hybrid process combining a membrane unit and a distillation column could lead, depending on the separation characteristics of the membrane material, to a significant reduction of the stream brought to the energy intensive splitter. Due to the fact that the separation train is more than half of the total cost of an olefin plant, a reduction of the splitter column is of high interest.

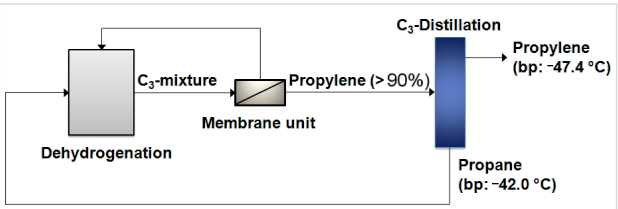


Figure 6: Hybrid process for the separation of propylene/propane.

However, membrane based processes for olefin/paraffin separations are currently not possible because suitable membrane materials are not commercially available. It has been found that polymeric membranes, e.g., silicone rubber, polysulfone, cellulose acetate, PDMS, 1,2-polybutadiene and polyethylene are not suitable for this kind of separation because the separation factors are far too low [44-46]. Much better separation characteristics were achieved with polyimides as membrane materials [11,45,47-49].

Unfortunately, polyimides are sensitive to plasticization due to higher hydrocarbons. It has been previously shown that neither ethane nor ethylene plasticize polyimide membranes but propane, propylene and higher hydrocarbon do [25,45,48,49]. In order to avoid undesirable plasticization effects, cross-linkable copolyimides have been synthesized, and their separation properties characterized. In Figure 7 the experimenstal data for the separation of a 50:50 propylene/propane mixture are shown. The temperature was 35 °C and the feed pressure was varied between 1 and 4.5 bar. In Figure 7, left-hand side, the total permeability is plotted versus the feed pressure, whilst on the right-hand side, the selectivity calculated from Equation 6 is shown as a function of the feed pressure.

As reference material, the 6FDA-4MPD was used as non cross-linkable membrane. In order to compare the propylene/propane separation characteristics of a 6FDA-4MPD polyimide membrane with a cross-linked copolyimide membrane, a copolyimide was synthesized substituting 20% of the 4MPD by the DABA diamine. The copolyimide obtained was the 6FDA-4MPD/6FDA-DABA 4:1. The structure is shown in Figure 4. Cross-linking of this type of polymer is possible due to the free carboxy groups and was performed by ethylene glycol treatment. As shown in Figure 7 for the reference polyimide 6FDA-4MPD, the permeability increases by 25% if the feed pressure is changed from 1.5 to 4 bar. Simultaneously, the selectivity for the propylene/propane separation decreases. This is caused by the increased mobility of the polymer chains during the swelling process as shown schematically in Figure 3. For the ethylene glycol cross-linked 6FDA-4MPD/6FDA-DABA 4:1 copolyimide, no plasticization effects were observed, since the mobility of the polymer chains is limited due to the cross-linking units. Therefore, the permeability as well as the selectivity remains constant. It should be also noted that a high selec-

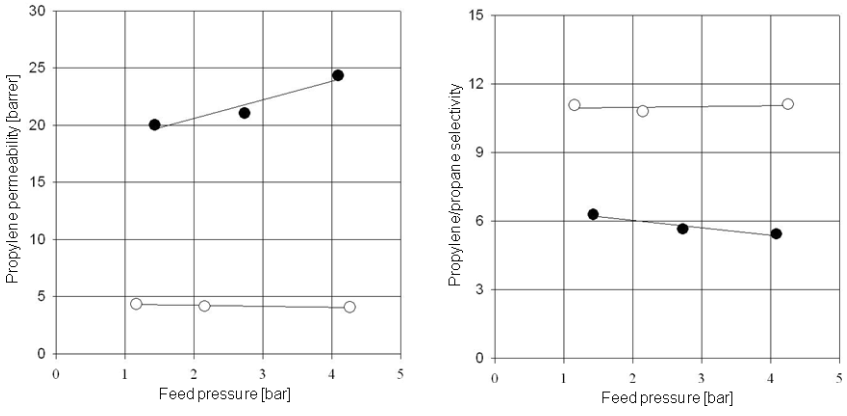


Figure 7: Total permeability (left) and selectivity (right) for the 6FDA-4MPD (●) and the 6FDA-4MPD/6FDA-DABA 4:1 copolyimide cross-linked with ethylene glycol (○) using a 50:50 propylene/propane feed mixture at 35 °C.

tivity of approximately 11 was found for the 6FDA-4MPD/6FDA-DABA 4:1 cross-linked with ethylene glycol, which means that with a 50:50 propylene/propane feed mixture a permeate concentration of more than 90% propylene can be achieved. This makes the membrane material very attractive for industrial applications.

Aromatics/aliphatics separation

The separation of aromatics/aliphatics is receiving more and more attention, as the benzene content in gasoline is, by law in Europe, limited to less than 1%. Discussions on the reduction of toluene and polynuclear aromatic compounds in gasoline are ongoing. Figure 8 shows the conventional separation process for separating a reformate stream containing 40–50% aromatics in which the aromatics are mainly benzene, toluene with small amounts of xylenes. As shown in the process scheme, in the first step the extracting column separates the reformate stream into aliphatic and aromatic streams. The separation factor for the aromatics, using a TETRA (tetraethylene glycol)/water mixture as the extracting solvent, is between 2 and 3. The main disadvantage of the extracting unit is that a huge amount of TETRA/water is necessary, e.g., the ratio of aromatics/extracting solvent is 1:10. In the next process step a stripping unit is necessary, not only to separate the aromatics from TETRA but also to separate the aliphatics, which are still present in the extracting unit due to the low separation factor. The stream on top of the stripper column consists mainly of aliphatics but also contains aromatics as well as TETRA and therefore it has to be returned to the extraction column.

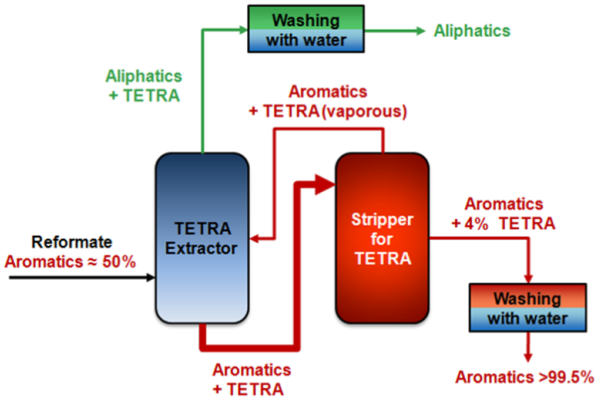


Figure 8: Conventional separation process for reformates containing extraction and stripping unit.

Figure 9 shows how a membrane separation unit might be implemented into a conventional aromatic/aliphatic separation process. This design is advantageous because the complete extracting column is replaced by a single membrane unit. Therefore the process itself requires only minor changes, i.e. the splitting ratio of the streams coming from the splitter does not have to be changed. In the proposed hybrid process, the separation factors for the aromatics are twice as high using a membrane compared to the extractor running with TETRA. Furthermore, the membrane unit will drastically reduce the stream to the splitter as well as the stream coming out on top of the splitter.

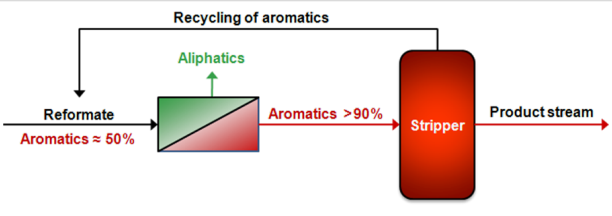


Figure 9: Hybrid process for the separation of aromatics/aliphatics.

Although the feed concentration for the aromatics in reformate streams is usually between 40% and 50%, it sometimes happens that much higher concentrations occur over a short time period. Therefore it is important to ensure that the membrane material is stable and additionally, that the separation characteristics – especially the selectivity – will not change drastically. It has been demonstrated that polyimides in principle are suitable for the separation of aromatic/aliphatic mixtures but unless they are cross-linked, the stability is poor especially at high aromatic concentrations and elevated feed temperatures. In order to circumvent these problems in practical applications, different copolyimides have been synthesized and their stabilities after exposure to high benzene concentrations tested. Figure 10 shows the 6FDA-6FpDA/6FDA-4MPD/6FDA-DABA 3:1:1 cross-linked with ethylene glycol in a stability experiment. This experiment was started by running pervaporation experiments, with benzene/cyclohexane mixtures with benzene concentrations of 50 and 80 wt %. After the membrane was exposed to 80% benzene, the feed mixture was exchanged and then the separation characteristics for benzene concentrations of 10 wt % up to 100 wt % in the feed were investigated. In this experiment it can be clearly seen that covalently cross-linked copolyimides are very stable towards high benzene concentrations [28]. No change in selectivity was observed after the cross-linked membrane was exposed to high aromatic concentrations in the feed. It has been found that cross-linked copolyimide membranes can even be exposed to 100% aromatics before starting separation experiments without any loss in selectivity. In certain cases even increased permeability without any loss in selectivity has been observed.

Pre-treatment of the membrane material prior to its use is referred to as conditioning. The effects of varying the composition of the conditioning agent were also investigated in this

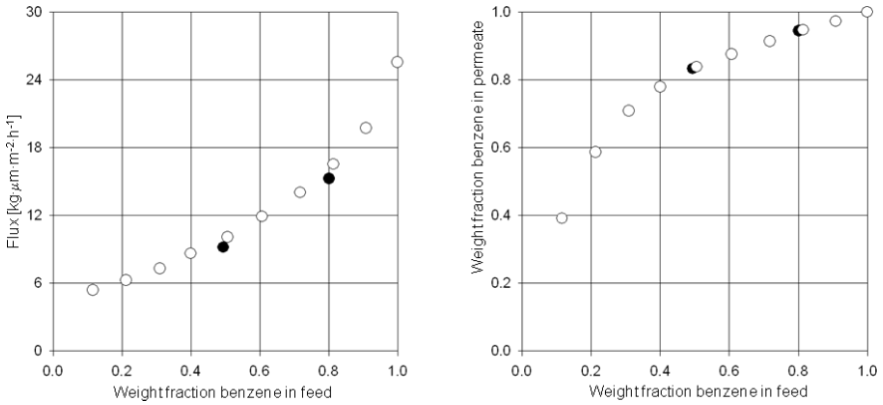


Figure 10: Pervaporation results for the 6FDA-6FpDA/6FDA-4MPD/6FDA-DABA 3:1:1 copolyimide cross-linked with ethylene glycol (first run (●) and second run (○) using benzene/cyclohexane mixtures at 60 °C and a permeate pressure of 10–20 mbar (data taken from [28]).

work. 6FDA-4MPD/6FDA-DABA 4:1 was used as the basic membrane material and non cross-linked membranes were prepared and conditioned in pure toluene and in a mixture of 90:10 toluene/cyclohexane, respectively. The results of the pervaporation experiments at 60 °C and at a permeate pressure of 20–25 mbar are shown in Figure 11.

It can be seen clearly that the membrane conditioned in pure toluene shows a much higher flux than the one conditioned in 90:10 toluene/cyclohexane. This effect is even more pronounced at higher toluene concentrations in feed. Remarkably, there is no significant difference in the selectivity for the different conditioned membranes within experimental error. From our experience in pervaporation experiments, the error range for the selectivity is ±10%, whereas for the flux it could be as much as 15%, depending on the homogeneity of the membranes. However, from the experiments performed, it can be concluded, that with appropriate conditioning, fluxes can be increased without any loss in selectivity.

Further experiments have been carried out in order to investigate the separation characteristics for covalently cross-linked copolyimide membranes compared to ionically cross-linked copolyimide membranes and non cross-linked membranes prepared from the same type of polymer. The polymer 6FDA-4MPD/6FDA-DABA 4:1 copolyimide was used and the covalent cross-linker was 1,4-butanediol. An ionically cross-linked membrane was prepared from the basic polymer material by adding 10% of the stoichiometric amount of cross-linker (based on the free carboxy groups of the polymer). For the ionic cross-linking, zircon(IV) acetylacetonate was used since it was expected to be more efficient than aluminium acetylacetonate because of the higher charge of the cation formed during the cross-linking reaction. The mixture to be separated consisted of toluene and cyclohexane and the experiments were carried out at 60 °C at a permeate pressure of 20–25 mbar.

The results obtained (Figure 12) show that the flux of a non cross-linked 6FDA-4MPD/6FDA-DABA 4:1 membrane is

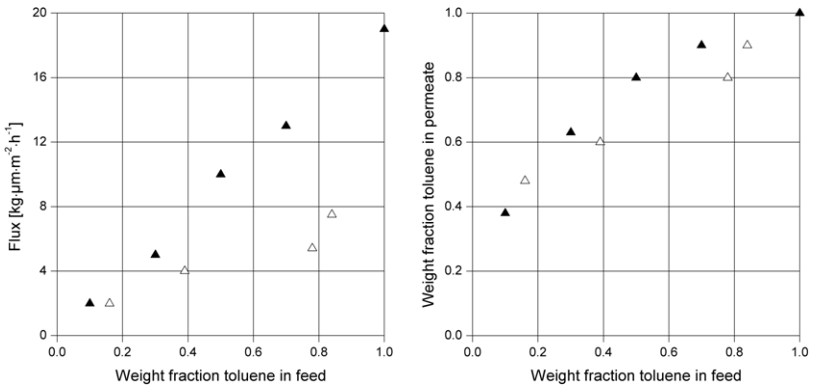


Figure 11: Pervaporation results for 6FDA-4MPD/6FDA-DABA 4:1 copolyimide (non cross-linked) conditioned in pure toluene (▲) and in a mixture of 90:10 toluene/cyclohexane (Δ). After conditioning, the measurements were performed using toluene/cyclohexane mixtures at 60 °C and a permeate pressure of 20–25 mbar.

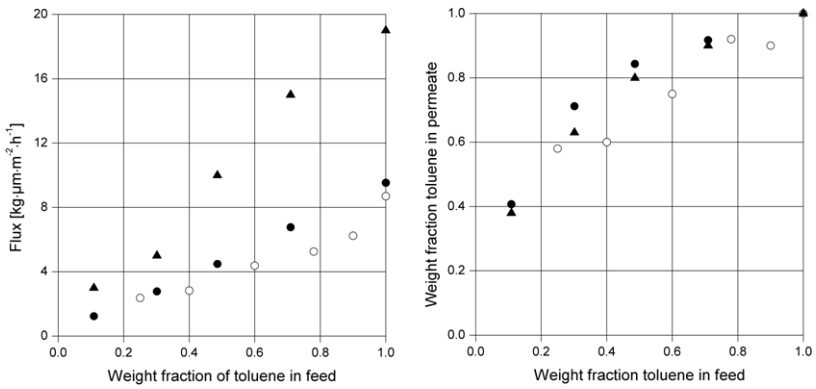


Figure 12: Pervaporation results for conditioned 6FDA-4MPD/6FDA-DABA 4:1 copolyimide membranes, 100% cross-linked with 1,4-butanediol (●) and 10% cross-linked with zircon(IV) acetylacetonate (○) and non cross-linked (▲) using a toluene/cyclohexane mixture at 60 °C. Permeate pressure was kept between 20 and 25 mbar.

much higher than the fluxes of the covalently and the ionically cross-linked membranes. In addition, it can be seen that the separation properties of the ionically cross-linked 6FDA-4MPD/6FDA-DABA 4:1 membrane is significantly lower, especially at higher aromatic feed concentrations compared to the covalently cross-linked membrane and the non cross-linked membrane.

From the experiments it can be concluded that conditioning of the membrane material is favourable since the flux can be increased without a loss in selectivity. It can be also seen that cross-linking is not necessary for the aromatic/aliphatic separation at moderate temperatures, e.g. 60 °C, but it presumably will increase the life time of the membrane with respect to the proposed hybrid process shown in Figure 9. It is obvious that if a 50:50 aromatic/aliphatic mixture is treated with a membrane unit (as shown in Figure 9), this could lead according to the results presented in Figure 12 to a 90% aromatics containing stream on the back side of the membrane. As a result the stream to the extraction column can be reduced by half, with a reduction of both extracting solvents and energy.

Natural gas treatment

In the area of natural gas treatment a number of different applications are of great interest. In tertiary oil production supercritical CO_2 is introduced into the oil field, especially if the oil is distributed in porous layers. As shown in Figure 13, the stream coming out of the oil field then contains the crude oil as well as gaseous compounds e.g. natural gas, higher hydrocarbons, H_2S and a small amount of water. However, it is important to hold back the CO_2 present in this stream because it is well known that CO_2 is one of various compounds responsible for the greenhouse effect. Figure 13 shows how a membrane unit can be implemented in such a process, so that the CO_2 is removed through the membrane and can then be re-used after compression. With this process not only could the emission of CO_2 be drastically reduced but also the natural gas can be recovered in this case instead of burning it which is generally carried out if the quantity and quality are too low.

Another very interesting application is the treatment of natural gas in offshore deposits. So far a huge number of gas resources are known worldwide, which cannot be exploited because of the high CO_2 content and the high pressure of the mixture. For economic reasons more and more membrane based processes in natural gas treatments are operated with polyimides as the membrane material instead of cellulose derivatives, since the intrinsic transport properties for the polyimides are much better. However, strong plasticization effects occur with non cross-linked polyimides generally at 10–20 bar partial CO_2 pressure in the feed. Therefore, in this context cross-linkable copolyimides are of interest because they offer plasticization resistance up to much higher CO_2 pressures and, in addition, they have better chemical resistance. In Figure 14 the higher plasticization resistance of cross-linked copolyimides compared to

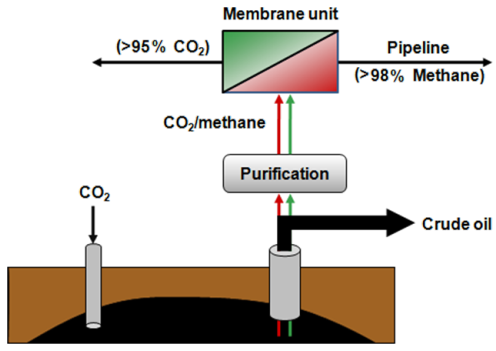


Figure 13: Hybrid process for the removal of CO_2 in tertiary oil production processes.

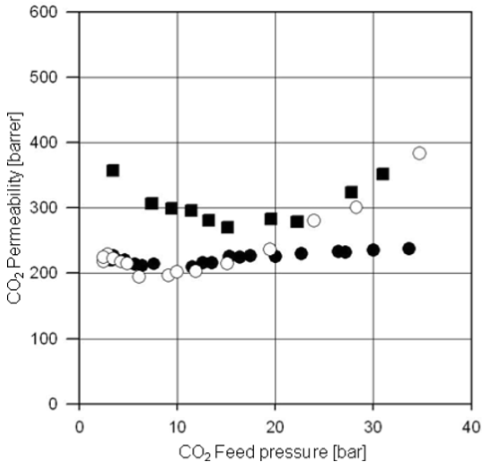


Figure 14: Pure CO_2 permeabilities at 35 °C for the 6FDA-4MPD (■), the 6FDA-4MPD/6FDA-DABA 4:1 copolyimide ionically cross-linked with aluminium acetylacetonate (○) and covalently cross-linked with ethylene glycol (●).

non cross-linked polyimides is illustrated. Plasticization resistance for different cross-linked copolyimides (covalently versus ionically) has been investigated in order to ascertain the most suitable cross-linking technique for this particular application.

It can be seen that the non cross-linkable reference polyimide, 6FDA-4MPD indeed starts plasticizing at a pure CO_2 pressure of approximately 15 bar. The plasticization is indicated by a large increase in permeability caused by increasing segmental motion of the polymer chains. Figure 14 shows that the ionically cross-linked material also plasticizes at very low CO_2 pressures whereas the covalently cross-linked membrane is resistant to plasticization up to a CO_2 pressure of approximately 30 bar. Similar effects have been found for different copolyimide structures [40].

It is assumed that ionic cross-linking leads to a much lower plasticization resistance compared to covalent cross-linking because ionic aggregates are formed due to electrostatic interactions, in this case between aluminium cations and carboxylate anions. Thus, heterogeneous regions with ionic and non-ionic domains are produced. The non-ionic regions consist mainly of polymer chains which are sensitive to plasticization in the presence of strong plasticization agents such as CO_2. Another plausible reason might be that the CO_2 with its strong solvation effect is able to weaken the ionic interactions in the ionic regions.

In Table 2 pure CO_2 permeabilities and ideal CO_2/CH_4 selectivities, which are the ratio of pure gas permeabilities, are reported for experiments performed at 10 bar feed pressure and 35 °C. Compared to the reference polyimide 6FDA-4MPD, the modified but non cross-linked 6FDA-4MPD/6FDA-DABA 4:1 copolyimide shows a much lower permeability but higher selectivity. The lower permeability results because the DABA in the polymer structure provides a much lower free volume than the 4MPD. With both cross-linked versions of the 6FDA-4MPD/6FDA-DABA 4:1, the permeability can be increased whereas the selectivity is not changed significantly compared to the non cross-linked 4:1 copolyimide. However, the ideal selectivities obtained with the different cross-linked 6FDA-4MPD/6FDA-DABA 4:1 copolyimides are not high enough to be commercially attractive. It should be noted that these are ideal selectivities and often the selectivities obtained with feed mixtures are even lower due to the fact that the diffusivity of the individual components are influenced by each other. This leads to effects where the slower permeating component is accelerated whereas the faster permeating component is slowed down.

In order to increase the selectivity the basic polymer structure was slightly modified. Thus, part of the 4MPD was substituted by the 6FpDA which is well known for both its high selectivity and high permeability due to the $–CF_3$ groups, which being bulky groups cause restricted rotation around the main polymer chain and also provide a high free volume.

In Figure 15 the mixed gas results obtained with a CO_2/CH_4 feed mixture at 35 °C are presented for the 6FDA-6FpDA/6FDA-4MPD/6FDA-DABA 3:1:1 cross-linked covalently with ethylene glycol and the ionically cross-linked with aluminium acetylacetonate. The results mirrored those found for the 4:1 copolyimide. The ionically cross-linked structure began to plasticize very early (approximately at a CO_2 partial pressure of 20 to 25 bar), whereas the ethylene glycol cross-linked structure shows nearly constant permeability and a selectivity which is

Table 2: CO_2 Permeability for different copolyimides at 35 °C and 10 bar feed pressure.

Polymer	$P(CO_2)$ [Barrer]	$\alpha^* = P(CO_2)/P(CH_4)$
6FDA-4MPD	300.0	15.6
6FDA-4MPD/6FDA-DABA 4:1	129.3	23
6FDA-4MPD/6FDA-DABA 4:1(covalently cross-linked)	221.1	23
6FDA-4MPD/6FDA-DABA 4:1 (ionically cross-linked)	200.5	20

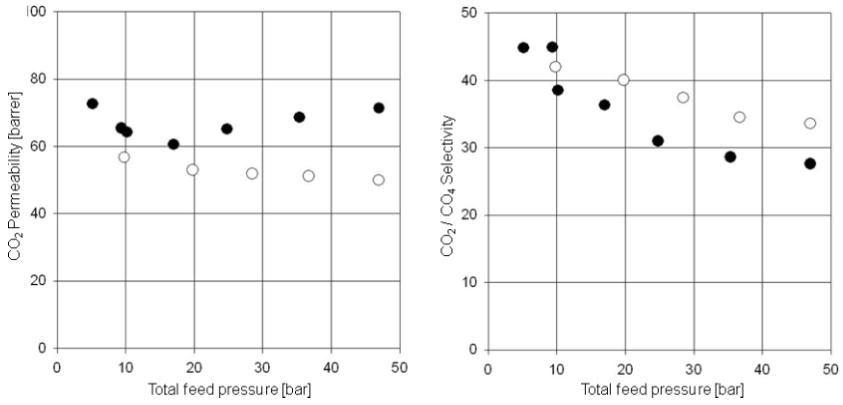


Figure 15: CO_2/CH_4 separation characteristics for the 6FDA-4MPD/6FDA-DABA 4:1 copolyimide ionically cross-linked with aluminium acetylacetonate (●) and covalently cross-linked with ethylene glycol (○) at 35 °C using a 50:50 CO_2/CH_4 feed gas mixture.

approximately 20% higher than the selectivity achieved with the ionically cross-linked structure. From the separation diagram it is also obvious that the selectivity is dependent on the feed pressure. With increasing feed pressure the usual decrease in selectivity was found, which is due to the interactions between the single components in the feed mixture as previously discussed. However, the modified polymer structure shows good selectivity for CO_2 over methane between 30 and 40, which indeed is attractive for commercial applications because it is much higher than the separation factors of the cellulose derivatives in current use.

Conclusion

It has been shown for the separation of high-pressure mixtures of CO_2/CH_4 as well as propylene/propane mixtures that the prepared cross-linked copolyimide membranes are much more plasticization resistant than non cross-linkable polyimide membranes used as reference substances. In the separation of aromatic/aliphatic mixtures, it was found that with conditioning, high fluxes combined with high selectivities can be achieved, e.g., with a 50:50 toluene/cyclohexane mixture a toluene concentration in permeate of approximately 85% can be reached. In the propylene/propane separation a 50:50 feed mixture could be concentrated to more than 90% propylene in permeate with a covalently cross-linked copolyimide structure of 6FDA-4MPD/6FDA-DABA 4:1. It was found that in the pressure range investigated (up to 4.2 bar) no plasticization was found with the cross-linked structures, whereas for the non cross-linked structure plasticization starts at a very low feed pressure of around 2 bar.

For the removal of CO_2 from natural gas, experiments with different cross-linked membranes showed that the covalently cross-linked copolyimide structure shows a much higher plasticization resistance and better selectivity in mixed gas experiments compared to the ionically cross-linked structures.

References

1. Ullman's Encyclopedia of Industrial Chemistry. *C. Judson King University of California;* Wiley-VCH Verlag GmbH & Co. KGaA: Berkeley, 2002.
2. Davis, J. C.; Valus, R. J.; Eshragi, R.; Velikoff, A. E. *Sep. Sci. Technol.* **1993,** *28,* 463–476. doi:10.1080/01496399308019500
3. Strathmann, H. *AIChE J.* **2001,** *47,* 1077–1087. doi:10.1002/aic.690470514
4. Ohlrogge, K.; Stürken, K. In *The separation of organic vapors from gas streams by means of membrane technology, Membrane technology in the chemical industry;* Nunez, S. P.; Peinemann, K.-V., Eds.; Wiley-VCH: Weinheim, 2001.
5. Baker, R. W. *Ind. Eng. Chem. Res.* **2002,** *41,* 1393–1411. doi:10.1021/ie0108088
6. http://www.borsig-china.com/#productrecovery.
7. http://www.sulzerchemtech.com.
8. Graham, T. *Phil. Trans./Ann. Chem. Pharm.* **1867,** *1* (Suppl. V).
9. Xiao, Y.; Low, B. T.; Hosseini, S. S.; Chung, T. S.; Paul, D. R. *Prog. Polym. Sci.* **2009,** *34,* 561–580. doi:10.1016/j.progpolymsci.2008.12.004
10. Maier, G. *Angew. Chem., Int. Ed.* **1998,** *37,* 2960–2974. doi:10.1002/(SICI)1521-3773(19981116)37:21<2960::AID-ANIE2960>3.0.CO;2-5
11. Koros, W. J.; Mahajan, R. *J. Membr. Sci.* **2000,** *175,* 181–196. doi:10.1016/S0376-7388(00)00418-X
12. Lin, L.; Kong, Y.; Yang, J.; Shi, D.; Xie, K.; Zhang, Y. *J. Membr. Sci.* **2007,** *298,* 1–13. doi:10.1016/j.memsci.2007.03.052
13. Lipnizki, F.; Field, R. W.; Ten, P. K. *J. Membr. Sci.* **1999,** *153,* 183–210. doi:10.1016/S0376-7388(98)00253-1
14. Robeson, L. M. *J. Membr. Sci.* **1991,** *62,* 165–185. doi:10.1016/0376-7388(91)80060-J
15. Stern, S. A. *J. Membr. Sci.* **1994,** *94,* 1–65. doi:10.1016/0376-7388(94)00141-3
16. Robeson, L. M. *J. Membr. Sci.* **2008,** *320,* 390–400. doi:10.1016/j.memsci.2008.04.030

17. Ohya, H.; Kudryavtsev, V. V.; Semenova, S. I., Eds. *Polyimide Membranes – Applications, Fabrications and Properties;* Gordon and Breach Publishers, 1996.
18. Tanaka, K.; Okano, M.; Kita, H.; Okamoto, K.-i.; Nishi, S. *Polym. J.* **1994,** *26,* 1186–1189. doi:10.1295/polymj.26.1186
19. Coleman, M. R.; Koros, W. J. *J. Membr. Sci.* **1990,** *50,* 285–297. doi:10.1016/S0376-7388(00)80626-2
20. Mikawa, M.; Nagaoka, S.; Kawakami, H. *J. Membr. Sci.* **1999,** *163,* 167–176. doi:10.1016/S0376-7388(99)00165-9
21. Lin, W.-H.; Chung, T.-S. *J. Membr. Sci.* **2001,** *186,* 183–193. doi:10.1016/S0376-7388(01)00333-7
22. Tanaka, K.; Kita, H.; Okano, M.; Okamoto, K.-i. *Polymer* **1992,** *33,* 585–592. doi:10.1016/0032-3861(92)90736-G
23. Staudt-Bickel, C.; Koros, W. J. *J. Membr. Sci.* **1999,** *155,* 145–154. doi:10.1016/S0376-7388(98)00306-8
24. Wessling, M.; Schoeman, S.; van der Boomgaard, T.; Smolders, C. A. *Gas Sep. Purif.* **1991,** *5,* 222–228. doi:10.1016/0950-4214(91)80028-4
25. Staudt-Bickel, C.; Koros, W. J. *J. Membr. Sci.* **2000,** *170,* 205–214. doi:10.1016/S0376-7388(99)00351-8
26. Kim, J. H.; Koros, W. J.; Paul, D. R. *J. Membr. Sci.* **2006,** *282,* 21–31. doi:10.1016/j.memsci.2006.05.004
27. Schiewe, B.; Staudt-Bickel, C.; Vuin, A.; Wegner, G. *ChemPhysChem* **2001,** *2,* 211–218. doi:10.1002/1439-7641(20010417)2:4<211::AID-CPHC211>3.0.CO;2-F
28. Jizhong, R.; Staudt-Bickel, C.; Lichtenthaler, R. N. *Sep. Purif. Technol.* **2001,** *22–23,* 31–43. doi:10.1016/S1383-5866(00)00155-6
29. Inui, K.; Noguchi, T.; Miyata, T.; Uragami, T. *J. Appl. Polym. Sci.* **1999,** *71,* 233–241. doi:10.1002/(SICI)1097-4628(19990110)71:2<233::AID-APP6>3.0.CO;2-M
30. Cao, B.; Hinode, H.; Kajiuchi, T. *J. Membr. Sci.* **1999,** *156,* 43–47. doi:10.1016/S0376-7388(98)00327-5
31. Fang, J.; Tanaka, K.; Kita, H.; Okamoto, K. *Polymer* **1999,** *40,* 3051–3059. doi:10.1016/S0032-3861(98)00523-0
32. *AICHE Annual Meeting,* Los Angeles, CA, Nov 16–21, 1997; 1997.
33. Matsui, S.; Paul, D. R. *J. Membr. Sci.* **2002,** *195,* 229–245. doi:10.1016/S0376-7388(01)00560-9
34. Rezac, M. E.; Sorensen, E. T.; Beckman, H. W. *J. Membr. Sci.* **1997,** *136,* 249–259. doi:10.1016/S0376-7388(97)00170-1
35. Rezac, M. E.; Schoberl, B. *J. Membr. Sci.* **1999,** *156,* 211–222. doi:10.1016/S0376-7388(98)00346-9
36. Bos, A.; Punt, I. G.; Wessling, M.; Strathmann, H. *J. Polym. Sci., Polym. Phys. Ed.* **1998,** *36,* 1547.
37. McCaig, M. S.; Paul, D. R. *Polymer* **1999,** *40,* 7209–7225. doi:10.1016/S0032-3861(99)00125-1
38. Wright, C. T.; Paul, D. R. *J. Membr. Sci.* **1997,** *124,* 161–174. doi:10.1016/S0376-7388(96)00215-3
39. Kita, H.; Inada, T.; Tanaka, K.; Okamoto, K.-i. *J. Membr. Sci.* **1994,** *87,* 139–147. doi:10.1016/0376-7388(93)E0098-X
40. Wind, J. D.; Staudt-Bickel, C.; Koros, W. J.; Paul, D. R. *Ind. Eng. Chem. Res.* **2002,** *41,* 6139–6148. doi:10.1021/ie0204639
41. Pithan, F.; Staudt-Bickel, C.; Heß, S.; Lichtenthaler, R. N. *ChemPhysChem* **2002,** *3,* 856–862. doi:10.1002/1439-7641(20021018)3:10<856::AID-CPHC856>3.0.CO;2-H
42. Funke, H. Sorption von Reingasen in Polymeren und an Zeolithen bei Drücken. Ph.D. Thesis, University of Heidelberg, Germany, 1991.
43. Cen, Y.; Staudt-Bickel, C.; Lichtenthaler, R. N. *J. Membr. Sci.* **2002,** *206,* 341–349. doi:10.1016/S0376-7388(01)00767-0
44. Ito, A.; Hwang, S.-T. *J. Appl. Polym. Sci.* **1989,** *38,* 483–490. doi:10.1002/app.1989.070380308
45. Tanaka, K.; Taguchi, A.; Hao, J.; Kita, H.; Okamoto, K. *J. Membr. Sci.* **1996,** *121,* 197–207. doi:10.1016/S0376-7388(96)00182-2
46. Shimazu, A.; Ikeda, K.; Hachisuka, H. Method of selectively separating unsaturated hydrocarbon.. U.S. Patent 5 749,943, Dec 5, 1998.
47. Lee, K. R.; Hwang, S.-T. *J. Membr. Sci.* **1992,** *73,* 37–45. doi:10.1016/0376-7388(92)80184-L
48. Krol, J. J.; Boerrigter, M.; Koops, G. H. *J. Membr. Sci.* **2001,** *184,* 275–286. doi:10.1016/S0376-7388(00)00640-2
49. Shimazu, A.; Miyazaki, T.; Maeda, M.; Ikeda, K. *J. Polym. Sci., Part B: Polym. Phys.* **2000,** *38,* 2525–2536. doi:10.1002/1099-0488(20001001)38:19<2525::AID-POLB40>3.0.CO;2-2

License and Terms

This is an Open Access article under the terms of the Creative Commons Attribution License (http://creativecommons.org/licenses/by/2.0), which permits unrestricted use, distribution, and reproduction in any medium, provided the original work is properly cited.

The license is subject to the *Beilstein Journal of Organic Chemistry* terms and conditions: (http://www.beilstein-journals.org/bjoc)

The definitive version of this article is the electronic one which can be found at: doi:10.3762/bjoc.6.86

Beilstein Journal of Organic Chemistry

Conjugated polymers containing diketopyrrolopyrrole units in the main chain

Bernd Tieke*, A. Raman Rabindranath, Kai Zhang and Yu Zhu

Review

Open Access

Address:
Department of Chemistry, University of Cologne, D-50939 Cologne, Germany

Email:
Bernd Tieke* - tieke@uni-koeln.de

* Corresponding author

Keywords:
conjugated polymer; diketopyrrolopyrrole; electroluminescence; photoluminescence; solar cell

Beilstein J. Org. Chem. **2010,** *6,* 830–845.
doi:10.3762/bjoc.6.92

Received: 21 May 2010
Accepted: 09 August 2010
Published: 31 August 2010

Guest Editor: H. Ritter

© 2010 Tieke et al; licensee Beilstein-Institut.
License and terms: see end of document.

Abstract

Research activities in the field of diketopyrrolopyrrole (DPP)-based polymers are reviewed. Synthetic pathways to monomers and polymers, and the characteristic properties of the polymers are described. Potential applications in the field of organic electronic materials such as light emitting diodes, organic solar cells and organic field effect transistors are discussed.

Introduction

A useful strategy in the design of new polymers for electronic applications is to incorporate chromophores which are highly absorbing and emitting in the visible and near infrared region into π-conjugated polymers chains. Potentially useful chromophores for electronic applications can be found among the various organic colourants, especially in the field of so-called "high-performance pigments" developed in the last two or three decades [1]. Among these pigments are 2,5-diketopyrrolo-[3,4-c]pyrrole (DPP) derivatives, which were commercialized in the 1980s [2,3]. DPPs are the subject of many patents, despite the fact that for a considerable time there were only a few publications that dealt with these compounds.

In recent years, a growing number of polymer chemists and physicists have become interested in DPPs since it was shown that DPP-containing polymers exhibit light-emitting and photovoltaic properties. The purpose of the present article is to review recent activities regarding the deeply coloured, and in many cases, fluorescing polymers. Synthetic pathways, characteristic properties, and possible applications are described.

Review

DPP-based monomers

After the 3,6-diphenyl-substituted DPP (diphenylDPP) (Figure 1) was first synthesized in low yield by Farnum et al. in 1974 [4], Iqbal, Cassar, and Rochat reported an elegant synthetic pathway for DPP derivatives in 1983 [5,6]. It was discovered that DPP derivatives could be prepared in a single reaction step in high yield by the reaction of benzonitrile (or other aromatic nitriles) with succinic acid diesters. Numerous DPP derivatives have since been synthesized, their colours ranging from orange yellow via red to purple. Many DPP derivatives

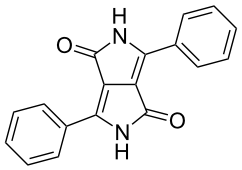


Figure 1: Structure of 3,6-diphenyl-substituted 2,5-diketopyrrolo-[3,4-c]pyrrole (DPP).

exhibit a high photostability in the solid state, weather fastness, deep colour, luminescence with large Stokes-shifts, and a brilliant red colour enabling technical applications in colouring of fibers, plastics and surface coatings such as prints or inks.

The electron-withdrawing effect of the lactam units causes the chromophore to have a high electron affinity. Strong hydrogen bonding between the lactam units favors the chromophores forming physically cross-linked chain structures in the solid state, which is the origin for the poor solubility [7,8]. Short distances between the chromophore planes (0.336 nm) and phenyl ring planes (0.354 nm) enable π-π-interactions via molecular orbital overlapping and excition coupling effects [7-9], whilst electronic interactions and strong intermolecular forces lead to a high thermal stability of up to 500 °C.

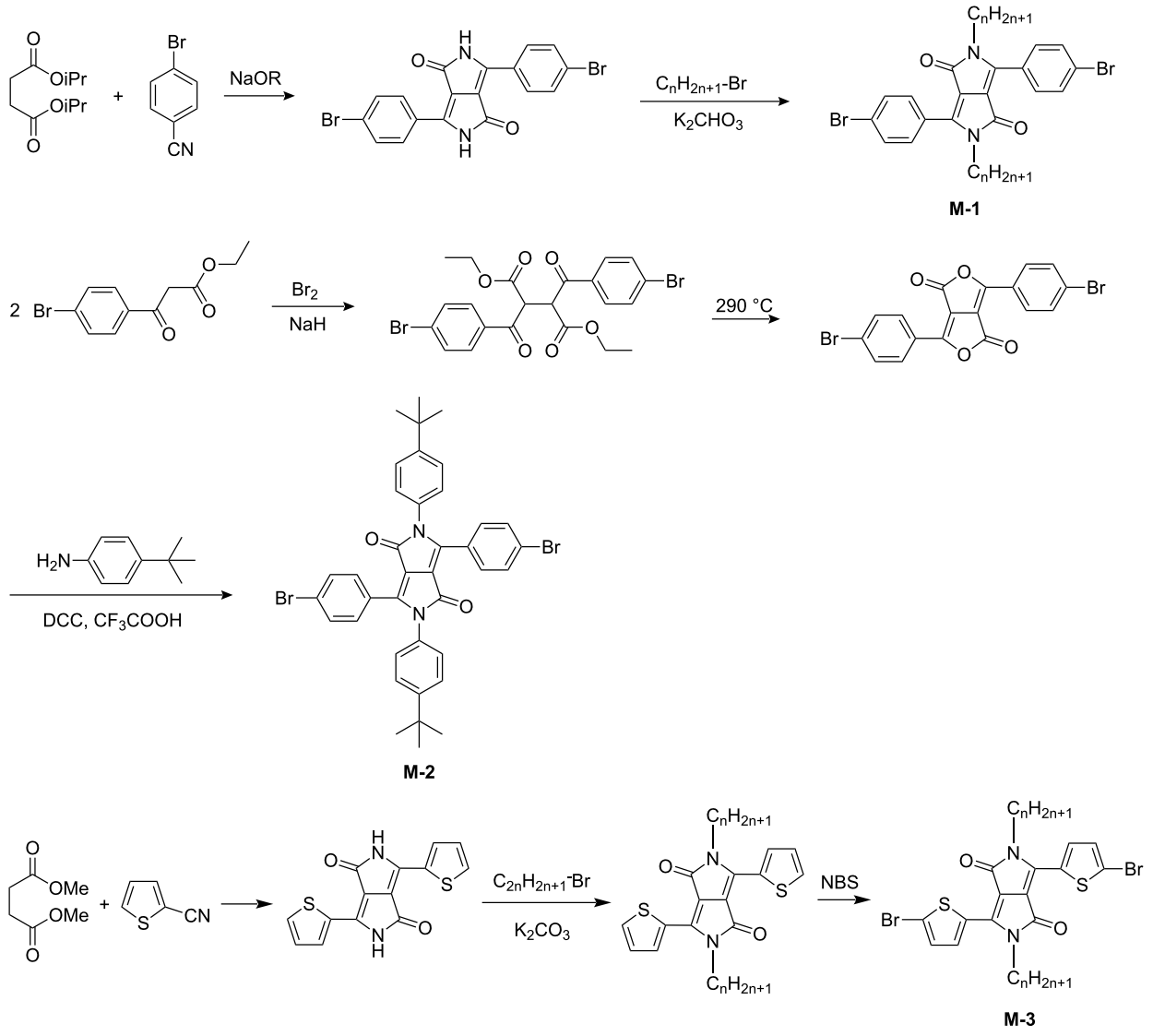
For chemical incorporation into conjugated polymers, the solubility of the DPP compound needs to be increased, and the chromophore requires to be functionalized with polymerizable groups. The solubility can be increased by *N*-alkylation [10], arylation [11] or acylation [12] of the lactam units thus preventing hydrogen bond formation between the chromophores. Polymerizable groups can be attached to the aryl units in the 3- and 6-positions of the central DPP chromophore [13], or to the lactam substituent groups [14,15]. Suitable polymerizable groups are halogen atoms (especially bromine and iodine), hydroxyl, trifluoromethylsulfonate, or aldehyde groups. Synthetic strategies recently described are outlined in Scheme 1. For the preparation of brominated diphenyl-DPPs it is necessary to start from bromobenzonitrile and a succinic acid ester and to prepare first the dibromophenyl-DPP pigment, which is subsequently N-alkylated to yield the soluble dibromodialkyl-DPP monomer **M-1**. While the N-alkylation of DPP proceeds directly in good yield, the introduction of aryl units in most cases requires a specific synthetic pathway. First, the corresponding diketofurofuran (lactone) compound has to be synthesized [11]. The lactone is subsequently converted into the N-aryl-lactam **M-2** by reaction with an arylamine. The bromination of aryl units is important for the subsequent palladium-catalyzed coupling reaction. If the aryl unit is thiophene, direct bromination with N-bromosuccinimide is possible to yield monomer **M-3** [16].

For the preparation of conjugated DPP-based polymers, palladium-catalyzed polycondensation reactions such as Suzuki [17], Stille [18] and Heck [19] coupling are especially useful. Other suitable reactions are Ni-mediated Yamamoto coupling [20], Sonogashira coupling [21], or electrochemical polymerization [22]. In the following, a brief review of recently prepared DPP based polymers is presented.

DPP-based polymers

The first DPP-based polymer was described by Yu et al. in 1993 [13]. Conjugated block copolymers containing phenylene, thienylene and N-alkyl substituted diphenyl DPP units in the main chain were synthesized by Stille coupling. Photorefractive polymers were prepared containing a conjugated main chain and nonlinear optically active (nlo) chromophores in the side chain. DPP was incorporated in the polymers as a sensitizer for charge carrier generation. Some years later, Eldin and coworkers described DPP-containing polymers obtained by radical polymerization of bis-acryloyl-substituted DPP derivatives [14,15]. Polymer networks containing non-conjugated, copolymerized DPP units were prepared, whilst linear DPP-containing polyesters and polyurethanes were first described by Lange and Tieke in 1999 [23]. The polymers were soluble and could be cast into orange films that exhibited a strong fluorescence with maxima at 520 nm and a large Stokes-shift of 50 nm. However, due to the aliphatic structure of the main chain, the thermal stability was rather poor. Photoluminescent polyelectrolyte-surfactant complexes were obtained from an amphiphilic, unsymmetrically substituted DPP-derivative upon complex formation with polyallylamine hydrochloride or polyethyleneimine [24]. The complexes exhibit a mesomorphous structure with the glass transition temperatures dependent on the structure of the polyelectrolyte.

The first synthesis of conjugated DPP-polymers and copolymers via Pd-catalyzed Suzuki coupling was reported by Tieke and Beyerlein in 2000 [25]. The polymers contained *N*-hexyl-substituted diphenylDPP units and hexyl-substituted 1,4-phenylene units in the main chain and molecular weights of up to 21 kDa were determined. Compared with the monomer, the optical absorption of the polymer in solution was bathochromically shifted by 12 nm with the maximum at 488 nm. The polymer also showed a bright red fluorescence with the maximum at 544 nm. In addition to the alternating copolymer, copolymers with lower DPP content were also prepared. All copolymers showed the DPP absorption at 488 nm, the ε-value being a linear function of the DPP content. Upon UV irradiation the copolymers gradually decomposed. The rate of



Scheme 1: Synthesis of DPP monomers.

photodecomposition was found to increase with decreasing DPP phenylene comonomer ratio. Two different photoprocesses were recognized: a slow process originating from the absorption of visible light by the DPP chromophore, and a rapid one arising from additional absorption of UV-light by the phenylene comonomer unit followed by energy transfer to the DPP chromophore. The actual mechanism of photodecomposition remains unclear. Comparative studies indicated that conjugated DPP-containing polymers are considerably more stable than the DPP monomers or non-conjugated DPP-polymers.

Dehaen et al. used a stepwise sequence of Suzuki couplings to prepare rod-like DPP-phenylene oligomers with well-defined lengths [26]. The resulting oligomers contained three, five and seven DPP units, respectively. Unfortunately, the effect of the chain length on absorption and emission behaviour was not reported. A study on thermomesogenic polysiloxanes containing DPP units in the main chain was published in 2002 [27]: Investigations on the thermotropic phase behaviour using polarizing microscopy revealed nematic and smectic enantiotropic phases. In the same year, the first study on electroluminescent (EL) properties of a DPP-containing conjugated polymer was reported by Beyerlein et al. [28] who studied a DPP-dialkoxyphenylene copolymer in a multilayer device of ITO/DPP-polymer/OXD7/Ca/-Mg:Al:Zn and observed a red emission with maximum at about 640 nm. A relevant plot of current density and light intensity vs. voltage is reproduced in Figure 2. DeSchryver et al. synthesized dendrimer macromole-

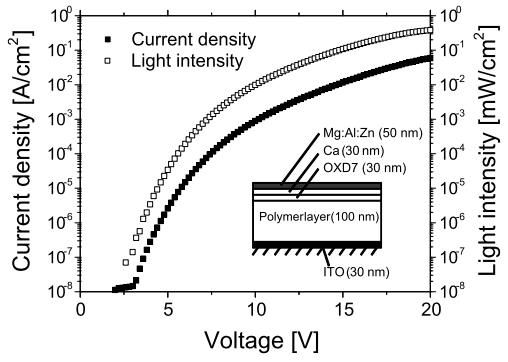
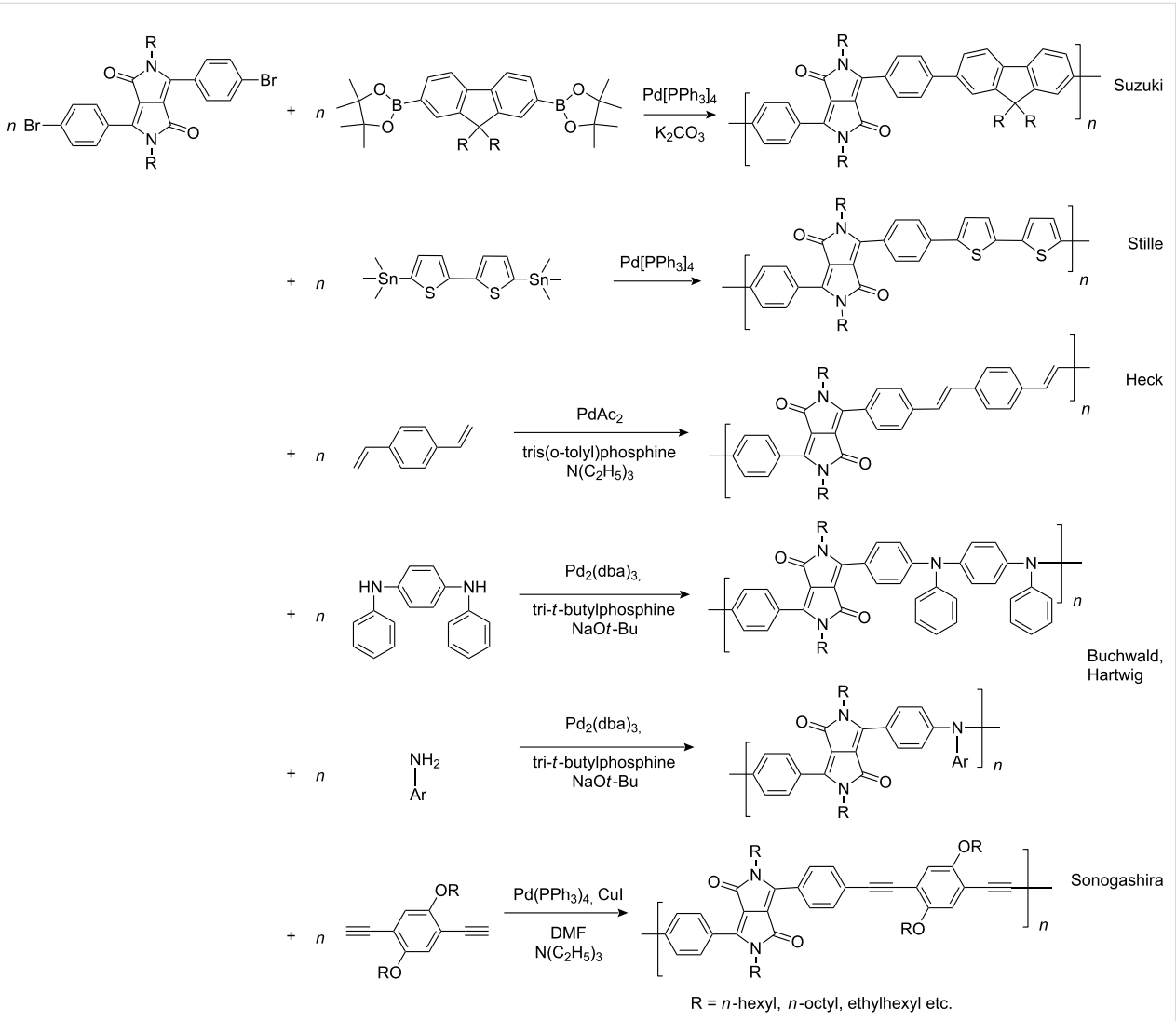


Figure 2: Plot of current density and light intensity versus voltage of polymer light-emitting diode containing **P-5**: ITO/**P-5**/OXD7/Ca/Mg:Al:Zn (from [28]).

cules with a DPP core [29]. Embedded in a spin-coated polystyrene film, single dendrimer molecules could be imaged via a confocal microscope by utilizing the strong fluorescence of the DPP core. It could be shown that the orientation of the absorption transition dipole of single dendrimer molecules in the film changed in a time window of seconds.

Recent work on diphenylDPP-based polymers

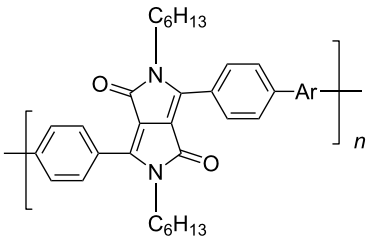
In recent years a number of studies were reported on synthesis, optical, electrochemical, and electroluminescent properties of conjugated DPP polymers. The polymers were prepared by Suzuki, Heck, and Stille coupling and other catalytic polycondensation reactions. Typical examples are shown in Scheme 2. Rabindranath et al. [30] synthesized a new DPP polymer consisting entirely of aryl-aryl coupled diphenyl-DPP units

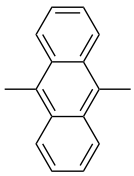
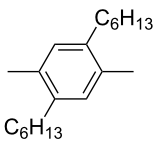
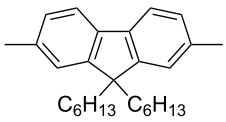
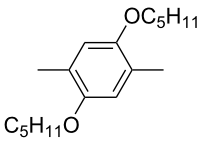
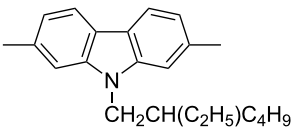
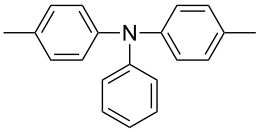
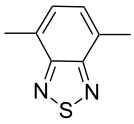


Scheme 2: Pd-catalyzed coupling reactions for preparation of DPP-containing polymers.

(poly-DPP, **P-1**, see Table 1). The polymer was prepared by three different reactions. Pd-catalyzed and Ni-mediated one-pot coupling reactions were carried out starting from dibrominated DPP **M-1** as the sole monomer as well as conventional Pd-catalyzed coupling of **M-1** and the 3,6-diphenyl(4,4′-bis(pinacolato)boron ester) derivative of DPP. The polymer exhibits a bordeaux-red colour in solution with absorption maxima of about 525 nm, and a purple luminescence with a maximum around 630 nm with a Stokes-shift of about 105 nm. Cyclovoltammetric studies indicated quasi-reversible oxidation and reduction behaviour, the band gap being about 2 eV. Characteristic properties of **P-1** are listed in Table 1. In a compre-

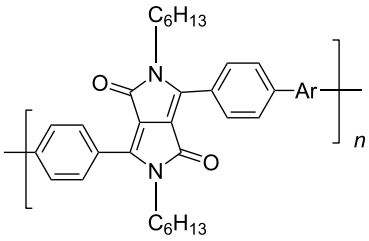
Table 1: List of diphenylDPP-based polymers prepared upon Suzuki coupling and their characteristic properties.

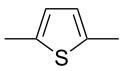
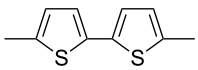
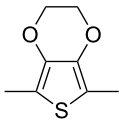
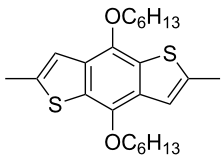
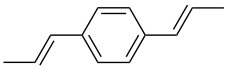
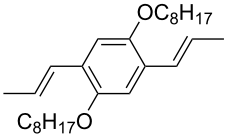
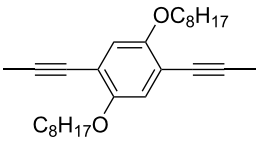


Polymer	Ar	UV [nm] in solution	PL [nm] in solution	PL quantum yield Φ	HOMO [eV]	LUMO [eV]	MW [kDa]	Ref.
P-1	none	528	631	0.13	−5.39	−3.46	8.7	30
P-2		479	552	0.79	−5.60	−3.30	6.0	31
P-3		488	544	0.62	−5.40	−3.40	24.0	25
P-4		500	574	0.79	−5.30	−3.60	20.0	31
P-5		503	565	0.72	−5.30	−3.50	21.0	28
P-6		506	585	0.46	−5.33	−3.43	15.5	31
P-7		511	587	0.85	−5.37	−3.55	7.4	31
P-8		515	600	0.19	−5.57	−3.57	7.0	31

hensive study, Zhu et al. prepared a number of highly luminescent DPP-based conjugated polymers [31]. The polymers consisted of dialkylated DPP units and carbazole, triphenylamine, benzo[2,1,3]thiadiazole, anthracene, or fluorene units in alternating fashion. They were prepared via Suzuki coupling, from the DPP monomers **M-1** or DPP-3,6-diphenyl(4,4′-bis(pinacolato)boron ester. A number of readily soluble polymers **P-2** to **P-8** exhibiting yellow to red absorption and emission colours, and fluorescence quantum yields of up to 86% were obtained. Characteristic properties are compiled in Table 1. Compared with the DPP monomers, the absorption of most of the polymers was bathochromically shifted by 24 to 39 nm. The small shift of **P-2** was ascribed to a large tilt angle between the π-planes of DPP and the adjacent comonomer units, in this case the anthracene unit, which strongly reduces the conjugation length [32]. EL devices prepared with **P-4** exhibited an external quantum efficiency (EQE) of 0.5% and a brightness at 20 V of 50 cd m^{-2} without much optimization. The maximum emission was at 600 nm, the turn-on voltage was 3.5 V. Cao et al. [33] prepared DPP-fluorene copolymers with a DPP content of between 0.1 and 50%. It was found that absorption and emission spectra, both in solution and thin film, varied regularly with the DPP content in the copolymers. On increasing the DPP content, the absorption only shifted by a few

Table 2: List of DPP-polymers prepared upon Stille, Heck and Sonogashira coupling and their characteristic properties.



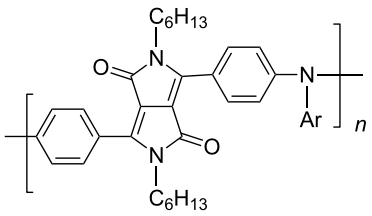
Polymer	Ar	UV [nm] in solution	PL [nm] in solution	PL quantum yield Φ	HOMO [eV]	LUMO [eV]	MW [kDa]	Ref.
P-9		545/558	635/704	0.13	−5.26	−3.69	12.2	36
P-10		558/570	616/699	0.15	−5.15	−3.68	9.1	36
P-11		560/581	624/723	0.36	−5.411	−3.65	6.7	36
P-12		539/563	-	-	−5.47	−3.74	9.7	51
P-13		529/539	598/685	0.23	−5.75	−3.51	31.0	36
P-14		540/553	617/726	0.31	−5.61	−3.45	-	52
P-15		510/525	585/649	0.66	−5.80	−3.68	-	52

nanometers to longer wavelengths, whereas the emission was bathochromically shifted by more than 40 nanometers. EL properties of the copolymers were also studied: With increasing DPP content the EL colours varied from orange to red corresponding to CIE coordinates from (0.52, 0.46) to (0.62, 0.37). The best performance was achieved for an orange emitting device with a copolymer containing only 1% DPP units. The EQE was 0.45%, the maximum brightness 520 cd m^{-2}. At high DPP content, the EQE was lowered to 0.14%, and the brightness to 127 cd m^{-2}, similar to the results reported by Zhu et al. [31]. Cao et al. [34] also studied DPP-fluorene alternating copolymers with the fluorene unit being attached to the *m*-position of the phenyl groups in DPP (in contrast to the usual *p*-position). While the optical properties were quite similar, the EL properties were inferior. This was ascribed to a reduced conjugation length in these polymers.

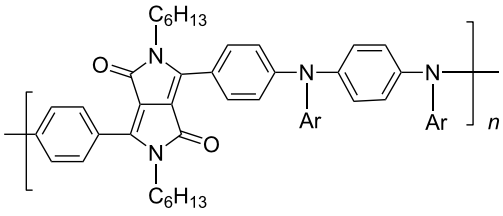
Novel vinyl ether-functionalized polyfluorenes for active incorporation in common photoresist materials were described by Kühne et al. [35] Among the polymers investigated was a diphenylDPP-fluorene copolymer, the fluorene units carrying ethyl vinylether groups in the 9,9´-position. The vinyl ether functionality allowed for active incorporation of the light emitting polymers into standard vinyl ether or glycidyl ether photoresist materials, the polymers retaining their solution fluorescence characteristics. This enabled photopatterning of light-emitting structures for application in UV-down-conversion, waveguiding, and laser media.

Using Stille coupling, Zhu et al. [36] first succeeded in the synthesis of copolymers **P-9** to **P-11** containing diphenylDPP and thiophene, bisthiophene, or 3,4-ethylenedioxythiophene (EDOT) units in alternating fashion (Table 2). Because of the strong donor-acceptor interaction between the thiophene and the DPP units, the absorption and emission maxima were shifted to longer wavelength: A solution of EDOT-DPP copolymer **P-11** exhibited a maximum absorption at 560 nm, and a solution-cast film of the same polymer had a λ_{max}-value of 581 nm. The band gaps were between 1.5 and 1.7 eV, i.e., considerably smaller than for the previously reported DPP-based polymers. The fluorescence quantum yields Φ of the copolymers were rather weak (Φ ~15–35%), the maximum appeared at about 700–720 nm in the solid state. By Heck coupling it was possible to synthesize a polyarylenevinylene-type polymer **P-13**, the arylene units alternatingly being phenylenevinylene and diphenylDPP (Table 2) [36]. The polymer was obtained upon Pd-catalyzed reaction of

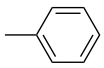
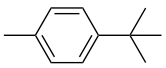
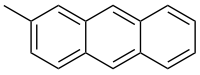
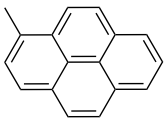
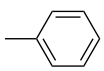
Table 3: List of DPP-based polyiminoarylenes and their characteristic properties [37].



I



II

Polymer	Ar	Type of polymer	UV [nm] in solution	PL [nm] in solution	PL quantum yield Φ	HOMO [eV]	LUMO [eV]	MW [kDa]
P-16		I	522/534	619/624	0.52	−5.24	−3.33	8.8
P-17		I	552/558	633/650	0.19	−5.41	−3.50	35.8
P-18		I	543/552	631/654	0.38	−5.41	−3.28	10.2
P-19		I	527/564	607	0.62	−5.24	−3.40	4.3
P-20		II	539/544	608	0.68	−5.06	−3.30	14.0

dibromoDPP derivatives such as **M-1** and divinylbenzene. The resulting polymer had a molecular weight of about 30 kDa, was readily soluble in common organic solvents and its solutions exhibited a bright red colour with red light emission.

A further study [37] focused on the incorporation of arylamine units in the main chain. Due to presence of electron-rich nitrogen atoms it was hoped that donor-acceptor interactions along the main chain would be enhanced and lead to a red-shift of the absorption and emission. Furthermore, the presence of easily oxidizable nitrogen in the main chain should give rise to a lower oxidation potential of the polymer. Relevant polymers **P-16** - **P-20** (Table 3) were synthesized using Pd-catalyzed aryl amination reactions as reported by Hartwig [38,39], Buchwald [40-42], and Kanbara [43-47]. As shown in Scheme 2, DPP monomers such as **M-1** were copolymerized with primary or

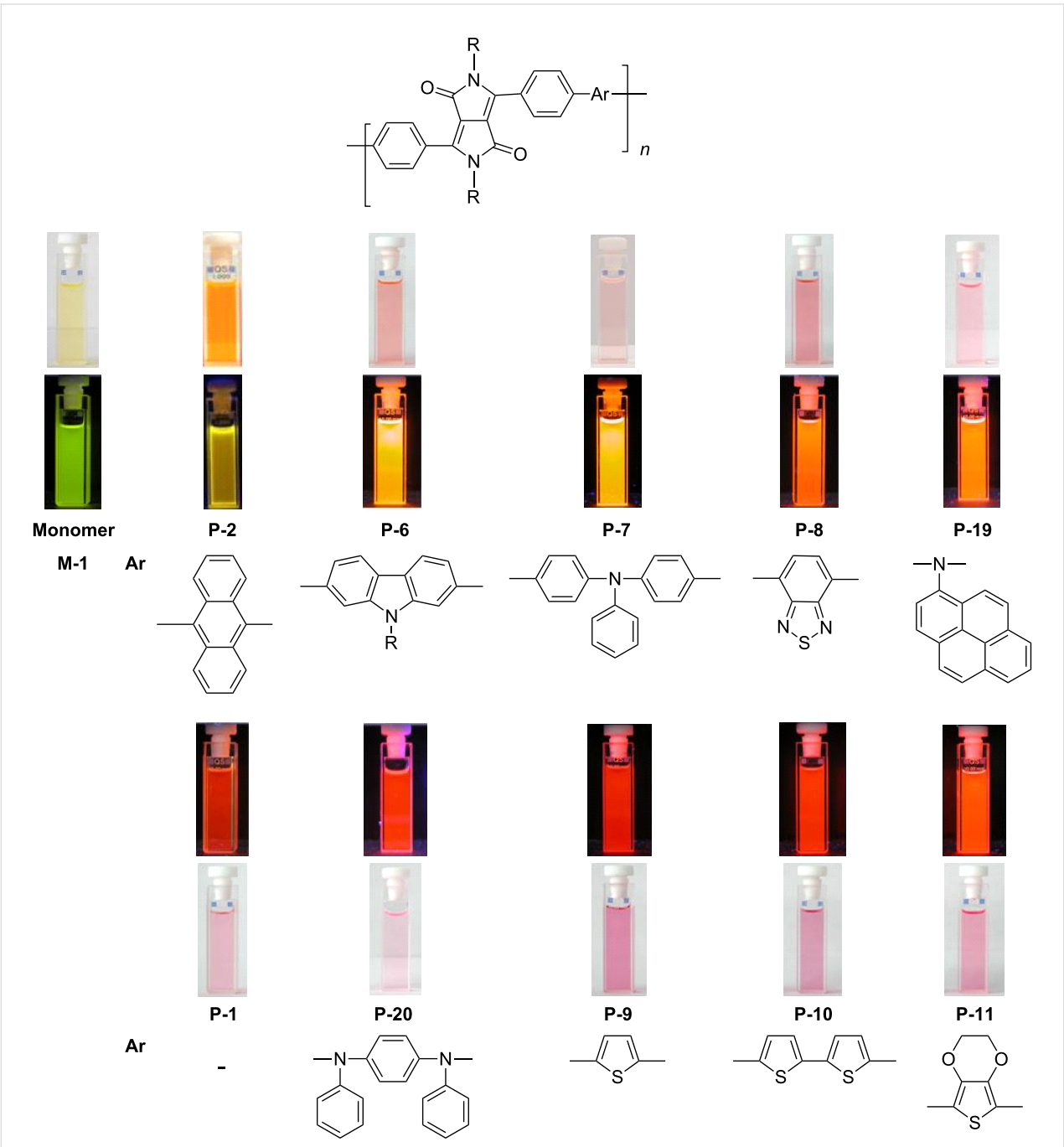


Figure 3: Optical properties of some diphenylDPP-based conjugated polymers.

secondary arylamines to yield DPP-containing polyiminoarylenes. The solutions of the polymers in chloroform exhibited a purple red colour with absorption maxima between 530 and 550 nm, and emission maxima from 610 to 630 nm. Fluorescence quantum yields were moderate (20 to 60%) (see also Table 3). The nitrogen atoms in the backbone lower the band gap of the polymers to approximately 1.9 eV. The band gaps are lower than for the conjugated DPP-arene copolymers prepared

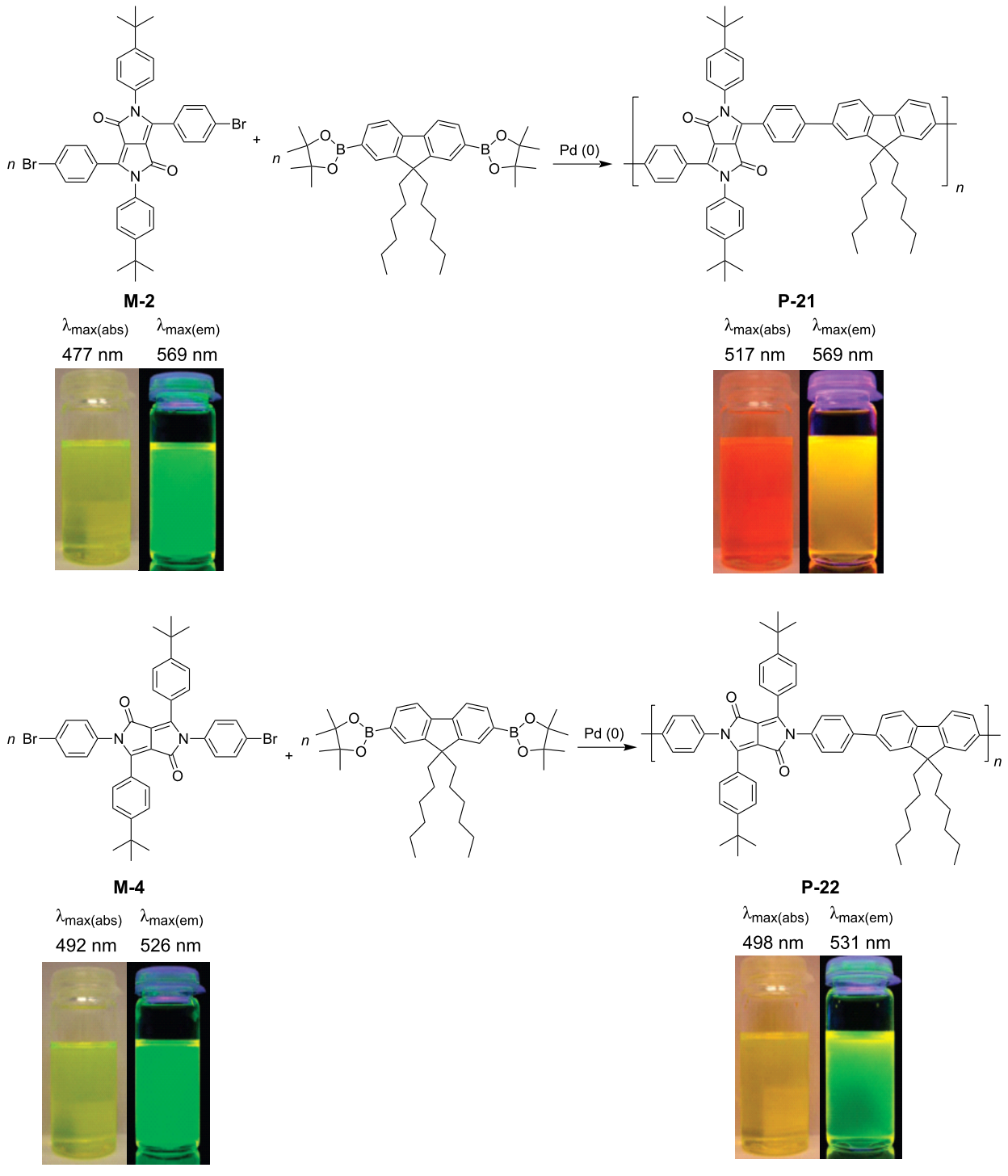


Figure 4: Optical properties of copolymers **P-21** and **P-22** based on two isomeric diphenylDPP monomer units (from [48]).

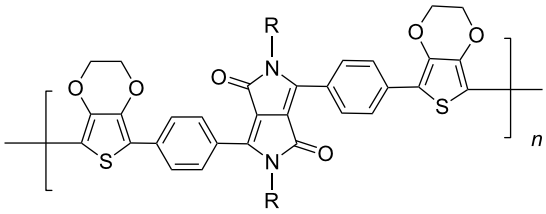
upon Suzuki coupling [31] but higher than for the DPP-thiophene copolymers made by Stille coupling [36]. Except for **P-16** and **P-18**, the polymers exhibit quasi reversible oxidation behaviour. A spectroelectrochemical study revealed that some of the polymers exhibited a reversible colour change between purple in the neutral state and a transparent greenish grey in the oxidized state. The electrochromism was very pronounced for **P-19** and **P-20**. Typical absorption and emission colours of several DPP-containing conjugated polymers are shown in Figure 3.

The synthesis of *N*-arylated diphenylDPP derivatives (also denoted as 2,3,5,6-tetraarylated DPP derivatives) such as **M-2** requires a different synthetic pathway outlined in Scheme 1. Direct *N*-arylation of the lactam group of DPP is only possible for activated arene units containing trifluoromethyl or nitro substituent groups. The common synthetic pathway first requires the synthesis of a diphenyldiketofurofuran derivative, which subsequently is reacted with an arylamine to yield the desired tetraarylated DPP derivative [11]. Using this approach, Zhang and Tieke [48] were able to prepare the two isomeric monomers **M-2** and **M-4** and their corresponding alternating copolymers **P-21** and **P-22** containing fluorene as the comonomer unit. While the properties of the two monomers are very similar, the optical and electrochemical properties of the two isomeric polymers are quite different. Suzuki coupling of **M-2** and a fluorene diboron ester derivative resulted in polymer **P-21** with fully conjugated main chain, the absorption being shifted by 15–25 nm compared with the monomer (Figure 4). The same coupling reaction of **M-4** resulted in polymer **P-22**, its π-conjugation being interrupted at the *N*-lactam units. Consequently, the absorption and emission behaviour were not much different from the corresponding monomer, the band gaps of the two isomers being 2 and 2.3 eV, respectively. The absorption and emission colours are shown in Figure 4.

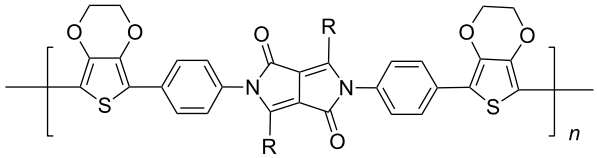
Stille coupling of **M-1** and 2-(tributylstannyl)-3,4-ethylenedioxythiophene gave the corresponding bis(thienyl)-substituted monomer [49]. Due to presence of the EDOT units, the monomer exhibited a rather low oxidation potential and could be easily electropolymerized by anodic oxidation. An insoluble, non-luminescent polymer film formed at the electrode that exhibited reversible electrochromic properties (Table 4). The film could be switched from blue in the neutral state via transparent grey to purple red in the oxidized state. The stability of the film was good, the switching could be repeated many times retaining 96% of the original absorption intensity after 100 cycles, without any protection against air or moisture. K. Zhang et al. [52] continued the studies and converted isomeric monomers **M-2** and **M-4** into corresponding bis-EDOT-substituted monomers. Both monomers could be electropolymerized, but the optical and electronic properties differed greatly between the two polymers. The polymers with EDOT-phenyl groups in the 3- and 6-positions (structure I in Table 4) represent conjugated polymers with low oxidation potentials and reversible electrochromic properties whereas the polymer with EDOT-phenyl groups in the 2- and 5- positions (structure II in Table 4) is non-conjugated, possesses a high oxidation potential and is not electrochromic (Figure 5).

Our activities have stimulated several other groups to synthesize diphenylDPP-containing conjugated polymers and to investigate their potential use in optoelectronic devices. Kanimozhi et al. [51] prepared alternating copolymers of diphenylDPP and 4,8-dihexylbenzo[1,2-b;3,4-b]dithiophene (**P-12**, Table 2) by Stille coupling and studied their optical and

Table 4: List of DPP-polymers prepared upon electrochemical polymerization.



I



II

Polymer	Type	R	λ_{max} of film [nm]	Half-wave oxidation potentials [V] E_1	E_2	E_3	E_4	HOMO [eV]	LUMO [eV]	Ref.
P-23	I	*n*-hexyl	626	0.15	0.46	-	−1.70	−4.85	−3.39	49
P-24	I	(2-hexyl)decyl	588	0.28	0.54	0.97	−1.59	−4.88	−3.32	50
P-25	I	4-*t*-butylphenyl	648	0.21	0.50	-	−1.52	−4.85	−3.48	50
P-26	II	4-*t*-butylphenyl	510	1.61	-	-	-	−6.21	−2.89	50

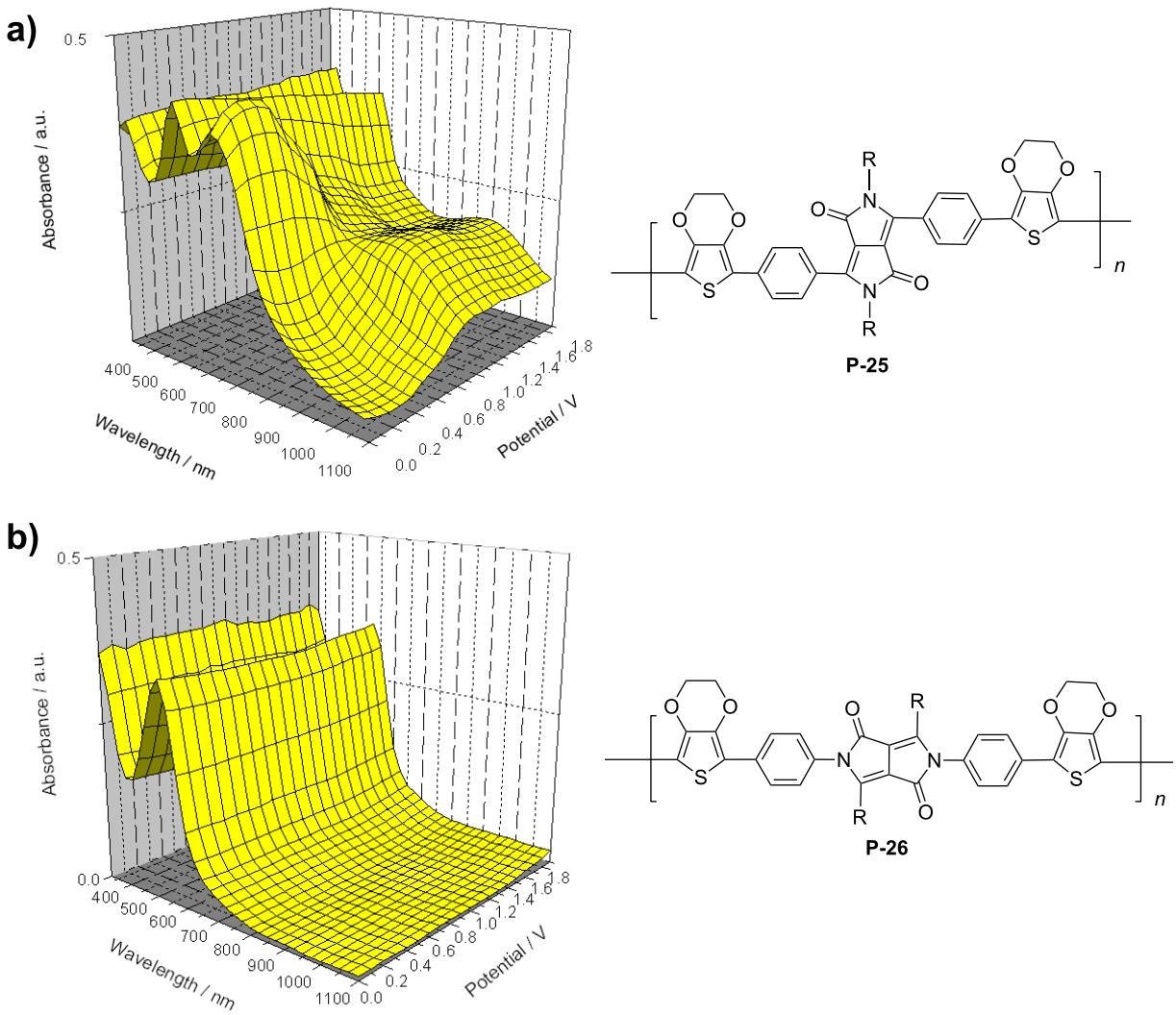
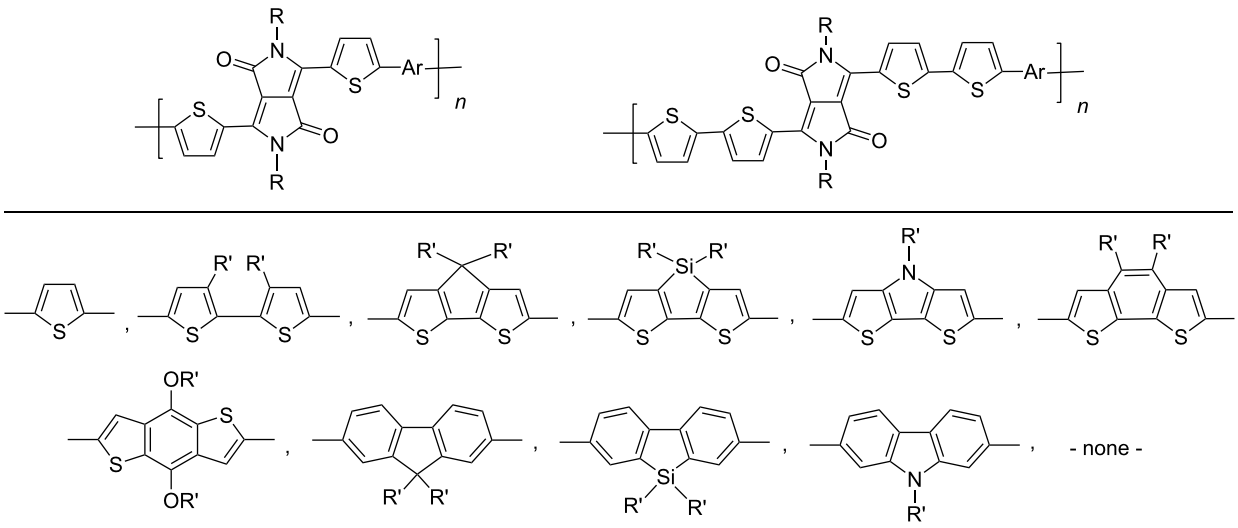


Figure 5: Absorption spectroelectrochemical plots of **P-25** and **P-26** as thin films on ITO glass. Scan rate: 100 mVs^{-1}; potential vs. ferrocene (from [50]).

photovoltaic properties. Polymer-sensitized solar cells were fabricated with **P-12** as active layer. A power conversion efficiency of 1.43% was reached. G. Zhang et al. [52] synthesized diphenylDPP-containing polyphenylene-vinylene (PPV)- and polyphenylene-ethynylene (PPE)-type conjugated polymers via Heck- and Sonogashira coupling, respectively. PPV-type polymers such as **P-14** (Table 2) exhibit good solubility in common organic solvents, high thermal stability and a broad UV/visible absorption between 300 and 600 nm in films. Bulk heterojunction solar cells were fabricated and showed a power conversion efficiency of 0.01%. A PPE-type polymer such as **P-15** (Table 2) exhibited absorption and fluorescence maxima of 510 and 585 nm, respectively, the fluorescence quantum yield being 66%. Polymer/PCBM bulk heterojunction solar cells exhibited a power conversion efficiency of 0.16%. Cao et al. [53] prepared new fluorene-DPP-phenothiazine terpolymers by Suzuki coupling, and studied the EL properties. The best EL performance was achieved by a fluorene:DPP:phenothiazine 50:30.30 polymer with a maximum EQE of 0.25% and a maximum brightness of 259 cd m^{-2} in the device configuration of ITO/PEDOT/PVK/terpolymer/Ba/Al. DPP units effectively improved the electron affinity, and phenothiazine significantly enhanced the hole injection ability.

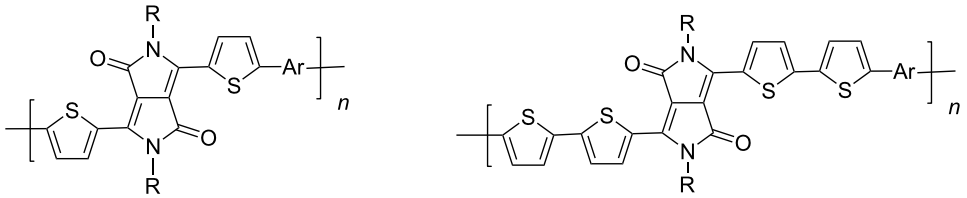
ThiophenylDPP-based copolymers

The replacement of the phenyl groups in 3,6-diphenyl-substituted DPP derivatives by thiophenyl groups resulted in 3,6-(2-thiophenyl)-substituted DPP derivatives (thiophenylDPPs) with absorption maxima at about 530 nm, i.e., more than 50 nm bathochromically shifted compared to diphenylDPP. Corresponding comonomer and polymer structures are listed in Scheme 3. Conjugated polymers containing thiophenylDPP in



Scheme 3: Thiophenyl-DPP-based polymers.

Table 5: Structure of thienyl-substituted DPP polymers used in photovoltaic devices.



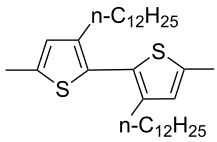
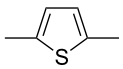
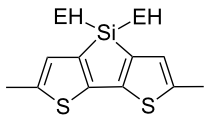
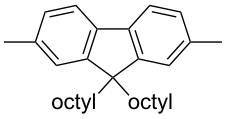
Polymer	Type	R	Ar[a]	MW [kDa]	Ref.
P-27	I	2-ethylhexyl		67	55
P-28	I	2-hexyldecyl		54	56
P-29	I	2-ethylhexyl		31.1	60
P-30	I	2-ethylhexyl		18.6	60

Table 5: Structure of thienyl-substituted DPP polymers used in photovoltaic devices. (continued)

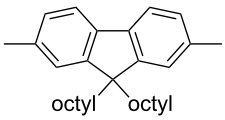
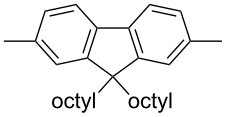
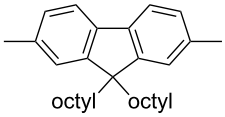
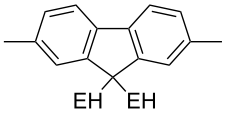
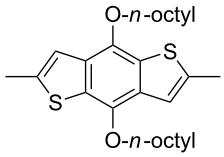
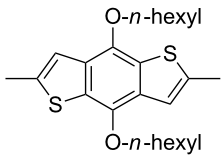
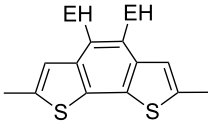
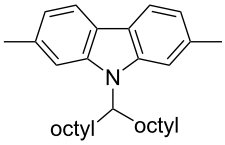
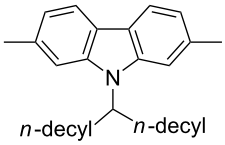
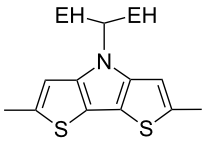
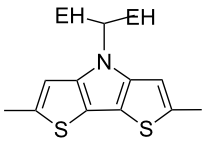
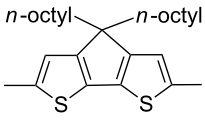
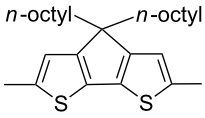
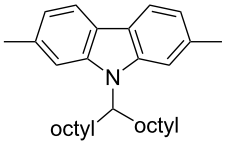
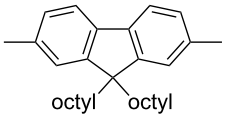
P-31	I	2-hexyldecyl		62	63
P-32	I	2-butyloctyl		31	63
P-33	I	2-ethylhexyl		17	63
P-34	I	2-ethylhexyl		15.3	61
P-35	I	2-ethylhexyl		20.4	60
P-36	I	hexyl		19	51,64
P-37	I	2-ethylhexyl		47.7	60
P-38	I	*n*-octyl		30	58,59
P-39	I	2-ethylhexyl		91.3	61
P-40	I	2-ethylhexyl		15.3	61
P-41	I	*n*-butyl		18.9	62

Table 5: Structure of thienyl-substituted DPP polymers used in photovoltaic devices. (continued)

P-42	I	2-butyloctyl		68	63
P-43	I	2-ethylhexyl		12	63
P-44	I	2-hexyldecyl	none	322	63
P-45	II	octyl		8	58
P-46	II	octyl		5	58

[a]EH = 2-ethylhexyl.

the main chain exhibited absorption maxima between 600 and 900 nm. Because of their small band gaps and high charge carrier mobilities, the polymers are interesting for applications in field effect transistors (FETs) and organic photovoltaic cells.

Winnewisser et al. [54] succeeded in preparing the thiophenylDPP-based polymer, poly[3,6-bis(4′-dodecyl[2,2′]bithiophenyl)DPP] by Yamamoto coupling of a dibrominated thiophenylDPP derivative such as **M-3**. An ambipolar near-infrared

Table 6: Thienyl-substituted DPP polymers and their use in photovoltaic devices (properties that are of interest with regard to photovoltaic devices).

Polymer	λ_{max} (abs.) film [nm]	E_g^{el} [eV]	HOMO(LUMO) [eV]	donor/PCBM ratio (w/w)	PCE [%]
P-27	-(810)	1.4	-	1:2	3.2
P-28	-	1.5	−5.17(−3.61)	1:2	4.9
P-29	798(796)	1.57	−5.04(−3.47)	1:2	2.1
P-30	649(652)	1.63	−5.23(−3.60)	1:2	0.78
P-31	663(664)	1.79	-	1:3	0.6
P-32	657(652)	1.79	-	1:4	0.8
P-33	658(656)	1.79	-	1:4	0.9
P-34	653(654)	1.78	−5.42(−3.64)	1:2	0.88
P-35	750(750)	1.65	−5.16(−3.51)	1:2	2.53
P-36	638(656)	1.46	−5.15(−3.69)	1:1	2.93
P-37	727(722)	1.58	−5.21(−3.63)	1:2	4.31
P-38	642(680)	1.52	−5.44(−3.92)	1:2	1.6
P-39	658(676)	1.69	−5.35(−3.62)	1:2	2.26
P-40	852(852)	1.17	−5.02(−3.64)	1:3	1.12
P-41	-(~770)	1.27	−4.90(−3.63)	1:2	2.71[a]
P-42	788(920)[b]	1.45	-	1:4	0.9
P-43	773(916)[b]	1.49	-	1:3	1.7
P-44	926(993)[b]	1.30	-	1:4	0.3
P-45	631(660)	1.46	−5.26(−3.80)	-	-
P-46	629(639, 678)	1.60	−5.40(−3.80)	-	-

[a]$PC_{70}BM$; [b]solution in o-dichlorobenzene, film cast from o-dichlorobenzene solution.

light-emitting transistor (LET) could be prepared from this material which exhibited hole and electron mobilities of 0.1 $cm^2\ V^{-1}\ s^{-1}$ and up to 0.09 $cm^2\ V^{-1}\ s^{-1}$, respectively. These values were higher than any other ones previously reported for solution-processed ambipolar transistors. Janssen et al. [55] demonstrated the utility of thiophenylDPP-containing conjugated polymers for application in photovoltaic devices. From a mixture of C_{70}PCBM and thiophenylDPP-based polymer **P-27** (Table 5) as active layer, solar cells with a power conversion efficiency up to 4.0% could be fabricated. The polymer exhibited a band gap of 1.4 eV, the maximum is shifted to 810 nm indicating chain aggregation and ordering, which is an important prerequisite for the preparation of films with good photovoltaic performance. In subsequent studies the efficiency could be further increased, e.g., by using **P-28** [56], or by the preparation of so-called 'polymer tandem solar cells' consisting of two subcells converting different parts of the solar spectrum [57]. For such a cell, an efficiency of 4.9% could be achieved (Table 6). Encouraged by the good performance of thiophenylDPP-based solar cells, further polymers **P-29** - **P-46** were recently synthesized and their photovoltaic properties investigated. Among these were alternating copolymers containing the thiophenylDPP, or bithiophenylDPP unit [58], and carbazole [58,59,61], fluorene [58,60,61,63], dibenzosilole, dithienosilole [58], benzo[1,2-b;3,4-b]dithiophene [63], benzo[2,1-b;3,4-b′]dithiophene [60], dithieno[3,2-b;2′,3′-d]pyrrole [61,62] and cyclopenta[2,1-b;3,4-b′]-dithiophene [63] as comonomer units (see Scheme 3). Some of the polymers were suited for the preparation of highly efficient polymer solar cells [60], some also exhibited ambipolar charge transport [62] with hole and electron transport mobilities up to 0.04 $cm^2\ V^{-1}\ s^{-1}$ and 0.01 $cm^2\ V^{-1}\ s^{-1}$, respectively [56]. Characteristic properties of photovoltaic devices are compiled in Table 6.

Conclusion

Diaryldiketopyrrolopyrroles are insoluble red pigments, which on *N*-alkylation of the lactam groups and bromine substitution of the aryl groups can be converted into readily soluble monomers suitable for Pd-catalyzed polycondensation reactions. Using Suzuki, Stille, Heck and other aryl-aryl coupling reactions, new conjugated polymers with good solubility in common organic solvents, high molecular weight, high thermal stability and application potential for optoelectronic devices became accessible. Polymers containing diphenylDPP units in the main chain exhibit brilliant orange, red or purple colours, intense luminescence, high luminescence quantum yields, and Stokes-shifts up to 110 nm. Some of the polymers were studied as active layers in electroluminescent devices and showed a brightness up to 500 cd m^{-2}. Polymers with dithiophenylDPP moieties in the main chain show broad absorption in the visible exhibiting blue or dark green colours, small band gaps and high charge carrier mobilities. They are suitable as electron donor in bulk heterojunction solar cells with PC_{60}BM or PC_{70}BM as electron acceptors to give maximum power conversion efficiencies of about 5%. In field-effect transistors they exhibit ambipolar charge transport with large hole and electron mobilities. Variation of comonomer units or aryl groups in DPP monomers might further improve the device properties.

References

1. Hao, Z.; Iqbal, A. *Chem. Soc. Rev.* **1997,** *26,* 203. doi:10.1039/cs9972600203
2. Iqbal, A.; Jost, M.; Kirschmayr, R.; Pfenniger, J.; Rochat, A.; Wallquist, O. *Bull. Soc. Chim. Belg.* **1988,** *60,* 37.
3. Iqbal, A.; Cassar, L.; Rochat, A. C.; Pfenniger, J.; Wallquist, O. J. *Coat. Technol.* **1988,** *60,* 37.
4. Farnum, D. G.; Metha, G.; Moore, G. G. I.; Siegal, F. P. *Tetrahedron Lett.* **1974,** *29,* 2549. doi:10.1016/S0040-4039(01)93202-2
5. Iqbal, A.; Cassar, L. Process for dyeing high-molecular organic material, and novel polycyclic pigments. U.S. Patent 4,415,685, Nov 15, 1983.
6. Rochat, A. C.; Cassar, L.; Iqbal, A. 1,4-Dioxopyrrolo [3,4-c] pyrroles. EP 94911, Nov 23, 1983.
7. Mizuguchi, J.; Rihs, G. *Ber. Bunsen-Ges. Phys. Chem.* **1992,** *96,* 597.
8. Mizuguchi, J.; Grubenmann, A.; Wooden, G.; Rihs, G. *Acta Crystallogr.* **1992,** *B48,* 696.
9. Mizuguchi, J. *J. Phys. Chem. A* **2000,** *104,* 1817. doi:10.1021/jp992302x
10. Potrawa, T.; Langhals, H. *Chem. Ber.* **1987,** *120,* 1075. doi:10.1002/cber.19871200702
11. Langhals, H.; Grundel, T.; Potrawa, T.; Polborn, K. *Liebigs Ann.* **1996,** 679.
12. Zombounis, J. S.; Hao, Z.; Iqbal, A. *Nature* **1997,** *388,* 131. doi:10.1038/40532
13. Chan, W. K.; Chen, Y.; Peng, Z.; Yu, L. *J. Am. Chem. Soc.* **1993,** *115,* 11735. doi:10.1021/ja00078a012
14. Eldin, S. H.; Iqbal, A.; Hao, Z. Polymerisable diketopyrrolopyrroles and polymers prepared with same. EP 0787730, Jan 22, 1997.
15. Eldin, S.; Iqbal, S. H. Polymerizable diketopyrrolopyrroles and polymers thereof. EP 0787731, Jan 22, 1997.
16. Tamayo, A. B.; Tantiwiwat, M.; Walker, B.; Nguyen, T. Q. *J. Phys. Chem. C* **2008,** *112,* 15543. doi:10.1021/jp804816c
17. Miyaua, N.; Suzuki, A. *Chem. Rev.* **1995,** *95,* 2457. doi:10.1021/cr00039a007
18. Stille, J. K. *Angew. Chem., Int. Ed. Engl.* **1986,** *24,* 508. doi:10.1002/anie.198605081
19. Heck, R. K. *Org. React.* **1982,** *27,* 345.
20. Yamamoto, T.; Morita, A.; Miyazaki, Y.; Maruyama, T.; Wakayama, H.; Zhou, Z.-H.; Nakamura, Y.; Kanbara, T. *Macromolecules* **1992,** *25,* 1214. doi:10.1021/ma00030a003
21. Sonogashira, K.; Tohnda, Y.; Hagihara, N. *Tetrahedron Lett.* **1975,** *16,* 4467. doi:10.1016/S0040-4039(00)91094-3
22. Danieli, R.; Ostoja, R.; Tiecco, M.; Zamboni, C.; Taliani, C. *J. Chem. Soc., Chem. Commun.* **1986,** 1473.
23. Lange, G.; Tieke, B. *Macromol. Chem. Phys.* **1999,** *200,* 106. doi:10.1002/(SICI)1521-3935(19990101)200:1<106::AID-MACP106>3.0.CO;2-W
24. Behnke, M.; Tieke, B. *Langmuir* **2002,** *18,* 3815. doi:10.1021/la011773j

25. Beyerlein, T.; Tieke, B. *Macromol. Rapid Commun.* **2000,** *21,* 182. doi:10.1002/(SICI)1521-3927(200003)21:4<182::AID-MARC182>3.0.CO;2-O
26. Smet, M.; Mellen, B.; Dehaen, W. *Tetrahedron Lett.* **2001,** 42. doi:10.1016/S0040-4039(01)01305-3
27. Horn, M.; Hepuzer, Y.; Yagci, Y.; Bilgin-Eran, B.; Cernenco, U.; Harabagiu, V.; Pinteala, M.; Simionescu, B. C. *Eur. Polym. J.* **2002,** *38,* 2197. doi:10.1016/S0014-3057(02)00124-6
28. Beyerlein, T.; Tieke, B.; Forero-Lenger, S.; Brütting, W. *Synth. Met.* **2002,** *130,* 115. doi:10.1016/S0379-6779(02)00058-9
29. Hofkens, J.; Verheijen, W.; Shukla, R.; Dehaen, W.; De Schryver, F. C. *Macromolecules* **1998,** *31,* 4493. doi:10.1021/ma980346i
30. Rabindranath, A. R.; Zhu, Y.; Heim, I.; Tieke, B. *Macromolecules* **2006,** *39,* 8250. doi:10.1021/ma061024e
31. Zhu, Y.; Rabindranath, A. R.; Beyerlein, T.; Tieke, B. *Macromolecules* **2007,** *40,* 6981. doi:10.1021/ma0710941
32. Potrawa, T.; Langhals, H. *Chem. Ber.* **1987,** *120,* 1075. doi:10.1002/cber.19871200702
33. Cao, D.; Liu, Q.; Zeng, W.; Han, S.; Peng, J.; Liu, S. *Macromolecules* **2006,** *39,* 8347. doi:10.1021/ma0615349
34. Cao, D.; Liu, Q.; Zeng, W.; Han, S.; Peng, J.; Liu, S. *J. Polym. Sci., Part A: Polym. Chem.* **2006,** *44,* 2395. doi:10.1002/pola.21354
35. Kuehne, A. J. C.; Mackintosh, A. R.; Pethrick, R. A.; Tieke, B. *Tetrahedron Lett.* **2008,** *49,* 4722. doi:10.1016/j.tetlet.2008.05.133
36. Zhu, Y.; Heim, I.; Tieke, B. *Macromol. Chem. Phys.* **2006,** *207,* 2206. doi:10.1002/macp.200600363
37. Rabindranath, A. R.; Zhu, Y.; Zhang, K.; Tieke, B. *Polymer* **2009,** *50,* 1637. doi:10.1016/j.polymer.2009.02.012
38. Louie, J.; Hartwig, J. F. *J. Am. Chem. Soc.* **1997,** *119,* 11695. doi:10.1021/ja972806d
39. Doodson, F. E.; Hartwig, J. F. *Macromolecules* **1998,** *31,* 1700. doi:10.1021/ma980027r
40. Guram, A. S.; Rennels, R. A.; Buchwald, S. L. *Angew. Chem., Int. Ed. Engl.* **1995,** *34,* 1348. doi:10.1002/anie.199513481
41. Marcoux, J.-F.; Wagaw, S.; Buchwald, S. L. *J. Org. Chem.* **1997,** *62,* 1568. doi:10.1021/jo9622946
42. Wolfe, J. P.; Wagaw, S.; Buchwald, S. L. *J. Am. Chem. Soc.* **1996,** *118,* 7215. doi:10.1021/ja9608306
43. Kanbara, T.; Honma, A.; Hasegawa, K. *Chem. Lett.* **1996,** 1135. doi:10.1246/cl.1996.1135
44. Kanbara, T.; Izumi, K.; Nakadimi, Y.; Narice, T.; Hasegawa, K. *Chem. Lett.* **1997,** 1185. doi:10.1246/cl.1997.1185
45. Kanbara, T.; Izumi, K.; Narice, T.; Hasegawa, K. *Polym. J.* **1998,** *30,* 66. doi:10.1295/polymj.30.66
46. Kanbara, T.; Oshima, M.; Hasegawa, K. *Macromolecules* **1998,** *31,* 8725. doi:10.1021/ma981085f
47. Kanbara, T.; Nakadimi, Y.; Hasegawa, K. *Polym. J.* **1999,** *31,* 206. doi:10.1295/polymj.31.206
48. Zhang, K.; Tieke, B. *Macromolecules* **2008,** *41,* 7287. doi:10.1021/ma801376r
49. Zhu, Y.; Zhang, K.; Tieke, B. *Macromol. Chem. Phys.* **2009,** *210,* 431. doi:10.1002/macp.200800507
50. Zhang, K.; Tieke, B.; Forgie, J. C.; Skabara, P. J. *Macromol. Rapid Commun.* **2009,** *30,* 1834. doi:10.1002/marc.200900442
51. Kanimozhi, C.; Baljaru, D.; Sharma, G. D.; Patil, S. *J. Phys. Chem. B* **2010,** *114,* 3095. doi:10.1021/jp909183x
52. Zhang, G.; liu, K.; Fan, H.; Li, Y.; Zhan, X.; Li, Y.; Yang, M. *Synth. Met.* **2009,** *159,* 1991. doi:10.1016/j.synthmet.2009.07.005
53. Qiao, Z.; Peng, J.; Jin, Y.; Liu, Q.; Weng, J.; He, Z.; Han, S.; Cao, D. *Polymer* **2010,** *51,* 1016. doi:10.1016/j.polymer.2009.12.044
54. Bürgi, L.; Turbiez, M.; Pfeiffer, R.; Bienewald, F.; Kirner, H.-J.; Winnewisser, C. *Adv. Mater.* **2008,** *20,* 2217. doi:10.1002/adma.200702775
55. Wienk, M. M.; Turbiez, M.; Gilot, J.; Janssen, R. A. J. *Adv. Mater.* **2008,** *20,* 2556. doi:10.1002/adma.200800456
56. Bijleveld, J. C.; Zoombelt, A.; Mathijssen, S. G. J.; Wienk, M. M.; Turbiez, M.; de Leeuw, D. M.; Janssen, R. A. J. *J. Am. Chem. Soc.* **2009,** *131,* 16616. doi:10.1021/ja907506r
57. Zou, Y. P.; Gendron, D.; Neagu-Plesu, R.; Leclerc, M. *Macromolecules* **2009,** *42,* 6361. doi:10.1021/ma901114j
58. Zou, Y. P.; Gendron, D.; Badrou-Aïch, R.; Najari, A.; Tao, Y.; Leclerc, M. *Macromolecules* **2009,** *42,* 2891. doi:10.1021/ma900364c
59. Huo, L.; Hou, J.; Chen, H.-Y.; Zhang, S.; Jiang, Y.; Chen, T.; Yang, Y. *Macromolecules* **2009,** *42,* 6564. doi:10.1021/ma9012972
60. Zhou, E.; Yamakawa, S.; Tajima, K.; Yang, C.; Hashimoto, K. *Chem. Mater.* **2009,** *21,* 4055. doi:10.1021/cm901487f
61. Zhou, E.; Wei, Q.; Yamakawa, S.; Zhang, Y.; Tajima, K.; Yang, C.; Hashimoto, K. *Macromolecules* **2010,** *43,* 821. doi:10.1021/ma902398q
62. Zoombelt, A. P.; Mathijssen, S. G. J.; Turbiez, M. G. R.; Wienk, M. M.; Janssen, R. A. J. *J. Mater. Chem.* **2010,** *20,* 2240. doi:10.1039/b919066j
63. Kanimozhi, C.; Baljaru, D.; Sharma, G. D.; Patil, S. *J. Phys. Chem. C* **2010,** *114,* 3287. doi:10.1021/jp909353s

License and Terms

This is an Open Access article under the terms of the Creative Commons Attribution License (http://creativecommons.org/licenses/by/2.0), which permits unrestricted use, distribution, and reproduction in any medium, provided the original work is properly cited.

The license is subject to the *Beilstein Journal of Organic Chemistry* terms and conditions: (http://www.beilstein-journals.org/bjoc)

The definitive version of this article is the electronic one which can be found at: doi:10.3762/bjoc.6.92

Beilstein Journal of Organic Chemistry

Hybrid biofunctional nanostructures as stimuli-responsive catalytic systems

Gernot U. Marten[1,2], Thorsten Gelbrich[1,3] and Annette M. Schmidt[*1,2]

Full Research Paper

Open Access

Address:
[1]Institut für Organische Chemie und Makromolekulare Chemie, Heinrich-Heine-Universität Düsseldorf, Universitätsstr. 1, D-40225 Düsseldorf, Germany, [2]Department of Chemistry, Universität zu Köln, Luxemburger Str. 116, D-50923 Köln, Germany and [3]present address: Qiagen GmbH Hilden, Germany

Email:
Annette M. Schmidt[*] - annette.schmidt@uni-koeln.de

* Corresponding author

Keywords:
biocatalysis; biolabelling; core–shell nanoparticles; immobilization matrix; thermoflocculation

Beilstein J. Org. Chem. **2010,** *6,* 922–931.
doi:10.3762/bjoc.6.98

Received: 01 June 2010
Accepted: 09 August 2010
Published: 16 September 2010

Guest Editor: H. Ritter

© 2010 Marten et al; licensee Beilstein-Institut.
License and terms: see end of document.

Abstract

A novel active biocatalytic reaction system is proposed by covalently immobilizing porcine pancreas trypsin within the thermoresponsive polymer shell of superparamagnetic Fe_3O_4 nanoparticles.

Active ester-functional nanocarriers suitable for the immobilization of amino functional targets are obtained in a single polymerization step by grafting-from copolymerization of an active ester monomer from superparamagnetic cores. The comonomer, oligo(ethylene glycol) methyl ether methacrylate, has excellent water solubility at room temperature, biocompatibility, and a tunable lower critical solution temperature (LCST) in water. The phase separation can alternatively be initiated by magnetic heating caused by magnetic losses in ac magnetic fields.

The immobilization of porcine pancreas trypsin to the core–shell nanoparticles results in highly active, nanoparticulate biocatalysts that can easily be separated magnetically. The enzymatic activity of the obtained biocatalyst system can be influenced by outer stimuli, such as temperature and external magnetic fields, by utilizing the LCST of the copolymer shell.

Introduction

The use of an external stimulus for the activation of (bio)chemical reaction processes can be a valuable tool in fundamental research and in applications such as reaction kits or lab-on-a-chip systems, as it allows for on-demand triggering of an active catalyst, and ideally can be limited, if necessary, to a geometrical confinement. By controlling the catalytic activity of a

particulate carrier by a switchable stimulus, the reaction rate of the catalysed process can be significantly accelerated or slowed down. One promising stimulus in this respect is the change of temperature. Polymeric materials show a wide range of thermoresponsive effects that can be explored for a discontinuous change of diffusion or reaction rate [1-3]. The temperature increase can for example be restricted locally by using near infrared (NIR) irradiation [4]. Other systems use a photodynamic process to force a medical effect by the photochemical drug release during light irradiation [5].

By combining thermoresponsive polymers with magnetic nanoparticles, hybrid materials become accessible that can be manipulated by two different stimuli, temperature and magnetic fields. Such dual responsive materials are of interest for a variety of applications ranging from magnetic separation or drug release systems to sensors and actuation [6-13]. We, and other groups, have demonstrated that magnetite nanoparticles decorated with a stabilizing shell composed of LCST or upper critical solution temperature (UCST) polymers lead to nanocomposites that show thermally inducible flocculation behavior in the carrier medium [14-21]. The particles agglomerate at a critical temperature resulting in an enhanced magnetic response. Thus the agglomerated particles can be separated easily by low magnetic field gradients, and facilitate, for instance, the separation process in purification applications of biomolecules.

Reversible thermoflocculation of magnetic colloids by encapsulation with thermoresponsive polymers has been proposed based on thermoresponsive polymers such as poly(*N*-isopropylamide) (PNiPAAm) [15,21-24] and (oligoethylene glycol) methacrylate copolymers (POEGMA) [25], which both show an LCST type behavior, and on glycinamide copolymers with an UCST behavior at around 10 °C [20,26]. The formation of a polymer brush on the surface of single nanoparticles has proved to be a valuable tool for the design of single-cored hybrid structures with tailored dispersion behavior [17-19,21,27-30]. Magnetic polymer brushes with thermoflocculation behavior have been reported for organic solvents by our group [17-19]. Lately, hydrophilic brush shells have been described [31-34], prepared either by surface-initiated polymerization or by a "grafting to" approach of tailored copolymers from oligo(ethyleneglycol) methacrylates with adjustable and narrow flocculation temperature and low unspecific adsorption [25,35]. The ability of magnetic nanoparticles to show considerable heat dissipation due to relaxation processes is recently employed in the combination with thermoresponsive polymers [34,36-39]. In ac magnetic fields in the kHz range, the nanoparticles transform magnetic energy to heat energy due to relaxation processes and hysteresis losses [40-42].

Here, we report the investigation of a biocatalytically active carrier system that can be tuned by temperature or external magnetic fields. The hybrid nanostructures are obtained by the combination of magnetic nanoparticle cores with a thermoresponsive poly[oligo(ethylene glycol) methyl ether methacrylate] copolymer shell [17,18,33,34] and covalently attached protease trypsin as the biocatalytically active species. A reversible shell collapse at elevated temperatures is made responsible for significantly enhanced protease activity.

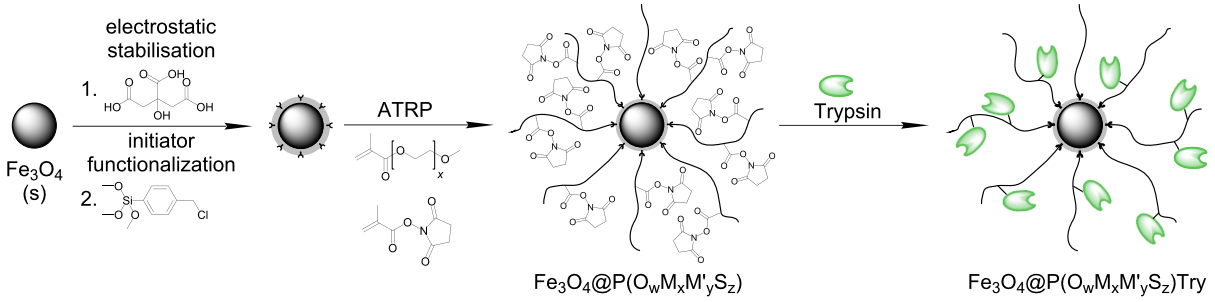
Results and Discussion

The target of the present study is the development of magnetic nanocarriers with tunable enzymatic activity. For the realization of such a system, we use several components, each performing a specific function. The iron oxide magnetic core allows positioning and heat generation, owing to its behavior in static and dynamic magnetic fields. The polymer shell is the anchor for covalent attachment of the enzyme, and allows the introduction of thermoresponsive behavior. At the same time, it improves biocompatibility and stabilization against agglomeration. Finally, the immobilization of trypsin as a serine protease introduces biocatalytic activity. These components result in hybrid nanostructures, which serve as a recoverable reaction system that can be activated reversely by external ac magnetic fields, by using the thermal energy developed by magnetic heating of the superparamagnetic cores in combination with the thermoresponse of the shell.

These multifunctional hybrid particles are formed by surface initiated copolymerization of oligo(ethylene glycol) methyl ether methacrylates (labeled as MEMA (M), MEEMA (M') and OEGMA (O)) with *N*-succinimidyl methacrylate (SIMA (S), Figure 1) as an active ester-functional monomer in DMSO by using surface-modified Fe_3O_4 nanoparticles as macroinitiators (Scheme 1). Subsequently, subunits carrying primary amine groups, such as proteins or enzymes, can be immobilized via the active ester pendant groups of the brush-type shell.

Synthesis of functional core–shell nanostructures

In the first step, Fe_3O_4 nanoparticles are prepared by alkaline precipitation based on a method of Cabuil and Massart [43] and surface-functionalized with (*p*-chloromethyl)phenyltrimethoxysilane (CTS) [44] in order to introduce benzylic chlorine groups for subsequent initiation of atom transfer radical polymerization (ATRP). Oligo(ethylene glycol) methyl ether methacrylates with different length of the hydrophilic side chain are used as the main monomer to generate a hydrophilic polymer shell with tunable critical solution behavior in water. By proper choice of the copolymer composition, the thermoflocculation temperature of the core–shell particles can be adjusted [34,35].



Scheme 1: Synthesis of magnetic biocatalyst particles.

The biocompatibility of poly(ethylene glycol) derivates is helpful to obtain nanoparticles acceptable for use in in vitro biological systems.

The direct introduction of carboxy functions to the polymer shell by surface-initiated ATRP involving (meth)acrylic acid is hindered by catalyst poisoning, resulting in a loss of reaction control. To overcome this, the protection of the carboxy group is useful [45], and in our approach, we employed succinimidyl methacrylate (SIMA) as a methacrylic acid derivative suitable for ATRP [46-48]. We have initially investigated the copolymerization behavior of the two monomers in model copolymerization experiments in solution, to ensure proper incorporation of the functional groups and stability of the active ester functionality under the polymerization conditions [33].

The catalytic system employed in the synthesis is based on copper(I) bromide and 2,2′-bipyridine in a DMSO solution. After 24 h of stirring at ambient temperature, viscous, deep brown magnetic dispersions are obtained. The success of the surface-initiated ATRP is qualitatively analyzed by transmission electron microscopy (TEM) and ATR-IR spectroscopy [33] on carefully washed and dried particles. TEM images (Figure 2) of the obtained nanoparticles demonstrate strongly contrasting Fe_3O_4 cores surrounded by less contrasting polymer shells. The nearly spherical nanoparticles are separately covered with a polymer layer of an average thickness of 3 nm, independent of the core size.

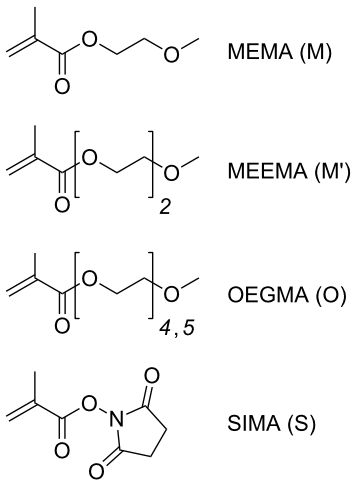


Figure 1: Structures of comonomers employed in the synthesis of functional core–shell particles.

ATR-IR spectra (Figure 3b) of the dry Fe_3O_4@P($O_xM_yS_z$) nanoparticles feature signals relating to the vibrational absorption of polymeric methyl and methylene groups (ν = 2800 cm^{-1}–3050 cm^{-1}), carbonyl double bond (ν = 1722 cm^{-1}), C–O deformation (ν = 1099 cm^{-1}) and N–O deformation (ν = 1025 cm^{-1}), which clearly reveals the presence of P(OEGMA-*co*-SIMA). The three distinct peaks at ν = 1807 cm^{-1}, 1778 cm^{-1} and 1722 cm^{-1} are characteristic of the vibrational absorption of the three carbonyl double bonds of the SIMA function, indicating that the succinimidyl ester is still existent and is neither hydrolysed nor deactivated [33]. The composition of the obtained hybrid materials is determined from mass loss between 150 °C and 480 °C in thermogravimetric analysis (TGA) (Table 1).

The hydrodynamic diameter of the core–shell nano-objects in aqueous dispersion can be detected by dynamic light scattering (DLS). A significant increase of the hydrodynamic diameter can be observed (Table 1), compared to electrostatic stabilized particles, and to CTS functionalized particles with a number average hydrodynamic diameter $d_{h,n}$ of 14 nm and 21 nm, respectively.

Hybrid particle characteristics

The magnetic properties of the nanoparticles at different points within the synthesis were investigated via vibrating sample magnetometry (VSM). In Figure 4a the magnetization curves of electrostatically stabilized nanoparticles Fe_3O_4@CA, initiator

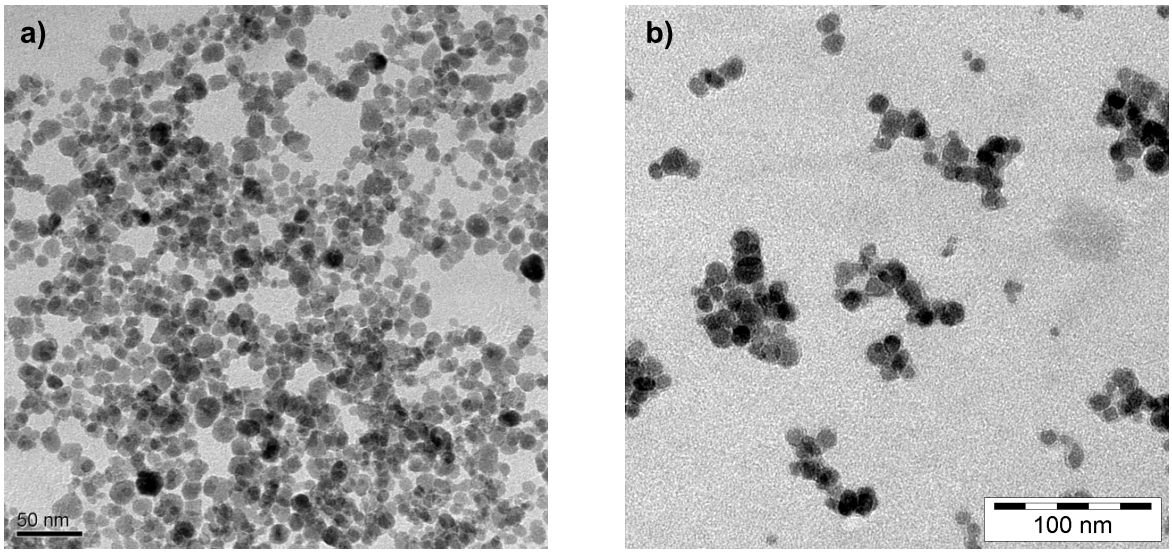


Figure 2: TEM images of a) Fe_3O_4 nanoparticles electrostatically stabilized by citric acid; b) Fe_3O_4@P(M_{100}) nanoparticles after surface-initiated ATRP.

functionalized nanoparticles Fe_3O_4@CPS and magnetic polymer brushes Fe_3O_4@P(O_{100}) are shown. Obviously, the graphs are almost perfectly matched after normalization by the saturation magnetization M_s, demonstrating that the magnetization behavior of the magnetic cores does not change during the synthesis of the polymer brushes. Furthermore, it can be observed from the graphs that the particles' cores are superparamagnetic and show no hysteresis in all investigated samples. By employing Chantrell´s method [49], we extract values for the core diameter between 10.2 nm and 10.7 nm from the initial slope (Table 1) [36].

As a consequence of the surface-initiated polymerization process, the polymer shells are end tethered to the particle surface in high density, as it has been previously shown by us and others [15,17]. When exposed to a suitable solvent, the polymer chains are highly solvated and protrude out from the surface in form of a polymer brush. In this state, the shell readily serves as a steric stabilizer for the particle dispersion, as the solvated brush surfaces result in a short-range repelling potential between individual particles. In contrast, when exposed to a bad solvent, the shell collapses, and particle agglomeration is observed.

In the present case, the polymer shell displays a reversible LCST behavior in water with a thermoflocculation temperature T_c that can be adjusted by the copolymer composition, as we have shown in a recent paper [34]. Thus, in aqueous media, the hybrid particles show thermoresponsive behavior [25]: while readily dispersible at low temperature, they reversibly flocculate when the dispersion temperature reaches the T_c of the shell, and therefore form a separate phase.

In the agglomerated state above the LCST, simple permanent magnets with magnetic field gradients below 50 $mT \cdot cm^{-1}$ are sufficient to separate the magnetic polymer brush particles from the carrier medium. We have shown that this behavior is of use for the easy magnetic separation of amino-functional probes and magnetically labeled biomolecules [33]. In this respect it is of

Table 1: Physical and chemical composition of investigated multifunctional core–shell nanoparticles.

Sample[a]	μ_P [wt %]	$d_{h,n}$ [nm]	d_c [nm]	μ_{MF} [wt %]	T_c [°C]
Fe_3O_4@P(O_{100})	62.9	169	10.2	2.10	61.2
Fe_3O_4@P($O_{82}M_{18}$)	43.8	127	10.7	1.91	53.4
Fe_3O_4@P($O_{64}M_{36}$)	62.8	171	10.5	2.48	43.7
Fe_3O_4@P($O_{47}M_{53}$)	33.8	113	10.3	1.22	36.6
Fe_3O_4@P($O_{75}S_{25}$)	40.4	79	12.1	2.14	59.4
Fe_3O_4@P($O_{80}S_{20}$)	49.9	47	10.3	1.54	57.8
Fe_3O_4@P($O_{85}S_{15}$)	41.3	73	12.0	2.33	60.8
Fe_3O_4@P($O_{90}S_{10}$)	52.1	49	10.4	1.51	57.9
Fe_3O_4@P($O_{95}S_5$)	43.9	48	10.4	1.91	—
Fe_3O_4@P($O_8M'_{84}S_8$)	39.8	75	11.3	1.56	32.3

[a]Sample annotation: Fe_3O_4@P($O_wM_xM'_yS_z$) with molar fraction of w: OEGMA, x: MEMA, y: MEEMA, and z: SIMA in the polymer shell; μ_P: mass fraction of copolymer in dry particle powder (TGA), $d_{h,n}$: number average hydrodynamic diameter (DLS), d_c: volume average core diameter (VSM), μ_{MF}: mass content of Fe_3O_4 in saturated DMSO dispersion (VSM), T_c: cloud point temperature (CPP).

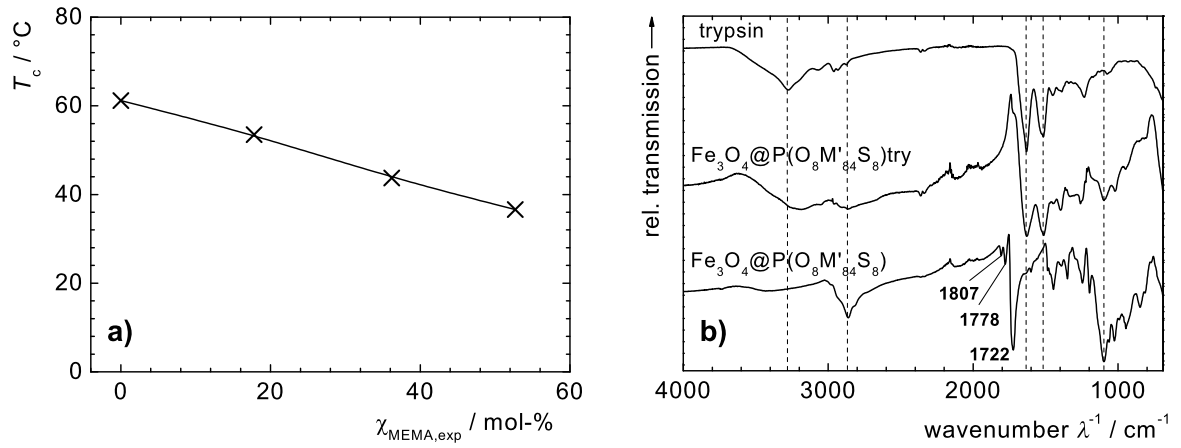


Figure 3: a) Cloud point temperature T_c of Fe_3O_4@P(O_xM_y) in water in relation to molar fraction of MEMA $\chi_{M,exp.}$ in the polymer shell. b) ATR-IR spectra of trypsin, Fe_3O_4@P($O_8M'_{84}S_8$); and Fe_3O_4@P($O_8M'_{84}S_8$)-Try (dry powders).

interest to note, that the cloud point temperature can be adjusted by copolymerization in a wide range, including temperatures acceptable for biomolecules and biological species (Figure 3a) [34]. Furthermore, it has been shown that thermoflocculation of core–shell particles can be induced by magnetic heating of the particle cores in suitable ac magnetic fields [34,38].

The ability of superparamagnetic nanoparticles to locally develop heat when exposed to external ac magnetic fields in the kHz range is of considerable interest to activate physical or chemical processes in the vicinity of the particles, e.g., in hyperthermia [50,51], and for the remote operation of thermoresponsive soft actuators [39,52]. The heat development occurs due to relaxational processes (Néel and Brown) as well as hysteresis effects that results in considerable losses during the dynamic magnetic response of the materials [40,53-55].

We investigated the behavior of Fe_3O_4@P(O_{100}) dispersions in an oscillating magnetic field (250 kHz, H = 31.5 kA·m^{-1}) by recording the sample temperature with time (Figure 4b). The temperature of all samples increases within minutes to temperatures up to 80 °C depending on the FeO_x content. A higher Fe_3O_4 content leads to faster heating, and a specific heat power (SHP) = 86.5 W·g^{-1} of the particle cores can be extracted from the data. The generated heat flux is strong enough to reach the cloud point temperature T_c of 61 °C in the dispersions at magnetic fractions of $\mu(Fe_3O_4)$ = 0.5 mass % and higher. In this temperature range, we observe a slight deviation from the

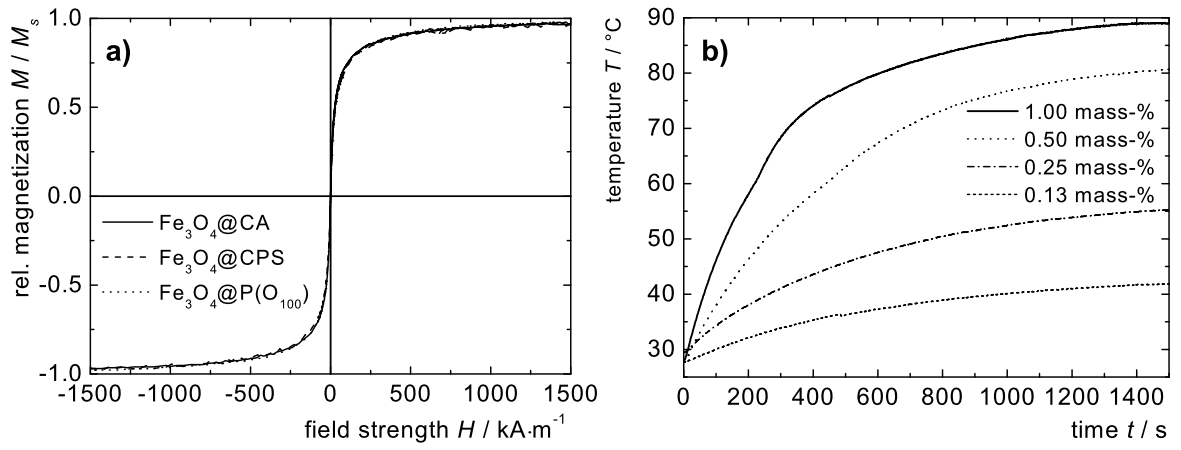


Figure 4: a) Normalized magnetization loops of dispersions based on Fe_3O_4@CA in water (solid line), Fe_3O_4@CPS in DMSO (dashed line), and Fe_3O_4@P($M_{90}C_{10}$) in DMSO (dotted line); b) sample temperature T vs irradiation time t for Fe_3O_4@P(O_{100}) nanoparticle dispersions in ac magnetic fields (250 kHz, H = 31.5 kA·m^{-1}).

expected logarithmic deceleration of the heating rate (Figure 4b). We attribute the deviation to the heat consumption caused by the phase transition process.

Enzyme immobilization and activity

The immobilization of biomacromolecules on magnetic carriers is of interest for separable biocatalytic systems. We successfully immobilized trypsin as a model enzyme on the shell of Fe_3O_4@P($O_8M'_{84}S_8$) nanoparticles. Particles with low SIMA functionality have been chosen to avoid particle cross-linking or agglomeration due to multiple attachment of a single protein molecule by several nano-objects. Figure 3b compares the ATR-IR spectra of trypsin-functional nanoparticles (Fe_3O_4@P($M_8O_{84}S_8$)-Try) to free trypsin. In both samples, we observe similar amide signals (ν = 1620, 1578 cm^{-1}), and also the NH-signal (ν = 3284 cm^{-1}) of the trypsin peptide sequence is visible in both spectra. From the nitrogen content obtained by elemental analyses (EA), the amount of trypsin bound to the polymer surface of the nanoparticles is calculated to 111 mg trypsin per g particle (4.76 µmol·g^{-1}), compared to commercially available magnetic particles for the protein binding with reported capacities between 1.5 mg·g^{-1} and 20 mg·g^{-1} [33,56]. The catalytic activity of trypsin, a protease for hydrolysis of specific peptide bonds (chain scission after the amino acids arginine and lysine), is investigated by the classical BAPNA method [57] and is compared to the native protein. Trypsin-catalyzed hydrolysis of benzoyl-Arg *p*-nitroanilide (BAPNA) results in the formation of *p*-nitroaniline that can be quantified by UV–vis spectroscopy at 410 nm (Scheme 2) [58].

The increase of relative absorption A_{410} is observed over time for different substrate concentrations c_{BAPNA}. A_{410} is directly correlated to the *p*-nitroaniline concentration, thus the reaction rate $v = d[P]/dt$ can be obtained from the initial slopes [2]. As a control experiment the primarily FeO_x@P($O_8M'_{84}S_8$) nanoparticle dispersion without trypsin bound to the polymer shell is also used; no increase in UV absorption over time was detected in the control experiment. In every run employing either trypsin or immobilized trypsin, a linear increase of absorption with time can be detected in UV experiments for initial stages. To exclude possible trypsin leaching from the carriers, we continued the data collection for a couple of minutes after magnetic separation of the magnetic nanoparticles from the BAPNA solution. No further increase in adsorption was detected.

By linearly plotting the reaction rates vs the BAPNA concentration c_{BAPNA} (Cornish-Bowden plot, Figure 5a), a hyperbolic behavior is observed that can nicely be fitted by the Michaelis Menten equation. The graph trends towards the saturation rate v_{max}, and the Michaelis constant K_m, respectively; where

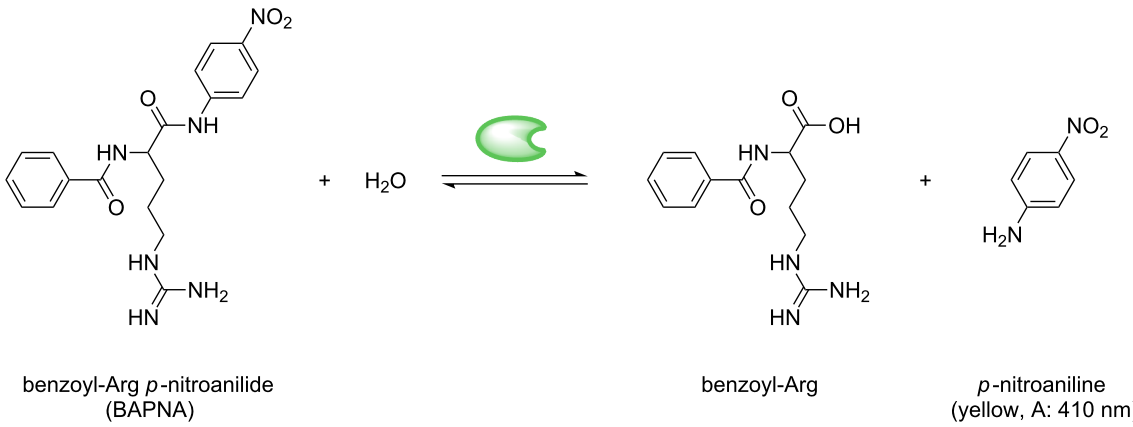
$$v = \frac{v_{max} \cdot c_{BAPNA}}{K_m + c_{BAPNA}} \quad (1)$$

Data linearization can be achieved by the Eadie–Hofstee method [59] (Figure 5b) by plotting v against $v \cdot c_{BAPNA}^{-1}$, and using the Michaelis–Menten equation in the form:

$$v = -K_m \frac{v}{c_{BAPNA}} + v_{max} \quad (2)$$

K_m and v_{max} can be determined from the negative slope and the intercept of the linear plots, respectively. A discontinuous behavior can be observed in the range of the LCST temperature (32.3 °C, see above) for aqueous Fe_3O_4@P($O_8M'_{84}S_8$)-Try dispersions.

While the Michaelis constant K_m of free trypsin decreases slowly with temperature, for particle-immobilized trypsin a strong increase is observed for temperatures above the T_c of the



Scheme 2: Reaction scheme of the enzymatic digestion of BAPNA catalyzed by magnetically labeled trypsin ( ).

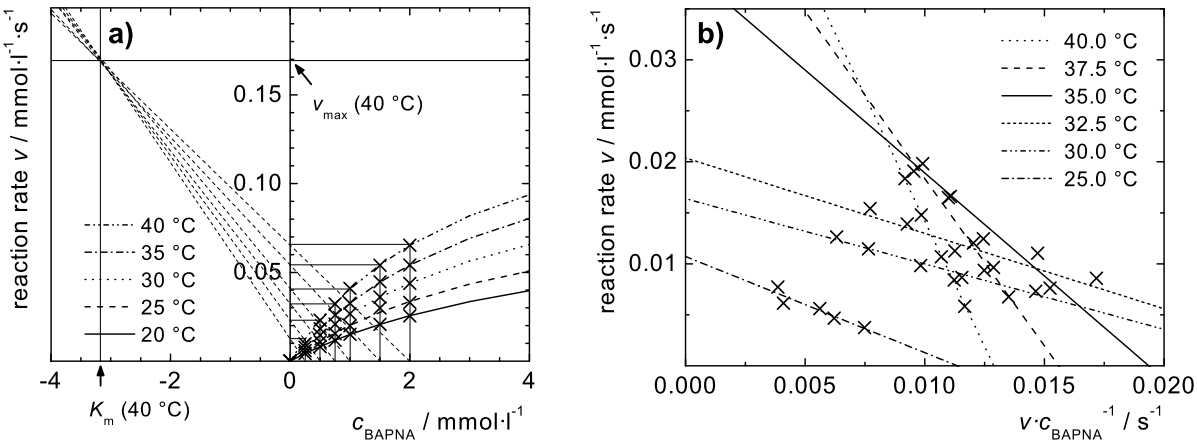
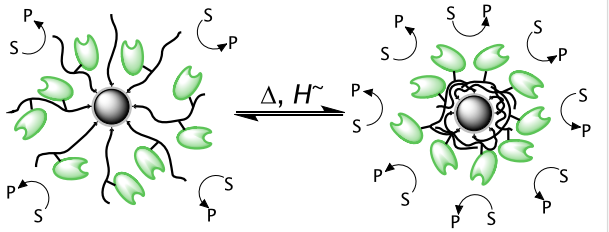


Figure 5: a) Cornish-Bowden diagram for the temperature-dependent kinetic data of trypsin activity, and b) Eadie–Hofstee diagram for the temperature-dependent kinetic data of nanocarrier activity.

polymer, indicating a decrease in complex stability, probably due to shell collapse or particle precipitation, or both (Figure 6b). Nevertheless, the turnover number $k_{cat} = v_{max}/c_{trypsin}$ that is comparably low for particle-bound trypsin below T_c, indicates a considerable acceleration of the particle-catalyzed reaction at temperatures above the T_c of the particle dispersion (Figure 6a). Probably, the shell collapse eases access to the enzyme for the substrate, considering that with a molar mass of 23,300 g·mol^{-1} the molecule size of trypsin is of the same order as M_n of the surface immobilized polymer chains (Scheme 3). In an upcoming study, the influence of diffusion and the extraction of thermodynamic parameters will give more insight to this process.



Scheme 3: Proposed mechanism of catalytic activity after heating magnetic biocatalyst particles above T_c.

Conclusion

In summary the presented results show that the combination of magnetic cores with a biocatalytically active, thermoresponsive polymer shell is a promising approach for nanoscopic carrier systems that allow an external reaction control and magnetic recovery of the catalyst. Fe_3O_4 nanoparticles with a brush shell composed of poly(oligo(ethylene glycol) methacrylates) and functionalized with porcine pancreas trypsin show temperature-tunable activity. Kinetic experiments on the catalytic activity by

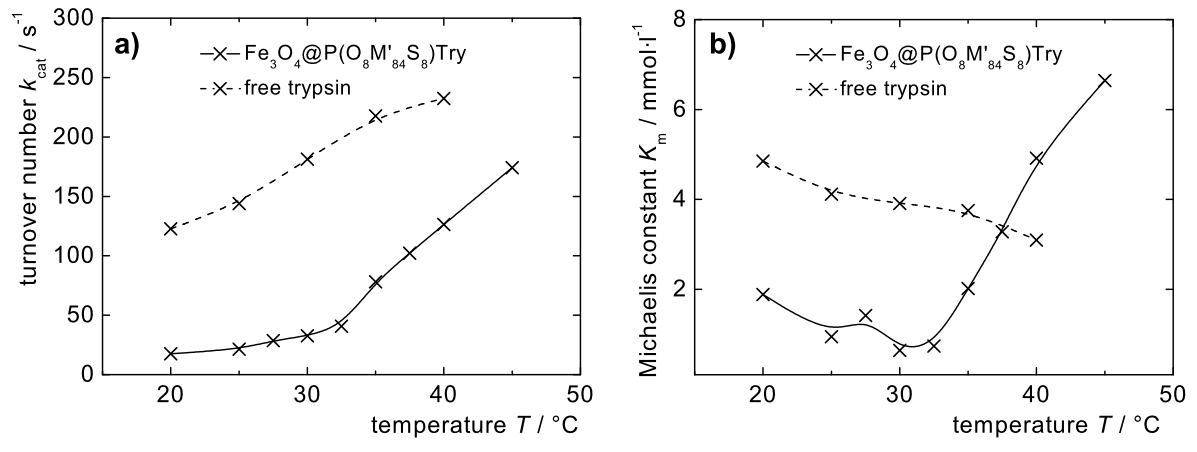


Figure 6: a) Turnover number k_{cat} and b) Michaelis constant K_m of particle- immobilized trypsin vs free trypsin.

the BAPNA method support the reaction acceleration in particle-immobilized trypsin when the particles are heated across the transition temperature of the polymer shell, an effect that is attributed to the shell collapse. The particles can be heated by ac magnetic fields, resulting in remotely controlled biocatalytic systems. The principle described here is applicable to the modification of other biologically or catalytically relevant groups, and will therefore open new ways for the design of multifunctional hybrid nanostructures with different property portfolios.

Experimental

Materials: Ammonium hydroxide aqueous solution (Fluka, 25%), N_α-benzoyl-D,L-arginin-4-nitroanilide hydrochloride (BAPNA) (Sigma, 98%), benzylamine (BzA) (Janssen Chimica), 2,2′-bipyridine (bpy) (Aldrich, 99%), citric acid monohydrate (Grüssing GmbH, 99,5%), (4-(chloromethyl)phenyl)trimethoxysilane (CPS) (ABCR, 95%), copper(I) bromide (CuBr) (Aldrich, 98%), 1-(3-dimethylaminopropyl)-3-ethylcarbodiimide hydrochloride (EDC) (ABCR, 98%), *N*-hydroxy succinimide (NHS, Fluka), iron(III) chloride hexahydrate, iron(II) chloride tetrahydrate (Fluka, 98%), ninhydrin (Riedel-de-Haen), oligo(ethylene glycol) methylether methacrylate (OEGMA, Aldrich, M_n = 290 g·mol^{-1}), 2-(2-methoxyethoxy)-ethyl methacrylate (MEEMA), porcine pancreas trypsin type IX-S (Aldrich), tetramethylammonium hydroxide aqueous solution (25%) were used as received without further purification. Ethanol, diethyl ether and acetone were purified by distillation before use. Dimethyl sulfoxide (DMSO; min. 99.5%, Riedel-de-Haen) was distilled under reduced pressure from calcium hydride and stored under argon and molecular sieve (3A). HEPES buffer was prepared from 11 mM HEPES (Sigma), 140 mM NaCl (Merck), 4 mM KCl (Merck), 10 mM D(+)-glucose, and dissolved in deionized water. 2-Methoxyethyl methacrylate (MEMA, Aldrich, 99%) was distilled under reduced pressure and stored under argon. Nitric acid (conc., p.a., Merck) was diluted with distilled water resulting in a 2 N solution. Succinimidyl methacrylate (SIMA) was synthesized by a method by Gatz et al [26,60].

Synthesis and stabilization of Fe_3O_4 nanoparticles: The synthesis of magnetite nanoparticles on the gram scale was carried out by alkaline precipitation of iron(III) and iron(II) chloride following a method of Cabuil and Massart and is described in detail elsewhere [43]. For stabilization, the freshly synthesized nanoparticles were stirred with 420 mL 2 N nitric acid for 5 min. After washing with distilled water, 90 mL 0.01 N citric acid (CA) was added to the nanoparticles and stirred for 5 min. The particles were magnetically separated from the supernatant and 15 mL of tetramethyl ammonium hydroxide aqueous solution was added to obtain 3.32 g magnetic nanoparticles Fe_3O_4@CA in 92 mL of a stable dispersion at pH 8–9 (yield: 42.5%).

The Fe_3O_4 content $\mu(Fe_3O_4)$ in dispersion and the magnetic core diameter d_c were determined via VSM ($\mu(Fe_3O_4)$ = 2.55 mass%, d_c = 11.7 nm). DLS: $d_{h,n}$ = 14.3 nm (25 °C in H_2O). FT-IR (Diamond): ν (cm^{-1}) = 2357, 2335 (C-N), 1247 (OH), 1098 (C-O), 1080 (OH).

Surface modification of Fe_3O_4 nanoparticles: For the immobilization of initiator sites on the particle surface of Fe_3O_4@CA, the dispersion was diluted with ethanol to a mass content of 1.0 g·l^{-1}, and 1.80 mmol CPS per gram of Fe_3O_4 was added. After stirring for 24 h at ambient temperature, ethanol was removed under reduced pressure at 40 °C and the particles were washed with ethanol/acetone (1:1) five times. The particles were then redispersed in DMSO, resulting in a Fe_3O_4 content $\mu(Fe_3O_4)$ of 6.44 mass % (VSM) in dispersion (yield: 46.4%). The magnetic core diameter d_c was measured to be 11.1 nm (VSM). The functionalization degree of CPS was determined by EA to be 0.87 mmol CTS on 1.94 g Fe_3O_4@CPS. FT-IR (Diamond): ν (cm^{-1}) = 2357, 2335 (C–N), 1241 (OH), 1115 (Si–O), 1011, 948 (Si–C).

Surface-initiated ATRP of functional polymer shells: The obtained CPS coated particles served as a macroinitiator for the following ATRP. The synthesis of Fe_3O_4@P(O_{100}) is described, representatively. Therefore 6 mL of the DMSO-based particle dispersion (0.65 g Fe_3O_4@CPS) was mixed with 5 mL of a DMSO solution of 37.3 mg (0.26 mmol) CuBr and 101 mg (0.65 mmol) bpy. The polymerization was started by adding 5.83 mmol of the monomer (here: OEGMA). The mixture was stirred for 24 h at ambient temperature. The obtained viscous magnetic fluid was diluted with 10 ml DMSO to the final ferrofluid. The Fe_3O_4 content $\mu(Fe_3O_4)$ in dispersion and the magnetic core diameter d_c were determined via VSM. The polymer content χ_{Pol} in the dried particles was obtained from EA and TGA.

Particle transfer to water/buffer: The DMSO-based particle dispersion was added dropwise to diethyl ether (Et_2O). The precipitate was washed five times with Et_2O/Acetone (1:1) and was redispersed in distilled water or buffer to obtain an aqueous magnetic fluid.

Immobilization of trypsin: 30 mg trypsin was dissolved in 6 mL HEPES buffer and mixed with 6 mL of a HEPES buffer-based Fe_3O_4@P($O_{85}S_{15}$) particle dispersion ($\mu(FeO_x)$ = 0.15 mass %). In order to allow reactivation of active ester functions that may have hydrolyzed during storage, 6 mL of 2.21 μM EDC/NHS solution was added. The binding reaction

was carried out for 6 h at ambient temperature on a shaker. The obtained trypsin functionalized particles were separated and washed carefully with water to remove any residues of free trypsin, and redispersed in HEPES buffer.

Determination of immobilized enzyme kinetics and activity: BAPNA was used as the model substrate. Four HEPES buffered BAPNA solutions with concentrations between 2.0 mM and 0.5 mM, and a 6.0 μM trypsin solution were prepared and tempered to the desired temperature. The respective BAPNA solution was added to a cuvette and mixed with 100 μL of FeO_x@POEGMA-trypsin nanoparticle dispersion or with 50 μL trypsin solution. The cuvette was placed into the spectrophotometer and tempered. Starting with the addition of the enzyme, the change in absorption at 410 nm was detected over a period of up to 20 min by UV–vis spectroscopy.

Analytic methods and instrumentation: ATR-IR spectra were measured on a Nicolet 6700 spectrometer. Elemental analyses were performed on a Perkin-Elmer 2400 CHN analyzer. The organic content was calculated through C content. For TGA, a Netzsch STA 449c in a He atmosphere was used with a heating rate of 10 $K \cdot min^{-1}$ between 30 and 600 °C. Gel permeation chromatography (GPC) elugrams were collected on THF (300 × 8 mm^2 MZ Gel Sdplus columns, Waters 410 RI-detector) relative to polystyrene standards. NMR spectroscopy was performed on a Bruker DRX500 at 500 MHz and ambient temperature. DLS experiments and zeta potential measurements were performed on a Malvern Zetasizer Nano ZS at 25 °C. The particle size distribution was derived from a deconvolution of the measured intensity autocorrelation function of the sample by the general purpose mode (non-negative least-squares) algorithm included in the DTS software. Each experiment was performed at least three times. Cloud point photometry of aqueous particle dispersions was performed on a Tepper TP1 cloud point photometer at 1 $K \cdot min^{-1}$ in HEPES buffer. From the turning point of the turbidity curves, the cloud point temperature T_c was obtained. Vibrating sample magnetization (VSM) measurements were implemented on an ADE Magnetics vibrating sample magnetometer EV7. Induction heating experiments were performed on a Hüttinger HF generator Axio 5/450T equipped with a copper inductor (l = 50 mm, dI = 35 mm, n = 5), and operating at 250 kHz and at a magnetic field of 31.5 $kA \cdot m^{-1}$. The experiments were performed in a vacuum-isolated glass sample container. Different samples with varying magnetite concentrations $\mu(Fe_3O_4)$ of Fe_3O_4@P(O_{100})-based magnetic fluid in water were exposed to the oscillating magnetic field. Via a fiber-optical sensor the fluid temperature T was measured against time t. For UV–vis spectroscopy, a Nicolet UV 540 spectroscope, a Unicam UV 500 or a Perkin Elmer Lambda19 with a thermostat Colora NBDS was used. Differential scanning calorimetry thermograms were collected on a Mettler-Toledo DSC 822^e at 5 $K \cdot min^{-1}$. TEM pictures were taken on a Hitachi H 600.

Acknowledgements

Thanks to Prof. T. J. J. Müller, HHU Düsseldorf, for the use of the temperature controlled UV–vis spectrometer and Prof. H. Ritter, HHU Düsseldorf for generous support. We also thank C. Schlemmer, ALU Freiburg, for recording TEM pictures. We gratefully acknowledge DFG (Emmy Noether Program, priority program SPP 1259) and FCI (A. M. Schmidt, G. U. Marten) for financial support.

References

1. Tokarev, I.; Minko, S. *Adv. Mater.* **2009,** *21,* 241–247. doi:10.1002/adma.200801408
2. Keurentjes, J. T. F.; Kemmere, M. F.; Bruinewoud, H.; Vertommen, M. A. M. E.; Rovers, S. A.; Hoogenboom, R.; Stemkens, L. F. S.; Péters, F. L. A. M. A.; Tielen, N. J. C.; van Asseldonk, D. T. A.; Gabriel, A. F.; Joosten, E. A.; Marcus, M. A. E. *Angew. Chem., Int. Ed.* **2009,** *48,* 9867–9870. doi:10.1002/anie.200904172
3. Kawaguchi, H.; Kisara, K.; Takahashi, T.; Achiha, K.; Yasui, M.; Fujimoto, K. *Macromol. Symp.* **2000,** *151,* 591–598. doi:10.1002/1521-3900(200002)151:1<591::AID-MASY591>3.0.CO;2-P
4. Weissleder, R. *Nat. Biotechnol.* **2001,** *19,* 316–317. doi:10.1038/86684
5. Sun, Y.; Chen, Z.; Yang, X.; Huang, P.; Zhou, X.; Du, X. *Nanotechnology* **2009,** *20,* 135102–135110. doi:10.1088/0957-4484/20/13/135102
6. Pankhurst, Q. A.; Thanh, N. K. T.; Jones, S. K.; Dobson, J. *J. Phys. D: Appl. Phys.* **2009,** *42,* 224001–224016. doi:10.1088/0022-3727/42/22/224001
7. Misra, R. D. K. *Mater. Sci. Technol.* **2008,** *24,* 1011–1019. doi:10.1179/174328408X341690
8. Horák, D.; Babič, M.; Macková, H.; Beneš, M. J. *J. Sep. Sci.* **2007,** *30,* 1751–1772. doi:10.1002/jssc.200700088
9. Gu, H.; Xu, K.; Xu, C.; Xu, B. *Chem. Commun.* **2006,** 941–949. doi:10.1039/b514130c
10. Franzreb, M.; Siemann-Herzberg, M.; Hobley, T. J.; Thomas, O. R. T. *Appl. Microbiol. Biotechnol.* **2006,** *70,* 505–516. doi:10.1007/s00253-006-0344-3
11. Safarik, I.; Safarikova, M. *Biomagn. Res. Technol.* **2004,** *2,* No. 7. doi:10.1186/1477-044X-2-7
12. Pankhurst, Q. A.; Connolly, J.; Jones, S. K.; Dobson, J. *J. Phys. D: Appl. Phys.* **2003,** *36,* R167–R181. doi:10.1088/0022-3727/36/13/201
13. Safarik, I.; Safarikova, M. *J. Chromatogr., B: Biomed. Sci. Appl.* **1999,** *722,* 33–53. doi:10.1016/S0378-4347(98)00338-7
14. Wakamatsu, H.; Yamamoto, K.; Nakao, A.; Aoyagi, T. *J. Magn. Magn. Mater.* **2006,** *302,* 327–333. doi:10.1016/j.jmmm.2005.09.032
15. Sun, Y.; Ding, X.; Zheng, Z.; Cheng, X.; Hu, X.; Peng, Y. *Chem. Commun.* **2006,** 2765–2767. doi:10.1039/b604202c
16. Brazel, C. *Pharm. Res.* **2009,** *26,* 644–656. doi:10.1007/s11095-008-9773-2

17. Gelbrich, T.; Feyen, M.; Schmidt, A. M. *Macromolecules* **2006,** *39,* 3469–3472. doi:10.1021/ma060006u
18. Kaiser, A.; Gelbrich, T.; Schmidt, A. M. *J. Phys.: Condens. Matter* **2006,** *18,* S2563–S2580. doi:10.1088/0953-8984/18/38/S03
19. Schmidt, A. M. *Macromol. Rapid Commun.* **2005,** *26,* 93–97. doi:10.1002/marc.200400426
20. Ohnishi, N.; Furukawa, H.; Hideyuki, H.; Wang, J.; An, C.; Fukusaki, E.; Kataoka, K.; Ueno, K.; Kondo, A. *NanoBiotechnology* **2006,** *2,* 43–49. doi:10.1007/s12030-006-0006-7
21. Lai, J. J.; Hoffman, J. M.; Ebara, M.; Hoffman, A. S.; Estournès, C.; Wattiaux, A.; Stayton, P. S. *Langmuir* **2007,** *23,* 7385–7391. doi:10.1021/la062527g
22. Kondo, A.; Kamura, H.; Higashitani, K. *Appl. Microbiol. Biotechnol.* **1994,** *41,* 99–105. doi:10.1007/BF00166089
23. Heskins, M.; Guillet, J. E. *J. Macromol. Sci., Part A: Pure Appl. Chem.* **1968,** *2,* 1441–1455. doi:10.1080/10601326808051910
24. Schild, H. G. *Prog. Polym. Sci.* **1992,** *17,* 163–249. doi:10.1016/0079-6700(92)90023-R
25. Chanana, M.; Jahn, S.; Georgieva, R.; Lutz, J.-F.; Bäumler, H.; Wang, D. *Chem. Mater.* **2009,** *21,* 1906–1914. doi:10.1021/cm900126r
26. Magnetic Beads Therma-Max. http://www.magnabeat.com/e_index.html (accessed June 1, 2010).
27. Perruchot, C.; Khan, M. A.; Kamitsi, A.; Armes, S. P.; von Werne, T.; Patten, T. E. *Langmuir* **2001,** *17,* 4479–4481. doi:10.1021/la0102758
28. Chen, X. Y.; Randall, D. P.; Perruchot, C.; Watts, J. F.; Patten, T. E.; von Werne, T.; Armes, S. P. *J. Colloid Interface Sci.* **2003,** *257,* 56–64. doi:10.1016/S0021-9797(02)00014-0
29. Li, D.; Sheng, X.; Zhao, B. *J. Am. Chem. Soc.* **2005,** *127,* 6248–6256. doi:10.1021/ja0422561
30. Li, D.; Jones, G. L.; Dunlap, J. R.; Hua, F.; Zhao, B. *Langmuir* **2006,** *22,* 3344–3351. doi:10.1021/la053103+
31. Wang, S.; Zhou, Y.; Guan, W.; Ding, B. *Appl. Surf. Sci.* **2008,** *254,* 5170–5174. doi:10.1016/j.apsusc.2008.02.021
32. Gou, Z.; Chen, Y.; Zhou, W.; Huang, Z.; Hu, Y.; Wan, M.; Bai, F. *Mater. Lett.* **2008,** *62,* 4542–4544. doi:10.1016/j.matlet.2008.08.035
33. Gelbrich, T.; Reinartz, M.; Schmidt, A. M. *Biomacromolecules* **2010,** *11,* 635–642. doi:10.1021/bm901203z
34. Gelbrich, T.; Marten, G. U.; Schmidt, A. M. *Polymer* **2010,** *51,* 2818–2824. doi:10.1016/j.polymer.2010.02.032
35. Lutz, J.-F.; Stiller, S.; Hoth, A.; Kaufner, L.; Pison, U.; Cartier, R. *Biomacromolecules* **2006,** *7,* 3132–3138. doi:10.1021/bm0607527
36. Kaiser, A.; Liu, T.; Richtering, W.; Schmidt, A. M. *Langmuir* **2009,** *25,* 7335–7341. doi:10.1021/la900401f
37. Schmidt, A. M. *Colloid Polym. Sci.* **2007,** *285,* 953–966. doi:10.1007/s00396-007-1667-z
38. Schmidt, A. M. *J. Magn. Magn. Mater.* **2005,** *289,* 5–8. doi:10.1016/j.jmmm.2004.11.003
39. Schmidt, A. M. *Macromol. Rapid Commun.* **2006,** *27,* 1168–1172. doi:10.1002/marc.200600225
40. Hergt, R.; Dutz, S.; Müller, R.; Zeisberger, M. *J. Phys.: Condens. Matter* **2006,** *18,* S2919–S2934. doi:10.1088/0953-8984/18/38/S26
41. Müller, G.; Dutz, S.; Hergt, R.; Schmidt, C.; Steinmetz, H.; Zeisberger, M.; Gawalek, W. *J. Magn. Magn. Mater.* **2007,** *310,* 2399–2401. doi:10.1016/j.jmmm.2006.10.772
42. Glöckel, G.; Hergt, R.; Zeisberger, M.; Dutz, S.; Nagel, S.; Weitschies, W. *J. Phys.: Condens. Matter* **2006,** *18,* S2935–S2949. doi:10.1088/0953-8984/18/38/S27
43. Massart, R.; Cabuil, V. J. *Chim. Phys. Phys.-Chim. Biol.* **1987,** *84,* 967–973.
44. Frickel, N.; Messing, R.; Gelbrich, T.; Schmidt, A. M. *Langmuir* **2010,** *26,* 2839–2846. doi:10.1021/la902904f
45. Matyjaszewski, K.; Davis, T. P., Eds. *Handbook of Radical Polymerization;* Wiley-Interscience: New York, 2002.
46. Rathforn, J. M.; Tew, G. N. *Polymer* **2008,** *49,* 1761–1769. doi:10.1016/j.polymer.2008.01.071
47. Shunmugam, R.; Tew, G. N. *J. Polym. Sci., Part A: Polym. Chem.* **2005,** *43,* 5831–5843. doi:10.1002/pola.21102
48. Monge, S.; Haddelton, D. M. *Eur. Polym. J.* **2004,** *40,* 37–45. doi:10.1016/j.eurpolymj.2003.08.003
49. Chantrell, R.; Popplewell, J.; Charles, S. *IEEE Trans. Magn.* **1978,** *14,* 975–977. doi:10.1109/TMAG.1978.1059918
50. Gneveckow, U.; Jordan, A.; Scholz, R.; Brüß, V.; Waldöfner, N.; Ricke, J.; Feussner, A.; Wust, P.; Hildebrandt, B.; Rau, B. *Med. Phys.* **2004,** *31,* 1444–1451. doi:10.1118/1.1748629
51. Falk, M. H.; Issels, R. D. *Int. J. Hyperthermia* **2001,** *17,* 1–18. doi:10.1080/02656730118511
52. Kaiser, A.; Winkler, M.; Krause, S.; Finkelmann, H.; Schmidt, A. M. *J. Mater. Chem.* **2009,** *19,* 538–543. doi:10.1039/b813120c
53. Néel, L. *C. R. Hebd. Seances Acad. Sci.* **1949,** *228,* 64–66.
54. Brown, W. F. *J. Appl. Phys.* **1959,** *30,* S130–S132. doi:10.1063/1.2185851
55. Feyen, M.; Heim, E.; Ludwig, F.; Schmidt, A. M. *Chem. Mater.* **2008,** *20,* 2942–2948. doi:10.1021/cm703419t
56. Chemagen AG: activated M-PVA Magnetic Beads AK11, protein binding capacity 8–20 $mg \cdot g^{-1}$. http://www.chemagen.com/activated-m-pva-magnetic-beads.html (accessed June 1, 2010); micromod: nanomag®-D (streptavidin), streptavidin functionality 1.5–2.0 $mg \cdot g^{-1}$ (http://www.micromod.de/scripts/datasheet.asp?sid=929022981&prod=09-19-252&lng=g&typ=1, accessed June 1, 2010).
57. Asgeirsson, B.; Cekan, P. *FEBS Lett.* **2006,** *580,* 4639–4644. doi:10.1016/j.febslet.2006.07.043
58. Erlanger, B. F.; Kokowsky, N.; Cohen, W. *Arch. Biochem. Biophys.* **1961,** *95,* 271–278. doi:10.1016/0003-9861(61)90145-X
59. Lineweaver, H.; Burk, D. *J. Am. Chem. Soc.* **1934,** *56,* 658–666. doi:10.1021/ja01318a036
60. Batz, H.-G.; Franzmann, G.; Ringsdorf, H. *Angew. Chem.* **1972,** *24,* 1189–1190. doi:10.1002/ange.19720842410

License and Terms

This is an Open Access article under the terms of the Creative Commons Attribution License (http://creativecommons.org/licenses/by/2.0), which permits unrestricted use, distribution, and reproduction in any medium, provided the original work is properly cited.

The license is subject to the *Beilstein Journal of Organic Chemistry* terms and conditions: (http://www.beilstein-journals.org/bjoc)

The definitive version of this article is the electronic one which can be found at: doi:10.3762/bjoc.6.98

Beilstein Journal of Organic Chemistry

Formation of epoxide-amine oligo-adducts as OH-functionalized initiators for the ring-opening polymerization of ε-caprolactone

Julia Theis and Helmut Ritter*

Full Research Paper

Open Access

Address:
Institut für Organische Chemie und Makromolekulare Chemie, Heinrich-Heine-Universität Düsseldorf, Universitätsstraße 1, 40225 Düsseldorf, Germany

Email:
Julia Theis - julia.theis@uni-duesseldorf.de; Helmut Ritter* - h.ritter@uni-duesseldorf.de

* Corresponding author

Keywords:
addition oligomerization; epoxide-amine adducts; microwave; ring-opening polymerization; transfer hydrogenation

Beilstein J. Org. Chem. **2010,** *6,* 938–944.
doi:10.3762/bjoc.6.105

Received: 15 July 2010
Accepted: 15 September 2010
Published: 01 October 2010

Editor-in-Chief: J. Clayden

© 2010 Theis and Ritter; licensee Beilstein-Institut.
License and terms: see end of document.

Abstract

Epoxide-amine oligo-adducts were synthesized via a one-pot microwave assisted heterogeneous catalytic transfer hydrogenation. Accordingly, 4-nitroanisole was reduced under microwave conditions to give 4-aminoanisole which reacted immediately with the diglycidyl ether of bisphenol A in an addition polymerization reaction to yield oligo(amino alcohol)s. The hydroxy groups of the new formed oligomers were used as the initiator for the ring-opening polymerization of ε-caprolactone to produce a graft copolymer.

Introduction

In the last decade the use of microwave (MW) irradiation in organic, pharmaceutical and polymer chemistry has become a well-established technique to promote chemical reactions. In many cases, the main advantages of this physical heating method over traditional heating in an oil bath are increases in reaction speed, product yields and purity [1-10].

Some previous works discussed the effective experimental procedure of metal-catalyzed reactions inside a MW oven [11,12]. Among the several types of these catalytic reactions, hydrogenation is probably one of the most useful in synthetic chemistry. Since many laboratory MW reactors are constructed to work under pressure, the MW tube can be regarded as a small autoclave. Therefore, this reaction can be performed either by using gaseous hydrogen [13,14] or by addition of a hydrogen source such as ammonium formate [15-19] or methylcyclohexenes [20].

Furthermore, the addition polymerization of primary amines with diepoxides forming linear adducts has been intensively studied [21]. Linear epoxide-amine addition polymers can be obtained for instance by the addition reaction of diglycidyl

ethers and aromatic primary amines in equimolar amounts. With regard to our former work on the formation of hyperbranched epoxide-amine adducts via microwave-assisted heterogeneous catalytic transfer hydrogenation [22], we report herein the synthesis of an linear oligo(amino alcohol). The hydroxy groups of the latter were then used as an initiator for the ring-opening polymerization (ROP) of ε-caprolactone to construct a new class of graft copolymers.

Results and Discussion

Formation of epoxide-amine adducts

Epoxide-amine adducts based on diglycidyl ether of bisphenol A (**1**) and 4-aminoanisole (**3**) were synthesized in a MW-assisted one-pot reaction. Thus, 4-nitroanisole (**2**) was reduced to the corresponding amine **3** via catalytic transfer hydrogenation. In presence of **1**, a simultaneous addition reaction of the freshly formed amine groups took place (Scheme 1). The reaction was carried out using 4-methyl-1-cyclohexene as a source of hydrogen in bulk. To prevent overheating, the reaction was carried out under simultaneous cooling with 5 psi of compressed air.

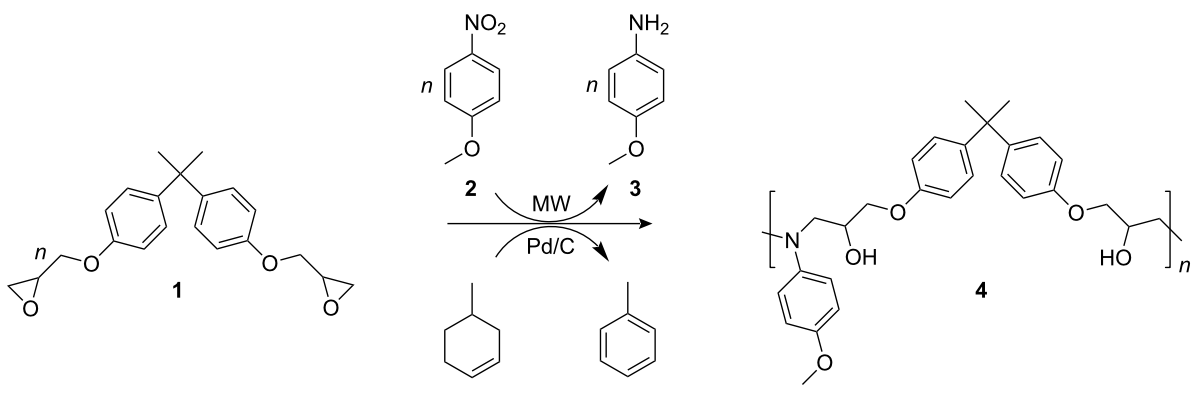
The obtained epoxide-amine addition product **4** was characterized by ^{13}C NMR, Fourier transform infrared (FT-IR) spectroscopy and matrix-assisted laser desorption-ionization time-of-flight (MALDI-TOF) mass spectrometry. The successful reduction of the nitroaromatic compound **2** was proven by IR spectroscopy by the disappearance of the asymmetric and symmetric NO_2 stretching vibration absorption bands at 1589 and 1329 cm^{-1}, respectively. The addition reaction of the new formed primary aromatic amine **3** with diepoxide **1** was proven by the complete disappearance of the absorption band at 911 cm^{-1} associated with the C–H stretching vibration of the epoxide group. Furthermore, the formation of amino alcohol units was confirmed by the appearance of a broad band in the range of 3600–3150 cm^{-1} with a maximum at 3370 cm^{-1} corresponding to the O–H stretching vibration. The absence of both epoxide and N–H-amine absorption bands indicates the formation of some cyclic compounds [23].

The ^{13}C NMR spectra of **4** (Figure 1) was compared with the data given in Ref. [24]. All characteristic signals of the formed addition product **4** were observed. Two signals for C-atom 6 appear due to the diastereomeric erythro and threo amino-diol units. Additionally, two signals for C-atom 7 were observed. The signals of the epoxide groups which should appear at about 44 and 50 ppm were faintly visible. In addition, new signals at about 18, 65 and 72 ppm appeared.

It is known, that epoxide-compounds can be reduced under palladium catalysis to form alcohols [25,26]. The new signals at 18, 65 and 72 ppm suggest the formation of a secondary alcohol formed by the reduction of the epoxide end groups under the reaction conditions.

The presence of some epoxide groups was also established by ^{1}H NMR spectroscopy. Because of overlap in the region between 3 and 4.5 ppm and the highly complex splitting of signals, ^{1}H NMR spectra were of little use for an analysis of this kind of polymer. However, the existence of intact epoxide groups was proven by means of two very weak signals, which were difficult to discern, at 2.81 and 2.66 ppm, corresponding to the CH_2 of the epoxide group.

MALDI-TOF MS measurements (Figure 2) definitely indicated the formation of an oligomer homologous series of epoxide-amine addition products of **1** and **3**. The amino alcohol repetitive unit (green) has a molecular mass of 463.56 g/mol and the molecule with the highest assignable molecular mass is the n = 13 oligomer with [M + Na$^+$] = 6049 *m/z*. Furthermore, the mass to charge ratios (*m/z*) of the repetitive unit containing epoxide (blue) and amine (red) end groups were observed.



Scheme 1: One-pot synthesis of epoxide-amine adducts via MW-assisted transfer hydrogenation.

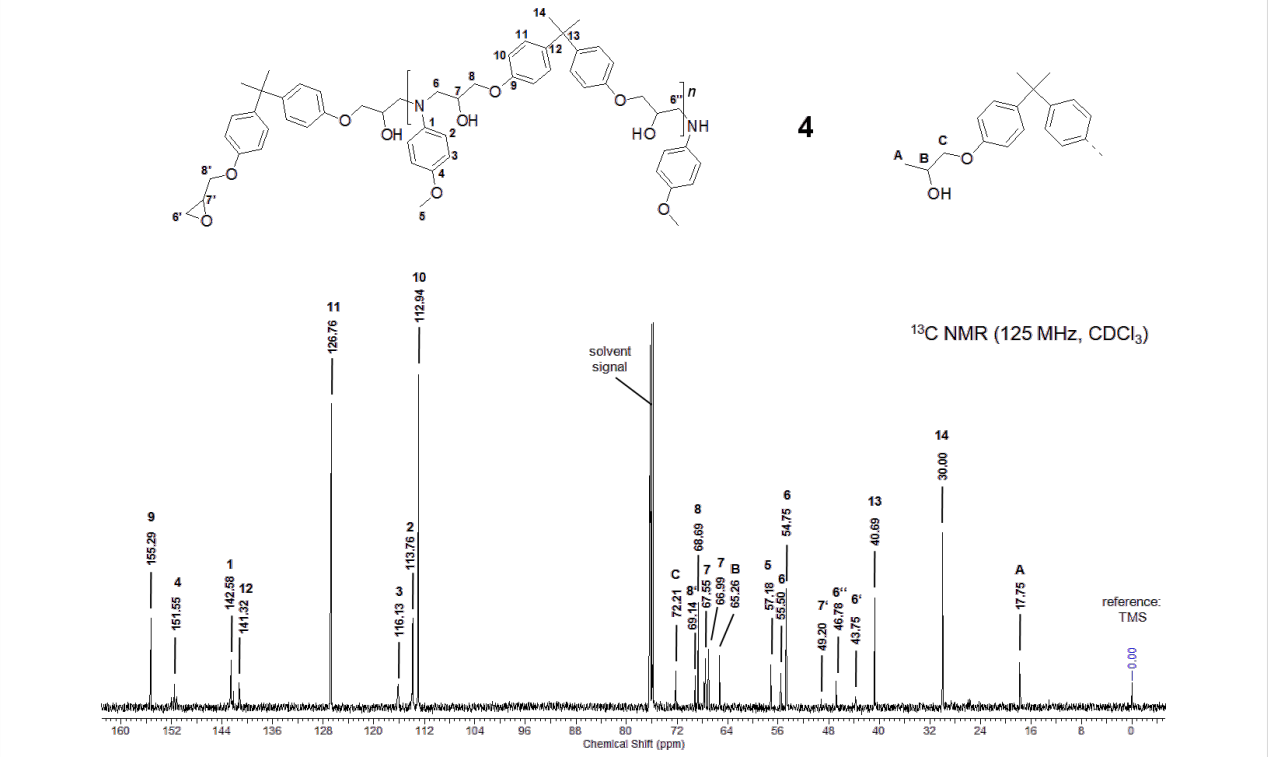


Figure 1: ^{13}C NMR spectra of **4**, measured in $CDCl_3$.

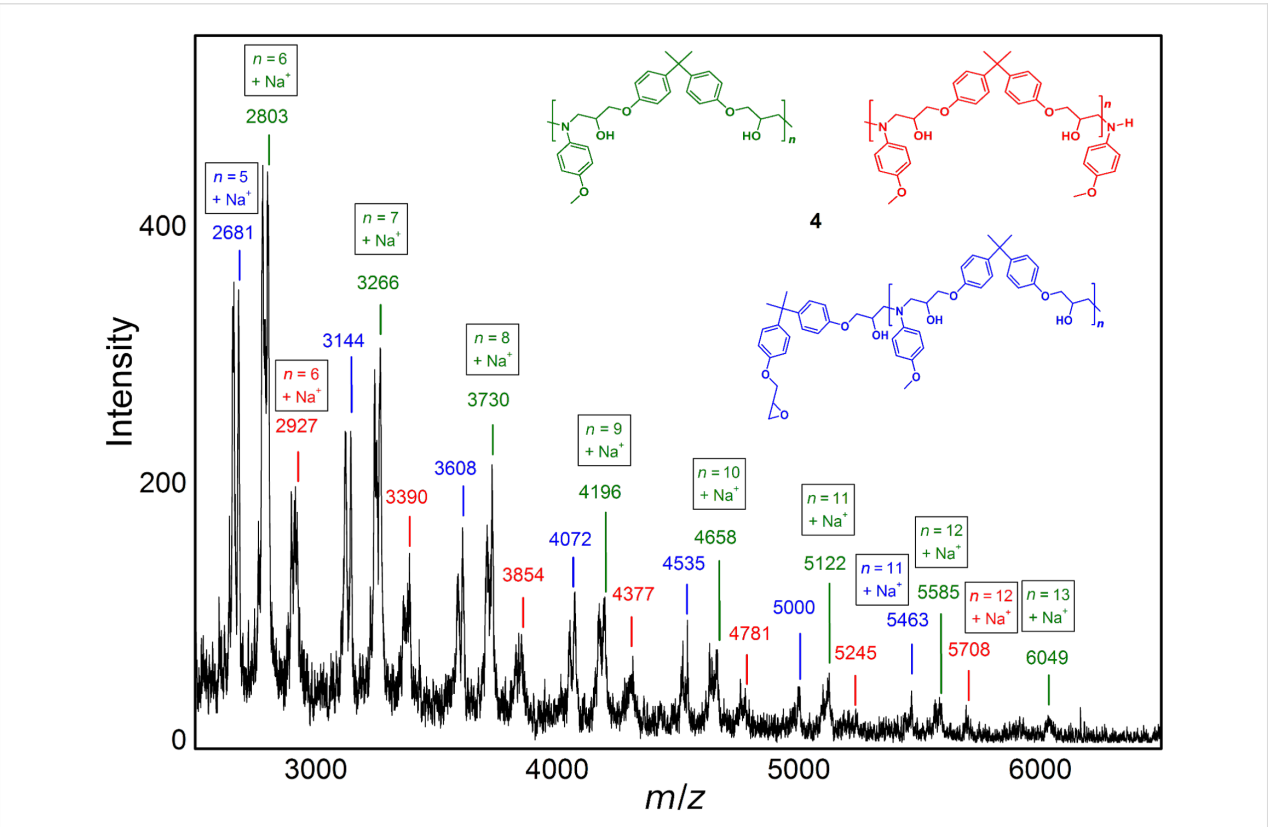


Figure 2: MALDI-TOF MS spectra (linear mode) of epoxide-amine product **4**.

The presence of oligomeric compounds was also confirmed by dynamic light scattering (DLS) measurements in dimethylformamide which indicated a number-average hydrodynamic diameter of 1.45 nm. Moreover, the gel permeation chromatography (GPC) diagram (Figure 3) clearly illustrates the formation of oligomers with repetitive units.

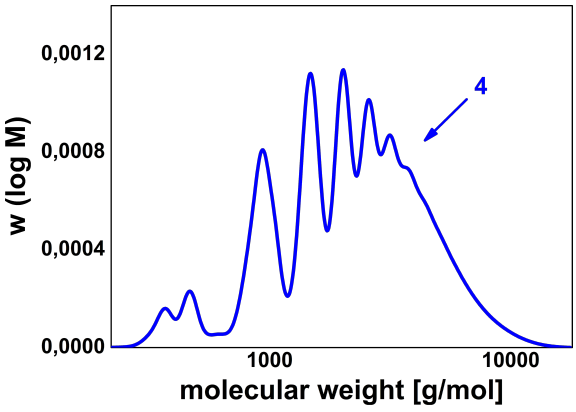


Figure 3: GPC curve of epoxide-amine product **4** detected by UV absorption.

Molecular weights calculated from the GPC curve are about 1700 g mol^{-1} for M_n and 2600 g mol^{-1} for M_w. The molecular weight distribution of the addition polymer **4** is relatively narrow (M_w/M_n = 1.6) which is typical for low molecular weight polymers.

The differential scanning calorimetry (DSC) curve of compound **4** shows a glass transition temperature (T_g) at 63 °C. The low molecular weight epoxide-amine adduct **4** is soluble, e.g., in tetrahydrofuran (THF), methanol, chloroform but insoluble in *n*-hexane and water.

We also carried out the above described one-pot reaction in THF as solvent. Surprisingly, in this process only reduction of the nitro groups took place, but no formation of oligomers was observed. Performing the solvent-free one-pot synthesis with reaction times up to 1 h did not lead to higher molecular weights. The formation of low molecular weight adducts **4** here is probably a result of the hydrogenation of some of the epoxide groups. Due to this side reaction, epoxide and amine compounds are not present in equimolar amounts so that the formation of higher sequences is prevented. To investigate this point, the addition polymerization was also carried out as a two-pot synthesis in bulk. Thus in the first step nitro compound **2** was reduced to the amine **3** according to Ref. [20]. Then, the crude product **3** was allowed to react with an equimolar amount of **1** for 10 min at 120 °C in the MW oven. As expected, the M_n and M_w values of the resulting product are about 4300 and 9300 g mol^{-1}, respectively which are clearly higher than the values achieved in the one-pot synthesis as described above. The DSC curve of the addition product **4** synthesized via two-pot reaction shows a T_g at 76 °C which is an increase of 7 °C compared with the product obtained via the one-pot synthesis (T_g: 63 °C). Figure 4 shows the number-average hydrodynamic diameters of addition product **4** prepared via the one-pot synthesis (continuous line) and via the two-pot synthesis (dashed line). Consistent with the GPC findings noted above, the number-average hydrodynamic diameter increases from 1.45 nm (one-pot) to 2.00 nm (two-pot).

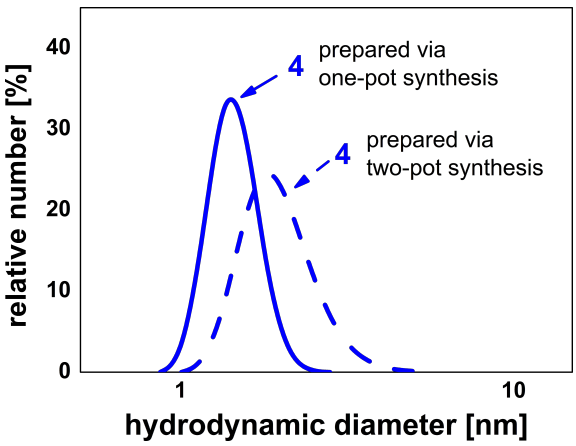
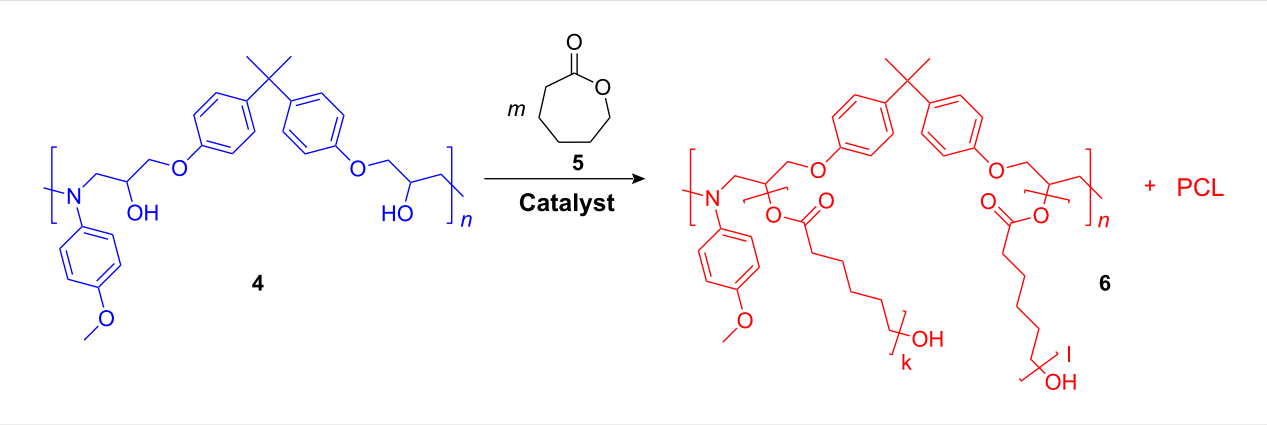


Figure 4: Number-average hydrodynamic diameters of compound **4** prepared via the one-pot (continuous line) and the two-pot (dashed line) synthesis.

Both FT-IR and ^{13}C NMR spectra clearly show signals of epoxide end groups so that probably linear epoxide-amine adducts were formed under the two-step reaction conditions. In addition, the ^{13}C NMR signals at about 18, 65 and 72 ppm which suggest the formation of a secondary alcohol formed by reduction of the epoxide end groups were absent in the ^{13}C NMR spectra of **4** synthesized in the two-pot reaction. These findings indicate that in case of the one-pot synthesis the epoxide reduction to alcohols may take place as a significant side reaction which prevents the formation of higher molecular weight products.

Ring-opening polymerization of ε-caprolactone

The epoxide-amine adduct **4** was used for preparation of graft copolymer **6** via ring-opening polymerization (ROP) of ε-caprolactone (ε-CL, **5**), where the secondary hydroxy groups of **4** act as the initiator. This ROP was catalyzed by bismuth(III) trifluoromethanesulfonate, which is known as effective catalyst for ROP [27] (Scheme 2).



Scheme 2: Ring-opening polymerization of ε-CL using alcohol units as initiator.

The dilution of the hydroxy groups in the obtained product **6** was proven by IR spectroscopy by the nearly complete disappearance of the OH-related absorption band at 3370 cm^{-1}. Furthermore, the formation of ester units was confirmed by the appearance of two strong bands at 1721 and 1176 cm^{-1} associated with C=O and C-O stretching vibrations, respectively.

To prove the existence of grafted polymer **6**, GPC-measurements were carried out. Figure 5 shows the GPC curves of copolymer **6** detected by UV absorption (continuous line) and by RI (dashed line).

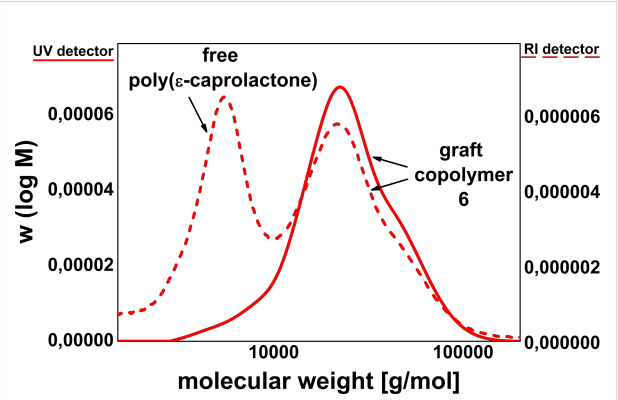


Figure 5: GPC curves of the new formed graft copolymer **6** detected by UV absorption (continuous line) and RI (dashed line).

The UV absorption of **6** in the GPC diagram (continuous line) clearly indicates the appearance of the aromatic compounds in a higher molecular weight area in comparison with the original polymer **4**. The molecular weights of polymer **6** are about 18000 g mol^{-1} for M_n and 27000 g mol^{-1} for M_w with a molecular weight distribution of $M_w/M_n = 1.5$. Additionally, the RI curve (dashed line) shows the existence of some non grafted poly(ε-caprolactone) (PCL) fractions. PCL is probably formed as a side product since one water molecule in the reaction mixture suffices to start this side reaction.

The significant increase of molecular weight in comparison with compound **4** was also confirmed by DLS measurements. As shown in Figure 6, the number-average hydrodynamic diameter increases after grafting from 1.45 nm (**4**) to 3.33 nm (**6**).

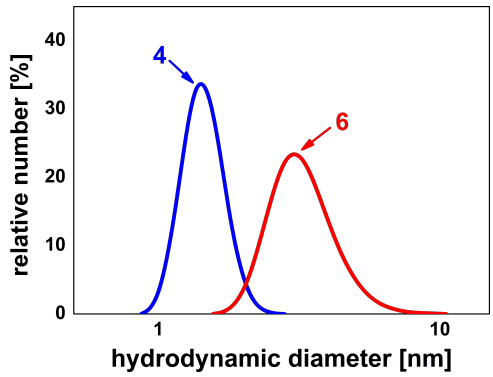


Figure 6: Number-average hydrodynamic diameters of compounds **4** (left) and **6** (right).

The DSC curve of grafted compound **6** shows a melting point (T_m) at 50 °C while PCL homopolymer crystallizes at about 55 °C. Obviously the backbone of copolymer **6** reduces the crystalline order.

Conclusion

A graft copolymer (**6**) was synthesized via ring-opening polymerization of ε-caprolactone using an epoxide-amine addition product **4** as an oligomeric initiator. This oligomer can be obtained in a one-pot microwave assisted heterogeneous catalytic transfer hydrogenation, starting from 4-nitroanisole (**2**) in the presence of the diglycidyl ether of bisphenol A (**1**). Pro-

duct **4** consists of oligomers because of some side reactions. The hydroxy groups of the obtained epoxide-amine adduct **4** were suitable for initiating the ring-opening polymerization of ε-caprolactone.

Experimental

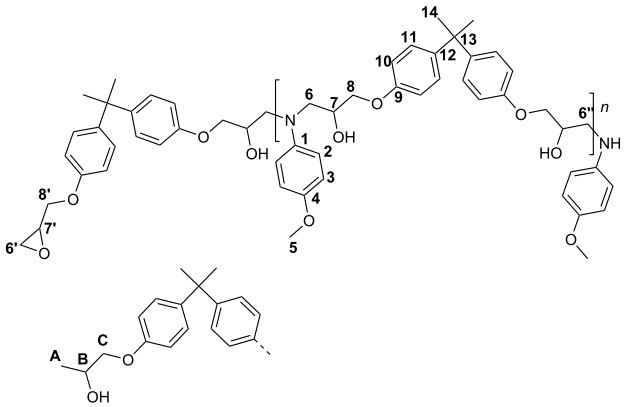
The following commercial products were used: 4-Nitroanisole (97%, Aldrich), 4-methyl-1-cyclohexene (TCI), palladium on activated carbon (Pd/C, 10% Pd, Alfa Aesar) and bismuth(III) trifluoromethanesulfonate (Aldrich) were used without further purification. Diglycidyl ether of bisphenol A (Sigma) was recrystallized from an acetone-methanol mixture (20:80, v/v); mp 44 °C [28]. ε-CL was purchased from Aldrich, dried over calcium hydride, distilled under reduced pressure and stored over 0.4 nm molecular sieves under an argon atmosphere. Chloroform-*d* (99.8% d, water <0.01%) was purchased from Eurisotop (France). The solvents obtained were of analytical grade and used as received.

The hydrogenation was performed in a monomodal microwave reactor (CEM Discover S-Class), equipped with an infrared pyrometer for temperature-control and a 300 W power source. Reactions were performed in closed vessels under controlled pressure. Infrared (IR) spectra were recorded on a Nicolet 6700 FT-IR (Fourier transform infrared) spectrometer, equipped with an ATR unit. The measurements were performed in the range of 4000–300 cm^{-1} at room temperature. ^1H and ^{13}C NMR spectra were obtained using a Bruker Avance DRX 500 spectrometer at 20 °C operating at 500.13 MHz for proton and 125.77 MHz for carbon, using deuterated chloroform as solvent. The chemical shift (δ-scale) was calibrated to TMS. Elemental analysis (EA) was carried out with a Perkin-Elmer Analyzer 2400 with an accuracy of measurement of ±0.3%. Differential scanning calorimetry (DSC) measurements were performed using a Mettler Toledo DSC 822 controller apparatus equipped with a sample robot TSO801RO. The apparatus was controlled over a temperature range between −40 and 120 °C at a heating rate of 10 K min^{-1}. For calibration, standard tin, indium and zinc samples were used. Three heating cycles were conducted. The glass-transition temperature (T_g) values are reported as the average of the second and the third heating cycle using the midpoint method. The melting point (T_m) values are reported as the average peak maxima of the second and the third heating cycle. Matrix-assisted laser desorption-ionization time-of-flight mass spectrometry (MALDI-TOF MS) was performed on a Bruker Ultraflex TOF mass spectrometer. Ions formed with a pulsed nitrogen laser (25 Hz, 337 nm) were accelerated to 25 kV, the molecular masses being recorded in linear mode. Dithranol was used as a matrix and sodium trifluoroacetate (NaTFA) as ionization reagent. The samples were dissolved in THF. Molecular weights and molecular weight distributions were measured by gel permeation chromatography (GPC) using a hydroxyethyl methacrylate (HEMA)-5 μm column set consisting of a precolumn of 4 nm and main colums of 10^3, 10^2 and 10 nm. Tetrahydrofuran (THF) was used as the eluent at a flow rate of 1 mL min^{-1}. For online detection, a Waters 486 tunable absorbance detector (λ = 256 nm) and a Waters 410 differential refractometer were used. The number average molecular weight (M_n), the weight average molecular weight (M_w) and the polydispersity (PD) were calculated by a calibration curve generated by polystyrene standards with a molar mass range from 580 to 1 186 000 Da. Dynamic light scattering (DLS) experiments were implemented on a Malvern HPPS-ET apparatus at a temperature of 25 °C using dimethylformamide (DMF) as solvent. Hellma Suprasil precision cells (110-QS) were used. The particle size distribution was derived from a deconvolution of the measurement number-average autocorrelation function of the sample by the general purpose mode algorithm included in the DTS software. Each experiment was performed five times to obtain statistical information.

Synthesis of epoxide-amine addition product 4

A 35 mL pressure-resistant microwave test tube provided with a magnetic stirring bar was loaded with diglycidyl ether of bispenol A (**1**) (1.702 g, 5.00 mmol) and 4-nitroanisole (**2**) (0.766 g, 5.00 mmol). The solids were dissolved in 4-methyl-1-cyclohexene (2.404 g, 25.0 mmol). After the addition of 10% Pd/C (125 mg) the tube was sealed with a silicon septum and the mixture irradiated for 5 min at a temperature of 120 °C using a maximum power of 100 W in the monomode microwave reactor. To prevent overheating, the reaction was performed under simultaneous cooling with compressed air (5 psi). After cooling to room temperature, the reaction mixture was dissolved in about 10 mL THF to remove the catalyst by filtration. The solution was concentrated under reduced pressure to give product **4**. The crude product was dissolved in 40 mL THF and precipitated into 400 mL of cold *n*-hexane. The polymer was isolated by filtration and dried under vacuum. A yield of 1.73 g (75%) was obtained.

EA $(C_{28}H_{33}NO_5)_n$ $(463.57)_n$: Calc. C 72.55, H 7.18, N 3.02; Found C 72.40, H 7.26, N 2.92. FT-IR (diamond): 3370 ν(OH), 2963, 2930, 2870 $\nu(CH)_{CH3,\ CH2}$, 2832 $\nu(CH)_{Ar\text{-}O\text{-}CH3}$, 1607, 1582, 1509 $\nu(C{=}C)_{aromatic}$, 1462 δ(CH), 1362 δ_s(CH), 1296 δ(OH), 1237 $\nu(CO)_{ArOCH2}$ cm^{-1}, no absorptions at 1589 $\nu_{as}(NO_2)$, 1329 $\nu_s(NO_2)$ and 911 $\nu(CH)_{epoxide}$ cm^{-1}. ^{13}C NMR ($CDCl_3$, 125 MHz): δ (ppm): 155.29 (9), 151.55 (4), 142.58 (1), 141.32 (12), 126.76 (11), 116.13 (3), 113.76 (2), 112.94 (10), 72.21 (C), 69.14 (8'), 68.69 (8), 67.55 (7), 66.99 (7), 65.26 (B), 57.18 (5), 55.50 (6), 54.75 (6), 49.20 (7'), 46.78 (6''), 43.75 (6'), 40.69 (13), 30.00 (14), 17.75 (A).



Synthesis of graft copolymer 6

57.9 mg (0.125 mmol) of the epoxide-amine addition product **4** and 1.142 g (10 mmol) of ε-CL (**5**) were mixed with 0.05 mol % of the catalyst bismuth(III) trifluoromethanesulfonate in a 10 mL vial sealed with a septum. The stirred reaction mixture was kept at 100 °C for 4 days. After cooling to room temperature, the reaction mixture was dissolved in 5 mL chloroform and precipitated into 150 mL of cold methanol. The polymer was isolated by filtration and dried under vacuum. A yield of 0.83 g was obtained.

IR (diamond): 2944, 2895, 2865 $\nu(CH)_{CH3,\ CH2}$, 1721 $\nu(CO)$, 1512 $\nu(C{=}C)_{aromatic}$, 1471 $\delta(CH)$, 1365 $\delta_s(CH)$, 1293 $\delta(OH)$, 1239 $\nu(CO)_{ArOCH2}$, 1176 $\nu(CO)$ cm^{-1}.

References

1. Loupy, A., Ed. *Microwaves in Organic Synthesis,* 2nd ed.; Wiley-VCH: Weinheim, Germany, 2006.
2. Kappe, C. O.; Stadler, A. *Microwaves in Organic and Medicinal Chemistry;* Wiley-VCH: Weinheim, Germany, 2005.
3. Lidström, P.; Tierney, G. P. *Microwave-Assisted Organic Synthesis;* Blackwell Publishing Ltd: Oxford, UK, 2005.
4. Hayes, B. L. *Microwave Synthesis: Chemistry at the Speed of Light;* CEM Publishing: Matthews, NC, USA, 2002.
5. Bardts, M.; Gonsior, N.; Ritter, H. *Macromol. Chem. Phys.* **2008,** *209,* 25–31. doi:10.1002/macp.200700443
6. Dallinger, D.; Kappe, C. O. *Chem. Rev.* **2007,** *107,* 2563–2591. doi:10.1021/cr0509410
7. Kappe, C. O. *Angew. Chem.* **2004,** *116,* 6408–6443. doi:10.1002/ange.200400655
   Angew. Chem., Int. Ed., **2004,** *43,* 6250–6285. doi:10.1002/anie.200400655
8. Xu, Y.; Guo, Q.-X. *Heterocycles* **2004,** *63,* 903–974. doi:10.3987/REV-03-574
9. Desai, B.; Kappe, C. O. *Top. Curr. Chem.* **2004,** *242,* 177–208. doi:10.1007/b96876
10. Wiesbrock, F.; Hoogenboom, R.; Schubert, U. S. *Macromol. Rapid Commun.* **2004,** *25,* 1739–1764. doi:10.1002/marc.200400313
11. Appukkuttan, P.; Van der Eycken, E. *Eur. J. Org. Chem.* **2008,** 1133–1155. doi:10.1002/ejoc.200701056
12. Nicks, F.; Borguet, Y.; Delfosse, S.; Bicchielli, D.; Delaude, L.; Sauvage, X.; Demonceau, A. *Aust. J. Chem.* **2009,** *62,* 184–207. doi:10.1071/CH08510
13. Piras, L.; Genesio, E.; Ghiron, C.; Taddei, M. *Synlett* **2008,** 1125–1128. doi:10.1055/s-2008-1072717
14. Vanier, G. S. *Synlett* **2007,** 131–135. doi:10.1055/s-2006-958428
15. Dayal, B.; Ertel, N. H.; Rapole, K. R.; Asgaonkar, A.; Salen, G. *Steroids* **1997,** *62,* 451–454. doi:10.1016/S0039-128X(97)00010-X
16. Banik, B. K.; Barakat, K. J.; Wagle, D. R.; Manhas, M. S.; Bose, A. K. *J. Org. Chem.* **1999,** *64,* 5746–5753. doi:10.1021/jo981516s
17. Daga, M. C.; Taddei, M.; Varchi, G. *Tetrahedron Lett.* **2001,** *42,* 5191–5194. doi:10.1016/S0040-4039(01)00969-8
18. Berthold, H.; Schotten, T.; Hönig, H. *Synthesis* **2002,** 1607–1610. doi:10.1055/s-2002-33349
19. Stiasni, N.; Kappe, C. O. *ARKIVOC* **2002,** *(Part viii),* 71–79.
20. Chapman, N.; Conway, B.; O'Grady, F.; Wall, M. D. *Synlett* **2006,** 1043–1046. doi:10.1055/s-2006-939062
21. Klee, J. E.; Hörhold, H. H. Epoxide-amine addition polymers, linear. In *Polymeric Materials Encyclopedia;* Salamone, J. C., Ed.; CRC Press: Boca Raton, Florida, USA; Vol. 3, D-E, pp 2182–2192. And references therein.
22. Theis, J.; Ritter, H.; Klee, J. E. *Macromol. Rapid Commun.* **2009,** *30,* 1424–1427. doi:10.1002/marc.200900157
23. Klee, J. E.; Flammersheim, H.-J. *Macromol. Chem. Phys.* **2002,** *203,* 100–108. doi:10.1002/1521-3935(20020101)203:1<100::AID-MACP100>3.0.CO;2-J
24. Klee, J. E.; Hörhold, H.-H.; Schütz, H. *Acta Polym.* **1987,** *38,* 293–299. doi:10.1002/actp.1987.010380509
25. Rylander, P. N. *Hydrogenation Methods;* Academic Press: London, UK, 1985; pp 137–139.
26. Kropf, H.; Thiem, J.; Nimz, H. In *Methoden der Organischen Chemie (Houben-Weyl);* Kropf, H., Ed.; Stuttgart, Germany, 1979; Vol. VI/1a, Part 1, pp 338–342.
27. Zhou, J.; Schmidt, A. M.; Ritter, H. *Macromolecules* **2010,** *43,* 939–942. doi:10.1021/ma901402a
28. Lastovica, J. E., Jr. Method for purifying diglycidyl ether of bisphenol A. U.S. Patent 3,142,688 July 28, 1964.

License and Terms

This is an Open Access article under the terms of the Creative Commons Attribution License (http://creativecommons.org/licenses/by/2.0), which permits unrestricted use, distribution, and reproduction in any medium, provided the original work is properly cited.

The license is subject to the *Beilstein Journal of Organic Chemistry* terms and conditions: (http://www.beilstein-journals.org/bjoc)

The definitive version of this article is the electronic one which can be found at: doi:10.3762/bjoc.6.105

Beilstein Journal of Organic Chemistry

Miniemulsion polymerization as a versatile tool for the synthesis of functionalized polymers

Daniel Crespy and Katharina Landfester*

Full Research Paper

Open Access

Address:
Max Planck Institute for Polymer Research, Ackermannweg 10, 55128 Mainz, Germany

Email:
Daniel Crespy - crespy@mpip-mainz.mpg.de; Katharina Landfester* - landfest@mpip-mainz.mpg.de

* Corresponding author

Keywords:
functionalized polymers; heterophase polymerization; miniemulsion; polymer colloids; polymerization

Beilstein J. Org. Chem. **2010,** *6,* 1132–1148.
doi:10.3762/bjoc.6.130

Received: 22 July 2010
Accepted: 10 November 2010
Published: 01 December 2010

Guest Editor: H. Ritter

© 2010 Crespy and Landfester; licensee Beilstein-Institut.
License and terms: see end of document.

Abstract

The miniemulsion technique is a particular case in the family of heterophase polymerizations, which allows the formation of functionalized polymers by polymerization or modification of polymers in stable nanodroplets. We present here an overview of the different polymer syntheses within the miniemulsion droplets as reported in the literature, and of the current trends in the field.

Review

Introduction

Miniemulsions are a special class of emulsions that are stabilized against coalescence (by a surfactant) and Ostwald ripening (by an osmotic pressure agent). The miniemulsions are produced by high-energy homogenization and usually yield stable and narrowly distributed droplets with a size ranging from 50 to 500 nm. Apolar droplets can be dispersed in a polar liquid to give direct miniemulsions (most classically oil-in-water), whereas the contrary (polar droplets in a non-polar liquid) leads to inverse miniemulsions (e.g., water-in-oil, w/o). Water-free miniemulsions can be formed in direct or inverse systems. Polymers can be synthesized in a miniemulsion system in the dispersed phase, at the interface of the droplets, or in the continuous phase, although only the two first possibilities are usually found in the literature. In principle, the synthesis of functionalized polymers in miniemulsion can occur either by (co)polymerizing one or several functional monomers, or by the modification of polymers present in the dispersed phase of a miniemulsion. In the latter case, the functionalization can occur by the reaction or the assembly of small molecules on the polymer, by the grafting of macromolecules or by degradation of the polymer. The functionalized polymer originates therefore from one or several reactive monomers or is the product of the transformation of a non-functional polymer to a functional polymer. The IUPAC recommendation for the term "functional polymer" is very broad since it includes polymers bearing "specified chemical groups" and polymers having "specified

physical, chemical, biological, pharmacological, or other uses which depend on specific chemical groups" [1]. Reviews on miniemulsion have recently been published, focusing on the kinetics of polymerization [2,3], the structure of the obtained nanoparticles [4], and their applications in medicine [5] as well as for catalysis [6]. As a consequence of the mechanism of the formation of miniemulsions, and due to their colloidal properties and stability, a large range of different polymers colloids can be generated using a miniemulsion. Table 1 shows some important references for the synthesis of commercially important polymers.

Table 1: Important polymer classes produced by miniemulsion polymerization.

Polymer class	Polymerization	Year	Ref.
polystyrene	radical	1973	[7]
polyvinyl chloride	radical	1984	[8]
silicone	anionic	1994	[9]
polyethylene	catalytic	2000	[10]
epoxy	polyaddition	2000	[11]
polyurethane	polyaddition	2001	[12]
saturated polyester	polycondensation	2003	[13]
polyamide	anionic	2005	[14]
polyimide	polycondensation	2009	[15]

In this review, we will focus on the description of the possibilities offered by the miniemulsion process to carry out chain polymerization, polyaddition, polycondensation, and modifications of polymers, and the trends followed in this research field. The so-called "artificial miniemulsions", i.e., the miniemulsion of preformed polymer, are not described in this review.

Free-radical polymerization

Most of the reported polymer syntheses in miniemulsion are performed via free-radical polymerization. In fact, the polymerization is very simple to perform and yields are usually high. Moreover, the polydispersity in size of the miniemulsion particles and the dispersity of the polymer are not directly correlated, and for applications the focus is in many cases on the nanoparticles themselves, i.e., size and size distribution or morphology, and not on the characteristics of the polymer chains (for a given polymer). Functionalized polymers can be obtained by the homopolymerization of a functional monomer or its copolymerization with another (non-functional) monomer. The generation of functional (and therefore often hydrophilic) (homo)polymer particles in inverse miniemulsion is more straightforward than direct miniemulsions, since the presence of functional groups such as amino, hydroxy, or carboxylic acid groups tends to increase the hydrophilicity of the monomer. The polymerization of hydrophilic monomers in inverse miniemulsions was recently reviewed by Capek [16]. The functional groups that can be introduced in latexes by free-radical polymerization in inverse miniemulsion are overviewed in Table 2.

Table 2: Functional monomers or comonomers polymerized in inverse miniemulsion (crosslinkers are not mentioned here).

Functional group	(co)Monomer	Ref.
carboxylic acid	methacrylic acid	[17,24]
	acrylic acid	[18-20,23]
hydroxy	2-hydroxyethyl methacrylate	[18,21]
	vinyl gluconamide	[28]
sulfonate	2-acrylamido-2-methyl-1-propanesulfonic acid	[25,26]

Homopolymers of crosslinked polymethacrylic acid [17], polyacrylic acid, i.e., poly(acrylic acid) and poly(acrylic acid sodium salt) [18-20], and poly(2-hydroxyethyl methacrylate) [18,21] were synthesized in inverse w/o miniemulsions. The polymerization of 2-hydroxyethyl methacrylate could be performed in inverse miniemulsion with a surface active initiator or an oil-soluble initiator. The initiator potassium peroxodisulfate (KPS) could not be used due to its low solubility in the 2-hydroxyethyl methacrylate monomer. Similarly, sodium acrylate was polymerized in inverse miniemulsion and was crosslinked with diethylene glycol diacrylate to yield, after the transfer to water, stable microgels. Monodisperse latexes could be obtained with the poly(2-hydroxyethyl methacrylate) when water, methanol, ethanol, ethylene glycol, or water/ethanol mixtures were used as the dispersed phase in the presence of cobalt tetrafluoroborate [21]. This approach is particularly interesting to encapsulate large amounts of metal salts. Indeed, up to 22.6 wt % of the cobalt salt compared to the monomer content could be encapsulated. Monodisperse latexes of silver–polymer particles were also obtained upon reduction of silver nitrate in the monomer droplets followed by polymerization of the dispersed phase [22]. The reduction reaction was performed at high temperature and miniemulsions were kept stable. This novel system opens up the area of high temperature reactions in miniemulsion. Acrylic acid was also copolymerized with trivinylacrylic acid in inverse minemulsion [23]. The non-reacted vinyl groups, detected by NMR spectroscopy, could be subsequently further crosslinked. The syntheses of temperature-responsive microgels in inverse miniemulsion have also been reported [24]. *N*-isopropylacrylamide and methacrylic acid were polymerized in the presence of Fe_3O_4 ferrofluid to yield superparamagnetic particles. Wiechers et al. investigated

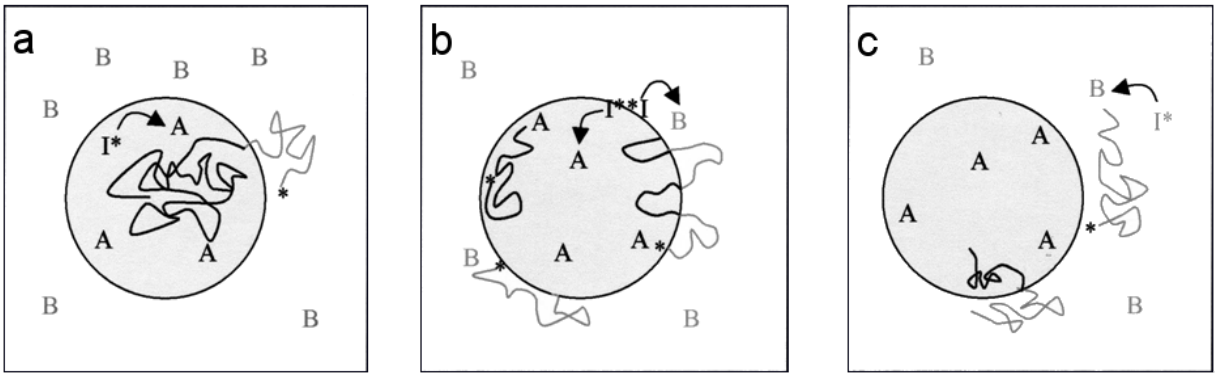


Figure 1: Copolymerization of 2 monomers A and B with different polarities in direct miniemlusions with the decomposed initiators $I^{\bullet}$ which are **a:** oil-soluble, **b:** surface active, **c:** water-soluble (reproduced with permission from [27]. Copyright (2002) Wiley-VCH Verlag GmbH & Co, KGaA).

the copolymerization of 1-vinylimidazole and 2-acrylamido-2-methyl-1-propanesulfonic acid in inverse miniemulsion with an oil-soluble initiator at different pH values [25]. The polymerization was found to be faster at neutral pH values and higher molecular weight polymers were produced in miniemulsion compared to solution polymerization as a result of the confinement effect. The same group carried out a similar study with the copolymerization of 2-acrylamido-2-methyl-1-propanesulfonic acid and 2-(dimethylamino)ethyl methacrylate [26].

In the copolymerization approaches discussed previously, the comonomers were present in the dispersed phase. Willert et al. studied the copolymerization of monomers with opposite polarity, i.e., one comonomer in each phase, in direct and inverse miniemulsion [27]. Water-soluble, surface active, and oil-soluble initiators were employed to initiate the polymerizations as shown in Figure 1. Oil-soluble initiators were found to give a higher yield of copolymers of acrylamide and methyl methacrylate with a low extent of blockiness than with a water-soluble initiator or surface active initiator. By contrast, the surface active polyethylene glycol azo-initiator yielded polymers almost free of homopolymers with a low blockiness when acrylamide and styrene were copolymerized. Wu et al. used the same principle but with monomers having the ability to copolymerize alternately [28]. Thus water-soluble poly(hydroxy vinyl ether)s were copolymerized with oil-soluble maleate esters to yield polymer particles with capsular morphology as shown in Figure 2.

While the formation of (hydrophilic) functionalized particles is straightforward in inverse miniemulsions, it most often required the presence of a second hydrophobic monomer when the polymerization was performed in direct miniemulsions. The hydrophilic acrylic acid or methacrylic acid was successfully polymerized in direct miniemulsion with the hydrophobic octadecyl methacrylate to yield functionalized comb-like polymers [29]. Acrylic acid was copolymerized with styrene to improve the hydrophilicity of the resultant polymer with phase separation of the polymer in oil nanodroplets, to form nanocapsules (and not hemispheres or separate nanoparticles of each phase) [30]. Particles with capsular morphologies suitable for the encapsulation of hydrophobic substances could be obtained. Capsules could be also obtained when methacrylic acid was used instead of acrylic acid [31]. Wu and Schork investigated the copolymerization between the functional *n*-methylol acrylamide and vinyl acetate in batch and semi-batch processes [32]. For a batch process with an initiator in the aqueous phase, it was found that the copolymerization followed the Mayo–Lewis equation despite the huge difference of solubility of the monomers in the aqueous continuous phase. Fluorinated monomers (fluoroalkyl acrylates) could be easily polymerized when dispersed in water in a miniemulsion system [33]. These monomers are typically difficult to polymerize in traditional

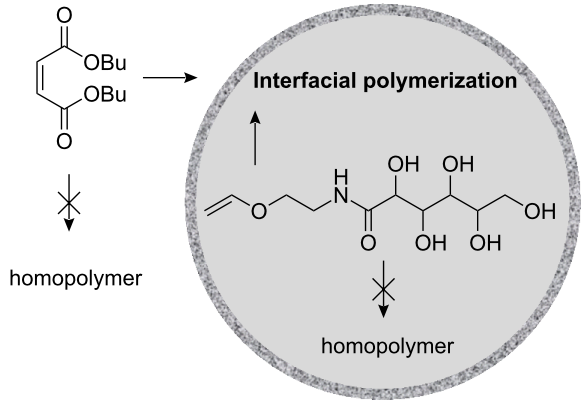


Figure 2: Interfacial alternating radical copolymerization between dibutyl maleate and vinyl gluconamide for building capsules (from [28]).

emulsion polymerizations because of the very low water solubility of the monomers and the oligomers. Functionality was introduced via copolymerization with protonated monomers such as acrylic acid and methacryloxyethyltrimethyl ammonium chloride (MADQUAT).

Styrene was copolymerized with various functional comonomers to be used as model systems for nanoparticles–cell interaction. In fact, a fluorescent marker suitable for FACS and LSM measurements could be encapsulated in the monodisperse nanoparticles with a controlled density of functionalization of the surface. Thus, the influence of the surface functionality nature and density of the nanoparticles on their uptake by different cell lines could be investigated. 2-Aminoethyl methacrylate (0–20 wt %) or acrylic acid were copolymerized with styrene to yield functionalized particles [34,35] and their uptake by cells was studied [34]. In general, with increased functional groups, an increase in the uptake into cells could be observed. Copolymer particles of styrene and acrylic acid were used to encapsulate a platinum(II) complex for photolithographic applications [36], magnetite [37], and as templates for the mineralization on the surface of particles [38]. Ethirajan et al. showed, for instance, that it was possible to use the surface of nanoparticles with carboxylate groups and calcium counterions to mineralize hydroxyapatite on the surface of the particles. Methyl methacrylate, butyl acrylate, and acrylic acid were copolymerized in the presence of alkyd resins to yield hybrid latexes [39]. Similar copolymerizations were carried out with styrene, tetraethylene glycol diacrylate as crosslinker, and up to 20 mol % of 2-hydroxyethyl methacrylate, 2-aminoethyl methacrylate or styrene sulfonic acid [40]. 2-Hydroxyethyl methacrylate and 2-hydroxypropyl methacrylate were copolymerized with styrene and the influence of the functional comonomers on the nucleation mechanism was investigated [41]. A mixture of styrene, butyl acrylate, and butyl methacrylate was also copolymerized with 2-aminoethyl methacrylate by the same authors [42]. Cell–particle investigations were performed with polyisoprene and copolymers of styrene and isoprene fluorescent particles. Their uptake was found to be faster in comparison to polystyrene particles [43]. Such particles can be considered as reactive latexes since they can be easily crosslinked in a subsequent step due to the presence of the double bond. In the case of vinylphosphonic acid, the monomer was added to styrene or MMA with an oil-soluble initiator to form the dispersed phase [44]. In contrast to latexes with styrene as monomer, the use of MMA led to an increase of coagulum by increasing the amount of vinylphosphonic acid. This is explained by the higher solubility of MMA in water as compared to styrene which leads to polymerization of MMA in the continuous phase via homogeneous nucleation. On the other hand, latexes with MMA and 10 wt % vinylphosphonic acid showed the highest density of phosphonate functionality (0.66 group/nm²) at pH = 10. Lu et al. introduced the term "emulsifier-free miniemulsion polymerization" for the copolymerization of styrene and sodium *p*-styrene sulfonate in the presence of magnetite stabilized by oleic acid [45]. The term "emulsifier-free" is debatable since oleic acid possesses surface activity. The concept of copolymerizing with a functional comonomer that is soluble in the continuous phase can be obviously extended to virtually any vinyl functional monomers provided that the copolymerization parameters under such conditions allow copolymerization. The functionalities available using hydrophobic monomers with functional monomers in direct miniemulsions are summarized in Table 3.

We have already mentioned above that latexes can be prepared from polyisoprene and that these can be further crosslinked. Latexes with double functionality were also prepared by the free-radical polymerization of divinylbenzene in miniemulsion [46,47]. The remaining vinyl group after polymerization could be, for instance, reacted with thiol-functionalized PEG via the thiol–ene chemistry [47].

Controlled radical polymerizations

Controlled radical polymerization techniques are suitable for synthesizing polymers with a high level of architectural control. They not only allow the copolymerization with functional monomers as discussed previously for free-radical polymerization, but also simple functionalization of the chain end by the initiator. Miniemulsion systems were found to be suitable to conduct controlled radical polymerizations [48-51] including atom transfer radical polymerization (ATRP), reversible addition fragmentation transfer (RAFT), degenerative iodine transfer [48], and nitroxide mediated polymerization (NMP). ATRP in miniemulsions was recently described in several reviews [52,53]. The kinetics of RAFT polymerization in miniemulsion has been discussed by Tobita [54] and thus no detailed description is required here.

*Sur*factant mono*mer* (surfmer) in radical miniemulsion polymerization

The presence of the surfactant used to stabilize the latexes can have an unfavorable effect on surface properties of films prepared from these latexes. Therefore the use of copolymerizable surfactants was investigated for a number of different polymerization systems. For some step-growth polymerizations in inverse miniemulsions, the surfactant is incorporated into the particle as a result of the end functional groups. Because there is usually only one reactive group in the surfactant, reaction with the surfactant is detrimental for the molecular weight of the polymer. We will focus here only on radical polymerization processes, for which the copolymerization is directed by the co-

Table 3: Functional comonomers employed in polymerizations with styrene, (meth)acrylates, and vinyl acetate in direct miniemulsion.

Main monomer	Functional comonomer	Functional group	Ref.
styrene	acrylic acid	carboxylic acid	[30,34-38]
	methacrylic acid	carboxylic acid	[31]
	2-aminoethyl methacrylate	amino	[34,35,40]
	isoprene	double bond	[43]
	vinylphosphonic acid	phosphonate	[44]
	2-hydroxyethyl methacrylate	hydroxy	[40,41]
	2-hydroxypropyl methacrylate	hydroxy	[41]
	styrene sulfonic acid	sulfonate	[40,45]
methyl methacrylate	vinylphosphonic acid	phosphonate	[44]
styrene, butyl acrylate, butyl methacrylate	2-aminoethyl methacrylate	amino	[42]
methyl methacrylate, butyl acrylate	acrylic acid	carboxylic acid	[39]
vinyl acetate	*n*-methylol acrylamide	hydroxy	[32]
octadecyl methacrylate	acrylic acid, methacrylic acid		[29]
fluoroalkyl acrylates	acrylic acid	carboxylic acid	[33]
	methacryloxyethyltrimethyl ammonium chloride	ammonium	[33]

polymerization parameters of the monomers. The functionalities available from the literature are listed in Table 4 and the chemical structures are displayed in Figure 3.

Table 4: Functionalities of polymerizable surfactants used for the stabilization miniemulsions.

Functionality	Ref.
sulfosuccinate	[55]
sulfate	[58]
carboxylate	[56]
phosphate	[46]
hydroxy	[46]
fluorinated	[57]
quaternary ammonium	[58-60]

Styrene and methyl methacrylate were copolymerized with the sodium salt of vinylbenzylsulfosuccinic acid [55]. Stable latexes were obtained with oil-soluble or water-soluble initiators. The authors estimated that 50 to 75% of the surfactant was efficiently grafted onto the surface of the particles. A polymerizable surfactant was formed by the esterification of hydroxypropyl methacrylate or hydroxyethyl methacrylate with succinic anhydride [56]. SDS was added to the surfmers to give sufficient stability to the latexes. A mono-fluorooctyl maleate surfactant has been used to stabilize the polymerization of styrene in miniemulsion [57]. Although the polymerizable moiety was not fixed at the end of the fluorinated chain (the hydrophobe part), the authors claimed that the surfactant was copolymerized with the styrene monomer. They compared the IR spectra (vibration of $–CF_2$ and $–CF_3$) before and after dialysis and estimated that 92% of the surfactant remained grafted after dialysis.

Nanoparticles and nanocapsules from polymerization of styrene and/or divinylbenzene in miniemulsion could be produced in the presence of a polymerizable derivative of polyethylene oxide/polypropylene oxide which was used to stabilize the droplets [46]. XPS measurements on dialyzed samples confirmed the grafting of the polymerizable surfactant onto the surface of the particles. Matahwa et al. synthesized one cationic and one anionic polymerizable surfactant and copolymerized these with styrene and methyl methacrylate by RAFT in miniemulsion [58]. The rate of polymerization for the systems stabilized by the non-polymerizable surfactants was similar to systems for which polymerizable surfactants were employed. Cao et al. synthesized and measured the CMC of another cationic polymerizable surfactant and copolymerized it with styrene [59]. Fluorescent particles of polystyrene were created in miniemulsion by copolymerizing styrene, the cationic polymerizable surfactant *N,N*-dimethyl-*N*-*n*-dodecyl-*N*-2-methacryloyloxyethyl ammonium bromide, and eventually the polymerizable dye 1-pyrenylmethyl methacrylate [60]. The pyrene dye encapsulated in the particles displayed an excitation lifetime 17 times longer than pyrene dissolved in THF.

Metal-catalyzed polymerizations

At the end of the last century, many groups focused their research on the production of polyolefins in aqueous media. Ethylene as one of the most industrially relevant monomers was polymerized via various heterophase polymerizations, including

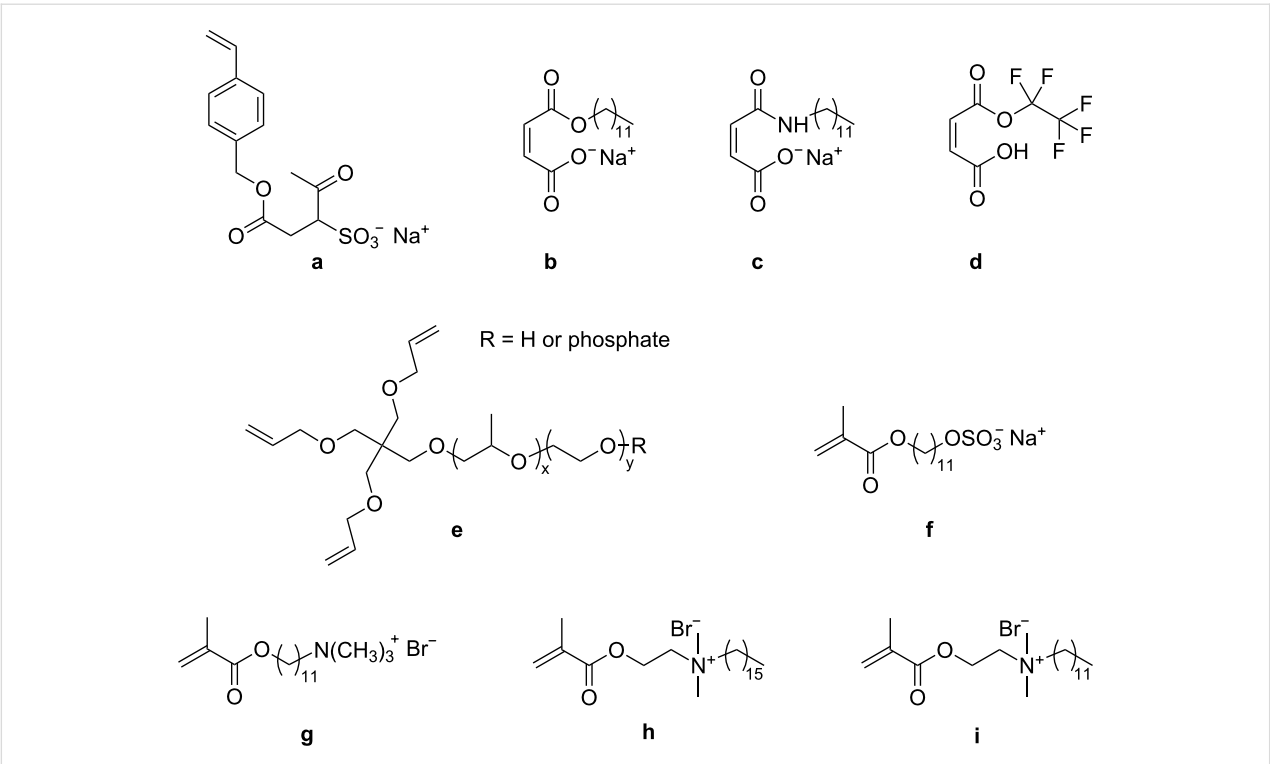


Figure 3: Chemical structures of the surfmers for radical polymerization in miniemulsions: **a:** sodium vinylbenzylsulfosuccinate [55], **b:** hemiester and **c:** hemiamide derivatives of maleic acid [56], **d:** mono-fluorooctyl maleate [57], **e:** PEO/PPO containing surfactant [46], **f:** 11-methacryloyloxyundecan-1-yl sulfate [58], **g:** 11-methacryloyloxyundecan-1-yl trimethyl ammonium bromide [58], **h:** *N,N*-dimethyl-*N*-*n*-hexadecyl-*N*-methacryloyloxyethyl ammonium bromide [59], **i:** *N,N*-dimethyl-*N*-*n*-dodecyl-*N*-methacryloyloxyethyl ammonium bromide [60].

polymerization in miniemulsion. The first report on polymerization of ethylene in miniemulsion describes the synthesis of polyethylene nanoparticles in the presence of a nickel–ylide complex [10]. The catalyst was dissolved in toluene and hexadecane as hydrophobe and the solution was dispersed in an aqueous solution of surfactant (SDS). The mixture was homogenized and ethylene was subsequently added to the system. In this example, the homogenization was by simple mechanical stirring and the droplet size was not measured prior to polymerization. Therefore it is difficult to know if the experiment represented a "true" miniemulsion polymerization process. A similar process was employed but with homogenization of catalyst/hexadecane/toluene, which was performed with either ultrasonication or high-pressure homogenizer in order to obtain a stable miniemulsion [61]. High molecular weight polyethylene (140,000 g·mol^{-1}) could be obtained in stable latexes with particles having a hydrodynamic diameter between 90 and 330 nm. The same principle was used with various catalysts from commercial sources [62]. It was also possible to copolymerize ethylene and up to 3 mol % 1-butene. Small nanoparticles (~200 nm) could be obtained by ethylene polymerization with a nickel(II) keto–ylide complex with 10% solids content in direct miniemulsion [63]. The same group copolymerized ethylene and polar and non-polar α-olefins in miniemulsion with a *P*,*O*-chelated Ni(II) catalyst to obtain dispersions with up to 30% solid content [64]. The copolymerization of carbon monoxide with ethylene or 1-olefins with catalysts formed in situ from palladium(II) complexes gave aliphatic polyketones [65]. The catalyst activity was slightly higher as compared to non-aqueous polymerizations in methanol with the same catalysts.

The emulsion and miniemulsion processes were compared for the copolymerization of ethylene with vinyl acetate [66]. For batch processes, ethylene incorporation in the copolymer was found to be higher in miniemulsion than in emulsion due to the low solubility of ethylene in water and hence its poor transfer through the continuous phase. The use of semibatch processes reduced the difference between emulsion and miniemulsion polymerization in term of incorporation of ethylene in the copolymer. Instead of miniemulsified catalyst, functionalized polystyrene nanoparticles were synthesized in emulsion and miniemulsion by non-covalently immobilized metallocene catalysts [67]. The catalytic polymerization of butadiene with a cobalt catalyst was found to give highly crystalline 1,2-polybutadiene with a particle size of 150–200 nm [68]. The copolymerization of isoprene afforded low crystalline polymers. After Grubbs popularized water resistant catalysts for metathesis polymerizations, it became clear that metathesis could be also

performed in aqueous heterophase systems. Claverie et al. studied the ring-opening metathesis polymerization (ROMP) in emulsion and miniemulsion [69]. Water-soluble ruthenium alkylidene was used for emulsion polymerization of norbornene, whilst an oil-soluble catalyst was employed for the miniemulsion polymerization of norbornene, 1,5-cyclooctadiene, cyclooctene. Similar to the polymerization of ethylene, which is described above, an organic solution of the catalyst was first miniemulsified in water and then the monomer was added to the miniemulsion. The monomer conversion was found to be moderate for the two latter monomers, and relatively high (97%) in the case of norbornene with an obtained particle size of 250 nm.

Another group compared the dispersion, miniemulsion, and suspension polymerization for the ROMP of norbornene or cyclooctadiene [70]. For the miniemulsions, two approaches were followed, i.e., the addition of a catalyst solution to a miniemulsion of the monomer and the addition of monomer to miniemulsion of Grubbs catalyst in water. Although the first approach could yield simultaneously high conversion and stable latexes, particles with sizes above 400 nm without coagulum and 100% conversion could be obtained with the second approach. A water-soluble ruthenium carbene complex (PEO-based catalyst) was prepared as shown in Scheme 1 and used in the direct miniemulsion ROMP of norbornene [71]. Particles with sizes of 200–250 nm could be obtained. The catalytic polymerization of norbornene in direct miniemulsion was also carried out in the presence of an oil-soluble catalyst that was generated in situ, or with a water-soluble catalyst [72]. The reaction was faster when the oil-soluble catalyst was used.

Finally, helical substituted polyacetylene could be efficiently polymerized in direct miniemulsion to yield a latex displaying intense circular dichroism [73]. Particles from 60 to 400 nm could be prepared and the optical activity increased with decreasing particle size. Films were prepared from dried miniemulsion latexes which were then mixed with polyvinyl alcohol in order to preserve the optical activity.

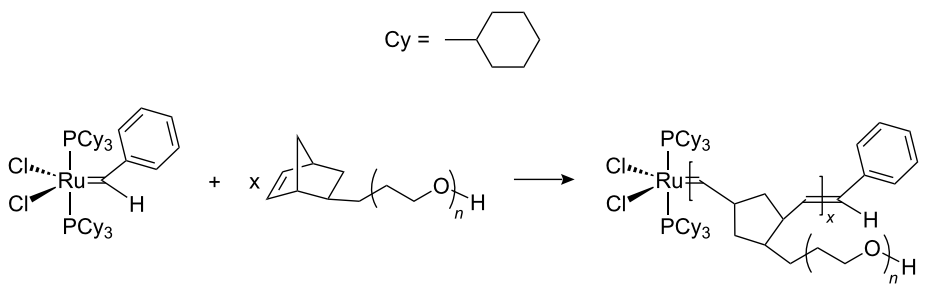
Ionic polymerizations

Although different ionic polymerizations in heterophase have been reported in the literature, they are scarcely described and can be hence still considered as unconventional systems. Ionic miniemulsion polymerizations were carried out either under mild conditions (e.g., in the presence of water) or in water-free conditions (see Figure 4). Historically, ionic polymerizations in miniemulsion under mild conditions were investigated before miniemulsion polymerization requiring water-free conditions (published in 2005). The monomers polymerized for both types of polymerization are listed in Table 5.

Table 5: Monomers employed for ionic polymerizations in miniemulsion.

Monomer	Ref.
octamethylcyclotetrasiloxane	[9,74]
1,3,5-tris(trifluoropropylmethyl)cyclotrisiloxane	[75]
2,4,6,8-tetramethylcyclotetrasiloxane	[76]
tetramethyltetravinylcyclotetrasiloxane	[77]
phenyl glycidyl ether	[78]
p-methoxystyrene	[79-81]
n-butyl cyanoacrylate	[82-90]
ε-caprolactam	[14]

Cyclosiloxanes, for instance, can also be easily polymerized in direct miniemulsion. Octamethylcyclotetrasiloxane, [9,74], 1,3,5-tris(trifluoropropylmethyl)cyclotrisiloxane [75], 2,4,6,8-tetramethylcyclotetrasiloxane [76], and tetramethyltetravinylcyclotetrasiloxane [77] were polymerized in miniemulsion to yield polydimethylsiloxane, poly(trifluoropropylmethyl)siloxane, poly(methylhydrogenosiloxane), and multiblock vinyl functionalized silicones, respectively. Oligomers of phenyl glycidyl ether were produced in direct miniemulsion initiated by the counter anion of the surfmer didodecyldimethyl ammmonium hydroxide [78]. Cationic polymerization can also be performed in direct miniemulsion in the presence of water. *p*-Methoxystyrene was polymerized using the inisurf dodecylbenzenesul-



Scheme 1: Synthesis of the macroinitiator for ROMP in direct miniemulsion [71].

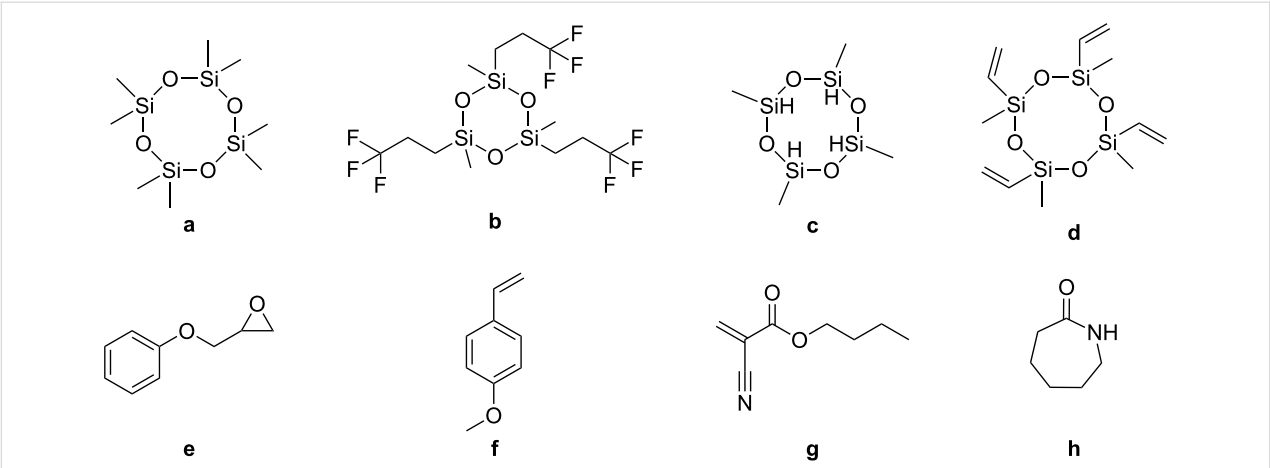


Figure 4: Monomers used in ionic miniemulsion polymerization. **a:** octamethylcyclotetrasiloxane [9,74], **b:** 1,3,5-tris(trifluoropropylmethyl)cyclotrisiloxane [75], **c:** 2,4,6,8-tetramethylcyclotetrasiloxane [76], **d:** tetramethyltetravinylcyclotetrasiloxane [77], **e:** phenyl glycidyl ether [78], **f:** *p*-methoxystyrene [79-81], **g:** *n*-butyl cyanoacrylate [82-90], **h:** ε-caprolactam [14].

fonic acid with a monomer content up to 40 wt % [79]. The same group also investigated the same system in the presence of ytterbium triflate and found that inverse systems were formed [80]. The rate of polymerization was found to be slower than for the direct system whereas the molecular weights obtained were larger. The polymerization was initiated by 1-chloro-1-(*p*-methoxyphenyl)ethane (*p*-MOS-HCl) and catalyzed by trisdodecyl sulfate ytterbium, which is both a surfactant and a Lewis acid [81]. The Lewis acid surfactant did not play the expected role, since the *p*-MOS-HCl was hydrolyzed. The resulting hydronium ion protonated the SDS surfactant, which acted as an inisurf in the interfacial cationic polymerization process.

Alkyl cyanoacrylate monomers are probably the simplest monomers to polymerize anionically since the monomer is very reactive and the polymerization can be conducted in the presence of a large amount of water. Moreover, the polymers were shown to be able to pass the blood brain barrier, making them ideal candidates as vectors for drug delivery. Therefore it is not surprising that several groups have reported the polymerization of cyanoacrylates in miniemulsion. Limouzin et al. obtained low molecular weight oligo(*n*-butyl cyanoacrylate) ($\leq$1,200 g·mol^{-1}) in the presence of a surfactant with a sulfonic acid group that slowed down the polymerization [82]. Altinbas et al. compared the polymerization of *n*-butyl cyanoacrylate both in macroemulsion and in miniemulsion in the presence of an oil (caprylic/capric triglyceride) with water as continuous phase [83]. The latter method yielded capsules with a higher stability. Solid-state NMR spectroscopy showed that the polymer was in contact with both water and oil, leading the authors to identify their particles as capsules (core–shell with oil as the core). Huang et al. showed that paclitaxel was encapsulated with high efficiency in poly(*n*-butyl cyanoacrylate) produced in miniemulsion [84]. Amino acids have been employed to initiate the polymerization of *n*-butyl cyanoacrylate in miniemulsion [85]. The nanoparticles were hence functionalized with carboxyl groups as shown by the pH dependence of the zeta potential. Functionalized nanoparticles of the same polymer were prepared by the polymerization of *n*-butyl cyanoacrylate in miniemulsion in the presence of methoxypoly(ethylene glycol) with the same oil used by Altinbas et al. [86]. Based on FT-IR and ^{1}H NMR measurements, the authors claimed that poly(ethylene gycol) (PEG) chains were connected to the poly(*n*-butyl cyanoacrylate). The same approach has been used by other authors with other surface active initiators based on PEG [87]. The hydrophilic layer thickness and surface coverage of non-dialyzed nanoparticles were estimated for various surfactant concentrations [88]. The investigation was carried out by the same group with a modified dextran as stabilizer [89].

An unconventional approach was reported by Musyanovych and Landfester for the polymerization of *n*-butyl cyanoacrylate [90]. The monomer was solubilized in the continuous phase and the polymer precipitated during the polymerization at the interface of aqueous droplets. The process could be successfully used for the encapsulation of DNA with an encapsulation efficiency of almost 100%. The method is particularly interesting since it allows the encapsulation of hydrophilic substances in the polymer capsules.

The "classical" miniemulsions described above are, however, limited to particular monomers for anionic polymerization. In fact in many cases, the initiator and active species are sensitive to water and hence cannot be polymerized in water-in-oil or oil-in-water miniemulsions. In 2005 we reported the anionic poly-

merization of ε-caprolactam in non-aqueous miniemulsion polymerization [14]. Since the monomer ε-caprolactam is hydrophilic, the polymerization had to be carried out in inverse miniemulsions. ε-Caprolactam-in-oil miniemulsions could not be stabilized efficiently in contrast to DMSO-in-oil miniemulsions. Thus, ε-caprolactam was dissolved in DMSO to build the dispersed phase and polyamide-6 nanoparticles could be obtained. The synthesis strategy paved the way for various water-free reactions to be performed in the miniemulsion nanodroplets, including the formation of hydrophilic polyurethane capsules and particles as discussed below.

Enzymatic polymerization

Enzymatic polymerization could be successfully performed in direct miniemulsion with significant advantages compared to the traditional bulk process. In fact, the bulk process yields only low molecular weight polymers and conversions are limited to 80% after 5 days (see Figure 5). Polyesters were polymerized by enzymatic polymerization of pentadecanolide in direct miniemulsions with amphiphilic lipases (e.g., lipase-PS^{TM}) [91]. Due to the very large interfacial area available, an apparent molecular weight as large as 200,000 g·mol^{-1} could be obtained with full conversion of the monomer after 2 h.

Another advantage of miniemulsion systems compared to solution polymerization was demonstrated by Qi et al. who were able to polymerize styrene with horseradish peroxidase, hydrogen peroxide, and a β-diketone in aqueous direct miniemulsion [92]. Normally, only hydrophilic monomers can be polymerized with this initiating system in water or a co-solvent, e.g. THF, is required, however, the yields of polymer are low. Although the conversion to polymer was moderate in miniemulsion, polymers with apparent molecular weight of up to 406,000 g·mol^{-1} could be obtained.

Oxidative polymerization

Semiconducting polymers are usually difficult to process due to their low solubilities and therefore several groups have investigated polymerization in miniemulsion to improve their processibilities. Oxidative polymerizations were carried out in miniemulsion either in the droplets or on the surface of nanoparticles to create an additional shell. The monomers polymerized are shown in Figure 6.

Aniline and anilium hydrochloride were polymerized in direct and in inverse miniemulsion, respectively [93]. The polymerization of anilium hydrochloride was initiated by hydrogen peroxide and gave highly crystalline emeraldine polyaniline. In direct miniemulsions, additional stabilizers such as poly(vinyl pyrrolidone) or poly(vinyl alcohol) were employed to preserve colloidal stability. The polymerization of aniline in direct miniemulsion has also been reported by other authors [94]. After polymerization, they treated the polymer with stannous chloride and doped the polymer with *p*-toluenesulfonic acid. The conductivity was increased dramatically when stannous chloride was employed, which the authors attributed to the reduction of part of pernigraniline in the emeraldine base structure. Such oxidative polymerization of aniline can be used to add an additional conductive shell to preformed latexes. For instance, Li et al. polymerized aniline in the presence of dodecylbenzesulfonic acid on the surface of polyurethane and polyurethane/polymethyl methacrylate nanoparticles prepared in miniemulsion [95]. The same approach was previously reported for the polymerization of pyrrole initiated by iron(III) chloride on polystyrene latexes produced in miniemulsion to yield particles with sizes ranging from 50 to 70 nm [96]. The conductivity of pellets prepared from the particles was found to be 15.4 S·cm^{-1}. Core–shell morphologies could be identified by selectively dissolving the polystyrene core in THF. Ham et al. dispersed single-wall carbon nanotubes and pyrrole before oxidative polymerization of the monomer [97]. The electric properties of the composite were investigated for application as electrode material for a supercapacitor. Ethylene dioxythiophene (EDOT) has also been polymerized on polystyrene latex in miniemulsion [98].

Polyaddition

Polyaddition and polycondensation reactions always yield functional polymers since the polymers produced are terminated with reactive functional groups. A higher degree of functionality is easily attained using monomers bearing additional reactive groups that do not participate in the step-growth polymerization. Polyaddition and polycondensation are probably the polyreactions for which miniemulsion systems are the most beneficial. An emulsion polymerization scenario where a mixture of micelles and monomer droplets coexist will probably yield polymer particles with a bimodal size distribution. The first polyadditions in miniemulsion carried out were the reactions of polyepoxides and hydrophobic diamines, bisphenols, and dimercaptans [11]. Stable latexes of epoxy resins could be obtained and apparent molecular weights up to 20,000 g·mol^{-1} were measured. Another group reported the reaction between chitosan oligosaccharide with ethylene glycol diglycidyl ether to encapsulate paclitaxel in methylene dichloride-water miniemulsions [99]. The encapsulation was determined by HPLC to be between ~84% and ~92% depending on the ratio and amount of the monomers used, and could be re-dispersed in water after removal of the solvent for release studies. Ethylene glycol diglycidyl ether and L-lysine were polymerized via interfacial polyaddition in inverse miniemulsion [100]. The particles were found to be amphoteric and bear positive charges from secondary amine groups below pH = 8.7, whereas nega-

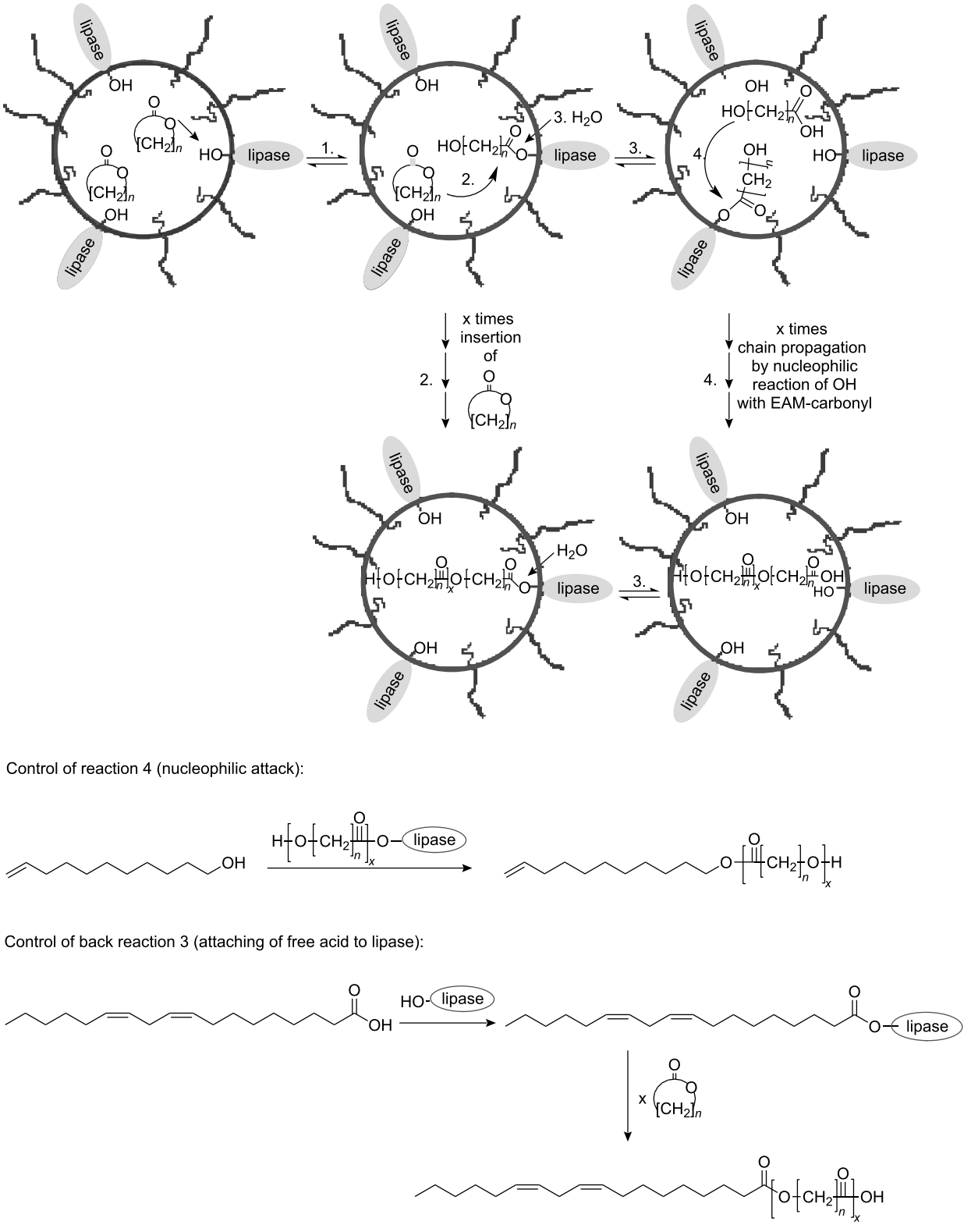


Figure 5: Enzymatic reactions in miniemulsion droplets (reproduced with permission from [91]. Copyright (2003) Wiley-VCH Verlag GmbH & Co, KGaA). EAM = enzyme-activated monomer.

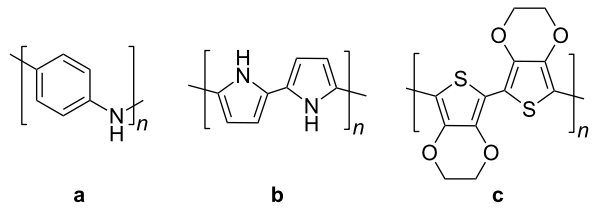


Figure 6: Chemical structure of **a:** polyaniline (leucoemeraldine), **b:** polypyrrole, **c:** poly(ethylene dioxythiophene).

tive charges from the carboxylate groups of the amino acid units were noted above this pH. ssDNA could be trapped at lower pH and could be subsequently released by increasing the pH to 11.0.

The most common miniemulsion polyaddition synthesis is the formation of polyurethanes. Originally, there was considerable interest in producing water-borne polyurethane dispersions to replace the solvent-borne formulations and therefore much effort was expended in investigating the synthesis of polyurethane in aqueous miniemulsions. Hydrophobic diols such as 1,12-dodecanediol, bisphenol A, and/or neopentyl glycol, and the slow reacting isophorone diisocyanate (IPDI) were reacted in miniemulsion droplets [12]. Similar reactions were performed but in the presence of an organotin catalyst [101]. Relatively high apparent molecular weight polyurethane could be obtained. The molecular weight could be increased by the use of an organotin catalyst, a solvent in the dispersed phase and an excess of diisocyanate compared to diol. Instead of synthetic polyols, it is possible to employ polyols from renewable resources to synthesize polyurethane in miniemulsion. For example, castor oil (a triol) has been used as the monomer [102]. Li et al. showed that short diols can be also replaced efficiently by poly(tetramethylene glycol) [103]. The polyaddition reaction to form urethane bonds was also carried out with a cyclodextrin derivative and IPDI as the diisocyanate component [104]. The particles were used to encapsulate nimodipine, a calcium channel blocker.

A popular method to form polyurethane latexes in direct aqueous miniemulsions is to dissolve a reactive preformed prepolymer in the dispersed phase and subsequently carry out the polyaddition. The molecular weights obtained are usually higher for these two-step methods than for the one-pot method described above. Poly(propylene glycol) terminated polyurethane particles with IPDI were polymerized with a diol, an organotin catalyst, and a triol as crosslinker in miniemulsion [105]. Such prepolymers were also polymerized in the presence of monomers, which can be polymerized under radical conditions to yield hybrid latexes [106,107]. Li et al. showed that homogeneous or core–shell morphologies could be obtained depending on the diol added and on the location of the initiator (water-soluble versus oil-soluble) [107]. Another prepolymer used is polydimethylsiloxane terminated by hydroxy groups; this was reacted with IPDI to yield silicone/polyurethane hybrid latexes [108]. An interesting approach is to polymerize a monomer for polyaddition possessing an additional functionality. For instance, the acyl chloride of the azo-initiator 4,4'-azobis(4-cyanopentanoic acid) was reacted with 2,4-diethyl-1,5-pentanediol to yield a diol functionalized with an azo-bond [109]. The functionalized diol was subsequently polymerized with a diisocyanate to yield particles of cleavable polyurethanes. In a second step it was possible to cleave the azo-bonds and polymerize styrene in the nanodroplets. This approach hence combines free-radical polymerization and polyaddition for the production of hybrid block-copolymer particles. Polyurethanes can also be prepared in inverse miniemulsion if the monomers or prepolymers are sufficiently hydrophilic. Polymerizations in non-aqueous inverse miniemulsions are even possible as was previously demonstrated [79]. Polyurethanes free from any urea could be hence produced in non-aqueous inverse miniemulsions in a one-pot process [110]. In this case the miniemulsions of dimethylformamide in hexane were stabilized by a copolymer surfactant with isoprene and methyl methacrylate blocks. A shell of polymethyl methacrylate could be subsequently added after the polyaddition [111]. One of the techniques associated with step-growth polymerizations is the so-called interfacial polyaddition or polycondensation (Table 6). Since the surface generated by the miniemulsion droplets is extremely large, fast reactions are expected to occur in such systems. The formation of a thin film around the nanodroplets allow the creation of core–shell or capsular morphologies.

Polystyrene–polyurea core–shell particles were prepared by miniemulsifying the styrene and a hydrophobic diisocyanate monomer followed by the addition of a diamine to the miniemulsion, and then the radical polymerization of styrene [112]. The presence of the polyurea shell was shown to prevent migration of encapsulated dye. Torini et al. carried out the reaction between a diisocyanate dissolved in oil and a diol dissolved in water and added after miniemulsification of the first monomer in the aqueous continuous phase [113]. Owing to the side reaction with water, only an oligomer with molecular weight ranging from 500 to 3000 $g \cdot mol^{-1}$ could be obtained. The same procedure was used by Johnsen et al. with a different polyol, i.e., propanetriol instead of 1,6-hexanediol [114]. A biocompatible hydrophobic liquid core, Myglyol 812 triglyceride, was used in the droplets to yield core–shell polyurethane/urea for the encapsulation of ibuprofen [115].

Table 6: Polymer obtained by interfacial polyaddition in miniemulsion.

Miniemulsion	Polymer obtained	References
direct	epoxy	[100]
	polyurea	[112]
	poly(urethane-urea)	[113-115]
inverse	epoxy	[116]
	polyurea	[116-118,120]
	poly(urethane-urea)	[116-119,122]
	polyurethane	[116]
	polythiourea	[116]
	crosslinked dextran	[116-118]
	crosslinked starch	[116,121]
	crosslinked polyethyleneimine	[116]

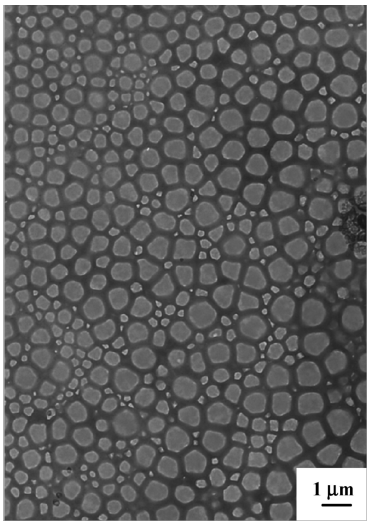


Figure 7: Transmission electron micrograph of polyurethane capsules synthesized by interfacial polyaddition in inverse miniemulsion (reprinted with permission from [116]. Copyright (2007) American Chemical Society).

Interfacial polyaddition in inverse miniemulsions is becoming especially popular since it allows the encapsulation of hydrophilic substances in various polymeric capsules. The method allows the formation of particles with capsular morphology consisting of a liquid core and a polymeric shell in comparison to the traditional monolithic morphology. Such capsular morphologies are suitable for drug delivery applications since the liquid in the core (e.g., water) has usually a higher solvent power than hydrophilic monomers. As for other techniques used to encapsulate drugs such as vesicle or liposome formation or solvent evaporation, the solvent used initially can be removed by dialysis or evaporation and exchanged with water to build the new dispersion medium. The capsules could be obtained with different wall thicknesses depending on the concentration of monomers and with a large variety of polymers, e.g., with epoxy, polyurethane (Figure 7), and polyurea, or based on synthetic polyamines, polythiourea, crosslinked starch, dextran or polyethylene imine [116]. Therefore, the functionality can be directly implemented in the capsules by using an excess of one of the monomers, or by using functionalized monomers or copolymers with additional functionality that do not participate in the polyaddition, in this case, e.g., amino, carboxylic, hydroxy, epoxide, isocyanate, or isothiocyanate.

Such capsules could be used to encapsulate contrast agents (Magnevist®, Gadovist®) for magnetic resonance imaging (MRI) in polyurethane, polyurea, and crosslinked dextran shells [117,118]. No significant difference in the relaxation time (T_1) between the encapsulated agent and the contrast agent in solution could be detected therefore making the capsules good candidates for MRI. Fluorescent dyes as markers are suitable for particle–cell interactions and can be followed by LSM and FACS measurements. Thus, polyurethane/urea capsules produced in inverse miniemulsion were used to encapsulate a fluorescent dye with 90% efficiency [119]. Carboxymethylation was performed on the particle surface followed by physical adsorption of poly(2-aminoethyl methacrylate) or polyethylene imine polycations. As expected, the uptake of the capsules modified by the polycation was found to be higher than for non-modified capsules. Rosenbauer et al. used the same route but in the presence of a surfactant which crosslinked the shell [120]. The commercially available surfactant polyisobutylene-succinimide pentamine was reacted with the diisocyanate monomer. The capsule shell wall was found to be less permeable than for capsules synthesized with a non-crosslinkable surfactant. Baier et al. used the previously described synthesis to carry out a polymerase chain reaction (PCR) in crosslinked starch nanocapsules [121]. The permeability of the shell was also evaluated by fluorescence spectroscopy. The combination of cleavable polyurethane [109] with the interfacial polyaddition described above [116] afforded polymer shells that could be cleaved by UV-irradiation, temperature, or by pH change [122]. In order to study the release of encapsulated sulforhodamine dye from the capsules, polyurethane with and without cleavable functionalities were synthesized. Fluorescence spectroscopy of the supernatant obtained by the centrifugation of both polymer capsules submitted to different stimuli was recorded and the release of the dye was found to occur on different time-scales in the case of the cleavable shells, i.e., minutes for UV-irradiation, hours for a temperature increase, and days for a pH change.

Polycondensation

In aqueous miniemulsion, polycondensations are even more demanding than polyadditions since the water formed in the condensation reaction has to be transported away from the reaction locus. Barrere et al. showed that esterification polyreactions could be efficiently performed in aqueous miniemulsion droplets, even in the presence of a large amount of water (continuous phase), since the reaction locus (the droplets) are hydrophobic and become even more hydrophobic throughout the condensation reaction (Figure 8) [13]. The size of the droplets had no influence on the equilibrium, i.e., similar yields were obtained. Two major parameters were found to play a role in increasing the yield. The yield was higher if a) more hydrophobic monomers and b) diols with electron-donating groups were polymerized. The polycondensation of a diamine and sebacoyl chloride was carried out in direct miniemulsions in the presence of silica nanoparticles prepared in inverse microemulsion [123]. The polyamide was identified by infrared spectroscopy.

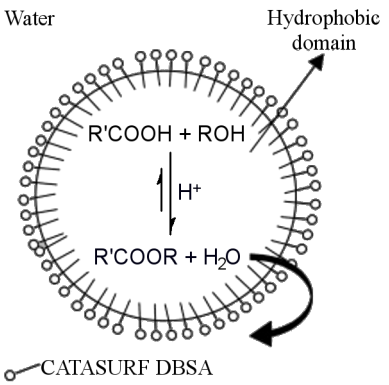
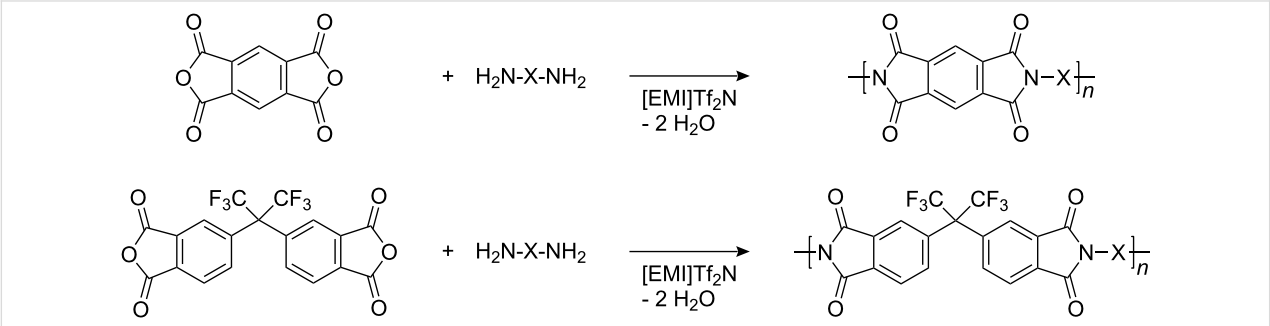


Figure 8: Schematics for the polycondensation reaction between hydrophobic alcohols and carboxylic acids surrounded by the aqueous continuous phase (not to scale for the surfactant) (reprinted with permission from [13]. Copyright (2003) Elsevier).

Polyimide nanoparticles could be synthesized in ionic liquids at temperatures up to 190 °C even although water is produced during the polycondensation as shown in Scheme 2 [15]. Here again, the reaction locus is hydrophobic and spills out the water into the continuous phase. The ionic liquid 1-ethyl-3-methylimidazolium bis(trifluoromethylsulfonyl)imide was used both as continuous phase and as stabilizer due to its amphiphilic properties. The approach is interesting for synthesizing polymers, which require very high polymerization temperatures. Star copolymers of polyethylene glycol and polypropylene glycol were crosslinked in inverse miniemulsion via an esterification reaction with a dithiodicarboxylic acid to yield nanogels [124]. The disulfide bonds were subsequently cleaved by reduction to yield thiols, whereas the nanogels were stable in PBS solution.

Radiation-induced polymerization

Miniemulsions initiated by ^{60}Co γ-rays are reported in a separate paragraph because of their peculiarities. The γ-ray initiated miniemulsion polymerization was conducted to synthesize polystyrene particles [125]. The dose rate and the total absorbed total dose were found to affect the particle size of the latex particles. Y-like branched surfactant were synthesized and used for γ-ray miniemulsion polymerization at room temperature [126]. Polyurethane (2 wt %) was used as the hydrophobe in the miniemulsion polymerization of styrene and was sufficient to ensure a shelf-life of 1 year for the miniemulsion [127]. In both cases [126,127], the particle size and distribution were preserved throughout the polymerization. The copolymerization of styrene with 1-vinyl-2-pyrrolidone as polar monomer in the presence of dodecane in the oil droplets also gave nanocapsules [128]. ^{1}H NMR spectroscopy measurements showed that graft copolymers were obtained by radiation-induced polymerization instead of random copolymers. Copolymers of butyl acrylate, acrylic acid, acrylonitrile, *N*-hydroxymethylacrylamide, and perfluoroalkylethyl methacrylate were prepared in direct miniemulsions with yields up to 96% within 34 h [129]. Functional polystyrene latexes were obtained by copolymerization of styrene with a polymerizable surfactant containing a



Scheme 2: Polyimide from the reaction performed in the ionic liquid 1-ethyl-3-methylimidazolium bis(trifluoromethylsulfonyl)imide [EMI]Tf_2N between a diamine H_2N-X-NH_2 and pyromellitic acid dianhydride, and 4,4'-(hexafluoroisopropylidene)diphthalic anhydride (from [15]).

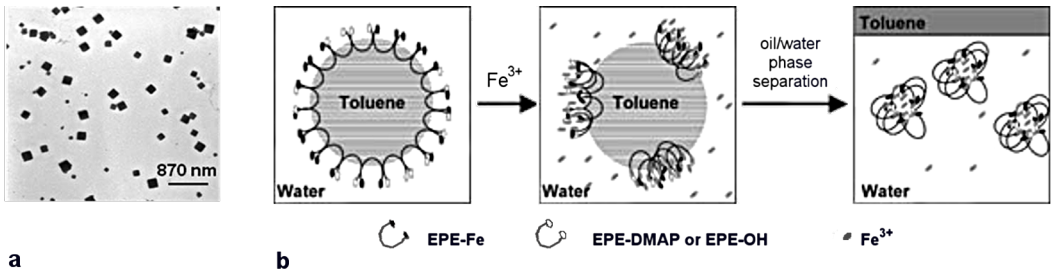


Figure 9: a: TEM micrograph of the cubic structures, **b:** proposed mechanism for the production of the nanocubes. The localized coordination polymerization is thought to destabilize the miniemulsion and nanocube growth is carried on in the aqueous phase (reproduced with permission from [136]. Copyright (2010) Wiley-VCH Verlag GmbH & Co, KGaA).

carboxylic acid group [130]. The authors reported a narrowly particle size distribution when the monomers were polymerized by γ-rays compared to initiation with potassium peroxodisulfate. The presence of carboxylic acid groups at the surface of the particles was confirmed by X-ray photoelectron and FT-IR spectroscopy. Finally, graft hybrid copolymers of polyurethane and polymers from vinyl monomers have also been reported [131]. In a first step, the polyaddition reaction was carried out between a polybutadiene terminated with hydroxy groups and the IPDI monomer in aqueous direct miniemulsion. The grafting of vinyl monomers on the PU backbone was then induced by γ-ray irradiation.

Coupling reactions

Pd-catalyzed cross-coupling reactions were carried out in direct aqueous miniemulsions with 1,2,4-tribromobenzene as crosslinker [132]. Aqueous latexes of crosslinked poly(*p*-phenylene ethynylene) were obtained and their opto-electronic properties were found to be similar to the linear polymer dissolved in toluene. The synthesis of fluorescent conjugated particles of poly(arylene diethynylenes) in direct miniemulsions by Glaser coupling has also been reported [133]. 4,4'-Dinonyl-2,2'-bipyridine was found to be a suitable ligand for solubilizing the copper(I) chloride catalyst in the toluene droplets. A solution of the monomers in toluene was mixed with the solution of the catalyst and then the reaction mixture was miniemulsified in an aqueous solution of a cationic surfactant. The miniemulsion was stirred for several days in the presence of air.

Particles from coordination polymers

Prussian blue shells were created by adding iron(III) ions to direct miniemulsions of toluene/hexadecane stabilized by the organometallic surfactant [PEG-*b*-PPG-*b*-PEG-pentacyano(4-dimethylamino)pyridine) ferrate] [134]. Interparticle coordination was identified by electron microscopy and dynamic light scattering experiments. Nanoboxes could be formed when the concentration of surfactant was 4 wt % at a toluene content of 5 wt % [135]. Forty percent of the organometallic surfactant was replaced by PEG-*b*-PPG-*b*-PEG terminated by bromine atoms. When more 40% of the organometallic was replaced, the synthesis yielded only irregular structures due to inadequate crosslinking. PEG-*b*-PPG-*b*-PEG was used in combination with the organometallic surfactant to reduce the concentration of the latter surfactant on the droplet surface [136]. When 20 wt % toluene was used with low concentration of the organometallic surfactant, cubic nanoparticles were produced instead of the spherical shells (Figure 9). Only irregular structures were obtained in control experiments performed in water, i.e., without oil nanodroplets. The authors deduced that the initial confinement of the coordination polymerization hence played a significant role. The proposed mechanism for the formation of the cubic structures is shown in Figure 9.

Conclusion

Compared to other heterophase polymerizations, miniemulsion polymerization offers an incomparable flexibility to create polymeric nano objects. Liquid or dissolved monomers can be polymerized by an unmatched variety of polymerization processes. The synthesis described above can be virtually extended to any polymerization or any polymer provided that the monomers can be emulsified, i.e., are not water- and oil-soluble. Even then, the monomers could be emulsified in sc-CO_2 or in fluorinated solvents with a suitable surfactant.

Acknowledgements

The image displayed as graphical abstract is a courtesy of the Empa, Switzerland, Laboratory for Protection and Physiology.

References

1. Horie, K.; Barón, M.; Fox, R. B.; He, J.; Hess, M.; Kahovec, J.; Kitayama, T.; Kubisa, P.; Maréchal, E.; Mormann, W.; Stepto, R. F. T.; Tabak, D.; Vohlidal, J.; Wilks, E. S.; Work, W. J. *Pure Appl. Chem.* **2004,** *76,* 889–906. doi:10.1351/pac200476040889
2. Tobita, H. *Macromol. Theory Simul.* **2009,** *18,* 108–119. doi:10.1002/mats.200800069

3. Tobita, H. *Macromol. Theory Simul.* **2009,** *18,* 120–126. doi:10.1002/mats.200800070
4. Landfester, K. *Angew. Chem., Int. Ed.* **2009,** *48,* 4488–4507. doi:10.1002/anie.200900723
5. Mailänder, V.; Landfester, K. *Biomacromolecules* **2009,** *10,* 2379–2400. doi:10.1021/bm900266r
6. Striegler, S. *Mini-Rev. Org. Chem.* **2009,** *6,* 234–240. doi:10.2174/157019309788922757
7. Ugelstad, J.; El-Aasser, M. S.; Vanderhoff, J. W. *J. Polym. Sci., Polym. Lett. Ed.* **1973,** *11,* 503–513.
8. Dewald, R. C.; Hart, L. H.; Carroll, W. F. *J. Polym. Sci., Part A: Polym. Chem.* **1984,** *22,* 2923–2930. doi:10.1002/pol.1984.170221115
9. De Gunzbourg, A.; Favier, J.-C.; Hémery, P. *Polym. Int.* **1994,** *35,* 179–188. doi:10.1002/pi.1994.210350208
10. Tomov, A.; Broyer, J.-P.; Spitz, R. *Macromol. Symp.* **2000,** *150,* 53–58. doi:10.1002/1521-3900(200002)150:1<53::AID-MASY53>3.0.CO;2-8
11. Landfester, K.; Tiarks, F.; Hentze, H.-P.; Antonietti, M. *Macromol. Chem. Phys.* **2000,** *201,* 1–5. doi:10.1002/(SICI)1521-3935(20000101)201:1<1::AID-MACP1>3.0.CO;2-N
12. Tiarks, F.; Landfester, K.; Antonietti, M. *J. Polym. Sci., Part A: Polym. Chem.* **2001,** *39,* 2520–2524. doi:10.1002/pola.1228
13. Barrere, M.; Landfester, K. *Polymer* **2003,** *44,* 2833–2841. doi:10.1016/S0032-3861(03)00151-4
14. Crespy, D.; Landfester, K. *Macromolecules* **2005,** *38,* 6882–6887. doi:10.1021/ma050616e
15. Frank, H.; Ziener, U.; Landfester, K. *Macromolecules* **2009,** *42,* 7846–7853. doi:10.1021/ma901392h
16. Capek, I. *Adv. Colloid Interface Sci.* **2010,** *156,* 35–61. doi:10.1016/j.cis.2010.02.006
17. Capek, I. *Cent. Eur. J. Chem.* **2003,** *156,* 35–61. doi:10.2478/BF02476230
18. Landfester, K.; Willert, M.; Antonietti, M. *Macromolecules* **2000,** *33,* 2370–2376. doi:10.1021/ma991782n
19. Luo, Y. D.; Dai, C. A.; Chiu, W. Y. *J. Colloid Interface Sci.* **2009,** *330,* 170–174. doi:10.1016/j.jcis.2008.10.036
20. Luo, Y.-D.; Dai, C.-A.; Chiu, W.-Y. *J. Polym. Sci., Part A: Polym. Chem.* **2008,** *46,* 8081–8090. doi:10.1002/pola.23105
21. Cao, Z.; Wang, Z.; Herrmann, C.; Ziener, U.; Landfester, K. *Langmuir* **2010,** *26,* 7054–7061. doi:10.1021/la904380k
22. Crespy, D.; Landfester, K. *Polymer* **2009,** *50,* 1616–1620. doi:10.1016/j.polymer.2009.02.003
23. Szaloki, M.; Skribanek, R.; Dudas, Z.; Hartmann, J. F.; Hegedus, C.; Borbely, J. *Colloid Polym. Sci.* **2008,** *286,* 435–444. doi:10.1007/s00396-007-1790-x
24. Lin, C.-L.; Chiu, W.-Y.; Don, T.-M. *J. Appl. Polym. Sci.* **2006,** *100,* 3987–3996. doi:10.1002/app.23084
25. Wiechers, S.; Schmidt-Naake, G. *Macromol. React. Eng.* **2008,** *2,* 126–134. doi:10.1002/mren.200700036
26. Wiechers, S.; Schmidt-Naake, G. *Macromol. Symp.* **2009,** *281,* 47–53. doi:10.1002/masy.200950706
27. Willert, M.; Landfester, K. *Macromol. Chem. Phys.* **2002,** *203,* 825–836. doi:10.1002/1521-3935(20020401)203:5/6<825::AID-MACP825>3.0.CO;2-R
28. Wu, D.; Scott, C.; Ho, C.-C.; Co, C. C. *Macromolecules* **2006,** *39,* 5848–5853. doi:10.1021/ma060951i
29. Baskar, G.; Landfester, K.; Antonietti, M. *Macromolecules* **2000,** *33,* 9228–9232. doi:10.1021/ma0009146
30. Tiarks, F.; Landfester, K.; Antonietti, M. *Langmuir* **2001,** *17,* 908–918. doi:10.1021/la001276n
31. Luo, Y.; Zhou, X. *J. Polym. Sci., Part A: Polym. Chem.* **2004,** *42,* 2145–2154. doi:10.1002/pola.20065
32. Wu, X. Q.; Schork, F. J. *Ind. Eng. Chem. Res.* **2000,** *39,* 2855–2865. doi:10.1021/ie990861k
33. Landfester, K.; Rothe, R.; Antonietti, M. *Macromolecules* **2002,** *35,* 1658–1662. doi:10.1021/ma011608a
34. Holzapfel, V.; Musyanovych, A.; Landfester, K.; Lorenz, M. R.; Mailänder, V. *Macromol. Chem. Phys.* **2005,** *206,* 2440–2449. doi:10.1002/macp.200500372
35. Musyanovych, A.; Rossmanith, R.; Tontsch, C.; Landfester, K. *Langmuir* **2007,** *23,* 5367–5376. doi:10.1021/la0635193
36. Manzke, A.; Pfahler, C.; Dubbers, O.; Plettl, A.; Ziemann, P.; Crespy, D.; Schreiber, E.; Ziener, U.; Landfester, K. *Adv. Mater.* **2007,** *19,* 1337–1341. doi:10.1002/adma.200601945
37. Ramirez, L. P.; Landfester, K. *Macromol. Chem. Phys.* **2003,** *204,* 22–31. doi:10.1002/macp.200290052
38. Ethirajan, A.; Ziener, U.; Landfester, K. *Chem. Mater.* **2009,** *21,* 2218–2225. doi:10.1021/cm9001724
39. Wu, X. Q.; Schork, F. J.; Gooch, J. W. *J. Polym. Sci., Part A: Polym. Chem.* **1999,** *37,* 4159–4168. doi:10.1002/(SICI)1099-0518(19991115)37:22<4159::AID-POLA15>3.0.CO;2-N
40. Töpfer, O.; Schmidt-Naake, G. *Macromol. Symp.* **2007,** *248,* 239–248. doi:10.1002/masy.200750225
41. Chern, C.-S.; Sheu, J.-C. *J. Polym. Sci., Part A: Polym. Chem.* **2000,** *38,* 3188–3199. doi:10.1002/1099-0518(20000901)38:17<3188::AID-POLA180>3.0.CO;2-Y
42. Grabs, I.-M.; Schmidt-Naake, G. *Macromol. Symp.* **2009,** *275–276,* 133–141. doi:10.1002/masy.200950115
43. Lorenz, M. R.; Kohnle, M.-V.; Dass, M.; Walther, P.; Höcherl, A.; Ziener, U.; Landfester, K.; Mailänder, V. *Macromol. Biosci.* **2008,** *8,* 711–727. doi:10.1002/mabi.200700336
44. Ziegler, A.; Landfester, K.; Musyanovych, A. *Colloid Polym. Sci.* **2009,** *287,* 1261–1271. doi:10.1007/s00396-009-2087-z
45. Lu, S.; Ramos, J.; Forcada, J. *Langmuir* **2007,** *23,* 12893–12900. doi:10.1021/la702281k
46. Crespy, D.; Musyanovych, A.; Landfester, K. *Colloid Polym. Sci.* **2006,** *284,* 780–787. doi:10.1007/s00396-005-1446-7
47. Van Berkel, K. Y.; Hawker, C. J. *J. Polym. Sci., Part A: Polym. Chem.* **2010,** *48,* 1594–1606. doi:10.1002/pola.23917
48. Butté, A.; Storti, G.; Morbidelli, M. *Macromolecules* **2000,** *33,* 3485–3487. doi:10.1021/ma991866w
49. Cunningham, M. F. *Prog. Polym. Sci.* **2002,** *27,* 1039–1067. doi:10.1016/S0079-6700(02)00008-4
50. Oh, J. K. *J. Polym. Sci., Part A: Polym. Chem.* **2008,** *46,* 6983–7001. doi:10.1002/pola.23011
51. Zetterlund, P. B.; Kagawa, Y.; Okubo, M. *Chem. Rev.* **2008,** *108,* 3747–3794. doi:10.1021/cr800242x
52. Qian, T.; Wang, J. J.; Zhang, Q. H.; Zhan, X. L.; Chen, F. Q. *Progress in Chemistry* **2010,** *22,* 663–668.
53. Oh, J. K.; Bencherif, S. A.; Matyjaszewski, K. *Polymer* **2009,** *50,* 4407–4423. doi:10.1016/j.polymer.2009.06.045

54. Tobita, H. *Macromol. Symp.* **2010,** *288,* 16–24. doi:10.1002/masy.201050203
55. Boisson, F.; Uzulina, I.; Guyot, A. *Macromol. Rapid Commun.* **2001,** *22,* 1135–1142. doi:10.1002/1521-3927(20011001)22:14<1135::AID-MARC1135>3.0.CO;2-X
56. Guyot, A.; Graillat, C.; Favero, C. *C. R. Chim.* **2003,** *6,* 1319. doi:10.1016/j.crci.2003.07.018
57. Pich, A.; Datta, S.; Musyanovych, A.; Adler, H.-J. P.; Engelbrecht, L. *Polymer* **2005,** *46,* 1323–1330. doi:10.1016/j.polymer.2004.11.065
58. Matahwa, H.; McLeary, J. B.; Sanderson, R. D. *J. Polym. Sci., Part A: Polym. Chem.* **2006,** *44,* 427–442. doi:10.1002/pola.21071
59. Cao, N.; Wang, X.; Song, L.; Zhang, Z. C. *J. Polym. Sci., Part A: Polym. Chem.* **2007,** *45,* 5800–5810. doi:10.1002/pola.22330
60. Taniguchi, T.; Takeuchi, N.; Kobaru, S.; Nakahira, T. *J. Colloid Interface Sci.* **2008,** *327,* 58–62. doi:10.1016/j.jcis.2008.08.003
61. Bauers, F. M.; Mecking, S. *Angew. Chem., Int. Ed.* **2001,** *40,* 3020–3022. doi:10.1002/1521-3773(20010817)40:16<3020::AID-ANIE3020>3.0.CO;2-7
62. Bauers, F. M.; Chowdhry, M. M.; Mecking, S. *Macromolecules* **2003,** *36,* 6711–6715. doi:10.1021/ma034164m
63. Soula, R.; Novat, C.; Tomov, A.; Spitz, R.; Claverie, J.; Drujon, X.; Malinge, J.; Saudemont, T. *Macromolecules* **2001,** *34,* 2022–2026. doi:10.1021/ma0017135
64. Soula, R.; Saillard, B.; Spitz, R.; Claverie, J.; Llauro, M. F.; Monnet, C. *Macromolecules* **2002,** *35,* 1513–1523. doi:10.1021/ma011366e
65. Held, A.; Kolb, L.; Zuideveld, M. A.; Thomann, R.; Mecking, S.; Schmid, M.; Pietruschka, R.; Lindner, E.; Khanfar, M.; Sunjuk, M. *Macromolecules* **2002,** *35,* 3342–3347. doi:10.1021/ma0120411
66. Guo, J.; Choi, K. Y.; Schork, F. J. *Macromol. React. Eng.* **2009,** *3,* 412–418. doi:10.1002/mren.200900023
67. Klapper, M.; Jang, Y.-J.; Bieber, K.; Nemnich, T.; Nenov, N.; Müllen, K. *Macromol. Symp.* **2004,** *213,* 131–146. doi:10.1002/masy.200450914
68. Monteil, V.; Bastero, A.; Mecking, S. *Macromolecules* **2005,** *38,* 5393–5399. doi:10.1021/ma050621i
69. Claverie, J. P.; Viala, S.; Maurel, V.; Novat, C. *Macromolecules* **2001,** *34,* 382–388. doi:10.1021/ma001570m
70. Quémener, D.; Chemtob, A.; Héroguez, V.; Gnanou, Y. *Polymer* **2005,** *46,* 1067–1075. doi:10.1016/j.polymer.2004.11.096
71. Quémener, D.; Héroguez, V.; Gnanou, Y. *J. Polym. Sci., Part A: Polym. Chem.* **2006,** *44,* 2784–2793. doi:10.1002/pola.21370
72. Chemtob, A.; Gilbert, R. G. *Macromolecules* **2005,** *38,* 6796–6805. doi:10.1021/ma050558x
73. Luo, X.; Kang, N.; Li, L.; Deng, J.; Yang, W. *J. Polym. Sci., Part A: Polym. Chem.* **2010,** *48,* 1661–1668. doi:10.1002/pola.23924
74. Barrère, M.; Ganachaud, F.; Bendejacq, D.; Dourges, M. A.; Maitre, C.; Hémery, P. *Polymer* **2001,** *42,* 7239–7246. doi:10.1016/S0032-3861(01)00207-5
75. Barrère, M.; Maitre, C.; Dourges, M. A.; Hémery, P. *Macromolecules* **2001,** *34,* 7276–7280. doi:10.1021/ma010559z
76. Yactine, B.; Ganachaud, F.; Senhaji, O.; Boutevin, B. *Macromolecules* **2005,** *38,* 2230–2236. doi:10.1021/ma047912w
77. Ivanenko, C.; Maitre, C.; Ganachaud, F.; Hémery, P. *e-Polym.* **2003,** No. 010.
78. Maitre, C.; Ganachaud, F.; Ferreira, O.; Lutz, J. F.; Paintoux, Y.; Hémery, P. *Macromolecules* **2000,** *33,* 7730–7736. doi:10.1021/ma0007132
79. Cauvin, S.; Sadoun, A.; Dos Santos, R.; Belleney, J.; Ganachaud, F.; Hemery, P. *Macromolecules* **2002,** *35,* 7919–7927. doi:10.1021/ma0202890
80. Cauvin, S.; Ganachaud, F.; Touchard, V.; Hémery, P.; Leising, F. *Macromolecules* **2004,** *37,* 3214–3221. doi:10.1021/ma035942d
81. Touchard, V.; Graillat, C.; Boisson, C.; D'Agosto, F.; Spitz, R. *Macromolecules* **2004,** *37,* 3136–3142. doi:10.1021/ma0355352
82. Limouzin, C.; Caviggia, A.; Ganachaud, F.; Hémery, P. *Macromolecules* **2003,** *36,* 667–674. doi:10.1021/ma0257402
83. Altinbas, N.; Fehmer, C.; Terheiden, A.; Shukla, A.; Rehage, H.; Mayer, C. *J. Microencapsulation* **2006,** *23,* 567–581. doi:10.1080/02652040600776424
84. Huang, C.-Y.; Chen, C.-M.; Lee, Y.-D. *Int. J. Pharm.* **2007,** *338,* 267–275. doi:10.1016/j.ijpharm.2007.01.052
85. Weiss, C. K.; Ziener, U.; Landfester, K. *Macromolecules* **2007,** *40,* 928–938. doi:10.1021/ma061865l
86. Zhang, Y.; Zhu, S.; Lin, L.; Qian, F.; Tang, C.; Yin, C. *Eur. Polym. J.* **2008,** *44,* 1654–1661. doi:10.1016/j.eurpolymj.2008.03.019
87. Wu, M.; Frochot, C.; Dellacherie, E.; Marie, E. *Macromol. Symp.* **2009,** *281,* 39–46. doi:10.1002/masy.200950705
88. Wu, M.; Dellacherie, E.; Durand, A.; Marie, E. *Colloids Surf., B* **2009,** *69,* 147–151. doi:10.1016/j.colsurfb.2008.10.003
89. Wu, M.; Dellacherie, E.; Durand, A.; Marie, E. *Colloids Surf., B* **2009,** *69,* 141–146. doi:10.1016/j.colsurfb.2008.12.010
90. Musyanovych, A.; Landfester, K. *Prog. Colloid Polym. Sci.* **2008,** *134,* 120–127. doi:10.1007/978-3-540-68023-9
91. Taden, A.; Antonietti, M.; Landfester, K. *Macromol. Rapid Commun.* **2003,** *24,* 512–516. doi:10.1002/marc.200390079
92. Qi, G.; Jones, C. W.; Schork, J. F. *Biomacromolecules* **2006,** *7,* 2927–2930. doi:10.1021/bm0605816
93. Marie, E.; Rothe, R.; Antonietti, M.; Landfester, K. *Macromolecules* **2003,** *36,* 3967–3973. doi:10.1021/ma0257550
94. Bhadra, S.; Singha, N. K.; Khastgir, D. *Synth. Met.* **2006,** *156,* 1148–1154. doi:10.1016/j.synthmet.2006.08.002
95. Li, C. Y.; Chiu, W. Y.; Don, T. M. *J. Polym. Sci., Part A: Polym. Chem.* **2007,** *45,* 3902–3911. doi:10.1002/pola.22140
96. Cho, S. H.; Kim, W. Y.; Jeong, G. K.; Lee, Y. S. *Colloids Surf., A* **2005,** *255,* 79–83. doi:10.1016/j.colsurfa.2004.12.025
97. Ham, H. T.; Choi, Y. S.; Jeong, N.; Chung, I. J. *Polymer* **2005,** *46,* 6308–6315. doi:10.1016/j.polymer.2005.05.062
98. Joo, Y. T.; Jin, S. M.; Kim, Y. *Polymer (Korea)* **2009,** *33,* 452–457.
99. Du, Y.-Z.; Wang, L.; Dong, Y.; Yuan, H.; Hu, F.-Q. *Carbohydr. Polym.* **2010,** *79,* 1034–1039. doi:10.1016/j.carbpol.2009.10.032
100. Taira, S.; Du, Y. Z.; Kodaka, M. *Biotechnol. Bioeng.* **2006,** *93,* 396–400. doi:10.1002/bit.20711
101. Barrère, M.; Landfester, K. *Macromolecules* **2003,** *36,* 5119–5125. doi:10.1021/ma025981+
102. Zanetti-Ramos, B. G.; Lemos-Senna, E.; Soldi, V.; Borsali, R.; Cloutet, E.; Cramail, H. *Polymer* **2006,** *47,* 8080–8087. doi:10.1016/j.polymer.2006.09.057
103. Li, C.-Y.; Li, Y.-H.; Hsieh, K.-H.; Chiu, W.-Y. *J. Appl. Polym. Sci.* **2008,** *107,* 840–845. doi:10.1002/app.25164
104. Du, Y.-Z.; Xu, J.-G.; Wang, L.; Yuan, H.; Hu, F.-Q. *Eur. Polym. J.* **2009,** *45,* 1397–1402. doi:10.1016/j.eurpolymj.2009.01.031

105. Li, C.-Y.; Chiu, W.-Y.; Don, T.-M. *J. Polym. Sci., Part A: Polym. Chem.* **2005,** *43,* 4870–4881. doi:10.1002/pola.20959
106. Wang, C.; Chu, F.; Guyot, A.; Gauthier, C.; Boisson, F. *J. Appl. Polym. Sci.* **2006,** *101,* 3927–3941. doi:10.1002/app.22889
107. Li, C.-Y.; Chiu, W.-Y.; Lee, C.-F. *e-Polym.* **2007,** 015.
108. Landfester, K.; Pawelzik, U.; Antonietti, M. *Polymer* **2005,** *46,* 9892–9898. doi:10.1016/j.polymer.2005.07.080
109. Koenig, A.; Ziener, U.; Schaz, A.; Landfester, K. *Macromol. Chem. Phys.* **2007,** *208,* 155–163. doi:10.1002/macp.200600448
110. Müller, K.; Klapper, M.; Müllen, K. *Colloid Polym. Sci.* **2007,** *285,* 1157–1161. doi:10.1007/s00396-007-1670-4
111. Haschick, R.; Mueller, K.; Klapper, M.; Muellen, K. *Macromolecules* **2008,** *41,* 5077–5081. doi:10.1021/ma800550z
112. Takasu, M.; Kawaguchi, H. *Colloid Polym. Sci.* **2005,** *283,* 805–811. doi:10.1007/s00396-004-1248-3
113. Torini, L.; Argillier, J. F.; Zydowicz, N. *Macromolecules* **2005,** *38,* 3225–3236. doi:10.1021/ma047808e
114. Johnsen, H.; Schmid, R. B. *J. Microencapsulation* **2007,** *24,* 731–742. doi:10.1080/02652040701585179
115. Gaudin, F.; Sintes-Zydowicz, N. *Colloids Surf., A* **2008,** *331,* 133–142. doi:10.1016/j.colsurfa.2008.07.028
116. Crespy, D.; Stark, M.; Hoffmann-Richter, C.; Ziener, U.; Landfester, K. *Macromolecules* **2007,** *40,* 3122–3135. doi:10.1021/ma0621932
117. Jagielski, N.; Sharma, S.; Hombach, V.; Mailänder, V.; Rasche, V.; Landfester, K. *Macromol. Chem. Phys.* **2007,** *208,* 2229–2241. doi:10.1002/macp.200700254
118. Sharma, S.; Paiphansiri, U.; Hombach, V.; Mailander, V.; Zimmermann, O.; Landfester, K.; Rasche, V. *Contrast Media Mol. Imaging* **2010,** *5,* 59–69. doi:10.1002/cmmi.364
119. Paiphansiri, U.; Dausend, J.; Musyanovych, A.; Mailander, V.; Landfester, K. *Macromol. Biosci.* **2009,** *9,* 575–584. doi:10.1002/mabi.200800293
120. Rosenbauer, E. M.; Landfester, K.; Musyanovych, A. *Langmuir* **2009,** *25,* 12084–12091. doi:10.1021/la9017097
121. Baier, G.; Musyanovych, A.; Dass, M.; Theisinger, S.; Landfester, K. *Biomacromolecules* **2010,** *11,* 960–968. doi:10.1021/bm901414k
122. Rosenbauer, E.-M.; Wagner, M.; Musyanovych, A.; Landfester, K. *Macromolecules* **2010,** *43,* 5083–5093. doi:10.1021/ma100481s
123. Boutti, S.; Bourgeat-Lami, E.; Zydowicz, N. *Macromol. Rapid Commun.* **2005,** *26,* 1860–1865. doi:10.1002/marc.200500518
124. Groll, J.; Singh, S.; Albrecht, K.; Moeller, M. *J. Polym. Sci., Part A: Polym. Chem.* **2009,** *47,* 5543–5549. doi:10.1002/pola.23595
125. Wang, S.; Wang, X.; Zhang, Z. *Eur. Polym. J.* **2007,** *43,* 178–184. doi:10.1016/j.eurpolymj.2006.09.010
126. Qian, Z.; Chen, J.; Chen, Y.; Zhang, Z.; Liu, H. *Colloids Surf., A* **2007,** *295,* 7–15. doi:10.1016/j.colsurfa.2006.08.051
127. Wang, H.; Ge, X.; Song, L.; Liu, H. *Colloid Polym. Sci.* **2007,** *285,* 1093–1100. doi:10.1007/s00396-007-1659-z
128. Chen, Y.; Liu, H. R.; Zhang, Z. C.; Wang, S. J. *Eur. Polym. J.* **2007,** *43,* 2848–2855. doi:10.1016/j.eurpolymj.2007.04.013
129. Li, J.; Wang, Q. J.; Su, C. H.; Chen, Q. M. *Eur. Polym. J.* **2007,** *43,* 2928–2934. doi:10.1016/j.eurpolymj.2007.04.028
130. Chen, J.; Zhang, Z.; Zhang, Q. *Radiat. Phys. Chem.* **2009,** *78,* 906–909. doi:10.1016/j.radphyschem.2009.06.014
131. Wang, H.; Wang, M.; Ge, X. *Radiat. Phys. Chem.* **2009,** *78,* 112–118. doi:10.1016/j.radphyschem.2008.08.005
132. Hittinger, E.; Kokil, A.; Weder, C. *Angew. Chem., Int. Ed.* **2004,** *43,* 1808–1811. doi:10.1002/anie.200352863
133. Baier, M. C.; Huber, J.; Mecking, S. *J. Am. Chem. Soc.* **2009,** *131,* 14267–14273. doi:10.1021/ja905077c
134. Liang, G.; Xu, J.; Wang, X. *J. Am. Chem. Soc.* **2009,** *131,* 5378–5379. doi:10.1021/ja900516a
135. McHale, R.; Ghasdian, N.; Liu, Y.; Ward, M. B.; Hondow, N. S.; Wang, H.; Miao, Y.; Brydson, R.; Wang, X. *Chem. Commun.* **2010,** *46,* 4574–4576. doi:10.1039/c0cc00003e
136. McHale, R.; Ghasdian, N.; Liu, Y.; Wang, H.; Miao, Y.; Wang, X. *Macromol. Rapid Commun.* **2010,** *31,* 856–860. doi:10.1002/marc.200900875

License and Terms

This is an Open Access article under the terms of the Creative Commons Attribution License (http://creativecommons.org/licenses/by/2.0), which permits unrestricted use, distribution, and reproduction in any medium, provided the original work is properly cited.

The license is subject to the *Beilstein Journal of Organic Chemistry* terms and conditions: (http://www.beilstein-journals.org/bjoc)

The definitive version of this article is the electronic one which can be found at: doi:10.3762/bjoc.6.130